

UNCLASSIFIED

AD NUMBER

ADB012310

LIMITATION CHANGES

TO:

Approved for public release; distribution is unlimited.

FROM:

Distribution authorized to U.S. Gov't. agencies only; Proprietary Information; 08 DEC 1975. Other requests shall be referred to Aeronautical Systems Div., Wright-Patterson AFB, OH 45433.

AUTHORITY

ASD ltr 8 Dec 1976

THIS PAGE IS UNCLASSIFIED

THIS REPORT HAS BEEN DELIMITED  
AND CLEARED FOR PUBLIC RELEASE  
UNDER DOD DIRECTIVE 5200.20 AND  
NO RESTRICTIONS ARE IMPOSED UPON  
ITS USE AND DISCLOSURE.

DISTRIBUTION STATEMENT A

APPROVED FOR PUBLIC RELEASE;  
DISTRIBUTION UNLIMITED.

UNCLASSIFIED

SECURITY CLASSIFICATION OF THIS PAGE (When Data Entered)

B.S. 00067654  
Vol-1

REPORT DOCUMENTATION PAGE

READ INSTRUCTIONS  
BEFORE COMPLETING FORM

1. REPORT NUMBER <b>14</b> GSE/SE/75-2	2. GOVT ACCESSION NO.	3. RECIPIENT'S CATALOG NUMBER
4. TITLE (and Subtitle) <b>6</b> VERY LOW COST EXPENDABLE HARASSMENT SYSTEM DESIGN STUDY, <del>XXXXXXXXXX</del> Volume III.	5. TYPE OF REPORT & PERIOD COVERED <b>9</b> MASTERS THESIS	
7. AUTHOR(s) <b>10</b> J. A. BRADBURY, II, J. E. HATLELID, M. H. LONG, III, P. M. MOORE, JR., D. C. MORRIS, R. W. PLANT, R. J. ROBBINS, L. J. WILLIAMS	8. CONTRACT OR GRANT NUMBER(s)	
9. PERFORMING ORGANIZATION NAME AND ADDRESS School of Engineering AIR FORCE INSTITUTE OF TECHNOLOGY (AFIT/EN) WRIGHT-PATTERSON AFB OH 45433	10. PROGRAM ELEMENT, PROJECT, TASK AREA & WORK UNIT NUMBERS <b>12</b> 457P	
11. CONTROLLING OFFICE NAME AND ADDRESS AERONAUTICAL SYSTEMS DIVISION (ASD/YRPM) WRIGHT-PATTERSON AFB OH 45433	12. REPORT DATE <b>11</b> DEC 1975	13. NUMBER OF PAGES 452
14. MONITORING AGENCY NAME & ADDRESS (if different from Controlling Office)	15. SECURITY CLASS. (of this report) UNCLASSIFIED	
15a. DECLASSIFICATION/DOWNGRADING SCHEDULE		

AD B O I 2310

AD B O I  
DDC FILE COPY

16. DISTRIBUTION STATEMENT (of this Report)  
DISTRIBUTION LIMITED TO U.S. GOV'T AGENCIES ONLY; PROPRIETARY INFO; 8 DECEMBER 1975. OTHER REQUESTS FOR THIS DOCUMENT MUST BE REFERRED TO ASD/YRPM, WRIGHT-PATTERSON AFB OH 45433.

17. DISTRIBUTION STATEMENT (of the abstract entered in Block 20, if different from Report)  
APPROVED FOR PUBLIC RELEASE; DISTRIBUTION UNLIMITED

DDC  
JUL 21 1976  
A

18. SUPPLEMENTARY NOTES

19. KEY WORDS (Continue on reverse side if necessary and identify by block number)  
MINI-DRONE, MINI-RPV, DRONE, RPV, 2-CYCLE ENGINE, HARASSMENT VEHICLE, MINI-DRONE LAUNCHER, MINI-RPV LAUNCHER, RPV MATERIALS, LIFE-CYCLE COST, RPV DESIGN, DRONE DESIGN.

20. ABSTRACT (Continue on reverse side if necessary and identify by block number)  
This study investigated the design and implementation of a decoy mini-drone (Type II) when employed with an attack vehicle (Type I) under the very low-cost harassment vehicle concept. A systems approach was used with the harassment system divided into eight areas of analysis: Mission, Airframe, Stability, Propulsion, Navigation, Electrical Power, Launcher, and Cost. The overriding constraint of this study was low cost.

Form a variety of possible missions, an area targeted, defense suppression mission was selected for the purpose of establishing a point design. A 125-pound, twin-boom pusher airframe, constructed of polyurethane foam, was designed as the common vehicle airframe. It is powered by a McCulloch MC101B engine. Type II vehicle stabilization is accomplished without a rate sensor. A dead-reckoning navigation system was designed and evaluated as the most cost-effective Type II navigation method. The analysis of launcher candidates indicated that a spring powered launcher was the most cost-effective launch concept. An extensive computer simulation of harassment vehicle employment results in a methodology for mix determination, and a 4.5 to 1 ratio of Type II to Type I vehicles maximizes the given measure of effectiveness. For this mix, the 12-year life cycle cost for 5000 mini-drones is \$18.95 million.

VERY LOW COST EXPENDABLE  
HARASSMENT SYSTEM DESIGN STUDY  
(VOLUME III)

Presented to the Faculty of the School of Engineering  
of the Air Force Institute of Technology  
Air University  
in Partial Fulfillment of the  
Requirements for the Degree of  
Master of Science

by

Capt James A. Bradbury II, USAF  
Capt John E. Hatlelid, USAF  
Capt Mahlon H. Long III, USAF  
Major Paul M. Moore, Jr., USAF  
Capt Douglas C. Morris, USAF  
Capt Richard W. Plant, USAF  
Capt Richard J. Robbins, USAF  
Capt Larry J. Williams, USAF

ACCESSION FOR	
NTIS	WPA/CS/DA <input type="checkbox"/>
DDC	DA/CS/DA <input checked="" type="checkbox"/>
UNANNOUNCED	<input type="checkbox"/>
JUSTIFICATION	
FY.....	
DIVISION.....	
F.O.	
B	

Graduate Systems Engineering

December 1975

## PREFACE

This academic study was prepared by the 1975 Graduate Systems Engineering Class (GSE 75D) at the Air Force Institute of Technology, Wright-Patterson AFB, Ohio. It is submitted in partial fulfillment of the requirements for the Master of Science degree and should not be construed to be an official Air Force Design Study. The work was sponsored by the Remotely Piloted Vehicle Systems Program Office (RPV SPO), Aeronautical Systems Division (ASD/YRP), Wright-Patterson AFB, Ohio. The authors of this report are the eight members of the AFIT GSE 75D class:

- Capt James A. Bradbury, II, USAF
- Capt John E. Hatlelid, USAF
- Capt Mahlon H. Long, III, USAF
- Maj Paul M. Moore, Jr., USAF
- Capt Douglas C. Morris, USAF
- Capt Richard W. Plant, USAF
- Capt Richard J. Robbins, USAF
- Capt Larry J. Williams, USAF

The AFIT Faculty advisors were:

- Maj Robert F. Bestgen, USAF
- Capt Richard D. Binkowski, USAF
- Dr. Charles J. Bridgman
- Maj Edward J. Dunne, Jr., USAF
- Lt Col Jon R. Hobbs, USAF
- Capt Thomas E. Moriarty, USAF
- Dr. Lynn E. Wolaver

Technical work was conducted during the period 2 April 1975 to 10 November 1975. The final report was submitted on 8 December 1975.

Special appreciation is given to Maj Robert E. Bowen, Mr. William J. Elsner, and Capt Heikki Joonsar of the RPV SPO for their support and cooperation in this study. Appreciation is also given to Professor Harold C. Larsen, AFIT; Maj Walter S. Hoy and staff of the Teleplane branch, Air Force Flight Dynamics Laboratory; Capt Frank Corvell, Aeronautical Systems Division, Staff Meteorologist Office; and Mr. Glen V. Pickwell, consultant, for their continued cooperation and technical support in the many phases of this study.

The report consists of three volumes, the first two of which are classified SECRET. Volume I, the Executive Summary, contains the major highlights of the design study. Volume II, the Final Report, contains mission analysis, costing, and a description of the vehicle and launcher. Volume III, the Unclassified Appendices, has the detailed design and iterative decisions associated with the airframe, flight control, propulsion, electrical power, navigation, and launcher.

Normally whenever reference is made to an appendix, it will be found in the same volume. When the referenced appendix is in a volume other than the one giving the reference, the volume number will also be given.

TABLE OF CONTENTS

	<u>Page</u>
List of Figures . . . . .	ix
List of Tables . . . . .	xiii
Appendix A     Airframe	
Introduction . . . . .	A- 1
Survey . . . . .	A- 4
Layout . . . . .	A-12
Preliminary Planform . . . . .	A-12
Preliminary Engine Layout . . . . .	A-21
Preliminary Fuselage Layout . . . . .	A-22
Preliminary Empennage Layout . . . . .	A-23
Preliminary Weight and Balance . . . . .	A-25
Final Weight and Balance . . . . .	A-26
Final Layout Estimate . . . . .	A-31
Structures . . . . .	A-37
Environment . . . . .	A-37
Materials . . . . .	A-39
Manufacturing Techniques . . . . .	A-44
Load Analysis . . . . .	A-46
Wing Loading . . . . .	A-47
Carry-Through Spar . . . . .	A-52
Booms . . . . .	A-54
Horizontal Tail Spar . . . . .	A-56
Vertical Tail . . . . .	A-60
Fuselage . . . . .	A-61
Weight Calculations . . . . .	A-66
Performance . . . . .	A-70
Mission Profile . . . . .	A-70
Power . . . . .	A-71
Wing Characteristics . . . . .	A-74
Time and Fuel . . . . .	A-75
Inputs to DESIGN . . . . .	A-78
Outputs from DESIGN . . . . .	A-79
Cost . . . . .	A-80
Conclusions . . . . .	A-81
Appendix A-1   Airfoil Characteristics . . . . .	A-83
A-2   Aspect Ratio Effects (CDVSAR) . . . . .	A-86
A-3   Wing Design (SHRENK) . . . . .	A-92
A-4   Fuselage Cross-Section (FUSLAG) . . . . .	A-100

TABLE OF CONTENTS

	<u>Page</u>
A-5 Weight and Balance (WTNBAL) . . . . .	A-102
A-6 Performance (DESIGN) . . . . .	A-107
Appendix B Flight Control Subsystem	
Introduction . . . . .	B- 1
Procedure . . . . .	B- 1
Discussion . . . . .	B- 2
Flight Conditions . . . . .	B- 2
Equations of Motion . . . . .	B- 2
Sensitivity Analysis . . . . .	B- 3
Servo and Sensor Model . . . . .	B- 4
Heading Control . . . . .	B- 4
Altitude Hold . . . . .	B- 6
Conclusions and Recommendations . . . . .	B- 7
Appendix B-1 Basis for the Equations of Motion . . . . .	B- 9
B-2 Nominal Flight Conditions for Analysis . . . . .	B-12
B-3 Evaluation of Nominal Longitudinal Stability Derivatives . . . . .	B-13
B-4 Evaluation of Nominal Lateral Stability Derivatives . . . . .	B-14
B-5 Longitudinal Dynamics and Characteristic Motion . . . . .	B-25
B-6 Lateral Dynamics and Characteristic Motion . . . . .	B-26
B-7 Sensitivity Analysis of Longitudinal Stability Coefficients . . . . .	B-27
B-8 Sensitivity Analysis of Lateral Stability Coefficients . . . . .	B-29
B-9 Neutral Point and Center of Gravity Location . . . . .	B-31
B-10 Servo Transfer Function . . . . .	B-34
B-11 Lateral Dynamics from Rudder Input . . . . .	B-35
B-12 Closed-Loop Heading-Control Dynamics . . . . .	B-37

TABLE OF CONTENTS

	<u>Page</u>
B-13 Best-Case and Worst-Case Closed-Loop Heading Control . . . . .	B-47
B-14 Longitudinal Dynamics for Elevator Input . . .	B-50
B-15 Closed-Loop Altitude Hold Dynamics . . . . .	B-52
B-16 Best-Case and Worst-Case Closed-Loop Altitude-Hold Dynamics . . . . .	B-60
B-17 Altitude Hold Circuit Details . . . . .	B-63
 Appendix C Propulsion Subsystem	
Introduction . . . . .	C-1
Scope . . . . .	C-1
Approach . . . . .	C-1
System Considerations . . . . .	C-2
Criteria . . . . .	C-3
Survey of Propulsion Devices . . . . .	C-3
Final Propulsion Subsystem Candidates . . . . .	C-6
Candidate Comparison with Decision Criteria . . . . .	C-13
Cost . . . . .	C-13
Weight . . . . .	C-15
Availability . . . . .	C-16
Power . . . . .	C-16
Specific Fuel Consumption . . . . .	C-17
Vibration . . . . .	C-18
Reliability . . . . .	C-19
Engine Selection . . . . .	C-20
Propeller Selection . . . . .	C-20
Engine Testings . . . . .	C-21
Background . . . . .	C-21
Test Objective . . . . .	C-21
Test Equipment . . . . .	C-21
Test Procedures . . . . .	C-22
Test Results . . . . .	C-23
 Appendix C-1 Engine Test . . . . .	C-24
 Appendix D Electrical Power	
Introduction . . . . .	D- 1
Power Requirements . . . . .	D- 1
Advantages of DM Generators . . . . .	D- 2
Excitation . . . . .	D- 2

TABLE OF CONTENTS

	<u>Page</u>
Selecting an Alternator . . . . .	D- 5
Batteries . . . . .	D- 6
Standard Cells vs Special-Purpose Batteries.	D- 6
Primary Cells vs Secondary Batteries . . . .	D- 7
Fuel Cells . . . . .	D- 7
Secondary Cells . . . . .	D- 7
Primary Cells . . . . .	D-10
Magnesium Batteries . . . . .	D-12
Alkaline Batteries . . . . .	D-12
Mercury Batteries . . . . .	D-12
Lithium Batteries . . . . .	D-14
Batteries vs Generators . . . . .	D-18
Conclusions . . . . .	D-18
Appendix E      Navigation Subsystem	
Introduction . . . . .	E- 1
System Selection . . . . .	E- 2
System Design . . . . .	E- 5
Pattern . . . . .	E- 5
Processing Network . . . . .	E- 5
Summary . . . . .	E- 7
E-1      Navigation Techniques . . . . .	E-12
E-2      Cost . . . . .	E-23
E-3      Wind Models . . . . .	E-27
E-4      Dead-Reckoning Circuit Details . . . . .	E-37
E-5      Reliability . . . . .	E-60
E-6      Accuracy . . . . .	E-64
E-7      CEP Analysis . . . . .	E-77
E-8      Launch Control Conditions . . . . .	E-81
E-9      Normalized Magnetometer Output . . . . .	E-82
Appendix F      Launcher	
Introduction . . . . .	F- 1
Approach . . . . .	F- 2
The Rocket Motor . . . . .	F- 3

TABLE OF CONTENTS

	<u>Page</u>
Sizing of Calapult . . . . .	F- 3
Rubber Launcher Element . . . . .	F- 4
Spring Launcher . . . . .	F- 5
Main Structure . . . . .	F- 8
The Spring . . . . .	F-10
Shock Absorber . . . . .	F-11
Shuttle . . . . .	F-12
Launch Specification . . . . .	F-16
Cost . . . . .	F-17
Conclusion and Recommendations . . . . .	F-18
Appendix F-1 Computation of Required Launcher Throw . . . . .	F-19
F-2 Evaluation of a Spring Launcher Capability . . . . .	F-26
F-3 Analysis of Main Structure . . . . .	F-30
F-4 Spring Design . . . . .	F-35
F-5 Shock Absorber Analysis . . . . .	F-40
F-6 Analysis of Critical Shuttle Components . . . . .	F-45

## LIST OF FIGURES

<u>FIGURE</u>		<u>PAGE</u>
A- 1	XBQM-106 . . . . .	A-11
A- 2	Canard Candidate . . . . .	A-11
A- 3	Twin-Boom Pusher Candidate . . . . .	A-11
A- 4	Preliminary Planform . . . . .	A-14
A- 5	Taper Ratio Drag Effect . . . . .	A-14
A- 6	Inboard Profile . . . . .	A-27
A- 7	Component Weight Locations . . . . .	A-29
A- 8	Center of Gravity Shift with Fuel Usage . . . . .	A-30
A- 9	Final Planform . . . . .	A-33
A-10	Vehicle External View . . . . .	A-35
A-11	Vehicle Assembly . . . . .	A-36
A-12	Package Size . . . . .	A-36
A-13	Primary Wing Section . . . . .	A-41
A-14	Alternate Wing Section . . . . .	A-45
A-15	Hinge Molding Scheme . . . . .	A-46
A-16	Loading Layout . . . . .	A-48
A-17	Structural Skeleton . . . . .	A-57
A-18	Horizontal Tail Loads . . . . .	A-58
A-19	Fuselage Schematic Loads . . . . .	A-58
A-20	Mission Profile . . . . .	A-72
A-21	NACA 2515 . . . . .	A-83
A-22	NACA 2518 . . . . .	A-84
A-23	NACA 0015 . . . . .	A-85
A-24	Aspect Ratio Effects . . . . .	A-91
A-25	Maximum Lift Coefficient vs Washout Angle . . . . .	A-99
A-26	Fuselage Section . . . . .	A-101
A-27	Center of Gravity Shift with Fuel Consumption . . . . .	A-106
A-28	Climb Angle and Rate of Climb . . . . .	A-118
A-29	Wing Area, Launch Speed, Weight . . . . .	A-119
A-30	Thrust-Horsepower Altitude . . . . .	A-120
A-31	Required Horsepower . . . . .	A-121
A-32	Lift and Drag Relationships . . . . .	A-121
A-33	Fuel Consumption Sensitivity . . . . .	A-122
B- 1	Preliminary Closed-Loop Heading Control (No Compensation) . . . . .	B- 4
B- 2	Comparison of Heading Control Step Response for Varying Aircraft Dynamics . . . . .	B- 5
B- 3	Preliminary Altitude Hold Block Diagram (No Compensation) . . . . .	B- 6
B- 4	Comparison of Step Response of Altitude Hold Circuit with Varying Aircraft Dynamics . . . . .	B- 7
B- 5	Aerodynamic Center, Neutral Point and Center of Gravity Locations . . . . .	B-31

LIST OF FIGURES

<u>FIGURE</u>		<u>PAGE</u>
B- 6	Exponential Approximation of the Linearized Response Curve of the KPS-16 Servo . . . . .	B-34
B- 7	Root Locus Plot of the Uncompensated Heading Control System . . . . .	B-39
B- 8	Unstable Time Response of the Heading Control System (No Compensation) . . . . .	B-38
B- 9	Heading Control Block Diagram with Compensation . . . . .	B-42
B-10	Root Locus Plot of the Compensated Heading Control System . . . . .	B-41
B-11	Time Response of Heading Angle for a Unit Step Input of Commanded Heading Angle . . . . .	B-42
B-12	Comparison of Heading Step Response for Two Values of Gain . . . . .	B-43
B-13	Time Response of Rudder Transients given a Unit Step Input of Commanded Heading Angle . . . . .	B-45
B-14	Time Response of Heading Angle Given a Unit Step Input of Heading Angle due to Gust . . . . .	B-46
B-15	Root Locus Plot of the Uncompensated Altitude Hold System . . . . .	B-54
B-16	Altitude Hold Block Diagram (with Compensation) . . . . .	B-55
B-17	Root Locus Plot of the Compensated Altitude Hold System . . . . .	B-56
B-18	Step Response of Aircraft Altitude Given a Commanded Altitude Change . . . . .	B-58
B-19	Comparison of Step Response in Altitude for Two Values of Gain . . . . .	B-58
B-20	Time Response of Elevator Transients Given a Unit Step Change of Commanded Altitude . . . . .	B-59
B-21	Time Response of Aircraft Altitude due to a Gust Change of Altitude . . . . .	B-57
B-22	Altitude Feedback Compensator . . . . .	B-63
B-23	Altitude Hold Forward Path Compensator . . . . .	B-65
B-24	Altitude Hold Circuit Diagram . . . . .	B-66
C- 1	Comparison of Power to Weight versus Power for Several Engines . . . . .	C-12
C- 2	Derived Altitude Test Data for MC 101 Engine in Lockheed Flight configuration . . . . .	C-26
C- 3	Mixture Ratio Effects . . . . .	C-27
C- 4	Disassembled View of the MC 101 . . . . .	C-30
C- 5	Test Bed Instrumentation Schematic . . . . .	C-32
C- 6	Front View of Engine in Altitude Chamber . . . . .	C-33
C- 7	Fuel Measurement System . . . . .	C-33

LIST OF FIGURES

<u>FIGURE</u>		<u>PAGE</u>
C- 8	Thrust Stand . . . . .	C-37
C- 9	Test Propeller Damage . . . . .	C-42
C-10	Thrust and Fuel Consumption Versus Engine Speed for Various Altitudes at 75 Miles Per Hour Tunnel Velocity . . . . .	C-44
C-11	Thrust and Fuel Consumption Versus Engine Speed for Various Altitudes at 100 Miles Per hour Tunnel Velocity . . . . .	C-46
C-12	Generic Performance Curves . . . . .	C-47
C-13	Design Chart for Propeller 5868-9, Clark Y Section, Two Blades . . . . .	C-53
C-14	Design Chart for Propeller 5868-R6, RAF-6 Section, Two Blades . . . . .	C-54
C-15	Design Chart for Propeller 37-3647, RAF-6 Section, Two Blades . . . . .	C-54
C-16	Power Coefficient Curves for Propeller 5868-9 Clark Y Section, Two Blades . . . . .	C-56
C-17	Thrust versus Velocity Curves, Fixed-Pitch Analysis Using NACA TR640 . . . . .	C-59
D- 1	Discharge Comparison of Secondary Batteries . . . . .	D- 9
D- 2	Discharge Characteristics of Lead-Acid Batteries . . . . .	D- 9
D- 3	Discharge Characteristics of Nickel-Cadmium Batteries . . . . .	D-11
D- 4	Temperature Discharge Characteristics of Carbon-Zinc Cells under Constant Load . . . . .	D-11
D- 5	Discharge Comparison of Primary Cells . . . . .	D-13
D- 6	Continuous Discharge Comparison of Carbon-Zinc and Alkaline Cells . . . . .	D-13
D- 7	Lithium D-Cell Discharge Curves . . . . .	D-15
D- 8	Lithium Battery Schematic for Type II Vehicle for 6-Hour Mission . . . . .	D-16
D- 9	Energy Capacity of D-Size Primary Cells (1 Ampere at 78°F) . . . . .	D-19
E- 1	Loiter Pattern Comparison . . . . .	E- 6
E- 2	Timer A for Final Circuit Design . . . . .	E- 8, 53
E- 3	Timers B through E, Navigation Circuit Final Design.	E- 9, 54
E- 4	Navigation Final Design . . . . .	E-10, 55
E- 5	View of Navigation Set . . . . .	E-11
E- 6	Three Station Loran Fix Using LOP's . . . . .	E-18
E- 7	Loran-C Coverage . . . . .	E-19
E- 8	Loran-D European Chain Under Construction . . . . .	E-20

LIST OF FIGURES

<u>FIGURE</u>		<u>PAGE</u>
E- 9	Prevailing Wind Direction (Central West Germany Using Weisbaden Germany 1946-1957) . . . . .	E-28
E-10	Mean Wind Speed (Wiesbaden, Germany, 1946-1957) . . . . .	E-29
E-11	Mesoscale Speed Prediction Error . . . . .	E-32
E-12	Mesoscale Direction Prediction Error . . . . .	E-32
E-13	Hourly Speed Change . . . . .	E-35
E-14	Hourly Direction Change . . . . .	E-35
E-15	Speed Change . . . . .	E-36
E-16	Direction Change . . . . .	E-36
E-17	Navigation Scheme . . . . .	E-38
E-18	Wind Triangle . . . . .	E-38
E-19(a)	Dead Reckoning Navigation Circuit . . . . .	E-39
E-19(b)	Dead Reckoning Navigation Circuit Diagram (Continued) . . . . .	E-40
E-20	Timer A, Monostable . . . . .	E-41
E-21	Timer B, Astable . . . . .	E-41
E-22	Karnaugh Map, Navigation Leg B . . . . .	E-46
E-23	Karnaugh Map, Navigation Leg C . . . . .	E-46
E-24	Prototype Timer Logic Diagram . . . . .	E-47
E-25	Heading Control Loop Compensator . . . . .	E-56
E-26	Relation of Desired Heading $\theta$ to Preset Values . . . . .	E-66
E-27	World Magnetic Chart of Surface Field Declination. . . . .	E-67
E-28	Values Seen by the Navigation System . . . . .	E-68
E-29	World Magnetic Chart of Horizontal Field Intensity . . . . .	E-71
E-30	Heading Error Due to Non-Horizontal Altitude . . . . .	E-73
E-31	Probability of Displacement is a Function of Time and Distance . . . . .	E-78
E-32	Probability of Error Less Than $r$ Versus Time . . . . .	E-79
F- 1	Launcher Mounted on M-36 Truck . . . . .	F- 6
F- 2	Major Launch Components . . . . .	F- 7
F- 3	Cross-Section of Launcher . . . . .	F- 8
F- 4(a)	Side View of Shuttle . . . . .	F-13
F- 4(b)	Front View of Shuttle . . . . .	F-13
F- 5	Oblique View of Shuttle and Drone . . . . .	F-14
F- 6	Views of the Thrust Lever Unlock Sequence . . . . .	F-15
F- 7	Beam Loads with Launcher Cocked . . . . .	F-30
F- 8	Spring Rate Versus Number of Coils or Spring Length. . . . .	F-37
F- 9	Minimum Launcher Length with Pulley Ratio of 4:1 Versus Spring Length . . . . .	F-38
F-10	Work Done by Linear Force . . . . .	F-41
F-11	Distance Required to Bring Shuttle Speed to Zero for Various Areas . . . . .	F-43
F-12	Capability and Electrical Requirements at 9 Volts dc . . . . .	F-51

LIST OF TABLES

<u>TABLE</u>		<u>PAGE</u>
A- 1	Preliminary Planform Parameters . . . . .	A-21
A- 2	Preliminary Empennage Parameters . . . . .	A-24
A- 3	Preliminary Weight and Balance . . . . .	A-25
A- 4	Final Weight and Balance . . . . .	A-28
A- 5	Final Wing Planform Estimate . . . . .	A-33
A- 6	Final Empennage Estimates . . . . .	A-34
A- 7	Aluminum/Polycarbonate Tradeoff . . . . .	A-43
A- 8	Wing Intersection Loading . . . . .	A-50
A- 9	Tube Properties . . . . .	A-51
A-10	Wing Root Loading . . . . .	A-52
A-11	Aluminum Structure Summary . . . . .	A-66
A-12	Foamed Component Weights . . . . .	A-67
A-13	Final Weight and Balance . . . . .	A-69
A-14	Recurring Airframe Cost Estimates . . . . .	A-80
B- 1	Nominal Flight Parameters . . . . .	B-12
B- 2	Nominal Longitudinal Stability Coefficients . . . . .	B-18
B- 3	Nominal Lateral Stability Coefficients . . . . .	B-24
B- 4	Longitudinal Characteristic Motion . . . . .	B-25
B- 5	Lateral Characteristic Motion . . . . .	B-26
B- 6	Longitudinal Sensitivity . . . . .	B-28
B- 7	Lateral Sensitivity . . . . .	B-30
B- 8	Dominant Heading Response for Various Values of Gain . . . . .	B-43
B- 9	Comparison of Best-Case, Baseline, and Worst-Case Heading-Control Dynamics . . . . .	B-49
B-10	Altitude Hold Settling Times . . . . .	B-62
C- 1	Comparison of Power Plants in Small Drones . . . . .	C- 7
C- 2	Comparison of Selected Engine Specifications based on Contractor Information . . . . .	C-14
C- 3	Estimated Propulsion Subsystem Costs for the Primary Candidates. . . . .	C-15
C- 4	Comparison of Rated Power and Net Power for the Primary Candidates Engines . . . . .	C-17
C- 5	MC 101B Specifications . . . . .	C-29
D- 1	Type I Power Requirements . . . . .	D- 3
D- 2	Type II Power Requirements . . . . .	D- 4
D- 3	Lithium Battery Requirements for Type II Vehicle with 6-Hour Missions . . . . .	D-17

LIST OF TABLES

<u>TABLE</u>		<u>PAGE</u>
E- 1	Summary of Coupled Approaches . . . . .	E- 3
E- 2	Summary of Independent Approaches . . . . .	E- 3
E- 3	Hours Downtime per Dollar . . . . .	E- 4
E- 4	Component Costs (2-Leg Pattern) . . . . .	E-23
E- 5	Component Costs (4-Leg Pattern) . . . . .	E-24
E- 6	Standard Deviation of Wind Prediction Error . . . . .	E-31
E- 7	Prototype Circuit Test Data . . . . .	E-50
E- 8	Failure Rate for Dead Reckoning Electronics . . . . .	E-61
E- 9	Failure Summary for Dead Reckoning . . . . .	E-62
E-10	Failure Rates for Omega . . . . .	E-63
E-11	Failure Summary for Omega . . . . .	E-63
E-12	Summary of Errors . . . . .	E-15
F- 1	Launcher Length and Spring Force for Differing Pulley Ratios . . . . .	F- 9
F- 2	Launch Weight, Number of Springs and G-load . . . . .	F-11
F- 3	Launch G and Velocity Versus Net Thrust . . . . .	F-17
F- 4	Kinetic Energy of Shuttle and Springs . . . . .	F-42
F- 5	Stiffening Rod Stresses . . . . .	F-44
F- 6	Material Cost for a Launcher . . . . .	F-52
F- 7	Fabrication Cost and Labor Hours . . . . .	F-52

APPENDIX A

AIRFRAME

## LIST OF SYMBOLS

A	wing cross-sectional area
$a_1$	spar support dimension
$a_2$	spar support dimension
AC	aerodynamic center
AR	aspect ratio
$A_v$	ventral stringer cross-sectional area
b	wingspan
$b_1$	spar support dimension
$b_2$	spar support dimension
$b_{ht}$	horizontal tail span
$b_{vt}$	vertical tail span
BHP	brake horsepower available
BHPR	brake horsepower required
c	chord
C	specific fuel consumption
$C_D$	drag coefficient
$C_{Di}$	induced drag coefficient
$C_{Dpe}$	parasite drag coefficient
$C_{Dt}$	tail drag coefficient
$C_{Dw}$	wing drag coefficient
CG	center of gravity
$c_{ht}$	horizontal tail chord
$C_L$	lift coefficient
$C_{Lmax}$	maximum lift coefficient

$C_{Lmaxvt}$	vertical tail maximum coefficient
$C_M$	moment coefficient
$c_{mac}$	mean aerodynamic chord
$c_{macvt}$	vertical tail mean aerodynamic chord
$c_r$	root chord
$c_t$	tip chord
$c_{vtr}$	vertical tail root chord
$c_{vtt}$	vertical tail tip chord
$D$	drag
$D_t$	tail drag
$D_w$	wing drag
$e$	span efficiency factor
$E$	endurance
$f_{ht}$	horizontal tail force distribution
$F_1$	launcher force
$f_y$	yield stress
$F_1$	U-bolt support force (foreward)
$F_2$	U-bolt support force (aft)
$g$	gravitational acceleration (32.2 ft/sec <sup>2</sup> )
$h$	operating altitude
$HP_{xs}$	excess thrust horsepower
$HP_{xs3}$	$HP_{xs}$ at 3000 ft
$HP_{xs10}$	$HP_{xs}$ at 10,000 ft
$HP_{xsavg}$	average $HP_{xs}$
$L$	lift
$l_b$	boom length

$l_t$	tail moment arm
$m$	number of maneuver g's
$M_a$	corner launch moment
MAC	mean aerodynamic center
$M_{bb}$	boom bending moment
$M_{bi}$	intersection bending moment
$M_{bs}$	sleeve bending moment
$M_{bt}$	tail bending moment
$M_e$	end moment
$M_L$	total launch moment
$M_{max}$	maximum moment
$M_{sb}$	boom torsional moment
$M_{si}$	intersection torsional moment
$M_{ss}$	sleeve torsional moment
$M_{st}$	tail torsional moment
$M_w$	wing moment
$M_{xb}$	x-axis boom moment
$M_{xi}$	x-axis intersection moment
$M_{xs}$	x-axis sleeve moment
$M_{xt}$	x-axis tail moment
$M_{yb}$	y-axis boom moment
$M_{yi}$	y-axis intersection moment
$M_{ys}$	y-axis sleeve moment
$M_{yt}$	y-axis tail moment
$M_{zb}$	z-axis boom moment
$M_{zi}$	z-axis intersection moment

$M_{zs}$	z-axis sleeve moment
$M_{zt}$	z-axis tail moment
$M_1$	end moment
$M_2$	end moment
$M_+$	wing support moment (ahead)
$M_-$	wing support moment (behind)
$n$	number of launch g's
$r$	range, turn radius
$RC$	rate of climb
$RC_{avg}$	average rate of climb
$R_e$	Reynold's number
$S$	wing area, section modulus
$S_b$	boom minimum section modulus
$SEM$	specific section modulus
$SFY$	specific yield strength
$S_{ht}$	horizontal tail area
$S_i$	intersection minimum section modulus
$S_r$	root minimum section modulus
$S_s$	sleeve minimum section modulus
$S_t$	tail area
$STIF\$\$	relative cost of stiffness
$STRONG\$\$	relative cost of strength
$S_v$	ventral stringer minimum section modulus
$S_{vt}$	vertical tail area
$S_w$	wing area

$t$	time
$t_{CL}$	time to climb
THP	thrust horsepower available
THPR	thrust horsepower required
$t_{ht}$	horizontal tail thickness
$T_L$	engine thrust at launch
$t_r$	root thickness
$t_t$	tip thickness
$t_{vtr}$	vertical tail root thickness
$t_{vtt}$	vertical tail tip thickness
$v$	airspeed
$v_{st}$	stall speed
$v_{term}$	terminal airspeed
$W$	weight
$W_{bd}$	dry weight less wings, booms, and empennage
$W_d$	dry weight
$W_f$	fuel weight
$W_g$	gross weight
$W_{ht}$	horizontal tail weight
$W_t$	boom plus empennage weight
$W_{vt}$	vertical tail weight (each)
$W_w$	wing weight (each)
$W_o$	beginning weight
$W_1$	ending weight
$X_a$	P/L bulkhead to wing spar distance
$X_b$	engine bulkhead to wing spar distance

$X_t$	boom to pivot distance
$X_w$	body GC to wing spar distance
$y_{ai}$	intersection to AC distance
$y_{ar}$	root to AC distance
$y_{bi}$	intersection to boom distance
$y_{br}$	root to boom distance
$y_{mac}$	spanwise location of MAC
$y_s$	spanwise location of stall onset
$y_{wi}$	intersection to wing CG distance
$y_{wr}$	root to wing CG distance
$Z_{ht}$	height of horizontal tail above wing spar
$Z_L$	height of CG above launcher probe
$\alpha_i$	wing incidence angle
$\alpha_{LO}$	zero-lift angle
$\alpha_{3D}$	three-dimensional lift-curve slope
$\epsilon$	washout angle
$\gamma$	specific weight
$\Gamma$	dihedral
$\eta$	propeller efficiency
$\theta_{CL}$	climb angle
$\theta_{vL}$	vehicle launch attitude
$\lambda$	taper ratio
$\Lambda$	wing sweep angle
$\sigma$	altitude density ratio
$\phi$	taper correction factor

## APPENDIX A

### Airframe

#### Introduction

The objectives of the airframe subsystem design effort are to define an airframe that can be used as a basis of comparison in the areas of cost, performance, handling, and technology and to provide representative data and parameter estimates to the other subsystem design efforts. This is motivated by the need to have what is considered a representative analysis of the capabilities, vulnerabilities, and problems involved with an aircraft of this class. This type of analysis is necessary for the definition of other subsystems, mission sensitivities, and concept practicality.

The actual effort put into generating an analysis of this type could be expanded into a fully funded program, complete with basic research and development. This approach would overlap the effort of Air Force Flight Dynamics Laboratory (AFFDL) and the Remotely Piloted Vehicle Program Office (RPV SPO), and is considerably beyond the capabilities of this group in the allotted time. The most useful alternative is considered to be an independent analysis of the problem using the same general requirements and limitations as the RPV SPO program. In this way, simultaneous and relatively independent solutions and recommendations can be developed.

Using the preceding argument, the actual scope of the effort is defined in the following way. Initially, a range of reasonable configurations of various components is surveyed to serve as guideline and source. Materials and manufacturing techniques that seem reasonably

common and applicable are discussed in order to point out any obvious pitfalls or solutions. The intended ground handling, packaging, and assembly methods are studied and combined with the materials and manufacturing considerations to illuminate one best candidate from the configurations considered. The estimated performance of this class of vehicle is then calculated and combined with an assessment of the simplest practical structural arrangement such that the maximum commonality between Type I (attack) and Type II (decoy) airframes might be realized. Engineering judgment, experience, and expert opinion are used to select the lowest cost approaches and to minimize complexity. The actual cost estimation is done by the cost estimation group, but it is included in this appendix.

In order to simplify and aid analysis, the following general assumptions are made. The design should be conventional and simple with emphasis on low-cost and hands-off operation. The layout of components and aerodynamics should be favorable to hands-off, no-autopilot considerations. The major parameters, supplied by the mission analysis group, are as follows:

Gross Weight	130 lbs maximum
Mission time	6 hours maximum (no recovery)
Payload	25 lbs, 7x7x11 inches
Assembly	One unskilled soldier
Launch	50 mph

The general approach of the design effort begins by considering the applicable configurations and technology encountered in the initial survey. Consideration is then given to special environments and requirements anticipated in the design development. A preliminary layout is established and used in a preliminary performance estimate. Incoming

information and data from other subsystems are incorporated into the estimates and multiple iterations made. Using the resulting layout, performance, packaging, handling, weight, and materials proposals, an appropriate structure is designed. All of the above information is combined in a final set of iterations to establish a reasonable estimate of layout and performance. The problems, unknowns, and questions generated are then considered and recommendations made.

The overall effort is consolidated into six major headings and presented in this appendix as follows: survey, layout, structure, performance, cost, and conclusions.

## Survey

A general survey was conducted in order to gain familiarity with available options, screen the various configurations, and develop a feel for the questions that need to be asked. As a result, various requirements are generated and applied.

First, the candidates must be as conventional as practical in configuration and technology. A major consideration is cost, and low cost necessitates the adoption of a low-risk approach to the technology. It would be of little value to this design problem to put all effort and foundation on a new and promising design if the risk of unsuccessful development was unreasonably high. Conventional aircraft layouts lend themselves to textbook and handbook analysis and visual verification, and properties of value in this type of approach.

Another requirement is to assure that the structural components and assembly can be manufactured easily. The emphasis is on minimizing hand operations, machining, and assembly time. Configurations that violate this rule are considered only if they strongly offset some disadvantage of another system.

The packaging requirements for storage and shipping to the launch site are significant. The vehicle package should be such that its bulk or shape lends itself to ease of shelf storage, hauling on an M-35/36 truck, and handling by two men. All components of one vehicle, except fuel, should be stored and shipped in one package.

At the launch site, the vehicle configuration should be compatible with a two-man launch crew. That is, one man should be able to uncrate and assemble the airframe, add fuel, and check the avionics. Both men should be able to mount the vehicle on the launcher, start the engine,

and launch. The above operations should be able to be accomplished quickly in unprepared areas by unskilled personnel.

Part of the payload is assumed to be a sensor which has look angles sensitive forward and down. This necessitates strong consideration of structural interference with the sensor. The obvious solution is to keep all metallic structure behind the payload, if possible, using only a non-metallic shroud to streamline the nose.

It is assumed that the vehicle will not be guided by an active remote operator, i.e., hands-off. The extension of this approach eliminates the need for a costly autopilot, and uses only heading and altitude sensors combined with rudder and elevator control for the Type II vehicle. The Type I vehicle has no such cost constraint, but the common airframe should conform to the no-autopilot approach if practical.

The aircraft should meet the anticipated requirements of mission time, payload, and mission profile. Any of these parameters are considered flexible in the presence of a favorable tradeoff.

The Type I and Type II airframes should be as similar as possible. There are two reasons for this, active decoy role and manufacturing cost. The two vehicles should fly, look, and reflect as similarly as possible, in order to satisfy the decoy role. Manufacturing cost dictates that all structural sub-assemblies (wings, fuselage, engine, and empennage) be identical, if possible, with the obvious exception of easily-deleted servos in the Type II or generator in the Type I. The only difference should be in the payload and avionics, and they should be easily changed at the storage site.

Although radar and optical visibility should be identical between the two vehicle types, no consideration is given to the actual level of visibility of the aircraft other than to note that low-visibility paint can be used. Justification or neglecting this consideration is given in the mission analysis, Chapter IV, Volume II.

Since both airframes are similar in layout, both must be capable of handling the maneuverability considerations of the attack role in the following ways. All control surfaces necessary to the Type I vehicle should be present on the Type II, but they may be pinned or fixed if not used. The Type I structural requirements are more severe than for the Type II, so the airframe is stressed for the attack role. The Type I also carries more equipment, necessitating ballast (or substitute payload) in the Type II.

The aircraft operates in an unusual Reynolds Number ( $Re$ ) regime, lower than light aircraft, but higher than model aircraft. This results in the problem of relating actual performance of airfoils to published higher- $Re$  data.

The configurations investigated are those that are commonly recognized, if not commonly used: They can be divided into six general categories: engine placement, fuselage layout, wing planform, airfoils, empennage, and roll control surfaces.

Engine placement is based on two overriding considerations, complexity and payload interference, with thought given to hands-off flying. Only single-engine configurations are considered because of their lower

complexity and cost. The tractor engine is ruled out because of obvious payload interference. The resulting solution is a single-engine pusher layout with the thrust line through the center of gravity (CG). The centerline-thrust configuration is used to preclude pitching moment ( $C_m$ ) changes with changes in the power setting. Hands-off, no-autopilot dynamics make the  $C_m$  changes very undesirable, and the first flight of the non-centerline thrust Teleplane XBQM-106 pointed out the presence of this pitching moment characteristic (Hoy, 1975).

The fuselage layout involves three major considerations; payload placement, fuel tank location, and overall size. The payload is placed in the nose as the most reasonable location; because no structure other than the support bulkhead, at the rear of the payload, interferes with the sensor. Simplicity dictates that the fuel tank be located in the fuselage, and the no-autopilot consideration specifies that the fuel CG be as close as possible to the aircraft CG to preclude stability changes as fuel is burned. Drag minimization dictates that the fuselage cross-section be as small as possible. Therefore, all components are laid out longitudinally, so that the fuselage covers the payload, avionics, fuel, and engine in as smooth a profile as possible. The result is a long and narrow, rather than stubby, profile. Balance is served if payload and engine are placed at the ends, with fuel and avionics shifted to balance as necessary.

The wing planform and layout choices are legion. The most obvious candidates are the high and low monoplane layouts. They are conventional, simple, well behaved, and well documented. A good alternative is the canard, not as widely used or commonly documented; but it offers an improvement in loiter capability for the same-weight aircraft. The

other common alternatives to the monoplane and canard are the biplane and boxwing. Both offer unique advantages in the realm of wingspan and efficiency, but both involve a higher complexity than the other alternatives. Another, uncommon configuration is the flying-wing which offers interesting manufacturing and ground-handling advantages, but it suffers from high-risk stability and control characteristics in an unpiloted situation. Wing sweep is considered unnecessary in this low-speed regime, and it requires a more complex wing structure than a zero or small-sweep wing. The delta wing is likewise discounted for its low-speed drag characteristics. Taper and twist offer substantial lift and drag advantages over straight wings, but they cannot be made by extrusion. The value of molding and extruding are considered as a tradeoff with performance requirements in the structures discussion.

The number of airfoils available to the aircraft designer are considerable. Therefore, it is thought most reasonable to use the advice of engineers familiar with the problem. The most promising airfoils are condensed into a list of five: NACA 230XX, NACA 25XX, NASA 65XX (Larsen, 1975a), GAW-1 and GAW-2 (Hoy and Early, 1975). Exotic high-lift sailplane wing sections are considered, but they do not appear to satisfy the maneuverability requirements of the attack role (Early, 1975). The NACA sections are well-known and have been used on many light aircraft. The GAW sections are recent developments and are being used on the initial flight version of the Teleplane XBQM-106. Unfortunately, the GAW sections are quite thin, and they do not seem to be performing as expected in this low-Re regime (Hoy and Early, 1975). The NACA 230XX has a good lift characteristic ( $C_{lmax}$ ) and a very small pitching moment ( $C_m$ ), but it loses performance in low-Re regions. The

NACA 65XX was originally considered for the AFIT Canard MRPRV (Rodenroth, 1975:9), but the most promising airfoil for this Re is considered to be the NACA 25XX which has a good  $C_{lmax}$  and a low  $C_m$  (Larsen, 1975a). It has a good, bulky cross-section with no exotic curves and seems well suited to ease of manufacture using a large wing spar. The curves for the NACA 25XX are shown in Appendix A-1.

Based on the indication that a single-engine pusher is desirable, various tail configurations are evident. For a monoplane, the empennage is supported by either one boom extending aft from the belly or two booms extending aft from the wings. A canard version can use a vertical tail mounted either above the rear-mounted engine or mounted as winglets on swept wings. The question of mounting empennage in the propwash is addressed in the stability and control discussion, Appendix B. The single-boom version easily places the surfaces in the free stream if desirable. The alternatives of elevator or stabilator (full-flying horizontal tail) are discussed and analyzed in Appendix B.

The two major types of roll-control surfaces, ailerons and spoilers, are considered since both have distinct advantages in this design. The spoilers are seen as a cheap and easy way to gain roll control without sacrificing wing structure integrity and by eliminating the mounting operation necessary for hinged ailerons. Spoilers also tend to induce favorable roll-yaw coupling, but they require a great deal of authority (deflection) and are plagued by boundary-layer deadband (Larsen, 1975a). Ailerons are highly conventional devices that assure well modelled dynamics. The added complexity of assembly can be overcome in an unmanned, lightweight aircraft of this type if some ingenuity is applied.

All of the preceding configurations are considered in the context of the requirements and considerations mentioned earlier. As a result, three major layouts seem to be the most promising.

The most conventional candidate is the single-boom pusher which has been flown as the Teleplane XBQM-106 (see Figure A-1). This layout has flown well and should be easy to assemble in a production version, but it is not packaged as small as the other versions. Unfortunately, this layout is not easily adapted to the centerline-thrust philosophy, and requires stability augmentation for both vehicle types.

Another very promising candidate is the canard, single-engine pusher seen in Figure A-2. This vehicle should have good loiter capability and be easily assembled, but it requires active control. There is also difficulty in arranging the layout to minimize sweep and winglet area, both of which are packaging and structural problems. The canard layouts developed contained at least one of the following unsatisfactory traits: long fuselage (packaging), large empennage area (weight), or an engine-to-propeller driveshaft (cost).

Since the single-boom pusher is already flying and the canard has basic layout difficulties, it was decided to concentrate the design effort on the twin-boom, single-engine, centerline-thrust pusher. Figure A-3 shows the final selected configuration. This arrangement seems like an interesting approach to the problem since it combines a short fuselage and conventionality with the problem of more complex assembly.

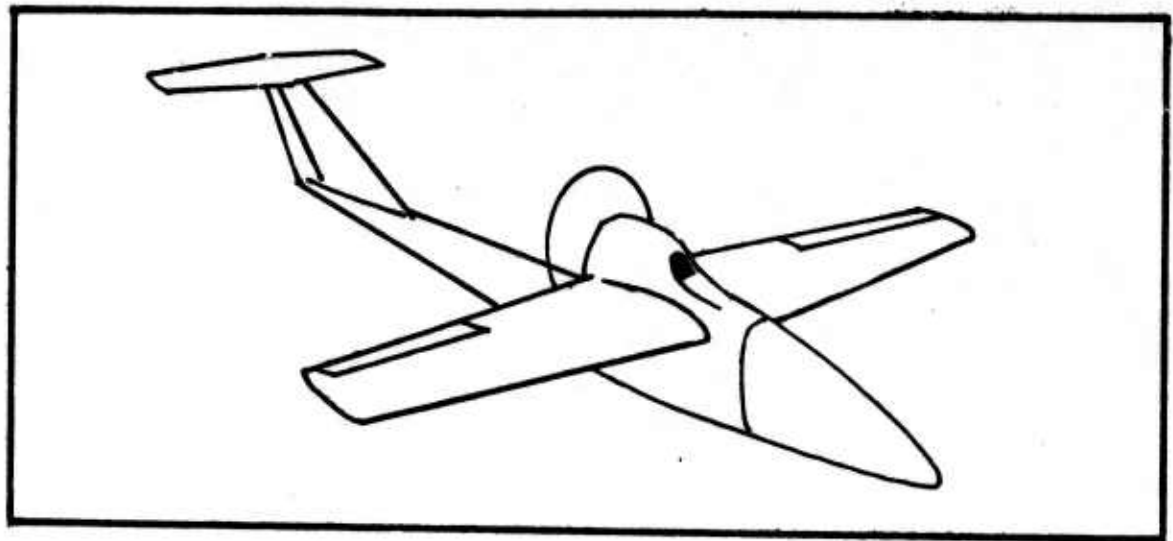


Figure A-1. XBQM-106 (Hoy, 1975)

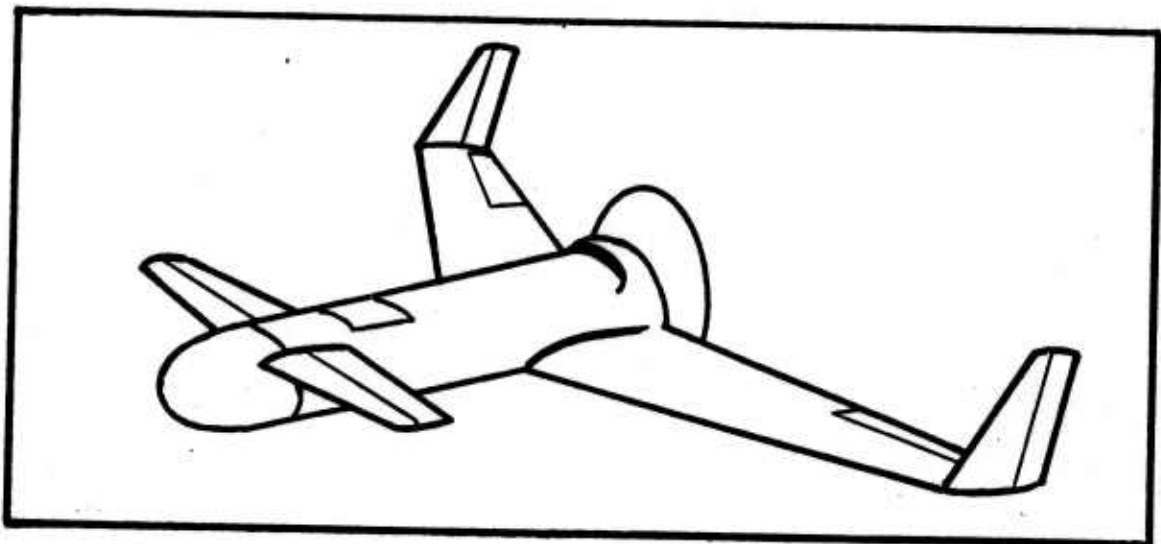


Figure A-2. Canard Candidate

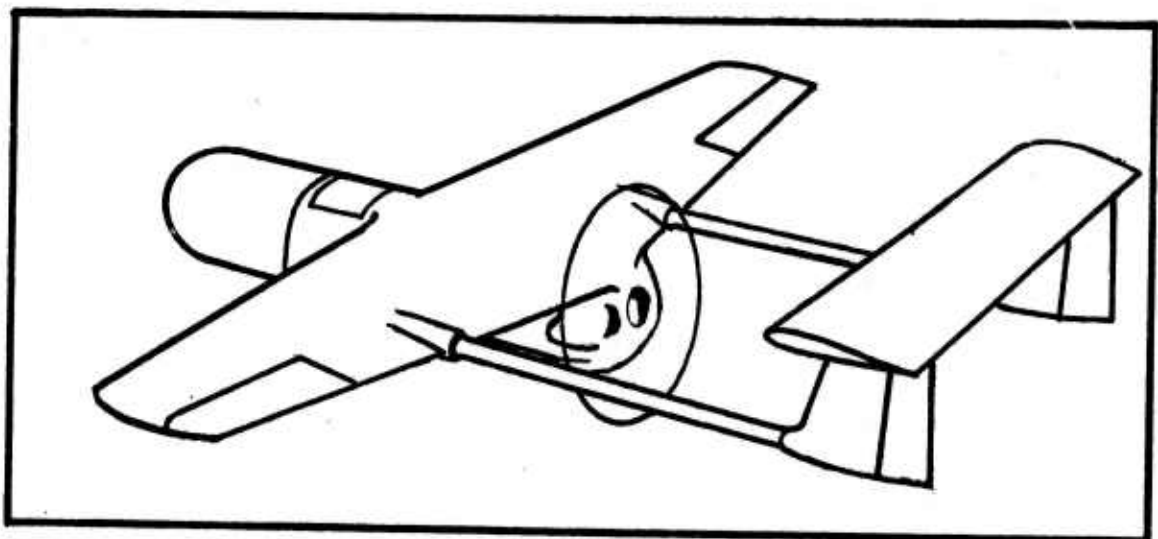


Figure A-3. Twin-Boom Pusher Candidate

## Layout

A preliminary version of the anticipated layout is generated to provide a basis for the design and selection efforts involved in the other subsystems. At the same time, it satisfies the need for a starting point for estimating the parameters of the aircraft itself and provides the necessary genesis for the prediction of promising materials, manufacturing techniques, and ground handling methods.

Preliminary Planform. Probably the most realistic starting place is the selection of a wing planform. The original wing structure is intended as a cast polyurethane foam molded around an aluminum tubular skeleton. Materials are discussed in the structures section, but the idea here is to incorporate the most promising material and process to assure simplicity and low cost from the very beginning. Using the idea of molded wing sections, the straight wing is abandoned since molding a twisted, tapered, and swept wing involves about the same cost as molding a straight wing (Morrissey, 1975). The planform selection will be developed in the following order: airfoil selection, sweep, spar placement, taper, aspect ratio, twist, area, dimensions, and dihedral.

As previously discussed, the most promising airfoil seems to be the NACA 25XX. In discussions with Major Hoy and Professor Larsen, the various aspects of wing thickness and Re effects were probed. As a result, the most reasonable approach is to use a thicker section at the tip than at the root. This allows the wing to carry a relatively large, say 2-inch diameter, wing spar without the necessity of tapering the spar cross-section or sacrificing the planform taper. The selected sections are: Roof, NACA 2515; Tip, NACA 2518. Using a taper ratio of 0.5 discussed

later, the wing thickness can easily carry a 2-inch diameter spar if necessary (see Table A-1).

The question of sweep is briefly mentioned in the survey, but the problems of spar placement and static margin need to be addressed here. Using the philosophy of minimum manufacturing cost, the most reasonable task is to place one straight, tubular spar through the center of the wing along the half-chord. This consideration blends well with the quest for a reasonable static margin. That is, as the wing is swept aft, the static margin is reduced. Having the half-chord unswept allows the aerodynamic center (AC) to remain forward as well as allowing the wing spar to be unbent. The consideration of structural torque due to wing spar placement is significant, and it is addressed in the structures section. Note, also, that launch speed is critical. This fact dictates that the line of ACs (quarter-chord) be swept as little as possible to minimize wing area. The result, then, is that the wing half-chord is unswept with the straight, tubular wing spar running down the half-chord (see Figure A-4). The most significant considerations with taper are structure and drag. Wing area and weight at the tips can be reduced with taper, thus reducing bending moment at the root; but excess taper forces the root chord ( $c_r$ ) into an unmanageable size or reduces tip thickness. The taper ratio may be adjusted in trapezoidal planforms in order to approach the idealized elliptical planform as seen in Figure A-5.

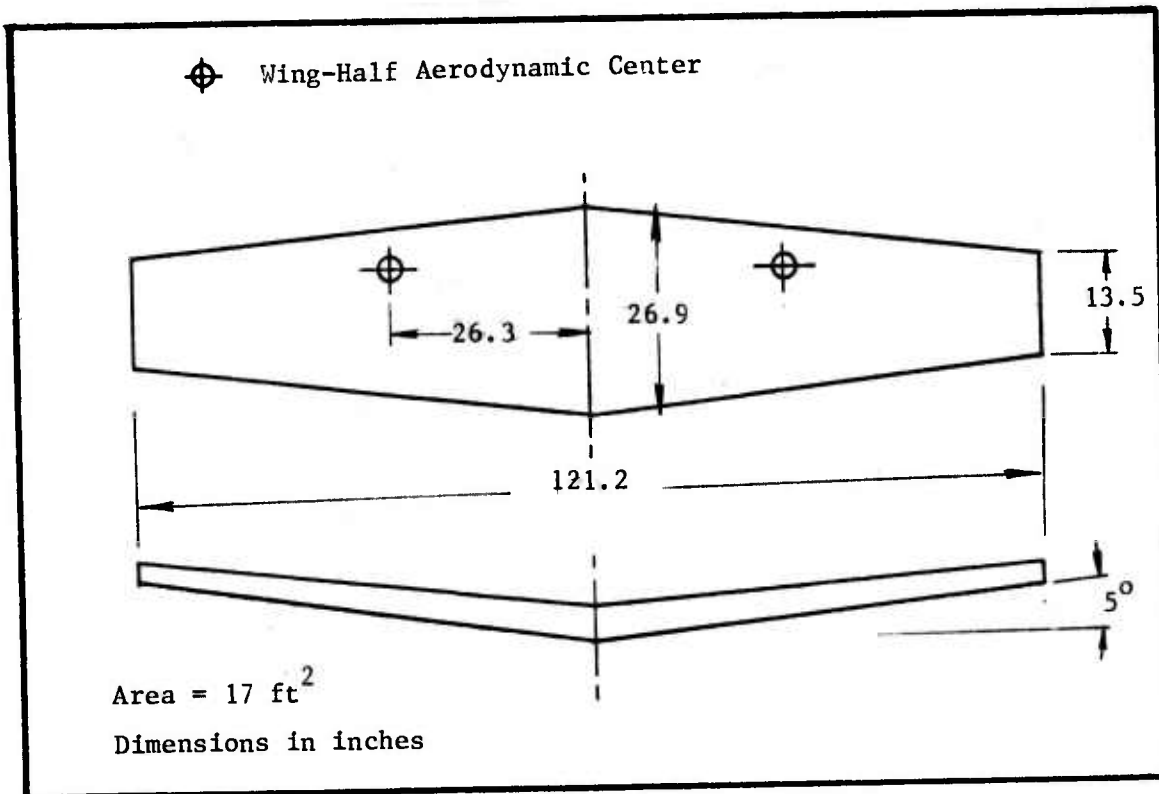


Figure A-4. Preliminary Planform

Wing taper is the ratio of tip chord to root chord.

$$\lambda = \frac{C_t}{C_r} \quad (A-1)$$

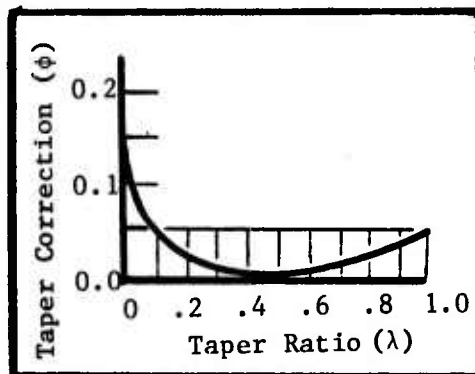


Figure A-5. Taper Ratio Drag Effect (Corning, 1953:3.3)

The intent is to reduce induced drag, which is defined by the following relation (Corning, 1953:5.12),

$$C_{D_i} = \frac{C_L^2}{\pi AR} (1+\phi) \quad (A-2)$$

$C_{D_i}$  = induced drag coefficient

$C_L$  = lift coefficient

AR = aspect ratio

$\phi$  = taper correction factor, from Figure A-5

Thus, induced drag is reduced by the selection of a taper ratio between 0.3 and 0.6 which keeps  $\phi$  below 0.01. Since the actual value of  $\phi$  is rather insensitive to  $\lambda$  in this bracket, 0.5 seems like a good compromise, insuring small  $\phi$  and reasonably thick wing tips. The resulting taper and tip thicknesses are shown in Table A-1. Note that Figure A-5 is presented for an aspect ratio of 6, where

$$AR = \frac{b^2}{S} \quad (A-3)$$

Thus, aspect ratio becomes another design parameter of importance. Large AR reduces  $C_{D_i}$  and thus increases endurance, but it also requires that wing span (b) and spar cross-section and weight be increased. The actual selection should be based on some objective tradeoff. Therefore, a measure of endurance, drag, and fuel requirements must be traded against reasonable aspect ratios, say between 5 and 8, with a target of 5 or 6, if practical. To accomplish this in a visual presentation, a plotting program, CDVSAR (Appendix A-2-1), is used. The basis of the program is the general maximum endurance equation (Perkins, 1949:188),

$$E = 37.9 \frac{\eta}{C} \frac{C_L^{1.5}}{C_D} \left( \frac{\sigma S}{W_0} \right)^{1/2} \left\{ \left( \frac{W_0}{W_1} \right)^{1/2} - 1 \right\} \quad (\text{A-4})$$

E = endurance (hrs)

$\eta$  = propeller efficiency

C = specific fuel consumption (lb/Bhp-hr)

$C_D$  = drag coefficient

$\sigma$  = altitude density ratio

S = wing area (ft<sup>2</sup>)

$W_0$  = beginning weight (lbs)

$W_1$  = ending weight (lbs)

where fuel load ( $W_f$ ) is

$$W_f = W_0 - W_1 \quad (\text{A-5})$$

and drag coefficient ( $C_D$ ) is calculated as

$$C_D = C_{D_{pe}} + C_{D_i} \quad (\text{A-6})$$

Using Eq (A-2), values for the important parameters,  $C_D$ ,  $C_L/C_D$ , and  $C_L^{1.5}/C_D$  are found and evaluated as a function of  $C_L$  and AR. The results are shown in Appendices A-2-2 and A-2-3. The input parameters are:

$$0.0 < C_L < 1.5 \quad (\text{Appendix A-1})$$

$$C_{d_{pe}} = 0.03 \quad (\text{Early, 1975})$$

$$5 < AR < 8$$

$$\phi = 0.01 \quad (\text{Table A-1})$$

For example, using  $C_L = 0.6$  and  $AR = 6$ , Eqs (A-2) and (A-6) give

$$C_D = 0.03 + \frac{(0.06)^2}{\pi(6)} (1 + 0.01)$$

$$= 0.049$$

$$C_L/C_D = \frac{0.06}{0.049}$$

$$= 12.1$$

$$C_L^{1.5}/C_D = \frac{(0.06)^{1.5}}{0.049}$$

$$= 9.4$$

The plots in Appendix A-2-3 show that  $C_L^{1.5}/C_D$  tends to decrease quickly below AR = 6, but it does not gain much above 6. In order to keep the wingspan and structural requirements within reason, an aspect ratio of 6 is used.

Twist ( $\epsilon$ ), or washout angle, is not considered quantitatively in the initial estimate other than to say it lies near Rodenroth's figure of 3 degrees (Rodenroth, 1975:11). The actual washout angle is calculated later as the planform is finalized. The other critical parameter involved with twist is the wing  $C_{Lmax}$ . This is calculated again later as parameters are finalized, but it is estimated at about 1.3 as indicative of this size aircraft from the estimate of the AFIT Canard MRPRV (Rodenroth, 1975:11).

Now that the planform of the wing is clear, the next major consideration is wing area. For a given wing planform, larger area reduces launch speed, increases loiter time, and adds to package size and vehicle weight. Therefore, the intent is to minimize wing area while assuming minimum launcher impact and fuel load. The equation used is that which calculates the wing area necessary to carry a given weight

at a given airspeed and altitude in straight and level flight (Corning, 1953:2-4) using acceleration and excess horsepower to provide climb.

$$S = \frac{391 W_g}{C_{Lmax} \sigma v^2} \quad (A-7)$$

where  $S$  = minimum required wing area ( $ft^2$ )

$W_g$  = launch weight = 130 lb

$C_{Lmax}$  = 1.3 from above

$v$  = launch airspeed = 50 mph

$\sigma$  = density ratio = 0.94 at 3000 ft MSL

The initial estimate is based on a 130-pound gross-weight vehicle, which is a conservative upper-limit. The mission analysis (Chapter II) estimates that the maximum expected altitude of launch operations would be about 3000 feet MSL. Therefore, the preliminary wing area estimate is

$$\begin{aligned} S &= \frac{(391)(130)}{(1.3)(0.94)(50)^2} \\ &= 16.64 \text{ ft}^2 \end{aligned}$$

This is rounded-off to 17 square feet for preliminary purposes (see Table A-1).

Wing planform dimensions are found using the following common relationships.

$$\begin{aligned} \text{wingspan, } b &= [S(AR)]^{1/2} \\ &= [17(6)]^{1/2} \\ &= 10.1 \text{ ft} \end{aligned} \quad (A-8)$$

$$\begin{aligned}
 h &= AR \left( \frac{c_r + c_t}{2} \right) \\
 &= \frac{1}{2} AR c_r (1 + \lambda) \qquad (A-9)
 \end{aligned}$$

$$\text{so } c_r = \frac{2b}{AR(1 + \lambda)} \qquad (A-10)$$

$$= \frac{2(10.1)}{6(1 + 0.5)}$$

$$= 2.24 \text{ ft}$$

$$= 26.88 \text{ in}$$

$$\begin{aligned}
 c_t &= \lambda c_r \\
 &= 0.5(2.24) \qquad (A-11)
 \end{aligned}$$

$$= 1.12 \text{ ft}$$

$$= 13.44 \text{ in}$$

The tip and root thicknesses are expressed as a percentage of chord derived from the last two digits of the NACA number, i.e., NACA 2515 means the maximum thickness is 15% of the chord length.

$$t_r = 0.15 c_r \qquad (A-12)$$

$$= 0.15 (2.24)$$

$$= 0.336 \text{ ft}$$

$$= 4.03 \text{ in}$$

$$t_t = 0.18 c_t \qquad (A-13)$$

$$= 0.18 (1.12)$$

$$= 0.202 \text{ ft}$$

$$= 2.42 \text{ in}$$

The length and location of the mean aerodynamic chord (MAC) are expressed as follows (Corning, 1953:3.3).

$$c_{mac} = \frac{2}{3} (c_r + c_t) - \left\{ \frac{c_r c_t}{c_r + c_t} \right\} \quad (A-14)$$

$$= \frac{2}{3} (2.44 + 1.12) - \frac{(2.24)(1.12)}{2.24 + 1.12}$$

$$= 1.783 \text{ ft}$$

$$= 21.39 \text{ in}$$

$$y_{mac} = \frac{b}{2} \left\{ \frac{1}{3} \right\} \frac{c_r + 2c_t}{c_r + c_t} \quad (A-15)$$

$$= \frac{10.1}{2} \left\{ \frac{1}{3} \right\} \frac{2.24 + 2(1.12)}{2.24 + 1.12}$$

$$= 2.194 \text{ ft}$$

$$= 26.33 \text{ in}$$

Dihedral ( $\Gamma$ ) is a parameter that is not easily quantified for this vehicle. Therefore, a value of 5 degrees is selected as representative for this anticipated type of hands-off flying. This number is selected as representative of many light aircraft now flying as well as suitable for maneuverability in the attack vehicle (Larsen, 1975a).

The wing sweep ( $\Lambda$ ) of the line of AC's is calculated geometrically from

$$A = \tan^{-1} \left\{ \frac{1}{4} \frac{(c_r - c_t)}{b/2} \right\} \quad (A-16)$$

$$= \tan^{-1} \left\{ \frac{1}{4} \frac{(2.24 - 1.12)}{10.1} \right\}$$

$$= 3.17 \text{ deg}$$

All of the above parameters are summarized in the following table of preliminary planform parameters and are intended for initial guidance and control calculations as well as for initial performance calculations. The planform is as presented in Figure A-4.

TABLE A-1. PRELIMINARY PLANFORM PARAMETERS

wingspan	$b = 10.1 \text{ ft}$
aspect ratio	$AR = 6$
wing area	$S = 17 \text{ ft}^2$
sweep	$\Lambda = 3.17 \text{ deg}$
dihedral	$\Gamma = 5 \text{ deg}$
twist	$\epsilon = -3 \text{ deg}$
mean aerodynamic chord	$c_{mac} = 21.39 \text{ in}$
MAC spanwise position	$y_{mac} = 26.33 \text{ in}$
root chord	$c_r = 26.88 \text{ in}$
root thickness	$t_r = 4.03 \text{ in}$
tip chord	$c_t = 13.44 \text{ in}$
tip thickness	$t_t = 2.42 \text{ in}$
maximum lift coefficient	$C_{L_{max}} = 1.3$

Preliminary Engine Layout. For the initial layout, the recommendation was to use the McCulloch 101B engine (see Appendix C). The engine is included in the layout without the stock shroud, magneto, or starting pulley. Orientation of the engine is arbitrary about the drive shaft axis, i.e., it can be mounted inverted, if necessary. Thus, changes in CG or thrustline are incorporated by rotating and/or translating the engine position.

The preliminary layout places the engine in a conventional, upright attitude with the drive shaft on the CG axis pointing aft with

the propeller mounted directly on the shaft without a spacer. The engine is mounted on a standard wire-loop vibration mount attached to the engine bulkhead just forward. The alternator is mounted on the forward face of the bulkhead and is attached to the starter pulley shaft via a flexible, clamped-tube coupling. When batteries are used (Type II), the alternator is not present, and the battery pack is located in the avionics bay (see Figure A-6).

The fuel is routed from the fuel tank through an end-weighted flexible tube. The weighted end is used to follow the motion of the fuel in the tank regardless of vehicle motion. The tube is attached to a standard fitting in the engine bulkhead, and another tube is then routed to the carburetor which is controlled by a servo link attached to the bulkhead. The initial propeller considered is 26 inches in diameter, and the initial thrust line is along the fuselage centerline.

Preliminary Fuselage Layout. The initial fuselage cross-section is somewhat oval, just large enough to enclose a 7 by 7 inch payload, fuel tank, avionics, and engine. Rodenroth's (1975:20) algorithm for generating fuselage cross-sectional shapes is used to find a section that encloses the above components while allowing adequate clearance for structure. The algorithm is presented in Appendix A-4-1 and the cross-section plot in Appendix A-4-2. It is based on the adjustment of parameters in Eq (A-17) to find a smooth, bulky shape.

$$\left\{ \frac{X}{A} \right\}^P + \left\{ \frac{Y}{B} \right\}^P = 1 \quad (\text{A-17})$$

A and B are semi-axes

p is a measure of severity of corner curve

For this fuselage,  $A = B = 5$  inches and  $p = 2.67$ .

The payload is mounted on the forward face of the payload bulkhead and consists of a 7 by 7 inch box. The avionics are mounted on the aft face of the payload bulkhead in the 6 by 6 by 7 inch avionics bay. The fuel tank is centered in the fuselage below the aircraft CG in a 7 by 7 inch cross-section cavity. The fuel cavity length is adjusted to fuel requirements and is 22 inches long in the preliminary layout. The alternator is located in a 6 by 6 by 7 inch cavity on the forward face of the engine bulkhead, with the engine mounted on the aft face. A small cooling-air scoop is located on the ventral cowling with a carburetor air intake on one side. The carry-through spar is mounted to the dorsal longitudinal stringers running just above the fuel cavity. All of the cavities mentioned are integrally-molded, having the same skinning properties as the external surface (see the materials discussion). These components are clearly seen in Figure A-6, the final layout.

Preliminary Empennage Layout. The horizontal tail is initially located between the booms and is configured as a conventional stabilizer-elevator. The initial sizing is done by visual comparison with the Teleplane Eagle, a somewhat larger RPV with a similar layout. The airfoil selected is the standard, commonly-used NACA 0009 symmetrical section, with rectangular planform: span 36 inches, chord 16 inches, and area 4 square feet (see Table A-2).

For launcher clearance, the vertical tails are moved on top of the booms. They have conventional stabilizer-rudder layouts with the dimensions noted in Table A-2. The total vertical tail area is 2.9 square feet. Both of the rudders and the elevator use one servo each, secured into a cavity in the stabilizers. The control surface hinges are extruded flexible plastic bonded to the skins.

The booms are estimated to be 2-inch-diameter aluminum tubes attached to the wings and are spaced about 36 inches apart, clearing the propeller by 4 inches on either side. The length of each boom is about 60 inches in order to generate a reasonable tail length. This dimension is readily changed for stability and control purposes, but it is limited due to packaging constraints.

TABLE A-2. PRELIMINARY EMPENNAGE PARAMETERS

Horizontal Tail Section	NACA 0009
Area	$S_{ht} = 4 \text{ ft}^2$
Span	$b_{ht} = 36 \text{ in}$
Chord	$c_{ht} = 16 \text{ in}$
Tail Length	$l_t = 60 \text{ in}$
Thickness	$t_{ht} = 1.44 \text{ in}$
Vertical Tail Section	NACA 0009
Area (each)	$S_{vt} = 1.46 \text{ ft}^2$
Height	$b_{vt} = 15 \text{ in}$
Root Chord	$c_{vtr} = 16 \text{ in}$
Tip Chord	$c_{vtt} = 12 \text{ in}$
Mean Aerodynamic Chord	$c_{mac} = 14.1 \text{ in}$
Root Thickness	$t_{vtr} = 1.44 \text{ in}$
Tip Thickness	$t_{vtt} = 1.08 \text{ in}$

Preliminary Weight and Balance. The initial estimates of component weights are listed in Table A-3. Component weights such as wings, fuselage, and tail correspond to the estimates of the Teleplane XBQM-106 (Early, 1975). Engine and propeller weights are from Appendix C. Alternator and avionics weights are from Appendices D and E, respectively. The coordinate system is a standard X-Y-Z aircraft layout with origin at the nose (X, forward; Y, right; Z, down). X-axis location estimates are taken from the preliminary layout with the fuel location adjusted by trial and error. The fuel weight is a preliminary estimate from the performance section.

TABLE A-3. PRELIMINARY WEIGHT AND BALANCE

Component	Weight (lbs)	X-axis CG location (in)
Shroud	1	7
Payload	25	9.5
Bulkhead	1	15
Avionics	10	20
Wings	18	41
Fuselage	9	38
Alternator	6	53
Bulkhead	1	56
Engine and Prop	15	60
Booms	3	64
Tail	4	100
Bulkhead	1	48
Fuel	<u>26</u>	<u>37</u>
TOTAL AIRCRAFT	120	37

In order to easily shift component locations, weights, and sizes, it is necessary to generate a weight-and-balance design tool. The Teleplane computer program, TEST (Hoy, 1975), is modified to account for fuel consumption, plots the X and Z shifts as a function of fuel weight (see Appendix A-5), and is called WTNBAL.

All of the above parameters and configurations are used in multiple iterations of the airframe parameters as well as a basis for decisions handled by other subsystems, launcher and flight control for example. Many changes are proposed and incorporated into the overall integration of the airframe, mission, and subsystems. Some of the more significant are noted below.

The horizontal tail is moved to the top of the vertical tail. This is done to minimize impingement of the propwash on the control surface and the resulting variation of dynamic pressure and control moment. The horizontal tail is also made into a full-flying stabilator to assure adequate control moment. The wingspan is moved forward along the line of AC's (the quarter-chord) to reduce internal torque due to wing moment. The boom-attachment sleeves and control surface hinges are also modified as discussed in the structures section. These, plus changes in fuel requirements, avionics weight, structural components, engine performance estimates, and other parameters result in a new, more realistic set of estimates for the actual vehicle layout. The above items are discussed later and incorporated into the final layout, Figure A-6 below.

Final Weight and Balance. The computer program WTNBAL (Appendix A-5) is used in conjunction with the following final weight estimates

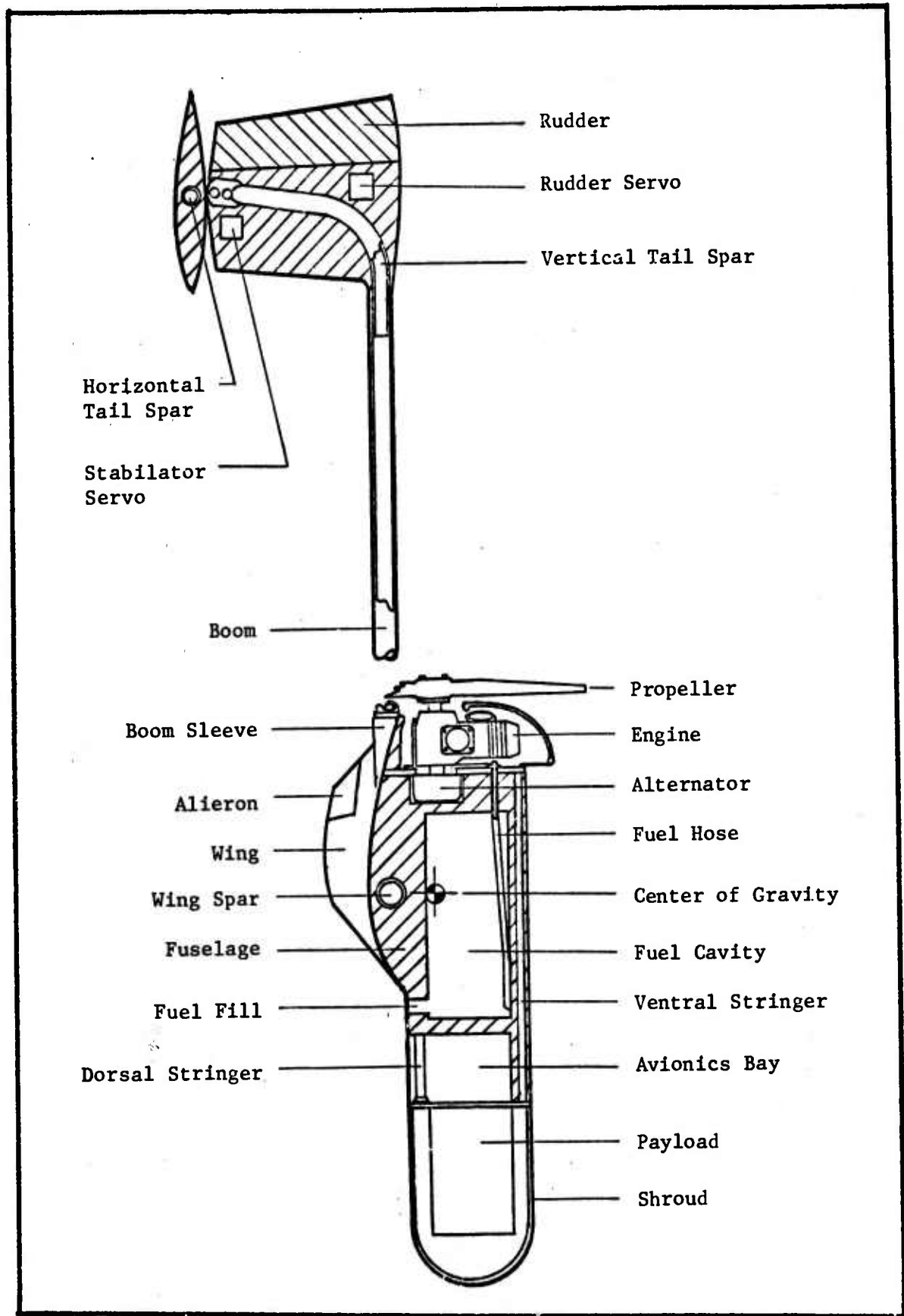


Figure A-6. Inboard Profile

in order to assure proper load distribution. The final component locations are listed in Appendix A-5-4 and shown in Figure A-7. The CG shift due to fuel consumption is shown in Appendix A-5-5 and in Figure A-8. The final weight estimate of each component is listed in Table A-4 and is clarified in the discussion that follows.

TABLE A-4. FINAL WEIGHT AND BALANCE

Component	Weight (lbs)	X-axis CG Location (in.)	Z-axis Location (in.)
Fuel	21.5	30.6	0.0
Payload	25.0	9.5	0.0
Fuselage	11.8	33.0	0.0
Wings	26.0	33.0	6.5
Horizontal Tail	3.75	92.0	23.0
Vertical Tails	2.4	92.0	12.0
Aileron Servos	0.4	33.0	6.0
Rudder Servos	0.4	93.0	8.0
Elevator Servo	0.2	93.0	20.0
Engine Servo	0.2	43.0	0.0
Shroud	1.4	5.0	0.0
Avionics	6.5	17.0	0.0
Propeller	2.0	50.0	0.0
Engine	12.0	46.0	0.0
Alternator	6.0	42.0	2.5
Booms	3.9	60.0	6.5
Payload Bulkhead	1.0	15.0	0.0
Engine Bulkhead	<u>1.0</u>	<u>43.0</u>	<u>0.0</u>
TOTAL VEHICLE	125.5	32.7	2.5

Fuel weight is calculated in the performance section and is a very flexible figure. It is positioned as close to the aircraft CG as practical based on the structural definition made just prior to the

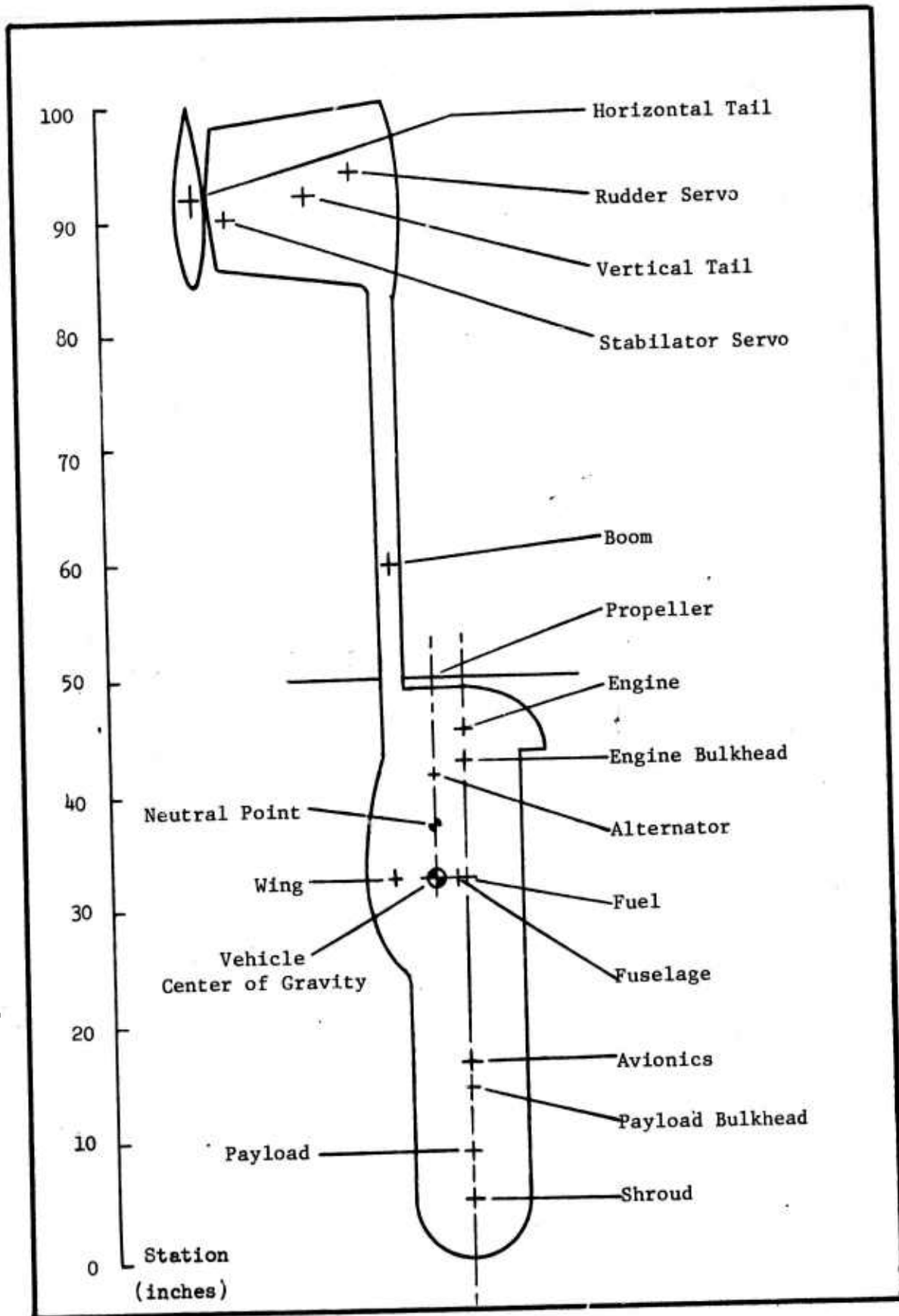


Figure A-7. Component Weight Locations

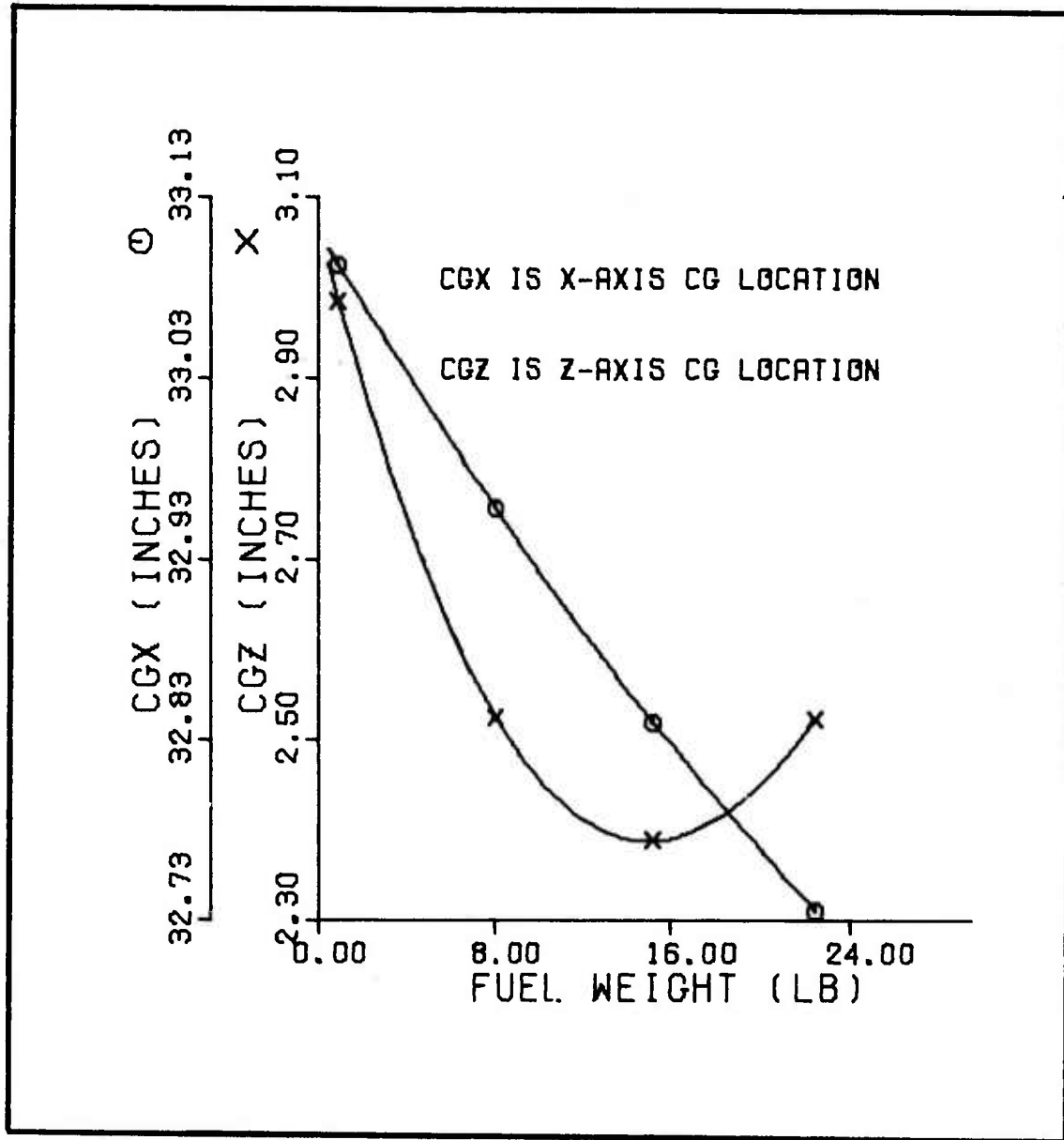


Figure A-8. Center of Gravity Shift with Fuel Usage

final performance estimate. Although aircraft CG shifts somewhat as fuel is burned, the actual longitudinal travel is insignificant, about 0.4 inch (Appendix A-5-5).

Payload weight and location are unchanged from the preliminary, since no alterations were input from the RPV SPO. The fuselage weight is based on structural requirements, the use of aluminum stringers and polyurethane foam filler, which are discussed in the structures section. Wing sections, empennage, and booms are also discussed in the structures section.

The bulkhead at the rear of the fuel cavity is deleted, and the estimated weight of the shroud is increased. The avionics weight is reduced to 6.5 pounds, based on design group estimates. The remaining components: engine, propeller, alternator, and servos remain unchanged from the preliminary estimates.

Final Layout Estimate. Based on the preceding discussion combined with structures, performance, and flight-control inputs, the final layout, planform, and internal profile are generated. The most significant item used by the structures analysis and the flight control analysis (Appendix B) is the wing planform. As mentioned in the preliminary discussion, the planform is based on consideration of launch speed, gross weight,  $C_{L_{max}}$ , taper, twist, airfoil selection, and sweep.

The discussion of the preliminary planform holds for the shape parameters: taper, sweep, and airfoils. The items that are modified are wing area, span, twist, and  $C_{L_{max}}$ .

$C_{L_{max}}$  and twist are closely related in any defined planform having known taper, sweep, airfoil, and Reynolds number.  $C_{L_{max}}$  of the wing

final performance estimate. Although aircraft CG shifts somewhat as fuel is burned, the actual longitudinal travel is insignificant, about 0.4 inch (Appendix A-5-5).

Payload weight and location are unchanged from the preliminary, since no alterations were input from the RPV SPO. The fuselage weight is based on structural requirements, the use of aluminum stringers and polyurethane foam filler, which are discussed in the structures section. Wing sections, empennage, and booms are also discussed in the structures section.

The bulkhead at the rear of the fuel cavity is deleted, and the estimated weight of the shroud is increased. The avionics weight is reduced to 6.5 pounds, based on design group estimates. The remaining components: engine, propeller, alternator, and servos remain unchanged from the preliminary estimates.

Final Layout Estimate. Based on the preceding discussion combined with structures, performance, and flight-control inputs, the final layout, planform, and internal profile are generated. The most significant item used by the structures analysis and the flight control analysis (Appendix B) is the wing planform. As mentioned in the preliminary discussion, the planform is based on consideration of launch speed, gross weight,  $C_{L_{max}}$ , taper, twist, airfoil selection, and sweep.

The discussion of the preliminary planform holds for the shape parameters: taper, sweep, and airfoils. The items that are modified are wing area, span, twist, and  $C_{L_{max}}$ .

$C_{L_{max}}$  and twist are closely related in any defined planform having known taper, sweep, airfoil, and Reynolds number.  $C_{L_{max}}$  of the wing

is a rather tedious function of the above parameters, so Professor Larsen's program SHRENK (Larsen,1975a) is modified for use as a design tool (see Appendix A-3-1). This algorithm uses a linearized  $C_L$ -versus- $Re$  relationship and standard aerodynamics to calculate  $C_{L_{max}}$  and spanwise position of stall onset ( $y_s$ ) as a function of aerodynamic and geometric twist (washout). The objective is to maximize  $C_{L_{max}}$  and to bring  $y_s$  inboard of the ailerons, so that roll control is not lost near stall. The results of using this algorithm are listed in Appendix A-3-2 and plotted in Appendix A-3-3 for launch, cruise, and terminal dive airspeeds. Again, twist is employed since it is assumed that a molded wing section is used. The resulting wing  $C_{L_{max}}$  is 1.223 for the launch airspeed of 50 mph. Using Eq (A-7) the required wing area is calculated.

$$S = \frac{391 W_g}{C_{L_{max}} \sigma v^2} \quad (A-7)$$

$$W_g = 120 \text{ lb}$$

$$C_{L_{max}} = 1.223$$

$$\sigma = 0.915 \text{ at } 3000 \text{ ft MSL}$$

$$v = 50 \text{ mph}$$

$$S = \frac{391(120)}{(1.223)(0.915)(50)^2}$$

$$= 16.77 \text{ ft}^2$$

Let  $S = 17 \text{ ft}^2$  to give some margin for gross-weight increase. This estimate matches the preliminary estimate, so all of the dimensions of Table A-1 apply for the final planform estimate as well, as seen in Table A-5 and Figure A-9.

TABLE A-5. FINAL WING PLANFORM ESTIMATE

wingspan	$b = 10.1 \text{ ft}$
aspect ratio	$AR = 6$
wing area	$S = 17 \text{ ft}^2$
sweep	$\Lambda = 3.17 \text{ deg}$
dihedral	$\Gamma = 5 \text{ deg}$
twist	$\epsilon = -4 \text{ deg}$
mean aerodynamic chord	$c_{mac} = 21.39 \text{ in}$
MAC spanwise position	$y_{mac} = 26.33 \text{ in}$
root chord	$c_r = 26.88 \text{ in}$
root thickness	$t_r = 4.03 \text{ in}$
tip chord	$c_t = 13.44 \text{ in}$
tip thickness	$t_t = 2.42 \text{ in}$
maximum lift coefficient	$C_{Lmax} = 1.223$

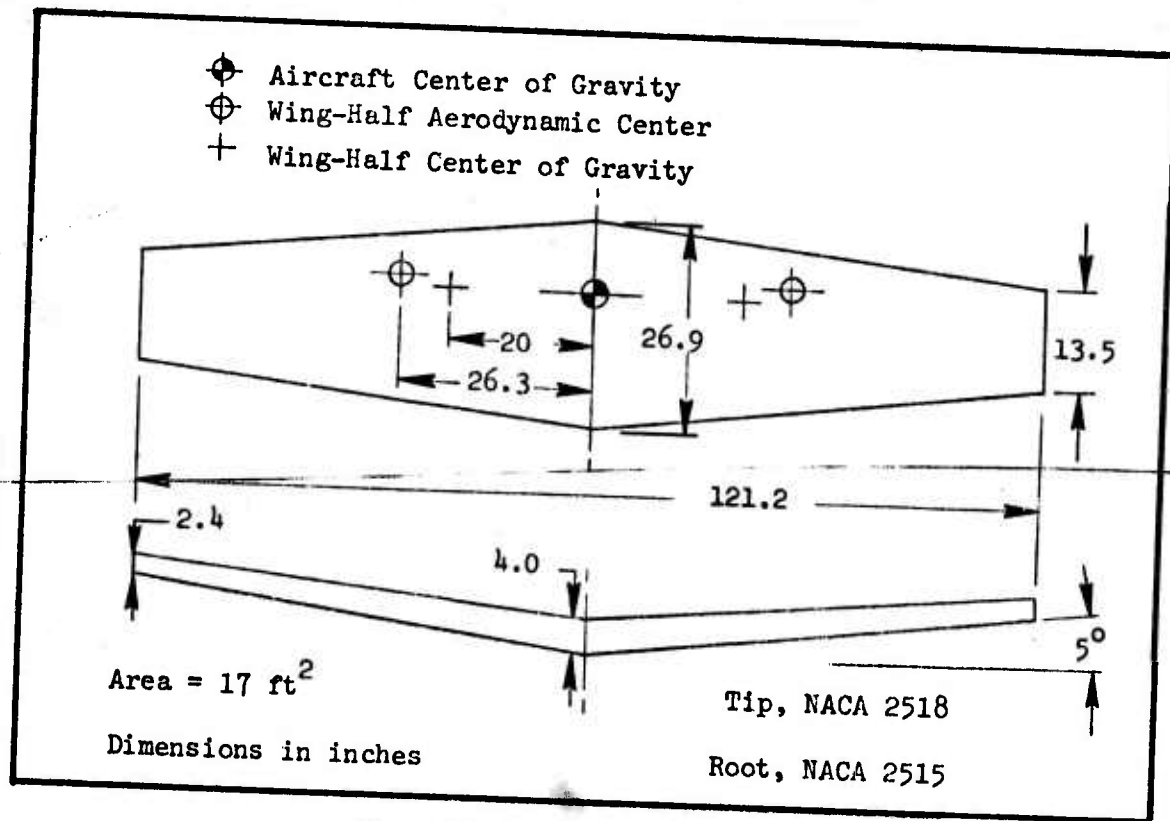


Figure A-9. Final Planform

The airfoil section for the empennage is thickened to a NACA 0015 symmetrical section to strengthen the foam and allow room for a larger spar. The planform areas are increased on advice from Flight Controls (Appendix B) to the values shown in Table A-6 below.

TABLE A-6. FINAL EMPENNAGE ESTIMATES

Horizontal Tail Section	NACA 0015
Area	$S_{ht} = 4.61 \text{ ft}^2$
Span	$b_{ht} = 41.5 \text{ in}$
Chord	$c_{ht} = 16 \text{ in}$
Tail Length	$l_t = 60 \text{ in}$
Thickness	$t_{ht} = 2.4 \text{ in}$
Vertical Tail Section	NACA 0015
Area (each)	$S_{vt} = 1.46 \text{ ft}^2$
Height	$b_{vt} = 15 \text{ in}$
Root Chord	$c_{vtr} = 16 \text{ in}$
Tip Chord	$c_{vtt} = 12 \text{ in}$
Mean Aerodynamic Chord	$c_{vmac} = 14.1 \text{ in}$
Root Thickness	$t_{vtr} = 2.4 \text{ in}$
Tip Thickness	$t_{vtt} = 1.8 \text{ in}$

The overall vehicle layout and dimensions are shown in Figure A-10, the package size is shown in Figure A-12 and the launch-site assembly is shown in Figure A-11.

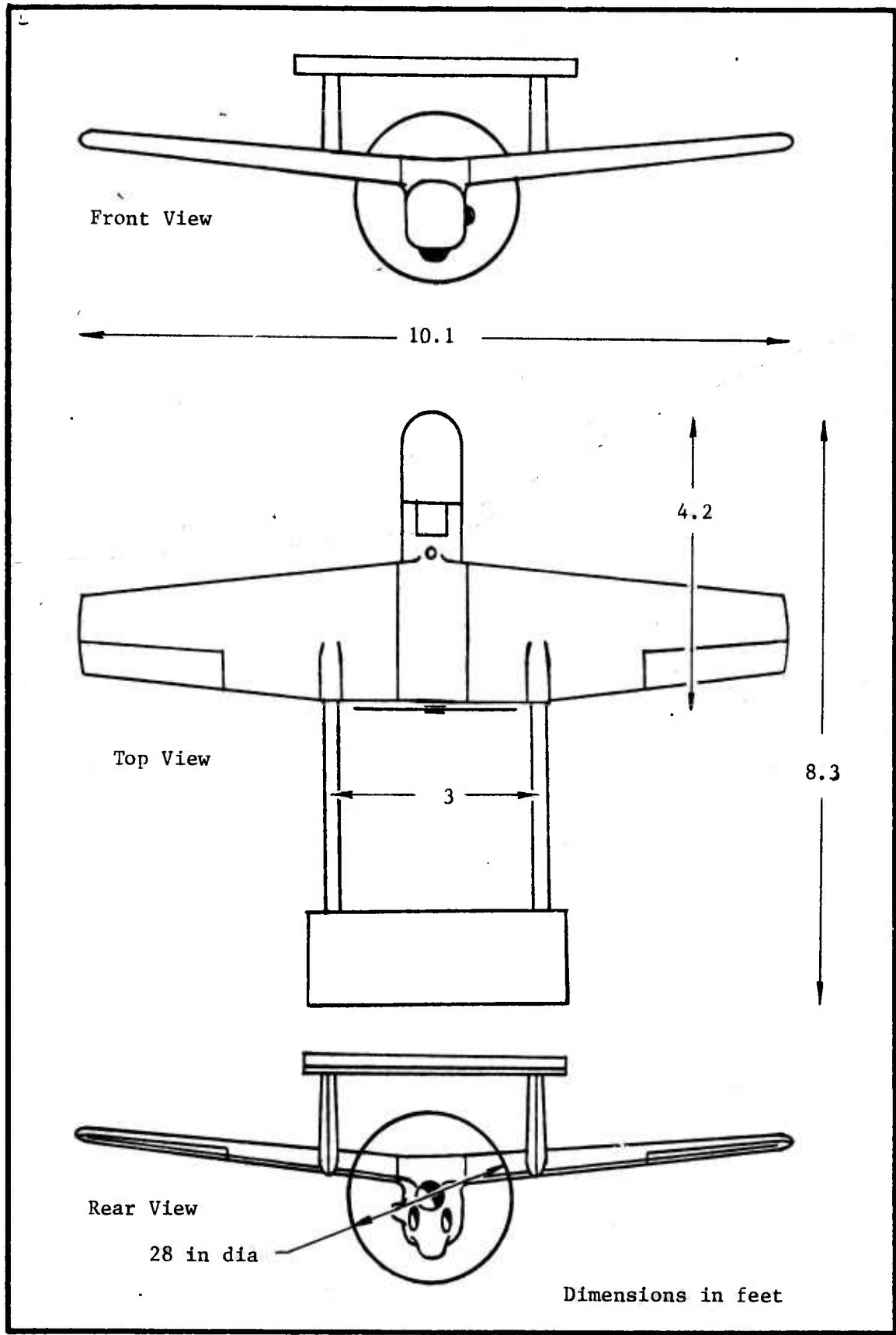


Figure A-10. Vehicle External View

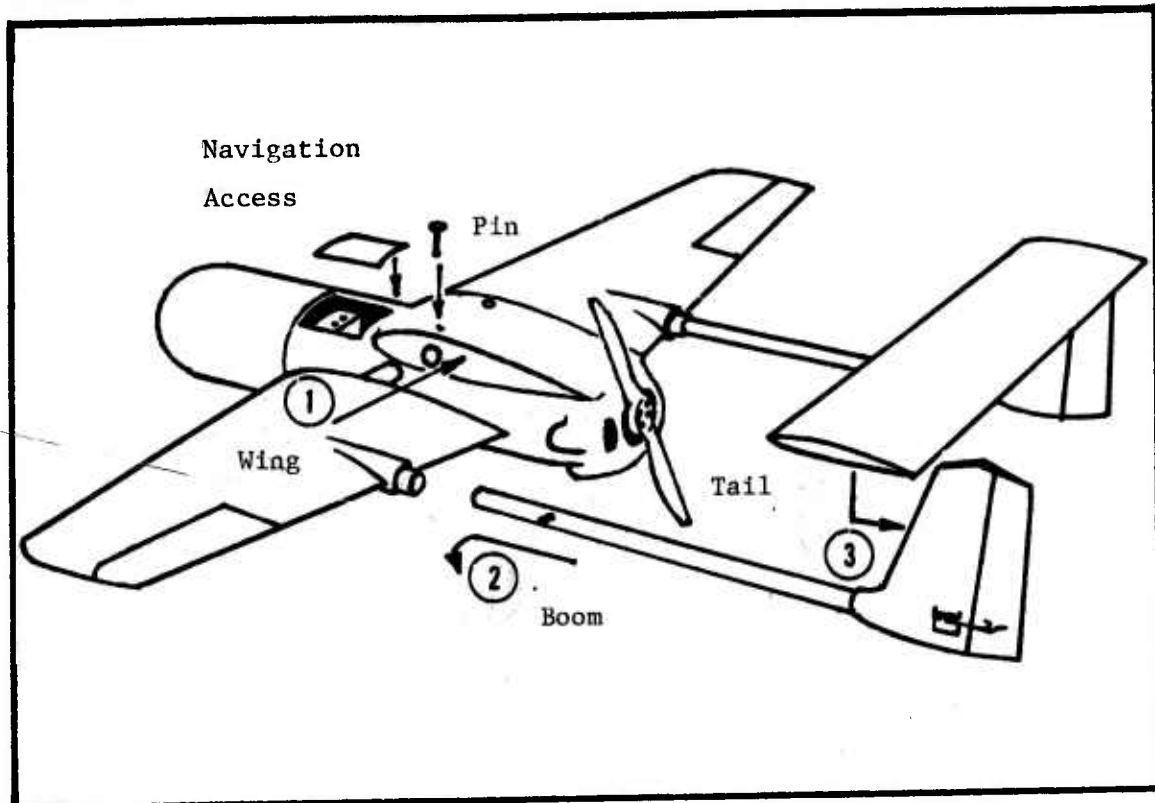


Figure A-11. Vehicle Assembly

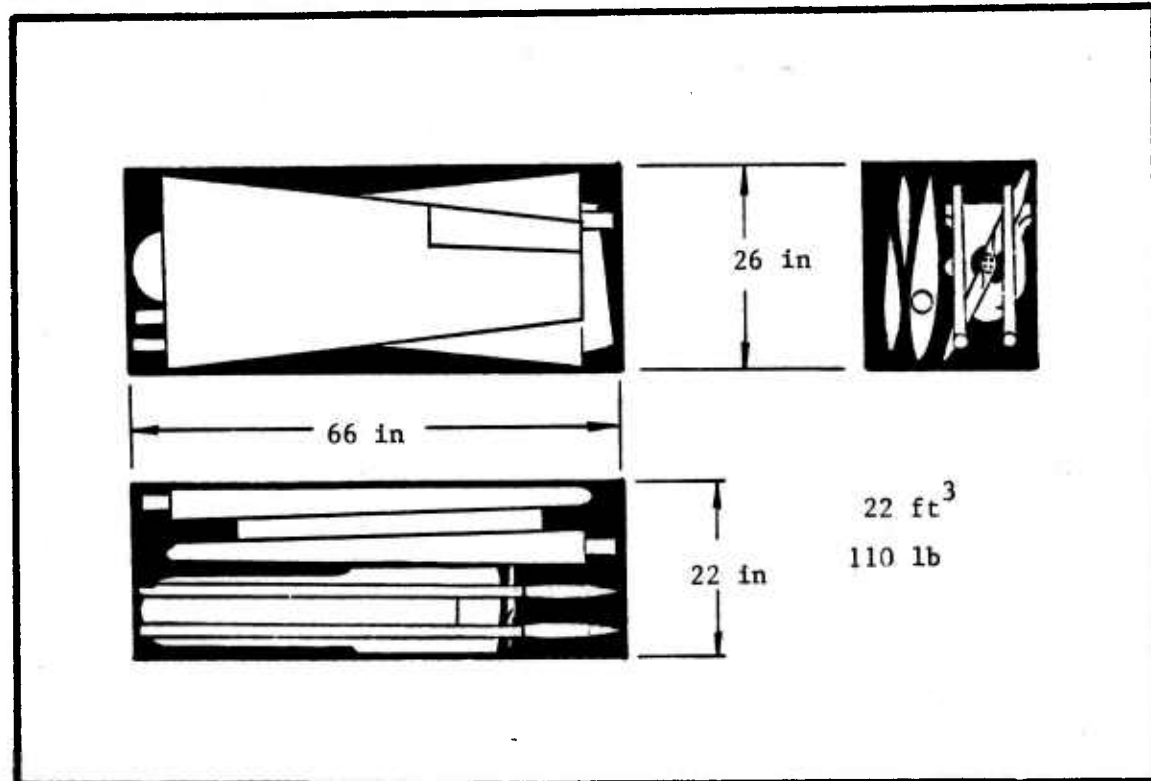


Figure A-12. Package Size

## Structures

Environment. The flight envelope of the Type I vehicle is divided into three main phases: launch and climb, cruise and loiter, and terminal dive. The Type II vehicle is concerned with only the first two since its fuel-depleted flight is of little value.

The launch-and-climb phase is significant in that the structure must endure an 8-g launch acceleration at full gross weight. It is anticipated that launch will occur somewhere between sea level and 3000 ft MSL, depending on the local altitude. The vehicle is pointed into the wind in unprepared areas, i.e., there may be obstacles to avoid locally. The attitude of the vehicle at release ( $\theta_{v1}$ ) is as near as possible to that which puts the wing at  $C_{Lmax}$ .

During the launch run and climb phase, the engine is running at the maximum power setting. The launcher pulls the vehicle by means of a fitting on the ventral side of the payload bulkhead. It is mounted there in order to utilize a tension-loaded ventral stringer in order to avoid buckling problems. The booms are supported by two "crutches" which are part of the launcher shuttle (Appendix F). Therefore, the special conditions encountered during launch need consideration. Specifically, the ventral stringer load and the bulkhead-stringer mounting point moments are the most stringent and are analyzed in a later section.

The conditions that the aircraft encounters during cruise and loiter are less stringent when compared to launch and dive. From the performance section, the cruise-loiter airspeed is 75 miles per hour at 10,000 feet MSL. Fuselage angle of attack is near zero, and turn loadings are well below those encountered during terminal dive.

Terminal dive is the most severe environment that almost all of the components face. This is due to the fact that an unmanned, sensor-guided vehicle gyrates beyond the conventional loading charts which use g-limits and standard wind shear. In this case, the maximum loading expected is the maximum that the aircraft can see, i.e., steady-state  $C_{Lmax}$  at terminal speed, 175 miles per hour.

Terminal dive speed, in this context, is the anticipated airspeed that the aircraft will encounter in a typical dive situation. Slope of dive is 45 degrees, control surfaces are continually deflecting, and the propeller is back-winded. Consequently, the steady-state force balances are applied as the vehicle reaches sea level,

$$D = W \sin 45^\circ \tag{A-18}$$

$$= \frac{\sigma}{391} v_{term}^2 C_D S$$

which is solved for  $v_{term}$

$$v_{term} = \left\{ \frac{391 (W \sin 45^\circ)}{\sigma C_D S} \right\}^{1/2} \tag{A-19}$$

where  $W$  is the aircraft weight at the dive. Dive does not occur before it cruises 100 miles, where the weight is about 120 pounds.  $C_D = 0.06$  for cruise, but it will vary somewhat due to control surface activity, backwash, and attitude change. The estimate is then  $C_D = 0.065$ .  $S$  is 17 square feet, and  $\sigma$  is 1.0 at sea level.

$$v_{term} = \left\{ \frac{391(120)(\sin 45^\circ)}{(1)(0.065)(17)} \right\}^{1/2}$$

$$= 173 \text{ mph}$$

Let  $v_{\text{term}} = 175$  mph as a conservative estimate. It will be somewhat lower for most cases.

The highest g-loading that the airframe will encounter (n) in a terminal maneuver is found from a balance of forces.

$$n = \frac{L_{\text{max}}}{W} \quad (\text{A-20})$$

$$= \frac{\sigma v_{\text{term}}^2 C_{L\text{max}} S}{391 W}$$

$$\sigma = 1.0 \text{ (sea level)}$$

$$v_{\text{term}} = 175 \text{ mph}$$

$$C_{L\text{max}} = 1.43 \text{ at } 180 \text{ mph (SHRENK)}$$

$$S = 17 \text{ ft}^2$$

$$W = 120 \text{ lb}$$

Therefore,

$$n = \frac{(1)(175)^2(1.43)(17)}{(391)(120)}$$

$$= 15.9 \text{ or, rounding off, } n = 16 \text{ g's.}$$

Materials. The low-cost and lightweight constraints are continuing adversaries in the search for realistic materials to be used in this vehicle. Therefore, the materials and manufacturing techniques were discussed in both general and specific terms with two very helpful engineers and chemists, Mr. Owens of AFFDL, and Mr. Morrissey of the Air Force Materials Laboratory (AFML).

The conventional methods used in making airframes, riveted metal and fabric-covered wood, put the price of this type of construction well

out of the \$100-\$200 price target. Super-lightweight model aircraft builders use materials like balsa, tissue, and hot-wired styrofoam. Unfortunately, these materials lose their weight advantage when high strength is required. The AFFDL Teleplane Project has been using styrofoam and plywood in RPV construction for many years, and it has proved very acceptable for prototypes in this weight class. However, this method requires a great deal of hand labor and is a very expensive approach in production.

The alternative suggested by Major Hoy and Mr. Lowe (AFFDL) is a self-skinning, medium-density, rigid polyurethane foam. The advantages of using this type of skin-support material are many. The foam, when molded, forms its own tough, colorable, rigid skin a few mils thick (Stengard, 1974:137). Skin thickness, foam density, and rigidity are readily controlled by proper mold temperature, chemistry, and pouring techniques (Morrissey, 1975). The Teleplane Program has samples of wing and fuselage sections made with this technique, and they appear quite satisfactory in use in this project.

The foam itself is stressed only to the extent that it carries the aerodynamic loading from its external skin to the spar. That is, the spar is assumed to transmit and resist all bending, shear, and torque encountered by the component (see Figure A-13). There are difficulties with this assumption, however. Data is not available to describe the mechanical properties of a skinned foam for any configuration remotely resembling the one anticipated. Consequently, the design approach depends on estimates that the qualitative evaluation of the technique is reasonable (Hoy and Morrissey, 1975). This caution is mentioned in the summary.

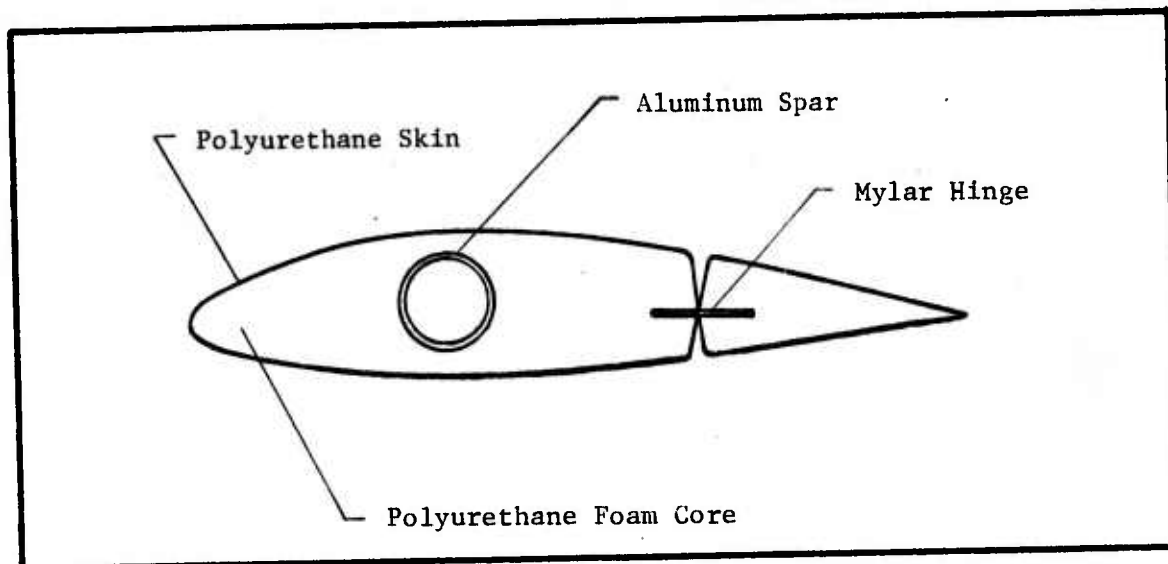


Figure A-13. Primary Wing Section

An alternative to the molded polyurethane foam is a blow-molded fiberglass reinforced plastic (FRP) such as polycarbonate (Owens, 1975 and Waterloo, 1974:278-284). This method is attractive for its ability to use the plastic as the major structure, possibly without using aluminum spars at all. Unfortunately, FRP blow molding appears to be quite a bit more expensive than simple polyurethane foam molding (Morrissey and Allinkov, 1975). This approach invites further work if the polyurethane foam approach fails or blow-molding becomes more cost-effective. But, for the purposes of this design effort, the molded-polyurethane, self-skinning foam approach is used.

The problem of supporting the loads encountered by the skinned-foam wings, empennage, and fuselage (E-Systems, 1974a) is solved by using tubular spars in areas where it is expected that the foam is insufficient. The most conventional spar material is aluminum; and it is very cheap, common, workable, and well-documented. Aluminum is available in a plethora of stock shapes and sizes. It is weldable, bendable,

affordable, and available. The most generally applicable shape is the circular tube which comes stocked in a wide range of sizes. The alloys of aluminum are many, but the one most applicable to this design is the 6061-T6 for three reasons: stiffness, workability, and availability in the stock sizes needed (Alcoa, 1956:53). Other alloys have favorable properties, but they are not available in the stock sizes necessary.

Composites, in general, are discouraged for this application on the basis of their higher cost. However, fiberglass-reinforced polycarbonate (FRP) is evaluated on the basis of cost for an aluminum-stiff structure and cost for an aluminum-strong structure. The basic structure weight involved is calculated later in this chapter under wing and fuselage structure requirements. It should also be noted that fiberglass-reinforced polycarbonate spars of the size required are not stock items. The reinforced polycarbonate cost estimate is based on the specific cost (dollars per pound) of a 2-inch diameter FRP rod. Unreinforced polycarbonate cost is based on 2-inch diameter, 1/8-inch wall tube (Dayton Plastics, 1975). Aluminum specific cost is based on large lots of stock extrusion (Alcoa, 1975). The comparison, shown in Table A-7, is based on the following relationships.

$$SEM = \frac{E}{\gamma} \quad (A-21)$$

$$SFY = \frac{fy}{\gamma} \quad (A-22)$$

$$STIF\$ = \frac{S\$}{SFY} \quad (A-23)$$

$$STRONG\$ = \frac{S\$}{SEM} \quad (A-24)$$

where  $S\$\$$  = specific cost of material  
 $SEM$  = specific elastic modulus  
 $SFY$  = specific yield strength  
 $STIF\$\$$  = relative cost of stiffness  
 $STRONG\$\$$  = relative cost of strength  
 $E$  = modulus of elasticity  
 $\gamma$  = specific weight  
 $f_y$  = yield stress

TABLE A-7. ALUMINUM/POLYCARBONATE TRADEOFF

	Specific Cost (\$/lb)	Specific Elastic Modulus	Specific Yield Strength	Relative Stiffness Cost	Relative Strength Cost
Aluminum	0.80	38.0	13.0	0.021	0.062
Unreinforced Polycarbonate	7.50	2.83	11.25	2.65	0.67
40% Fiberglass Polycarbonate	7.84	9.21	21.0	0.85	0.37

Plywood is a cheap and versatile material, but it suffers from high fabrication cost in that it requires cutting, finishing, and attaching. It is not cheap enough for use as a skin or strong enough for most structural components. However, it is ideal for use as bulkheads since it requires only one peripheral cut and is a common material for mounting boxes and flanges. Many other materials are available; but their cost, weight, or manufacturability leave a great deal to be desired in applications on slow, lightweight mini-drones of this type (Adams, 1971).

Manufacturing Techniques. The significant questions involved here are the problems of foam-spar adhesion and wing-aileron and stabilizer-rudder mating. The problem of adhesion of the polyurethane foam to an aluminum spar is not serious. The foam skins against the spar as well as the mold; and this skin adheres quite well since no release agent is used (Morrissey, 1975).

The problem arises when considering the stress flow from the aerodynamically loaded skin to the spar (see Figure A-13). The lower density foam between the skin and spar has questionable properties. Indeed, there appears to be no useable information available to conclusively describe the ability of this scheme to work in this configuration. Therefore, it must be assumed that, after a small amount of research and development, it will.

This assumption is made at some risk, but the alternative solution involves only a slightly higher cost. If the simple, cast-in spar arrangement proves unsatisfactory, it should be an easy matter to remedy. One attractive solution is to attach, by means of adhesive or spot-welding, an intermediate structure of light plastic or metal mesh about the wing spar in a manner shown in Figure A-14. The purpose of the mesh is to act as a skinning surface for the foam. The result is a foam cross-section that no longer depends on the strength of the lighter density core but is now able to transmit stresses through a stronger, higher density layer at the mesh. To repeat, this course adds little weight and some minor labor and materials cost, but it should only be necessary if the original foam-spar process proves inadequate during test.

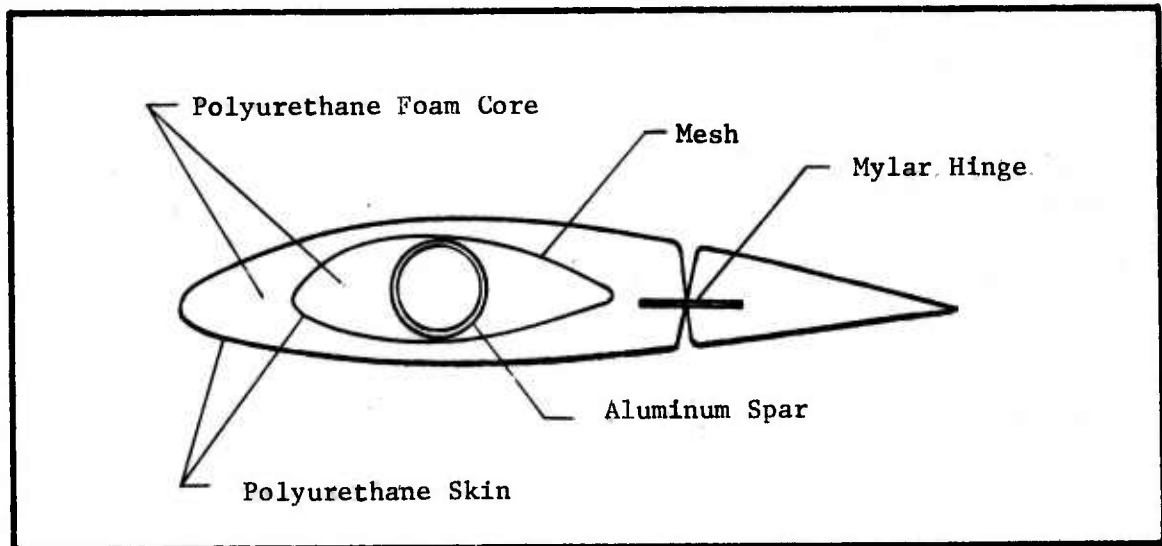


Figure A-14. Alternate Wing Section

The problem of cheaply mating the control surfaces is more easily solved. E-Systems (Morrissey, 1975) has demonstrated a technique for molding the wing and aileron as one piece, using a fiberglass hinge molded integrally with the foam. Unfortunately, their technique suffers from alignment and fatigue problems and is quite unsatisfactory. The approach seems valid, so this design effort includes this type of integral molding, except that the hinge is a perforated mylar strip. The perforations allow the foam to mechanically hold the strip, and the mylar is used since it is a very strong and flexible material. It can be easily and cheaply punched and cut. There are numerous ways of applying the mylar strip hinge, but this one seems most satisfactory (see Figure A-15).

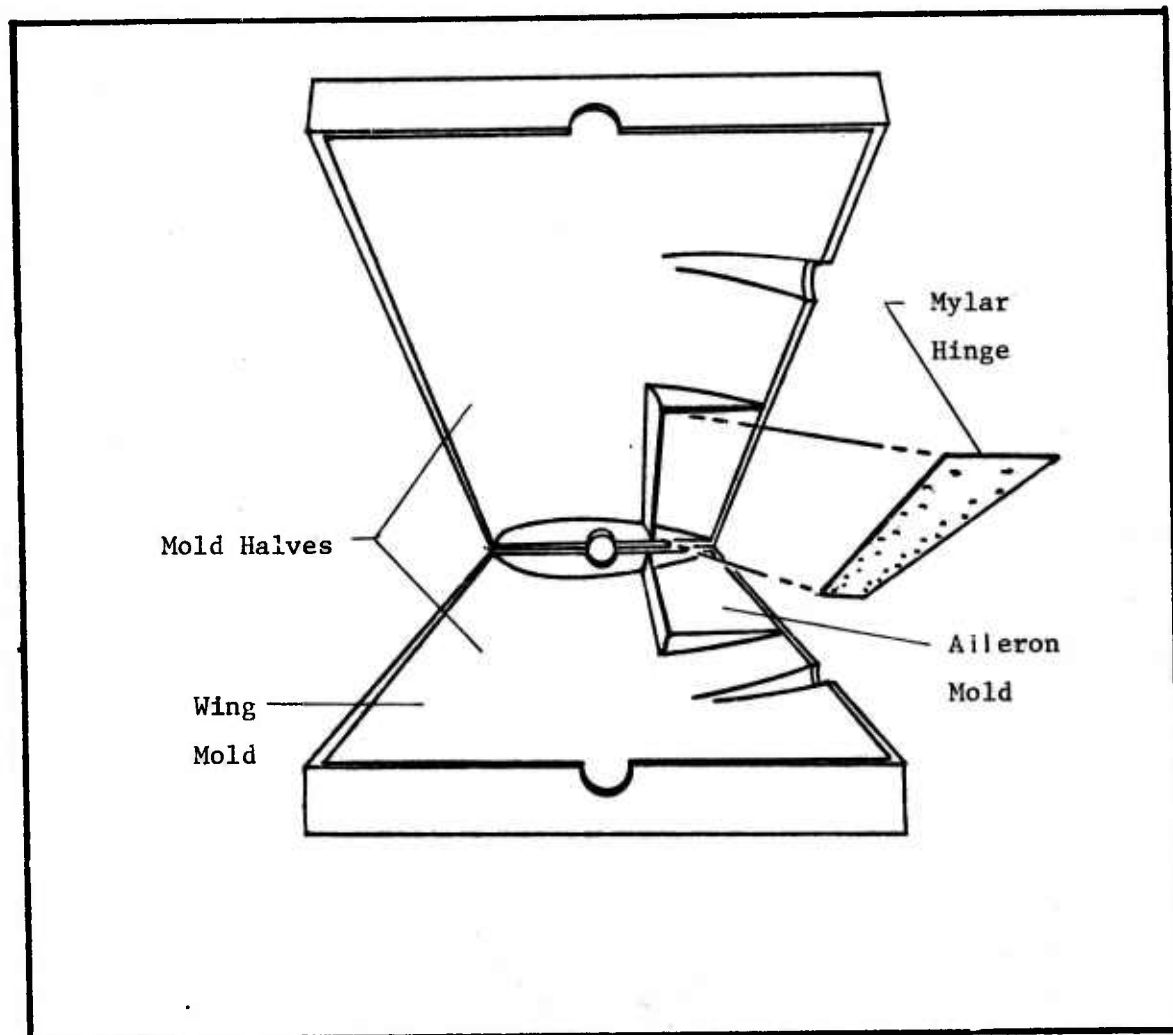


Figure A-15. Hinge Molding Scheme

Load Analysis. The general approach in analyzing the secondary structure required (spars, stringers, booms) is to select the critical loading and strength points, assess the nature and magnitude of the loads, and select the lightest-weight structure to handle it. As shown in the discussion of flight environments, the most critical points affecting structures are launch and terminal maneuvers. The most restrictive case is evaluated for each component examined. Safety factor

is ignored, since the vehicle is unmanned and usually encounters maximum loading on terminal dive where yielding is no longer important.

Wing Loading. Analysis of the more significant forces on the wings shows that the major area of concern is the strength of the spar at the point of fuselage intersection, i.e., where the carry-through spar ends. It is considered that each spar is cantilevered at that point and is acted upon by lift (L) at the AC, drag (D) at the AC, inertia at the wing CG, inertia of the body (without wing or tail), and inertia of the tail. This setup is shown in Figure A-16.

Looking first at the wing intersection moment about the X-axis ( $M_{xi}$ ) and using balance of moments (see Figure A-16),

$$M_{xi} = m \left[ \frac{1}{2} (W_d + W_f) y_{ai} - W_w y_{wi} - \frac{1}{2} W_t y_{bi} \right] \quad (A-25)$$

Likewise, the moment balance equation about the y-axis is

$$M_{yi} = m(W_{bd} + W_f) - n(W_{ht} Z_{ht} - W_{vt} Z_{ht}) \quad (A-26)$$

For the moment about the Z-axis,

$$M_{zi} = n Y_{wi} W_w + \frac{1}{2} Y_{bi} (D_t + W_t) + \frac{1}{2} Y_{ai} D_w \quad (A-27)$$

Using the standard drag relationship from Eq (A-18), Eq (A-28) is modified to

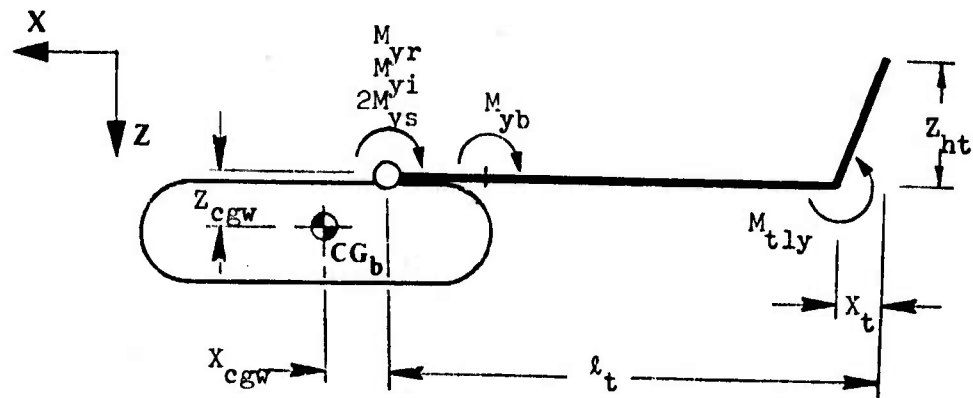
$$M_{zi} = n Y_{wi} W_w + \frac{1}{2} Y_{bi} \left( \frac{\sigma}{391} v^2 C_{Dt} S_t + W_t \right) + \frac{1}{2} Y_{ai} \frac{\sigma}{391} v^2 C_{Dw} S_w \quad (A-28)$$

where  $M_{xi}$  = moment about x-axis intersection

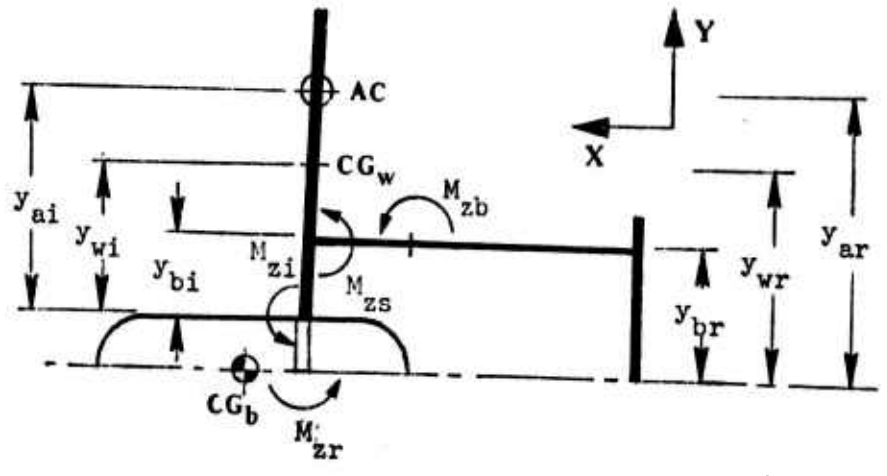
$M_{yi}$  = moment about y-axis intersection

$M_{zi}$  = moment about z-axis intersection

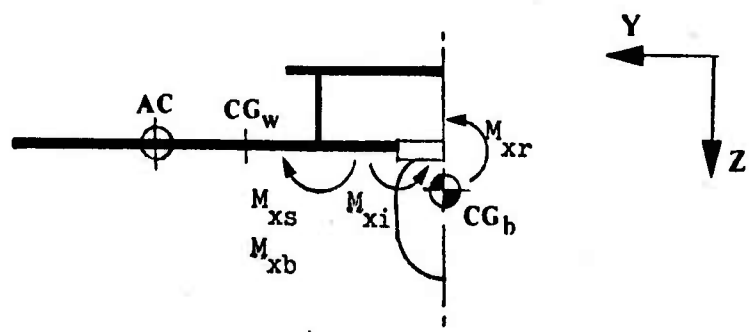
$C_{Dt}$  = tail drag coefficient



(a) X-Z Plane (Right Side)



(b) X-Y Plane (Right Side)



(c) Y-Z Plane (Right Side)

Figure A-16. Loading Layout

$C_{D_w}$  = wing drag coefficient  
 $D_t$  = tail drag  
 $D_w$  = wing drag  
 $m$  = number of maneuver g's  
 $n$  = number of launch g's  
 $S_t$  = tail area  
 $S_w$  = wing area  
 $v$  = airspeed  
 $W_{bd}$  = dry weight of body ( $W_g$  less wing and empennage)  
 $W_d$  = dry weight of vehicle ( $W_g$  less fuel)  
 $W_f$  = weight of fuel present  
 $W_{ht}$  = weight of horizontal tail  
 $W_t$  = weight of empennage  
 $W_{vt}$  = weight of vertical tail  
 $W_w$  = weight of one wing  
 $X_w$  = distance between body CG and spar  
 $Y_{ai}$  = distance from intersection to AC  
 $Y_{bi}$  = distance from intersection to boom  
 $Y_{wi}$  = distance from intersection to wing CG  
 $t_{ht}$  = height of horizontal tail above wing spar  
 $\sigma$  = altitude density ratio

The values used are:

$C_{D_t}$  = 0.05  
 $C_{D_w}$  = 1.223 (launch)  
           = 0.6 (terminal)  
 $m$  = 1 g (launch)  
       = 16 g (terminal)  
 $n$  = 8 g (launch)  
       = 0 g (terminal)  
 $S_t$  = 4 ft<sup>2</sup>  
 $S_w$  = 17 ft<sup>2</sup>

$v = 50$  mph (launch)  
 $= 175$  mph (terminal)  
 $W_{bd} = 70$  lb  
 $W_d = 100$  lb  
 $W_f = 15$  lb (at IP)  
 $W_{ht} = 4.2$  lb  
 $W_t = 10.4$  lb  
 $W_{vt} = 1.1$  lb  
 $W_w = 10.1$  lb  
 $X_w = 6.4$  in (launch)  
 $= 12$  in (terminal)  
 $Y_{ai} = 20.3$  in  
 $Y_{bi} = 12$  in  
 $Y_{wi} = 21.5$  in  
 $\sigma = 1.0$  (sea level)

The results are shown below in Table A-8.

TABLE A-8. WING INTERSECTION LOADING

Load Moment	Launch Value	Terminal Value
$M_{xi}$ (in-lb)	847	13,355
$M_{yi}$ (in-lb)	-138	10,192
$M_{zi}$ (in-lb)	1927	1,127

Table A-8 clearly shows that terminal-dive maneuvering is the dominant wing loading factor. Using the above terminal loads, Eqs (A-30), (A-31), and (A-33) are used to find bending moment ( $M_{bi}$ ), torque ( $M_{si}$ ), and minimum section modulus by using handbook examples ( $S_{imin}$ ) (Alcoa, 1956:88,97,98).

$$M_{bi} = (M_{xi}^2 + M_{zi}^2)^{1/2} \text{ (in-lb)} \quad (\text{A-29})$$

$$M_{si} = \frac{1}{2} M_{yi} \text{ (in-lb)} \quad (\text{A-30})$$

$$S_i = \frac{(M_{bi}^2 + 4M_{si}^2)^{1/2}}{f_y} \text{ (in}^3\text{)} \quad (\text{A-31})$$

Using the terminal numbers from Table A-8 and the common value  $f_y = 35,000$  pounds per square inch (Alcoa, 1956:53), the minimum required section modulus for the wingspan is  $S_i = 0.438$  inches cubed. The lightest aluminum tubes that satisfy this requirement are shown in Table A-9 (Alcoa, 1956:757).

TABLE A-9. TUBE PROPERTIES

Spar Diameter (in)	Wall Thickness (in)	Section Modulus (in <sup>3</sup> )	Total Spar Weight (lb)
2.0	3/16	0.443	12.1
2.25	1/8	0.420	9.5
2.25	3/16	0.579	13.8

From the data above, it is clearly advantageous to discount the anticipated leads slightly to gain a weight savings of 2.6 pounds in wing weight by choosing the second of the three spars listed. Since the actual attack loading is untested, this tradeoff seems reasonable.

In order to minimize the torsion loading encountered by the foam, it is decided to move the wing spar forward to the quarter-chord line. Since this airfoil section has a very low moment, the minimum-moment position is near the line of AC's.

Carry-through Spar. The wings are attached to the fuselage by sliding the wing-spar extensions into the carry-through spar mounted in the fuselage (see Figure A-11). The carry-through must be large enough to accommodate the wing-spar diameter and strong enough to carry the wing loading discussed above. The root (centerline) load analysis is similar to that of the intersection load analysis with the exception of the y-axis dimensions. Since the intersection is 6 inches out from the centerline, the following parameters are derived (see Figure A-16):

$$Y_{ar} = Y_{ai} + 6 \text{ in} = 26.3 \text{ in}$$

$$Y_{br} = Y_{bi} + 6 \text{ in} = 18 \text{ in}$$

$$Y_{wr} = Y_{wi} + 6 \text{ in} = 27.5 \text{ in}$$

Using Eqs (A-25), (A-26), and (A-28), the following equations are formed by similarity.

$$M_{xr} = m \left[ \frac{1}{2} (W_d + W_f) Y_{ar} - W_w Y_{wr} - \frac{1}{2} W_t Y_{br} \right] \quad (\text{A-32})$$

$$M_{yr} = M_{yi} \quad (\text{A-33})$$

$$M_{zr} = n Y_{wr} W_w + \frac{1}{2} Y_{br} \left( \frac{\sigma}{391} v^2 C_{Dt} S_t + W_t \right) + \frac{1}{2} Y_{ar} \frac{\sigma}{391} v^2 C_{Dw} S_w \quad (\text{A-34})$$

where  $M_{xr}$ ,  $M_{yr}$ , and  $M_{zr}$  are the components of the wing root moment.

The values for these three parameters are shown in Table A-10.

TABLE A-10. WING ROOT LOADING

Load Item	Launch Value	Terminal Value
$M_{xr}$ (in-lb)	1129	17,424
$M_{yr}$ (in-lb)	-138	10,192
$M_{zr}$ (in-lb)	2486	1,460

Eqs (A-29), (A-30), and (A-31) are used to find the minimum required section modulus for the carry-through spar ( $S_r$ ). The result is  $S_r = 0.439$  inches cubed. The section required to accompany the wing spar and root loading is a 2.5-inch diameter and  $\frac{1}{8}$  - inch wall thickness tube with a weight of 1.10 pounds.

Booms. Each boom is in the form of an aluminum tube connecting the leading edge of the vertical tail spar to the wing spar. This configuration results in a total boom spar length about the same as the tail moment arm, about 5 feet. The boom is attached to the vertical tail spar by means of rivets and to the wing spar via a sleeve welded to the spar. The boom slides into the sleeve and is held in place by a simple slot-pin detent. The pin is held in by pre-loading the horizontal tail spar (see Figure A-17). The result is that the boom is cantilevered at the sleeve end.

The critical stress areas are easily seen to be the points where the boom enters the sleeve and where the sleeve is attached to the wing spar. The conservative assumption made here is that during any portion of the flight, all balance forces are handled by the empennage. This is reasonable since this is a low-moment wing with the boom attachment at the wing quarter-chord. Again, referring to Figure A-16, the balance of moments equations for the sleeve at maximum terminal maneuver are

$$M_{xs} = \frac{\sigma}{391} v_{\text{term}}^2 C_{L_{\text{maxvt}}} S_{\text{vt}} \left\{ \frac{Z_{\text{ht}}}{2} \right\} \quad (\text{A-35})$$

$$M_{ys} = \frac{1}{2} M_{\text{yr}} \quad (\text{A-36})$$

$$M_{zs} = \frac{\sigma}{391} v_{\text{term}}^2 C_{L_{\text{maxvt}}} S_{\text{vt}} l_t \quad (\text{A-37})$$

where  $M_{xs}$ ,  $M_{ys}$ , and  $M_{zs}$  are the moments at the sleeve-spar interface,

$\sigma$  = density ratio, and  $v_{\text{term}}$  = terminal airspeed.

$C_{L_{\max vt}}$  = max  $C_L$  of the vertical tail

$S_{vt}$  = vertical tail area

$Z_{ht}$  = height of vertical tail above the wing spar

$M_{yR}$  = moment at the wing root at y-axis, Eq (A-33)

These moments are calculated using the attack conditions noted earlier.

That is,

$$\sigma = 1 \text{ (sea-level)}$$

$$v_{\text{term}} = 175 \text{ mph}$$

$$Z_{ht} = 16 \text{ in}$$

$$M_{yR} = 10,192 \text{ in-lb}$$

$$S_{vt} = 1.56 \text{ ft}^2$$

$$C_{L_{\max vt}} = 0.5 \quad (\text{Jacobs, 1934:42})$$

$$l_t = 60 \text{ in} \quad (\text{Appendix B})$$

The resulting attack moments are

$$M_{xs} = 489 \text{ in-lb}$$

$$M_{ys} = 5096 \text{ in-lb}$$

$$M_{zs} = 3666 \text{ in-lb}$$

Using the relationships from Eqs (A-29), (A-30), and (A-31),

$$M_{bs} = (M_{ys}^2 + M_{zs}^2)^{1/2}$$

$$= 6278 \text{ in-lb}$$

$$M_{ss} = M_{xs}$$

$$= 489 \text{ in-lb}$$

$$S_s = \frac{1}{f_y} (M_{bs}^2 + 4 M_{ss}^2)^{1/2}$$

$$= 0.182 \text{ in}^3$$

The minimum section modulus for the boom is now found by using similar equations and conditions but using the boom-sleeve intercept as the design point (see Figure A-16). This reduces the effective boom length ( $l_b$ ) by the sleeve length, 10 inches. The resulting moments are found using Eqs (A-35), (A-36), and (A-37). The results are

$$M_{xb} = 489 \text{ in-lb}$$

$$M_{yb} = 3055 \text{ in-lb}$$

$$M_{zb} = 4247 \text{ in-lb}$$

Applying these values to Eqs (A-29), (A-30), and (A-31) yield the values

$$M_{bb} = 5232 \text{ in-lb}$$

$$M_{sb} = 489 \text{ in-lb}$$

$$S_b = 0.152 \text{ in}^3$$

The minimum-weight, aluminum-tube section that satisfies this minimum section modulus has a 2-inch diameter, 1/16-inch wall thickness, 0.179-inch cubed section modulus, and weight of 1.94 pounds. The associated minimum-weight sleeve associated with that boom has a 2-1/4 inch diameter, 1/16-inch wall thickness, 0.229-inch cubed section modulus, and weight of 0.42 pounds (Alcoa, 1956:257).

Horizontal Tail Spar. Figure A-17 shows that the horizontal tail spar can be represented as shown in Figure A-18a.

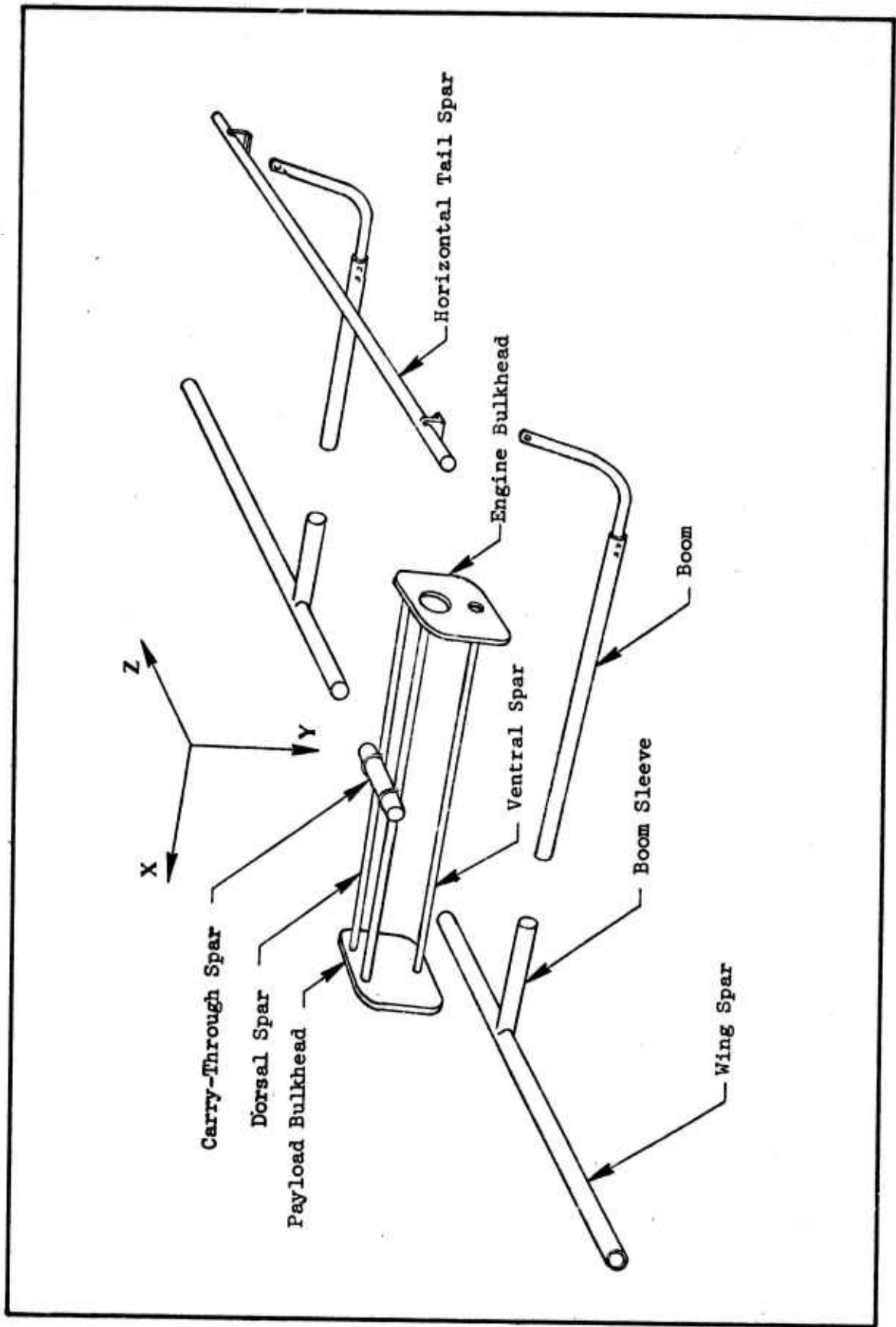


Figure A-17. Structural Skeleton

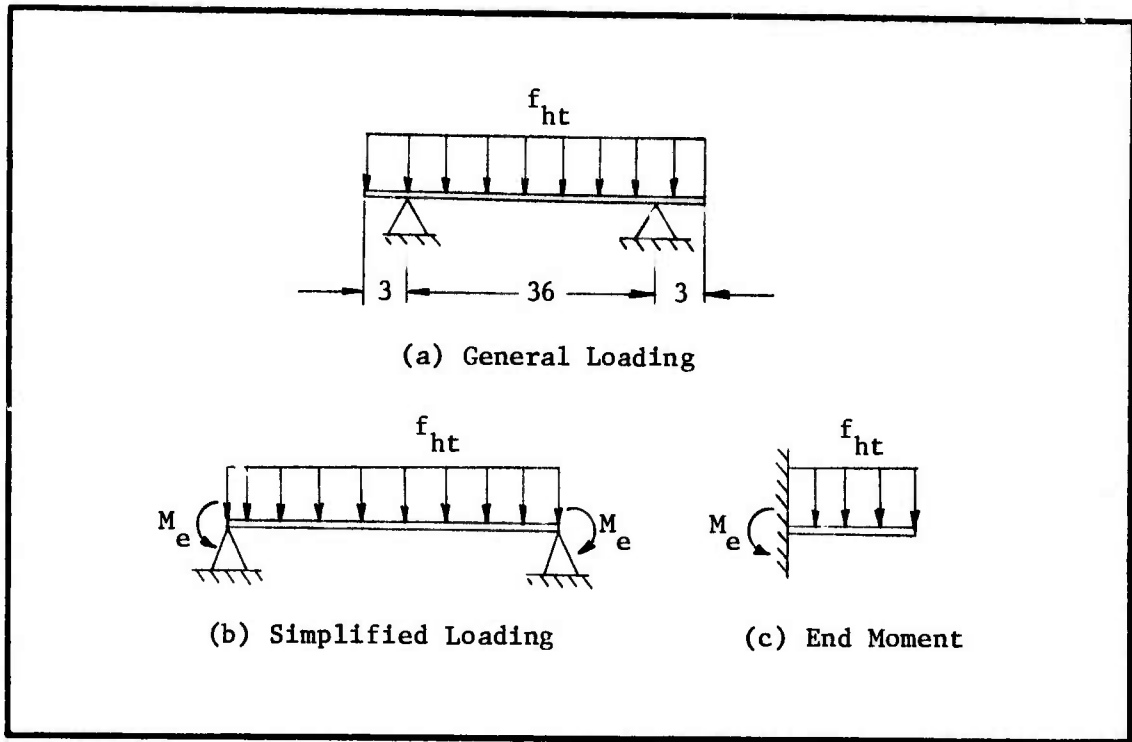


Figure A-18. Horizontal Tail Loads

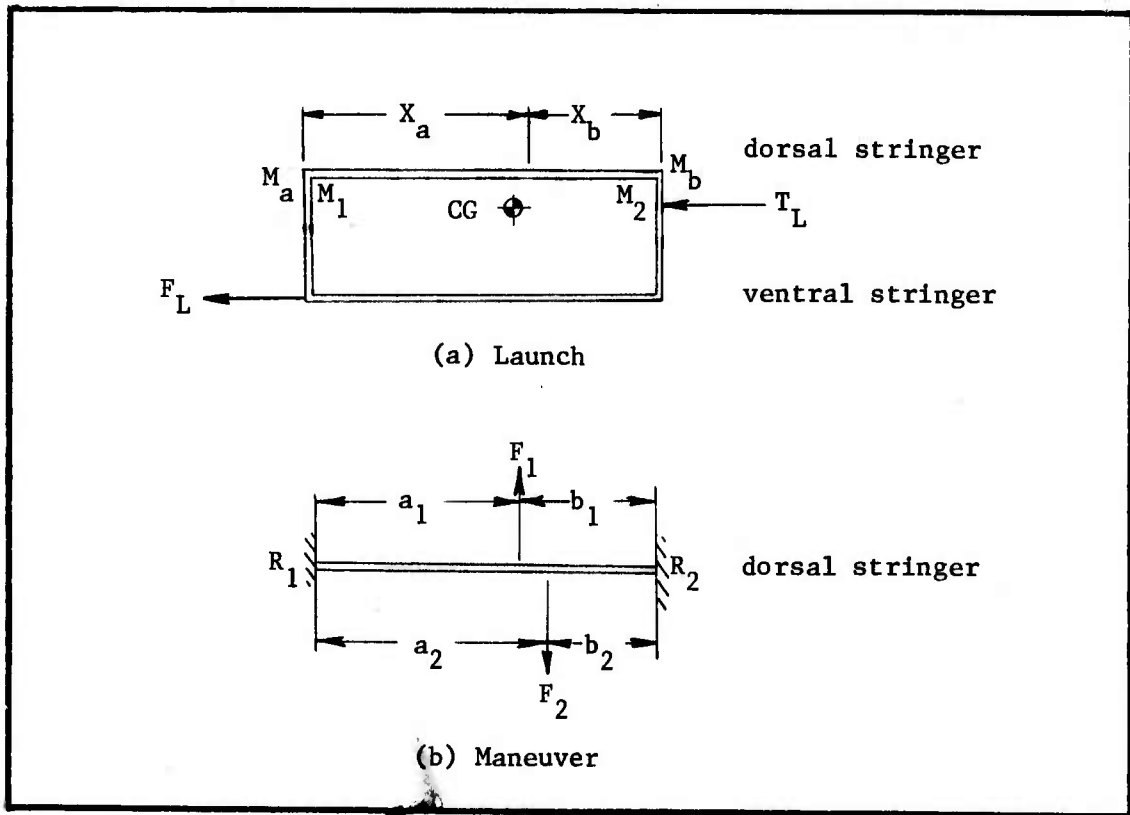


Figure A-19. Fuselage Schematic Loads

The loading is assumed to be uniform over the spar length. This layout is simplified as shown in Figure A-18b to a uniform load between pins with end moments. The total load is twice the end load seen by each boom, so the spanwise loading is shown by

$$f_{ht} = \frac{2 M_{yb}}{b_{ht} l_b} \quad (A-38)$$

$$= 2.72 \text{ lb/in}$$

where

$$M_{yb} = 3055 \text{ in-lb}$$

$$l_b = 50 \text{ in}$$

$$b_{ht} = 45 \text{ in}$$

The tail support pins are 36 inches apart with 4.5-inch overhangs, and the end moments ( $M_e$ ) are calculated using the diagram in Figure A-18c (American, 1965:2.126).

$$M_e = \frac{f_{ht} l_e^2}{2} \quad (A-39)$$

$$= \frac{(2.72)(4.5)^2}{2}$$

$$= 27.54 \text{ in-lb}$$

Using the diagram in Figure A-18b, the maximum moment encountered ( $M_{max}$ ) is found (American, 1965:131).

$$M_{max} = \frac{f_{ht} l_e^2}{8} - M_e \quad (A-40)$$

$$= 725.8 \text{ in-lb}$$

Using Eq (A-31) where  $M_b = M_{max}$  and  $M_s = 0$ ,

$$S = 0.021 \text{ in}^3$$

Since a NACA 0015 section is used with a chord of 16 inches, the largest-diameter tube useable is 2 inches. However, the lightest standard-size tube that meets the horizontal tail spar strength requirements has a 1-3/4 inch diameter, 1/32-inch wall, and weight of 0.75 pounds (Alcoa, 1956:257).

Vertical Tail. Using the dimensions shown in Figure A-16, the minimum useable spar for the vertical tail is found. Using the moment-balance method, the following relationships for bending moment ( $M_{bt}$ ) and torque ( $M_{st}$ ) are found

$$\begin{aligned} M_{bt} &= \frac{M_{bs} X_t}{l_t} & (A-41) \\ &= 837 \text{ in-lb} \end{aligned}$$

where  $M_{bt}$  = bending moment at boom intercept  
 $M_{bs}$  = sleeve-root moment = 6278 in-lb  
 $X_t$  = distance aft from boom to stabilator pivot = 8 in  
 $l_t$  = length of tail arm = 60 in

and  $M_{st} = M_{ss}$  (A-42)  
 $= 489 \text{ in-lb}$

Using Eq (A-31),

$$\begin{aligned} S &= \frac{1}{f_y} (M_{bs}^2 + 4 M_{ss}^2)^{1/2} \\ &= 0.037 \text{ in}^3 \end{aligned}$$

The lightest satisfactory stock tube has a 1-1/2 inch diameter, 1/32-inch wall, and weight of 0.34 pounds.

Fuselage. The fuselage loading and spar selection is based on the structure presented in Figures A-17 and A-19. The major items of interest are the launcher force ( $F_L$ ), the engine thrust at launch ( $T_L$ ) aircraft inertia ( $nw_g$ ), and wing lift ( $L$ ). The three stringer tubes (two dorsal, one ventral) are assumed to be cantilevered from the bulkheads, since they are mounted with flanges bolted to the bulkhead.

The launch loading on the dorsal stringer is decomposed into its major components (see Figure A-19a), wing moment ( $M_w$ ), inertia moments ( $M_a$ ), and end moments ( $M_1$  and  $M_2$ ). Since there are two dorsal stringers,  $M_w = \frac{1}{2} M_{ry}$ , and the inertia moments are distributed to the six flange mounts,  $M_a = \frac{1}{6} M_L$ . Therefore,

$$M_L = F_L Z_L - M_{ry} \quad (A-43)$$

where

- $M_L$  = total launcher moment
- $F_L$  = launcher force
- $M_{ry}$  = wing-root moment at y-axis
- $Z_L$  = height from launcher probe to CG

using the values

- $Z_L = 7$  in
- $F_L = 880$  lb (Appendix F)
- $M_{ry} = -138$  in-lb (at launch)

The results are  $M_L = -6022$  inch-pounds and  $M_a = -1004$  inch-pounds. End moments are calculated from the standard equations (Priest, 1965: 157).

$$M_1 = M_a - \frac{M_w X_b}{\ell^2} (\ell - 3X_a) \quad (A-44)$$

$$M_2 = M_a - \frac{M_w X_a}{\ell^2} (2\ell - 3X_a) \quad (A-45)$$

$$M_+ = M_1 + M_w + \frac{6M_w X_a^2 X_b}{\ell^3} \quad (A-46)$$

$$M_- = M_+ - M_w \quad (A-47)$$

where

$M_w$  = wing moment

$\ell$  = length of each stringer

$X_a$  = distance from payload bulkhead to carry-through spar

$X_b$  = distance from spar to engine bulkhead

$M_+$  = moment just ahead of spar

$M_-$  = moment just behind spar

Using the values  $M_w = \frac{1}{2} M_{ry} = -69$  in-lb

$$\ell = 27 \text{ in}$$

$$X_a = 17.5 \text{ in}$$

$$X_b = 9.5 \text{ in}$$

the results are

$$M_1 = -1027 \text{ in-lb}$$

$$M_2 = -1002 \text{ in-lb}$$

$$M_+ = -1157 \text{ in-lb}$$

$$M_- = -1088 \text{ in-lb}$$

This shows that, for launch, the maximum dorsal moment is  $M_{\max} = 1157$  inch-pounds.

The loading on the ventral stringer is also of concern. The tension stress through the stringer during launch is calculated from

$$F_L = |M_a| S_v + \frac{F_L}{A_v} \quad (A-48)$$

where

- $F_L$  = ventral stringer launch stress
- $M_a$  = corner launch moment
- $S_v$  = ventral stringer section modulus
- $F_L$  = launch force
- $A_v$  = ventral stringer sectional area

Using the values:  $M_a = -1004$  in-lb

$F_L = 880$  lb

$S_v = 0.022$  in<sup>3</sup> for a one-inch diameter, 1/32-inch wall tube (Alcoa, 1956:257)

$A_v = 0.095$  in<sup>2</sup>

The resulting stress,  $F_L = 9285$  pounds per square inch is much less than the yield stress of the material (35,000 lb/in<sup>2</sup>), which means that the lightest 1-inch diameter tube is adequate.

The attack maneuver is another critical time for load analysis, as shown in Figure A-19b. This analysis is simplified by considering the dorsal load due to the wing lift (L) and moment ( $M_w$ ) as produced by two separate forces ( $F_1$  and  $F_2$ ). This is reasonable, since the carry-through spar is supported by U-bolts into each dorsal stringer. The dimension d is the distance between the U-bolt ends, 2.75 inches. The forces,  $F_1$  and  $F_2$ , are found from the balance equations,  $F_1 + F_2 = L$  and  $F_1 d - F_2 d = 2 M_w$ . The resulting values are  $F_1 = 2178$  pounds and  $F_2 = -1530$  pounds. The dimensions  $a_1$ ,  $a_2$ ,  $b_1$ , and  $b_2$  are

found by using  $X_a$  and  $X_b$  and centering the U-bolt. The values are as follows:

$$a_1 = 16.125 \text{ in}$$

$$a_2 = 18.875 \text{ in}$$

$$b_1 = 9.875 \text{ in}$$

$$b_2 = 7.125 \text{ in}$$

$$l = 27 \text{ in}$$

$$M_w = 5096 \text{ in-lb}$$

$$d = 2.75 \text{ in}$$

$$L = 648 \text{ lb}$$

$L$  and  $M_w$  are found for a 16-g terminal maneuver. Superimposing the single-force beam equations (American, 1965:2.125) yields

$$R_1 = \frac{F_1 b_1^2}{3} (3a_1 + b_1) + \frac{F_2 b_2^2}{l^3} (3a_2 + b_2) \quad (\text{A-49})$$

$$= 377 \text{ lb}$$

$$R_2 = \frac{F_1 a_1^2}{3} (a_1 + 3b_1) + \frac{F_2 a_2^2}{l^3} (a_2 + 3b_2) \quad (\text{A-50})$$

$$= 271 \text{ lb}$$

The corner moments are (AISC, 1965:2.125)

$$M_1 = \frac{F_1 a_1 b_1^2 + F_2 a_2 b_2^2}{l^2} \quad (\text{A-51})$$

$$= 2687 \text{ in-lb}$$

$$M_2 = \frac{F_1 a_1^2 b_1 + F_2 a_2^2 b_2}{l^2} \quad (\text{A-52})$$

$$= 2344 \text{ in-lb}$$

The moment at the carry-through spar is

$$M_c = \frac{2}{l^3} [R_1 a_1^2 b_1 + R_2 a_2^2 b_2] \quad (\text{A-53})$$

$$= 2800 \text{ in-lb}$$

The preceding calculations show that the maximum expected dorsal moment is 2800 inch-pounds at the carry-through attachment. The ventral stringer loading is much less, since the wing moment is not applied directly.

Looking at all of the above loadings, it is obvious that the most severe load is encountered during terminal maneuvers at the carry-through spar attachment,  $M_{\max} = 2800$  inch-pounds. Therefore, Eq (A-31) is used to show the minimum dorsal stringer section modulus.

$$S = \frac{M_{\max}}{f_y}$$

$$= 0.080 \text{ in}^3$$

This necessitates the use of a tube with a 1-inch diameter, 3/16-inch wall, and a weight of 1.3 pounds for each dorsal stringer. The total weight of the three stringers is 2.9 pounds. Tubing is not the most efficient cross-section for bending, but no other suitable stock sections fit this fuselage. Fuselage redesign might result in some weight savings but it is not expected to be significant.

The weight and section characteristics of the above structural components are listed below in Table A-11.

TABLE A-11. ALUMINUM STRUCTURE SUMMARY

Component	Number Used	Diameter (in)	Wall Thickness (in)	Length (in)	Weight, each (lb)	Total wt (lb)
Wing Spar	2	2-1/4	1/8	58	4.74	9.5
Carry-through	1	2-1/2	1/8	12	1.1	1.1
Boom	2	2	1/16	52	1.54	3.9
Boom Sleeve	2	2-1/4	1/16	12	0.51	1.0
Horiz. Tail Spar	1	1-3/4	1/32	45	0.75	0.8
Vertical Tail Spar	2	1-1/2	1/16	24	0.34	0.7
Dorsal Stringer	2	1	3/16	28	1.30	2.6
Ventral Stringer	1	1	1/32	28	0.30	0.3

Weight Calculations. The following discussions deal with estimating the weights of skinned-polyurethane foam parts cast around the associated aluminum structural member. The foam normally considered for this application is a rigid, freon-blown, 6 pound per cubic foot density foam commonly available (Morrissey, 1975). The approach is to find gross component volume, subtract cavity and spar volumes, and calculate the remaining weight of foam. These estimates are presented along with spar and total foam-component weights in Table A-12.

For example, the fuselage is composed of the following volume estimates (all data is in cubic feet):

overall fuselage, 1.31  
     avionics bay, 0.19  
     fuel tank, 0.37  
     alternator bay, 0.06  
     wing root hump, 0.51  
 carry-through spar, 0.03

The resulting foam volume is  $1.31 - 0.19 - 0.37 - 0.06 + 0.51 - 0.03 = 1.12$  cubic feet. Using 6 pound per cubic feet foam, the weight estimate of the foam is 6.77 pounds. This is added to the weights of the stringers, engine cowling, and carry-through spar to find the total fuselage weight of 11.8 pounds.

TABLE A-12. FOAMED-COMPONENT WEIGHTS

Component	Foam wt (lb)	Structure wt (lb)	Total Component wt (lb)
Fuselage	6.77	5.0	11.8
Wings	15.46	10.5	26.0
Horizontal Tail	3.00	0.75	3.8
Vertical Tails	1.70	0.68	1.2

The volume of foam required for the wings and empennage is based on a ratio of cross-sectional area to chord relationship,

$$V = b c_{mac}^2 \left\{ \frac{A}{c^2} \right\} \quad (A-54)$$

where  $\frac{A}{c^2}$  is estimated by trapezoidal rule from the station coordinates presented for each airfoil (Jacobs, 1935:17,18). The ratios  $A/c^2$  for the

wing and tail are:

$$\begin{aligned} \text{wing; } A/c^2 &= 0.117, \text{ tip} \\ &= 0.098, \text{ root} \\ \text{tail; } A/c^2 &= 0.078 \end{aligned}$$

Other component weights are discussed below. The known component weights, in pounds, are: payload, -25; servos, 0.2 each; engine, 12; and propeller, 2. Avionics weight is estimated at 6.5 pounds from the mission and navigation study as recommended by the RPV SPO. Bulkhead weights are estimated, using 1/2-inch standard plywood, at 1 pound each. A representative alternator weight is estimated in Appendix D at 6 pounds. The payload shroud is estimated at 1.4 pounds by using a 1/16-inch thick polycarbonate shell. Fuel weight is discussed in the following section (Performance).

The weight-and-balance estimate for the vehicle at launch is shown below in Table A-13. The changes in CG location as a function of fuel consumption are shown in Figure A-9 and are tabulated in Appendix A-5-5. The component CG's are illustrated in Figure A-7.

TABLE A-13. FINAL WEIGHT AND BALANCE

Component	Weight (lb)	X-axis Location (in)	Y-axis Location (in)	Z-axis Location (in)
Fuel	21.5	30.6	0.0	0.0
Payload	25.0	9.5	0.0	0.0
Fuselage	11.8	33.0	0.0	0.0
Left Wing	13.0	33.0	0.0	6.5
Right Wing	13.0	33.0	0.0	6.5
Horizontal Tail	3.75	92.0	0.0	23.0
Left Vertical Tail	1.2	92.0	-19.0	12.0
Right Vertical Tail	1.2	92.0	19.0	12.0
Aileron Servo L	0.2	33.0	-25.0	6.0
Aileron Servo R	0.2	33.0	25.0	6.0
Rudder Servo L	0.2	93.0	-19.0	8.0
Rudder Servo R	0.2	93.0	19.0	8.0
Elevator Servo	0.2	93.0	0.0	20.0
Engine Servo	0.2	43.0	0.0	0.0
Payload Shroud	1.4	5.0	0.0	0.0
Avionics	6.5	17.0	0.0	0.0
Propeller	2.0	50.0	0.0	0.0
Engine	12.0	46.0	0.0	0.0
Alternator	6.0	42.0	0.0	0.0
Left Boom	1.95	60.0	-18.0	6.5
Right Boom	1.95	60.0	18.0	6.5
Payload Bulkhead	1.0	15.0	0.0	0.0
Engine Bulkhead	1.0	43.0	0.0	0.0
TOTAL AIRCRAFT AT LAUNCH	125.0	32.68	0.0	2.54

## Performance

The approach used to estimating the vehicle performance and parameters necessary to satisfy the mission requirements is based on commonly used, preliminary-performance techniques employed at a basic level. In general, these techniques are derived from unpublished class notes supplied by Prof Harold E. Larsen of the Aero Mechanics Department of the Air Force Institute of Technology (Larsen, 1975 b).

The method generally involves applying the preliminary weight, layout, and planform parameters, discussed earlier, to the general-performance analysis. These results are then used to redesign or rearrange, if necessary, the airplane parameters in such a way as to produce acceptable results. The technique is basic, since confidence in many of the parameter values is questionable. That is, some initial values are desirables, some are estimates, and some are arbitrary.

This technique is mechanized by constructing a computer program, DESIGN (Appendix A-6), on the basis of the referenced notes and on an endurance estimating technique taken from NACA TR234 (Diehl, 1926). This program and the associated results and plots are presented in Appendices A-6-1, A-6-2, and A-6-3, respectively.

Mission Profile. The quantitative aspects of vehicle performance are closely related to the environments and flight profiles which the vehicle encounters. Therefore, it is reasonable to base the software design tool on one basic mission profile that reasonably simulates the expected vehicle situation. In discussions with System Analysis,

Chapters II and IV, Volume II, the following profile seems reasonable.

Launch occurs at 3000 feet MSL (worst case) at 50 miles per hour with no wind. Launch is into the wind if there is any. It occurs in an unprepared area, thus necessitating quick climb to clear any surrounding obstacles, such as trees, hills, wires, buildings, etc. Time to reach cruise altitude of 10,000 feet MSL is not specified, but mountains might need to be crossed. Therefore, time to altitude should be minimized. The distance from launcher to target is a maximum of 100 miles, and the cruise to the target is at 75 miles per hour at 10,000 feet. In the target area, the vehicle remains at 10,000 feet and 75 miles per hour until fuel depletion, occasionally turning full-about. The actual terminal phase is not included, except to note terminal velocity and maneuver loading discussed previously.

The discussion above leads to the mission profile applied in DESIGN. Launch is at 50 miles per hour, 3000 feet altitude, and full power. Climb is at 60 miles per hour at the best climb angle for that speed. Upon reaching an altitude of 10,000 feet, throttle is reduced and the vehicle remains straight-and-level at 75 miles per hour for the rest of the 100-mile leg. Further specification of conditions here would make the design tool too closely coupled with navigation, flight control, and servo loops. Loiter over the target area is based on the same conditions as cruise. No turns are included since the frequency of turns is small. The preceding discussion is illustrated in Figure A-20.

Power. It is assumed that an alternator uses power (HPGEN) driven from the engine (for the Type I), and the available thrust horsepower decreases with altitude by the simple 4-cycle relationship shown

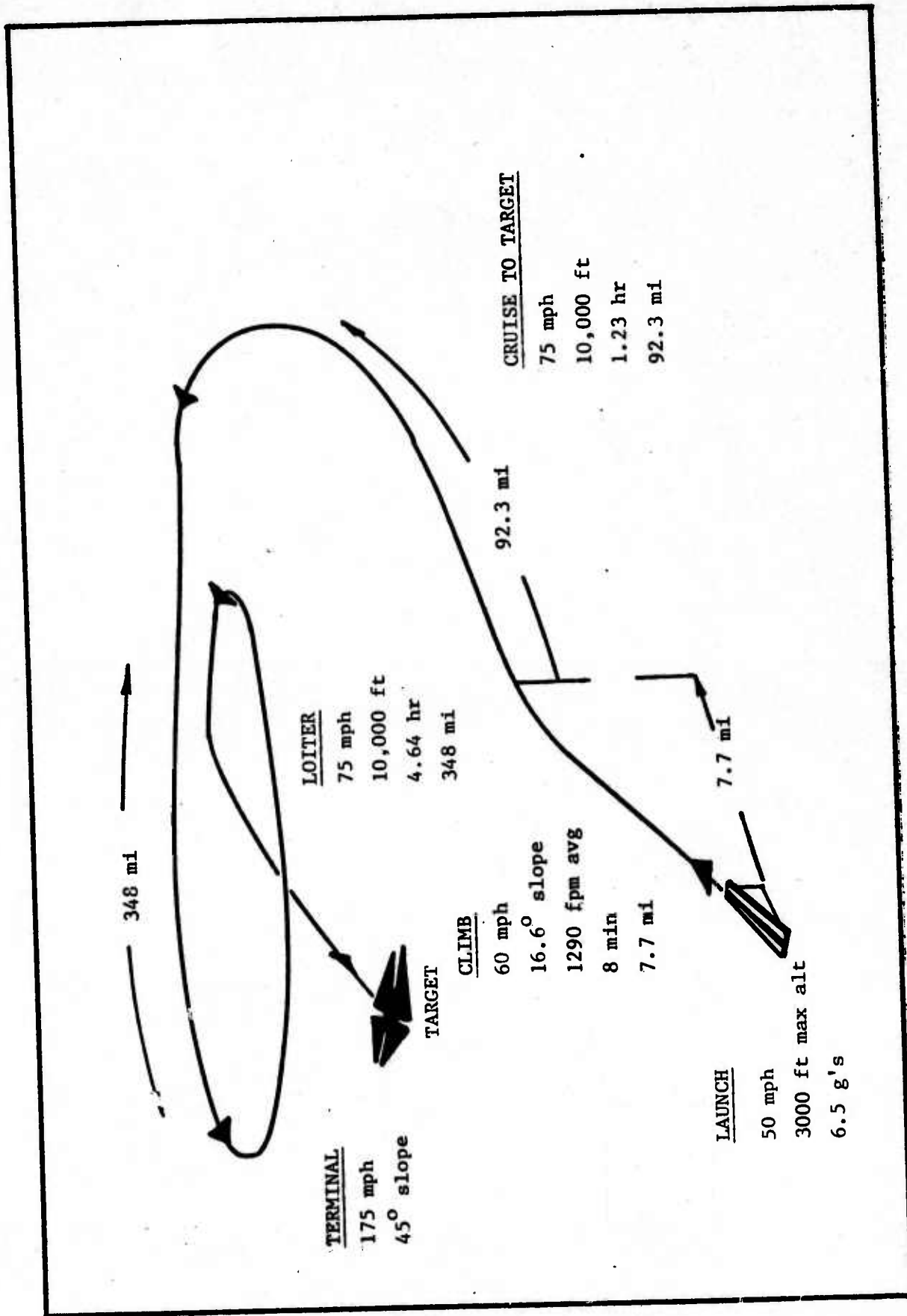


Figure A-20. Mission Profile

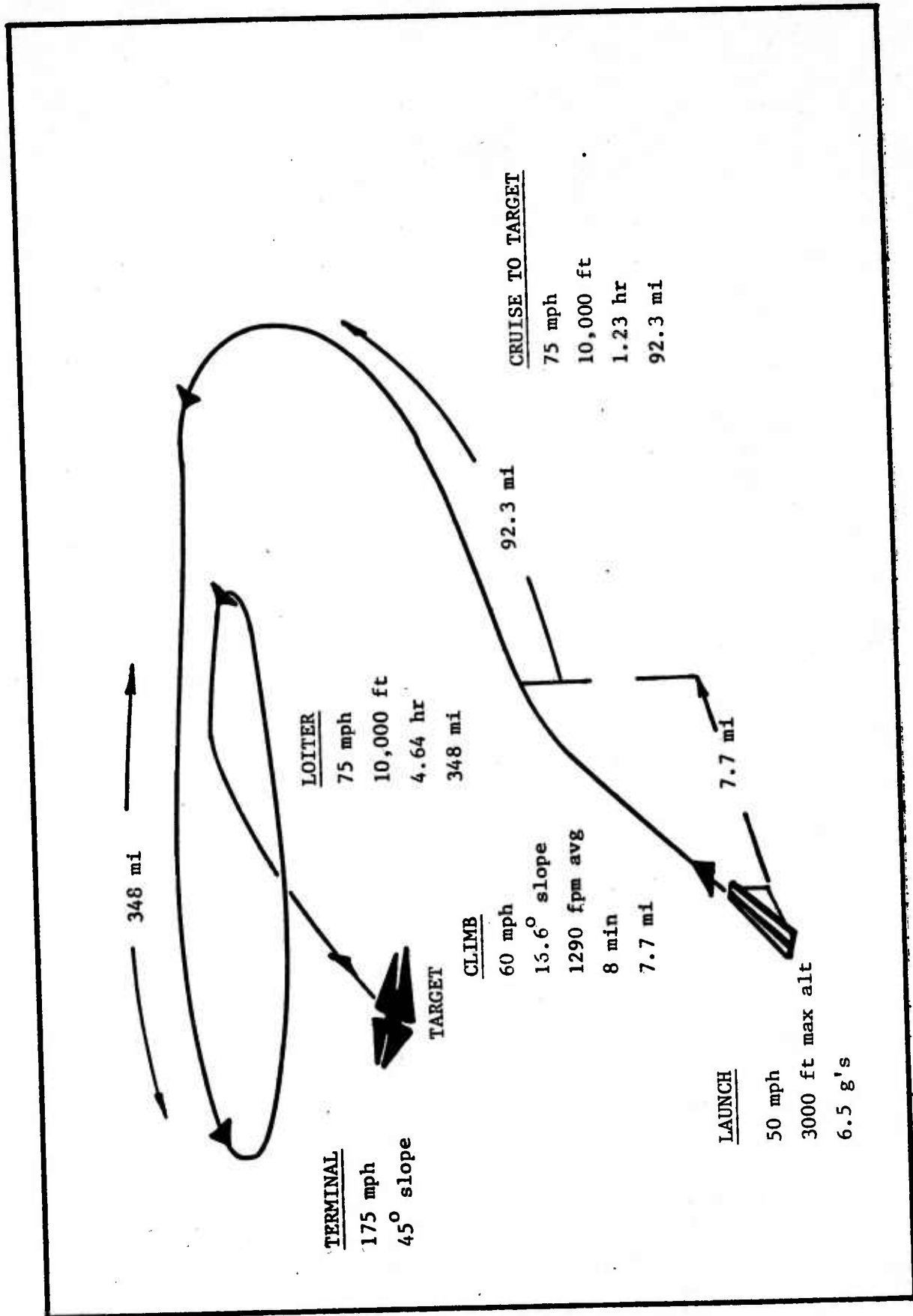


Figure A-20. Mission Profile

in Eq (A-55) since 2-cycle data is unavailable. Engine performance data is taken from calculations by Early (1975) in connection with the Teleplane XBQM-106. Available thrust horsepower,

$$THP = THP_{SL} (1.132\sigma - 0.132) \quad (A-55)$$

Required thrust horsepower,

$$THPR = 4.65 \times 10^{-6} \left\{ C_{Dpe} S v^3 + \frac{0.226}{b} \frac{Wg}{b} \right\}^2 + HP_{gen} \quad (A-56)$$

Required brake horsepower,

$$BHPR = \frac{THPR}{\eta} \quad (A-57)$$

Excess horsepower,

$$HP_{xs} = THP - THPR \quad (A-58)$$

Average excess horsepower is assumed to be a linear average of excess horsepower from 3000 feet to 10,000 feet.

$$HP_{xsavg} = \frac{1}{2} (HP_{xs3} + HP_{xs10}) \quad (A-59)$$

Rate of climb,

$$RC = \frac{33,000 HP_{xs}}{Wg} \quad (A-60)$$

Angle of Climb,

$$\theta_{CL} = \sin^{-1} \left\{ \frac{RC}{88 V} \right\} \quad (A-61)$$

Wing Characteristics.

Stall speed,

$$V_{st} = \left\{ \frac{391 Wg}{C_{L_{max}} \sigma S} \right\}^{1/2} \quad (A-62)$$

Wing area required for launch at 50 miles per hour at 3000 feet,

$$S = \frac{391 Wg}{C_{L_{max}} \sigma V^2} \quad (A-7)$$

Drag coefficient,

$$C_D = C_{Dpe} + \frac{C_L^2}{\pi e AR} \quad (A-63)$$

Lift-to drag ratio,

$$L/D = \frac{C_L}{C_D} \quad (A-64)$$

Endurance ratio,

$$\frac{L^{1.5}}{D} = \frac{C_L^{1.5}}{C_D} \quad (A-65)$$

Maximum lift-to-drag,

$$\left. \frac{L}{D} \right|_{max} = \frac{1}{2} \left\{ \frac{\pi e AR}{C_{Dpe}} \right\}^{1/2} \quad (A-66)$$

Airspeed at  $\left. \frac{L}{D} \right|_{max}$ ,

$$V = \left\{ \frac{\left( \frac{391 Wg}{S} \right)^2}{C_{Dpe} \pi e AR} \right\}^{1/2} \quad (A-67)$$

Minimum turn radius,

$$r_t = \frac{391 Wg}{Sog C_{L_{max}} \left[1 - \left(\frac{V_{st}}{V}\right)^4\right]^{1/2}} \quad (A-68)$$

Angle of incidence,

$$\alpha_i = \frac{C_{L_{cruise}}}{\alpha_{3D}} + \alpha_{LO} \quad (A-69)$$

Time and Fuel.

Time to climb,

$$t_{CL} = \frac{h}{60 RC_{avg}} \quad (A-70)$$

Fuel for climb,

$$W_f = \frac{THP C t_{CL}}{\eta} \quad (A-71)$$

Fuel for cruise,

$$W_f = W \left\{ 1 - \exp \left\{ \frac{\Gamma_{cruise} \eta}{326 C(L/D)} \right\} \right\} \quad (A-72)$$

Fuel for loiter,

$$W_f = \frac{t W V C}{400(L/D)\eta} \quad (A-73)$$

Time over target with a given remaining fuel supply,

$$t = \frac{400 W_f \eta}{W(L/D)C V} \quad (A-74)$$

The preceding equations use the following general terminology:

- AR = aspect ratio
- b = wingspan (ft)
- BHP = brake horsepower available (hp)
- BHPR = brake horsepower available (hp)
- C = specific fuel consumption (lb/hp-hr)
- $C_D$  = drag coefficient
- $C_{Dpe}$  = profile drag coefficient
- $C_L$  = lift coefficient
- $C_{Lmax}$  = maximum lift coefficient
- D = drag (lb)
- e = span efficiency factor
- g = gravitational acceleration (32.2 ft/sec<sup>2</sup>)
- h = cruise-loiter altitude (ft)
- $HP_{xs}$  = excess thrust horsepower (hp)
- $HP_{xs3}$  =  $HP_{xs}$  at 3000 ft (hp)
- $HP_{xs10}$  =  $HP_{xs}$  at 10,000 ft (hp)
- $HP_{xs_{avg}}$  = average  $HP_{xs}$  (hp)
- L = lift (lb)
- r = range (mi), turn radius (ft)
- RC = rate of climb (ft/min)
- $RC_{acg}$  = average RC (ft/min)
- S = wing area (ft<sup>2</sup>)
- t = time (hr)
- $t_{CL}$  = time to climb to h (hr)

THP = thrust horsepower available (hp)

THPR = thrust horsepower required (hp)

V = airspeed (mph)

$V_{st}$  = stall speed (mph)

W = aircraft weight (lb)

$W_f$  = fuel weight (lb)

$W_g$  = gross weight (lb)

$\alpha_i$  = wing incidence (deg)

$\alpha_{3D}$  = 3-dimensional lift curve slope ( $\text{deg}^{-1}$ )

$\alpha_{LO}$  = zero-lift angle (deg)

$\eta$  = propeller efficiency

$\sigma$  = altitude density ratio

$\theta_{CL}$  = angle of climb (deg)

Inputs to DESIGN. The labels of the variables, as listed in the program, are explained in Appendix A-6-1. The values of the input variables are listed below.

$W_g = 126$  lb (structures)  
 $CL_{max} = 1.223$  (SHRENK, Appendix A-3)  
 $S = 17$  ft<sup>2</sup> (layout)  
 $AR = 6$  (layout)  
 $e = 0.95$  (layout)  
 $C_{Dpe} = 0.03$  (layout)  
 $\alpha_{3D} = 0.08133$  deg (SHRENK)  
 $\alpha_{LO} = -2$  deg (Jacobs, 1935:17)  
 $\eta = 0.75$  (cruise and loiter) (Appendix C)  
 $\eta = 0.6$  (climb) (Appendix C)  
 $C = 1.25$  lb/bhp-hr (cruise and loiter) (Appendix C)  
 $C = 1.50$  lb/bhp-hr (climb) (Appendix C)  
 $h = 10,000$  ft (Chapter II, Volume II)  
 $t(\text{mission}) = 6$  hr (Chapter II, Volume II)  
 $r = 100$  mi (to target) (Chapter II, Volume II)  
Alternator power = 300 watts (Appendix D)  
 $v = 50$  mph (launch) (Appendix F)  
 $v = 60$  mph (climb)  
 $v = 75$  mph (cruise)

Climb speed is found by taking a compromise between climb angle and rate of climb (Appendix A-6-3). Cruise speed is taken as the highest airspeed practical without significantly adding to fuel consumption (Appendix A-6-3). This is done by taking the minimum-horsepower required point (maximum endurance) and running the airspeed up until no more than about 1/2 horsepower extra is necessary. The speed is purely arbitrary at this point, but the system analysis (Chapter II, Volume II) indicates that increasing speed increases survivability.

Outputs from DESIGN. DESIGN was built as a design tool to be used continually to update the estimates as new data and requirements came to light. The final performance parameter estimates are tabulated and plotted in Appendices (A-6-2) and (A-6-3), and the more significant parameter estimates are presented below.

Climb Angle	16.6 deg at launch
Rate-of-Climb	1290 fpm average
Cruise Brake Horsepower	2.3 hp
Fuel Weight	2.4 lb climb
	2.1 lb cruise
	18.0 lb loiter
	22.5 lb total mission
Fuel Fraction	17.9%
Time	0.13 hr climb
	1.23 hr cruise
	4.64 hr loiter
	6.0 hr total mission
Distance	7.74 mi climb
	92.25 mi cruise
	348.06 mi loiter
using 15.5 lb fuel,	2.84 hr loiter time
	212.65 mi loiter coverage

Fuel consumption sensitivity is illustrated in Appendix A-6-4.

### Cost

The airframe cost estimate is based on the structure and molding techniques discussed earlier in the structures section, pages A-37 to A-46. The estimates (Stansberry, 1975) are separated into two areas, non-recurring and recurring production costs.

The non-recurring cost is composed of the costs of die-cast molds, pouring apparatus, feed and take-away tables, and assembly equipment. The low, most-likely, and high estimates of non-recurring costs are \$202,000, \$230,000, and \$248,000, respectively.

Recurring production costs are comprised of the cost of labor to assemble, connect, and test all components of the vehicles as well as the materials and labor associated with actual airframe construction. Table A-14 illustrates the recurring component and total recurring airframe cost estimates.

TABLE A-14. RECURRING AIRFRAME COST ESTIMATES (EACH)

<u>Component</u>	<u>Low (\$)</u>	<u>Most Likely (\$)</u>	<u>High (\$)</u>
Fuselage	147	167	180
Empennage	68	77	84
Wings (2)	61	69	74
Cowling and Shroud	<u>21</u>	<u>24</u>	<u>26</u>
Total Recurring	297	337	364

## Conclusions

The basic result of the airframe design and analysis is that this configuration is indeed suitable for the class of vehicle presented. All significant design goals are met, all operating constraints are satisfied, and most listed desirable characteristics are included. The concept of a low-cost airframe common to both Type I and II vehicles is realistic. It seems unlikely that any real cost-saving can be had by constructing different airframes for each of the two types. There are some difficulties, however.

The bulk of a 126-pound vehicle indicates that there may be ground-handling problems using a two-man crew. The solution might be to add the 23 pounds of fuel while the vehicle sits on the launcher. This impacts launch rate, but it eliminates the need for a handling cart or costly weight reduction program.

The performance (and therefore fuel) estimates are based on questionable data for both fuel consumption and power output of the McCulloch MC 101 engine. The data used is reasonable; but it is clear, from many runs of DESIGN, that the fuel weight and other parameters are sensitive to engine performance (see Appendix A-6-4).

The aircraft structure presented here is the simplest scheme that seems realistic. However, the unknowns discussed in Manufacturing Techniques lead to the conclusion that further research and development efforts are required in skinned foams in this configuration. The recommendation, then, is to fund studies of this material in wing-spar combinations with major emphasis on wind-tunnel and flight testing. The alternate meshing approach should also be considered in the above tests.

In consideration of all of the assumptions and estimates made in the preceding discussions, it is advisable that they be tested by building and flying a prototype aircraft based on the proposed design. The concepts of hands-off, no-stability-augmentation flight in conjunction with this configuration can only be considered valid in the presence of some hard test results.

To recapitulate, this airframe configuration meets the design goals satisfactorily and should prove a realistic basis for cost analysis, operations, and technology; but further testing is required to validate the results.

APPENDIX A-1

AIRFOIL CHARACTERISTICS

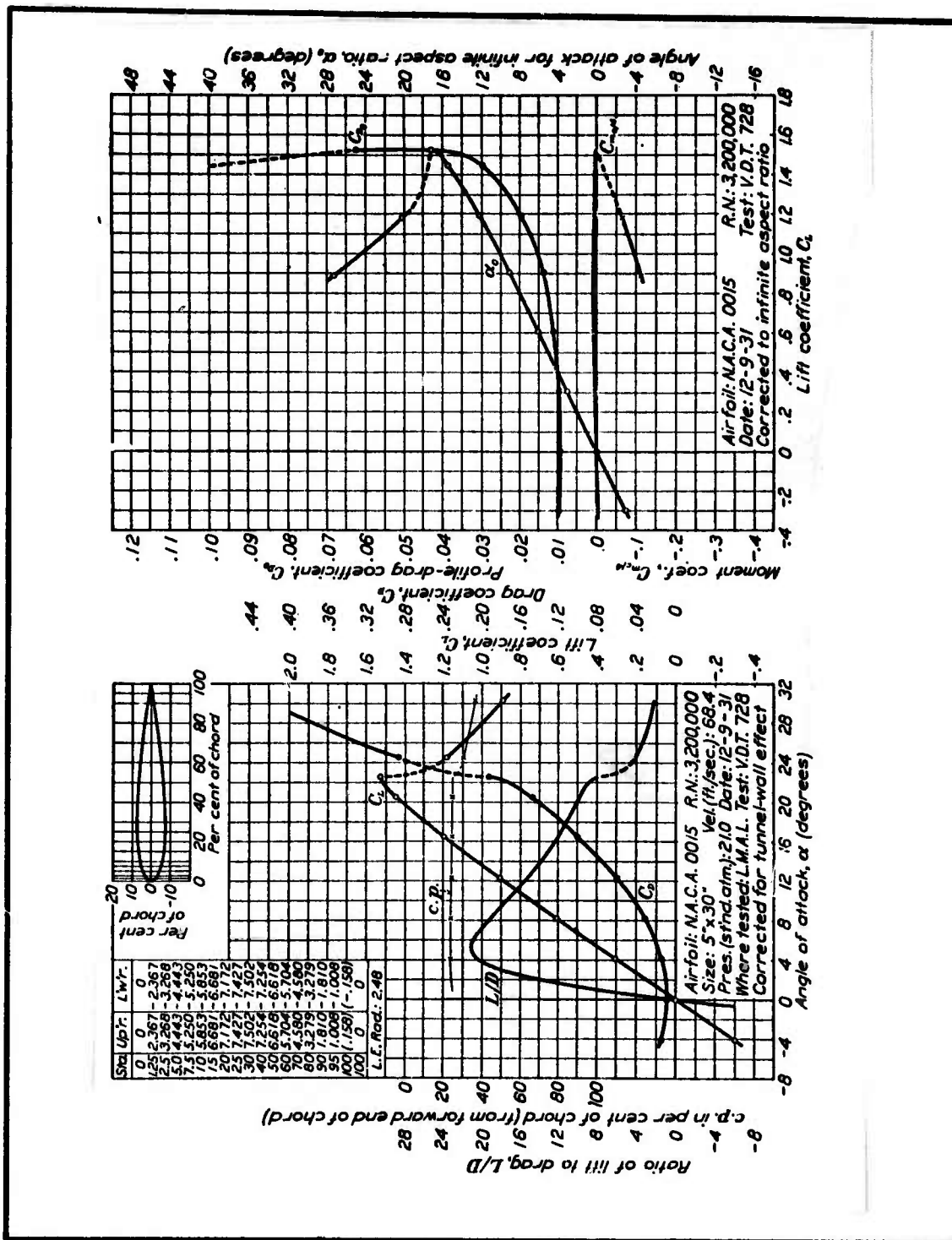


Figure A-21. NACA 2515 (Jacobs, 1935:17)

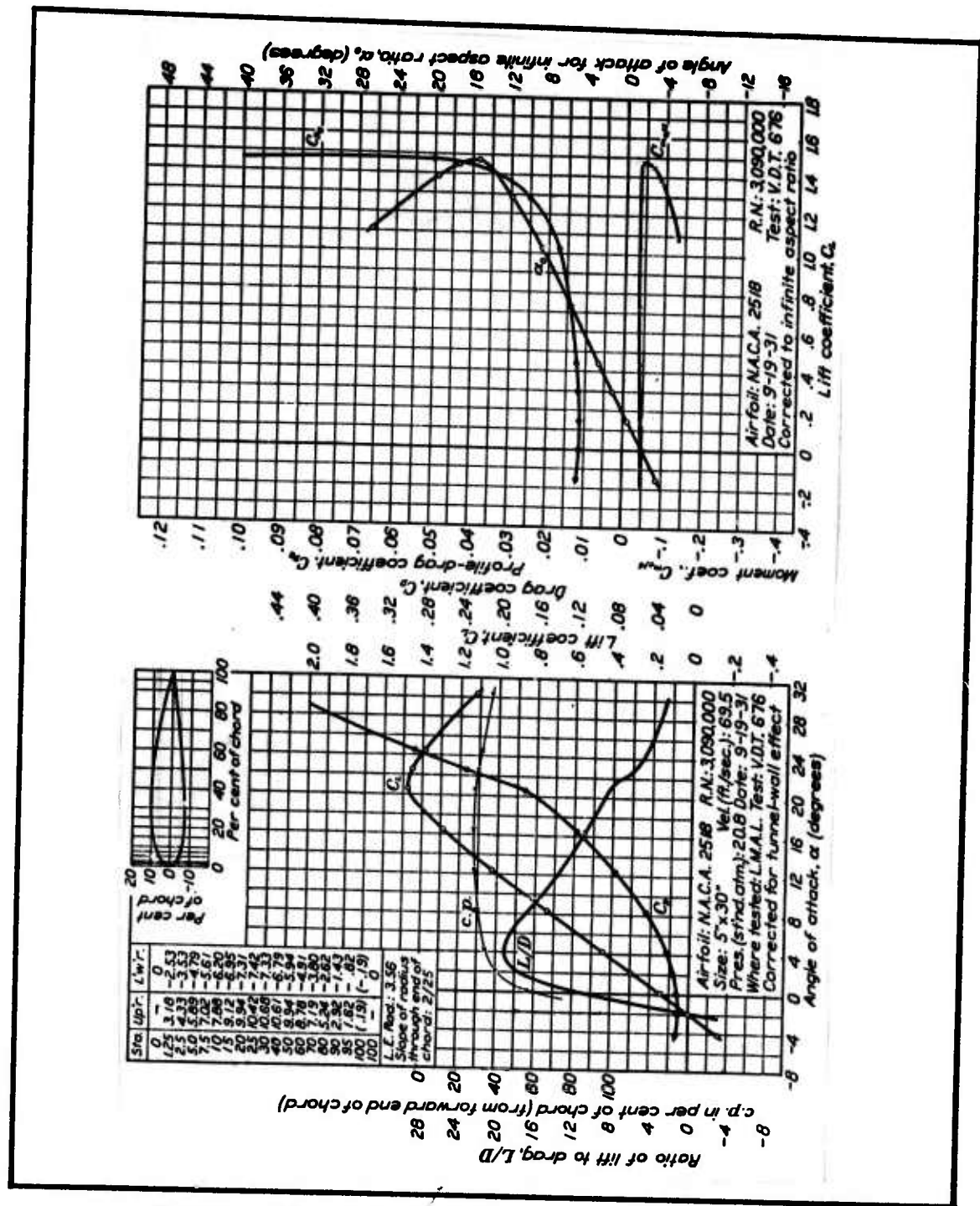


Figure A-22. NACA 2518 (Jacobs, 1935:18)

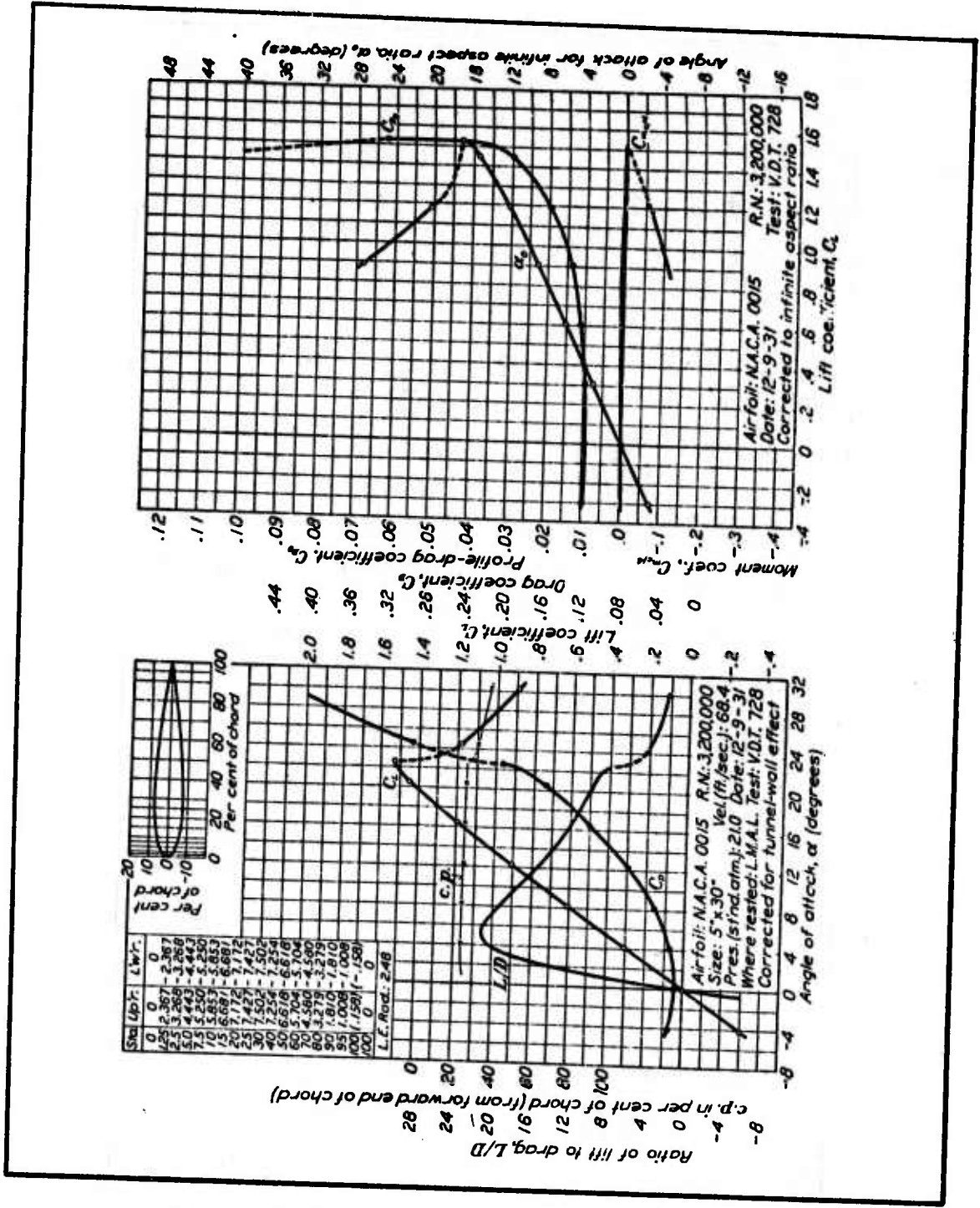


Figure A-23. NACA 0015 (NACA TR460, 1935:19)

## ASPECT RATIO EFFECTS (CDVSAR)

```

PROGRAM CDVSAR(INPUT, OUTPUT, TAPE1=INPUT, TAPE2=OUTPUT)
DIMENSION CLW(60), CNIW(60), ARW(10), B1(60), B2(60),
1 B3(60), B4(60), C0(60), A1(60), A2(60), A3(60), A4(60), C1(60), C2(60),
2 C3(60), C4(60)
DELTA=.01 $PI=4.*ATAN(1.) $CDP=.03
ARW(1)=5.
DO 500 I=1,4
PRINT(2,600)ARW(I)
CLW(1)=0.
DO 400 J=1,50
CDIW(J)=CLW(J)**2*(1.+DELTA)/(PI*ARW(I))
CD(J)=CNIW(J)+CDP
A=CLW(J)/CD(J) $C=CLW(J)**1.5/CD(J)
IF(I.EQ.1) GO TO 100 $IF(I.EQ.2) GO TO 110
IF(I.EQ.3) GO TO 120
B4(J)=CD(J) $A4(J)=A $C4(J)=C $G0 TO 300
B1(J)=CD(J) $A1(J)=A $C1(J)=C $G0 TO 300
B2(J)=CD(J) $A2(J)=A $C2(J)=C $G0 TO 300
B3(J)=CD(J) $A3(J)=A $C3(J)=C
300 CLW(J+1)=CLW(J)+.03
400 PRINT(2,700)CLW(J), CD(J), A, C
500 ARW(I+1)=ARW(I)+1.
600 FORMAT(//'"AR="',F4.0,T12,'"CL"',T22,'"C0"',T32,'"L/D"',T42,'"L1.5/D"',/)
700 FORMAT(T10,F5.3,T20,F5.3,T30,F6.3,T40,F6.3)
CALL DRAWZ(CLW,B1,B2,B3,B4,4,4,50,1,1)
CALL DRAWZ(CLW,A1,A2,A3,A4,4,4,50,1,1)
CALL DRAWZ(CLW,C1,C2,C3,C4,-4,4,50,1,1)
END

```

## APPENDIX A-2-2

## CDVSAR OUTPUT

AR= 5.	CL	CD	L/D	L1.5/D
	0.000	.030	0.000	0.000
	.030	.030	.998	.173
	.060	.030	1.985	.486
	.090	.031	2.949	.885
	.120	.031	3.880	1.344
	.150	.031	4.770	1.847
	.180	.032	5.610	2.380
	.210	.033	6.396	2.931
	.240	.034	7.121	3.489
	.270	.035	7.784	4.045
	.300	.036	8.383	4.592
	.330	.037	8.918	5.123
	.360	.038	9.391	5.635
	.390	.040	9.804	6.123
	.420	.041	10.159	6.584
	.450	.043	10.460	7.017
	.480	.045	10.711	7.421
	.510	.047	10.915	7.795
	.540	.049	11.077	8.140
	.570	.051	11.200	8.456
	.600	.053	11.289	8.745
	.630	.056	11.347	9.007
	.660	.058	11.378	9.243
	.690	.061	11.384	9.456
	.720	.063	11.369	9.647
	.750	.066	11.335	9.816
	.780	.069	11.285	9.967
	.810	.072	11.221	10.099
	.840	.075	11.145	10.215
	.870	.079	11.059	10.315
	.900	.082	10.965	10.402
	.930	.086	10.863	10.476
	.960	.089	10.755	10.538
	.990	.093	10.643	10.590
	1.020	.097	10.527	10.631
	1.050	.101	10.407	10.664
	1.080	.105	10.286	10.689
	1.110	.109	10.163	10.707
	1.140	.114	10.039	10.718
	1.170	.118	9.914	10.723
	1.200	.123	9.789	10.723
	1.230	.127	9.664	10.718
	1.260	.132	9.540	10.708
	1.290	.137	9.410	10.695
	1.320	.142	9.294	10.677
	1.350	.147	9.172	10.657
	1.380	.152	9.052	10.634
	1.410	.158	8.934	10.608
	1.440	.163	8.817	10.580
	1.470	.169	8.701	10.550

AR= 6.	CL	CD	L/D	L1.5/D
	0.000	.030	0.000	0.000
	.030	.030	.998	.173
	.060	.030	1.987	.487
	.090	.030	2.957	.887
	.120	.031	3.900	1.351
	.150	.031	4.807	1.862
	.180	.032	5.672	2.406
	.210	.032	6.489	2.974
	.240	.033	7.254	3.554
	.270	.034	7.963	4.138
	.300	.035	8.615	4.719
	.330	.036	9.209	5.290
	.360	.037	9.744	5.847
	.390	.038	10.223	6.384
	.420	.039	10.646	6.899
	.450	.041	11.016	7.390
	.480	.042	11.335	7.853
	.510	.044	11.608	8.289
	.540	.046	11.836	8.697
	.570	.047	12.023	9.077
	.600	.049	12.173	9.429
	.630	.051	12.289	9.754
	.660	.053	12.373	10.052
	.690	.056	12.430	10.325
	.720	.058	12.462	10.574
	.750	.060	12.471	10.800
	.780	.063	12.460	11.005
	.810	.065	12.432	11.189
	.840	.068	12.388	11.354
	.870	.071	12.331	11.501
	.900	.073	12.261	11.632
	.930	.076	12.182	11.748
	.960	.079	12.094	11.849
	.990	.083	11.998	11.938
	1.020	.086	11.895	12.014
	1.050	.089	11.788	12.079
	1.080	.092	11.676	12.134
	1.110	.096	11.560	12.179
	1.140	.100	11.442	12.216
	1.170	.103	11.321	12.245
	1.200	.107	11.198	12.267
	1.230	.111	11.075	12.282
	1.260	.115	10.950	12.291
	1.290	.119	10.825	12.295
	1.320	.123	10.700	12.294
	1.350	.128	10.575	12.288
	1.380	.132	10.451	12.277
	1.410	.137	10.328	12.263
	1.440	.141	10.205	12.246
	1.470	.146	10.083	12.225

AR= 7.	CL	CD	L/D	L1.5/D
	0.000	.030	0.000	0.000
	.030	.030	.999	.173
	.060	.030	1.989	.487
	.090	.030	2.963	.889
	.120	.031	3.914	1.356
	.150	.031	4.834	1.872
	.180	.031	5.716	2.425
	.210	.032	6.557	3.005
	.240	.033	7.352	3.602
	.270	.033	8.096	4.207
	.300	.034	8.789	4.814
	.330	.035	9.428	5.416
	.360	.036	10.013	6.008
	.390	.037	10.545	6.585
	.420	.038	11.023	7.144
	.450	.039	11.450	7.681
	.480	.041	11.828	8.195
	.510	.042	12.159	8.683
	.540	.043	12.445	9.145
	.570	.045	12.689	9.580
	.600	.047	12.894	9.988
	.630	.048	13.063	10.368
	.660	.050	13.198	10.722
	.690	.052	13.303	11.051
	.720	.054	13.381	11.354
	.750	.056	13.433	11.633
	.780	.058	13.462	11.889
	.810	.060	13.470	12.123
	.840	.062	13.460	12.336
	.870	.065	13.434	12.530
	.900	.067	13.393	12.705
	.930	.070	13.339	12.863
	.960	.072	13.273	13.005
	.990	.075	13.198	13.131
	1.020	.078	13.113	13.244
	1.050	.081	13.022	13.343
	1.080	.084	12.923	13.430
	1.110	.087	12.819	13.506
	1.140	.090	12.711	13.571
	1.170	.093	12.598	13.627
	1.200	.096	12.482	13.674
	1.230	.099	12.364	13.712
	1.260	.103	12.243	13.743
	1.290	.106	12.121	13.767
	1.320	.110	11.997	13.784
	1.350	.114	11.873	13.795
	1.380	.117	11.748	13.801
	1.410	.121	11.623	13.802
	1.440	.125	11.498	13.798
	1.470	.129	11.374	13.790

AR= 8.	CL	CO	L/D	L1.5/D
	0.000	.030	0.000	0.000
	.030	.030	.999	.173
	.060	.030	1.990	.488
	.090	.030	2.968	.890
	.120	.031	3.924	1.359
	.150	.031	4.854	1.880
	.180	.031	5.750	2.440
	.210	.032	6.610	3.029
	.240	.032	7.427	3.638
	.270	.033	8.199	4.260
	.300	.034	8.924	4.888
	.330	.034	9.600	5.515
	.360	.035	10.225	6.135
	.390	.036	10.800	6.744
	.420	.037	11.324	7.339
	.450	.038	11.799	7.915
	.480	.039	12.226	8.471
	.510	.040	12.607	9.003
	.540	.042	12.944	9.512
	.570	.043	13.238	9.995
	.600	.044	13.493	10.452
	.630	.046	13.711	10.882
	.660	.048	13.893	11.287
	.690	.049	14.044	11.665
	.720	.051	14.164	12.019
	.750	.053	14.257	12.347
	.780	.054	14.325	12.652
	.810	.056	14.370	12.933
	.840	.058	14.394	13.193
	.870	.060	14.400	13.431
	.900	.063	14.388	13.650
	.930	.065	14.361	13.850
	.960	.067	14.321	14.031
	.990	.069	14.268	14.196
	1.020	.072	14.204	14.345
	1.050	.074	14.131	14.480
	1.080	.077	14.049	14.600
	1.110	.080	13.960	14.708
	1.140	.082	13.864	14.803
	1.170	.085	13.763	14.887
	1.200	.088	13.657	14.960
	1.230	.091	13.547	15.024
	1.260	.094	13.433	15.078
	1.290	.097	13.316	15.124
	1.320	.100	13.197	15.162
	1.350	.103	13.076	15.193
	1.380	.107	12.954	15.217
	1.410	.110	12.830	15.235
	1.440	.113	12.706	15.247
	1.470	.117	12.581	15.254

APPENDIX A-2-3

CDVSAR PLOTS

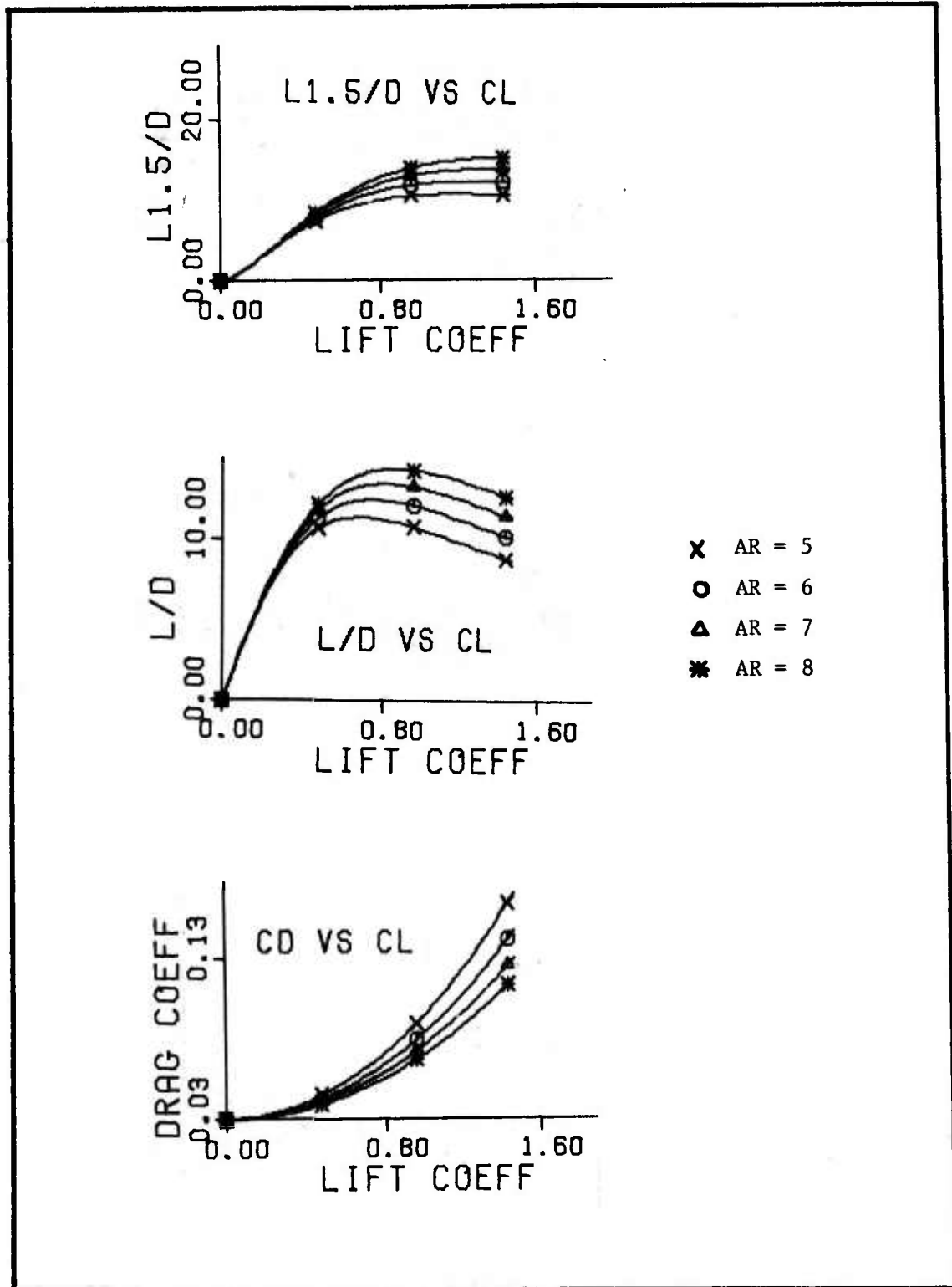


Figure A-24. Aspect Ratio Effects

APPENDIX A-3-1

WING DESIGN (SCHRENK)

```

PROGRAM SCHRENK(INPUT, OUTPUT, TAPE9=INPUT)
DIMENSION C(51), YBAR(51), TOC(51), CLB(51), CCLB(51), CLAI(51),
+CCLAI(51), CLMR(51), CLX(51), EPS0(51), T(51), TI(51), CL(7),
+CCL(7), X(7), CLMAX(51), Y(51), YI(51), CI(51), CL1(51)
DIMENSION EP(20), YB(20), CLMY(20), XC(20), VEL(30)
REAL LAMBDA, MAC, MACI
DATA PI/3.14159265359/

C      RRAD = PI/180.
C      PI2 = PI**2
C      PIT2 = PI**2.

C      FOR A SINGLE GIVEN WING, TWIST, AND AIRSPEED...SET LP=0
C      LP=0

C      C1 = 4./((3.*SQRT(3.))
1 READ 2, S, A, LAMBDA, CLMAXR, CLMAXT, ALFALOP, ALFALOT, TOCR, TOCT,
+EPSTU0, EPSTL, ROOTSEC, TIPSEC, VEL(1), WG, SIGMA
IF(EOF(9)) 3, 8
8 EPS=EPSTL $MP=0

C      7 NN=1 $XC(1)=0.
      LL=0 $LM=0
      EPSTL=EPS
      IF(EOF(9)) 3, 4

C      4 OPL = 1. + LAMBDA
      OPL2 = OPL**2
      OPLPL2 = OPL + LAMBDA**2
      V=VEL(NN)*5280./3500.
      OML = 1. - LAMBDA
      C2 = (1. + 2.*LAMBDA)/(3.*OPL)
      C3 = 2.*LAMBDA/OPL
      C4 = 2.*OPL/PI
      C5 = 4.*SQRT(S/A)/PI

```

```

TAU = TOCT/TOCR
OMTL = 1. - TAU*LAMBDA
B = SORT(A*S)
BI = 12.*B
BO2 = B/2.
RO22 = BO2**2
RSOA = SORT(S/A)
CR = 2.*RSOA/OPL
CPI = 12.*CR
TR = CR*TOCP
TRI = 12.*TR
CT = CR*LAMBDA
CTI = 12.*CT
TT = CT*TOCT
TTI = 12.*TT
MAC = (2.*OPLPL2/(3.*OPL2) + 16./(3.*PI2))*RSOA
MACI = MAC*12.
YBARMAC = 0.5*(C2 + 4./(3.*PI))
YMAC = BO2*YBARMAC
YMACI = 12.*YMAC
TOCMAC = TOCR*(1. - OMTL*YBARMAC)/(1. - OMTL*YBARMAC)
TMAC = MAC*TOCMAC
TMACI = 12.*TMAC
ACR = PIT2*(1. + C1*TOCR)/(1. + (C1*TOCR)**2)
ACT = PIT2*(1. + C1*TOCT)/(1. + (C1*TOCT)**2)
ACRARR = (ACR + LAMBDA*AJT)/OPL
ACRARRD = AOBARRRAD
GTAU = 0.001 + 0.07*(A/16.)**2
E = (CT + SORT((OML*CR/4)**2 + RO22) + SQRT((3.*OML*CR/4)**2 +
+BO22))/R
A3 = AOBARR/(E + AOBARR*(1. + 5TAU)/(PI*A))
A3D = A3*RRAD
EPSTU = EPSTU0 + ALFALOR - ALFALOT
ALFALOW = C3*EPSTU + C2*EPSTL
IF(LP.EQ.0) PRINT 6

```

```

00 10 I = 1,51
YBAR(I) = 0.02*(I-1)
Y(I) = 802*YBAR(I)
YI(I) = 12.*Y(I)
TOC(I) = TOCR*(1. - OML*YBAR(I))/(1. - OML*YBAR(I))
C(I) = CR*(1. - OML*YBAR(I))
CI(I) = 12.*C(I)
Y(I) = YOC(I)*C(I)
YI(I) = 12.*Y(I)
AD = PIT2*(1. + C1*TOC(I))/(1. + (C1*TOC(I))**2)
ADD = A0*RPAD
EPS0(I) = (EPSTL + EPSTU*CT/C(I))*YBAR(I)
IF (I - 46) 11, 11, 12
11 CLR(I) = 0.5*ADD*(EPS0(I) - ALFALOW)
CCLR(I) = C(I)*CLR(I)
CLA1(I) = 0.5*A0/A0BAR*(1. + C4*SQRT(1. - YBAR(I)**2)/(1. - OPL*
+YBAR(I)))
CCLA1(I) = C(I)*CLA1(I)
CL1(I) = CLA1(I) + CLB(I)
GO TO 13
12 CLB(I) = CLB(46)*(1. - 100.*(YBAR(I) - YBAR(46))**2)
CCLR(I) = C(I)*CLB(I)
CLA1(I) = CLA1(46)*(1. - 100.*(YBAR(I) - YBAR(46))**2)
CCLA1(I) = C(I)*CLA1(I)
CL1(I) = CLA1(I) + CLR(I)
13 IF(TOC(I) - 0.12) 31,31,32
31 CLMAX(I)=1.60-0.57*((0.12-TOC(I))/0.06)**2
GO TO 33
32 CLMAX(I)=1.60-0.22/0.09*(TOC(I)-0.12)
33 CLMR(I) = CLMAX(I)*(0.0021312873*V*C(I))**0.125
CLX(I) = CLMR(I)/CL1(I) + (CLMR(I)/CL1(I) - 1.)*CLB(I)/CL1(I)
IF(LP.NE.0) GO TO 10
PRINT 14, I, YBAR(I), Y(I), YI(I), C(I), CI(I), TOC(I), Y(I), YI(I)
10 CONTINUE

```

```

IF(LP.NE.0) GO TO 40
PRINT 17
DO 18 I = 1,51
18 PRINT 19, I, EPS0(I), CCLB(I), CLR(I), CCLAI(I), CLAI(I), CL(I),
+CLMP(I), CLX(I)
40 SMALL = ABS(CLX(1))
J = 1

00 15 K = 2,50
IF(CLX(K) .GT. SMALL) GO TO 15
SMALL = ABS(CLX(K))
J = K
15 CONTINUE
YBARX = 0.02*(J-1)
IF(LP.NE.0) GO TO 50
00 20 K = 1,2
PRINT 21
00 20 I = 1,51
00 30 J = 1,7
X(J) = 0.1*(J-1) + 0.7*(K-1)
CCL(J) = X(J)*CCLAI(I) + CCLB(I)
30 CL(J) = CCL(J)/C(I)
PRINT 22, I, X(L), CCL(L), CL(L), L = 1,7)
20 CONTINUE

IF(NN.NE.1) GO TO 51
IF(LL.NE.0) GO TO 52
IF(MP.NE.0) GO TO 52
MP=1
PRINT 5, ROOTSEC, TIPSEC, S, A, B, BI, CR, CRI, TR, TPI, CT, CII,
+TT, TTI, MAC, MACI, TMAC, TMACI, YBARMAC, YMAC, YMACI, AOR, AOT,
+AOBAR,A3,A3D,ALFALOW,TOCR,TOCT,VEL(1),EPSTU,EPSTL,CLMAXP,CLMPXT
52 PRINT 16, YBARX, SMALL,EPSTL

51 IF(LP.E0.0) GO TO 1
IF(MN-1) 45,45,55
45 EP(LL)=-EPSTL $YR(LL)=YBARX $CLMX(LL)=SMALL
IF(SMALL-XC(NN)) 43,43,42

```

C

C

C

```

42 MM=LL      $XC(NN)=SMALL
43 LL=LL+1
   EPSTL=EPSTL-0.5

C
   IF(LL.LE.15) GO TO 4
   VTO=SQRT(391.*WG/(XC(NN)*SIGMA*S))
   IF (ABS(VTO-VEL(NN)).LE.(0.5)) GO TO 54
   PRINT 41,VEL(NN),XC(NN),EP(1M),VTO
   VEL(NN)=VTO
   GO TO 7
54 PRINT 41,VEL(NN),XC(NN),EP(MM),VTO
   CALL DRAWZ(FP,CLMX,DUM,DUM,-1,1,15,1,1)
   GO TO 60
55 PRINT 56, VFL(NN)
   XC(NN)=SMALL
60 GO TO 1

C
2 FORMAT(F10.4, F5.2, 3F5.3, 2F5.2, 2F5.3, 2F5.2, 2A10/3F10.5)
5 FORMAT(//, "AIRFOIL AT THE ROOT = ", A10, /, "AIRFOIL AT THE TIP
+=", A10 / "WING AREA-SQ.FT. = ", F10.4, /, "ASPECT RATIO = ",
+F5.2, /, "SPAN-FT. = ", F7.3, /, "SPAN-IN. = ", F8.3, /, "ROOT
+CHORD-FT. = ", F6.3, / "ROOT CHORD-IN. = ", F7.3, /, "ROOT THICKNE
+SS-FT. = ", F6.3, /, "ROOT THICKNESS-IN. = ", F7.3, /, "TIP CHOR
+D-FT. = ", F6.3, /, "TIP CHORD-IN. = ", F7.3, / "TIP THICKNESS-FT.
+=", F6.3, /, "TIP THICKNESS-IN. = ", F7.3, /, "MAC-FT. = ", F6.
+3, /, "MAC-IN. = ", F7.3, /, "MAC THICKNESS-FT. = ", F6.3, / "MAC
+THICKNESS-IN. = ", F7.3, /, "YBARMAC = ", F8.6, /, "Y AT MAC-FT.
+=", F9.6, /, "Y AT MAC-IN. = ", F9.5, / "A0R-/RAD. = ", F9.6, /,
+"A0T-/RAD. = ", F9.6, /, "A0BAR-/RAD. = ", F9.6, /, "A3-/RAD. =
+", F9.6, /, "A3D-/DEG. = ", F9.7, / "ANGLE OF ZERO LIFT-DEG. =
+", F9.6, /, "T/C AT ROOT = ", F5.3, /, "T/C AT TIP = ", F5.3, /,
+"AIRSPEED (MPH)=", F8.3, / "EPSTU-DEG. = ", F9.6, /, "EPSTL-DEG. = ",
+F9.6, /, "CLMAX ROOT = ", F9.7, /, "CLMAX TIP = ", F9.7, //)

```

CHORD-FT. CHORD-

```

6 FORMAT( /, " I YRAP Y-FT. Y-IN.
+IN. T/C THICK.-FT. THICK.-IN.", /)
14 FORMAT(1H , I2, 2X, F4.2, 2X, 7(F10.7, 2X)) CCLA1
17 FORMAT( /, " I EPS0 CCLB CLX", /)
+ CCLA1 CLMP CLB
19 FORMAT(1H , I2, 2X, 8(F10.7, 2X))
21 FORMAT(//, " I X CCL CL CCL X CCL X CCL X
+ CL X CCL CL X CCL X CCL X CCL X CCL X
+ CCL CL", /)
22 FORMAT(1H , I2, 1X, 7(F4.2, 1X, F6.3, 1X, F6.4, 1X))
16 FORMAT( /, "YRAP FOR CLMAX = ", F5.3, /,
+ COEFFICIENT = ", F9.7, /, "GEOM TWIST=", F9.5)
41 FORMAT(//, " AND OCCURS AT WASHOUT ANGLE OF ", F9.3, " DEG", /,
+ "SPEED IS ", F10.3, "MPH", /, "*****", /,
56 FORMAT( "AT", F9.4, " MPH", /, /)
3 STOP
END

```

## APPENDIX A-3-2

## SHRENK OUTPUT

AIRFOIL AT THE ROOT = NACA--2515  
AIRFOIL AT THE TIP = NACA--2518  
WING AREA-SQ.FT. = 17.0000  
ASPECT RATIO = 6.00  
SPAN-FT. = 10.100  
SPAN-IN. = 121.194  
ROOT CHORD-FT. = 2.244  
ROOT CHORD-IN. = 26.932  
ROOT THICKNESS-FT. = .337  
ROOT THICKNESS-IN. = 4.040  
TIP CHORD-FT. = 1.122  
TIP CHORD-IN. = 13.466  
TIP THICKNESS-FT. = .202  
TIP THICKNESS-IN. = 2.424  
MAC-FT. = 1.782  
MAC-IN. = 21.389  
MAC THICKNESS-FT. = .282  
MAC THICKNESS-IN. = 3.386  
YBARMAC = .434429  
Y AT MAC-FT. = 2.193758  
Y AT MAC-IN. = 26.32510  
ADR-/RAD. = 6.916485  
ADT-/RAD. = 7.019043  
ADBAR-/RAD. = 6.950671  
A3-/RAD. = 4.660119  
A3D-/DEG. = .0813344  
ANGLE OF ZERO LIFT-DEG. = -1.777778  
T/C AT ROOT = .150  
T/C AT TIP = .180  
AIRSPEED (MPH) = 50.000  
EPSTU-DEG. = 0.000000  
EPSTL-DEG. = -4.000000  
CLMAX ROOT = 1.3000000  
CLMAX TIP = 1.2500000

YBAR FOR CLMAX = .420  
WING MAXIMUM LIFT COEFFICIENT = 1.2198276  
GEOM TWIST = -4.00000

SCHRENK PLOT

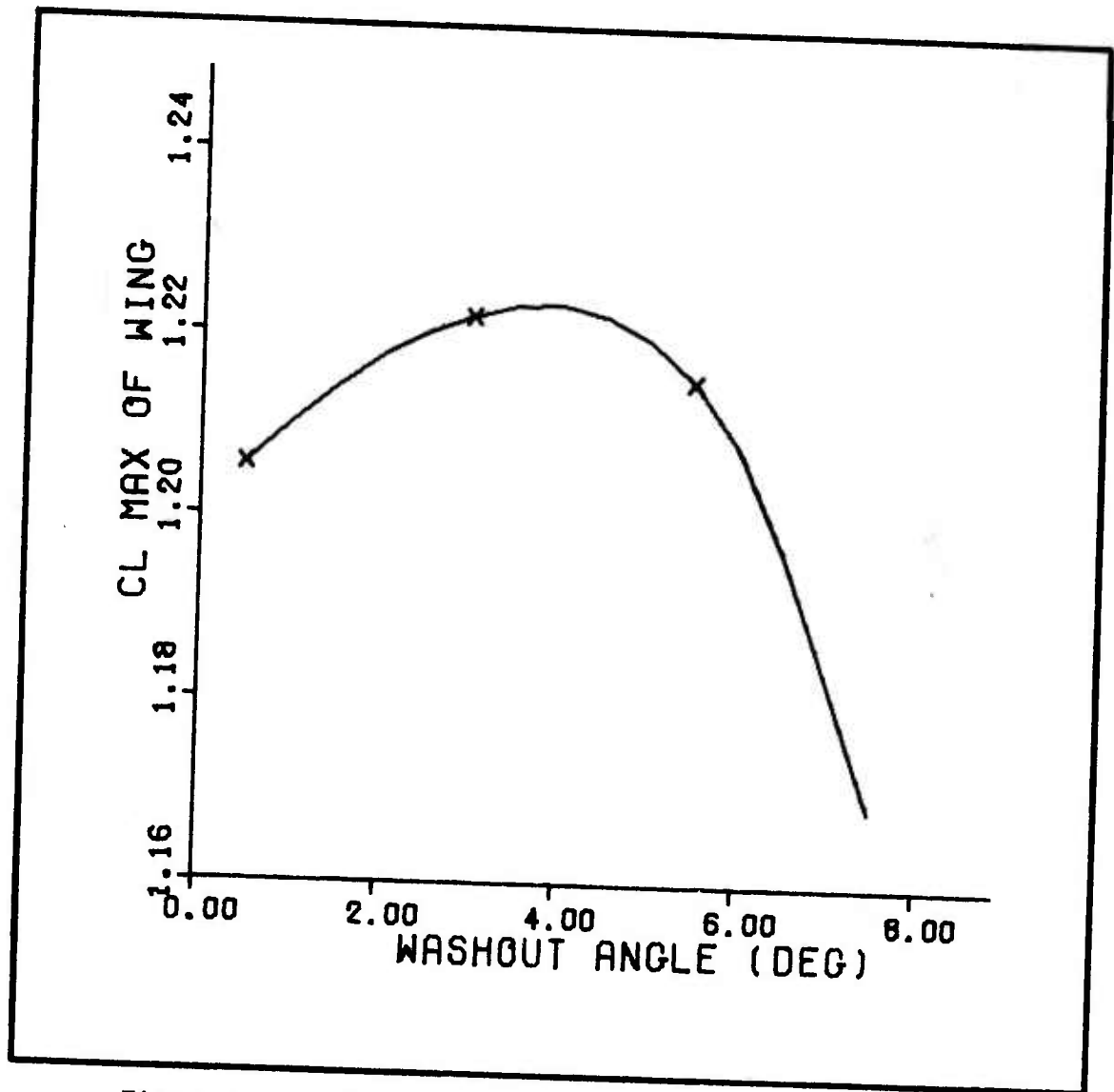


Figure A-25. Maximum Lift Coefficient vs Washout Angle

## APPENDIX A-4-1

## FUSELAGE CROSS-SECTION (FUSLAG)

```

PROGRAM FUSLA J(INPUT, OUTPUT, TAPES=INPUT, TAPES=OUTPUT)
DIMENSION X(250), Y(250), R(250)
A=5.5 $R=5.5 $C=2.67 $DEL=8/50.
XROX=3.5 $YBOX=3.5 $XLNTH=28.
RMAX=0. $J=1 $I=1 $PI=I
RBOX=SQRT(XBOX**2+YBOX**2)
50 RI=I
X(I)=A*(ABS(1.- (ABS(Y(I)/R)**C))**(1./C))
IF(J.EQ.0) GO TO 100
Y(I+1)=Y(I)+DEL
IF(I.GE.50.AND.I.LE.150) J=0
GO TO 200
100 X(I)=-X(I)
Y(I+1)=Y(I)-DEL
IF(I.GE.150) J=1
200 R(I)=SQRT(ABS(X(I))**2+ABS(Y(I))**2)
IF(R(I).GT.RMAX) L=I
RMAX=R(L)
XMAX=ABS(X(L))
YMAX=ABS(Y(L))
DIFF=RMAX-RBOX
IF(I.GT.200) GO TO 300
PRINT*, " I=", I, " X=", X(I), " Y=", Y(I)
I=I+1
GO TO 50
300 PRINT*, " DIFF=", DIFF, " XM=", XMAX, " YM=", YMAX
X(0)=5. $CIRCUM=0.
DO 400 I=1,50
DLTA=SQRT(DEL**2+ABS(X(I)-X(I+1))**2)
CIRCUM=CIRCUM+DLTA
CIRCUM=CIRCUM*4.
AREA=CIRCUM*XLNTH
PRINT*, " CIRCUM=", CIRCUM, " AREA=", AREA, "
CALL DRAWZ(Y, X, DUM, DUM, -1, 1, 200, 1, 1)
STOP $END
LENGTH=", XLNTH

```

FUSLAG PLOT

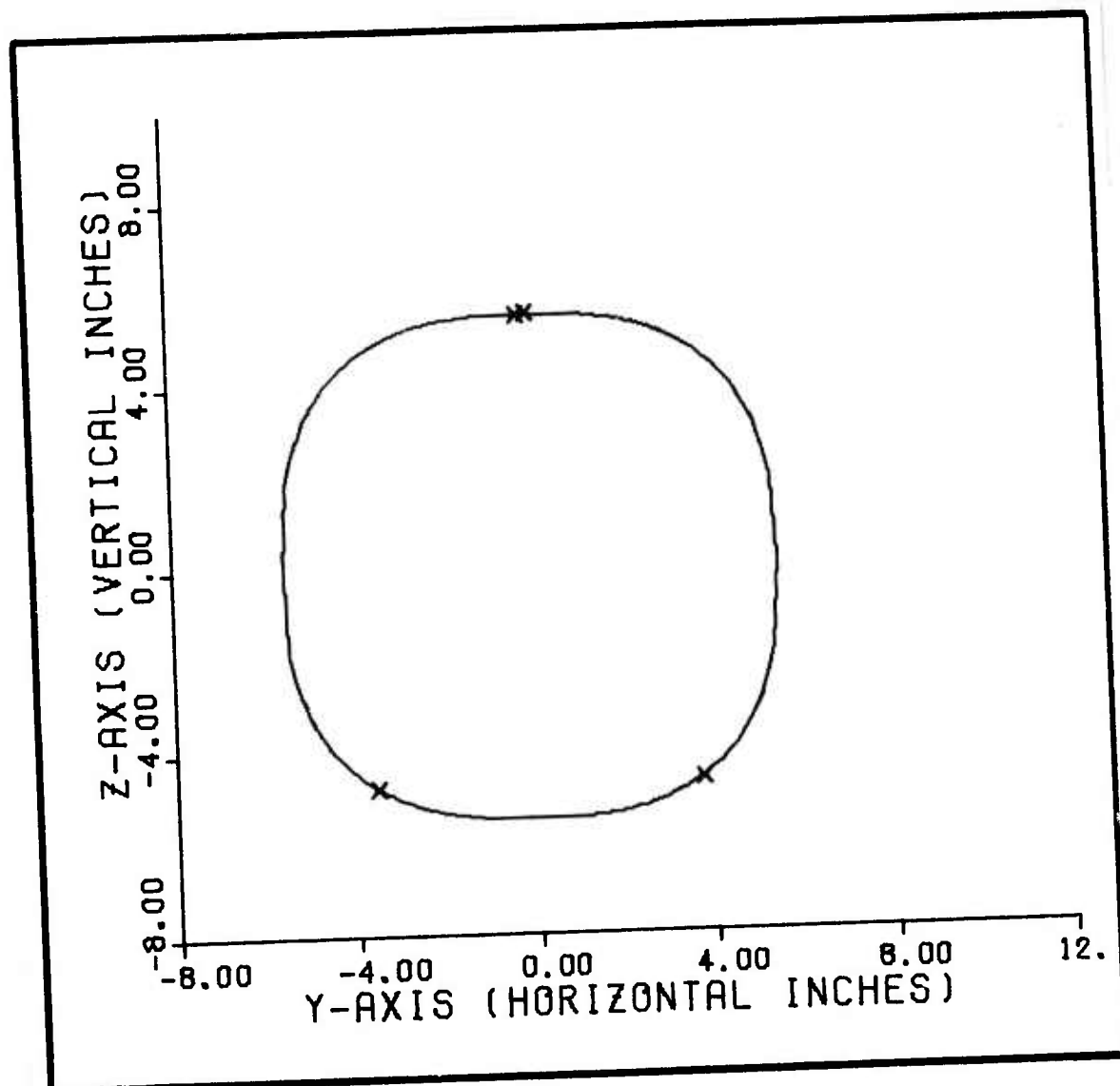


Figure A-26. Fuselage Section

## WEIGHT AND BALANCE (WTNBAL)

```

PROGRAM WTNBAL(INPUT, OUTPUT, TAPE1=INPUT, TAPE2=OUTPUT)
REAL MOMX, MOMY, MOMZ, MASS, IX, IY, IZ, I7, I8, I9
DIMENSION X(50), Y(50), Z(50), A(50), B(50), WT(50)
DIMENSION XG(60), YG(60), ZG(60), WF(60)

C SET INM= NUMBER OF ITEMS INPUT
C INM=23
C
K=1 $HTNK=7. $DGAS=42./12./144. $WTNK=7. $L=1
WRITE(2, 107)
500 DO 108 I=1, INM
READ(1, 105) A(I), B(I), WT(I), X(I), Y(I), Z(I)
IF (EOF(1)) 150, 111
111 MW1=WT(1) $ZZ1=Z(1)
108 WRITE(2, 100) A(I), B(I), WT(I), X(I), Y(I), Z(I)
ATNK=WT(1)/DGAS/HTNK
TNKL=ATNK/WTNK
PRINT 1000, WT(1), HTNK, WTNK, TNKL, ATNK
120 IF (L.EQ.1) GO TO 130
WT(2)=0.
Z(1)=ZZ1 $WT(1)=MW1
DO 160 I=1, INM
160 WRITE(2, 400) A(I), B(I), WT(I), X(I), Y(I), Z(I)
130 WRITE(2, 200)
DELWF=WT(1)/50.
DELH=DELWF/DGAS/ATNK
110 TOTWT=MOMX=MOMY=MOMZ=0.0
DO 109 I=1, INM
MOMX=MOMX + WT(I)*X(I)
MOMY=MOMY + WT(I)*Y(I)
MOMZ=MOMZ + WT(I)*Z(I)
109 TOTWT=TOTWT + WT(I)
TWTLBS=TOTWT
XCG=MOMX/TOTWT
YCG=MOMY/TOTWT
ZCG=MOMZ/TOTWT

```

```

XG(K)=XCG
YG(K)=YCG
ZG(K)=ZCG
WF(K)=WT(1)
IX=IY=IZ=IX7=0.0
DO 101 I=1,INM
MASS=(WT(I))/32.174
IXZ=IXZ-MASS*(X(I)-XCG)*(Z(I)-ZCG)+((Z(I)-ZCG)*(Z(I)-ZCG))
IX=IX+MASS*((Y(I)-YCG)*(X(I)-XCG))+((Z(I)-ZCG)*(Z(I)-ZCG))
IY=IY+MASS*((X(I)-XCG)*(X(I)-XCG))+((Y(I)-YCG)*(Y(I)-YCG))
IZ=IZ+MASS*((X(I)-XCG)*(X(I)-XCG))+((Y(I)-YCG)*(Y(I)-YCG))
WRITE(2,300) K,TMTLBS,WT(1),Z(1),XCG,YCG,ZCG
IF(L.GT.1) GO TO 50
Z(1)=Z(1)-DELH
WT(1)=WT(1)-DELWF
K=K+1
IF(K.LE.50) GO TO 110
CALL DRAW7(WF,ZG,XG,DUM,DUM,-2,1,50,1,1,2)
CALL DRAWZ(WF,ZG,XG,DUM,DUM,-2,1,50,1,1,2)
L=L+1
K=1
GO TO 120
100 FORMAT(" ",2A10,4G10.3)
105 FORMAT(2A10,4G10.3)
107 FORMAT("//",T9,"ITEM",X,Y,Z,"/")
200 FORMAT("//",K,"T5","A/C WT",T16,"FUEL WT",T27,"ZCG FUEL",T50,"XCG",
1T61,"YCG",T72,"ZCG",/)
300 FORMAT(I2,T5,6G10.4,T16,G10.4,T27,G10.4,T50,G10.4,T61,G10.4,T72,
1G10.4)
400 FORMAT(" ",2A10,4G10.3)
1000 FORMAT("//",FUEL WT (LB)=",F5.1,"TANK DIMENSIONS (IN) ",
+ F3.1," X ",F3.1," F4.1,/,BASE AREA=",F5.1," SQIN",//)
150 STOP
END

```

## APPENDIX A-5-2

## WTNBAL OUTPUT

K	A/C WT	FUEL WT	ZCG FUEL	XCG	YCG	ZCG
1	126.5	22.50	0.	32.73	0.	2.523
2	125.0	22.05	-.1400	32.74	0.	2.507
3	125.6	21.60	-.2800	32.75	0.	2.493
4	125.1	21.15	-.4200	32.75	0.	2.479
5	124.7	20.70	-.5600	32.76	0.	2.466
6	124.2	20.25	-.7000	32.77	0.	2.454
7	123.8	19.80	-.8400	32.77	0.	2.443
8	123.3	19.35	-.9800	32.78	0.	2.433
9	122.9	18.90	-1.120	32.79	0.	2.424
10	122.4	18.45	-1.260	32.79	0.	2.416
11	122.0	18.00	-1.400	32.80	0.	2.409
12	121.5	17.55	-1.540	32.81	0.	2.403
13	121.1	17.10	-1.680	32.81	0.	2.398
14	120.6	16.65	-1.820	32.82	0.	2.394
15	120.2	16.20	-1.960	32.83	0.	2.391
16	119.7	15.75	-2.100	32.83	0.	2.389
17	119.3	15.30	-2.240	32.84	0.	2.388
18	118.8	14.85	-2.380	32.85	0.	2.388
19	118.4	14.40	-2.520	32.85	0.	2.389
20	117.9	13.95	-2.660	32.86	0.	2.391
21	117.5	13.50	-2.800	32.87	0.	2.394
22	117.0	13.05	-2.940	32.87	0.	2.399
23	116.6	12.60	-3.080	32.88	0.	2.404
24	116.1	12.15	-3.220	32.89	0.	2.411
25	115.7	11.70	-3.360	32.90	0.	2.418
26	115.2	11.25	-3.500	32.90	0.	2.427
27	114.8	10.80	-3.640	32.91	0.	2.437
28	114.3	10.35	-3.780	32.92	0.	2.449
29	113.9	9.900	-3.920	32.93	0.	2.461
30	113.4	9.450	-4.060	32.93	0.	2.475
31	113.0	9.000	-4.200	32.94	0.	2.490
32	112.5	8.550	-4.340	32.95	0.	2.506
33	112.1	8.100	-4.480	32.96	0.	2.523
34	111.6	7.650	-4.620	32.97	0.	2.542
35	111.2	7.200	-4.760	32.97	0.	2.562
36	110.7	6.750	-4.900	32.98	0.	2.583
37	110.3	6.300	-5.040	32.99	0.	2.605
38	109.8	5.850	-5.180	33.00	0.	2.629
39	109.4	5.400	-5.320	33.01	0.	2.655
40	108.9	4.950	-5.460	33.01	0.	2.681
41	108.5	4.500	-5.600	33.02	0.	2.709
42	108.0	4.050	-5.740	33.03	0.	2.738
43	107.6	3.600	-5.880	33.04	0.	2.769
44	107.1	3.150	-6.020	33.05	0.	2.801
45	106.7	2.700	-6.160	33.06	0.	2.835
46	106.2	2.250	-6.300	33.07	0.	2.870
47	105.8	1.800	-6.440	33.07	0.	2.907
48	105.3	1.350	-6.580	33.08	0.	2.945
49	104.9	.9000	-6.720	33.09	0.	2.985
50	104.4	.4500	-6.860	33.10	0.	3.026

APPENDIX A-5-3

COMPONENT WEIGHTS AND LOCATIONS (WTNBAL)

ITEM	WEIGHT	X	Y	Z
FUEL	22.5	31.0	0.	0.
PAYLOAD	25.0	9.50	0.	0.
FUSELAGE	11.8	33.0	0.	0.
WING L	13.0	33.0	0.	6.50
WING R	13.0	33.0	0.	6.50
HORIZONTAL TAIL	3.75	92.0	0.	23.0
VERTICAL TAIL L	1.20	92.0	-19.0	12.0
VERTICAL TAIL R	1.20	92.0	19.0	12.0
ALIERON SERVO R	.200	33.0	25.0	6.00
ALIERON SERVO L	.200	33.0	-25.0	6.00
RUDDER SERVO R	.200	93.0	19.0	8.00
RUDDER SERVO L	.200	93.0	-19.0	8.00
ELEVATOR SERVO	.200	93.0	0.	20.0
ENGINE SERVO	.200	43.0	0.	0.
SHROUD	1.40	5.00	0.	0.
ELECTRONICS	6.50	17.0	0.	0.
PROPELLER	2.00	50.0	0.	0.
ENGINE	12.0	46.0	0.	0.
GENERATOR	6.00	42.0	0.	0.
BOOM L	1.95	60.0	-18.0	6.50
BOOM R	1.95	60.0	18.0	6.50
BULKHEAD A	1.00	15.0	0.	0.
BULKHEAD B	1.00	43.0	0.	0.

FUEL WT (LB) = 22.5 TANK DIMENSIONS (IN) 7.0 X 7.0 X 18.9  
 BASE AREA = 132.2 SQIN

APPENDIX A-5-4

CENTER OF GRAVITY SHIFT

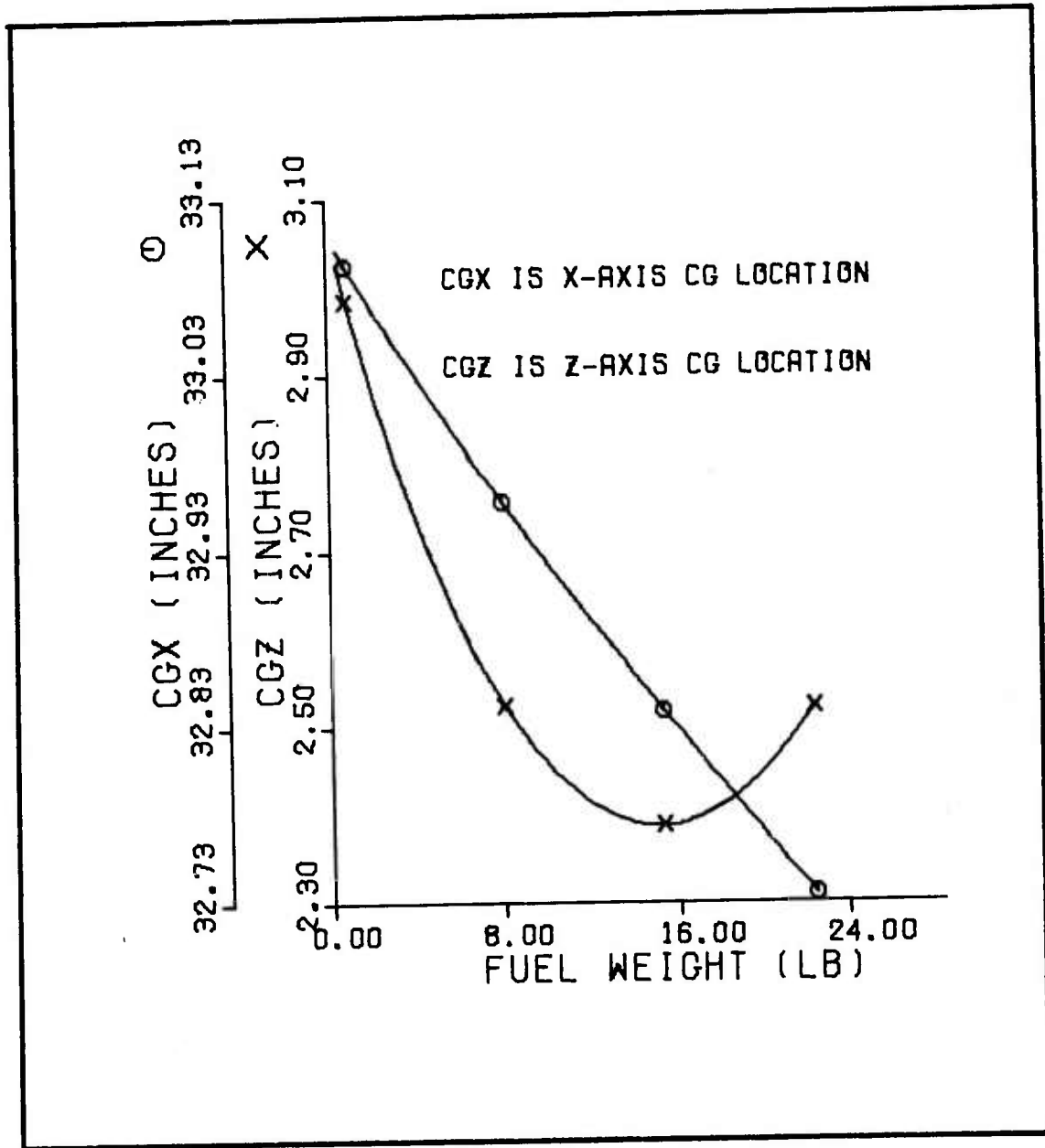


Figure A-27. Center of Gravity Shift With Fuel Consumption

PERFORMANCE (DESIGN)

PROGRAM DESIGN(INPUT, OUTPUT, TAPES=INPUT, TAPE6=OUTPUT)  
 DIMENSION SS(25), VSTSL(25), VST3K(25), H(25), VSTM(25),  
 +C1(20), W1(20), E1(20),  
 +CL(55), CD(55), LO(55), THP(25), THPR(25), HPEX(25),  
 +RC(25), THETA(25), V(25), S50(25), XLD(25), BHPR10(25),  
 +THPR10(25), THPRSL(25), THPSL(25), THP3(25), THP10(25), THPR3(25)  
 REAL LO, LOMAX

```

C C *****
C C INPUT PARAMETERS
C C
C C GROSS WEIGHT (LBS)
C C   WG=125.
C C
C C MAX LIFT COEFFICIENT
C C   CLMAX= 1.223
C C
C C WING AREA (SOFT)
C C   S= 17.
C C
C C ASPECT RATIO
C C   AR= 6.
C C
C C SPAN EFFICIENCY
C C   E= 0.95
C C
C C PARASITE DRAG COEFF
C C   CDPE= 0.03
C C
C C LIFT CURVE SLOPE (DEG -1)
C C   A30= 0.08133
C C
C C ZERO LIFT ANGLE (DEG)
C C   ALFLO= -2.
C C
C C PROP EFFICIENCY
C C   ETA= 0.75
    
```

```

C C PROP EFFICIENCY AT CLIMB
    ETACL=0.60
C C SPECIFIC FUEL CONS (LB/BHP-HR)
    C=1.0
C C FUEL CARRIED
    WFMAX=20.
C C OPERATING ALTITUDE (FT)
    ALTMX= 10000.
C C MISSION TIME (HRS)
    TMISSN= 6.
C C LAUNCH SPEED (MPH)
    VTO= 50.
C C TARGET DISTANCE (MI)
    RNGTGT= 100.
C C GENERATOR OUTPUT (WATTS)
    PWGEN= 300.
C C CLIMB SPEED (II=VCLIMB/5)
    II=12
C C CRUISE SPEED (IC=VCRUISE/5)
    IC=15
C *****
C C
C C AFTER THE FIRST PASS, PRINTS ONLY INPUT & OUTPUT PARAMETERS
C C

```

```

G=32.2 $PI=4.*ATAN(1.) $SIGMA10= 0.738
SIGMASL= 1. $SIGMA3K= 0.915 $HPTOWAT=745.7
RTOD=180./PI $DTOR=PI/180.
M=1 $JJ=0
1 J=0 $L=0
CCL=C+0.25
HPGEN=PWGEN/HPTOWAT
IF(M.NE.1) GO TO 4
3 DO 10 I=1,20
READ(5,9100) HP
THPSL(I)=HP
IF(THPSL(I).LE.0) THPSL(I)=0.
THP3(I)=THPSL(I)*(1.132*SIGMA3K-0.132)
10 THP10(I)=THPSL(I)*(1.132*SIGMA10-0.132)
4 SS(1)=12. $W(1)=WG+10.
DO 100 I=1,20
VSTSL(I)=SQRT(391.*WG/CLMAX/SIGMASL/SS(I))
VST3K(I)=SQRT(391.*WG/CLMAX/SIGMA3K/SS(I))
S50(I)=(391.*W(I)/CLMAX/SIGMA3K)/VTO**2
VSTW(I)=SQRT(391.*W(I)/CLMAX/SIGMA3K/S)
W(I+1)=W(I)-2.
100 SS(I+1)=SS(I)+0.5
VSTL=SQRT(391.*WG/CLMAX/SIGMA10/S)
IF(M.NE.1) GO TO 210
PRINT 1000,S
DO 200 I=1,20
200 PRINT 1100,I,SS(I),VSTSL(I),VST3K(I),W(I),VSTW(I)
210 B=SQRT(AR*S)
LDMAX=0.5*SQRT(PI*E*AR/CDPE)
VLDMX=((391.*WG/SIGMASL/S)**2/CDPE/PI/E/AR)**0.25
DO 300 I=1,50
CL(I)=I*CLMAX/50.
CD(I)=CDPE+CL(I)**2/PI/E/AR
LD(I)=CL(I)/CD(I)
300 XLD(I)=CL(I)**1.5/CD(I)
IF(M.NE.1) GO TO 360
PRINT 1110

```

```

DO 350 I=1, 50
350 PRINT 1120, CL(I), CO(I), LD(I), XLD(I)
360 ALFINC=CL(IC)/A3D+ALFLO
IM=1 $IN=1
DO 400 I=1, 20
V(I)=I*5.
THPRSL(I)=4.65E-6*CDPE*S*SIGMASL*V(I)**3+
+0.226*(WG/B)**2/E/SIGMASL/V(I)+HPGEN
THPR3(I)=4.65E-6*CDPE*S*SIGMA3K*V(I)**3+
+0.226*(WG/B)**2/E/SIGMA3K/V(I)+HPGEN
THPR10(I)=4.65E-6*CDPE*S*SIGMA10*V(I)**3+
+0.226*(WG/B)**2/E/SIGMA10/V(I)+HPGEN
BHPR10(T)=THPR10(I)/ETA
HPEX(I)=THP3(I)-THPR3(I)
RC(I)=33000./WG*HPEX(I)
IF(HPEX(I).LE.0.) RC(I)=0.
IF(RC(I).GT.RC(IN)) IN=I
THETA(I)=ASIN(RC(I)/88./V(I))*RTOD
400 IF(THETA(I).GT.THETA(IM)) IM=I
IF(M.NE.1) GO TO 610
PRINT 1200
DO 500 I=1, 20
500 PRINT 1210, V(I), THPSL(I), THP3(I), THP10(I), THPRSL(I), THPR3(I),
+THPR10(I), BHPR10(I)
PRINT 1220
DO 600 I=1, 20
600 PRINT 1230, V(I), RC(I), THETA(I), HPEX(I)
610 HPXAVG=(HPEX(II)+THP10(II)-THPR10(II))/2.
RCAVG=33000./WG*HPXAVG
WFCLM=THP3(II)/ETACL*CCL*ALTMX/60./RCAVG
TCLM=ALTMX/RCAVG/60.
RNGCLM=TCLM*V(II)
RNGCRZ=RNGTGT-RNGCLM
WFCRZ=(WG-WFCLM)*(1.-EXP(-RNGCRZ*ETA/326./C/LD(IC)))
TCRZ=RNGCRZ/V(IC)
ENDUR=TMISSN-TCLM-TCRZ
WFLOIT=ENDUR*(WG-WFCLM-WFCRZ)*V(IC)/400./LD(IC)*C/ETA

```

```

RNGLOIT=V(IC)*ENDUR
WFUEL=WFCLM+WFGRZ+WFLOIT
FRACTN=WFUEL/WG
ENRMAX=400.*(WFMAX-WFCLM-WFGRZ)/(WG-WFCLM-WFGRZ)*LD(IC)+
+ETA/C/V(IC)
RNGMAX=ENRMAX*V(IC)
RTMIN=391.*WG/S/SIGMA10/G/CLMAX/(1.-(VSTL/V(IC))**4)**0.5
IF(JJ.GE.1) GO TO 900
PRINT 1300, WG,S,AR,VTO,E,CLMAX,COPE,ETA,G,ALTMX,RNGTGT,TMISSN,
+PVRGEN
PRINT 1310, B,RTMIN,LDMAX,VLDMX,ALFLDMX,ALFINC,THETA(IM),V(IM),
+THETA(II),V(II),MPXAVG,RCAVG,V(IC),BHPR10(IC),
+WFCLM,WFGRZ,WFLOIT,WFUEL,FRACTN,TCLM,TCRZ,ENDUR,TMISSN,
+RNGCLM,RNGCRZ,RNGLOIT,WFMAX,ENRMAX,RNGMAX
899 IF(M.NE.1) GO TO 900
C
C ENTER CALL DRAWZ'S HERE
CALL DRAWZ(V,THPSL,THP10,THPRSL,THPR10,-4,4,20,1,1,4)
CALL DRAWZ(H,S50,DUM,DUM,DUM,-1,1,20,1,1,2)
CALL DRAWZ(SS,VSTSL,VST3K,DUM,DUM,-2,2,20,1,1,4)
CALL DRAWZ(V,RC,THETA,DUM,DUM,-2,1,20,1,1,2)
CALL DRAWZ(V,THPSL,THP3,THPRSL,THPR3,-4,4,20,1,1,4)
CALL DRAWZ(CL,CO,LO,DUM,DUM,-2,1,50,1,1,4)
CALL DRAWZ(V,THPRSL,THPR3,THPR10,BHPR10,-4,4,20,1,1,4)
C
C 900 M=M+1
C
C ENTER CHANGES TO INPUT PARAMETERS NOM
C
C IF(JJ.NE.0) GO TO 1399
C=0.7
PRINT 1400
GO TO 1398

```

```

1399 C1(JJ)=C
      W1(JJ)=WFUEL
      E1(JJ)=ENRMAX
      PRINT 1410, JJ, C1(JJ), W1(JJ), E1(JJ)
1398 JJ=JJ+1
      C=C+0.1
1400 FORMAT(/, "JJ", T8, "SFC", T15, "FUEL REQ", T25, "TARGET TIME", //)
1410 FORMAT(I2, T5, F8.3, T15, F8.3, T25, F8.3)
      IF (JJ.NE.11) GO TO 1420
      CALL DRAWZ(C1, W1, E1, DUM, DUM, 2, 1, 10, 1, 1, 2)
      MDES=1
C      SET MDES= NUMBER OF ITERATIONS DESIRED
C
1420 MDES=11
      IF (MDES-M) 2, 1, 1
C
1000 FORMAT(/, "I", T12, "S", T28, "VST SL", T42, "VST 3K", T60,
      + "WEIGHT", T70, "VST (S=", F4.1, ") ", //)
1100 FORMAT(I2, T10, F5.1, T25, F10.5, T40, F10.5, T60, F6.1, T70, F10.5)
1110 FORMAT(/, "CL", T18, "CO", T33, "L/D", T47, "L1.5/D", //)
1120 FORMAT(F6.4, T15, F7.5, T30, F9.5, T45, F9.5)
1200 FORMAT(/, "SPEED", T18, "THP SL", T33, "THP 3K", T48, "THP 10K", T62,
      + "THPREQ SL", T77, "THPREQ 3K", T91, "THPREQ 10K", T108, "BHPREQ", //)
1210 FORMAT(F5.1, T15, F10.5, T30, F10.5, T45, F10.5, T60, F10.5, T75, F10.5,
      + T90, F10.5, T105, F10.5)
1220 FORMAT(/, "SPEED", T16, "R/C (FPM)", T29, "CLIMB ANGLE", T46,
      + "EXCESS HP", //)
1230 FORMAT(F5.1, T15, F10.4, T30, F5.2, T45, F10.5)
1300 FORMAT(/, "INPUT PARAMETERS", //, "GROSS WEIGHT (LBS)", T30, F8.3, /,
1 "WING AREA (SQFT)", T30, F8.3, /, "ASPECT RATIO", T30, F8.3, /,
+ "LAUNCH SPEED (MPH)", T30, F8.3, /, "SPAN EFFICIENCY", T30, F8.3, /,
+ "MAX CL", T30, F8.3, /, "PARASITE CD", T30, F8.3, /,
+ "PROP EFFICIENCY", T30, F8.3, /, "SFC (LB/BHP-HR)", T30, F8.3, /,
+ "OPERATING ALT (FT)", T30, F8.2, /, "TARGET DIST (MI)", T30, F8.3, /,
+ "MISSION TIME (HR)", T30, F8.3, /, "GENERATOR PMR (WATTS)", T30, F8.3, /,
1310 FORMAT(/, "OUTPUT PARAMETERS", //,

```



## APPENDIX A-6-2

## DESIGN OUTPUT

S	VST SL	VST 3K	WEIGHT	VST (S=17.0)
12.0	57.70847	60.32940	135.0	52.67530
12.5	56.54252	59.11050	133.0	52.28366
13.0	55.44450	57.96261	131.0	51.88906
13.5	54.40806	56.87910	129.0	51.49144
14.0	53.42766	55.85417	127.0	51.09072
14.5	52.49841	54.88272	125.0	50.68683
15.0	51.61602	53.96025	123.0	50.27970
15.5	50.77668	53.08279	121.0	49.86925
16.0	49.97700	52.24679	119.0	49.45539
16.5	49.21395	51.44908	117.0	49.03804
17.0	48.48481	50.68683	115.0	48.61710
17.5	47.78715	49.95749	113.0	48.19249
18.0	47.11877	49.25875	111.0	47.76410
18.5	46.47766	48.58853	109.0	47.33184
19.0	45.86204	47.94494	107.0	46.89559
19.5	45.27025	47.32627	105.0	46.45525
20.0	44.70079	46.73095	103.0	46.01069
20.5	44.15229	46.15754	101.0	45.56180
21.0	43.62350	45.60474	99.0	45.10843
21.5	43.11327	45.07133	97.0	44.65047

SPEED	R/C (FPM)	CLIMB ANGLE	EXCESS HP
5.0	0.0000	0.00	-6.83166
10.0	0.0000	0.00	-2.12778
15.0	0.0000	0.00	-.08233
20.0	317.8762	10.41	1.20408
25.0	585.6714	15.44	2.21845
30.0	840.1300	18.56	3.18231
35.0	1024.2635	19.42	3.87979
40.0	1192.8723	19.81	4.51846
45.0	1301.9795	19.19	4.93174
50.0	1401.3786	18.57	5.30825
55.0	1468.3731	17.66	5.56202
60.0	1527.4553	16.82	5.78582
65.0	1555.0711	15.78	5.89042
70.0	1503.5964	14.13	5.69544
75.0	1396.8465	12.22	5.29109
80.0	1234.6807	10.10	4.67682
85.0	945.3107	7.26	3.58072
90.0	552.3386	4.00	2.09219
95.0	0.0000	0.00	-1.05518
100.0	0.0000	0.00	-2.97050

INPUT PARAMETERS

GROSS WEIGHT (LBS)	125.000
WING AREA (SQFT)	17.000
ASPECT RATIO	6.000
LAUNCH SPEED (MPH)	50.000
SPAN EFFICIENCY	.950
MAX CL	1.223
PARASITE CD	.030
PROP EFFICIENCY	.750
SFC (LB/BHP-HR)	1.000
OPERATING ALT (FT)	10000.00
TARGET DIST (MI)	100.000
MISSION TIME (HR)	6.000
GENERATOR PWR (WATTS)	300.000

OUTPUT PARAMETERS

SPAN (FT)	10.100
MIN TURN RADIUS (FT)	120.022
L/D MAX	12.216
AT SPEED (MPH)	62.630
AT ALPHA (DEG)	0.000
WING INCIDENCE (DEG)	2.511
MAX CLIMB ANGLE (DEG)	19.809
AT SPEED (MPH)	40.000
OPER CLIMB ANGLE (DEG)	16.816
AT SPEED (MPH)	60.000
HP EXCESS, AVG	4.940
R/C, AVG (FPM)	1304.180
CRUISE SPEED (MPH)	75.000
BHP AT CRUISE	2.399
FUEL WT CLIMB (LBS)	1.949
CRUISE	2.644
LOITER	14.286
TOTAL	18.879
FUEL FRACTION	.151
TIME TO CLIMB (HR)	.128
CRUISE	1.231
LOITER	4.641
TOTAL	6.000
DISTANCE, CLIMB (MI)	7.668
CRUISE	92.332
LOITER	348.083
FUEL CARRIED (LBS)	20.000
ENDURANCE (HRS)	5.005
COVERAGE (MI)	375.406

CL	CD	L70	L1.5/D
.0245	.03003	.81443	.12737
.0489	.03013	1.62343	.35907
.0734	.03030	2.42173	.65602
.0978	.03053	3.20424	1.00227
.1223	.03084	3.96624	1.38705
.1468	.03120	4.70343	1.80185
.1712	.03164	5.41199	2.23942
.1957	.03214	6.08869	2.69337
.2201	.03271	6.73082	3.15804
.2446	.03334	7.33629	3.62831
.2691	.03404	7.90360	4.09968
.2935	.03481	8.43178	4.56812
.3180	.03565	8.92039	5.03018
.3424	.03655	9.36946	5.48285
.3569	.03752	9.77945	5.92363
.3914	.03855	10.15117	6.35045
.4158	.03966	10.48574	6.76164
.4403	.04083	10.78453	7.15593
.4647	.04206	11.04910	7.53238
.4892	.04336	11.28115	7.89036
.5137	.04473	11.48249	8.22951
.5381	.04617	11.65497	8.54969
.5626	.04767	11.80047	8.85098
.5870	.04924	11.92088	9.13361
.6115	.05088	12.01805	9.39793
.6360	.05259	12.09377	9.64443
.6604	.05436	12.14978	9.87367
.6849	.05619	12.18775	10.08627
.7093	.05810	12.20925	10.28292
.7338	.06007	12.21579	10.46430
.7583	.06211	12.20876	10.63116
.7827	.06421	12.18948	10.78421
.8072	.06638	12.15917	10.92419
.8316	.06862	12.11897	11.05181
.8561	.07093	12.06993	11.16778
.8806	.07330	12.01301	11.27279
.9050	.07574	11.94911	11.36749
.9295	.07825	11.87905	11.45253
.9539	.08082	11.80356	11.52852
.9784	.08346	11.72334	11.59604
1.0029	.08616	11.63900	11.65564
1.0273	.08894	11.55112	11.70785
1.0518	.09178	11.46020	11.75316
1.0762	.09468	11.36671	11.79205
1.1007	.09766	11.27107	11.82496
1.1252	.10070	11.17367	11.85231
1.1496	.10380	11.07484	11.87448
1.1741	.10698	10.97489	11.89184
1.1985	.11022	10.87411	11.90474
1.2230	.11353	10.77274	11.91351

SPEED	THP SL	THP 3K	THP 10K	THPREQ SL	THPREQ 3K	THPREQ 10K	9HPREQ
5.0	1.70000	1.53643	1.19581	7.69104	8.36809	10.27846	13.70462
10.0	2.50000	2.25945	1.75854	4.04890	4.38723	5.34203	7.12270
15.0	3.30000	2.98247	2.32127	2.83979	3.06480	3.70019	4.93359
20.0	4.00000	3.61512	2.81366	2.24339	2.41104	2.88529	3.84706
25.0	4.70000	4.24777	3.30606	1.89705	2.02931	2.40484	3.20645
30.0	5.50000	4.97079	3.86879	1.68108	1.78848	2.09555	2.79407
35.0	6.10000	5.51306	4.29084	1.54519	1.63327	1.88819	2.51759
40.0	6.70000	6.05533	4.71289	1.46514	1.53687	1.74881	2.33175
45.0	7.10000	6.41684	4.99425	1.42824	1.48510	1.65912	2.21216
50.0	7.50000	6.77835	5.27562	1.42759	1.47010	1.60867	2.14489
55.0	7.80000	7.04948	5.48664	1.45945	1.48746	1.59130	2.12174
60.0	8.10000	7.32062	5.69767	1.52192	1.53480	1.60334	2.13778
65.0	8.30000	7.50137	5.83835	1.61423	1.61095	1.64263	2.19018
70.0	8.20000	7.41100	5.76801	1.73633	1.71555	1.70804	2.27738
75.0	7.90000	7.13986	5.55699	1.88868	1.84879	1.79905	2.39874
80.0	7.40000	6.68797	5.20528	2.07204	2.01115	1.91564	2.55418
85.0	6.40000	5.78419	4.50186	2.28744	2.20347	2.05807	2.74409
90.0	5.00000	4.51890	3.51708	2.53604	2.42671	2.22684	2.96912
95.0	1.80000	1.62680	1.26615	2.81917	2.68198	2.42264	3.23019
100.0	0.00000	0.00000	0.00000	3.13823	2.97050	2.64627	3.52836

APPENDIX A-6-3

DESIGN PLOTS

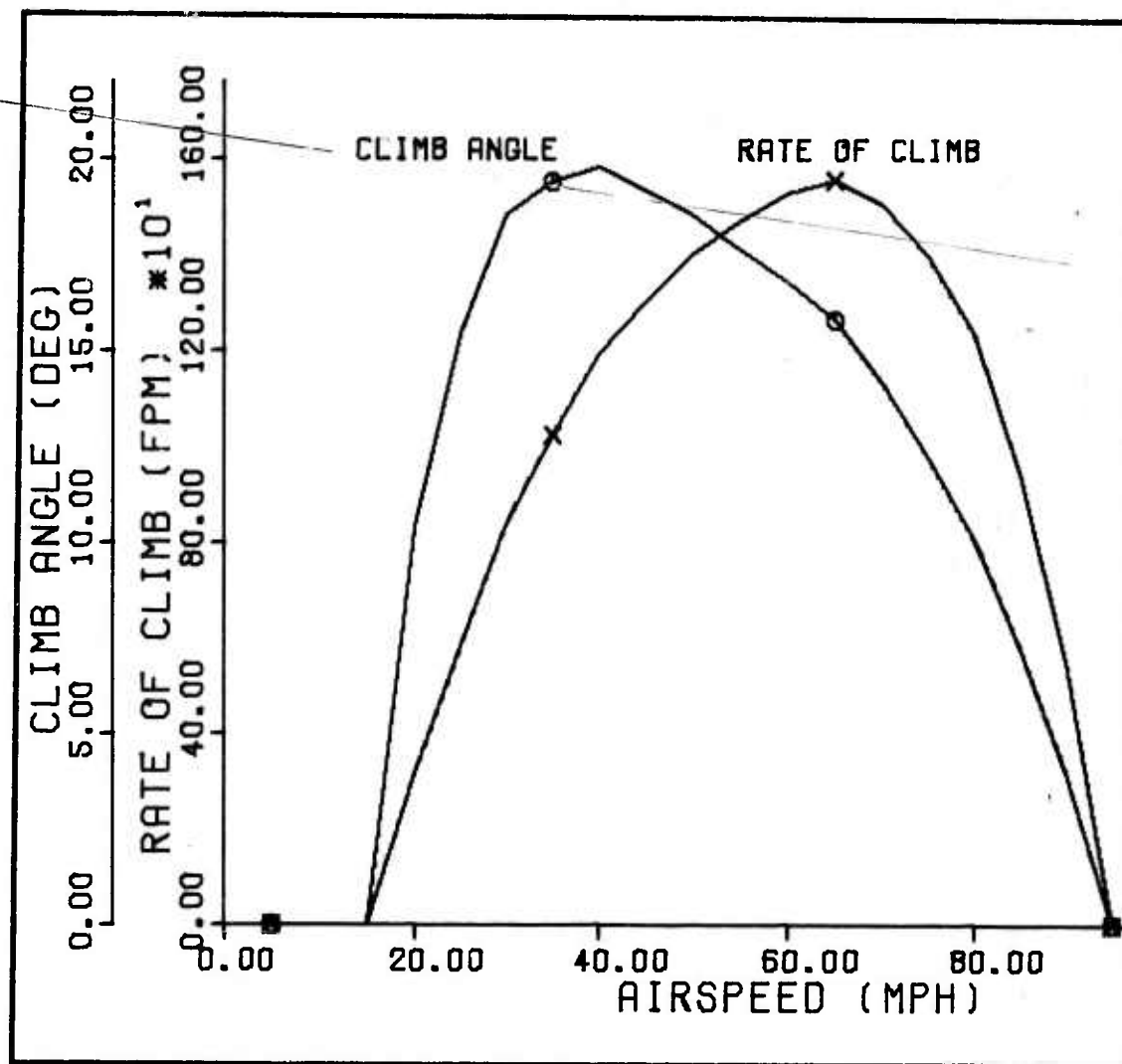


Figure A-28. Climb Angle and Rate of Climb

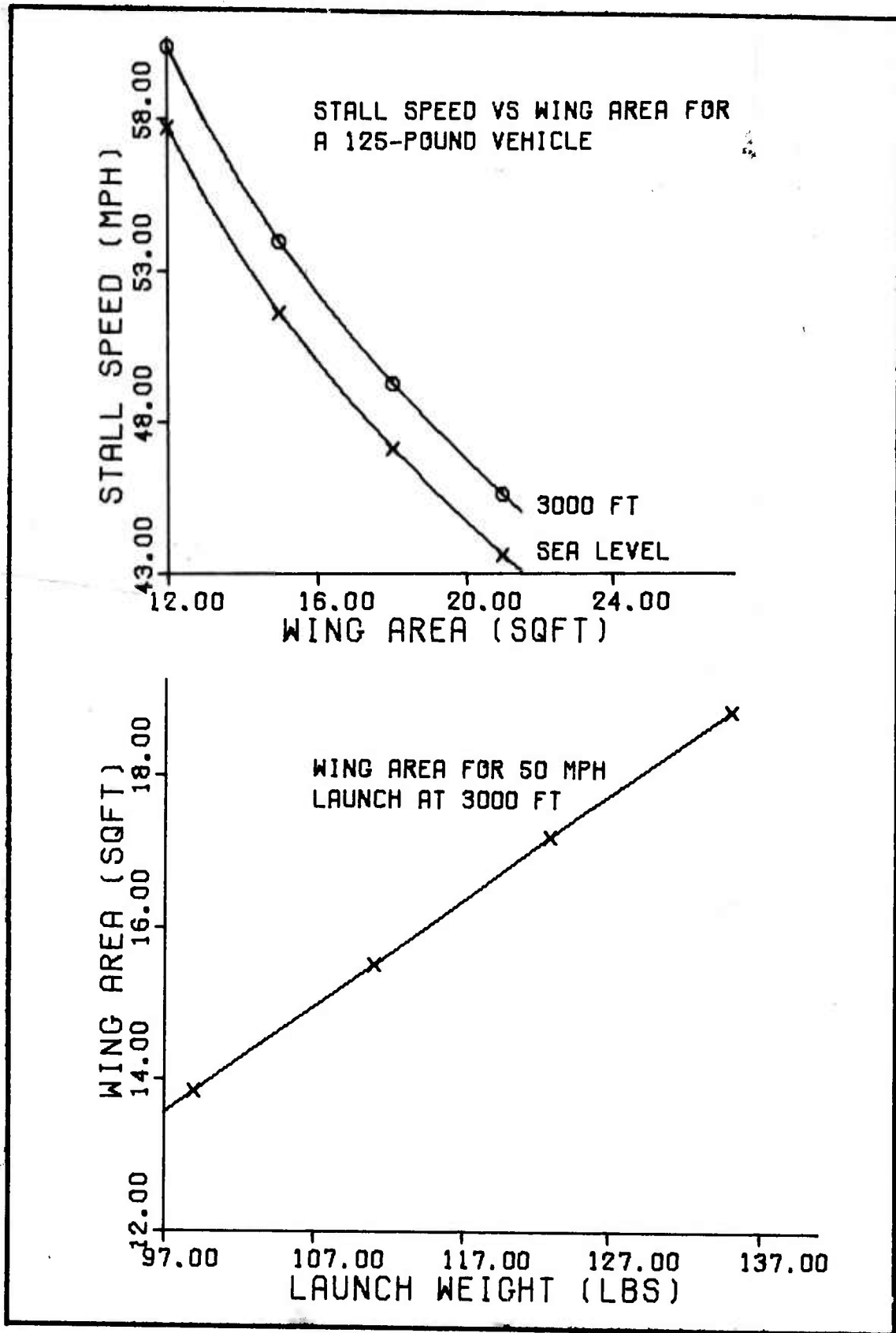


Figure A-29. Wing Area, Launch Speed, Weight

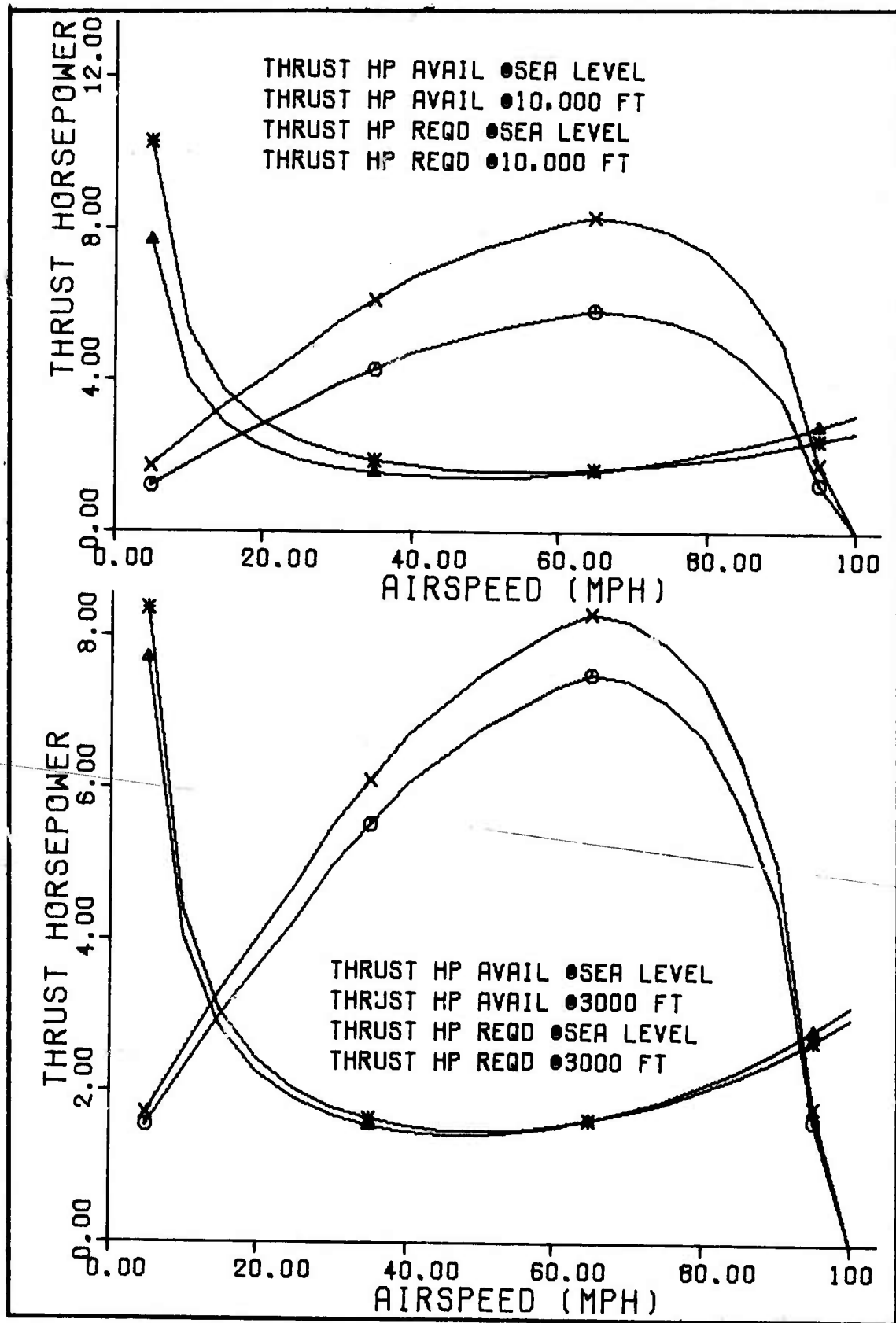


Figure A-30. Thrust Horsepower-Altitude

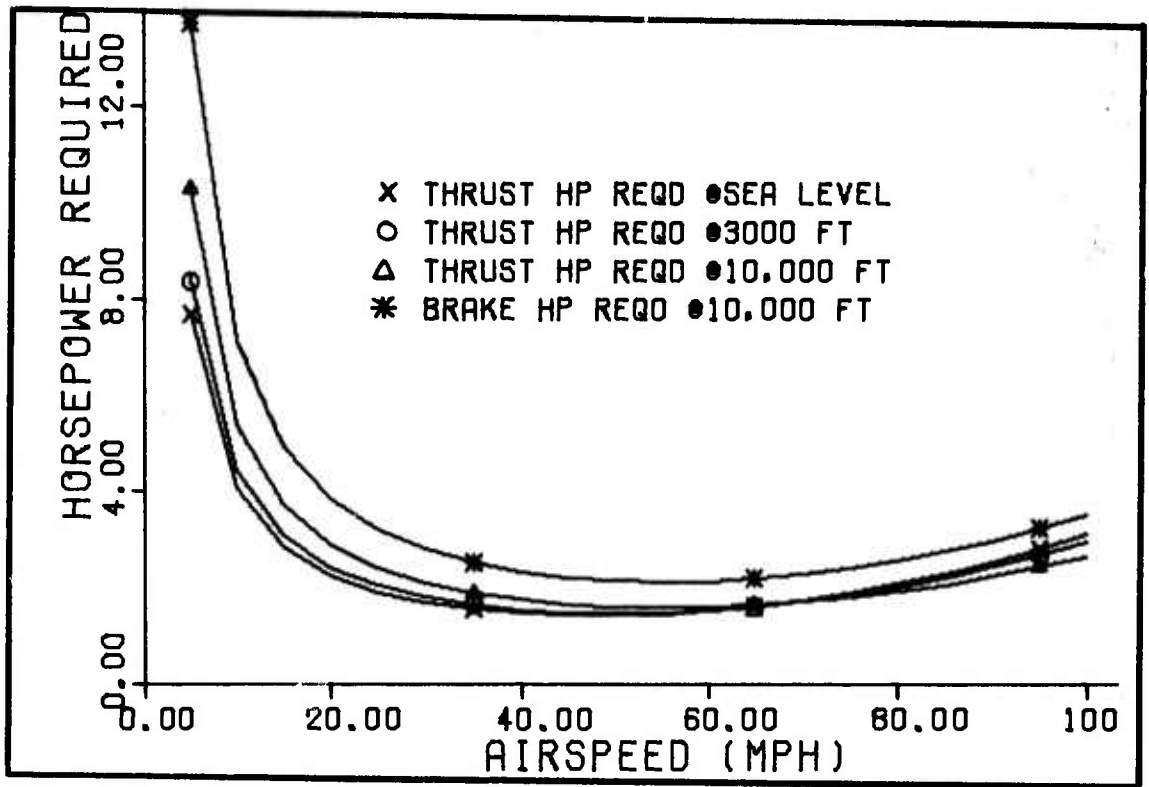


Figure A-31. Required Horsepower

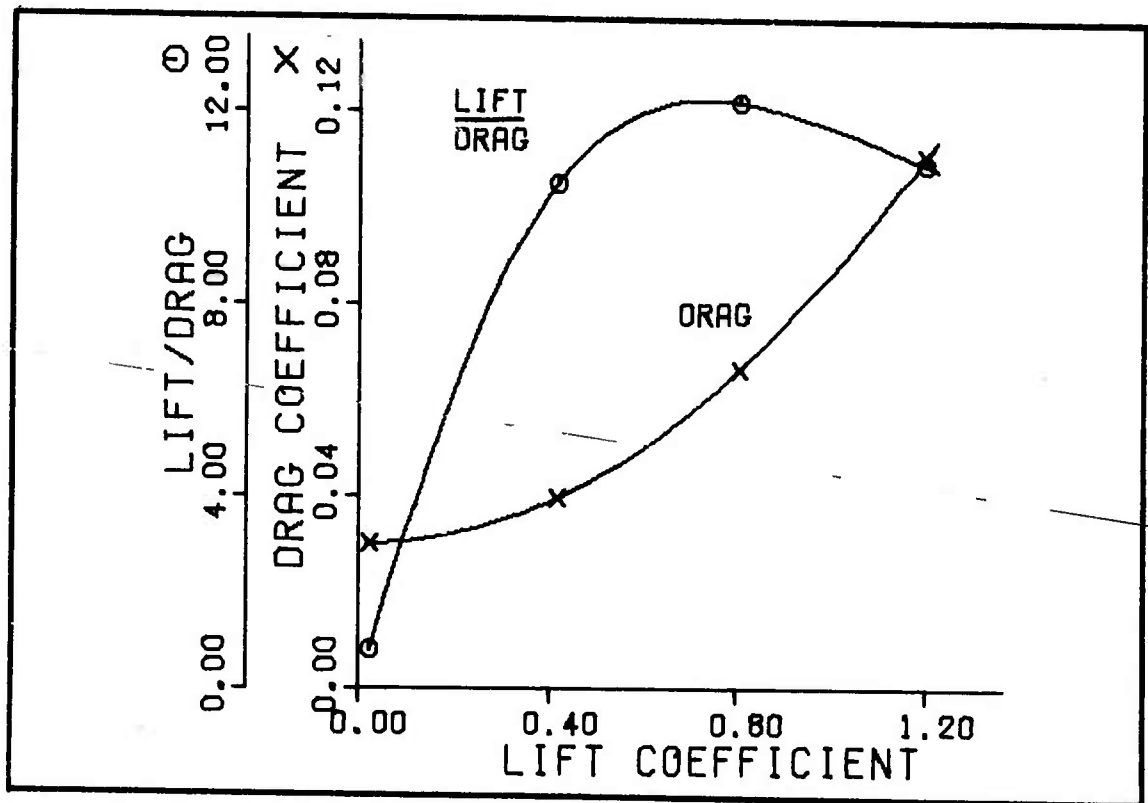


Figure A-32. Lift and Drag Relationships

FUEL CONSUMPTION SENSITIVITY

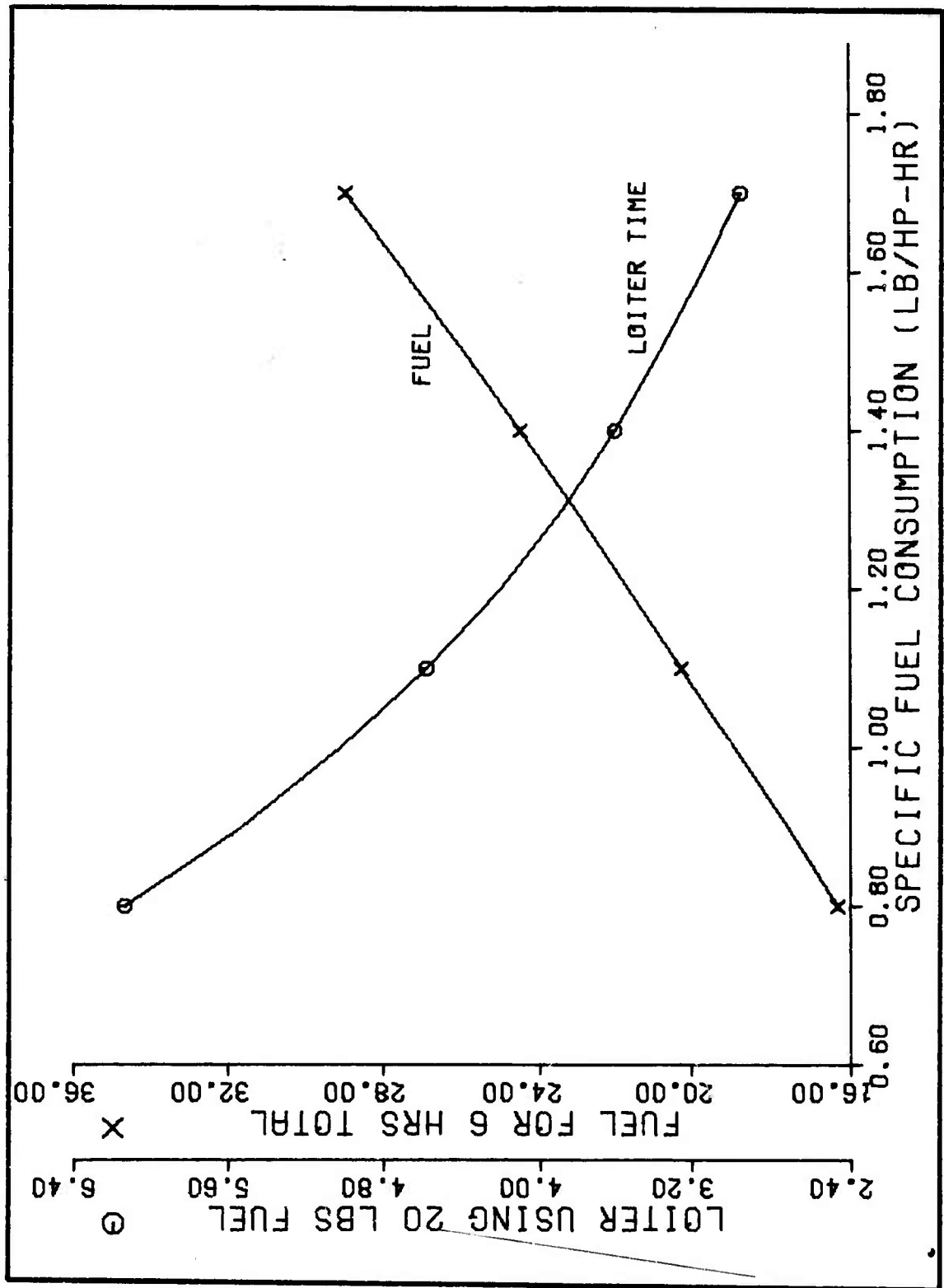


Figure A-33. Fuel Consumption Sensitivity

APPENDIX B

FLIGHT CONTROL

## LIST OF SYMBOLS

A	aspect ratio
$a_{ht}$	lift curve slope, horizontal tail
$A_{ve}$	effective aspect ratio of vertical tail
$a_{vt}$	lift curve slope, vertical tail
$a_z$	vertical acceleration with respect to Earth
b	wing span
$b_{vt}$	vertical tail span
c	mean aerodynamic chord
$C_D$	drag coefficient
$C_D^w$	drag coefficient of the wing
$C_{F_x a}$	coefficient of applied force in the x direction
$C_{F_z a}$	coefficient of applied force in the z direction
$C_L$	lift coefficient
$C_{l_a}$	coefficient of applied rolling moment
$C_{l_p}$	change of rolling moment from a change of roll angular velocity
$C_{l_r}$	change of rolling moment from a change in yaw angular velocity
$C_{l_\beta}$	change of rolling moment from a change in sideslip angle
$C_{l_{\delta r}}$	change of rolling moment from a change of rudder deflection
$C_{l_{\psi_{vert} tail}}$	change of yaw angle due to the vertical tail
$C_{l_{\psi} wing}$	change of rolling moment from a change of yaw angle due to the wing
$C_{l_\alpha}$	change of the lift coefficient due to a change of angle of attack
$C_{l_{\alpha t}}$	change of lift coefficient due to an change of angle of attack of the tail
$C_m$	pitch moment coefficient
$C_{m_a}$	coefficient of applied pitching moment

$C_{m_{it}}$	change of pitching moment coefficient due to an change of incidence of the tail
$C_{m_q}$	change of pitching moment due to a pitch angular velocity
$C_{m_u}$	change of pitching moment due to a change of forward velocity
$C_{m_\alpha}$	change of pitching moment due to a change of angle of attack
$C_{m_{\dot{\alpha}}}$	change of pitching moment due to a change of angle of attack rate
$C_{m_{\delta_e}}$	change of pitching moment due to a change of elevator deflection
$C_{n_a}$	change of yawing moment applied
$C_{n_p}$	change of yawing moment due to a change of roll angular velocity
$C_{n_\beta}$	change of yawing moment due to a change of sideslip angle
$C_{n_{\delta_r}}$	change of yawing moment due to a change of rudder deflection
$C_{n_{\psi_{fus}}}$	change of yawing moment due to yaw angle of the fuselage
$C_{n_{\psi_{prop}}}$	change of yawing moment due to yaw angle of the propeller
$C_{n_{\psi_{prop}}}$ cruise power	change of yawing moment due to yaw angle with the propeller at cruise power
$C_{n_{\psi_{prop}}}$ full power	change of yawing moment due to yaw angle with the propeller at full power
$C_{n_{\psi_{wing}}}$	change of yawing moment due to yaw angle of the wing
$C_w$	weight coefficient
$C_x$	coefficient of forces in the x direction
$C_{x_q}$	change in x force due to a change in pitch angular velocity
$C_{x_u}$	change in x force due to a change in forward velocity
$C_{x_\alpha}$	change in x force due to a change in angle of attack
$C_{x_{\dot{\alpha}}}$	change in x force due to a change in angle of attack rate
$C_{x_{\delta_e}}$	change in x force due to a change in elevator deflection
$C_{y_a}$	change in applied y force

$C_{y\beta}$	change in y force due to a change in sideslip angle
$C_{y\delta_r}$	change in y force due to a change in rudder deflection
$C_{y\phi}$	change in y force due to a change in roll angle
$C_{y\psi}$	change in y force due to a change in yaw angle
$C_{zq}$	change in z force due to a change in pitch angular rate
$C_{zu}$	change in z force due to a change in forward velocity
$C_{z\alpha}$	change in z force due to a change in angle of attack
$C_{z\dot{\alpha}}$	change in z force due to a change in angle of attack rate
$C_{z\delta_e}$	change in z force due to a change of elevator deflection
$e$	span efficiency factor
$g$	gravitational acceleration
$h$	altitude
$h_{CMD}$	commanded altitude
$i_t$	incidence angle of the horizontal tail
$I_x$	moment of inertia in x direction
$I_{xz}$	product of inertia
$I_y$	moment of inertia in y direction
$I_z$	moment of inertia in z direction
$j$	square root of -1
$K$	correction factor for roughness
$l_{ht}$	length from the aircraft center of gravity to the horizontal tail quarter chord point
$l_{vt}$	length from aircraft center of gravity to vertical tail quarter chord point
$m$	mass
$M$	Mach number
$q$	dynamic pressure
$Re$	Reynold's number

s	Laplace variable
S	wing area
$S_{ht}$	horizontal tail area
S.M.	static margin
$S_{vt}$	vertical tail area
t	time
T	thrust
T.F. O.L.	open-loop transfer function
T.F. servo	servo transfer function
$T_s$	settling time
u	perturbation of forward velocity
'u	ratio of perturbation of forward velocity to total forward velocity
U	total forward velocity
$U_o$	equilibrium forward velocity
w	weight
x	distance between the aircraft neutral point and the center of gravity
$x_o$	distance between the wing aerodynamic center and the aircraft neutral point
$z_{vt}$	vertical distance from the aircraft center of gravity and the quarter chord point of the vertical tail
$\alpha$	angle of attack
' $\alpha$	variation in angle of attack from equilibrium
$\beta$	sideslip angle
$\Gamma$	dihedral angle of the wing
$\delta_e$	elevator deflection
$\delta_r$	rudder deflection
$\Delta C_{l_{\psi 1}}$	correction factor 1 for the change in rolling moment due to a change in yaw angle

$\Delta C_{l_{\psi^2}}$	correction factor 2 for the change in rolling moment due to a change in yaw angle
$\Delta C_{n_{\psi}}$	correction factor 1 for the change in yaw moment due to a change in yaw angle
$\Delta C_{n_{\psi^2}}$	correction factor 2 for the change in yaw moment due to a change in yaw angle
$\epsilon$	downwash angle due to the wing
$\zeta$	damping ratio
$\eta_{ht}$	ratio of dynamic pressure at the horizontal tail to the free stream dynamic pressure
$\eta_{vt}$	ratio of dynamic pressure at the vertical tail to the free stream dynamic pressure
$\theta$	perturbation of the pitch angle
$\theta_o$	equilibrium pitch angle
$\theta_T$	total pitch angle
$\tau$	time constant
$\tau_{ht}$	efficiency of the horizontal tail
$\tau_{vt}$	efficiency of the vertical tail
$\phi$	roll angle
$\psi$	yaw angle or heading angle
$\psi_{CMD}$	commanded heading angle
$\psi_{GUST}$	perturbation to the heading angle due to a gust
$\omega_n$	natural <u>frequency</u>

## APPENDIX B

### FLIGHT CONTROL SUBSYSTEM

#### Introduction

The purpose of this section is to study the feasibility of very low-cost stability and control for the Type II vehicle. The profile and stability requirements of the Type I vehicle are more demanding of the control system than the Type II profile. Both the Type I dynamics and control tolerances are tighter than those of the Type II. Type II dynamics involve only launch-and-climb and cruise-and-loiter phases with no precise maneuvering required.

To achieve a very low cost system, as much commonality as possible is desired between the Type I and II vehicles. Therefore, common airframe, control surfaces and servos are assumed. No optimization or detailed design are used in picking the common items since the more demanding Type I requirements drive the selection. For this study, nominal airframe and control characteristics are used to model the recommended vehicle. A study is made of the feasibility of controlling the Type II vehicle without using rate sensors and rate feedback for stability.

#### Procedure

A digital simulation of the closed-loop heading control and altitude hold dynamics is developed to determine if the closed-loop time response is acceptable. The assumptions used in developing the equations of motion are detailed in Appendix B-1. The derivation

yields a set of equations that are linearized, decoupled approximations to the equations of motion, and the equations are valid for small perturbations from an equilibrium position.

The aircraft dynamics, in the form of a transfer function, are used with a servo and sensor model to simulate the closed-loop response. The closed-loop dynamics are studied on a digital computer. The AFIT ROOTL program (ROOTL, 1974) is used to plot the root locus which is used to determine the closed-loop poles and system stability. The AFIT PARTL program (PARTL, 1974) is used to determine the time response to various inputs, primarily to step inputs.

#### Discussion

Flight Conditions. Nominal flight conditions that are considered for this analysis are contained in Appendix B-2. Cruise and loiter dynamics are identical, therefore only the cruise condition is analyzed. Over 90% of the duration of the flight will be at the cruise condition. Therefore, cruise is used as the design condition.

Equations of Motion. The digital simulation of an aircraft comes from evaluating its equations of motion. The equations of motion are a system of equations that contain the aircraft's stability coefficients. The equations of motion have been de-coupled into sets of longitudinal (pitch) and lateral (roll-yaw) equations. Longitudinal and lateral stability coefficients are developed in Appendices B-3 and B-4, respectively. Cruise coefficients are developed in detail and the coefficients for all the conditions of flight (launch, climb, and cruise) are summarized in Tables B-2 and B-3, (in Appendices B-3 and B-4). The coefficients

are developed from analytical expressions since no wind-tunnel or flight test data are available on this airframe for comparison.

The equations of motion and characteristic motions of the airframe are developed in Appendices B-5 and B-6. The longitudinal characteristics include normal phugoid and short-period modes of oscillation. The phugoid oscillation is lightly damped ( $\zeta = 0.145$ ) and shows up as a slowly converging oscillation. The short-period mode is well damped ( $\zeta = 0.6$ ) and rapidly dies out.

The lateral motion includes a moderately damped Dutch-roll mode ( $\zeta=0.358$ ) and a rapidly convergent roll-subsidence mode. This aircraft also has a characteristic root indicating spiral stability.

Sensitivity Analysis. The equations of motion, as developed in Appendices B-5 and B-6, are used in the study as a baseline set of dynamics that are representative of an airframe that can be constructed. The actual airframe that is built would not perform exactly as the baseline dynamics predict. Therefore, a sensitivity analysis is done in Appendices B-7 and B-8 to determine how sensitive the baseline dynamics are to changes in input parameters. A best-case and worst-case set of dynamics are developed by looking only at changes in the damping ratio of the dominant oscillatory term in each of the longitudinal and lateral characteristic motions. A well-damped characteristic motion should provide well damped closed-loop dynamics. The best-case dynamics come from changes that increase the damping ratio and the worst-case results from a decreased damping ratio.

The dominant longitudinal oscillation is the phugoid oscillation. Combining terms that tend to increase the phugoid damping generate the

best-case dynamics. Worst-case dynamics result from combining all of the terms that tend to decrease the phugoid damping. Similarly, the damping ratio of the Dutch-roll mode in the lateral dynamics is used to generate the best and worst cases of lateral dynamics, see Appendix B-8.

Appendix B-7 shows that the aircraft can tolerate a 20% variation in  $C_{m\alpha}$ . This variation is converted to an allowable range of location for the center of gravity in Appendix B-9.

Servo and Sensor Models. Both a servo model and a sensor model are used to complete the closed-loop analysis. The servo model is developed in Appendix B-10. The sensors, a magnetometer for heading and a pressure transducer for altitude, are both solid-state devices and are modelled as unity gains. There are no lags associated with their measurements.

Heading Control. To close the heading control dynamics, the proper aircraft transfer functions are needed. Rudder-only turns are used for heading control. Appendix B-11 develops the lateral transfer functions for rudder inputs. The heading control loop to be analyzed is shown in Figure B-1.

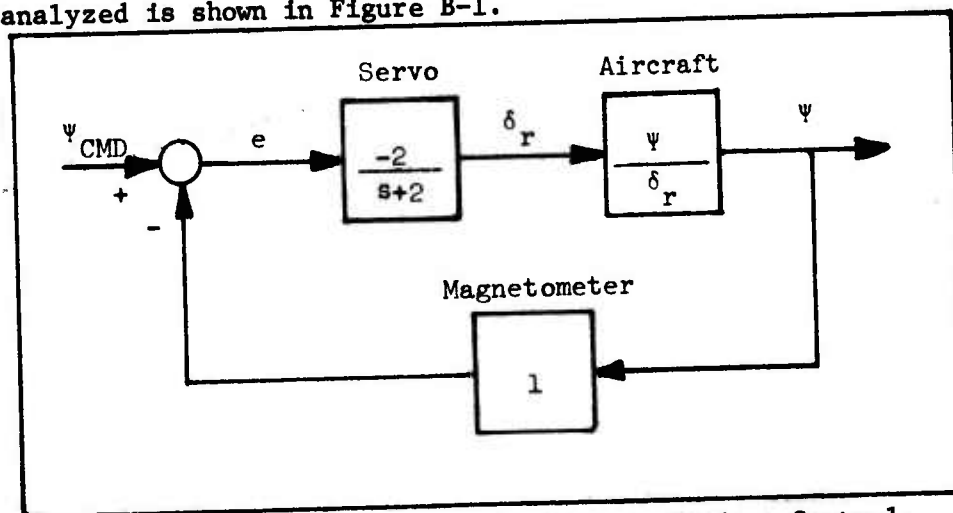


Figure B-1. Preliminary Closed-Loop Heading Control (No Compensation)

Appendix B-12 gives the details of the analysis of the closed-loop heading control. The lag of the servo drives the closed-loop dynamics unstable. A cascade lead-lag compensator and reduction of the gain are included in the forward path, as described in Appendix B-12, to stabilize the system. The resulting time response for the three sets of aircraft dynamics is shown in Figure B-2. The baseline airframe has a settling time, to within 5% of a commanded input, of less than 20 seconds. A complete heading control circuit description, including the lead-lag compensator, is presented in Appendix E-4.

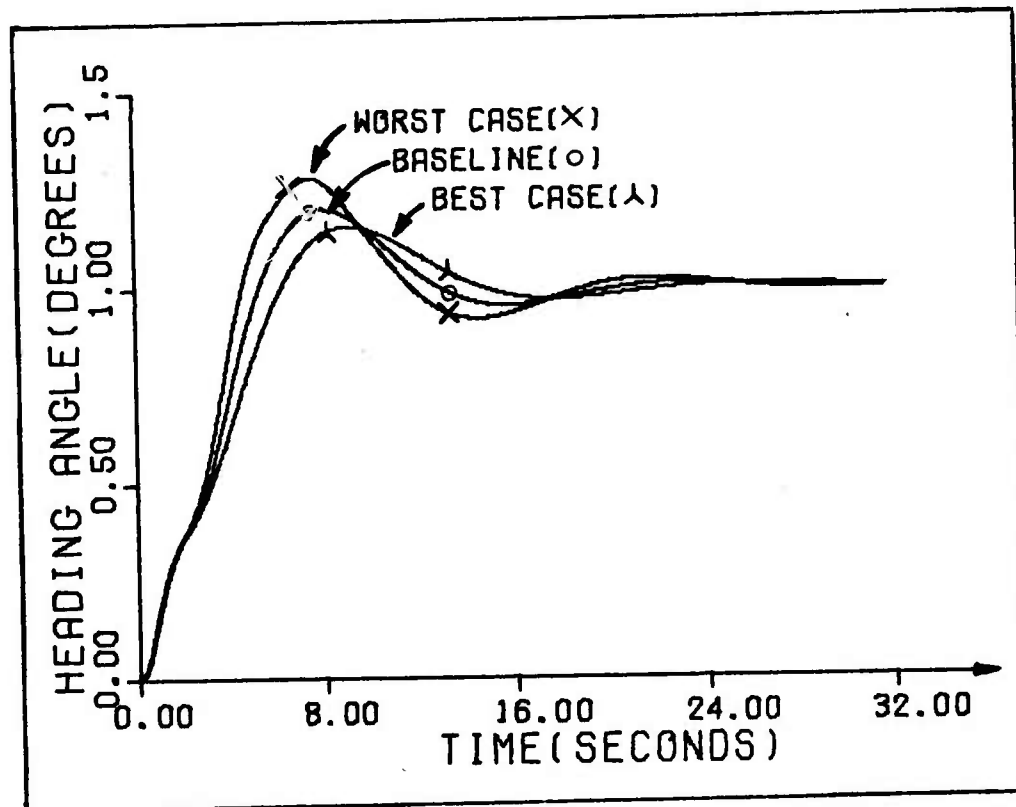


Figure B-2. Comparison of Heading Control Step Response for Varying Aircraft Dynamics

Altitude Hold. The longitudinal dynamics are developed and included in an altitude-hold system in Appendices B-14 and B-15. The elevator provides control inputs for the airframe and a solid-state pressure transducer senses and is used to feedback altitude. Figure B-3 is a block diagram description of the altitude-hold system.

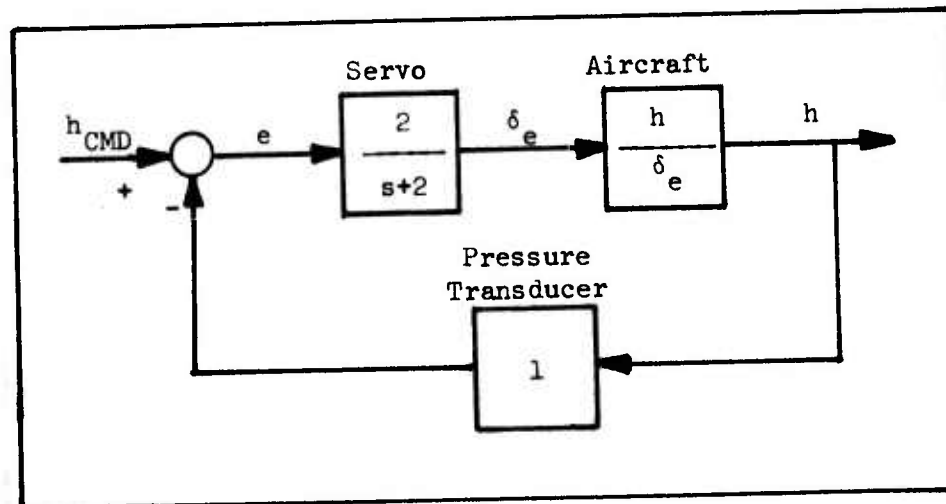


Figure B-3. Preliminary Altitude Hold Block Diagram (No Compensation)

The combination of servo lag and aircraft dynamics produces an unstable closed-loop system. To stabilize this system, a lead-lag compensator and reduction of gain are included in the forward path, and a lead-lag compensator is included in the feedback path (see Appendix B-15).

Figure B-4 shows a comparison of the best-case, worst-case and baseline time responses of the altitude hold system, (also see Appendix B-16). The dominant time response is an exponential growth to the final value. The baseline altitude-hold system requires 87 seconds to rise to 95% of the final value. The slow response is

acceptable in the altitude-hold loop since there will be few disturbances from the nominal altitude, and precise control is not required. A description of the altitude hold circuit is contained in Appendix B-17.

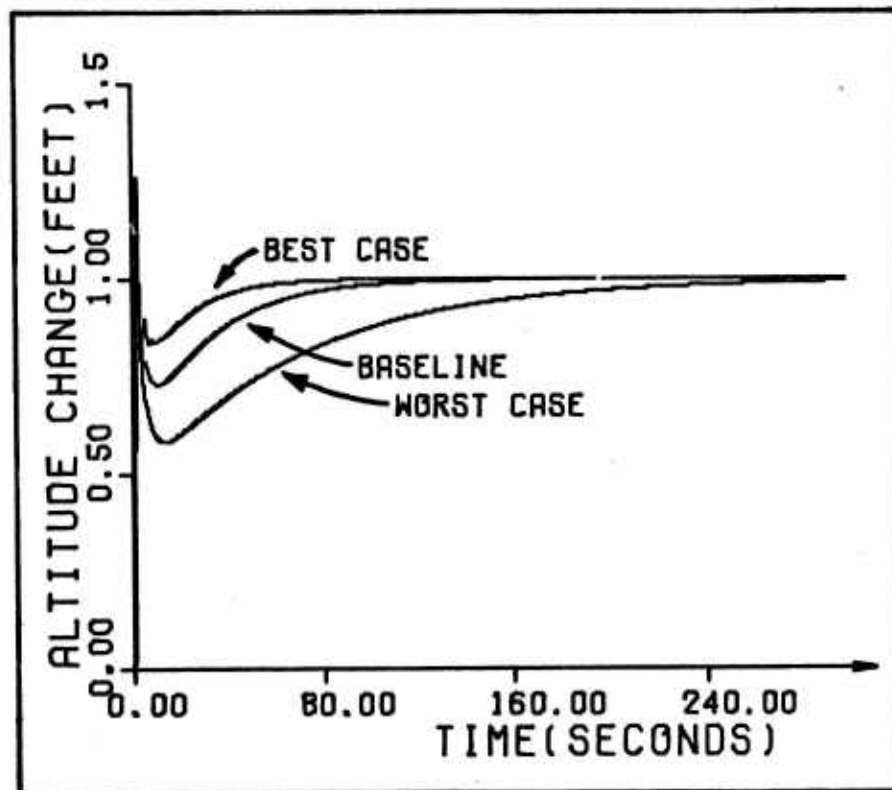


Figure B-4. Comparison of Step Response of Altitude Hold Circuit with Varying Aircraft Dynamics

#### Conclusions and Recommendations

Extended hands-off flying of mini-drones without a full-up autopilot, using rate sensors for stability, is feasible. Both heading and altitude control can be accomplished, given proper compensation for stability. The cascade compensators that have been selected are:

$\frac{(0.4)(s + 1)}{(s + 10)}$  in the forward path of the heading control loop

$\frac{(0.004)(s + 0.1)}{(s + 10)}$  in the forward path of the altitude-hold loop

$\frac{(10)(s + 4)}{(s + 40)}$  in the feedback path of the altitude-hold loop

The selected compensation techniques provide stability over a range of aircraft dynamics. It is recommended that wind-tunnel or flight testing be done to validate the simulation dynamics. This testing should be accomplished to confirm that the simulation that has been developed actually models the airframe that could eventually be built.

## APPENDIX B-1

### BASIS FOR THE EQUATIONS OF MOTION

The equations of motion that are used in this study are derived from Blakelock (1965). The derivation uses a body-fixed reference axis system with its origin fixed at the aircraft center of gravity (standard aircraft body-axis reference system).

#### Basic Assumptions

Aircraft has symmetry about the vertical plane through the center of gravity (left and right sides are symmetrical).

An earth-centered inertial reference is used on conjunction with a flat-earth assumption.

The mass of the aircraft remains fixed during the period of dynamic analysis (10-60 seconds).

The atmosphere is fixed and rotates with the earth.

The aircraft always starts in a condition of equilibrium, and disturbances arise from control inputs or other perturbations, such as gusting.

The aircraft is assumed to be a rigid body.

Perturbations from the equilibrium are assumed to be small, so the products of perturbations can be neglected, and small angle assumptions apply.

Quasi-steady flow exists (valid for low mach number ( $M < 0.8$ )).

These basic assumptions are used to generate a set of linear, decoupled equations of motion. The equations are decoupled into a

set of longitudinal (pitch dynamics) and lateral (roll and yaw dynamics) equations of motion.

The final form of the equation, as derived by Blakelock (1965:21), is as follows:

Longitudinal Equations of Motion:

$$\begin{aligned} \left( \frac{mU}{Sq} s - C_{x_u} \right) \dot{u}(s) + \left( -\frac{c}{2U} C_{x_d} s - C_{x_\alpha} \right) \dot{\alpha}(s) \\ + \left( -\frac{e}{2U} C_{x_q} s - C_w(\cos\theta_T) \right) \theta(s) = C_{F_{x_a}} \end{aligned} \quad (B-1)$$

$$\begin{aligned} \left\{ \left( \frac{mU}{Sq} - \frac{c}{2U} C_{z_\alpha} \right) s - C_{z_\alpha} \right\} \dot{\alpha}(s) \\ + \left\{ \left( -\frac{mU}{Sq} - \frac{c}{2U} C_{z_q} \right) s - C_w(\sin\theta_T) \right\} \theta(s) = C_{F_{z_a}} \end{aligned} \quad (B-2)$$

$$\begin{aligned} -C_{m_u} \dot{u}(s) + \left\{ \left( -\frac{c}{2U} C_{m_\alpha} \right) s - C_{m_\alpha} \right\} \dot{\alpha}(s) \\ + \left( \frac{I_y}{Sq c} s^2 - \frac{c}{2U} C_{m_q} s \right) \theta(s) = C_{m_a} \end{aligned} \quad (B-3)$$

Lateral Equations of Motion:

$$\begin{aligned} -C_{y_\phi} \phi(s) + \left( \frac{mU}{Sq} s - C_{y_\psi} \right) \psi(s) + \left( \frac{mU}{Sq} s - C_{y_\beta} \right) \\ \beta(s) = C_{y_a} \end{aligned} \quad (B-4)$$

$$\left( \frac{I_x}{Sq b} s^2 - \frac{b}{2U} C_{l_p} s \right) \phi(s) - \left( \frac{I_{xz}}{Sq b} s^2 + \frac{b}{2U} C_{l_r} s \right) \psi(s) \quad (B-5)$$

$$- C_{l\beta} \beta(s) = C_{l_a} \quad (B-5)$$

$$\left( -\frac{I_{xz}}{Sqb} s^2 - \frac{b}{2U} C_{n_p} s \right) \phi(s) - \left( \frac{I_z}{Sqb} s^2 - \frac{b}{2U} C_{n_r} s \right) \quad (B-6)$$

$$\psi(s) - C_{n\beta} \beta(s) = C_{n_a}$$

The coefficients of the above equations are non-dimensionalized coefficients, commonly referred to as "stability derivatives".

APPENDIX B-2

NOMINAL FLIGHT CONDITIONS FOR ANALYSIS

The three nominal flight conditions used in evaluation of the stability coefficients are launch, climb, and cruise. Some of the parameters associated with each of these conditions are contained in Table B-1.

TABLE B-1. NOMINAL FLIGHT PARAMETERS

	SPEED U (FT/SEC)	H (FT) ALTITUDE	DYNAMIC PRESSURE q (LB/FT <sup>2</sup> )	LIFT COEFFICIENT C <sub>L</sub>	DRAG COEFFICIENT C <sub>D</sub>	NOMINAL WEIGHT w (POUNDS)
Launch	73.33	0	6.394	1.22	0.118	120
Climb	88	5000	7.934	1.22	0.118	120
Cruise	110	10000	10.624	0.68	0.060	110

APPENDIX B-3

EVALUATION OF NOMINAL LONGITUDINAL STABILITY DERIVATIVES

The following equations come from Blakelock (1965) and Perkins and Hage (1949), except where noted. Aircraft planform and related characteristics are taken from the airframe design, Appendix A, and are summarized in Tables A-5 and A-6 and Figure A-10. Nominal cruise stability coefficients are developed in detail below:

$$\frac{C_{x_u}}{C_{x_u}} = \frac{U}{Sq} \frac{\partial T}{\partial u} - 2C_D - U \frac{\partial C_D}{\partial u} \quad (B-7)$$

where

$$\frac{\partial T}{\partial u} = -0.227 \text{ (from Figure C-17)}$$

so

$$C_{x_u} = \frac{110}{(17)(10.62)} (-0.227) - (2)(0.06) - (110)(0)$$

$$C_{x_u} = -0.258$$

$$\frac{C_{x_\alpha}}{C_{x_\alpha}} = C_L - \frac{\partial C_D}{\partial \alpha} \quad (B-8)$$

where

$$\frac{\partial C_D}{\partial \alpha} = \left( \frac{2C_L}{\pi eA} \right) \left( \frac{\partial C_L}{\partial \alpha} \right)$$

$$= \frac{(2)(0.68)(4.75)}{\pi(0.93)(6)}$$

$$= 0.369$$

so

$$C_{x_\alpha} = 0.68 - 0.369$$

$$C_{x_\alpha} = 0.311$$

$\frac{C_w}{C_w}$

$$C_w = - \frac{mg}{Sq} \quad (B-9)$$

$$= - \frac{110}{(17)(10.62)}$$

$$C_w = - 0.609$$

$\frac{C_{z_u}}{C_{z_u}}$

$$C_{z_u} = - 2 C_L - U \frac{\partial C_L}{\partial u} \quad (B-10)$$

$$= (-2)(0.68) - (110)(0)$$

$$C_{z_u} = - 1.36$$

$\frac{C_{z_\alpha}}{C_{z_\alpha}}$

$$C_{z_\alpha} = - C_D - \frac{\partial C_L}{\partial \alpha} \quad (B-11)$$

$$= - \frac{\partial C_L}{\partial \alpha} \quad \text{since } \frac{\partial C_L}{\partial \alpha} \gg C_D$$

$$C_{z_\alpha} = - 4.75$$

$\frac{C_{z_{\dot{\alpha}}}}{C_{z_{\dot{\alpha}}}}$

$$C_{z_{\dot{\alpha}}} = 2 \frac{\partial C_m}{\partial i_t} \frac{d\epsilon}{d\alpha} \quad (B-12)$$

with

$$\begin{aligned}\frac{\partial C_m}{\partial i_t} &= - \eta_{ht} \frac{l_{ht} s_{ht}}{cS} a_{ht} && \text{(Seckel, 1964:60)} \\ &= (-1) \frac{(4.58)(4.61)(3.09)}{(1.78)(17)} \\ &= - 2.16\end{aligned}$$

and

$$\begin{aligned}\frac{d\varepsilon}{d\alpha} &= \frac{4}{A+2} && \text{(Seckel, 1964:61)} \\ &= 0.5\end{aligned}$$

so

$$\begin{aligned}C_{z\alpha} &= (2)(-2.16)(.5) \\ &= - 2.16\end{aligned}$$

$\frac{C_{zq}}{C_{zq}}$

$$C_{zq} = (2)K \frac{\partial C_m}{\partial i_t} \quad \text{(B-13)}$$

with

$$K = 1.1 \quad \text{(Blakelock, 1965:30)}$$

so

$$\begin{aligned}C_{zq} &= (2)(1.1)(-2.16) \\ C_{zq} &= - 4.75\end{aligned}$$

$\frac{C_{m\alpha}}{C_{m\alpha}}$

$$C_{m\alpha} = (S.M.) \frac{\partial C_L}{\partial \alpha} \quad \text{(B-14)}$$

where

$$\begin{aligned} \text{S.M.} &= \text{Static Margin} \\ &= -0.2 \end{aligned}$$

so

$$\begin{aligned} C_{m_\alpha} &= (-0.2)(4.75) \\ &= -0.95 \end{aligned}$$

$$\begin{aligned} \frac{C_{m_\alpha}}{c} &= (2) \frac{\partial C_m}{\partial i_t} \frac{d\epsilon}{d\alpha} \frac{l_{ht}}{c} && \text{(B-15)} \\ &= 2(-2.16)(0.5) \frac{(4.58)}{1.78} \\ C_{m_\alpha} &= -5.56 \end{aligned}$$

$$\begin{aligned} \frac{C_{m_q}}{c} &= 2K \frac{\partial C_m}{\partial i_t} \frac{l_{ht}}{c} && \text{(B-16)} \\ &= (2)(1.1)(-2.16) \frac{(4.58)}{1.78} \\ C_{m_q} &= -12.23 \end{aligned}$$

$$\begin{aligned} \frac{C_{x_\alpha}}{c} &= 0 && \text{(B-17)} \end{aligned}$$

since drag changes are negligible (Blakelock, 1965:25)

$$\frac{C_{xq}}{q} = 0 \quad (B-18)$$

since drag changes are negligible (Blakelock, 1965:25)

$$\frac{C_{m_u}}{u} = 0 \quad (B-19)$$

since slipstream effects are negligible  
(Blakelock, 1965:26)

The same methodology is used to generate the coefficients for the other two flight conditions. The nominal longitudinal stability coefficients for the three flight conditions are summarized in Table B-2 (all coefficients are unitless or per radian).

TABLE B-2. NOMINAL LONGITUDINAL STABILITY COEFFICIENTS

	<u>LAUNCH</u>	<u>CLIMB</u>	<u>CRUISE</u>
$C_{x_u}$	-0.389	-0.384	-0.258
$C_{x_\alpha}$	-0.568	0.568	0.311
$C_w$	-1.105	-0.890	-0.609
$C_{z_u}$	-2.44	-2.44	-1.36
$C_{z_\alpha}$	-4.75	-4.75	-4.75
$C_{z_{\dot{\alpha}}}$	-2.16	-2.16	-2.16
$C_{z_q}$	-4.75	-4.75	-4.75
$C_{m_\alpha}$	-0.95	-0.95	-0.95
$C_{m_{\dot{\alpha}}}$	-5.56	-5.56	-5.56
$C_{m_q}$	-12.23	-12.23	-12.23

APPENDIX B-4

EVALUATION OF NOMINAL LATERAL STABILITY DERIVATIVES

The following equations come from Blakelock (1965) and Perkins and Hage (1949), except where noted. Airframe planform and related characteristics are from Appendix A and are summarized in Tables A-5 and A-6 and Figure A-10. Nominal cruise coefficients are generated in detail below.

$$\frac{C_{\ell P}}{C_{\ell P}} = -0.45 \quad (\text{Perkins, 1949:357}) \quad (\text{B-20})$$

$$\frac{C_{\ell \beta}}{C_{\ell \beta}} = -C_{\ell \psi} \quad (\text{B-21})$$

where

$C_{\ell \psi}$  is composed of the following four components

$$C_{\ell \psi} = C_{\ell \psi \text{ wing}} + C_{\ell \psi \text{ vert tail}} + \Delta C_{\ell \psi 1} + \Delta C_{\ell \psi 2} \quad (\text{B-22})$$

(Perkins, 1949:323)

with

$$\begin{aligned} C_{\ell \psi \text{ wing}} &= \frac{C_{\ell \psi}}{\Gamma} \Gamma + \Delta C_{\ell \psi \text{ tip shape}} \\ &= \frac{(0.75)(5)(57.3)}{3290} + 0.0 \\ &= 0.0653 \end{aligned}$$

and

$$\begin{aligned} C_{l\psi_{\text{vert tail}}} &= C_{n\psi_{\text{vert tail}}} \frac{z_{vt}}{l_{vt}} \\ &= -a_{vt} \frac{S_{vt}}{S} \frac{l_{vt}}{b} \eta_{vt} + \Delta_2 C_{n\psi} \frac{z_{vt}}{l_{vt}} \end{aligned}$$

where  $A_{ve}$ , the effective aspect ratio of the vertical tail is:

$$\begin{aligned} A_{ve} &= 1.55 \frac{b_{vt}^2}{S_{vt}} \quad (\text{Perkins, 1949:325}) \\ &= \frac{(1.55)(15)^2}{210} \\ &= 1.66 \end{aligned}$$

which yields

$$a_{vt} = 2.21 \quad (\text{Perkins, 1949:324})$$

also

$$\Delta_2 C_{n\psi} = .0287 \quad (\text{Perkins, 1949:324})$$

therefore

$$\begin{aligned} C_{l\psi_{\text{vert tail}}} &= \frac{(-2.21)(1.46)(4.59)(1)}{(17)(10.1)} + 0.0287 \frac{0.595}{4.58} \\ &= -.0149 \end{aligned}$$

also

$$\Delta C_{l\psi_1} = .0344$$

and

$$\Delta C_{l\psi_2} = -.0092$$

so

$$C_{l_{\psi}} = C_{l_{\psi_{\text{wing}}}} + C_{l_{\psi_{\text{vert tail}}}} + \Delta C_{l_{\psi_1}} + \Delta C_{l_{\psi_2}}$$

$$= 0.0633 - .0149 + .0344 - .0092$$

$$C_{l_{\psi}} = 0.0756$$

$$C_{l_{\beta}} = -0.0756$$

$$\frac{C_{l_r}}{C_{l_r}}$$

$$= \frac{C_L}{4}$$

(B-23)

$$= \frac{0.68}{4}$$

$$= 0.17$$

$$\frac{C_{n_p}}{C_{n_p}}$$

$$= \frac{-C_L}{8} \left(1 - \frac{d\epsilon}{d\alpha}\right)$$

(B-24)

$$= \frac{-0.68}{8} (1 - 0.5)$$

$$= -0.0425$$

$$\frac{C_{n_r}}{C_{n_r}}$$

$$= \frac{-C_D^*}{4} - 2n_{vt} \frac{S_{vt}}{S} \frac{l_{vt}}{b} (a_{vt})(2)$$

(B-25)

where the factor of 2 is for two tail surfaces

$$= -\frac{0.03}{4} - 2(1) \frac{(1.46)}{(17)} \frac{(4.58)^2}{(10.1)} (2.21)(2)$$

$$= -0.164$$

$$\begin{aligned}
 \frac{C_{y\phi}}{C_{y\phi}} &= \frac{mg}{Sq} \cos \theta_T && \text{(B-26)} \\
 &= \frac{(110)}{(17)(10.62)} \cos 0^\circ \\
 &= 0.609
 \end{aligned}$$

$$\begin{aligned}
 \frac{C_{y\psi}}{C_{y\psi}} &= \frac{mg}{Sq} \sin \theta_T && \text{(B-27)} \\
 &= \frac{110}{(17)(10.62)} \sin 0^\circ \\
 &= 0.0
 \end{aligned}$$

$$\begin{aligned}
 \frac{C_{n\beta}}{C_{n\beta}} &= -C_{n\psi} && \text{(B-28)}
 \end{aligned}$$

where

$$C_{n\psi} = C_{n\psi}^{\text{prop}} + \Delta_1 C_{n\psi} + C_{n\psi}^{\text{fus}} + C_{n\psi}^{\text{wing}}$$

$$C_{n\psi}^{\text{prop windmilling}} = -0.00573$$

$$C_{n\psi}^{\text{prop full power}} = (1.5)(-0.00573)$$

$$= -0.00745$$

$$\Delta_1 C_{n\psi} = -0.0115$$

$$C_{n\psi}^{\text{fus}} = 0.0195$$

$$C_{n\psi_{wing}} = -0.00613$$

so

$$C_{n\psi} = -0.00745 - 0.0115 + 0.0195 - 0.00613$$
$$= -0.0056$$

and

$$C_{n\beta} = 0.0056$$

$C_{y\beta}$

$C_{y\beta}$  has no simple equation, so use  $C_{y\beta} = -0.6$  (Blakelock, 1965:112)

The same methodology is used to generate the stability coefficients for the other two flight conditions. The nominal lateral stability coefficients for the three flight conditions are summarized in Table B-3 (all coefficients are unitless or per radian).

TABLE B-3. NOMINAL LATERAL STABILITY COEFFICIENTS.

	<u>LAUNCH</u>	<u>CLIMB</u>	<u>CRUISE</u>
$C_{\ell p}$	-0.45	-0.45	-0.45
$C_{\ell \beta}$	-0.0756	-0.0756	-0.0756
$C_{\ell r}$	0.31	0.31	0.17
$C_{n p}$	-0.0763	-0.0763	-0.0425
$C_{n r}$	-0.177	-0.177	-0.164
$C_{y \phi}$	1.08	0.87	0.609
$C_{y \psi}$	0.23	0.185	0.0
$C_{n \beta}$	0.0069	0.0069	0.0056
$C_{y \beta}$	-0.6	-0.6	-0.6

APPENDIX B-5

LONGITUDINAL DYNAMICS AND CHARACTERISTIC MOTION

The longitudinal stability coefficients are used in the appropriate non-dimensionalized equations of motion from Appendix B-1 to generate the following set of equations for cruise conditions:

$$(2.081s + 0.258) u(s) + (-.311) \alpha(s) + (.609) \theta(s) = C_{F_{x_a}} \quad (B-29)$$

$$(1.361) u(s) + (2.081s + 4.75) \alpha(s) + (-2.081) \theta(s) = C_{F_{z_a}} \quad (B-30)$$

$$(.045s + 0.95) \alpha(s) + (.0223s^2 + 0.099s) \theta(s) = C_{m_a} \quad (B-31)$$

Similar sets of equations can be generated for take-off and climb conditions. The characteristic equation is determined by setting the determinant of the coefficients of the above equations equal to zero. The characteristic equation of the homogeneous solution (zero forcing functions) for the system of equations is generated and factored to yield the characteristic motion.

The longitudinal characteristic motions for the three conditions of flight are summarized in Table B-4.

TABLE B-4. LONGITUDINAL CHARACTERISTIC MOTION

	<u>PHUGOID</u>		<u>SHORT PERIOD</u>	
	NATURAL FREQUENCY $\omega_n$ (rad/sec)	DAMPING RATIO $\zeta$	NATURAL FREQUENCY $\omega_n$ (rad/sec)	DAMPING RATIO $\zeta$
Take-off	0.559	0.053	5.8	0.67
Climb	0.528	0.077	6.35	0.64
Cruise	0.393	0.145	7.26	0.602

APPENDIX B-6

LATERAL DYNAMICS AND CHARACTERISTIC MOTION

The lateral stability coefficients are used in the corresponding non-dimensionalized equations of motion, from Appendix B-1, to generate the following set of equations for cruise conditions.

$$(-0.609) \phi(s) + (2.081s) + \psi(s) + (2.081s + 0.6) \beta(s) = C_{F_{y_a}} \quad (B-32)$$

$$(0.0024s^2 + 0.0207s) \phi(s) + (0.0002s^2 - 0.0142s) \psi(s) + (0.0756) \beta(s) = C_{l_a} \quad (B-33)$$

$$(0.0002s^2 + 0.0016s) \phi(s) + (0.0061s^2 + 0.0075s) \psi(s) + (0.0057) \beta(s) = C_{n_a} \quad (B-34)$$

Similar sets of equations can be generated for take-off and climb conditions. The characteristic equation arising from the system of equations with the forcing functions equal to zero is solved for the characteristic motion. The lateral characteristic motions for the three conditions of flight are summarized in Table B-5.

TABLE B-5. LATERAL CHARACTERISTIC MOTION

	<u>DUTCH ROLL</u>			
	NATURAL FREQUENCY $\omega_n$ (rad/sec)	DAMPING RATIO $\zeta$	SPIRAL STABILITY	ROLL SUBSIDENCE
Launch	1.621	0.375	-0.342	-7.78
Climb	1.767	0.381	-0.301	-8.12
Cruise	1.649	0.358	-0.409	-8.76

## APPENDIX B-7

### SENSITIVITY ANALYSIS OF LONGITUDINAL STABILITY COEFFICIENTS

Each of the longitudinal stability coefficients are changed from their nominal values. The resulting changes to the characteristic motion are contained in Table B-6. In general, plus and minus twenty percent changes are used. The weight terms and a lift related term,  $C_{z_u}$ , are varied only ten percent, since the weight change due to using fuel can only vary ten percent around the nominal.

The best case and worst case result from looking at the damping ratio of the phugoid. The phugoid is a long-period lightly-damped oscillation which is the dominant longitudinal characteristic motion. Increasing and decreasing the damping ratio of the phugoid are used to define the best-case and worst-case dynamics. The best case is a combination of all of the changes that increase the damping ratio. The worst case is a combination of all the terms that decrease the damping ratio. The best-case and worst-case characteristic motions are included in Table B-6.

TABLE B-6. LONGITUDINAL SENSITIVITY

STABILITY DERIVATIVE	PERCENT CHANGE	SHORT PERIOD		PHUGOID	
		NATURAL FREQUENCY $\omega_n$ (rad/sec)	DAMPING RATIO $\zeta$	NATURAL FREQUENCY $\omega_n$ (rad/sec)	DAMPING RATIO $\zeta$
	Baseline	7.264	0.602	0.393	0.145
Weight	+10%	7.200	0.593	0.378	0.136
	-10%	7.342	0.613	0.410	0.156
$C_{x_u}$	+20%	7.264	0.602	0.393	0.177
	-20%	7.264	0.602	0.393	0.113
$C_{z_u}$	+10%	7.264	0.602	0.412	0.137
	-10%	7.264	0.602	0.373	0.154
$C_{m_\alpha}$	+20%	7.828	0.559	0.399	0.143
	-20%	6.652	0.658	0.384	0.148
$C_{m_q}$	+20%	7.404	0.651	0.386	0.148
	-20%	7.121	0.551	0.401	0.142
$C_{x_\alpha}$	+20%	7.264	0.602	0.393	0.147
	-20%	7.264	0.602	0.393	0.143
$C_{m_{\dot{\alpha}}}$	+20%	7.264	0.630	0.393	0.145
	-20%	7.263	0.575	0.393	0.145
Best Case		7.684	0.791	0.370	0.215
Worst Case		6.948	0.457	0.409	0.096

## APPENDIX B-8

### SENSITIVITY ANALYSIS OF THE LATERAL STABILITY COEFFICIENTS

The sensitivity of the characteristic motion of the aircraft to changes in stability coefficients is determined by varying one coefficient at a time. In general, the changes are plus and minus 20% from the nominal. The weight terms are varied only 10%, which is the actual weight variation due to fuel flow.

There is no simple relationship to generate the  $C_{y\beta}$  term. A nominal value of  $C_{y\beta} = -0.6$  was selected (Blakelock, 1965:112). The sensitivity of  $C_{y\beta}$  is checked for an increase of 50% and a decrease of an order of magnitude.

The best case and worst case dynamics result from looking only at the damping ratio of the Dutch roll mode. The Dutch roll oscillation is the dominant characteristic oscillation of the lateral response. Therefore, increasing and decreasing its damping ratio is used to define the best and worst case dynamics. The best case is the combination that increases the damping ratio. The worst case is the combination of terms that decrease the damping ratio (see Table B-7).

TABLE B-7. LATERAL SENSITIVITY

STABILITY COEFFICIENT	CHANGE	DUTCH ROLL		SPIRAL STABILITY	ROLL SUBSIDENCE
		NATURAL FREQUENCY $\omega_n$ (rad/sec)	DAMPING RATIO $\zeta$		
BASELINE		1.649	0.358	-0.409	-8.760
Weight	+10%	1.559	0.295	-0.38	-7.294
	-10%	1.775	0.435	-0.442	-11.011
$C_{\ell p}$	+20%	1.564	0.391	-0.381	-10.453
	-20%	1.767	0.308	-0.440	-7.110
$C_{\ell \beta}$	+20%	1.751	0.318	-0.446	-8.782
	-20%	1.546	0.403	-0.358	-8.738
$C_{n_r}$	+20%	1.595	0.404	-0.539	-8.761
	-20%	1.688	0.307	-0.299	-8.760
$C_{n_p}$	+20%	1.713	0.355	-0.366	-8.760
	-20%	1.582	0.355	-0.459	-8.760
$C_{y \beta}$	+50%	1.698	0.394	-0.386	-8.762
	-90%	1.563	0.278	-0.455	-8.757
BEST CASE		1.536	0.597	-0.471	-13.164
WORST CASE		1.815	0.180	-0.325	-5.991

APPENDIX B-9

NEUTRAL POINT AND CENTER OF GRAVITY LOCATION

The locations and relationships of the wing aerodynamic center (quarter-chord point of the wing), the center of gravity of the aircraft and the neutral point (aerodynamic center) of the aircraft are shown in Figure B-5.

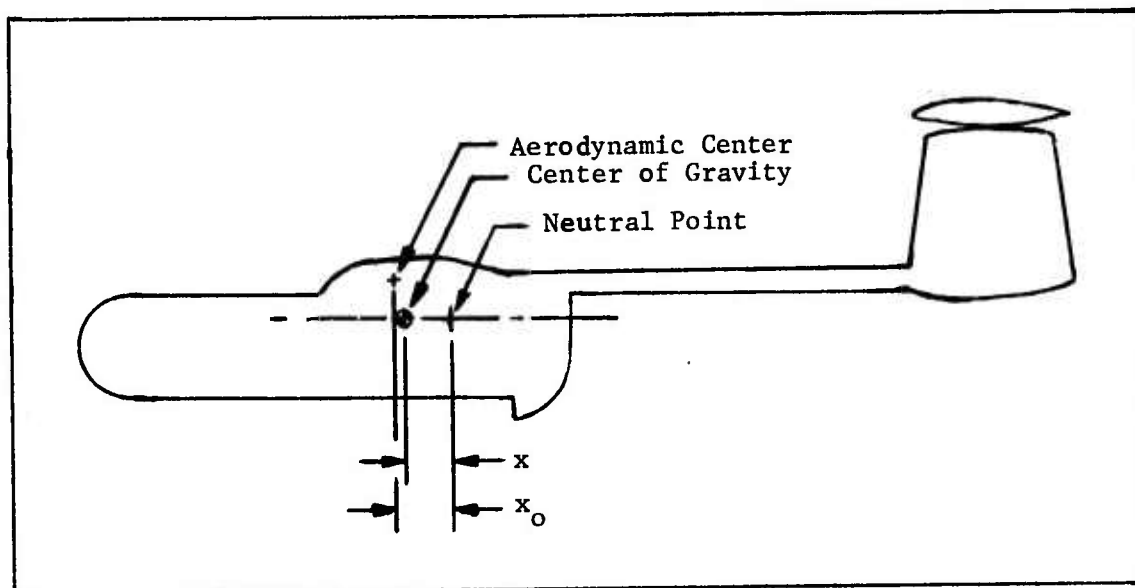


Figure B-5. Aerodynamic Center, Center of Gravity and Neutral Point Locations

The aircraft neutral point (aircraft aerodynamic center) is located the distance  $x_0$  behind the wing aerodynamic center. The distance,  $x_0$ , can be found using the following relationships:

$$\frac{x_0}{c} = \left(1 - \frac{d\epsilon}{d\alpha}\right) \frac{C_{L\alpha t}}{C_{L\alpha}} \eta_{vt} \frac{S_{vt} l_{vt}}{Sc} \quad (B-35)$$

(Dommasch, 1951:382)

$$= (1 - 0.5) \frac{3.09}{4.75} (1) \frac{4.61}{17} \frac{4.58}{1.78}$$

$$= 0.227$$

so

$$x_o = (0.227)(c)$$

$$= (0.227)(1.78)$$

$$= 0.404 \text{ feet}$$

$$= 4.85 \text{ inches}$$

The distance between the neutral point and the aircraft center of gravity,  $x$  is determined by the static margin. A static margin of -20% is recommended as a starting point for this type of vehicle (Bair, 1975:12). (The negative value of  $x$  indicates that the center of gravity is in front of the neutral point, which is required for a stable aircraft.)

$$\frac{x}{c} = \text{Static Margin}$$

$$= -0.20$$

so

$$x = (-0.20)(c)$$

$$= (-0.20)(1.78)$$

$$= -0.356 \text{ feet}$$

$$= -4.27 \text{ inches}$$

These calculations result in a theoretical difference between the center of gravity and the wing aerodynamic center of about one-half an inch. Therefore, the center of gravity of the aircraft is con-

sidered located at the wing aerodynamic center (quarter chord point of the wing).

Appendix B-7 shows that  $\pm 20\%$  changes in  $C_{m_\alpha}$  are not excessive and do not drastically affect the aircraft stability characteristics. A 20% change in  $C_{m_\alpha}$  directly relates to a 20% change in static margin, see Eq (B-14), which can be used to calculate the allowable range for center of gravity. For a 20% increase in static margin Eq(B-36) yields  $x = -5.13$  inches. For a 20% decrease in static margin Eq(B-36) gives  $x = -3.42$  inches. This indicates that the location of the center of gravity moves through 1.71 inches to vary the static margin by  $\pm 20\%$ . It is expected that the variation from aircraft to aircraft will be much less than this.

APPENDIX B-10

SERVO TRANSFER FUNCTION

The proposed control loops involve servos, which must be mathematically modelled to be included in the closed-loop analysis. The response of the Kraft KPS-16 servos, that are proposed, is highly non-linear. As a first order approximation the servos are modelled as a simple, linear, first-order time lag.

The servo response reaches 95% of the final value in one second and travels the last 5% in one-tenth of a second. Figure B-6 shows that an exponential of the form,  $f(t) = 1 - e^{-t/\tau}$  with  $\tau = 0.5$ , is an approximation to the response of the servo. The appropriate transfer function is:

$$\begin{aligned} \text{T. F. servo} &= \frac{K_s}{s + 1/\tau} \\ &= \frac{2}{s + 2} \end{aligned} \quad (\text{B-37})$$

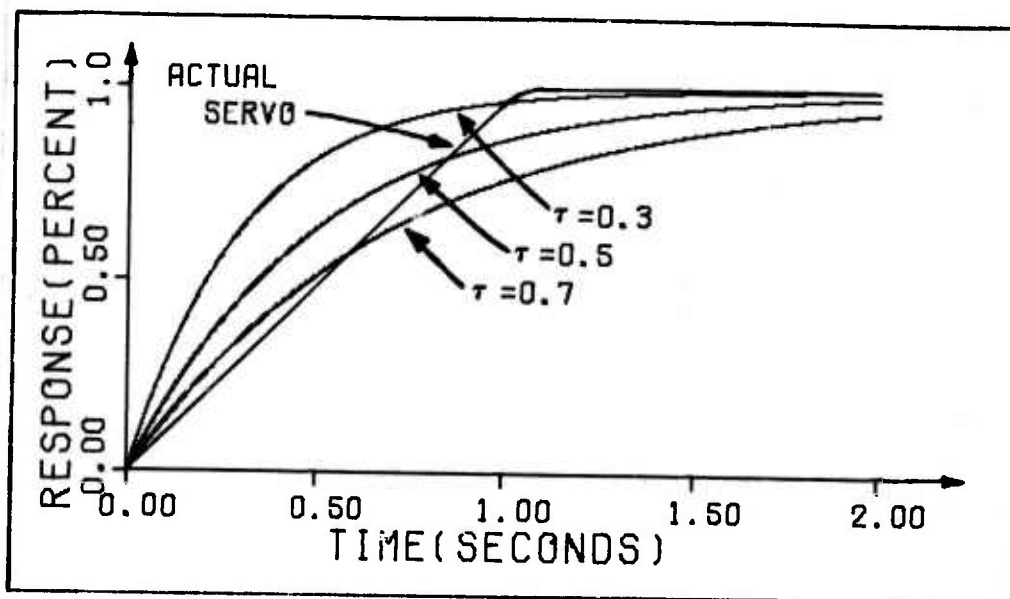


Figure B-6. Exponential Approximation of the Linearized Response Curve of the KPS-16 Servo

APPENDIX B-11

LATERAL DYNAMICS WITH RUDDER INPUT

The forcing functions involved with rudder inputs are evaluated to determine the lateral dynamics which result from rudder inputs.

$$\frac{C_{n\delta_r}}{C_{n\delta_r}} = -a_{vt}\tau_{vt} \frac{S_{vt}}{S} \frac{l_{vt}}{b} n_{vt}(2) \quad (\text{Perkins, 1949:250}) \quad (\text{B-38})$$

(The factor of two is included since this aircraft has two rudders)

$$\begin{aligned} \text{Using } A_{v_e} &= 1.55 \frac{b_{vt}^2}{S_{vt}} && (\text{Perkins, 1949:325}) \quad (\text{B-39}) \\ &= 1.55 \frac{15^2}{210} \\ &= 1.66 \end{aligned}$$

yields

$$a_{vt} = 2.21/\text{rad} \quad (\text{Perkins, 1949:250}) \quad (\text{B-40})$$

also

$$\tau_{vt} = 0.5 \text{ for 30\% rudder} \quad (\text{Perkins, 1949:25}) \quad (\text{B-41})$$

$$C_{n\delta_r} = -(2.21)(0.5) \frac{1.46}{17} \frac{4.58}{10.1} \quad (1) \quad (2) \quad (\text{B-42})$$

$$C_{n\delta_r} = -.0861$$

$$\begin{aligned}
 \frac{C_{y\delta_r}}{C_{y\delta_r}} &= \frac{b}{l_{vt}} C_{n\delta_r} & (B-43) \\
 &= -\frac{10.1}{4.58} (-0.861) \\
 C_{y\delta_r} &= 0.1898
 \end{aligned}$$

$$\begin{aligned}
 \frac{C_{\phi\delta_r}}{C_{\phi\delta_r}} &= a_{vt} \tau_{vt} \frac{z_{vt}}{b} \frac{S_{vt}}{S} \quad (2) & (B-44) \\
 &= -\frac{10.1}{4.58} (-0.0861) \\
 &= (2.21)(0.5) \left(\frac{1}{10.1}\right) \frac{1.46}{17} \quad (2) \\
 &= 0.0188
 \end{aligned}$$

The AFIT TRANFUN program (TRANFUN, 1974) is used to generate transfer functions given a system of equations. These forcing functions and the basic lateral equations of motion, that are developed in Appendix B-6, are used to generate the transfer functions associated with a rudder input.

The transfer functions are:

$$\frac{\phi(s)}{\delta_r(s)} = \frac{9.034 (s + 4.14) (s - 12.37)}{(s + 0.587 \pm 1.542j) (s + 0.409) (s + 8.76)} \quad (B-45)$$

$$\frac{\psi(s)}{\delta_r(s)} = \frac{-14.41 (s + 0.0779 \pm 1.007j) (s + 8.75)}{s (s + 0.587 \pm 1.542j) (s + 0.409) (s + 8.76)} \quad (B-46)$$

$$\frac{\beta(s)}{\delta_r(s)} = \frac{15.33 (s - 0.166) (s + 8.511)}{(s + 0.587 \pm 1.542j) (s + 0.409) (s + 8.76)} \quad (B-47)$$

APPENDIX B-12

CLOSED-LOOP HEADING CONTROL DYNAMICS

Closed-loop navigation is accomplished using a magnetometer to sense and continuously feedback the aircraft heading angle,  $\psi$ , while in flight. This is compared with a commanded heading angle,  $\psi_{CMD}$ , which comes from the navigation scheme, to generate an error signal  $e$ . The error signal drives a servo which generates a rudder deflection,  $\delta_r$ . The aircraft responds to these rudder reflections to produce a heading change. The transfer function for the heading response is  $\frac{\psi(s)}{\delta_r(s)}$  as developed in Appendix B-11. The closed loop system is shown in Figure B-1.

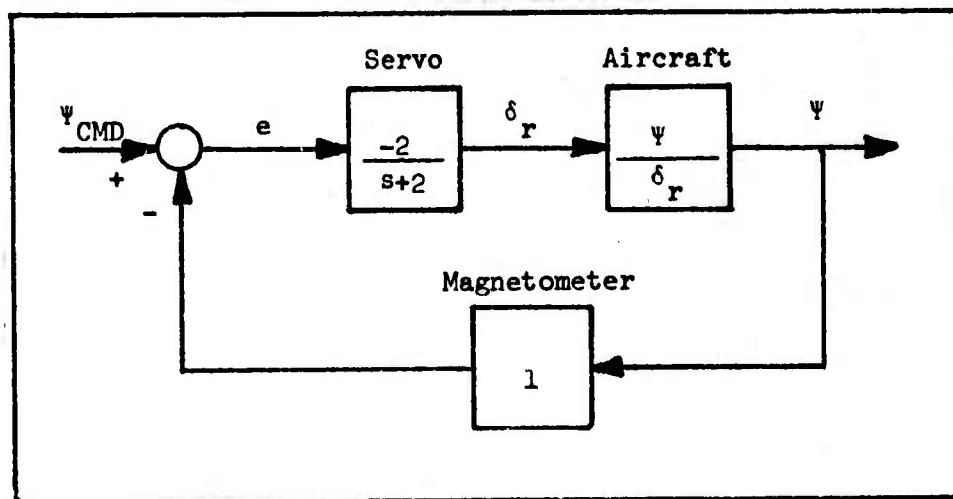


Figure B-1. Preliminary Closed-Loop Heading Control (No Compensation)

The open-loop transfer function, Eq(B-48), is used to plot a root locus of the closed-loop heading control system.

$$\text{T.F. O.L.} = \frac{(-2)(-41.41)(s+0.0779 \pm 1.007j)(s+8.74)}{(s)(s+2)(s+0.587 \pm 1.542j)(s+0.409)(s+8.76)} \quad (\text{B-48})$$

Figure B-7 is the associated root locus plot. The roots in the right-half s-plane indicate an unstable oscillating system. Figure B-8 shows the system response to a step change in commanded heading. These divergent oscillations in the time response are totally unacceptable. The inherent lag of the servo contributes to the unstable oscillations.

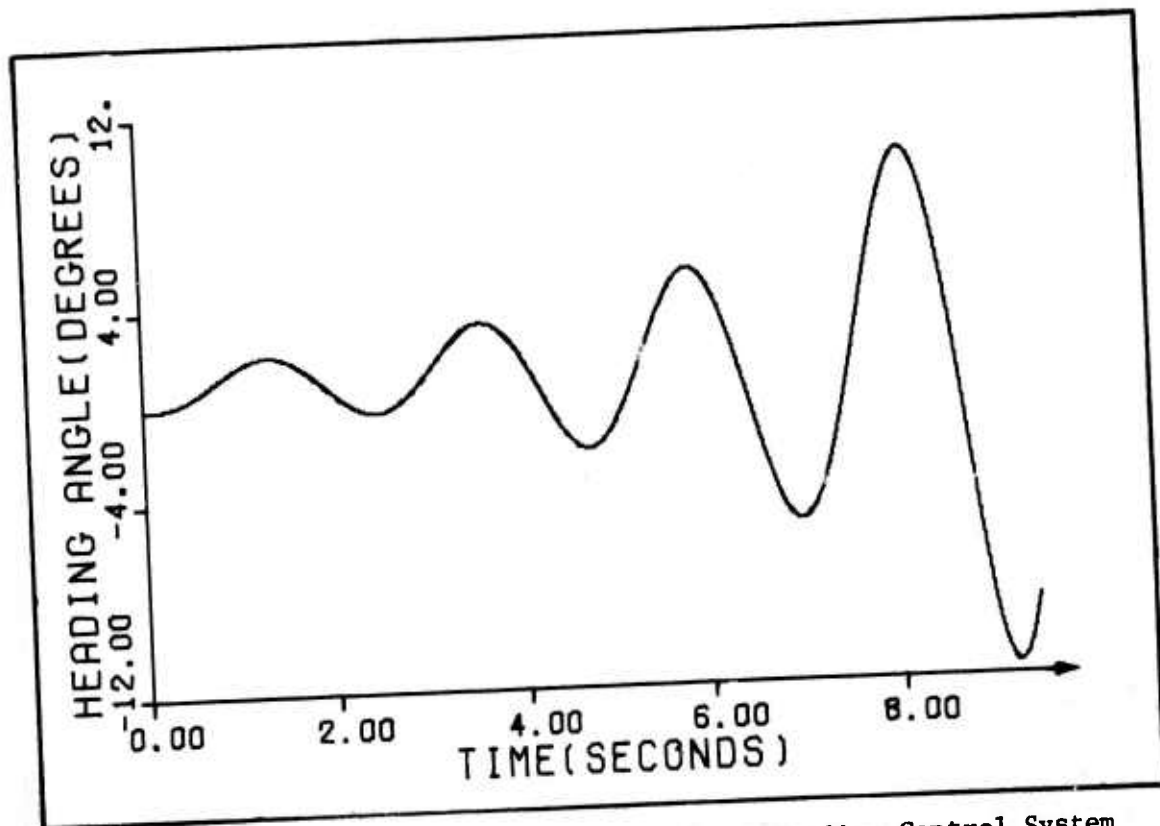


Figure B-8. Unstable Time Response of the Heading Control System (No Compensation)

The open-loop transfer function, Eq(B-48), is used to plot a root locus of the closed-loop heading control system.

$$T.F._{O.L.} = \frac{(-2)(-41.41)(s+0.0779 \pm 1.007j)(s+8.74)}{(s)(s+2)(s+0.587 \pm 1.542j)(s+0.409)(s+8.76)} \quad (B-48)$$

Figure B-7 is the associated root locus plot. The roots in the right-half s-plane indicate an unstable oscillating system. Figure B-8 shows the system response to a step change in commanded heading. These divergent oscillations in the time response are totally unacceptable. The inherent lag of the servo contributes to the unstable oscillations.

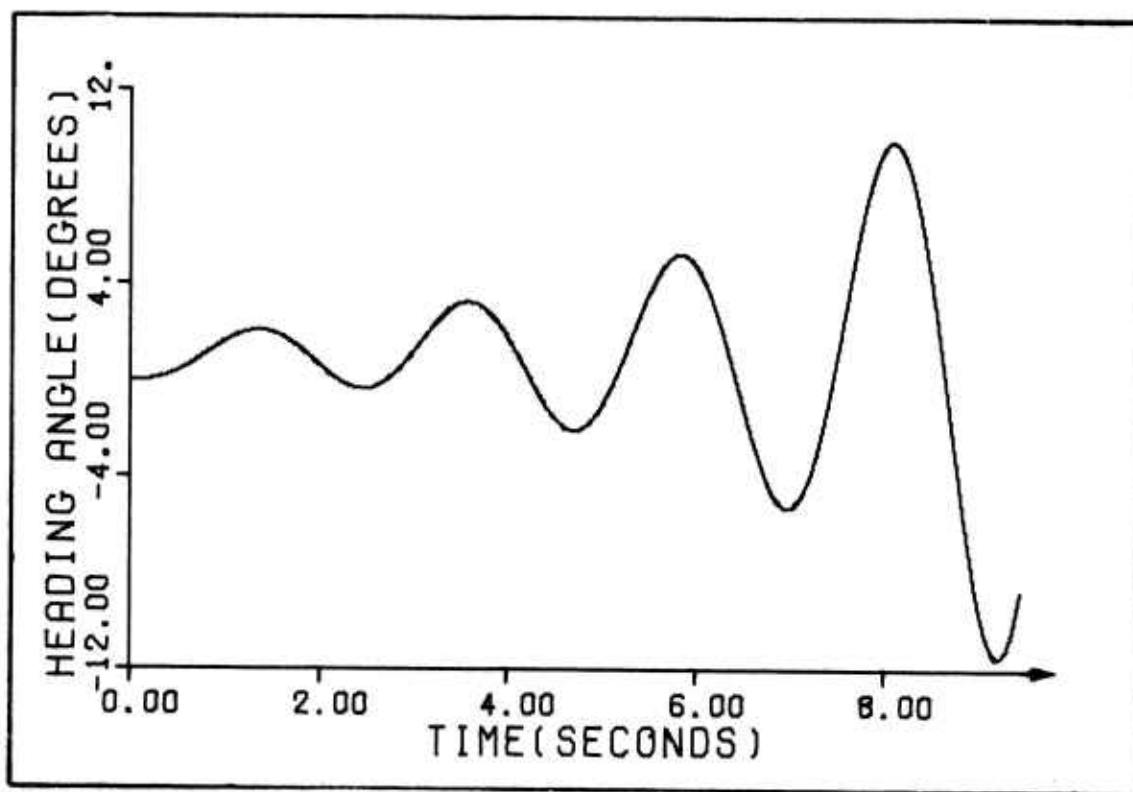


Figure B-8. Unstable Time Response of the Heading Control System (No Compensation)

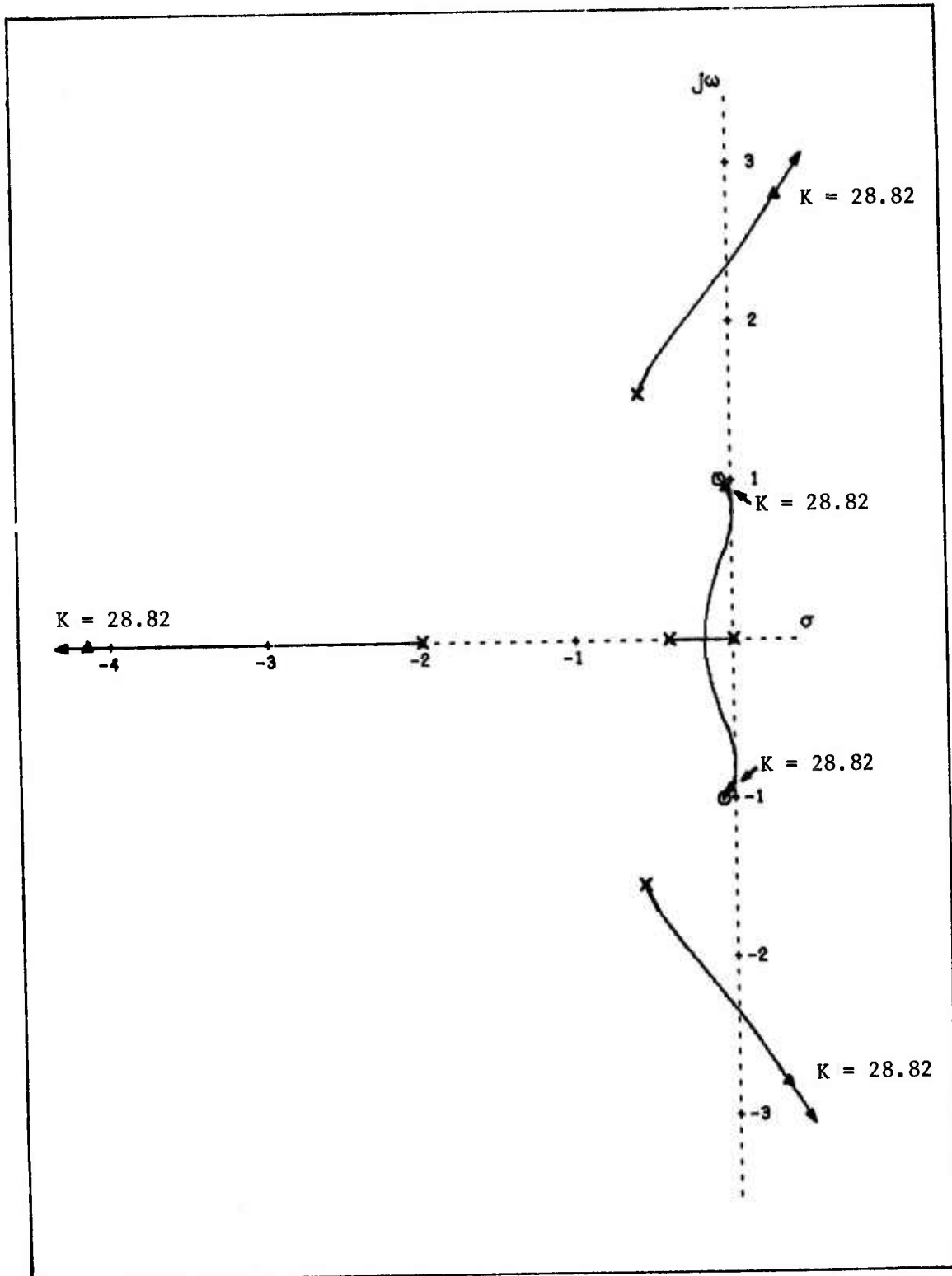


Figure B-7. Root Locus Plot of the Uncompensated Heading Control System.

Two methods that can be used to stabilize the system are: a reduction in gain, which moves the operating point along the original root locus, or a cascade compensator, which can vary the branches of the root locus and move them into the stable left-half s-plane. Cascade compensation, by moving them into the left-half s-plane, provides a larger gain margin than that which is provided by a gain reduction technique (gain margin is used here to mean the difference in gain required to move along a root locus branch from a satisfactory operating point to the imaginary axis, which is approaching an unstable operating point).

A lead-lag compensator of the form  $\frac{s + 1}{s + 10}$  provides for adequate time response of the system without the need for any other gain reduction. Various compensators are checked for adequate compensation using the ROOTL program. The above compensator is selected because it has the greatest effect on moving the root locus left to the stable region of the s-plane and provides a large gain margin. The resulting gain margin is slightly over one order of magnitude (3db). A block diagram of the closed-loop system, with the compensator included, is shown in Figure B-9.

The time response of the system comes from the closed-loop transfer function. The poles (denominator roots) of the closed-loop transfer function come from the operating points on the root locus, see Figure B-10. The zeros, or numerator roots of the closed loop transfer function, are a product of the forward path zeros, forward path gain, and feedback path poles (Houpis, 1960:206). The closed-loop transfer function for heading angle produced by the aircraft from a commanded heading input is Eq(B-49).

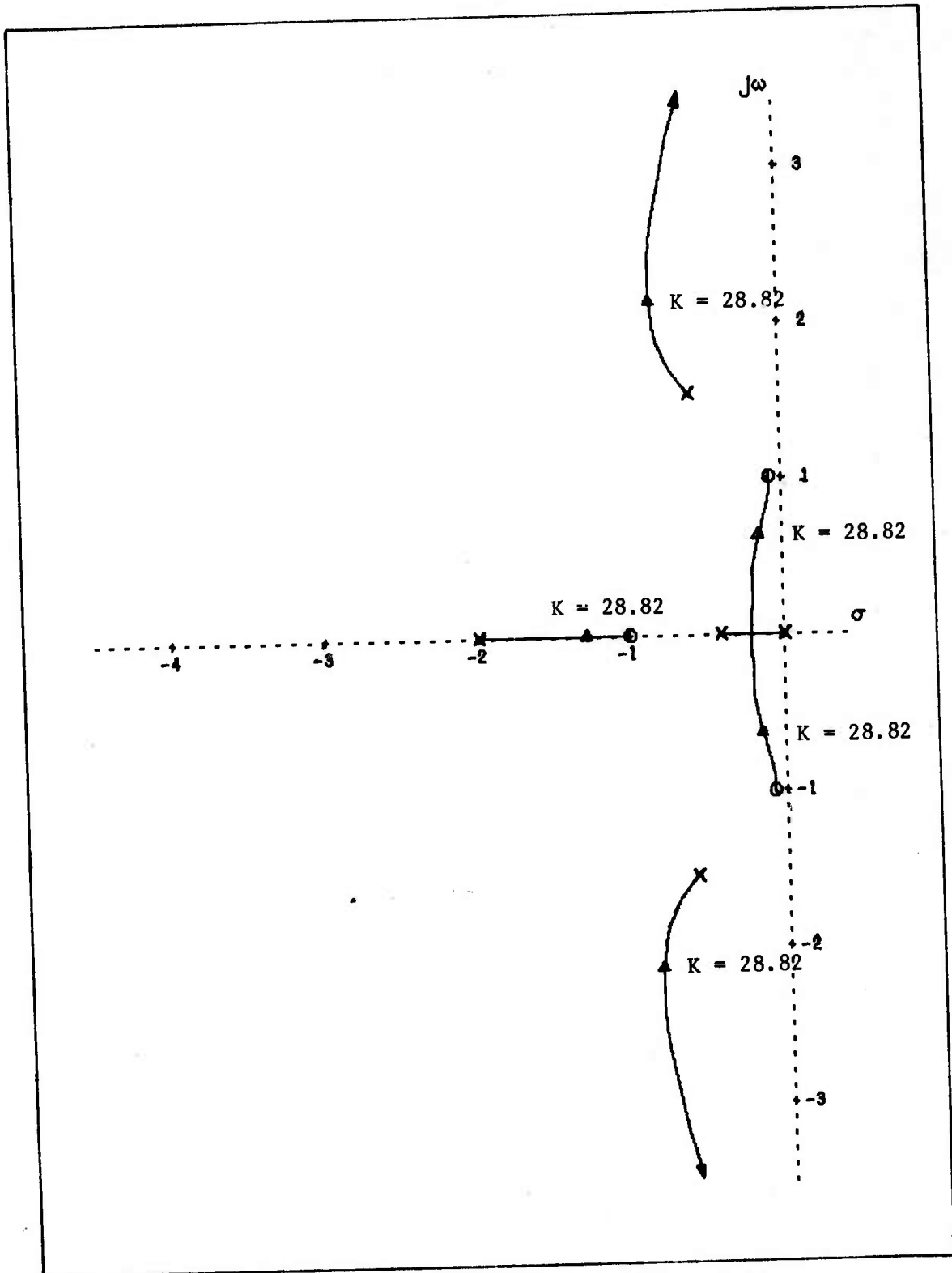


Figure B-10. Root Locus Plot of the Compensated Heading Control System.

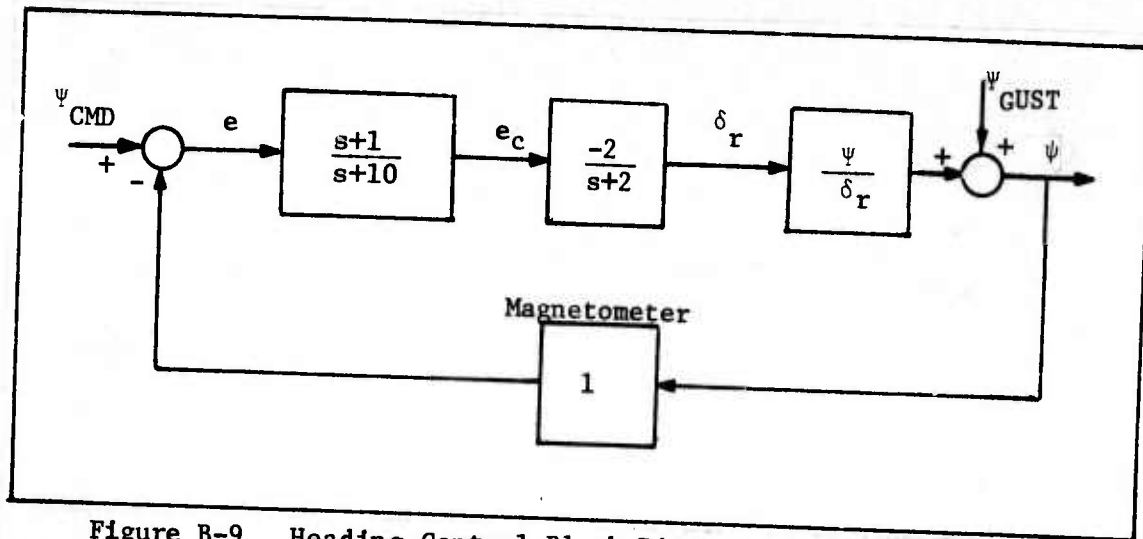


Figure B-9. Heading Control Block Diagram with Compensation.

$$\frac{\psi(s)}{\psi_{\text{CMD}}(s)} =$$

(B-49)

$$\frac{28.82 (s+0.0779 \pm 1.007j) (s+8.734) (s+1)}{(s+0.152 \pm 0.631j) (s+0.828 \pm 2.13j) (s+1.28) (s+10.3) (s+8.75)}$$

The PARTL program is used to get the time response of the system. The response to a step input, of the baseline aircraft in the closed-loop system, is shown in Figure B-11. The time response is a damped oscillation. The oscillations are well damped and the aircraft changes heading to within 5% of the commanded value within twenty seconds.

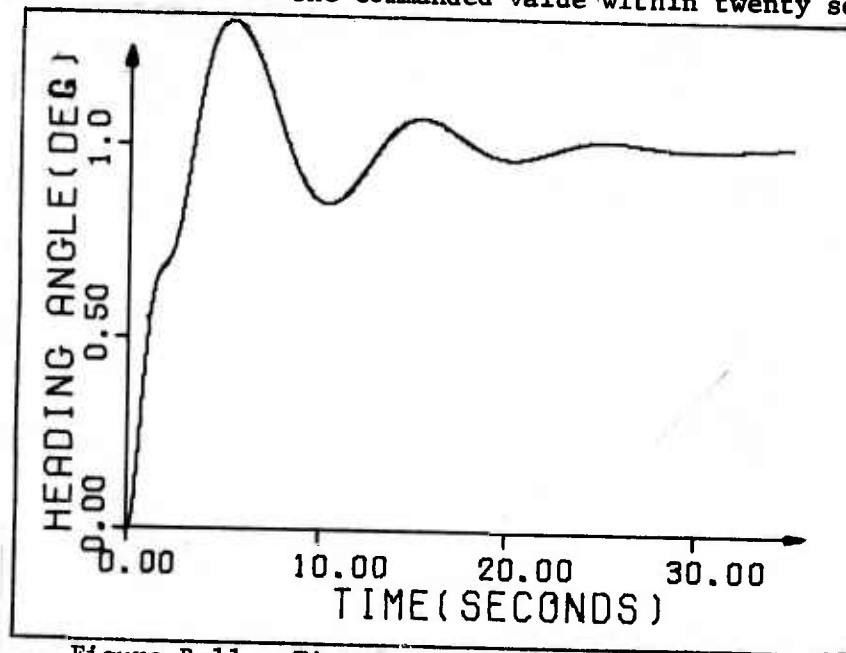


Figure B-11. Time Response of Heading Angle for a Unit Step Input of Commanded Heading Angle

Gain reduction is added to improve system response. Table B-8 shows the dominant oscillatory term and corresponding settling time which come from reducing the gain from the baseline of 28.82. Reducing the gain does reduce the settling time. Figure B-12 compares the system time response with the baseline gain of 28.82 and a 60% gain reduction to 11.53.

TABLE B-8. DOMINANT RESPONSE FOR VARIOUS VALUES OF GAIN

Open-Loop Gain	Duth Roll Natural Frequency $\omega_n$ (rad/sec)	Damping Ratio $\zeta$	Settling Time $T_s$ (sec)
28.82	0.65	0.23	20.1
17.29	0.54	0.34	16.3
11.53	0.45	0.43	15.5
5.76	0.33	0.63	14.4

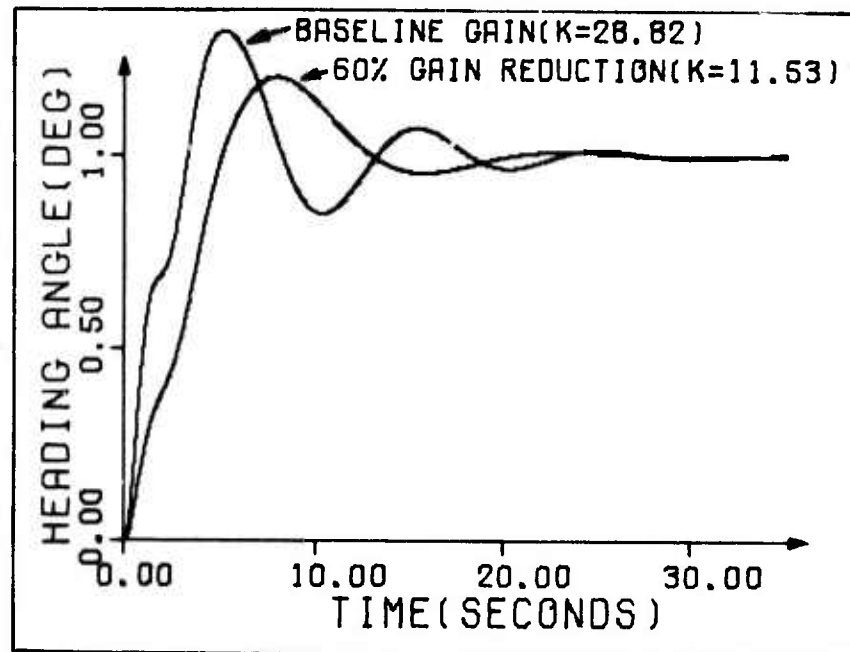


Figure B-12. Comparison of Heading Step Response for Two Values of Gain

Through block diagram manipulations, two more elements of the system are studied, rudder transients and response to gusts. The rudder deflection,  $\delta_r$ , is considered the output with aircraft dynamics and magnetometer in the feedback path. The transfer function in Eq(B-50) is generated and used to output the rudder transients.

$$\frac{\delta_r(s)}{\psi_{CMD}(s)} = \frac{-0.8(s)(s+1)(s+0.587 \pm 1.542j)(s+0.409)(s+8.76)}{(s+0.152 \pm 0.631j)(s+0.828 \pm 2.135j)(s+1.283)(s+8.753)(s+10.35)} \quad (B-50)$$

Figure B-13 shows the resulting time response of rudder deflection given in a unit-step change in heading command input. The rudder transients damp out with the same characteristic oscillation as the aircraft and the final value of rudder deflection is zero. So once the aircraft is stabilized on the commanded heading angle, no further rudder deflection is required. The peak rudder deflection required for a 10-degree change in commanded heading is about 0.6 degrees rudder deflection.

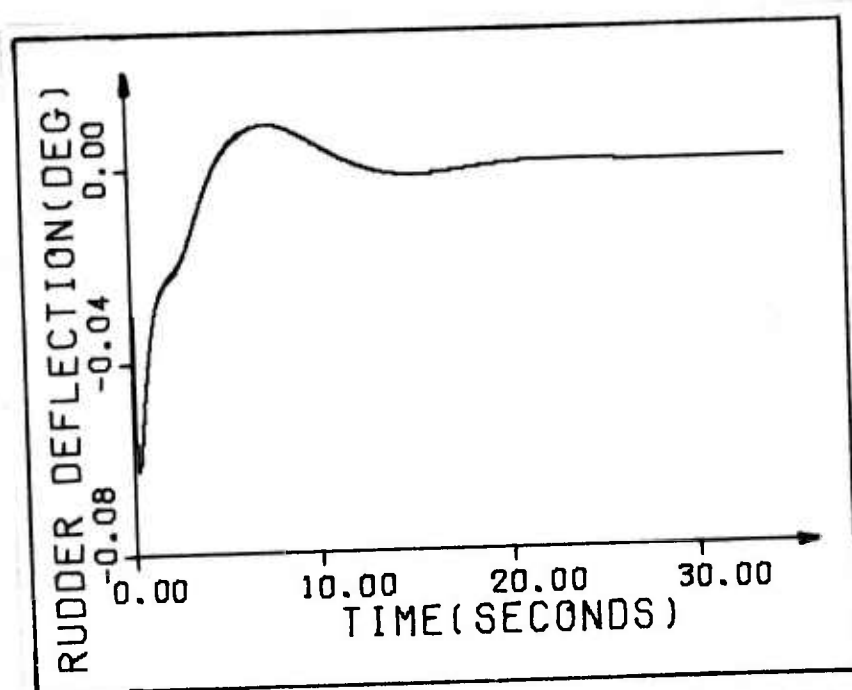


Figure B-13. Time Response of Rudder Transient Given a Unit Step Input of Commanded Heading Angle

Heading changes due to gusts are input, as shown in Figure B-9, as a direct change in the aircraft heading. This gives a forward path with a transfer function of one and the compensator, servo and aircraft considered in the feedback path. Eq(B-51) is the closed-loop transfer function for the gust dynamics and is used to generate the response of the system to gust inputs.

$$\frac{\psi(s)}{\psi_{\text{GUST}}(s)} = \quad (B-51)$$

$$\frac{(s)(s+2)(s+10)(s+0.587 \pm 1.542j)(s+0.409)(s+8.734)}{(s+0.152 \pm 0.631j)(s+0.828 \pm 2.135j)(s+1.283)(s+0.753)(s+10.35)}$$

Figure B-14 shows the closed-loop response to a step change in heading angle. Initially, the heading error equals the input gust and damps from there to zero. In a steady-state sense, the response to gust inputs is damped to zero and the aircraft responds only to the

commanded heading angle. The settling time for gust suppression is the same as the basic closed-loop settling time, less than 20 seconds.

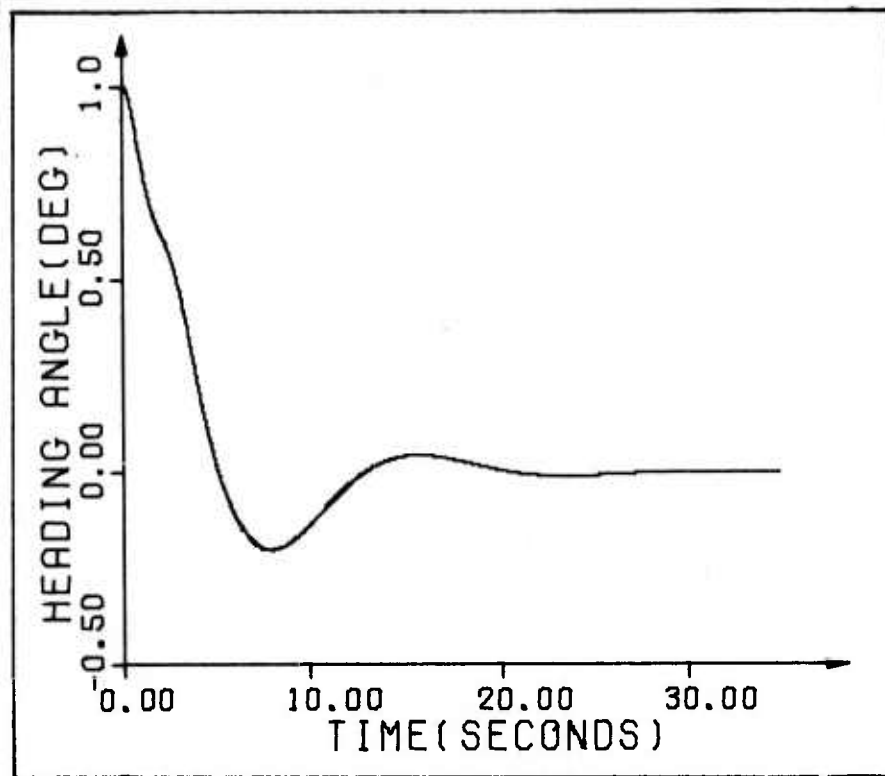


Figure B-14. Time Response of Heading Angle Given a Unit Step Input of Heading Angle Due to Gust

APPENDIX B-13

BEST-CASE AND WORST-CASE CLOSED-LOOP HEADING CONTROL DYNAMICS

The analysis in Appendix B-12 is repeated with the compensator and servo as developed there, while varying the aircraft dynamics from the baseline. The best-case and worst-case dynamics are defined in Appendix B-8. Techniques of Appendix B-11 are repeated for the best and worst case to generate the corresponding aircraft transfer functions as shown in Eq (B-52) and (B-53).

Best Case:

$$\frac{\psi(s)}{\delta_r(s)} = \frac{-17.94 (s + 0.128 \pm 0.819j) (s + 13.05)}{s (s + 0.917 \pm 1.232j) (s + 0.471) (s + 13.16)} \quad (B-52)$$

Worst Case:

$$\frac{\psi(s)}{\delta_r(s)} = \frac{-12.04 (s - 0.00429 \pm 1.216j) (s + 5.999)}{s (s + 0.325) (s + 0.326 \pm 1.785j) (s + 5.991)} \quad (B-53)$$

Closed-loop heading control transfer functions are given in Eq (B-54) and (B-55).

Best Case:

$$\frac{\psi(s)}{\psi_{CMD}(s)} = \frac{14.35 (s + 1) (s + 0.128 \pm 0.819j) (s + 13.05)}{(s+0.214 \pm 0.222j) (s+1.091 \pm 1.412j) (s+1.599) (s+10.09) (s+13.16)} \quad (B-54)$$

Worst Case:

$$\frac{\psi(s)}{\psi_{\text{CMD}}(s)} = \frac{9.63 (s + 1) (s - 0.00429 \pm 1.215j) (s + 5.999)}{(s+0.147 \pm 0.697j)(s+0.5 \pm 2.146)(s+1.405)(s+5.992)(s+10.28)} \quad (\text{B-55})$$

Figure B-2 shows a comparison of the best-case, baseline and worst-case time response to a step input. Table B-9 has a similar comparison.

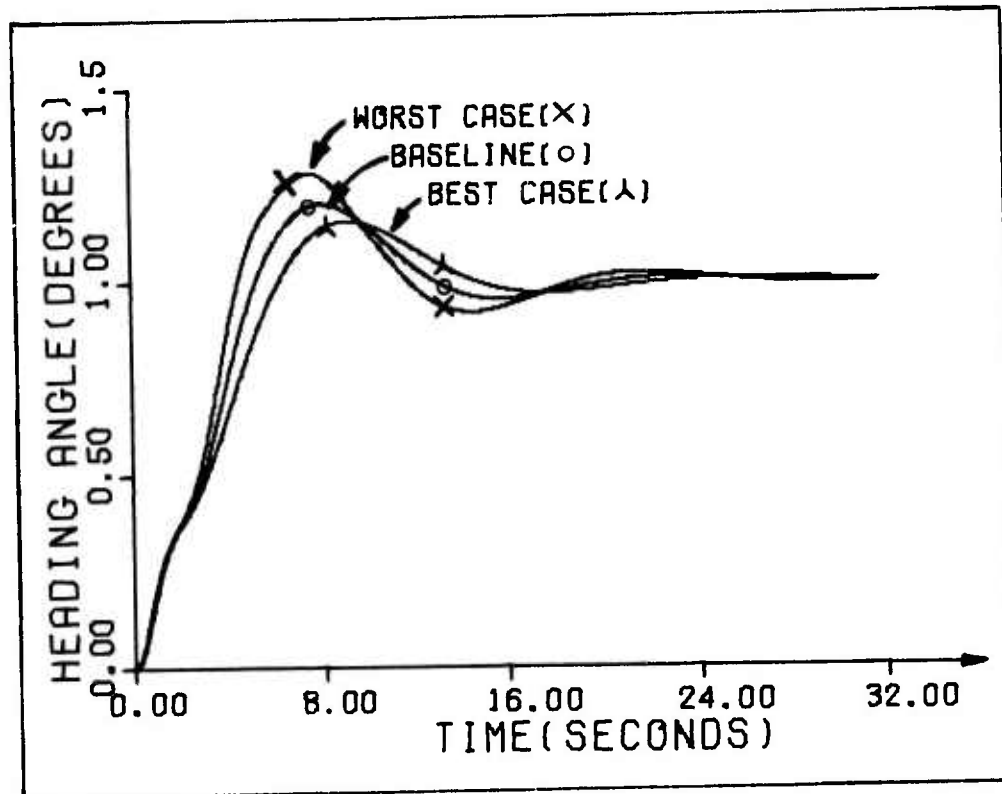


Figure B-2. Comparison of Heading Control Step Response for Varying Aircraft Dynamics

The combination of increasing natural frequency and decreasing damping ratio results in settling times approximately equal for all three sets of dynamics.

TABLE B-9. COMPARISON OF BEST-CASE, BASELINE,  
AND WORST-CASE HEADING CONTROL DYNAMICS

	DUTCH ROLL		SETTLING TIME $T_s$ (sec)
	NATURAL FREQUENCY $\omega_n$ (rad/sec)	DAMPING RATIO $\zeta$	
BEST CASE	0.56	0.27	19.8
BASELINE	0.65	0.23	20.0
WORST CASE	0.71	0.21	20.1

APPENDIX B-14

LONGITUDINAL DYNAMICS FOR ELEVATOR INPUT

The coefficients involved with elevator inputs are evaluated to determine the longitudinal dynamics that result from elevator inputs.

For the full-flying horizontal tail  $C_{m_{\delta_e}} = C_{m_{i_t}}$ .

$$\frac{C_{m_{\delta_e}}}{C_{m_{\delta_e}}} = -a_{ht} \frac{(l_{ht})}{(c)} \frac{(s_{ht})}{(s)} \eta_{ht} \quad (\text{Seckel, 1965:60}) \quad (\text{B-56})$$

$$\text{with } a_{ht} = \frac{\pi A_{ht}}{[1 + (A/2)^2]^{1/2}} \quad (\text{Seckel, 1964:60}) \quad (\text{B-57})$$

where

$$A_{ht} = \frac{41.5}{16} = 2.59$$

$$\text{so } a_{ht} = \frac{(\pi)(2.59)}{1 + [1 + (\frac{2.59}{2})^2]^{1/2}} = 3.09$$

$$\text{and } C_{m_{\delta_e}} = -3.09 \frac{(4.58)}{(1.78)} \frac{(4.61)}{(17)} \quad (1)$$

$$C_{m_{\delta_e}} = -2.16$$

$$\frac{C_{z_{\delta_e}}}{C_{z_{\delta_e}}} = \frac{c}{l_{ht}} C_{m_{\delta_e}} \quad (\text{Blakelock, 1965:31}) \quad (\text{B-58})$$

$$= \frac{1.78}{4.58} \quad (-2.16)$$

$$C_{z\delta_e} = -0.8395$$

$$C_{x\delta_e}$$

$$C_{x\delta_e} = 0 \text{ drag effects are negligible}$$

(Blakelock, 1965:31) (B-59)

The TRANFUN program is used with these forcing functions and the basic longitudinal equations of motion developed in Appendix B-5, to generate the transfer functions associated with an elevator input.

TRANFUN generates the following transfer functions:

$$\frac{u(s)}{\delta_e(s)} = \frac{-0.0603 (s + 4.378) (s - 226.06)}{(s + 0.0569 \pm 0.3888j) (s + 4.375 \pm 5.799j)} \quad (\text{B-60})$$

$$\frac{\alpha(s)}{\delta_e(s)} = \frac{-0.4034 (s + 0.0616 \pm 0.429j) (s + 244.5)}{(s + 0.0569 \pm 0.3888j) (s + 4.375 \pm 5.799j)} \quad (\text{B-61})$$

$$\frac{\theta(s)}{\delta_e(s)} = \frac{-96.05 (s + 0.175) (s + 2.072)}{(s + 0.0569 \pm 0.3888j) (s + 4.375 \pm 5.799j)} \quad (\text{B-62})$$

APPENDIX B-15

CLOSED-LOOP ALTITUDE HOLD DYNAMICS

Closed-loop altitude hold is accomplished by using a solid-state pressure transducer to sense and continuously feedback the aircraft altitude (h). Measured altitude is compared with a commanded altitude to generate an error signal (e). The error signal is the input to a servo which generates an elevator deflection ( $\delta_e$ ) resulting in aircraft pitch and angle of attack changes and finally the desired changes in altitude.

Aircraft response to elevator inputs is developed in the form of a transfer function. Eq (B-63) and Eq (B-64) are combined to form the necessary transfer function. The acceleration  $a_z$  is defined with respect to the earth.

$$h = -\frac{1}{s^2} a_z \quad (\text{Blakelock, 1965:97}) \quad (\text{B-63})$$

$$\text{with } \frac{a_z}{\delta_e} = U_0 \left( \frac{\dot{\alpha}}{e} - \frac{\dot{\theta}}{\delta_e} \right) \quad (\text{Blakelock, 1965:72}) \quad (\text{B-64})$$

$$\begin{aligned} \text{so } \frac{h}{\delta_e} &= -\frac{U_0}{s^2} \left( \frac{\dot{\alpha}}{\delta_e} - \frac{\dot{\theta}}{\delta_e} \right) \quad (\text{B-65}) \\ &= \frac{U_0}{s} \left( \frac{\theta}{\delta_e} - \frac{\alpha}{\delta_e} \right) \end{aligned}$$

$\frac{\theta}{\delta_e}$  and  $\frac{\alpha}{\delta_e}$  transfer functions, from Appendix B-14, are used to generate

Eq (B-66),

$$\frac{h(s)}{\delta_e(s)} = \frac{-44.33 (s + 0.0801) (s + 21.86) (s - 23.11)}{s (s + 0.0569 \pm .3888j) (s + 4.375 \pm 5.799j)} \quad (\text{B-66})$$

The closed loop altitude hold system is shown in Figure B-3.

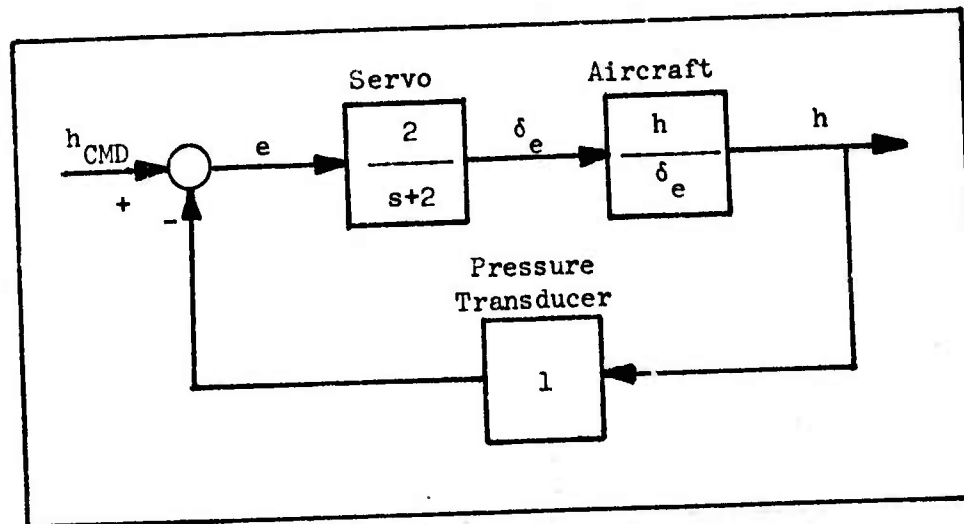


Figure B-3. Preliminary Altitude Hold Block Diagram (No Compensation)

The related open-loop transfer function, Eq (B-67), is used to plot a root locus of the closed-loop altitude-hold system.

$$T.F. \text{ O.L.} = \frac{(-2)(-44.33)(s+0.801)(s+21.86)(s-23.11)}{(s)(s+2)(s+0.0569 \pm .3888j)(s+4.375 \pm 5.799j)} \quad (B-67)$$

An unstable system is indicated by the associated root locus, Figure B-15, with branches in the right-half s-plane. As in the case in the heading control loop, the lag of the servo combined with the aircraft dynamics produces an unstable oscillatory system response.

Cascade compensation and gain reduction are used to generate a stable system response. Two lead-lag compensators are used, one in the forward path and one in the feedback path. Gain reduction anywhere from 60% to 80% is recommended and should be selected depending on the desired

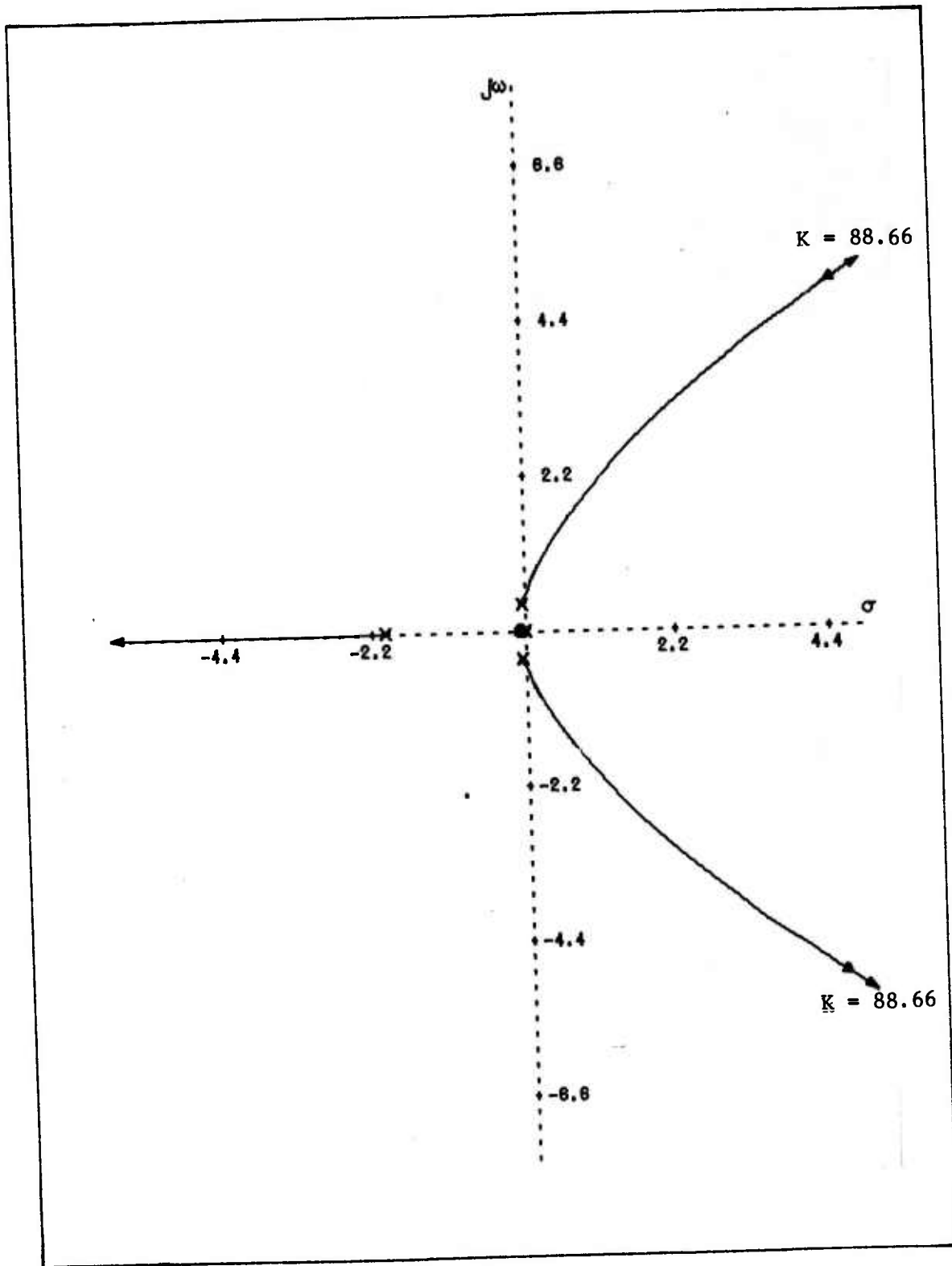


Figure B-15. Root Locus Plot of the Uncompensated Altitude Hold System.

system response and gain margin. The gain margin is just under one order of magnitude (3 db) for the 80% gain reduction and is only about a factor of four (1 db), less than half an order of magnitude, for a 60% gain reduction.

The lead-lag compensator for the feedback path is  $\frac{10(s + 4)}{s + 40}$  and it provides unity feedback for the steady-state system. A lead-lag compensator of the form  $\frac{0.04 (s + 0.1)}{(s + 10)}$  is included in the forward path which, combined with the factor of 10 in the feedback path, gives a gain reduction of 60%. The closed-loop system with compensation is shown in Figure B-16,

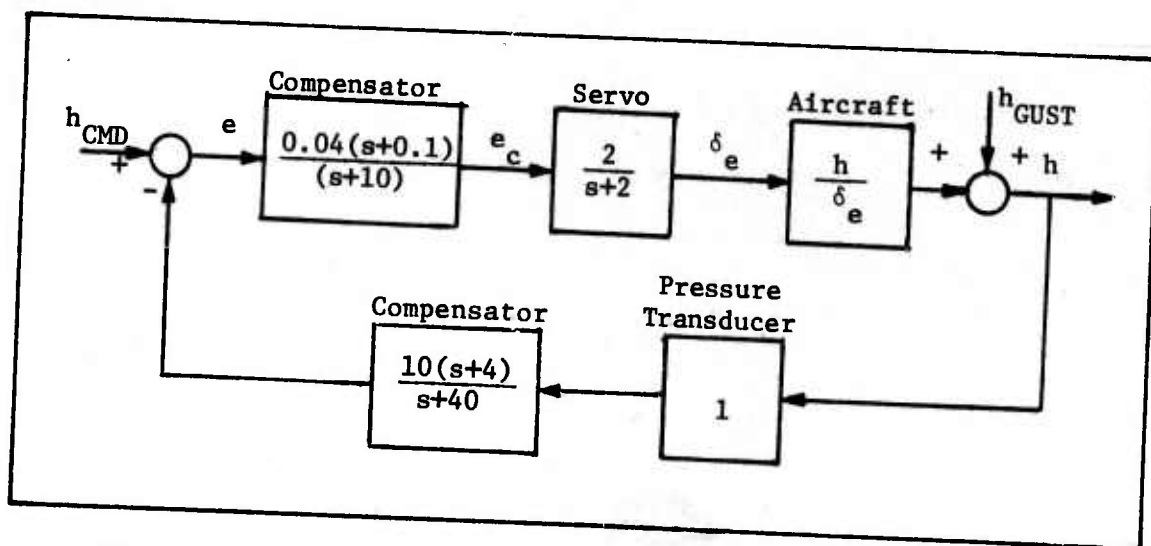


Figure B-16. Altitude Hold Block Diagram (with Compensation).

The closed-loop transfer function has as its poles the operating points of the root locus, Figure B-17. The numerator is a product of the forward path zeros, forward path gain and feedback poles. Eq(B-68) represents the closed-loop altitude-hold dynamics.

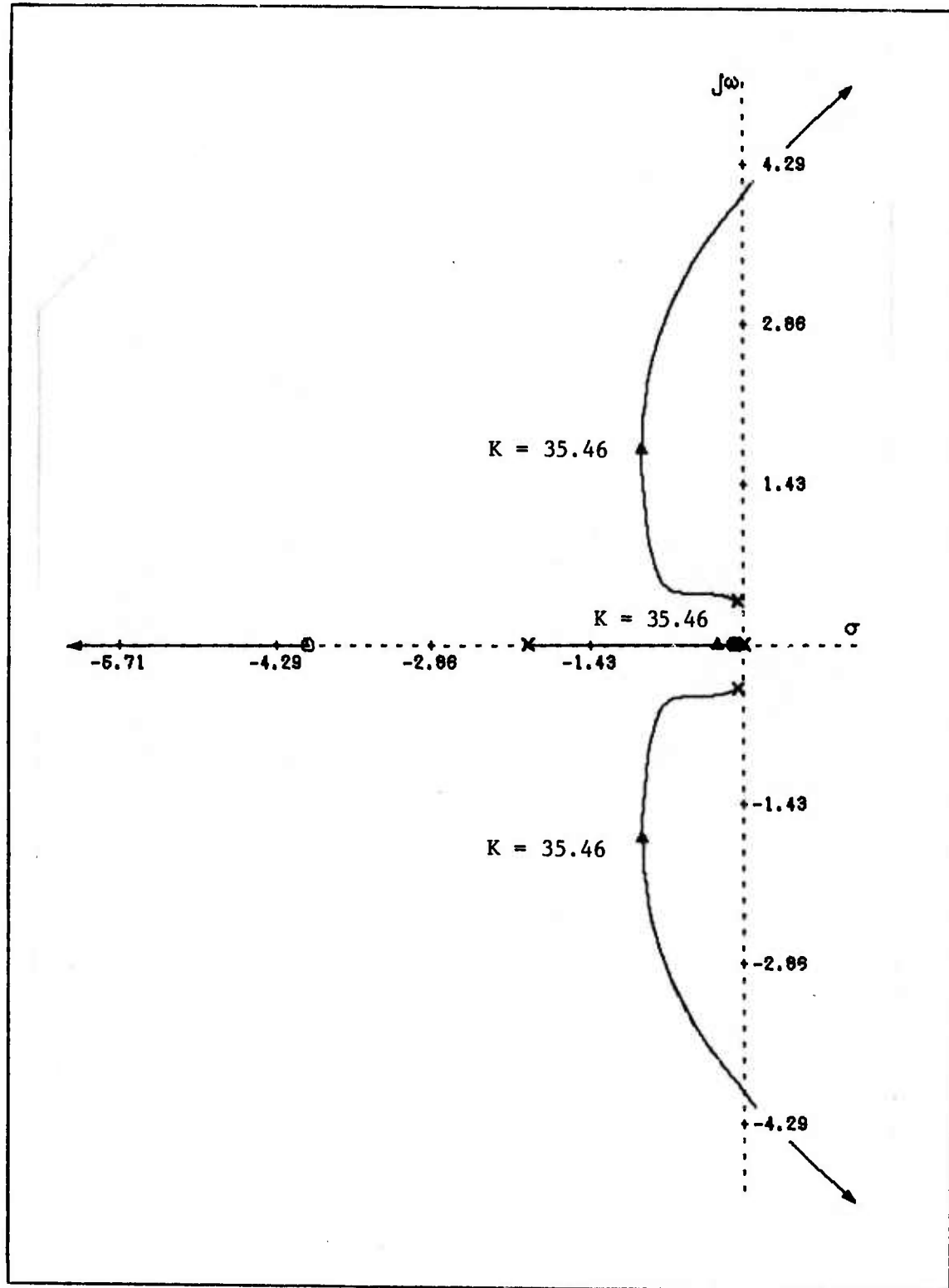


Figure B-17. Root Locus Plot of the Compensated Altitude Hold System.

$$\frac{h(s)}{h_{\text{cmd}}(s)} =$$

$$\frac{35.46 (s + .1)(s + 0.0801)(s + 21.86)(s - 23.11)(s + 40)}{(s+0.024)(s+0.424)(s+0.87+0.84j)(s+4.5+5.44j)(s+9.716)(s+39.99)} \quad (\text{B-68})$$

PARTL is used to find the time response of the system. The response to a step input is shown in Figure B-18. The dominant response is an exponential growth to the final value. About 90 seconds are required for the response to stay within 5% of the final value. If the 80% gain reduction is used, a slower time response is generated, and slightly over 2 minutes are required to achieve 95% of the commanded input. Figure B-19 shows a comparison of the time responses for these two levels of gain reduction.

Elevator transients and response to gusts is studied as in Appendix B-12 for the heading-control loop. Figures B-20 and B-21 contain the associated time-response curves. The settling time to damp out gust perturbations in altitude is 90 seconds.

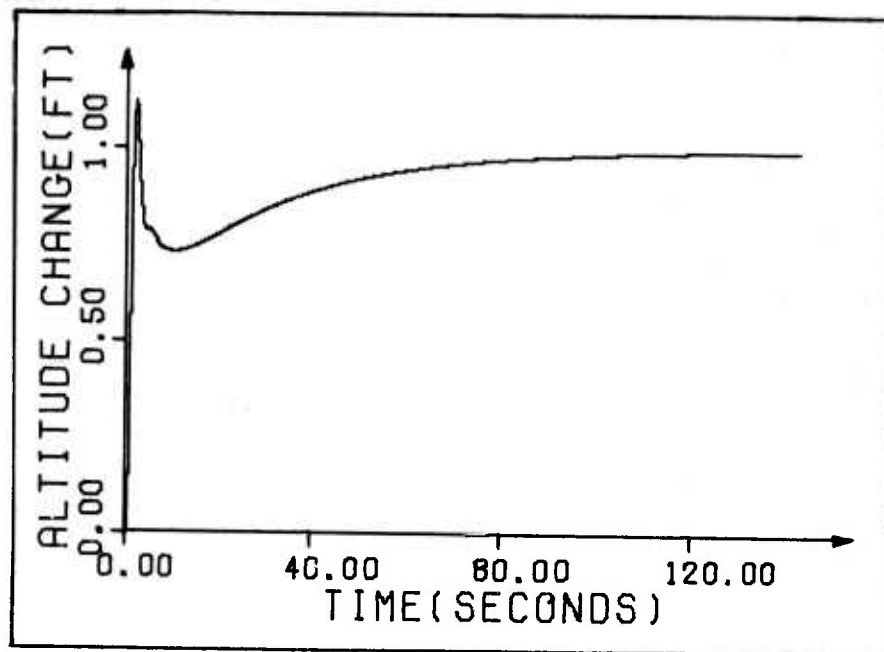


Figure B-18. Step Response of Aircraft Altitude Given a Commanded Altitude Change.

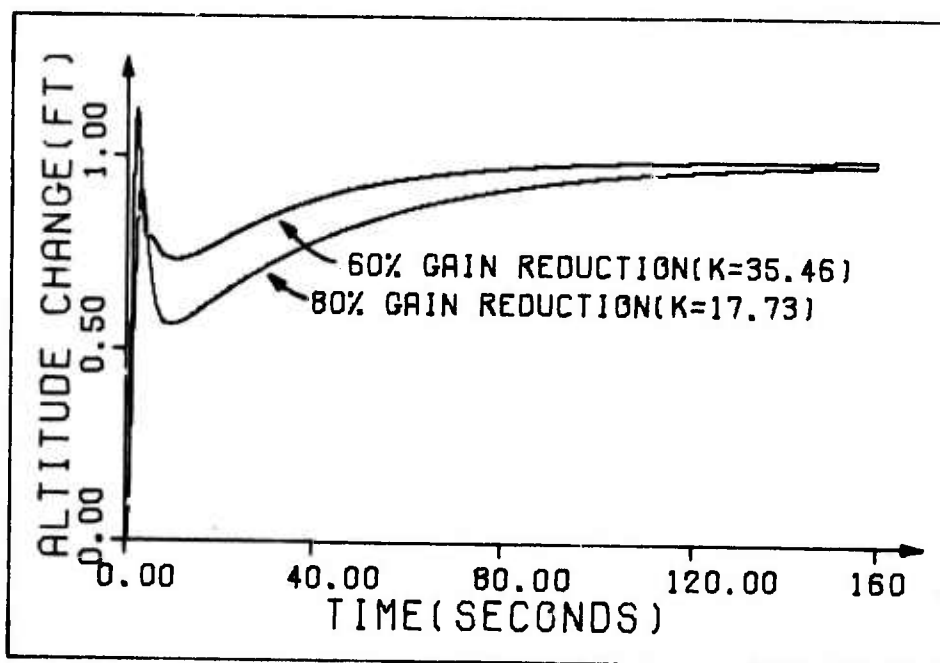


Figure B-19. Comparison of Step Response in Altitude For Two Values of Gain.

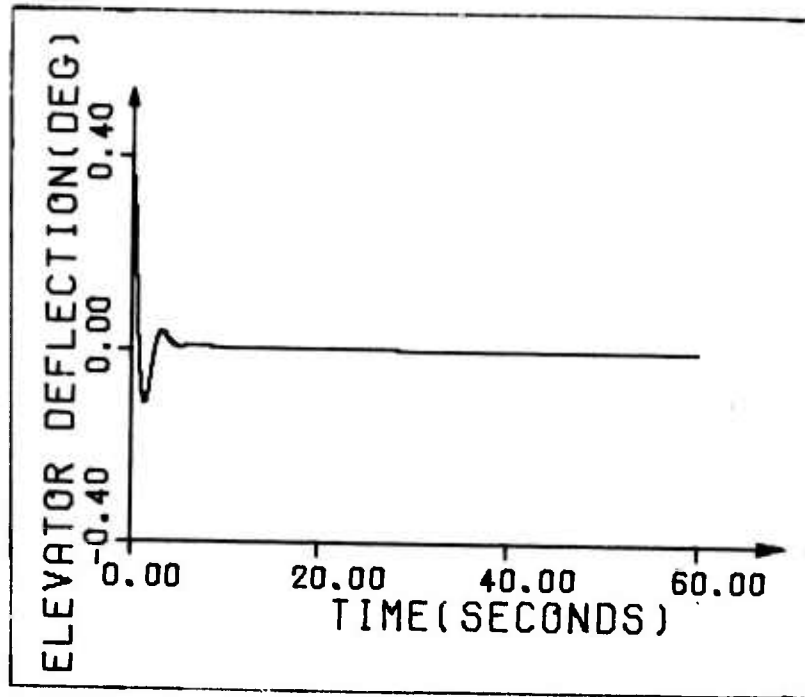


Figure B-20. Time Response of Elevator Transients Given a Unit Step Change of Commanded Altitude.

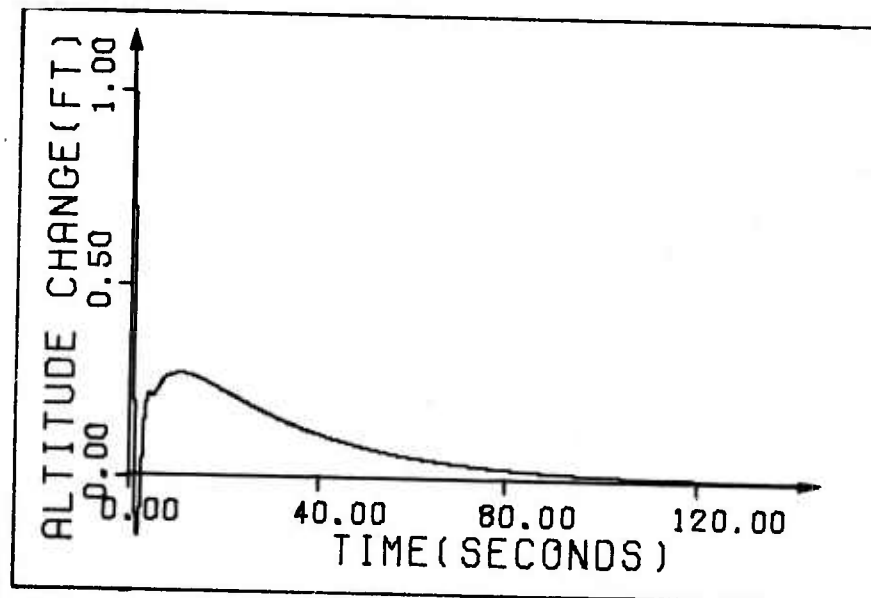


Figure B-21. Time Response of Aircraft Altitude Due to a Gust Change of Altitude.

APPENDIX B-16

BEST CASE AND WORST CASE CLOSED-LOOP ALTITUDE-HOLD DYNAMICS

The analysis in Appendix B-15 is repeated with the compensators and servos as developed there while varying the aircraft dynamics from the baseline. The best-case and worst-case dynamics are defined in Appendix B-7. The techniques of Appendix B-14 are repeated for the best and worst cases to generate the corresponding aircraft transfer functions. Then Eq(B-65) from Appendix B-15, is used to generate Eq(B-69) and Eq(B-70).

Best case is:

$$\frac{h(s)}{\delta_e(s)} = \frac{-49.29 (s + 30.43) (s + 0.131) (s - 20.92)}{s(s + 0.0795 \pm 0.361j) (s + 6.077 \pm 4.702j)} \quad (B-69)$$

Worst case is:

$$\frac{h(s)}{\delta_e(s)} = \frac{-40.37 (s + 0.0354)(s + 22.67)(s - 18.07)}{s(s + 0.393 \pm 0.407j)(s + 3.172 \pm 6.182j)} \quad (B-70)$$

Eq(B-71) and Eq(B-72) are the best-case and worst-case closed-loop transfer functions with 60% gain reduction, using the baseline compensators and servo.

Best case is:

$$\frac{h(s)}{h_{cmd}(s)} = \frac{3.961 (s + 0.1)(s + 30.57) (s - 20.99) (s + 40)}{(s+0.105)(s+0.724 \pm 2.028j)(s+7.699 \pm 3.769j)(s+7.125)(s+39.99)} \quad (B-71)$$

Worst case is:

$$\frac{h(s)}{h_{CMD}(s)} =$$

$$\frac{3.23 (s + 0.1)(s + 0.0354)(s + 22.67)(s - 18.07)(s + 40)}{(s + 0.0147)(s + 0.257)(s + 1.013 + 1.424j)(s + 3.254 + 5.623j)(s + 9.635)(s + 39.98)}$$

(B-72)

Figure B-4 shows the comparison of the time responses of the three sets of dynamics. Table B-10 lists the settling times for two values of gain reduction.

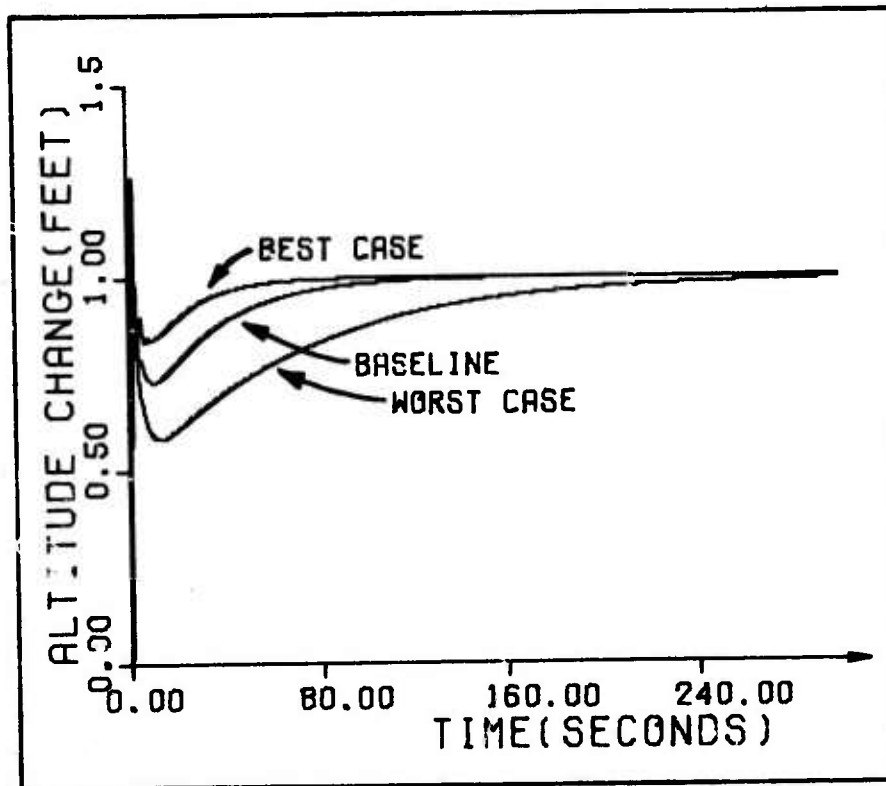


Figure B-4. Comparison of Step Response of Altitude Hold Circuit with Varying Aircraft Dynamics

TABLE B-10. ALTITUDE HOLD-SETTLING TIMES

	SETTLING TIME (60% GAIN REDUCTION) $T_s$ (sec)	SETTLING TIME (80% GAIN REDUCTION) $T_s$ (sec)
BEST-CASE	29	27
BASELINE	87	125
WORST-CASE	204	313

## ALTITUDE HOLD CIRCUIT DESCRIPTION

The altitude control diagram shown in Figure B-16 has two lead-lag compensators, one in the forward path and one in the feedback path. For the barostat, an integrated circuit pressure transducer is chosen. This is a fully temperature-compensated linear device using a piezo resistive strain sensor. It has an overall accuracy of  $\pm 0.075$  volts over its span of 2.5 volts to 12.5 volts (National, 1974:2-9).

In the feedback path, the barostat feeds a lead-lag compensator with the transfer function  $\frac{10(s+4)}{s+40}$ . An LM324 operational amplifier (op amp) is used to form the compensator (National, 1973:AN20-4).

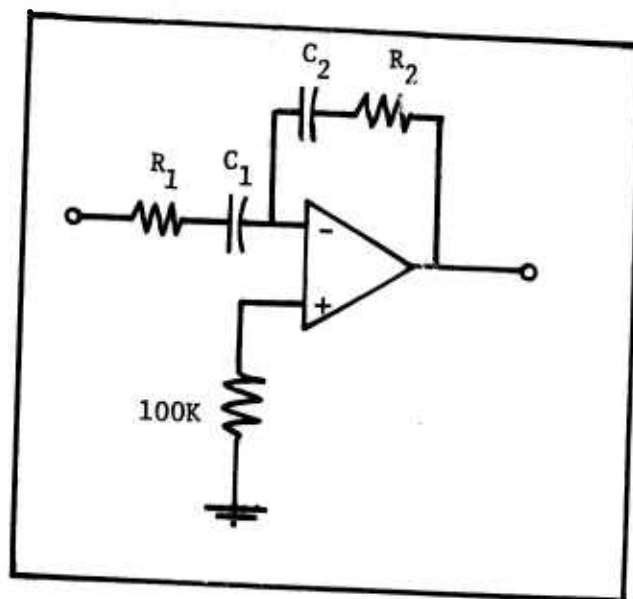


Figure B-22. Altitude Feedback Compensator

The transfer function is equal to the negative of the feedback impedance divided by the input impedance:

$$\frac{10(s+4)}{s+40} = - \frac{Z_f}{Z_i} \quad (\text{Carlson, 1967:207})$$

Manipulating this equation yields:

$$\frac{Z_f}{Z_i} = - \frac{100K + \frac{1}{2.5(10)^{-6}s}}{100K + \frac{1}{0.25(10)^{-6}s}}$$

From this equation:

$$R_1 = 100K \text{ ohm}$$

$$C_1 = 0.25 \text{ uf}$$

$$R_2 = 100K \text{ ohm}$$

and

$$C_2 = 2.5 \text{ uf}$$

The circuit to accomplish the feedback path transfer function is shown in Figure B-22. This signal must be subtracted from the commanded input. Since the output of the feedback compensator has a negative sign, this signal is added to the commanded input. The output of the adder feeds into the forward path compensator which has a transfer function of  $\frac{0.04(s+0.1)}{s+10}$ . The circuit for this transfer function is shown in Figure B-23. The complete altitude hold circuit is shown in Figure B-24. (Appendix E-4 contains a similar description of the complete heading control circuit).

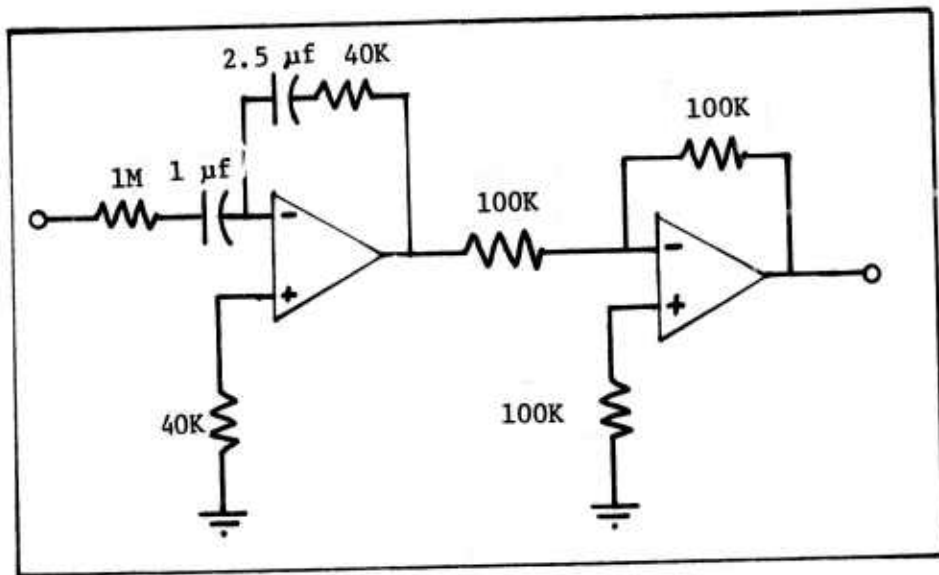


Figure B-23. Altitude Hold Forward Path Compensator

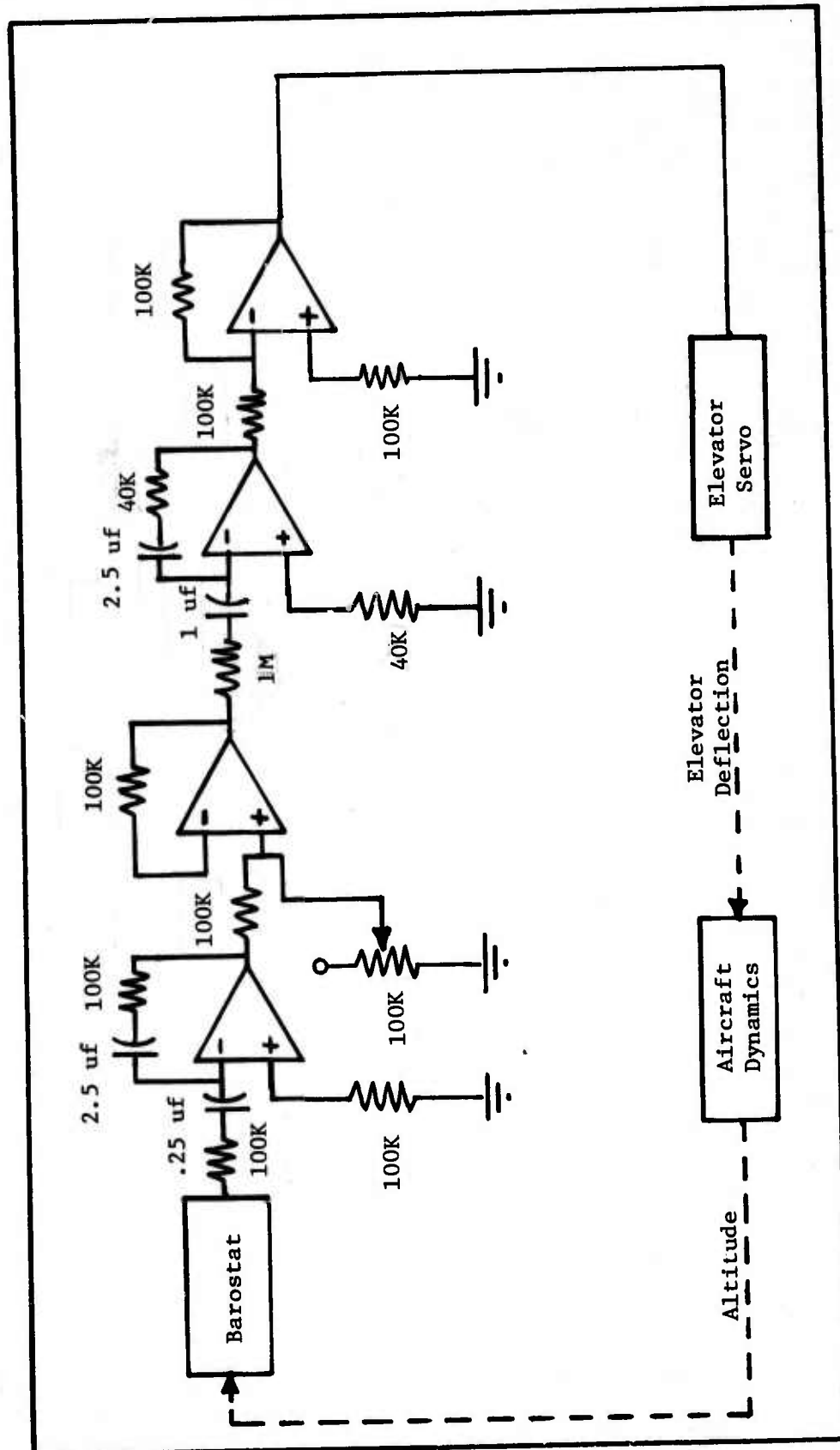


Figure B-24. Altitude Hold Circuit Diagram

APPENDIX C

PROPULSION SUBSYSTEM

## LIST OF SYMBOLS

A	area
BHP, bhp	brake horsepower
$C_D$	drag coefficient
$C_P$	power coefficient
$C_S$	speed-power coefficient
$C_T$	thrust coefficient
D	drag force
D, d	propeller diameter
F	force
$F_s$	scale force
h	altitude above ground level (AGL)
HP, hp	horsepower
J	propeller advance ratio
L	length of moment arm
lbf	pounds force
lbm	pounds mass
M	moment
N	engine speed, revolutions per minute
n	engine speed, revolutions per second
mph	miles per hour
$P_t, P_0$	total pressure
$P_s$	static pressure
q	dynamic pressure
$R_e$	Reynold's number

RPM, rpm	engine speed, revolutions per minute
SFC	specific fuel consumption
SHP	shaft horsepower
T	thrust
V	velocity
$V_d$	velocity at the disk
$V_0$	velocity of the unaffected air upstream
$V_s$	final velocity of the slipstream air
$\beta$	propeller blade angle
$\eta$	efficiency
$\nu$	kinematic viscosity
$\rho$	mass density ( $\rho_0$ is at sea-level)
$\sigma$	density ratio ( $\rho/\rho_0$ )

#### Subscripts

p	propeller
D	drag
adj	adjusted

## APPENDIX C

### PROPULSION SUBSYSTEM

#### Introduction

This appendix discusses the selection of a propulsion subsystem for a very low cost expendable harassment system (VLCEHS). The propulsion subsystem consists of the engine-propeller combination. The selection criteria is based on meeting performance specifications at minimum cost.

#### Scope

Since the entire study effort is driven by a minimum-cost concept, only low-cost, commercially-available engines are evaluated in depth.

#### Approach

Manufacturer data were analyzed to obtain generic performance curves which were used to determine the engine that best suited the chosen airframe. Once power and weight requirements were levied by the airframe considerations, the engine selection was made using the performance curves.

Where possible, the results of previous analyses are incorporated into the evaluation. For example, the Applied Physics Laboratory (APL) at John Hopkins University recently completed a study and evaluation of three candidate engines to be used in their RPV program. These reciprocating engines were made by Sakert-Riggs, Kolbo Korporation and the McCulloch Corporation. It was concluded that the McCulloch engine, with modifications made by the APL, is an ideal power plant for long flight-time RPV missions (Small, 1974:36).

### System Considerations

The accomplishment of the mission is affected by the range, endurance, and ceiling of the aircraft. These factors, in turn, affect the fuel consumption. The airframe designer's desired performance characteristics affect the required power of the engine and fuel consumption, since the rate of climb depends upon the reserve horsepower of the engine. Electrical power requirements for the vehicle, such as flight control servos and avionics, can drain power from the engine.

Airframe considerations determine the maximum allowable propeller diameter for a reciprocating engine and, therefore, can put constraints on the vehicle launching device. For example, an aircraft configuration with twin empennage-supporting booms attached to the wings fixes the maximum diameter of the propeller, not only from the vehicle and launcher structural-clearance standpoint, but also from the standpoint of tip-flow losses if the propeller gets too near the booms.

Clearly, the weight, physical size, and fuel consumption of the engine affect the airframe design. Engine weight, where the center of gravity of the engine is located, direction of rotation of the propeller and its configuration, tractor or pusher, affect the proper balance of the aircraft, statically and dynamically. Engine power and thrust available influence the airframe design.

The type of engine chosen affects the throttle control servo and its associated linkage. The approximate response time of the engine also helps to determine the design of the throttle control.

### Criteria

Although the engine should be as cheap as possible, the optimum upper cost limit for the engine is \$200, based on the design goal of a total system cost of \$1000 for the Type II vehicle. The engine must be available through shelf stock in the commercial market and must have easily replaceable parts. The total engine weight should be less than 30 pounds and the propulsion system should weigh no more than 35 pounds. The acceptable range of power is from 5 to 15 brake horsepower. The acceptable range of specific fuel consumption (SFC) is between 0.5 and 1.5 lbm/hp-hr. The vibrations that the engine transmits to the airframe should be minimal. Engine reliability must be compatible with the overall system, even though the active system life is short. Because of synchronization requirements and unnecessary redundancies which increase weight and cost, twin-engine concepts are not considered in the detailed evaluation.

### Survey of Propulsion Devices

Although several methods of providing propulsive power are available for aircraft, the limited size of the vehicle drone eliminated all but the simplest and least expensive propulsion systems. The following is a list of the different types of engines considered.

#### Jet Engines

1. Ramjet
2. Turbojet and Turbofan
3. Pulse-jet

#### Internal Combustion Engines

1. Rotary Combustion (Wankel)

2. Large recreational engines

- a. Motorcycle
- b. Snowmobile
- c. Outboard motor

3. Small recreational engines

- a. Chain-saw
- b. Go-kart
- c. Mini-bike
- d. Four-cycle horizontal shaft snowblower engine

The ramjet, turbojet, and turbofan engines were classed together in the analysis. All three types have more thrust than needed for the drone application. Also, their specific fuel consumption is higher than tolerable. The above factors coupled with the fact that these engines are heavy and involve high initial costs and considerable maintenance, eliminate jet engines from further consideration.

The rotary combustion engine (Wankel) is too heavy and its cost was considered excessive for this application. At the present time, a 5-horsepower engine that weighs about 35 pounds is about the best one can hope for from a rotary engine. Curtiss-Wright Corporation is working on prototype engines for the U.S. Army RPV program, but none are now commercially available (Alan, 1975).

Larger, internal-combustion engines, such as those used for motorcycles, snowmobiles and outboard motors, are high cost items, and exceed the weight restrictions even with aluminum engine blocks. Most snowmobile engines fall in this category. However, some can be grouped with the two-cycle engines and with the horizontal-shaft, four-cycle

engines due to their relatively light weight.

Two-cylinder engines are commercially available, but presently, not in large quantities, and they are cost prohibitive. Engines of this type, manufactured by Kolbo Korporation of Anaheim, CA, have been used in RPV applications; however, they were not considered for the harassment drone because of cost and production capability.

Smaller internal-combustion engines, such as those used for chainsaws, go-karts, and mini-bikes, were grouped together, since most are two-cycle, light-weight, and relatively inexpensive. The McCulloch go-kart engines are representative of this class of engines, having specific fuel consumptions (SFCs) in the range of 0.9 to 1.3 lbm/hp-hr (McCulloch, 1974). The cost of the McCulloch engines varies between \$100 and \$200 (Jacobs, 1975). Since the estimated total weight of the engine, propeller, and hub is approximately 20 pounds, this particular subsystem is very light. Reliability figures for these engines are not available. These engines are commercially available, with a production rate of several thousand engines per year.

Other small engines are the horizontal-shaft, four-cycle engines which are used in small generators, snowblowers, and lawnmowers. Four-cycle engine fuel consumption is characteristically less than that for two-cycle engines being approximately 1.0 lbm/hp-hr (Currie, 1975). The cost of these engines, depending on the manufacturer, is within the established criteria. Four-cycle engines are heavier than two-cycle engines, and the maximum horsepower attainable, with an aluminum engine block, is 8 horsepower. Above 5 horsepower, the engines become excessively heavy. The HSSK 50 weighs 24 pounds with an estimated unit retail cost of \$150 (Tecumseh, 1974:8).

Table C-1 shows a comparison of all known power plants that might be suitable for use in small drones or RPVs. Figure C-1 shows a comparison of the engine horsepower to weight ratio versus the horsepower for several engines that are representative of the general class that is considered in this design study.

#### Final Propulsion Subsystem Candidates

The McCulloch MC 101, the Tecumseh HSSK 50, and the Tecumseh HMSK 70 are the prime candidate engines and are representative of the respective engine types. The MC 101 is a go-kart engine rated at 12.5 horsepower at 9000 rpm and 88 inch-pounds of torque at 9000 rpm with an open exhaust. The total engine weight is 13.5 pounds resulting in a weight-to-horsepower ratio of about 1.08 at 9000 rpm. The displacement is 7.5 cubic inches with a bore of 2.280 inches and stroke of 1.835 inches. The unit retail cost of the MC 101B is \$205, but the unit cost for large orders is \$148 (Jacobs, 1975).

The Tecumseh HSSK 50 is a four-cycle, horizontal-shaft engine rated at 5.0 horsepower at 3600 rpm. It is designed to be used in small snowblowers. With all factory furnished parts installed, the engine weighs 24 pounds. The displacement is 12.0 cubic inches with a bore of 2-5/8 inches and a stroke of 1-15/16 inches. It is representative of most four-cycle engine models currently on the market with a 5 horsepower rating.

The Tecumseh HMSK 70 is similar to the HSSK 50 and is rated at 7.0 horsepower at 3600 rpm with a bore of 2-15/16 inches and a stroke of 2-17/32 inches. The engine weighs 47 pounds.

TABLE C-1. COMPARISON OF POWER PLANTS FOR USE IN SMALL DRONES

Manufacturer	Model Designation	Type	Weight (lb)	Horsepower @ RPM	Torque (in-lb) @ RPM
Curtiss-Wright	RCL-27P1	Wankel	55.0	29.0@5500	N/A
Curtiss-Wright (Sachs)	RCL-18.5	Wankel	56.0	20.0@5500	N/A
Clinton	502-0308	1 Cyl. 2 Cycle	22.5	7.0@6000	80.4@4500
Clinton	400-0305	1 Cyl. 4 Cycle	24.0	3.0@3600	58.8@2800
Clinton	404-0304	1 Cyl. 4 Cycle	24.5	3.5@3500	67.2@2800
Clinton	410-0305	1 Cyl. 4 Cycle	24.5	4.0@3600	6.05@3200
Hirth	82R	1 Cyl. 2 Cycle	39.0	12.5@5000	168 @4000
Hirth	192R	1 Cyl. 2 Cycle	50.0	20.5@5750	276 @5000
Hirth	193R	1 Cyl. 2 Cycle	57.0	19.0@5500	240 @4500
Hirth	194R	1 Cyl. 2 Cycle	51.0	28.0@6500	288 @6000
Hirth	210R	1 Cyl. 2 Cycle	70.0	22.0@5500	240 @4500
Hirth	211R	2 Cyl. 2 Cycle	70.0	24.0@5500	264 @4750
Hirth	220R	2 Cyl. 2 Cycle	69.0	27.0@5500	348 @4000
Hirth	261R	2 Cyl. 2 Cycle	69.0	26.0@6250	192 @6000

TABLE C-1 (Continued)

Manufacturer	Model Designation	Type	Weight (lb)	Horsepower @ RPM	Torque (in-lb) @ RPM
Hirth	261R4	2 Cyl. 2 Cycle	64.0	31.0@7750	N/A
Hirth	260R4	2 Cyl. 2 Cycle	63.0	36.0@7750	N/A
Hirth	277R4	2 Cyl. 2 Cycle	64.0	42.0@7500	N/A
Hirth	276R4	2 Cyl. 2 Cycle	64.0	46.0@7500	N/A
Hirth	279R0	2 Cyl.	70.5	36.0@6750	N/A
Hirth	281R0	2 Cyl.	82.5	55.0@6750	N/A
JLO	LB-600/2	2 Cyl. 2 Cycle	84.7	45.0@6000	N/A
JLO	L-230	1 Cyl. 2 Cycle #	29.0	15.5@6000	163 @5600
JLO	L-295	1 Cyl. 2 Cycle	48.5	21.5@6000	228 @5000
JLO	L-340	1 Cyl. 2 Cycle	49.7	23.5@6000	242 @6000
JLO	LR-399/2	2 Cyl. 2 Cycle	62.0	30.0@6250	302 @6000
JLO	LR-440/2	2 Cyl. 2 Cycle	62.0	35.0@6750	340 @6000
Kiekhaeffer	KAM-440-I/V	N/A	65.0	40.0@5500	N/A
Kiekhaeffer	290SS	N/A	51.0	25.0	N/A
Kiekhaeffer	400SS	N/A	72.0	45.0	N/A

TABLE C-1 (Continued)

Manufacturer	Model Designation	Type	Weight (lb)	Horsepower @ RPM	Torque (in-lb) @ RPM
Kiekhaeffer	440SS	N/A	72.0	55.0	N/A
Kiekhaeffer	575AERO	N/A	72.0	60.0	N/A
Kiekhaeffer	900SS	N/A	103.0	100.0	N/A
Kohler	K295-2AX	2 Cyl. 2 Cycle	54.0	24.0	N/A
Kohler	K340-2AX	2 Cyl. 2 Cycle	54.0	28.0	N/A
Kohler	K440-2AX	2 Cyl. 2 Cycle	65.0	37.0	N/A
Kolbo	D-238	2 Cyl. Glo-plug	4.5	5.0	N/A
Kolbo	D-274	2 Cyl. Glo-plug	7.5	10.0	N/A
Kolbo	Rhino 140	1 Cyl. Glo-plug	2.0	2.0	N/A
Kolbo	Super Rhino	1 Cyl. Glo-plug	2.0	3.0	N/A
Kolbo	D-2100	2 Cyl. Glo-plug #	9.3	16.0@8300	N/A
Kolbo	D-2118	2 Cyl. Glo-plug #	10.0	22.0@7800	N/A
Lycoming	Undesignated	2 Cyl. 4 Cycle #	13.5	4.5@4000	N/A
Lycoming	Undesignated	2 Cyl. 4 Cycle #	N/A	14.0	N/A

TABLE C-1 (Continued)

Manufacturer	Model Designation	Type	Weight (lb)	Horsepower @ RPM	Torque (in-lb) @ RPM
McCulloch	S210A	1 Cyl. 2 Cycle	4.5*	3.3@8000	N/A
McCulloch	7-10A	1 Cyl. 2 Cycle	5.75 4.0 *	4.2@8000	N/A
McCulloch	CP 80	1 Cyl. 2 Cycle	5.1 *	5.2@8000	N/A
McCulloch	MC 49C	1 Cyl. 2 Cycle	12.0	7.0@7500 5.5@7000**	59@7500 55@5000**
McCulloch	MC 91B	1 Cyl. 2 Cycle	11.6	10.6@8500 10.0@9000**	84@7500 82@6000**
McCulloch	MC 101A	1 Cyl. 2 Cycle	12.25 10.0 *	14.5@9500 13.5@8500**	105@7500 107@5500**
Nelson	H-63CP	4 Cyl. 2 Cycle	68.0	48.0@4400	N/A
Olson & Rice	13BA	1 Cyl. 2 Cycle	3.9	1.0@6300	N/A
Olson & Rice	20AB	1 Cyl. 2 Cycle	4.9	1.6@7200	N/A
Ross	525-05	4 Cyl. Glo-plug	7.0	10.0@4000	N/A
Ross	1.8 SIX	6 Cyl. Glo-plug	2.5	3.6@14000	N/A
Sachs	KM 48	Wankel	37.5	5.0@3000 (DIN) 8.0@4800 (DIN)	N/A N/A

TABLE C-1 (Continued)

Manufacturer	Model Designation	Type	Weight (lb)	Horsepower @ RPM	Torque (in-lb) @ RPM
Sachs	KM 914B	Wankel	61.7	21.0@5500	N/A
Sachs	KM 37	Wankel	34.0	5.0	N/A
Tecumseh	HSK 25	1 Cyl. 4 Cycle	22.25	2.5@3600	N/A
Tecumseh	HSK 30	1 Cyl. 4 Cycle	22.25	3.0@3600	N/A
Tecumseh	HSK 35	1 Cyl. 4 Cycle	22.25	3.5@3600	N/A
Tecumseh	HSSK 40	1 Cyl. 4 Cycle	24.0	4.0@3600	N/A
Tecumseh	HSSK 50	1 Cyl. 4 Cycle	24.0	5.0@3600	N/A
Tecumseh	HSK 60	1 Cyl. 4 Cycle	41.5	6.0@3600	N/A
Tecumseh	HMSK 70	1 Cyl. 4 Cycle	47.0	7.0@3600	N/A
Tecumseh	HMSK 80	1 Cyl. 4 Cycle	48.5	8.0@3600	N/A
Thermo-Jet	JS-104	Pulse-jet	12.9	Thrust = 30 lb SFC = 34.5	N/A

Legend: \* Stripped for Flight    \*\* Open Exhaust    # Horizontally Opposed Cylinders    N/A Information Not Available  
(Hoy, 1975)

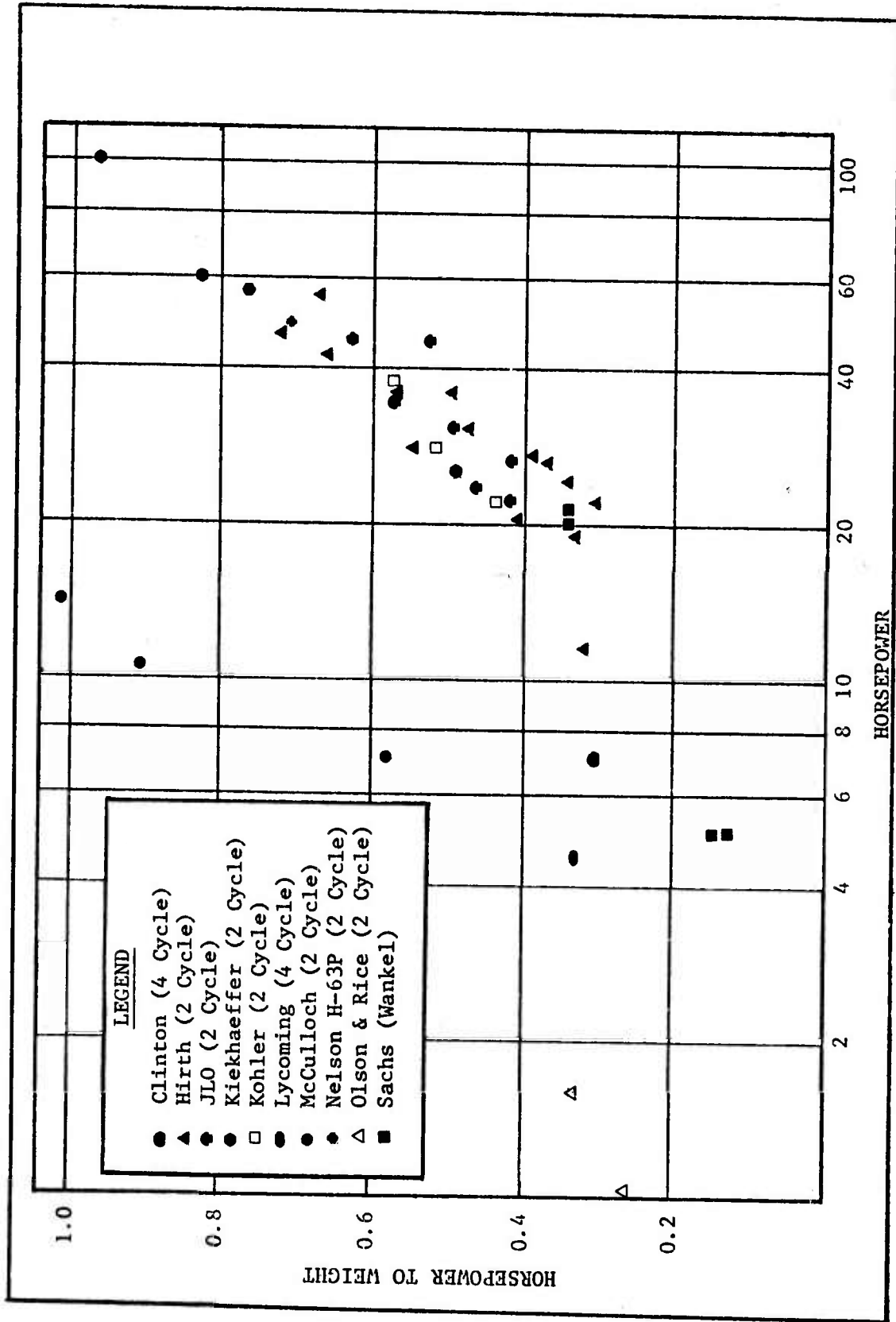


Figure C-1. Comparison of Power to Weight versus Power for Several Engines

### Candidate Comparison with Decision Criteria

In many cases, complexity of engine design is directly related to cost, weight, availability, power, fuel consumption, and, to a lesser extent, vibration and reliability. Table C-2 relates the relative merits of the three engines to the decision criteria.

#### Cost

The four-cycle engine design of the HSSK 50 and the HMSK 70, as opposed to the two-cycle design of the MC 101, requires intake and exhaust valves, rocker arms, push rods, camshaft and timing gears, and lubrication systems. Thus, both Tecumseh engines are more mechanically complex than the MC 101. Also, good quality control is necessary to maintain close tolerances on camshafts and valves which are required for the four-cycle Tecumsehs. A private study shows that production costs for a four-cycle engine are two or three times the cost of an equivalently horsepower-rated two-cycle design (Lockheed, 1975:5-4).

The unit retail costs (plus tax and freight) of the MC 101B, HSSK 50, and HMSK 70 are \$205, \$147, and \$165 respectively. The unit cost figures for large orders from the respective factories are \$148, \$55, and \$75 respectively.

The criterion of minimum cost suggests selection of the HSSK 50 as the engine for the propulsion subsystem; however, this study shows in the following sections that the HSSK 50 is not adequate to power the vehicle at the design cruise altitude. Further, the HMSK 70 is unacceptable from the allowable weight standpoint and contributes to increased life-cycle costs. If the MC 101 is chosen, the average

TABLE C-2. COMPARISON OF SELECTED ENGINE SPECIFICATIONS  
BASED ON CONTRACTOR INFORMATION

CRITERIA	SPECIFICATION	ENGINE		
		MC 101	HSSK 50	HMSK 70
Less than 200	Unit Retail Cost (dollars)	205	147	165
Less than 20	Weight (lb)	13.5	24.0	47.0
Commercial	Availability	Commercial	Commercial	Commercial
5-15	Maximum Rated Horsepower at rpm	12.5@9000	5.0@3600	7.0@3600
0.5-1.5	Specific Fuel Consumption	N/A	1.0	1.0

NOTE: N/A = Not Available from Manufacturers

large-order cost difference between it and the Tecumsehs is about \$40, but is only 3.33% of the total system cost.

Table C-3 shows approximate costs for the various propulsion subsystem components for the candidate engines. The costs are based on an order of thirty-four or more.

TABLE C-3. ESTIMATED PROPULSION SUBSYSTEM COSTS FOR THE PRIMARY CANDIDATES

Component	Engines		
	MC 101	HSSK 50	HMSK 70
Engine	\$148.00	\$ 55.00	\$ 75.00
Shock mounts	30.00	30.00	30.00
Propeller	62.00	62.00	62.00
Fuel System	8.00	8.00	8.00
Engine Run-in	<u>30.00</u>	<u>30.00</u>	<u>30.00</u>
	\$278.00	\$185.00	\$205.00

Weight. The weight per rated horsepower of the MC 101 is lower than that for the HSSK 50 or the HMSK 70; however, this is offset somewhat by the fact that the specific fuel consumption for the MC 101 is approximately 0.9 to 1.3 lbm/hp-hr as compared to approximately 1.0 lbm/hp-hr for the Tecumseh engines. Further details on fuel consumption are discussed in a later section.

The ratios of weight over rated horsepower for the MC 101, HSSK 50, and HMSK 70 are 1.08, 3.43, and 6.71 pounds per horsepower respectively. The weights of 13.5, 24.0, and 47.0 pounds, respectively,

are based on stock engines with cooling shrouds, recoil starters, and other items that are not needed for mini-drone application.

The weight of the HMSK 70 drives the total vehicle weight over the 130-pound limit, and the engine weight exceeds the maximum engine weight criterion of twenty pounds. Also, the HMSK 70 engine is about 30% of the vehicle gross weight. Therefore, the criteria of low weight and low weight-per-horsepower dictate the selection of the MC 101.

Availability. As noted earlier, engines for chain-saws, portable power units, and go-karts are produced in volumes of tens to hundreds of thousands per year. Manufacturers seem reluctant to supply a special run of engines for a drone RPV program (Lockheed, 1975: 5-4). As a result either: (a) stock engines should be installed in the aircraft with a minimum of pre-flight checkout or (b) if the weight and performance of the engine becomes critical, one could perform extensive quality control checks, performance modification and testing, and produce modified engines at greater cost. Again, since low cost is a primary consideration, stock engines are recommended.

Power. In considering how each of the three engines meets the power range criterion of 5-15 horsepower, the degradation of performance due to altitude, temperature, and continuous operation are considered. Typically, internal-combustion engines lose 3-1/2% of their power for each 1000 feet of altitude above sea level and 1% for each 10°F above standard temperature, 60°F. When engines are operated continuously, 20% is subtracted from the power as a safety factor. Also, most production engines develop at least eighty-five percent of their rated power as shipped; and when run-in to reduce friction,

they develop at least 95% of rated power (McCulloch, 1974). The correction factors are multiplied together and are equal to 0.494. For example, the altitude correction factor for 10,000 feet altitude is 35%; the temperature correction factor is not considered; the correction factors for continuous power operation and run-in are 80% and 95% respectively. Table C-4 below shows the net power at 10,000 feet for each engine when the correction factors are applied.

TABLE C-4. COMPARISON OF RATED POWER AND NET POWER FOR THE PRIMARY CANDIDATE ENGINES

ENGINE	HORSEPOWER
	RATED HP x CORRECTION FACTOR = NET POWER
MC-101	12 X 0.494 = 5.93
HSSK 50	7 X 0.494 = 2.47
HMSK 70	5 X 0.494 = 3.46

From these calculations, it is evident that the HSSK 50 does not meet the 3 brake horsepower requirement for the vehicle at the design cruise altitude of 10,000 feet (Appendix A).

Specific Fuel Consumption. Mission requirements dictate minimum specific fuel consumption (SFC) at all times to keep the fuel load down and, hence keep the vehicle weight low. The fuel consumption depends primarily on the heating value of the fuel, the air-fuel mixture, and engine efficiency (Lichty, 1951:455-456).

There are two basic types of fuel used in small internal-combustion engines. The first is glow plug fuel which is commonly used by airplane modelers for control-line and remote control aircraft.

Variations are also used in high performance racing cars. The fuel consists of 10% nitromethane, 80% methanol, and 10% castor oil. The ignition system is normally eliminated when operating with glow-plug fuel which reduces the engine weight and eliminates shielding against radio frequency interference (Lockheed, 1975:5-2). The SFC for glow-plug fuel is approximately twice that for gasoline and oil mixtures, which means that the fuel load increases and the available payload decreases. Ethanol (ethyl alcohol) fuel has 36% and 31% less heating value on a weight and volume basis, respectively, than gasoline (Lichty, 1951:455-456). Therefore, a larger fuel consumption exists with almost the same power output for a given engine using ethanol. Also, it is logistically difficult to provide an exotic fuel in the field.

The second type of fuel is a gasoline-oil mixture which is commonly used in two-cycle engines. The oil-to-gas mixture ratio can vary somewhat if long engine life is not a consideration. Also gasoline-oil fuel is logistically easier to supply to the field.

The type of engine cycle also has an effect on the SFC. It is estimated that a small four-cycle engine will have a cruise SFC of 1.0 lbm/hp-hr (Currie, 1975). This SFC range for the four-cycle engine should be compared to the two-cycle SFC range of 0.9 - 1.3 lbm/hp-hr (McCulloch, 1974).

Vibration. Single-cylinder engines vibrate severely and require vibration isolation mounts. Instances of nuts, bolts, and other parts shaking loose are well documented (Lockheed, 1975:5-11). Vibration problems for single-cylinder engines are more common in two-cycle engines than in four-cycle engines. Engine testing of the MC 101 without vibration mounts created vibration levels which caused the

vibration transducers to be shaken off the engine. Project Teleplane Design Group (AFFDL/PTT) uses cable-ring mounts in their vehicles, some of which are powered by the MC 101, to dampen vibrations.

Reliability. The mature, basic, proven designs of the MC-101 and the HSSK 50 have seen many years of service. Engines for chain-saws, go-karts, mini-bikes, snowblowers, and snowmobiles undergo reliability and developmental testing for years before they are offered for sale to the general public (Lockheed, 1975:5-3). As mentioned previously, reliability data for small internal combustion engines are, for the most part, unavailable to the general public; therefore, reliability testing should be performed on a representative group of these engines.

Additional factors were examined relative to the engine selection process. The splash lubrication system of the four-cycle Tecumseh is not suitable when the engine is inclined more than 30° from the vertical where the engine will not get proper lubrication. A similar problem exists with the float-type carburetor in the Tecumseh engines. Whenever the engine is tilted more than 25° from the vertical, a valve closes in the carburetor and the float ceases to operate, thus causing the engine to be starved for fuel.

The study conducted by the John Hopkins University Applied Physics Laboratory found that reliable engine starting is a problem in engines with magnetic ignition systems. Additionally, it was found that hand-starting was hazardous to personnel. The use of a modified Volkswagon starter, capable of spinning the McCulloch engine up to 3600 rpm assured rapid starts every time. The procurement of a device of this type solves the starting problem and increases personnel safety (Small, 1974:27).

### Engine Selection

Comparison of the candidate engines with criteria indicates that the McCulloch MC 101 engine is the most logical engine for the VLCEHS. Four considerations make it so. It has adequate reserve power, thus enabling the payload and power requirements to be changed. It has fewer parts than the four-cycle engines; therefore, it has less mechanical complexity. The MC 101 is lightest of the three primary candidates. And, the MC 101 is not restricted in orientation during maneuvering as are the four-cycle engines. These operational factors affect the decreased unit cost advantage of the four-cycle engines.

### Propeller Selection

A propeller selection is customarily made knowing the power and rpm of the engine that will be driving it. A suitable propeller can then be selected using the speed-power coefficient,  $C_s$  (Dommasch, 1951:199). The various parameters used in propeller design and selection are found in NACA TR640 by Hartman and Bierman (1938) where their use is discussed in relation to calculating the thrust-versus-flight-speed for propellers of the same plan form and twist distribution, but which use the Clark Y section and the RAF 6 section. The airfoil section that is used influences the propeller performance. Appendix C-2 includes sample calculations that show the 5868-9 Clark Y section superior to the RAF 6 in the design envelope for this drone.

Airfoil tests show that the Clark Y sections have lower minimum drag, lower maximum lift, and lower maximum lift-to-drag ratio than the RAF 6 section. The tests indicate that a fixed-pitch propeller with Clark Y section is superior at cruise and high speeds, but inferior

to the RAF 6 at takeoff and tests done in NACA TR378 (1931) demonstrate this fact (Nelson, 1944:46).

Sample propeller calculations produce parameters that are very close to those done by an independent investigator (Rose, 1975b). Although planform characteristics are not specified, they are not necessarily the driving function for a propeller design. Even though the two designs possess the same characteristics at the design point, off-design conditions can differ drastically (Larsen, 1975a). In spite of this, it is encouraging that the performance characteristics of the two designs are so close and indicates the design by the Sensenich Company is adequate.

Calculations using strip-analysis theory by Theodorsen for 75 mph, 10,000 feet altitude, and 3900 rpm engine speed require a Sensenich W28JX22 propeller with  $\beta = 18.25^\circ$  at 0.75R (75% of the propeller radius), with a chord width of 2.25 inches, and a camber of 3.5%. The efficiency of the W28JX22 propeller is 0.819 at a blade activity factor of 110 (Alan, 1975).

### Engine Testing

Background. Several agencies of the federal government and government contractors are involved in testing engines such as the McCulloch MC 101. The U.S. Army Mobility Equipment Research and Development Center is performing tests on the Lockheed "Little R" engine and several stock MC 101 engines. Lockheed Missiles and Space Company is involved in testing small internal-combustion engines for use in mini-RPVs.

Testing was done at Wright-Patterson Air Force Base, Ohio, by the AFIT Graduate Systems Engineering class in close cooperation with the

Air Force Aero-Propulsion Laboratory and the Air Force Flight Dynamics Laboratory. AFAPL has furnished an altitude chamber, instrumentation, and test personnel; AFFDL has furnished the engine, propeller, thrust stand, and test personnel for the tests performed during this study.

Test Objective. The objective of the AFIT engine test program was to obtain thrust and fuel-consumption data at various altitudes, air speeds, and engine speeds. Although the tests used the MC 101 engine, similar tests can be performed using other engines of the same class.

Test Equipment. The propeller used in the test is a 26GXL13 propeller with a 12° blade angle manufactured by the Sensenich Company. The propeller is made of laminated wood and has a diameter of 25 inches.

The thrust stand or engine mount is a tee-bar that rotates in the horizontal plane. The engine is mounted on one side. A wire is connected to the other side and then to a scale which measures the force transmitted by the arm of the bar. Instrumentation consists of an rpm readout, iron-constantan thermocouples, throttle control, mixture control, and vibration transducers.

Test Procedures. Fuel flow and thrust are measured at different altitudes while the engine rpm is varied. Cylinder head temperature is monitored to prevent overheating. The initial phase of testing requires that the mixture be adjusted to give the maximum thrust at cruise air velocity and altitude. The next phase requires that the fuel-to-air mixture be leaned to permit the cylinder head temperature to reach 400°F. Then, engine data are taken while the altitude is decreased. This procedure determines whether or not the engine will run at lower altitudes with a reduced fuel-to-air mixture. The last phase of testing involves placing a pitot tube rake in the plane of the propeller to determine

the velocity distribution.

Test Results. The data points show that the effects of scatter and repeatability of the test points was a problem. Only two readings were taken at each test point. Consequently, the statistical average is not significant.

While the thrust data is definitely conservative, it indicates that the engine and propeller will produce adequate thrust throughout the flight regime. Even larger values of thrust should result when the test is run in a wind tunnel using a nacelle-mounted engine. The data also shows that the engine can be de-rated to give it longer life.

Fuel consumption data shows that the specific fuel consumption is in the acceptable range of 0.5 to 1.5 lbm/hp-hr. The fuel consumption should also improve in wind-tunnel testing.

Inconclusive test results came from two areas. An estimate of the drag of the engine was not obtained due to the insensitivity of the equipment and lack of definition of the flow behavior. The attempt to measure the velocity distribution in the plane of the propeller yielded inconclusive data due to the arrangement of the equipment and non-uniform flow field in the region of the propeller.

## APPENDIX C-1

### ENGINE TEST

#### Introduction

A McCulloch MC 101 engine and 25 inch diameter Sensenich propeller were tested by the AFIT Graduate Systems Engineering class in cooperation with the Air Force Flight Dynamics Laboratory and the Air Force Aero-Propulsion Laboratory. The test gives thrust and fuel consumption data as a function of engine speed for different flight speeds and altitudes.

The U.S. Army is currently involved in testing several engines for possible use in RPVs. They are testing a stock MC 101 engine with a "double-pumper" carburetor which has a larger range of adjustment for altitude operations. The Army is also testing the engine for the Lockheed "Little R" vehicle. It is an MC 101B that has been modified to suit Lockheed's configuration by using a carburetor and intake manifold from an MC 49E engine.

Test data has not been received from the Army; however, their monthly reports of progress provide some valuable information. Use of Go-Power dynamometers are not suitable for testing this class of engines. The alignment between the engine and dynamometer is a problem due to flexing of the dynamometer mounts. The dynamometer mounted tachometer is not suitable due to excessive vibrations and variations in speed. The vibrations are greater than anticipated especially at light load and high speeds. Because of vibrations, optical speed pickups are unsatisfactory. The Army also found that the use of a six-tooth gear which was attached to the coupling and a magnetic pickup were not acceptable due to vibration. The use of a pressure pickup installed in the

reed box housing gave satisfactory engine speed results (Leggett, 1975).

The Sandia Crest Experiments conducted by Lockheed show the MC 101 to have 8.75 brake horsepower at 8250 rpm, which is more than adequate for the vehicle at 10000 feet altitude. If the engine is derated by running at a lower rpm, for example, 4000 rpm, the brake horsepower is approximately 3. Figure C-2 shows a family of curves at different altitudes for the brake horsepower versus engine speed for the Lockheed modified MC 101 in flight configuration. The curves are for static conditions.

Figure C-3 shows the effect of mixture ratio setting at sea-level conditions. The engine configurations has an eleven inch induction extension with no elbow; it also has a tuned exhaust with a 5/16 inch slot. The data points show that the high speed mixture setting does not appreciably affect the power.

The Teleplane Preliminary Design Study (AFFDL TM-71-1-PTB, December, 1971) shows performance curves for a McCulloch MC 101 engine equipped with the same Sensenich propeller as was used in this experiment. The method used to obtain the curves was to obtain performance data for the engine and then use the procedures outlined in NACA TR237, which deals with the Type A Navy Propeller, to obtain combined performance curves.

#### Test Objective

The objective of the test is to obtain tentative thrust and fuel consumption data at various altitudes, vehicle flight speeds, and engine speeds for a McCulloch MC 101 engine. The engine has a twenty-

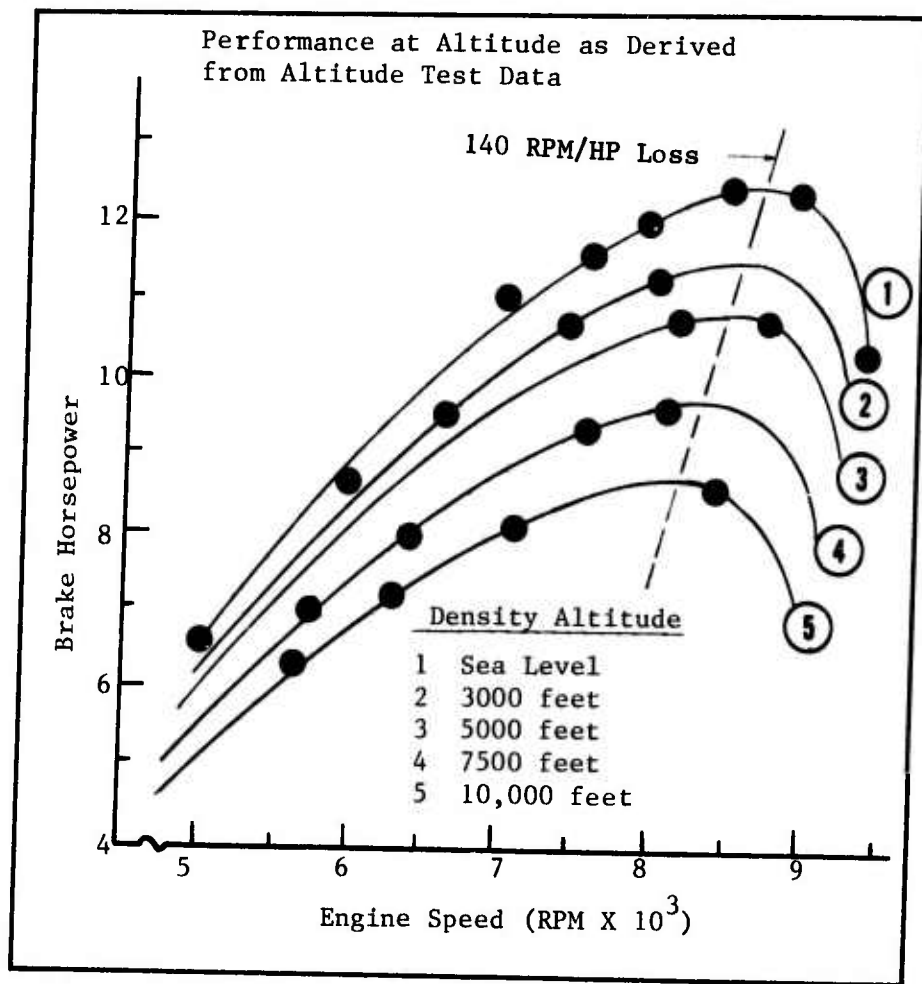


Figure C-2. Derived Altitude Test Data for MC 101 Engine in Lockheed Flight Configuration (Lockheed, 1974)

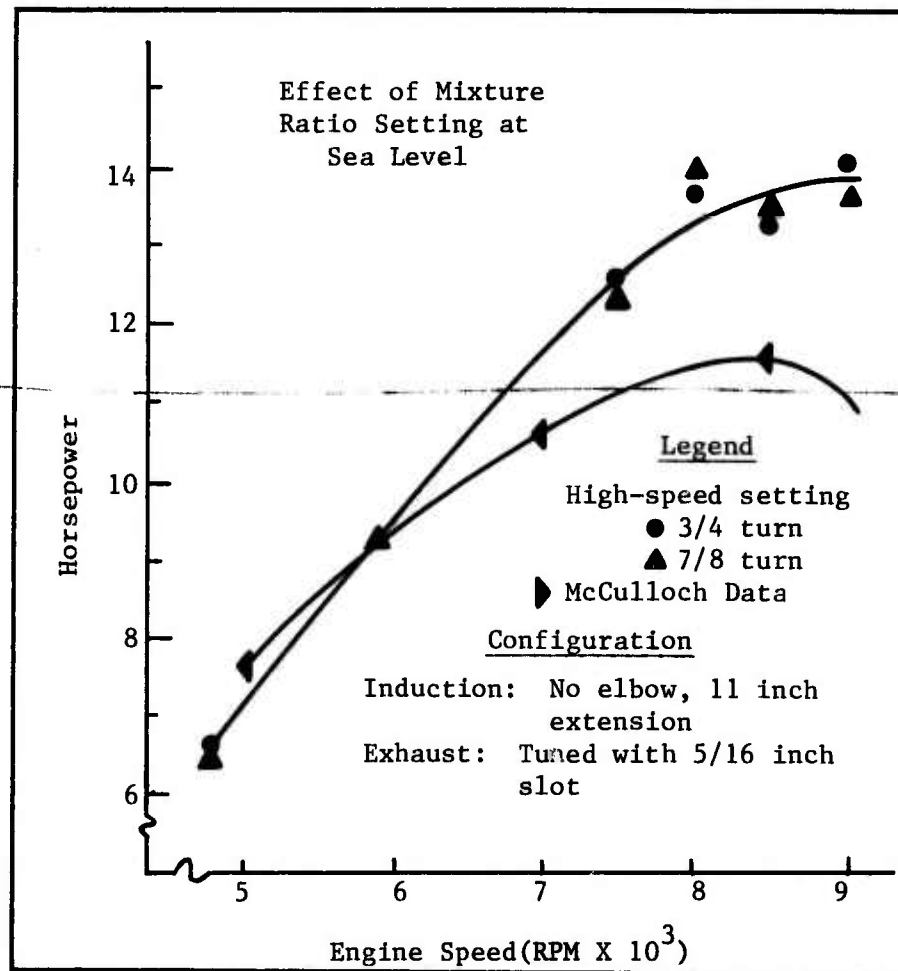


Figure C-3. Mixture Ratio Effects

five inch diameter propeller attached. Thrust and fuel consumption data will aid in refining airframe design and in sizing the fuel tank. In addition to the above, a measure of reliability of the engine is sought.

#### Scope of the Test

This experiment will show the procedures used in arriving at thrust and fuel consumption data and points out areas in the set-up that are questionable experimental practice and will show why the data are questionable. In addition, a procedure is recommended for further testing which should give more accurate and representative data. The data that are obtained should give a representative sampling of static performance data at various altitudes.

#### Equipment

Engine. Many of the engine specifications are given in the main text of Appendix C; however, Table C-5 gives the manufacturer's specifications.

Figure C-4 shows the McCulloch MC 101 engine disassembled. The small size of the stripped down version should be noted.

Propeller. The two-blade propeller used in the test is a 26GXL13 with a blade angle of  $12^\circ$ . It is manufactured by Sensenich Company of Lancaster, PA. This particular propeller is used in the experiment because there were no other representative propellers available at the time of the engine test. The 26GXL13 is a climb propeller that was designed about eight years ago for the Forrestal Laboratory at Princeton University. A McCulloch engine was derated

TABLE C-5. MC 101B SPECIFICATIONS

Displacement	7.5 in. <sup>3</sup> (123 cc)
Bore	2.280 in. (58mm)
Stroke	1.835 in. (4.6mm)
Compression Ratio	9.4:1
Weight	12 pounds 4 ounces (5.7 kg)
Carburetor	Twin stage integral fuel pump. Wide range high and low mixture needles.
Piston Rings	Two narrow steel racing type with chrome plated wear face for quick sealing, low friction and long life. Pinned.
Bearings Conn Rod	Full complement M-50 Tool Steel needle rollers, hardened shaft and rod ends.
Wrist Pin	<del>Two needle roller bearings in the piston. Extra length for additional lubrication and cooling.</del>
Main	Full complement high capacity Ball bearings (2)
Connecting Rod	Hot forged, hardened and ground alloy steel with removable cap and integral race. Oil slot in cap. Wrist pin pressed in place.
Crankshaft	Extensively glass bead shot peened, and tungsten counter- weights.
Cylinder-Crankcase	Die cast aluminum alloy with precision honed cast iron liner. Deep finned detachable head.
Direction of Rotation	All engines clockwise (facing power take off shaft)

Ignition	Waterproof high tension magneto. Advanced magnetic timing system. Moisture-proof coil bonded to special high rev lamination.
Spark Plug	Champion L-78
Fuel Oil Mixture	20:1 with McCulloch oil and automotive regular grade gasoline.
Flywheel	High pressure die cast aluminum alloy with integral magneto magnets, steel hub.
Mounting	Four bolt holes provided on bottom of crankcase, Engine operates in any position. (McCulloch, 1975)

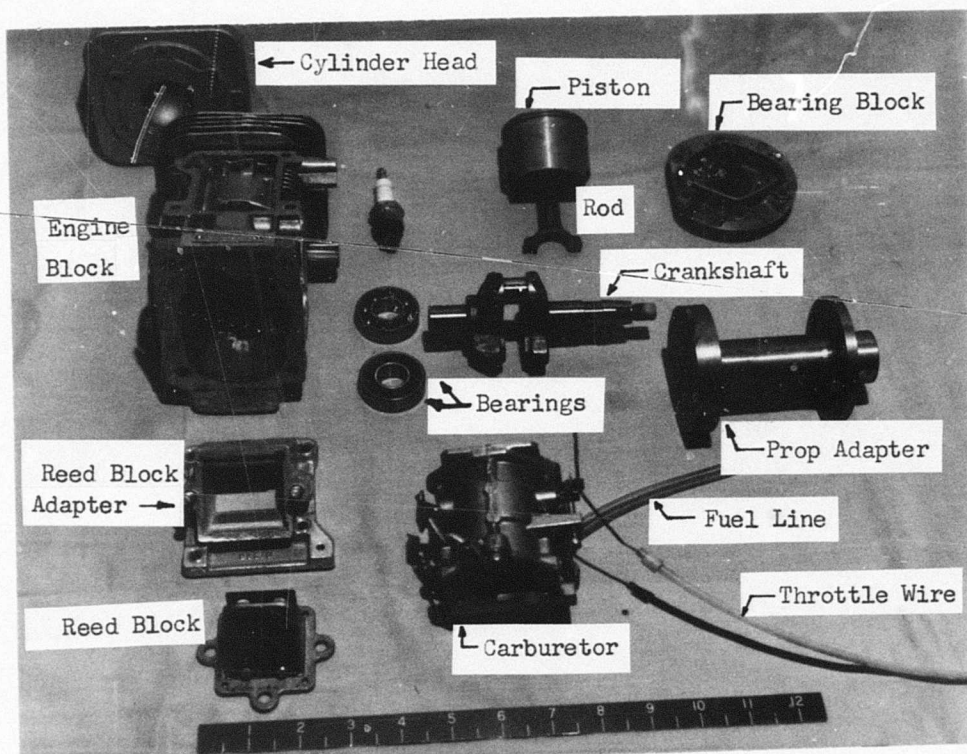


Figure C-4. Disassembled View of the MC 101

to 11-1/2 horsepower at 7200 rpm for a 60 knot flight speed in the design analysis at that time. The theory of "strip analysis", was used to design the propeller (Rose, 1975b). Although the Sensenich 26GXL13 propeller is not a cruise propeller, it is felt that it would give representative data.

Engine Thrust Stand. The stand is mounted in the tunnel with the "Tee" bar in the horizontal plane and perpendicular to the direction of airflow. The center line of the engine crankshaft is approximately nine inches below the center line of the exhaust bell-mouth; the plane of the propeller face is 3 feet 5 inches from the exhaust bell-mouth and is 5 feet 6 inches from the annular flange upstream of the engine. Figure C-5 shows the orientation of the engine and test stand relative to the altitude chamber and the instrumentation schematic.

Figure C-6 shows the existence of a great deal of drag-producing equipment and structural members upstream of the flow. The effects upon the flow velocities and pressures that exist in the plane of the propeller due to these devices will be treated in the theory section of this report. Figure C-6 also shows many of the pieces of equipment necessary to the test. Note the throttle linkage shown in the upper middle part of the figure.

Fuel System. Figure C-7 shows the one-liter graduated cylinder with twenty milliliter graduations situated approximately three feet below the carburetor intake. The fuel line is run from the graduated cylinder to the carburetor and a five gallon pressurized can containing a 9:1 ratio of regular gasoline and Klotz 30 weight motorcycle oil

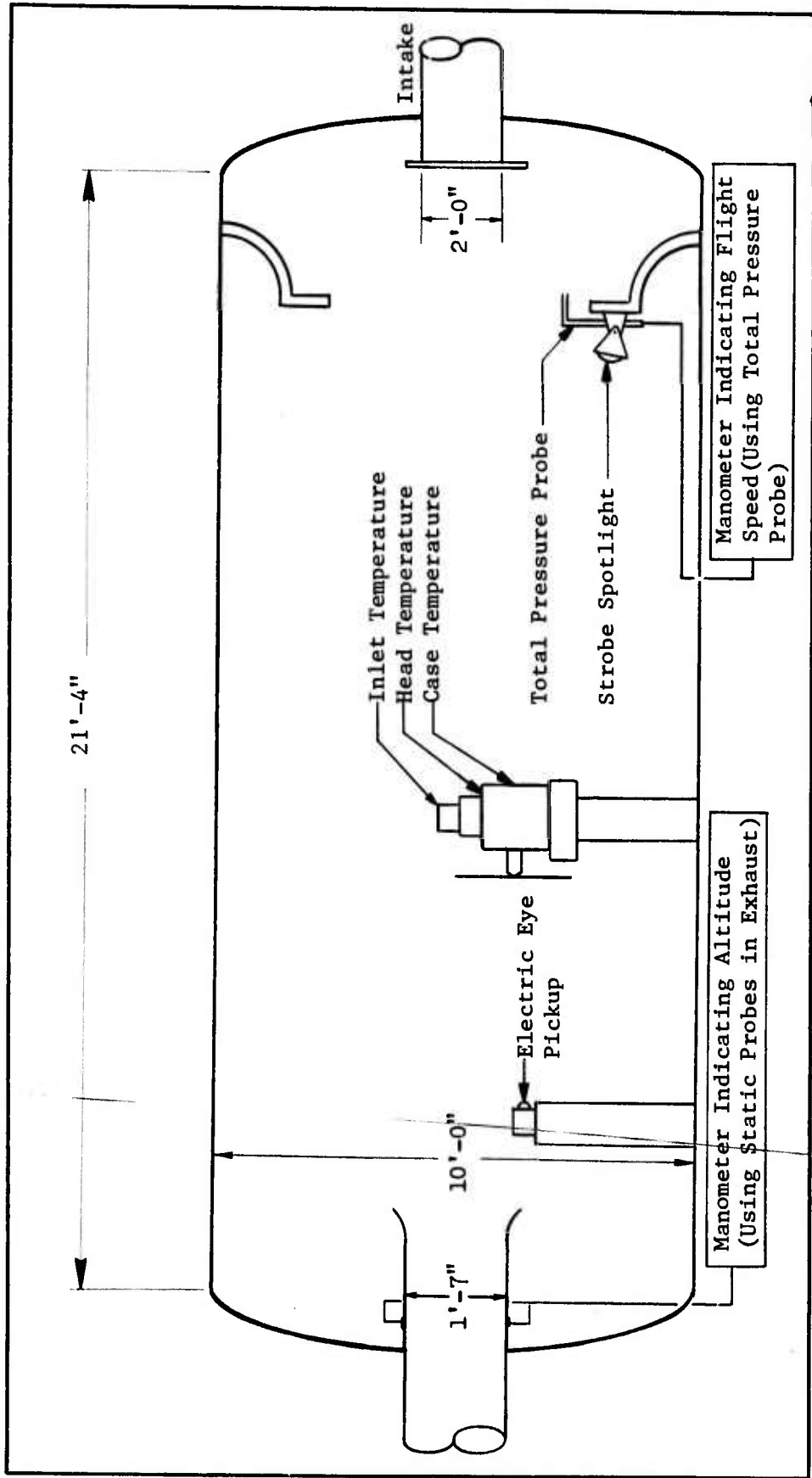


Figure C-5. Test Bed Instrumentation Schematic

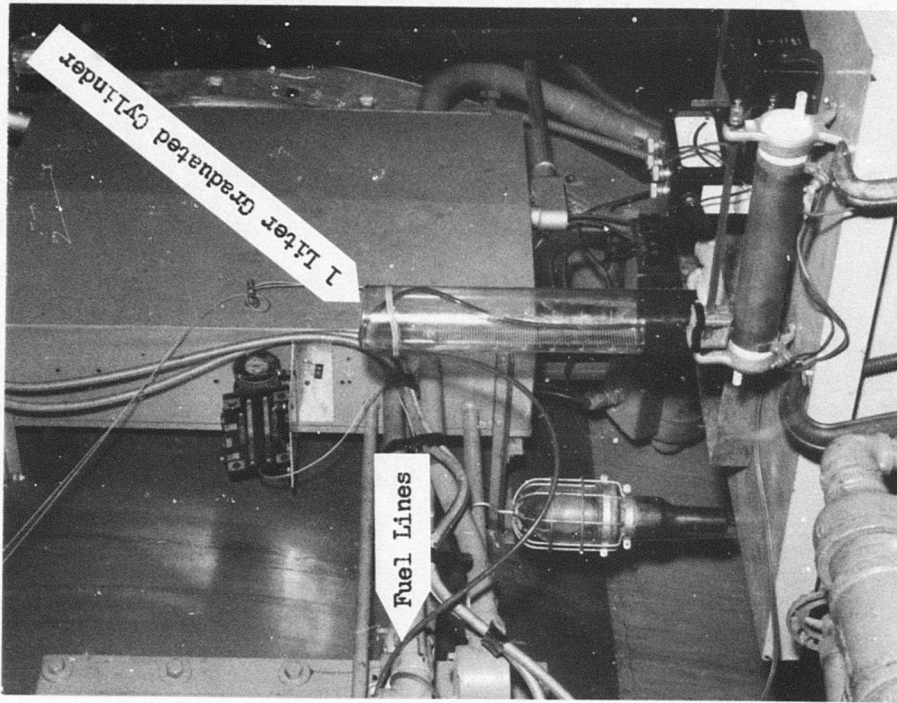


Figure C-7. Fuel Measurement System

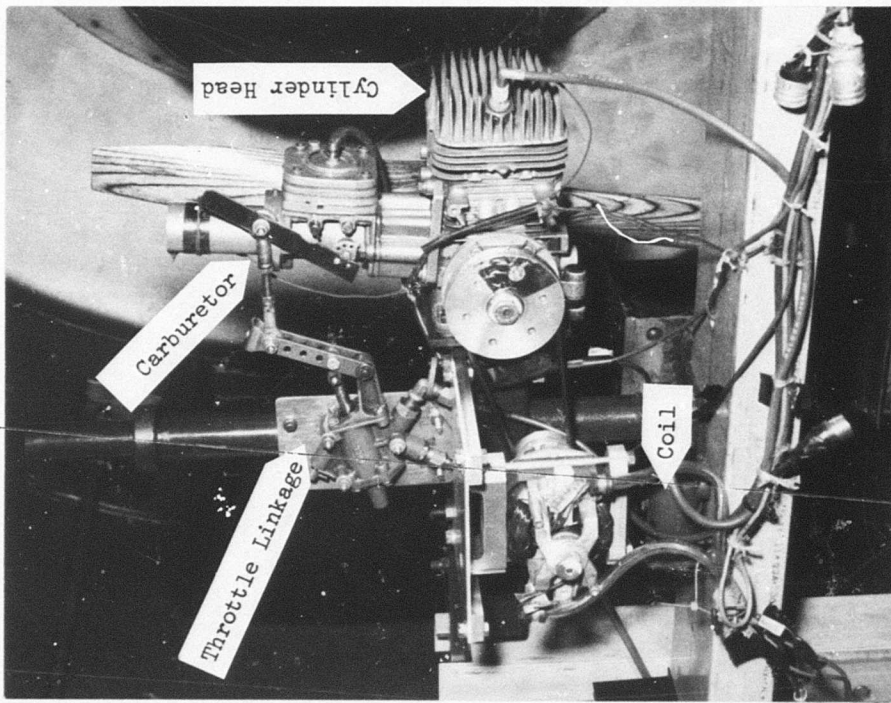


Figure C-6. Front View of Engine in Altitude Chamber

is connected to the graduated cylinder by a separate piece of fuel line. This procedure enables the operator to keep an adequate supply of fuel in the cylinder at all times.

The mixture to the carburetor is adjusted by means of a pulley wheel that is brazed to the mixture control needle valve. A wire is wrapped around the pulley wheel and is run through a small hole in the chamber so an operator can adjust the mixture from outside the chamber.

Instrumentation. Engine speed (rpm) is measured by shining a spotlight from the front of the chamber through the propeller onto a strobe pickup. Each time a blade breaks the light beam, the circuit is interrupted and a signal is relayed to the control room where a Beckman/Berkeley Preset EPUT Meter is used to measure rpm directly.

Three iron-constantan thermocouples are used to monitor temperatures of the engine. Since head temperature is so critical, a thermocouple is mounted near the spark plug. Another thermocouple is attached to the crankcase and a third is placed just inside the carburetor inlet tube to monitor inlet air temperature to the carburetor.

Vibration is monitored by two sensors. One is mounted to measure displacements parallel to the engine crankshaft centerline and the other is mounted to measure displacements in the vertical direction. Lack of suitable mounting locations precluded placing a sensor to measure horizontal displacements that are perpendicular to the axis of the crankshaft. Excessive vibration of the engine caused the sensors to break from their mountings early in the test and no attempt was made to re-connect them.

Altitude Chamber. The altitude chamber that is used for testing is located in room 24 of building 18E of the Aero-Propulsion Laboratory. The chamber is approximately 22 feet long and 10 feet in diameter.

The air flow is not refrigerated and is achieved by exhausters which are situated in the basement of building 18E. Air is pulled through the chamber and altitude and airspeed are adjusted by using static pressure probes in the exhaust and a total pressure probe which is mounted on the annular flange upstream of the engine. During testing, the exhaust gases are vented to the exhausters when the altitude runs are made and are vented through the open chamber door during static, sea-level tests, since the altitude chamber does not have provisions to simulate temperature effects for increased altitude. Therefore, ambient air flowing past the engine provides cooling to the engine during altitude runs. No cooling air is provided for static runs.

### Theory

Thrust Measurements. The thrust of the engine and propeller causes a moment which results in an opposing force that pulls the cable towards the rear of the chamber. The cable is attached by pulleys to the spring scale which measures the force. The ratio of the moment arms is 5:1 so the scale force reading is multiplied by five to obtain the net thrust value. Figure C-8 shows the relationship of the forces to the thrust stand.

Summing moments around the pivot point enables the determination of the force or thrust imparted to the air by the propeller and engine.

$$\Sigma M = 0$$

and

$$TL_1 - F_s L_2 = 0$$

so

$$T = F_s L_2 / L_1.$$

For the thrust stand the ratio of  $L_2$  to  $L_1$  is five.

$$\text{Thus} \quad T = 5F_s \quad (C-1)$$

where

$T$  = engine thrust, pounds

$F_s$  = scale reading of force, pounds

$L_1$  = distance from the centerline of the  
crankshaft to the pivot point, inches

$L_2$  = distance of the cable attachment point  
to the pivot point, inches

Propeller. Thrust can be calculated by finding the increase of axial momentum per unit time. When the propeller is treated as a disk, thrust equals the mass per unit time through the disk multiplied by the increase in velocity or

$$T = \rho V_d (V_s - V_0) \quad (C-2)$$

where

$T$  = thrust, pounds

$V_d$  = velocity at the disk, ft/sec

$V_0$  = velocity of the unaffected  
air upstream, ft/sec

$V_s$  = final velocity of the slipstream  
air, ft/sec

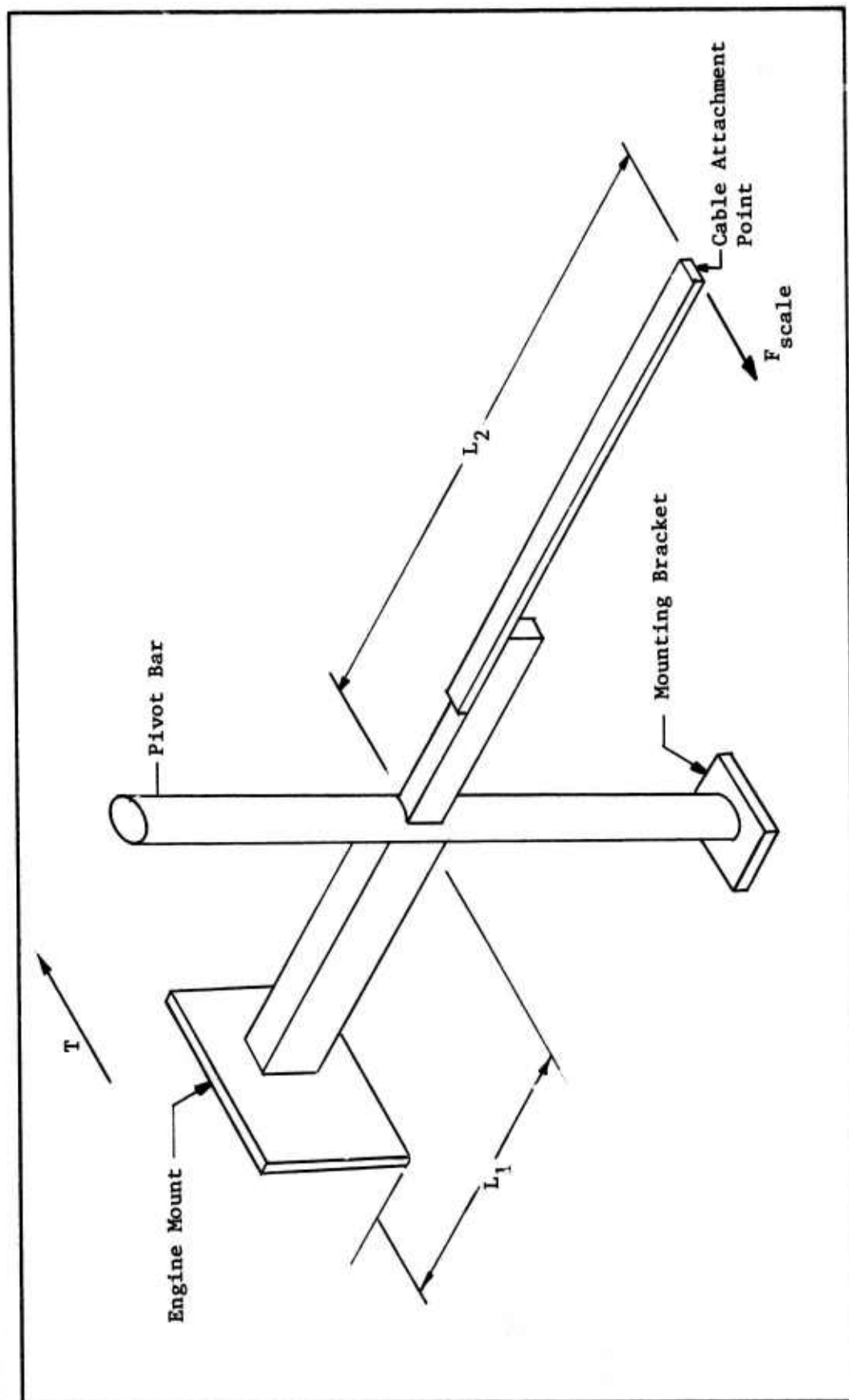


Figure C-8. Thrust Stand

$$A = \text{area of the disk} = \pi D^2/4,$$
$$\text{ft}^2$$

$$\rho = \text{mass density of air, slugs/ft}^3$$

Thrust can also be expressed as  $A\Delta p$  where  $\Delta p$  is the difference in total pressure head along a given stream tube both in back of and in front of the disk. Bernoulli's theorem does not apply because energy is added at the disk. Thus,  $P_0 + \rho V_0^2/2$  is a constant along a given stream line except in the plane of the disk (Nelson, 1944:4-5).

Momentum theory neglects some important items such as aerodynamic drag losses of the blades, energy loss due to slipstream rotation, compressibility losses, blade interference, and thrust pulsations due to the finite number of blades. In addition, the propeller or engine torque cannot be introduced into the analysis (Nelson, 1944:6-7).

Uniform flow is to be desired for propeller testing to obtain the best possible thrust versus velocity. Since there is a great deal of drag-producing equipment in front of the propeller in this test program (see Figure C-6), it is not in a uniform flow. The flow is asymmetric with vortices that are shed from the structural members upstream. Thrust readings indicate the net thrust because the air flow impacts against the engine and parts of the horizontal pivot bar causing a drag force. One phase of the experiment is to measure the drag force by reversing the pulleys so the scale indicates the drag force or the force of the air on the engine.

An analytical estimate of the drag was done to see if flow blockage was significant. Calculations were done for each separate

piece of equipment that could alter the measurements by creating a drag force. Since most of the apparatus is symmetric about the vertical pivot bar, the assumption is made that the engine and carburetor are the only contributors to drag. An individual Reynolds number ( $R_e$ ) is calculated for each piece of equipment which yields a value for the coefficient of drag ( $C_D$ ). Once the values for  $C_D$  are found, they are multiplied by the individual frontal areas to obtain the total drag force (D). Initial calculations show the carburetor and engine to be in the transition region from laminar to turbulent flow which yields relatively high values of  $C_D$  and a total estimated drag of 3.9 pounds force (lbf).

Calculations showed a 37% total flow blockage in the area that is swept out by the propeller. It was assumed, however, that only the non-moving structural members such as the horizontal support bar and pivot bar contributed to the drag. This assumption resulted in a 12% flow blockage and therefore, resulted in an adjusted propeller efficiency ( $\eta_{adj}$ ) of 0.71. The unadjusted efficiency was 0.81 for a cruise velocity of 75 miles per hour and an advance ratio, J, of 0.65.

$$\begin{aligned}\eta_{adj} &= 0.81 \times 0.88 && (C-3) \\ &= 0.71\end{aligned}$$

Fuel Consumption. Flow from the graduated cylinder is measured over a two minute interval and reduced to give readings in milliliters per minute. The number of liters per minute is multiplied by 91.1421 to obtain the number of pounds per hour of fuel flow.

## Test Procedures

Initial Calibration and Checkout of Equipment. A magnetic pickup was initially used with a toothed gear to measure the engine speed; however, vibration of the engine prevented accurate rpm readings on the digital output. The next method used to measure the rpm was an electrical pickup mounted on the spark plug connection. This method proved unreliable also. The most effective method to measure rpm was an optical pickup using a spotlight. Each time the propeller blade passed through the light beam a signal was relayed to the digital readout meter.

Static Data. Once the calibration and checkout phase was complete, data were obtained for static conditions. This part of the test determined "static sea-level" thrust and fuel consumption. Of course, the data are obtained at local conditions and elevation of the test chamber.

Varying Altitude and Engine Speed. The second phase of the actual testing yielded data at varying altitudes and different engine speeds. Initial runs were made at a fuel-to-air mixture setting which enabled the engine to develop maximum thrust at the design speed of 75 miles per hour and 9000 feet (the actual design point was 10,000 feet, but the chamber was restricted to an altitude of 9000 feet).

After the thrust was optimized for cruise, data were obtained for a range of flight velocities and various altitudes. Then the altitude was decreased to sea-level conditions to see if the engine would run at the fuel-to-air mixture that gave the maximum thrust at 9000 feet altitude.

The next phase of testing consisted of bringing the chamber to 100 miles per hour flight speed at 9000 feet altitude and leaning the mixture until a maximum head temperature of 404°F was obtained. This was the maximum head temperature that was considered to be safe for engine longevity. A report by T. R. Small of the Johns Hopkins University Applied Physics Laboratory recommends a maximum head temperature of 400°F for a McCulloch MC 91B/1 engine. The report also pointed out that the engine is susceptible to damage if it is run without an exhaust pipe (Small, 1974:34).

Problems Associated with the Test. During one experimental run, the condenser shook off the engine and had to be remounted. Repair was accomplished and testing was resumed. In another run, the carburetor air intake tube came off the carburetor and it hit the propeller. A one-half-inch chunk was knocked out of the leading edge of one of the blades. Figure C-9 shows a picture of the damaged test propeller. Subsequent testing used the same propeller.

During another test run, a diode shook loose in the rpm strobe pickup unit due to excessive vibration. At approximately the same time, it was noticed that fuel was leaking from around the carburetor. After the chamber was brought back to ambient conditions, the carburetor and reed block were removed from the engine and examined. One side of the reed block was cracked and was leaking fuel. Since a spare was unavailable, the reed block was reversed and re-installed with the carburetor on the engine. This action enabled the test to continue without further problems of fuel leakage. The same day an alternator belt broke so the rest of the runs that day were made without an alternator load on the engine.

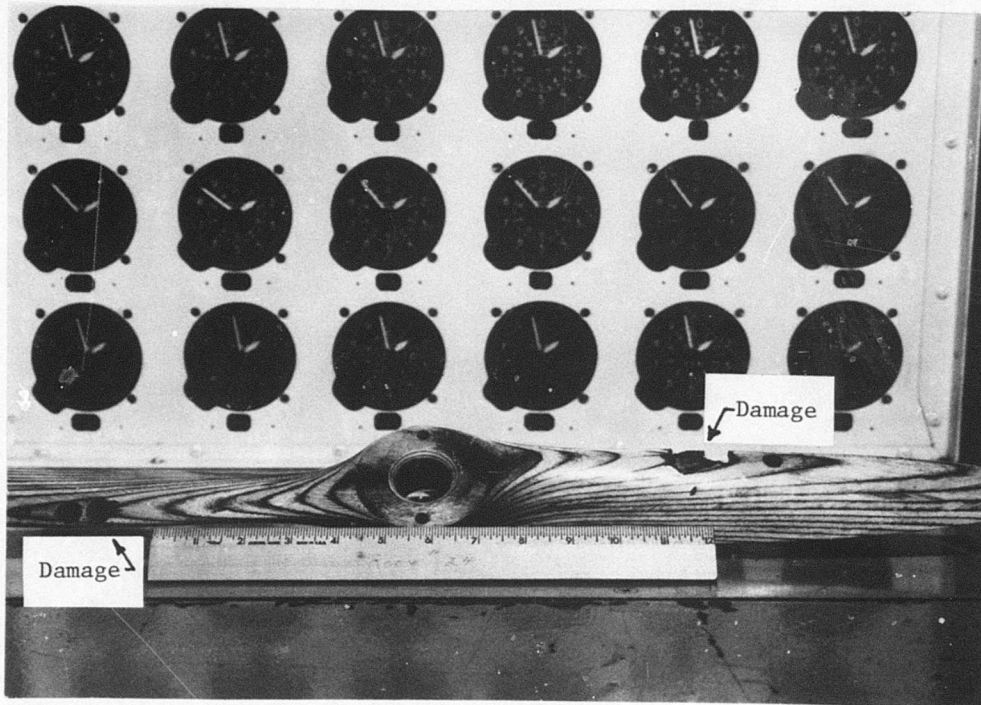


Figure C-9. Test Propeller Damage

Drag Measurement. Some assessment of the drag produced by this equipment and its effect upon the engine thrust becomes necessary. Consequently, the pulleys were altered to enable the pivot bar to rotate in the opposite direction from the usual.

The test procedures for this phase involved leaving the engine shut down and running the tunnel at different altitudes and tunnel velocities. Readings were taken from the force scale to determine the drag due to the air impacting on the equipment.

## Test Results

Discussion. The test results indicate a great deal of scatter in the data. Also, repeatability of the data is a problem. Examination of Figures C-10 and C-11 shows that the slopes of the lines through the data points are very similar for the various altitudes. Linearization is assumed since there are not enough data points collected to suggest otherwise.

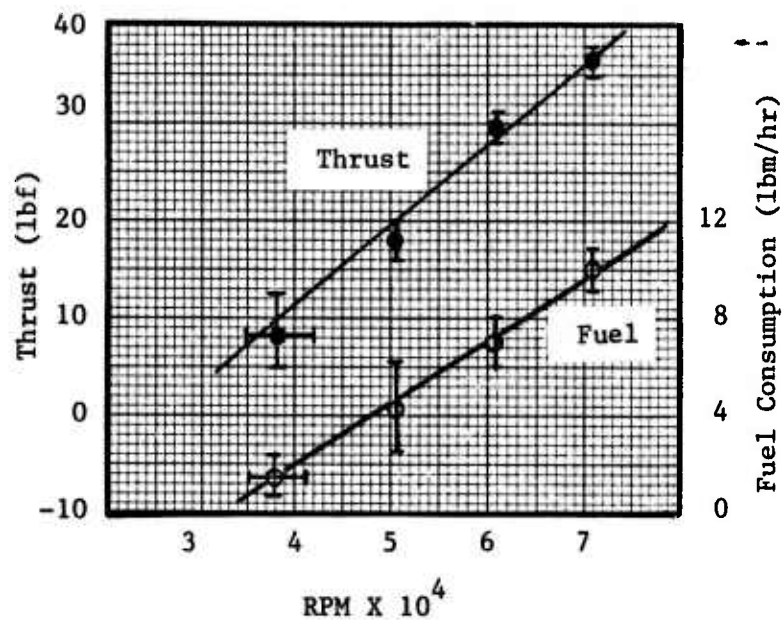
The data taken to estimate the drag indicates only 0.1 pound drag force acting on the assembly. This reading is due more to the vibration of the assembly than to an actual drag force. The relative insensitivity of the equipment makes it difficult to determine small changes in thrust.

Calculation at 75 miles per hour shows a drag force of approximately 3.9 pounds (Appendix C-2). The thrust measurements are very conservative yet provide ample thrust for the vehicle.

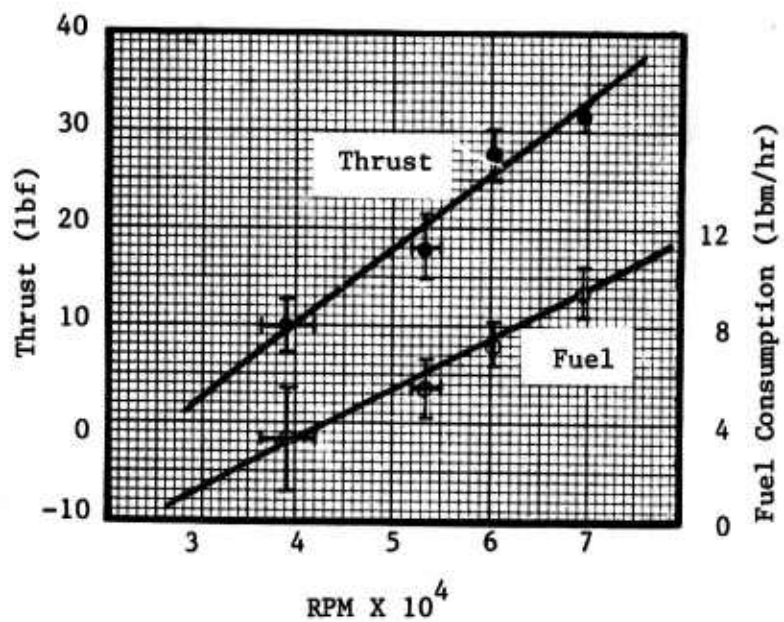
A pressure rake was fabricated to estimate the velocity distribution in the plane of the propeller. This was attempted because of the relatively high values of thrust that were obtained at 10,000 feet and 100 miles per hour tunnel velocity. The results of this part of the experiment did not yield conclusive data and the actual flow conditions in the chamber are unknown.

Errors in the Test. Possible errors associated with taking data may be due to the following:

1. Operator error when reading fuel consumption would be about  $\pm 10$  ml. since the graduated cylinder that is used has increments of 20 ml.

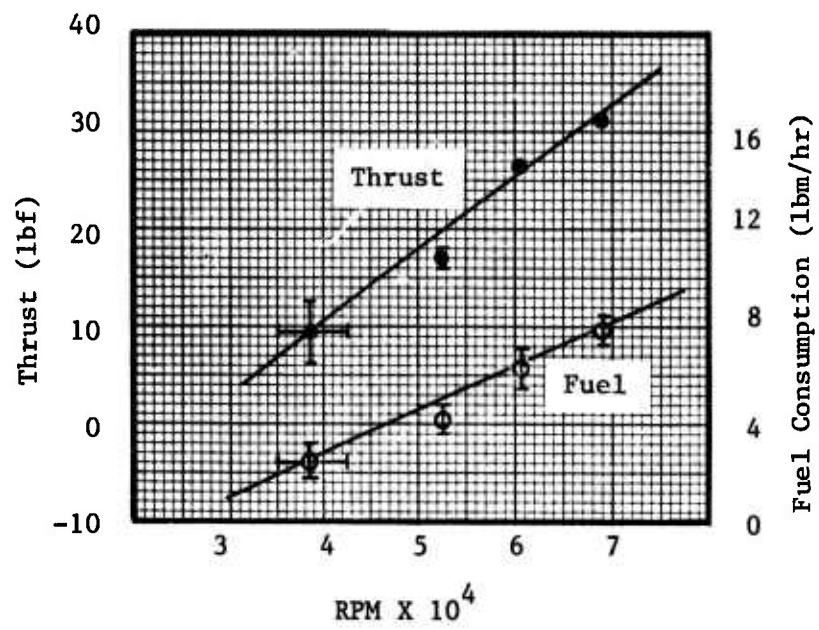


(a) 3000 feet

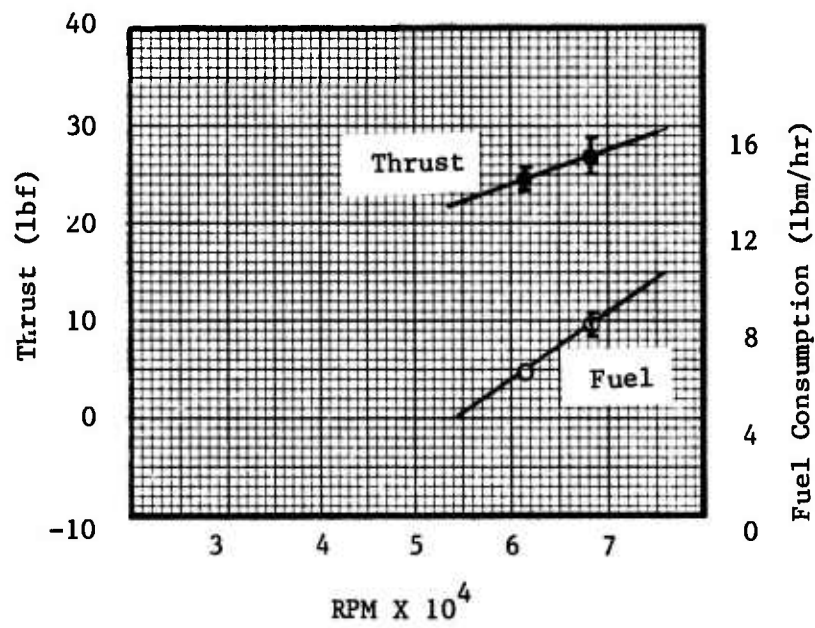


(b) 5000 feet

Figure C-10. Thrust and Fuel Consumption Versus Engine Speed for Various Altitudes at 75 Miles Per Hour Tunnel Velocity

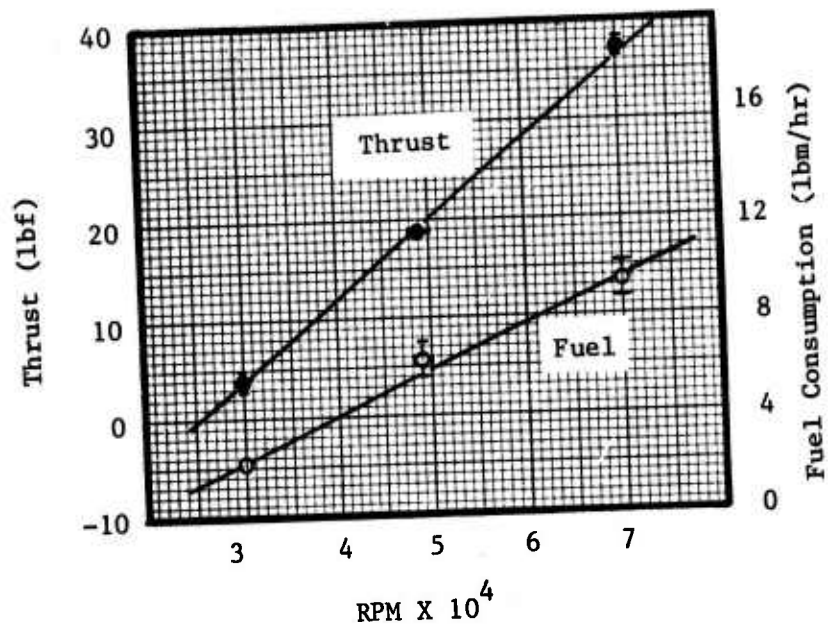


(c) 7000 feet

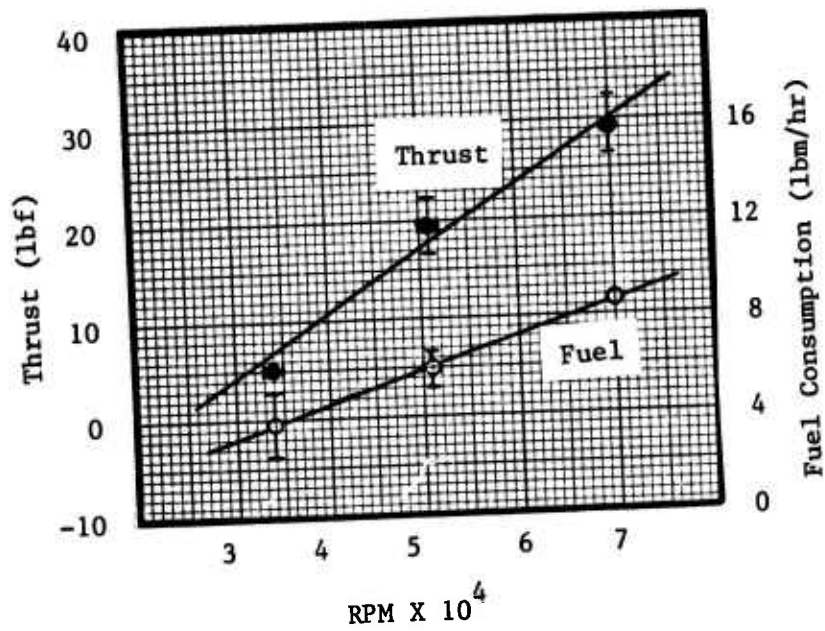


(d) 9000 feet

Figure C-10. Continued



(a) 3000 feet



(b) 5000 feet

Figure C-11. Thrust and Fuel Consumption Versus Engine Speed for Various Altitudes at 100 Miles Per Hour Tunnel Velocity

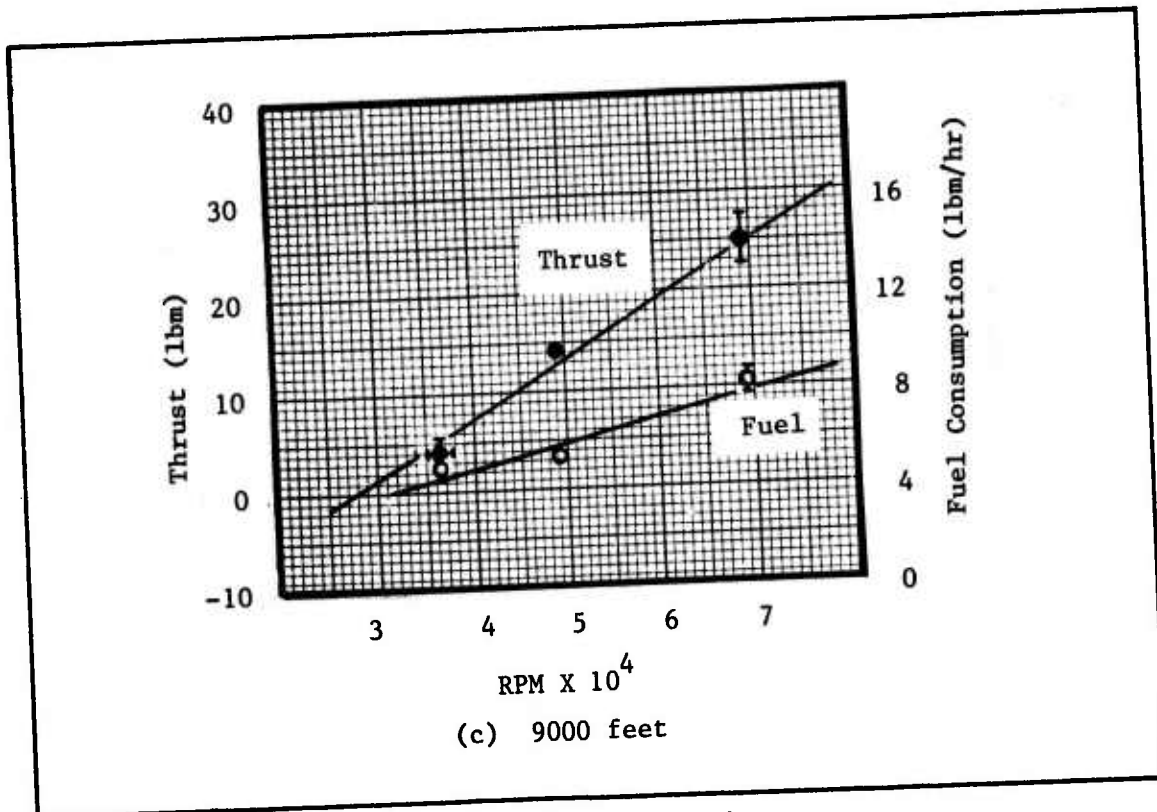


Figure C-11. Continued

Thrust and fuel consumption curves should resemble those found in Figure C-12 below.

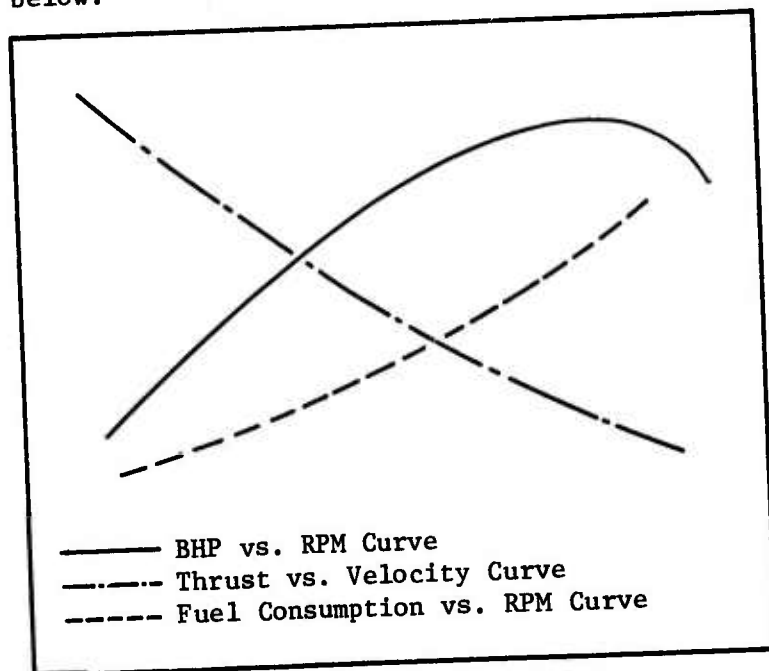


Figure C-12. Generic Performance Curves

2. Operator errors in reading the force scale could be  $\pm 0.5$  pound which, when multiplied by the pivot arm factor of five, yields  $\pm 2.5$  pounds error in the thrust values. The force scale is graduated into increments of 0.1 pound.
3. Inherent equipment error can also contribute to the data scatter. The engine speed digital readout meter has an error of  $\pm 5\%$  associated with it.
4. In calculating the thrust of the engine, the tacit assumption is made that the pivot bearing is frictionless, which is obviously not correct. The vibration of the assembly would help to make this a reasonable assumption.

In order to properly measure the thrust of the engine and propeller combination, a test bed would have to be fabricated and load cells used to measure the thrust. To reduce the drag, the engine should be mounted in a model of an actual aircraft nacelle. This procedure would reduce the expected error associated with the experiment.

The thrust can be calculated from the formula

$$T = \frac{\text{BHP}}{V} \eta \quad (\text{C-4})$$

where

- T = engine thrust, pounds
- BHP = brake horsepower
- V = flight velocity
- $\eta$  = propeller efficiency

A variety of explanations can be offered for the data obtained from this experiment. There are also some conclusions that can be drawn. They are listed as follows:

1. Due to the relatively small inlet expanding into the large, cavernous volume of the test chamber the possibility of an application of free-jet mixing theory becomes a possible explanation of the experiment. In which case, the pressure distribution at the propeller face should perhaps resemble a "flattened-out" Gaussian curve.
2. The initial feeling that the velocity data were incorrect is neither verified nor denied by the results of the pressure-rake part of the experiment. The data are inconclusive. On the other hand, since the attempt was made to use an altitude chamber as a wind tunnel, there is good reason to believe that the flow inside the chamber could be any value and could have any distribution. Also, to assume that the flow will behave similar to the way it would in a wind tunnel where the experiment has been correctly set up may be erroneous.
3. The data are very conservative and the engine-propeller combination should perform much better in an actual aircraft than it did in the test. This data should not be used for design purposes.

Engine Test Recommendations. In future experiments with small engines, several things should be done. The engine should be cali-

brated using a dynamometer or a prony brake to get partial and full throttle performance maps. Knowledge of the torque and brake horsepower versus engine speed curves determine what the output of the engine is. These performance maps could be obtained with the test bed in an altitude chamber which would give necessary altitude data.

Propeller testing should be performed in a wind tunnel using a variable-speed electric motor as the power source. The electric motor must be calibrated before using it with a propeller so the amounts of amperage, wattage, etc. are known. Once this has been done, the propeller and electric motor should be mounted in a model of the actual nacelle to facilitate adequate measurement of the thrust developed by the electric motor and propeller. If a curve of thrust versus velocity is developed for sea-level conditions, it is a relatively simple matter to generate curves for different altitudes. The only wind tunnel that is suitable for such tests on Wright-Patterson AFB is the AFIT Five-Foot Wind Tunnel.

Glauert suggested that the propeller diameter should be small relative to the jet diameter and that an open-throat wind tunnel should be used. With these conditions met, no boundary layer corrections are required (Pope, 1966:362-363). The propeller requires uniform flow in order to develop the maximum amount of thrust and to accurately determine its performance.

When data from the engine and propeller tests are obtained, they can be mated to obtain the various performance curves for the engine and propeller combination. The resulting performance maps can then be used in the design process for the airframe.

A plan should be developed that will permit reliability testing of a number of engines over the desired time interval of operation.

Weather effects of the propulsion system need to be studied. For example, the effects of carburetor icing at all altitudes within the flight regime, especially during periods of cold weather and humidity and temperature effects, on engine performance should be investigated.

The effects of engine vibration of the vehicle, when it is equipped with and without vibration isolation mounts, should be investigated. Also, safety wire should be used on nuts, bolts, etc. on the engine and airframe to preclude loosening from vibration.

APPENDIX C-2

SAMPLE CALCULATIONS

Propeller Calculations

These calculations use the fixed-pitch analysis from NACA TR640 (Hartman, 1938). The design calculations are as follows:

- V = flight speed
- = 75 miles per hour
- h = altitude above ground level (AGL)
- = 10,000 feet
- $\sigma = \rho/\rho_0 =$  density ratio = 0.7384
- $\rho = 0.001756$  slug/ft<sup>3</sup>
- N = engine speed
- = 4000 rpm (or RPM)
- BHP = 2.5 brake horsepower (input to the propeller shaft)

Using the above design parameter, a typical propeller is chosen. The Appendix in NACA TR640 illustrates the procedure for the sample calculations.

1. Calculate  $C_s$  (speed power coefficient).

$$\begin{aligned} C_s &= \frac{(0.638)(\text{mph})(\rho/\rho_0)^{0.2}}{(\text{BHP})^{0.2}(\text{RPM})^{0.4}} && \text{(C-5)} \\ &= \frac{(0.638)(75)(0.7384)^{0.2}}{(2.5)^{0.2}(4000)^{0.4}} \\ &= 1.36 \end{aligned}$$

a. Figure C-13 shows that for a 5868-9 Clark Y section with 2 blades  $\beta \approx 19^\circ$

$$\frac{V}{nD} = \text{advance ratio} = 0.7$$

$$\eta \approx \text{design efficiency} \approx 0.80$$

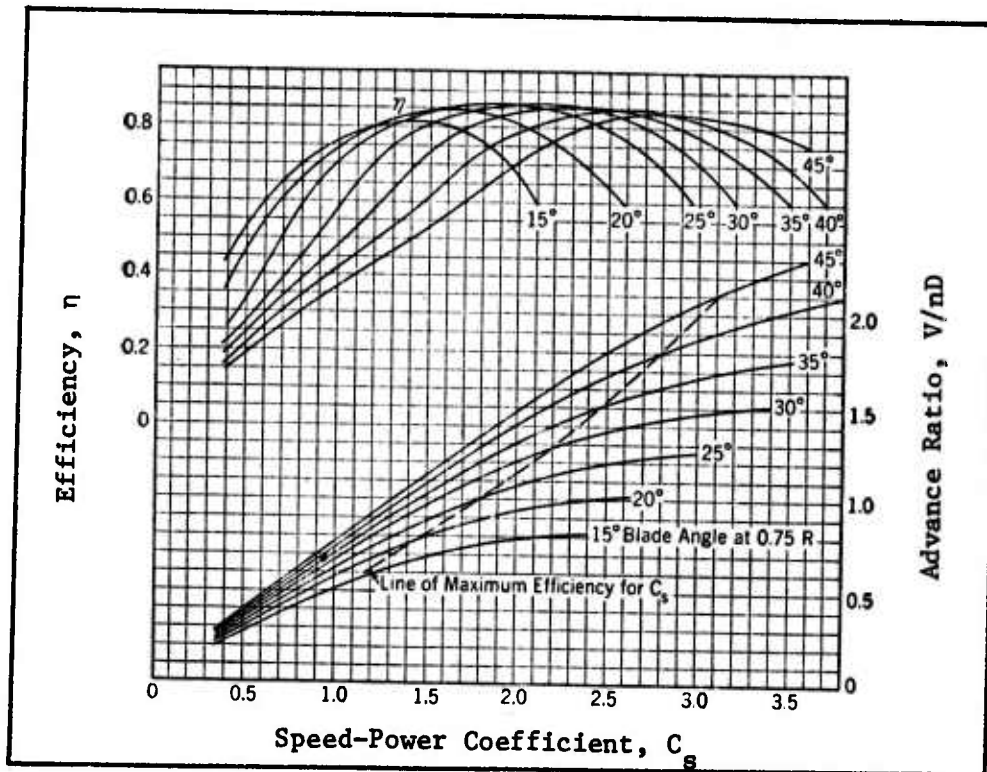


Figure C-13. Design Chart for Propeller 5868-9, Clark Y Section, Two Blades (Nelson, 1944:110)

b. Figure C-14 shows that for a 5868-9, RAF 6 section with 2 blades  $\beta \approx 20^\circ$

$$\frac{V}{nD} = 0.73$$

$$\eta \approx 0.82$$

c. Figure C-15 shows that for a 37-3647, RAF 6 section with 2 blades  $\beta \approx 23^\circ$

$$\frac{V}{nD} = 0.80$$

$$\eta \approx 0.80$$

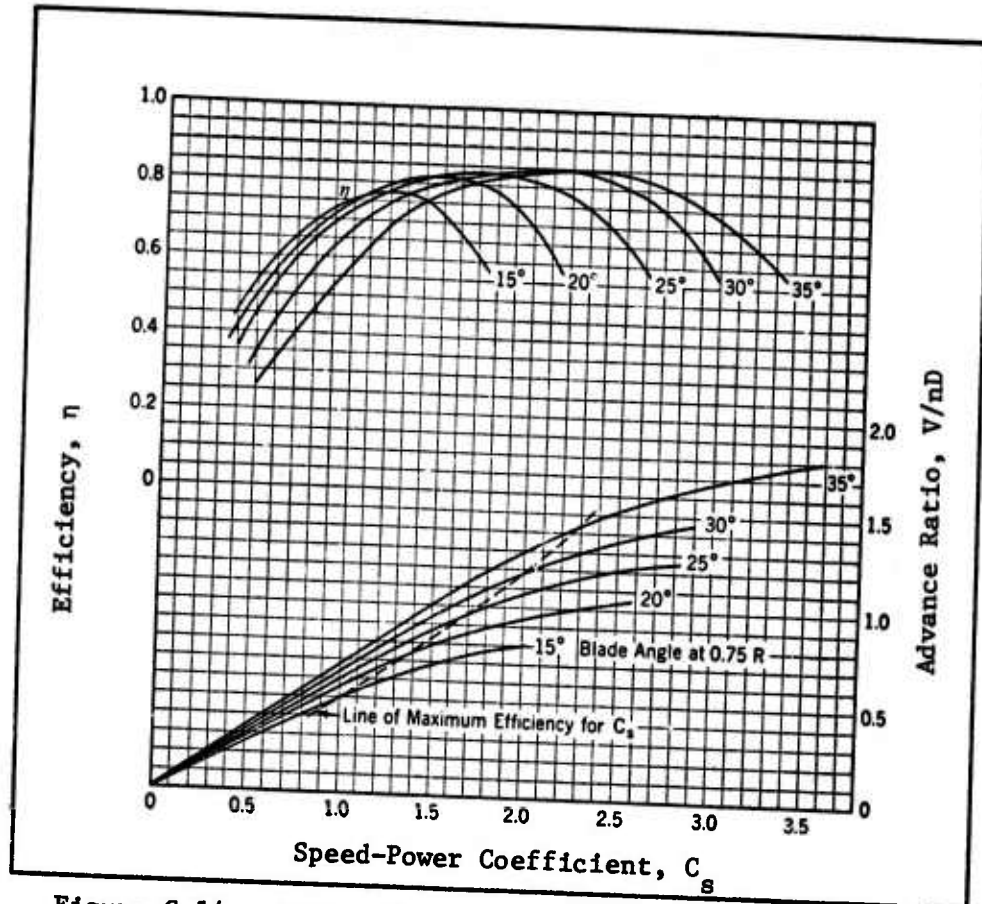


Figure C-14. Design Chart for Propeller 5868-R6, RAF-6 Section, Two Blades (Nelson, 1944:116)

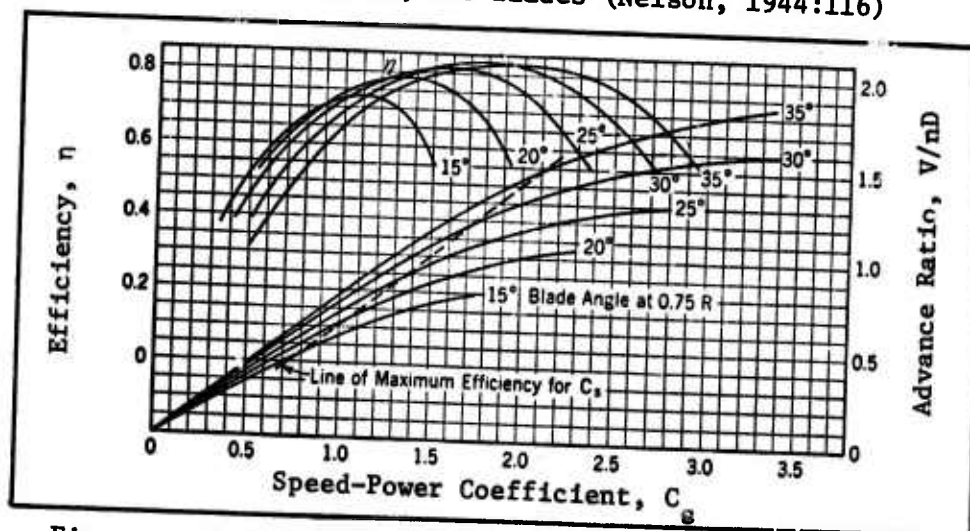


Figure C-15. Design Chart for Propeller 37-3647, RAF-6 Section, Two Blades (Nelson, 1944:121)

2. The diameter, D, knowing the advance ratio,  $J = V/nD$ , is found from

$$\begin{aligned}
 D &= \frac{(\text{mph})(88)}{(\text{RPM})(V/nD)} && \text{(C-6)} \\
 &= \frac{(75)(88)}{(4000)J} \\
 &= \frac{1.65}{J}
 \end{aligned}$$

Using the previous values of J, the corresponding diameters are

J	Diameter, D	
	Feet	Inches
0.70	2.357	28.286
0.73	2.260	27.123
0.80	2.063	24.750

For a fixed-pitch propeller, the following parameters are assumed:

$$\begin{aligned}
 V_0 &= \text{design air speed} \\
 &= 75 \text{ miles per hour} \\
 N_0 &= \text{design engine speed} \\
 &= 8000 \text{ rpm} \\
 (\text{bhp})_0 &= \text{design engine power (rated power)} \\
 &= 10 \text{ bhp} \\
 J_0 &= (V/nD)_0 = \text{design advance ratio} \\
 &= 0.73 \\
 \eta_0 &= \text{design efficiency} \\
 &= 0.80
 \end{aligned}$$

$D_0$  = design propeller diameter  
 = 2.357 ft

$\beta_0$  = design blade angle at 0.75R  
 = 19°

Note that the last three parameters are for the Clark Y section, and the sample calculations will be for that particular section.

1. Using  $J_0$  and  $\beta_0$  enter Figure C-16 and obtain values of  $C_{T0}$  and  $C_{P0}$  from the charts of  $C_P$  and  $C_T$  versus  $V/nD$ . This results in  $C_{T0} = 0.047$  and  $C_{P0} = 0.040$ .

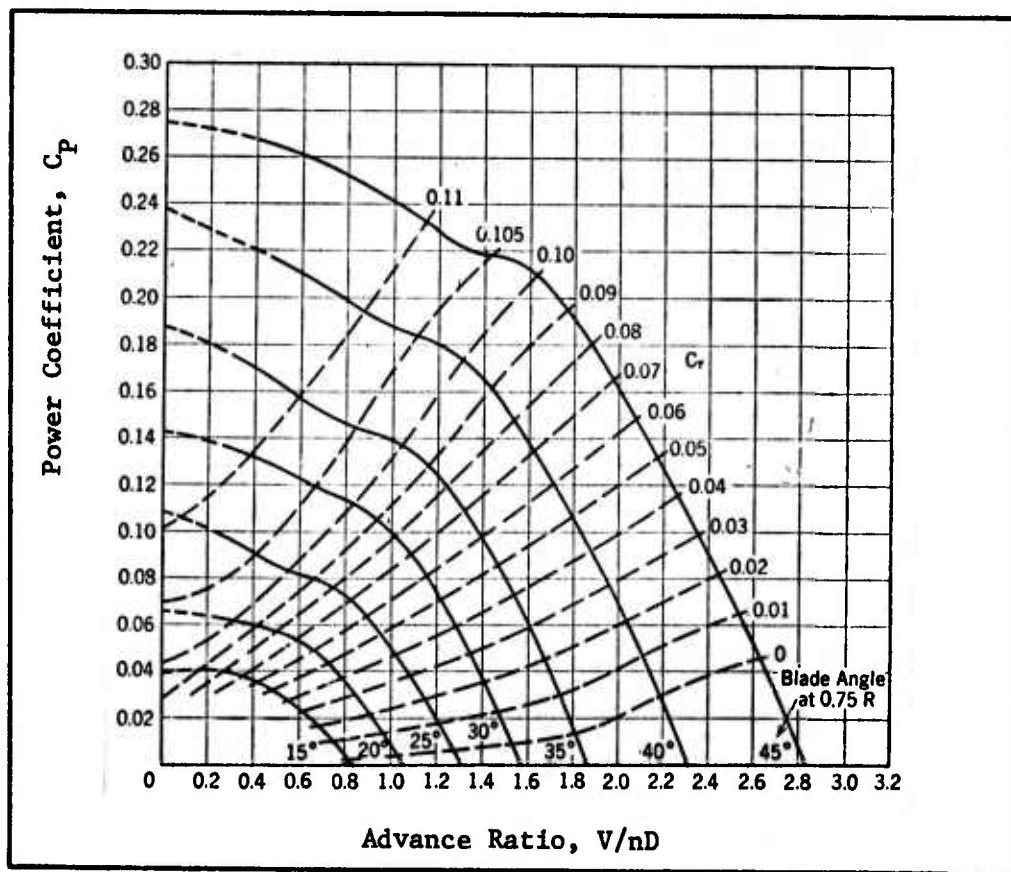


Figure C-16. Power Coefficient Curves for Propeller 5868-9, Clark Y section, Two Blades (Nelson, 1944:111)

2. For even values of  $J$ , values of  $C_T$  and  $C_P$  along a line of constant  $\beta_0$  are found.

$J$	$C_P$	$C_T$	$J/J_0$	$C_T/C_P$	$N/N_0$	$V$	$T$	$C_{P_0}/C_P$
0.6	0.050	0.065	0.857	1.31	0.8944	57.49	44.59	0.8000
0.4	0.058	0.090	0.571	1.55	0.8305	33.57	52.76	0.6897
0.2	0.060	0.103	0.286	1.72	0.8165	17.51	58.55	0.6667

3. Compute  $J/J_0$ ,  $C_T/C_P$ , and  $C_{P_0}/C_P$ .

4. Compute  $N/N_0 = (C_{P_0}/C_P)^{1/2}$

5. Compute

$$\begin{aligned}
 T_0 &= \frac{(\eta_0)(\text{bhp})(375)}{V_0} \\
 &= \frac{(0.80)(10)(375)}{75} \\
 &= 40 \text{ lb}
 \end{aligned}$$

6. Compute

$$\begin{aligned}
 V &= V_0 \times J/J_0 \times N/N_0 \\
 V_1 &= 75 \times 0.857 \times 0.8944 \\
 &= 57.49 \text{ mph} \\
 V_2 &= 75 \times 0.571 \times 0.8305 \\
 &= 35.57 \text{ mph} \\
 V_3 &= 75 \times 0.286 \times 0.8165 \\
 &= 17.51 \text{ mph}
 \end{aligned}$$

7. Compute the thrust,

$$\begin{aligned} T &= T_0 \times C_{P_0}/C_{T_0} \times C_T/C_P \\ &= K \times C_T/C_P \end{aligned} \quad (C-7)$$

where

$$K = \frac{T_0 \times C_{P_0}}{C_{T_0}}$$

Substituting values from step 2 into Eq (C-7) gives

$$\begin{aligned} K &= \frac{(40)(0.040)}{0.047} \\ &= 34.04 \text{ lb} \end{aligned}$$

and

$$\begin{aligned} T_1 &= (34.04)(1.31) \\ &= 44.59 \text{ lb} \\ T_2 &= (34.04)(1.55) \\ &= 58.55 \text{ lb} \end{aligned}$$

Figure C-17 shows the thrust versus velocity for the 5868-9 Clark Y section in the upper curve. Similar calculations give values that are plotted for the lower curve.

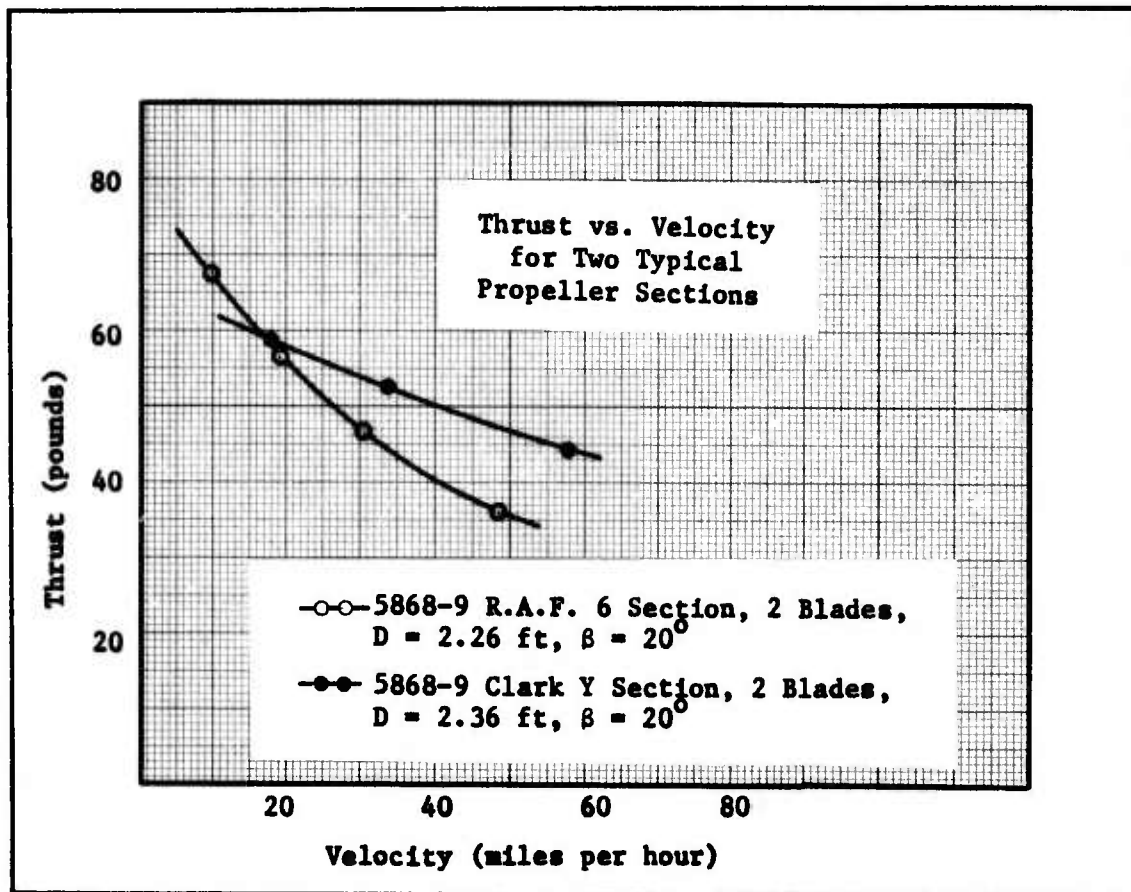


Figure C-17. Thrust Versus Velocity Curves, Fixed-Pitch Analysis Using NACA TR640

### Drag Calculations

Since most of the test apparatus is symmetric about the pivot bar, assume that the engine and carburetor with intake stack are the only contributors to the drag. The Reynolds number ( $R_e$ ) is based on the diameter or effective area for each piece of drag-producing equipment in the swept area of the propeller. The engine is treated as a circular cylinder with a 4-inch diameter and an 8-inch height and the carburetor and air intake are treated as a circular cylinder with a diameter of 2.5 inches and a height of 8.5 inches.

The drag force is found according to the formula

$$\sum D = q \sum_{i=1}^n C_{D_i} A_i \quad (C-8)$$

where

$D$  = drag force, pounds

$q$  = dynamic pressure, pounds,  $\text{ft}^2$

$C_{D_i}$  = coefficient of drag for each part  
of the apparatus

$A_i$  = area of each part of the apparatus,  
 $\text{ft}^2$

The Reynolds number,  $R_e$ , is calculated for each piece of drag producing equipment by the formula

$$R_e = \frac{Vx}{\nu} \quad (C-9)$$

where

$V$  = vehicle velocity, feet/second

x = effective length, feet

v = kinematic viscosity, feet<sup>2</sup>/second

For the engine,

$$\begin{aligned} R_e &= \frac{(110 \text{ ft/sec})(4 \text{ in.})(1 \text{ ft}/12 \text{ in.})}{2.004 \times 10^{-4} \text{ ft}^2/\text{sec}} \\ &= 1.83 \times 10^5 \end{aligned}$$

For the carburetor,

$$\begin{aligned} R_e &= \frac{(110 \text{ ft/sec})(2.5 \text{ in.})(1 \text{ ft}/12 \text{ in.})}{2.004 \times 10^{-4} \text{ ft}^2/\text{sec}} \\ &= 1.14 \times 10^5 \end{aligned}$$

Both values of Reynolds number are in the transition region from laminar to turbulent flow so a value of  $C_D = 1.0$  is used for both.

The effective areas are found as follows:

$$\text{Carburetor Area} = \frac{(8.5 \text{ in.})(2.5 \text{ in.})}{144 \text{ in.}^2/\text{ft}^2} = 0.1476 \text{ ft}^2$$

$$\text{Engine Area} = \frac{(4 \text{ in.})(8 \text{ in.})}{144 \text{ in.}^2/\text{ft}^2} = 0.222 \text{ ft}^2$$

Now the dynamic pressure,  $q = 0.5 \rho v^2$  where  $\rho$  is the density in slugs/ft<sup>3</sup>. At 10,000 feet of altitude,  $\rho = 0.001756$  slugs/ft<sup>3</sup> and the cruise velocity,  $V$  is 110 ft/sec.

$$\begin{aligned} \text{Then } q &= \frac{(0.5)(0.001756 \text{ slug/ft}^3)(110 \text{ ft/sec})^2}{144 \text{ in.}^2/\text{ft}^2} \\ &= 10.6238 \text{ lbf/ft}^2 \end{aligned}$$

Substituting values into Eq (C-8) gives the total drag force.

$$\begin{aligned} D &= (10.6238 \text{ lbf/ft}^2)(1.0)(0.3696 \text{ ft}^2) \\ &= 3.93 \text{ lbf} \end{aligned}$$

APPENDIX D

POWER SUPPLY

## APPENDIX D

### ELECTRICAL POWER

#### Introduction

The power sources available that may be able to power mini-drones are fuel cells, solar cells, alternators and batteries. Fuel cells of the type used on spacecraft are considered too exotic and costly for this application. Solar cells fastened to the external skin of the wings are not feasible because changing light intensities due to clouds or night flight would necessitate either on-board power storage (batteries) or a second power source. This leaves alternators or batteries as the only feasible power source.

In the systems approach to the design, the effects of this subsystem on the other subsystems are considered. Factors which are considered include: size, weight, placement, power required, radio frequency (RF) interference with on-board sensors, magnetic disturbance to the navigation subsystem magnetometer, reliability and power required from the engine. The most important single factor considered is cost.

#### Power Requirements

The original approach was to design a power system common to both Type I and Type II vehicles. The reason for this commonality was to facilitate addition of modules to a Type II vehicle to change it into a Type I vehicle at the launch site.

As the power requirements evolved, the common power subsystem became less and less attractive due to the great difference in the power requirements

for the Type I and Type II vehicles. As shown in Tables D-1 and D-2, the power requirement for the Type I vehicle is about ten times that for the Type II vehicle. In addition, a power requirement of up to 600 watts has been proposed to power an electronic counter measures (ECM) package (Maxwell, 1975). If this power requirement is added to the total in Table D-1, the ratio of power needed for the Type I vehicle to that of the Type II vehicle would be seventy to one. Unless the number of Type I vehicles required is much greater than the number of Type II vehicles, the common power subsystem is not feasible. Because a possible ECM mission and its requirements are as yet undefined, the power subsystem presented here applies only to the Type II vehicle.

#### Advantages of PM Generators

The main advantage is the absence of arcing. PM generators do not have the brushes, commutators, or slip rings which are found on dc generators and automotive-type alternators. These items cause arcing, and since the generator is in close proximity to the engine, this arcing is a fire/explosion hazard. Arcing also causes a wide-spectrum RF noise which can interface with any on-board sensors and with low-frequency radio-navigation equipment.

Excitation. In order to produce power, the generator must first produce a magnetic field. In automotive generators, where the field is created by a coil, an external battery is used to excite the generator. Since pm generators use permanent magnets to produce the field, no external excitation is needed to start the generator. Thus, pm generators are self-exciting.

TABLE D-1. TYPE I POWER REQUIREMENTS

Flight Control Servos

(Kraft KPS-16)

2 Aileron Servos	600ma @ 5.6v
2 Rudder Servos	600ma
Elevator Servo	300ma
Throttle Servo	300ma

---

1800ma @ 5.6v  
(10.08 watts)

Autopilot

+ 15v 4 - 8w 0.27a (max)

+ 5v 1 - 2w 0.2 a (max)

---

10 watts

Omega Navigation

+ 5v 2.1a = 21.0 w

- 5v 0.1a = 0.5 w

- 15v 0.1a = 1.5 w

---

23.00 watts

Sensor

+ 15v 10 w            15 w avg  
                                 30 w peak

+ 5v 5 w

+ 15v 0.667a = 20.1 w

+ 5v 1.000a = 10.0 w

---

60.1 watts

---

Total	10.08w
	10.00w
	23.00w
	60.10w

---

103.18 watts

TABLE D-2. TYPE II POWER REQUIREMENTS

Flight Control Servos

2 Rudder Servos	600ma @ 5.6v
Elevator Servo	300ma
Throttle Solenoid, nil	
<hr/>	
(5.04 watts)	900ma @ 5.6v

Altitude Control Circuit

16.8v    0.23 a    =    3.87 watts

D. R. Navigation Circuit

0.035a @ +8.4v = 0.3 w

0.020a @ 28 v = 0.56w

---

0.86 watts

Total	5.04 watts
	3.87
	<u>0.86</u>
	9.77 watts

TABLE D-2. TYPE II POWER REQUIREMENTS

Flight Control Servos

2 Rudder Servos	600ma @ 5.6v
Elevator Servo	300ma
Throttle Solenoid, nil	
(5.04 watts)	900ma @ 5.6v

Altitude Control Circuit

16.8v    0.23 a    =    3.87 watts

D. R. Navigation Circuit

0.035a @ +8.4v = 0.3 w

0.020a @ 28 v = 0.56w

---

0.86 watts

---

Total	5.04 watts
	3.87
	<u>0.86</u>
	9.77 watts

In generators with field windings, heat is generated by the current flowing through these windings. Also, these generators use a small percentage of their output to maintain the field. PM generators require none of their power for excitation. Therefore, they run cooler and are more efficient than generators excited by field windings.

#### Selecting an Alternator

In selecting an alternator, two alternatives are available. One alternative is to use an existing mass-produced alternator that can be adapted to the application. The other is to look for an alternator that is designed specifically for the application. Considering only the costs of the alternator, a mass-produced alternator is considered first.

A mass-produced alternator is less expensive, because design costs and production-tooling costs are already included in the sale price. For mass-produced units, good reliability figures and operating characteristics are known for mass-produced alternators because most have been produced for years.

With a single-voltage, mass-produced alternator, a transformer with a multi-tapped secondary is needed to provide the various voltages needed for the other vehicle subsystems. Transformers are undesirable because of additional cost and weight. Transformers have efficiencies between 60% and 90% (American, 1974:38), so as much as 40% of the alternator output can be lost in the transformer.

An alternator specifically designed for the application contains windings or voltage taps to yield the voltages at the power levels

required. Using an alternator that supplies the different voltages needed simplifies the power supply circuitry. The use of this type of alternator decreases the number of components needed, thus increasing the power-system reliability and efficiency.

### Batteries

Batteries are considered as a possible power source, because they are small, lightweight, and can be packaged as a self-sufficient subsystem. Batteries are electro-chemical energy storage devices, and require no energy input from outside as do alternators, which require mechanical energy from the engine. Batteries change stored chemical energy into electrical energy upon demand.

The objectives in finding a suitable battery are to find one having long life, high power output, low weight, good shelf life reliability, and low cost. Another objective is to find one that has a constant cell voltage. Ideally, the cell voltage remains constant over the discharge period and does not vary with changing temperature. Once the battery is determined, the battery pack may be made from either of two types of batteries, standard cells or special-purpose batteries.

Standard Cells versus Special-Purpose Batteries. Standard cell sizes, "D", "C", "AA", etc. are preferred because specially-fabricated batteries or battery packs cost much more. Standard cells are produced and marketed by battery manufacturers in tremendous quantities (in 1968 two-billion cells were being produced annually) (Morehouse, 1958:362). By buying off-the-shelf or commonly-produced items, no costs are incurred due to design, tooling, or production-line changes. For

specially-designed batteries, these costs have to be pro-rated over the number of batteries purchased.

Primary versus Secondary Batteries. Battery design literature (Union Carbide, 1971:25) (Lyman, 1975:79) refers to batteries as being either primary or secondary. Primary batteries are not rechargeable, and are discarded after depletion. Secondary batteries are batteries capable of being recharged again and again. For the application in the harassment vehicle, the batteries are used only once but stored a long time. However, secondary batteries cannot arbitrarily be ignored just because they may be used only once. They are evaluated with primary cells on the basis of cost, voltage versus time, and voltage-versus-temperature characteristics to find a type with the most desirable characteristics.

Fuel Cells. A fuel cell is a primary cell (non-rechargeable). In a fuel-cell, the chemical reactants are continuously fed through the cell (Messerle, 1969:223). This method brings fresh chemicals into the cell while removing the chemical products, mostly water. Fuel cells have reservoirs for holding the reactants and chemical products and have at least one pump to move the chemicals through the cell. This technology is too sophisticated, exotic, and costly for use in mini-drones.

Secondary Cells. The secondary cells considered are the silver-zinc, silver-cadmium, nickel-cadmium, lead-calcium, nickel-iron and types of lead-acid cells with liquid or gelled electrolyte. The discharge characteristics of these cells are shown in Figure D-1 (Lyman, 1975:81). Of these batteries, the lead-acid cell has the

highest cell voltage, 2.0 volts (Hedderson, 1969:24-5). The cell voltage of the lead-acid cell immediately starts to decline as the cell is discharged (see Figure D-2). From this fact alone, the lead-acid cell is unacceptable. The lead-calcium cell has the same cell structure as the lead-acid cell. The difference between the two types of cells is that in the lead calcium cell, calcium is used to harden the lead instead of the antimony used in lead-acid cells (Hedderson, 1969:24-28). Calcium decreases the corrosion rate and increases the battery life. The voltage-versus-time plot is the same for the two cells. Again, the lead-calcium voltage drops almost linearly with time. This type of cell does not perform well at low temperatures and, therefore, it is unacceptable for use at high altitudes.

The silver-zinc cells discharge at 1.8 volts for approximately one-fourth of their lifetime, and they drop to an almost constant voltage of 1.55 volts for the rest of their discharge period (Figure D-1). Their high cost and short life, relative to other battery types, prevents the silver-zinc cells from being used in many applications (Lander, 1969:24-55).

The silver-cadmium battery is the most expensive secondary battery (Lyman, 1957:181). As of 1969, it was the newest secondary battery (Howard, 1969:24-42). The voltage-discharge curves for the silver-cadmium batteries are similar to those of the silver-zinc cells (see Figure D-1). Silver cadmium cells do not perform well at low temperatures. A temperature of 0°C is a minimum for high-discharge rates.

Nickel-cadmium batteries, referred to as Nicads, are in the middle of the price range for secondary batteries (Lyman, 1975:81). Nicads

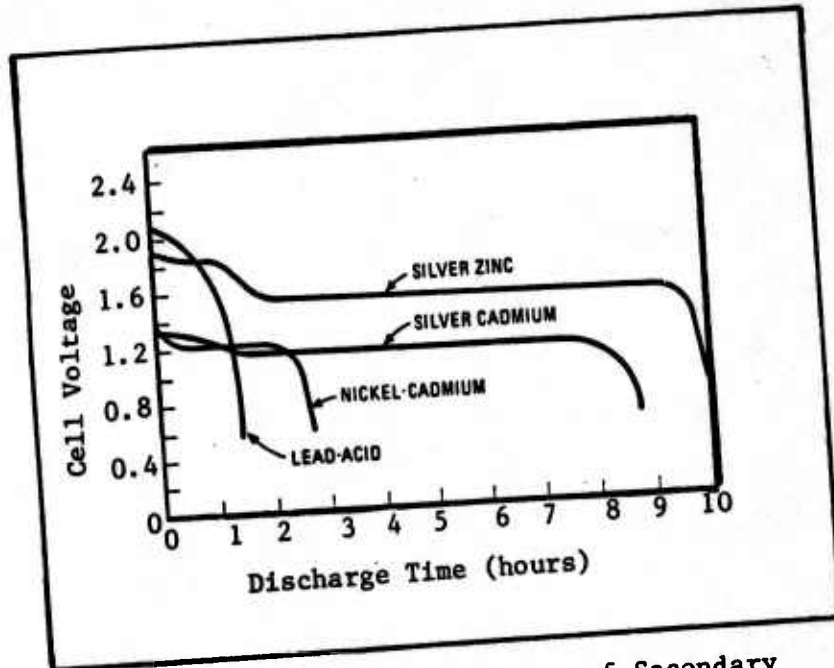


Figure D-1. Discharge Comparison of Secondary Batteries

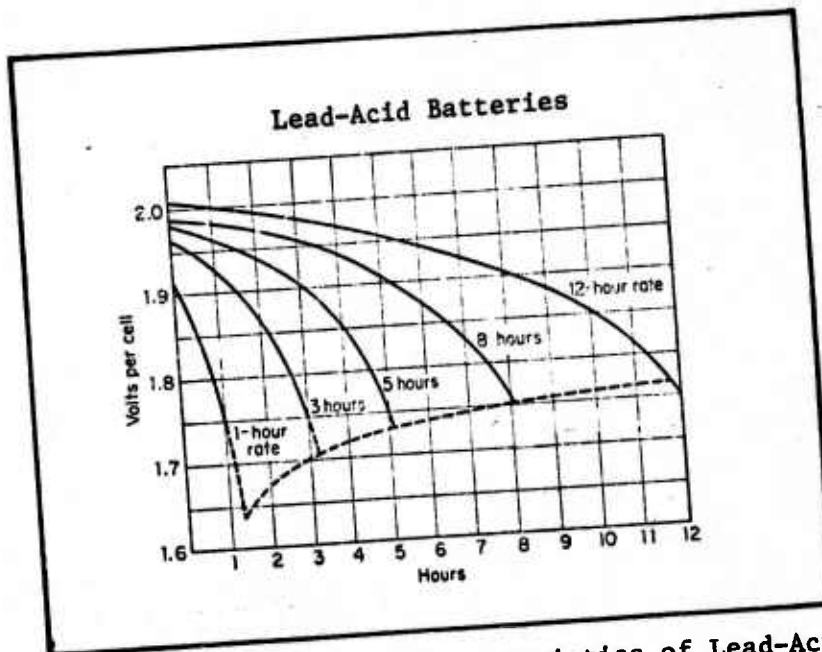


Figure D-2. Discharge Characteristics of Lead-Acid Batteries

have a nearly flat voltage curve throughout their discharge but are sensitive to temperature changes. The power capacity of these cells at 0°F is only 55 percent of the capacity at 70°F (see Figure D-3), (Donahue, 1969:24-57).

Nicads have a characteristic that is called a "memory effect". If the cell is operated for short discharge levels or is kept charged for long periods of time, it "forgets" its designed capacity. When the battery is then used it only produces what it "remembers", only a portion of its rated capacity. For this reason, nicads are periodically cycled - charged and discharged to prevent them from developing this "memory". Because of the characteristics mentioned above, they are unacceptable.

Primary Cells. The primary cells considered were the carbon-zinc (Laclanche), magnesium, alkaline-manganese, mercury-zinc, and a newcomer to the battery industry, the lithium cell. The carbon-zinc cell is a modified Laclanche cell which, as made by Laclanche in 1868, had a liquid electrolyte (Morehouse, 1958:358-362). The modern carbon-zinc cell is of the same type. The only difference is that the carbon-zinc has a paste electrolyte. The carbon-zinc is designed for intermittent use, and under heavy current drains the efficiency of the electrolyte drops to less than 10%. This cell is also very sensitive to temperature changes. At 0°F, the output power available drops to about one-fourth that at 70°F (see Figure D4). Also, under a constant load, the output voltage declines almost linearly, which makes this type of cell undesirable.

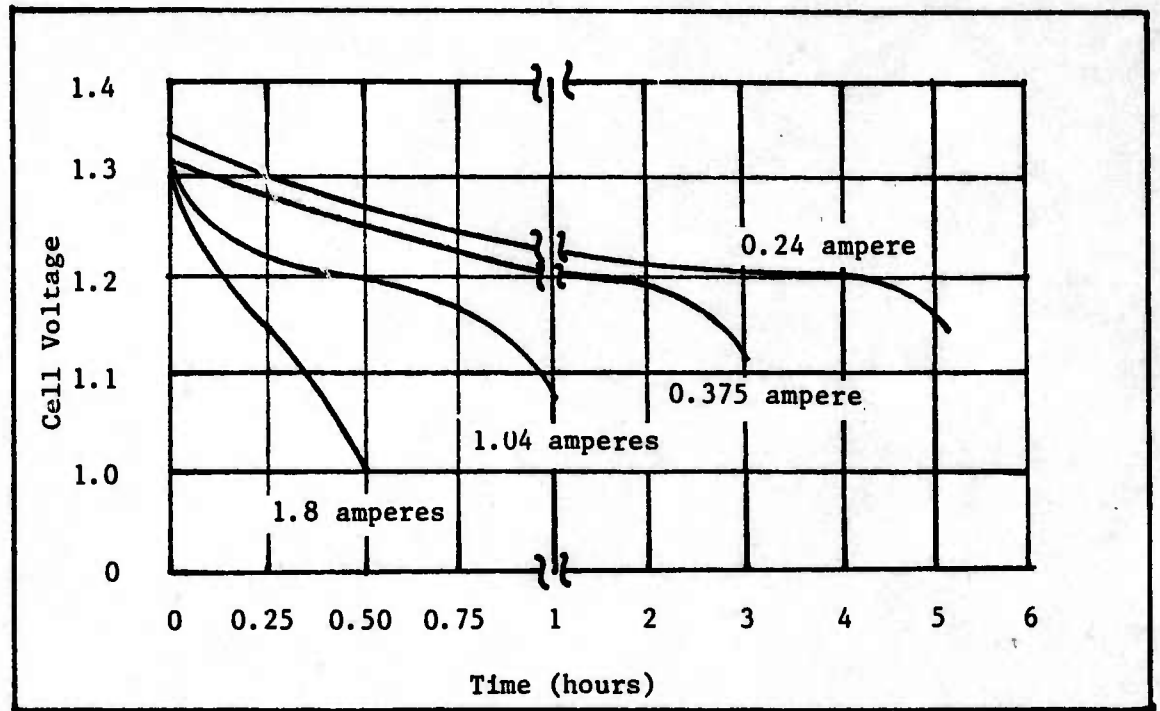


Figure D-3. Discharge Characteristics of Nickel-Cadmium Batteries

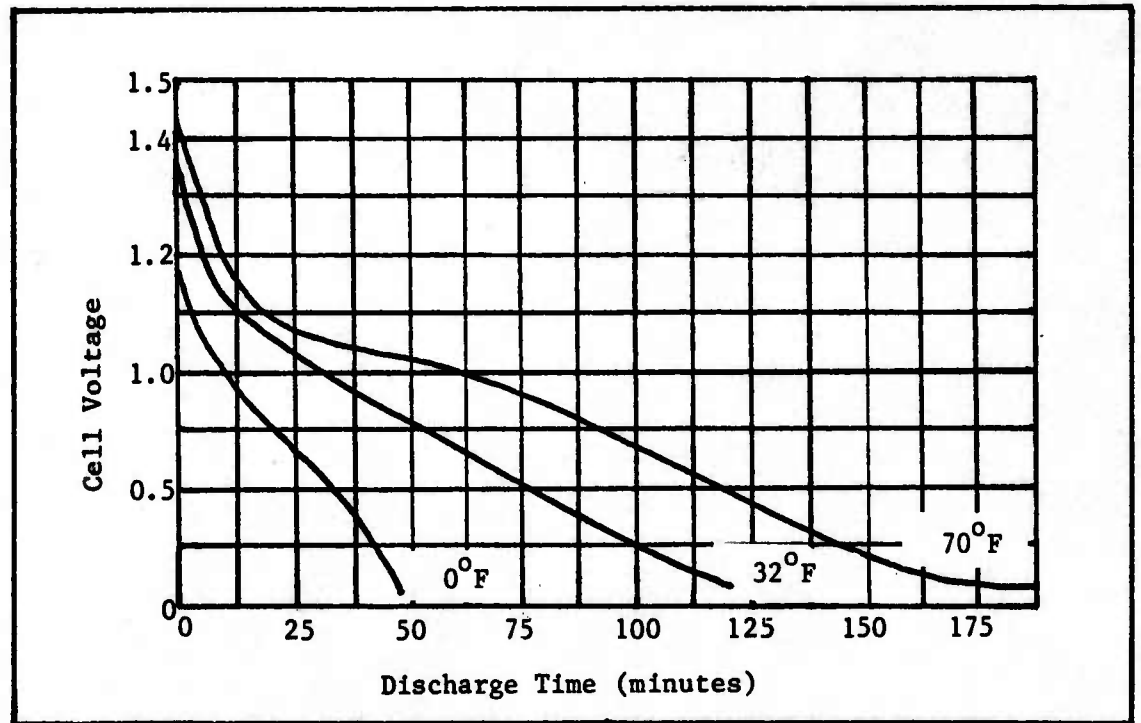


Figure D-4. Temperature Discharge Characteristics of Carbon-Zinc Cells under Constant Load

Magnesium Batteries. Silver chloride-magnesium and cuprous-chloride-magnesium cells are stored dry, and the electrolyte is added just before use. The reason for this is that the batteries become exhausted within one to ten days from self-discharge. Thus, these batteries are called "one-shot" batteries (Coleman, 1969:24-40). They are efficiency discharged in short periods of time at high current rates. These cells use saline water for an electrolyte and, therefore, find application in sonobuoys and torpedoes. Magnesium batteries have a shelf life of two to three years but do not operate well at low temperatures. They also have an undesirable, sloping discharge curve (Figure D-5) (Lyman, 1975:76, 80).

Alkaline Batteries. Zinc-Alkaline-Manganese dioxide batteries have the capability for high current delivery and have excellent shelf-life characteristics of 3 to 5 years (Errico, 1969:24-52 and Lyman, 1975:76). Alkaline cells contain 50% to 100% more energy than carbon-zinc cells of the same size (Figure D-6). These batteries show an excellent advantage over conventional carbon-zinc cells on a performance-per-unit-of-cost basis (Union Carbide, 1971:239). In a typical application, a 75-cent AA alkaline cell lasts four times as long as a 30-cent carbon-zinc cell of the same size (Lyman, 1976:76).

Mercury Batteries. Zinc-Mercury cells have a good shelf life of 3 to 5 years. They have good temperature characteristics, and the cell voltage of the mercury cells remains fairly constant under light loads, enough so that mercury cells are used as voltage references. Zinc-mercury cells hold approximately twice the power-per-cell as carbon-zinc cells (Ruben, 1975:24-32).

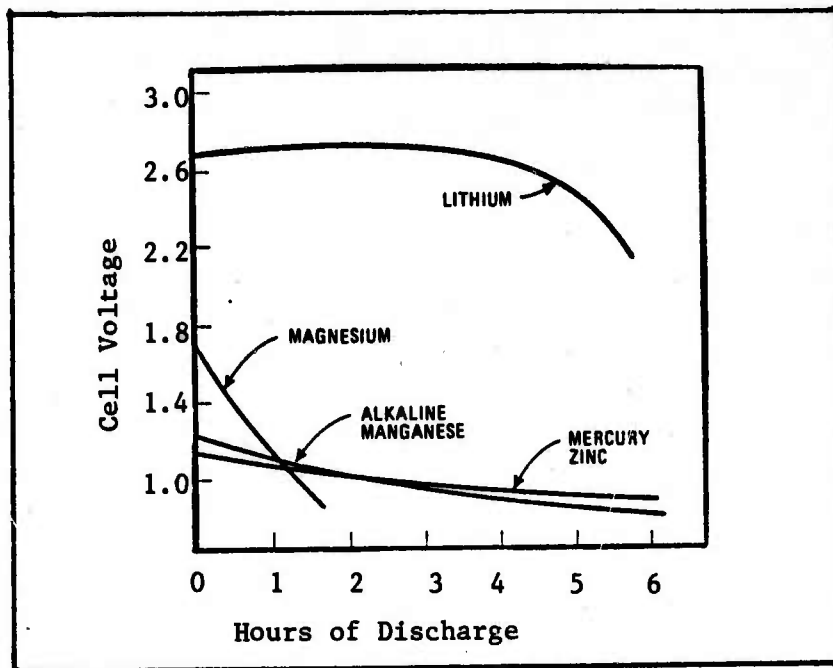


Figure D-5. Discharge Comparison of Primary Cells

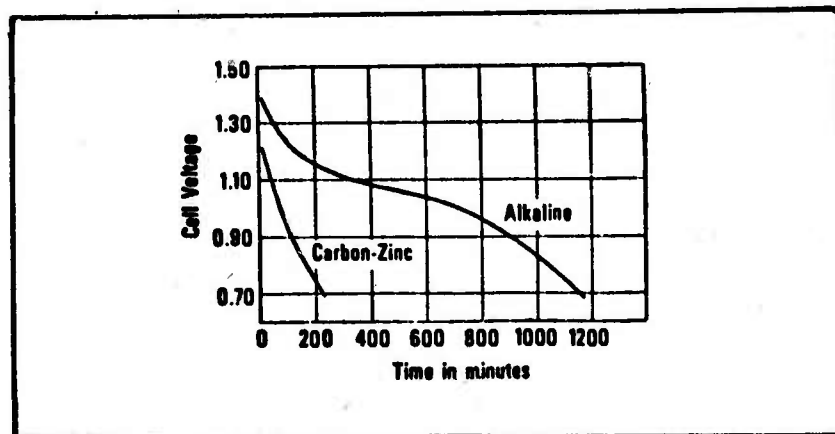


Figure D-6. Continuous Discharge Comparison of Carbon-Zinc and Alkaline Cells

The mercury cell has the best voltage, temperature, and storage characteristics of those cells examined thus far. The lithium cell, however, has a greater energy storage capacity.

Lithium Batteries. Lithium batteries are the newest type of primary cells that are commercially available. Power Conversion, Inc. has been producing Lithium cells for about two years and Mallory Battery Company is scheduled to start production this year. Since these batteries are new, adequate shelf-life data is not available; however, these cells have a projected shelf life of three to five years, or longer (Lyman, 1975:76). The Power Conversion Original Equipment Manufacturer Price List states:

"The lithium primary battery with organic electrolyte is the most significant improvement in battery technologies in the past 25 years.

Compared with all other primary battery types, the lithium system is markedly superior in every aspect of battery performance."

The discharge curves for the lithium cell are shown in Figure D-7. The lithium battery has a nominal operating voltage of 2.8 volts-per-cell which is twice that of other cells. It has extremely good low-temperature characteristics and will operate at  $-65^{\circ}\text{F}$ . The lithium cell handles high discharge rates with almost no degradation of its output voltage. The output voltage stays almost constant over the discharge (Power, 1975 and Mallory, 1975).

The lithium cell has the best characteristics of any battery considered. A power supply using lithium cells was designed so that a cost comparison could be made with a generator (Figure D-3). With a one-ampere current drain at  $70^{\circ}\text{F}$ , one lithium cell is equivalent to

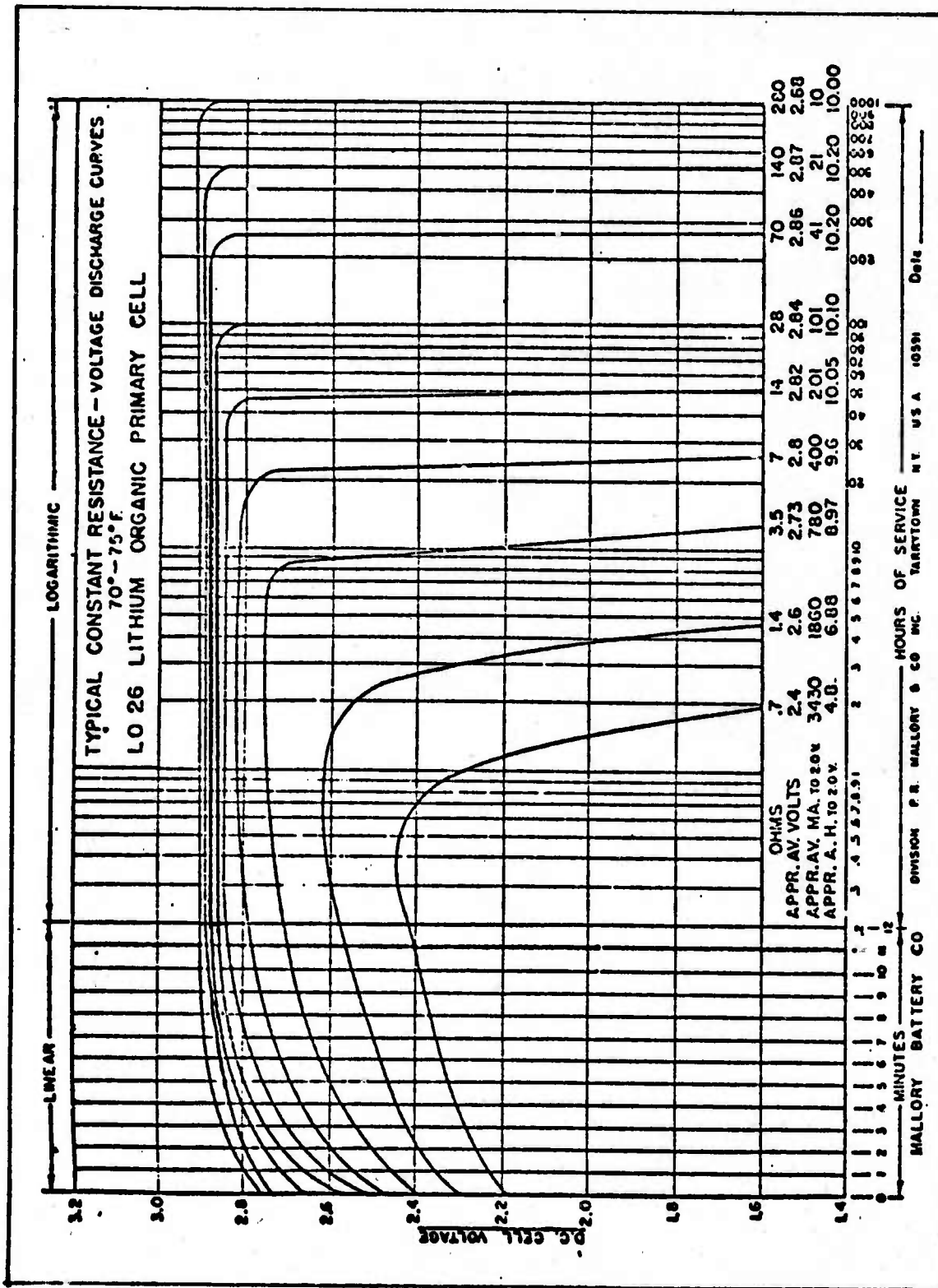


Figure D-7. Lithium D Cell Discharge Curves.

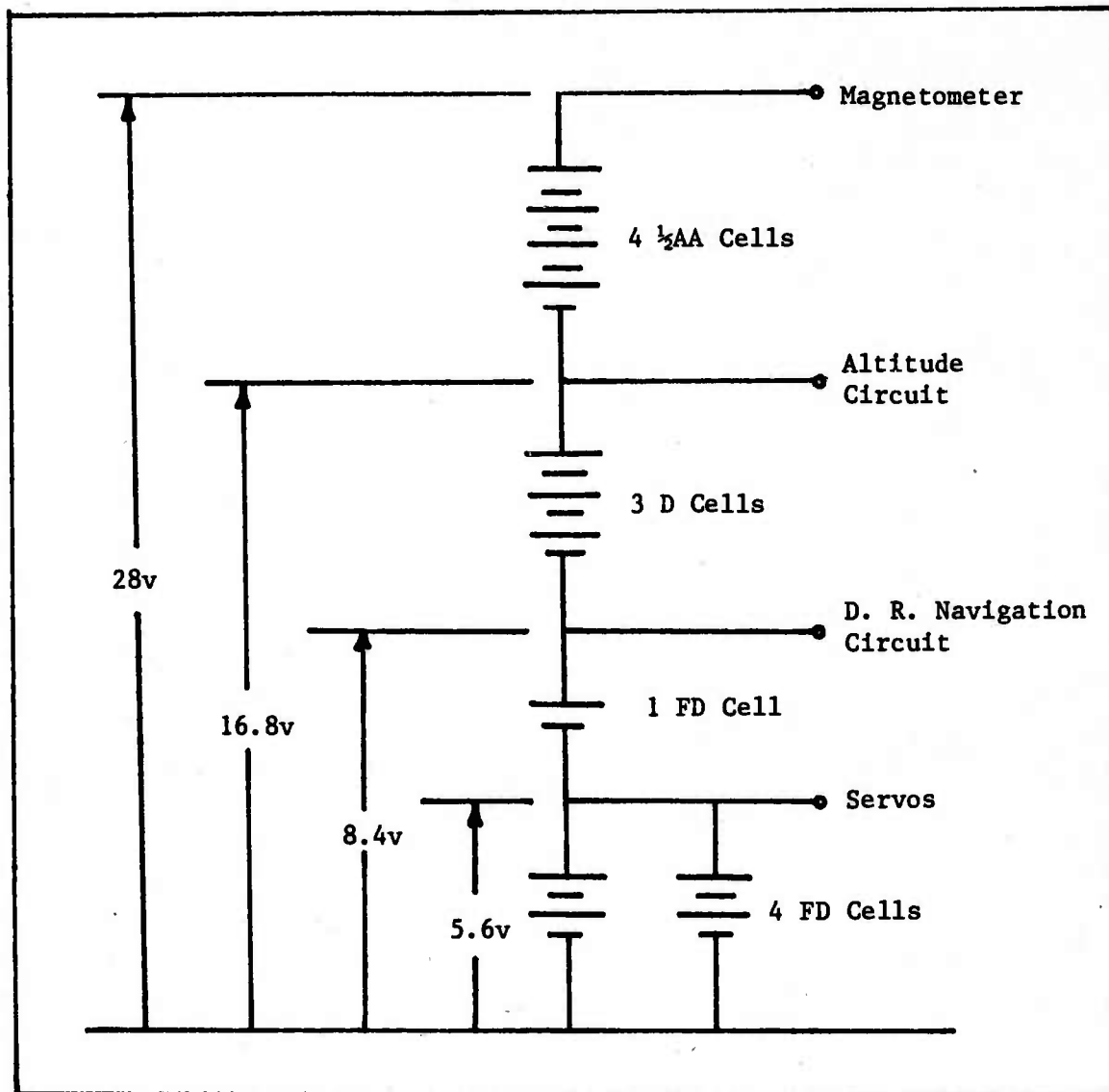


Figure D-8. Lithium Battery Schematic for Type II Vehicle for Six Hour Mission

TABLE D-3. LITHIUM BATTERY REQUIREMENTS FOR  
TYPE II VEHICLES WITH SIX HOUR MISSIONS

No.	Cell Size	Weight (oz)		Volume (in <sup>3</sup> )		Cost (\$)	
		each	total	each	total	each	total
5	FD	3.52	17.60	4.09	20.45	3.45	17.25
3	D	2.92	8.76	3.10	9.30	3.08	9.24
4	½AA	0.26	1.04	0.22	0.88	1.05	4.20
<b>Totals</b>		27.40 oz		30.63 in <sup>3</sup>		\$30.69	

four mercury-zinc cells, five alkaline cells, seven magnesium cells, or 30 carbon-zinc cells, all of equal size (Lyman, 1975:78) (Figure D-9).

#### Batteries versus Generators

The cost of the lithium-battery power supply, from Table D-3, is approximately one-fifth that of the estimated low-cost, permanent-magnet generator which Gecrator can produce. (Trefzger,1975) With the estimated life cycle of 10 years, two or three sets of batteries must be purchased because of the three to five year estimated shelf-life of the batteries. Even with three sets of batteries, they are still cheaper than the low-cost generator.

Another factor which discounts the use of a generator is the effect of the generator field, either changing in intensity or rotating, on the magnetometer in the navigation subsystem. The changing magnetic field of a generator may severely affect a magnetometer, causing it to be inoperable. This will have to be verified by experimentation before a generator is used in the Type I vehicle.

#### Conclusions

Lithium batteries were chosen over a permanent-magnet alternator to power the Type II vehicle. The factors considered were cost and possible effect of generator on navigation accuracy.

Since the power required for the Type I vehicle is at least ten times that of the Type II vehicle, a generator is the most likely choice for the Type I vehicle. However, before this choice is made, tests should be conducted to determine the effect a generator will have on the navigation subsystem's and the propulsion system's performance.

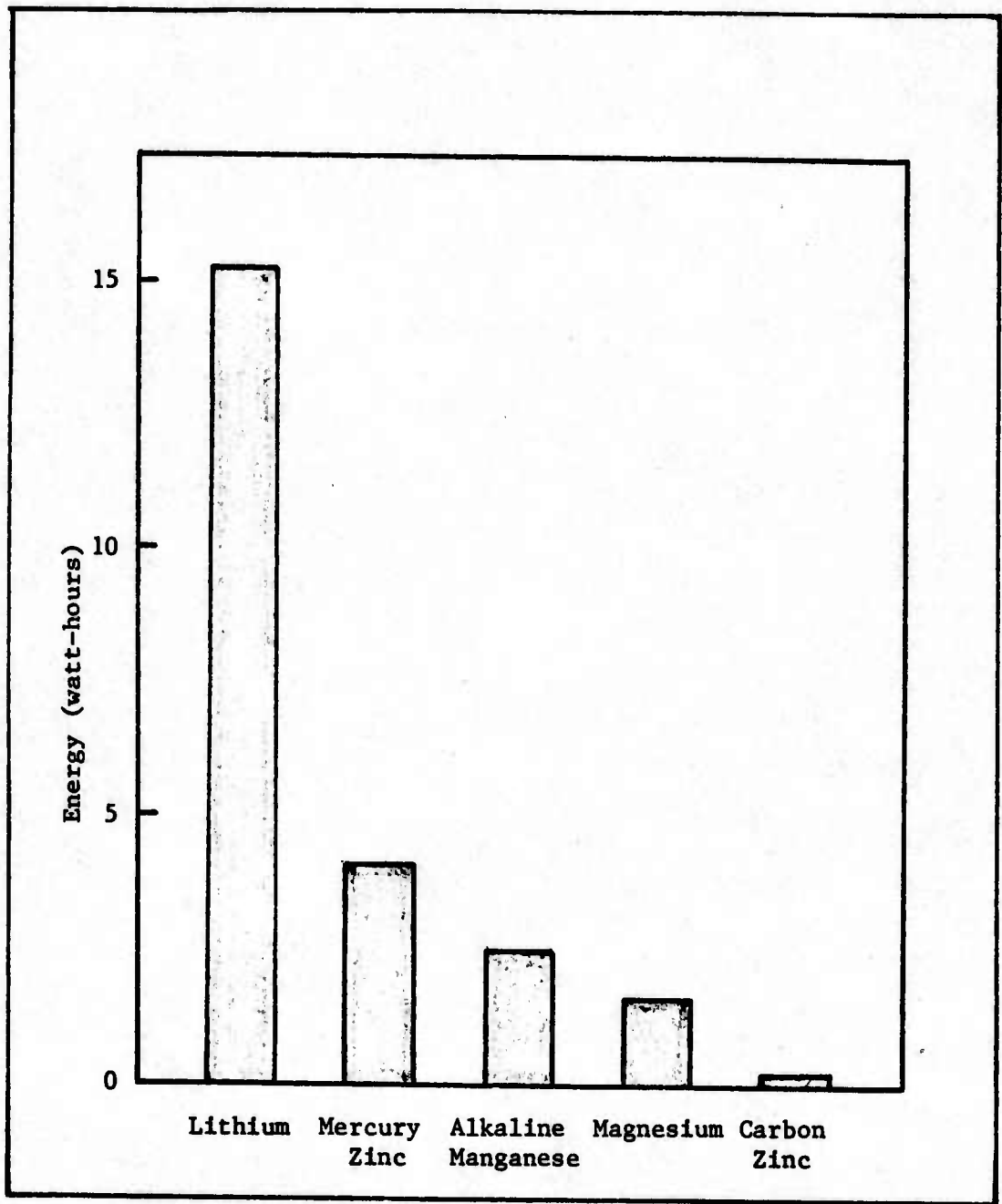


Figure D-9. Energy Capacity of D Size Primary Cells  
( 1 ampere at 70°F )

APPENDIX E

NAVIGATION

AND

STATIONKEEPING

## APPENDIX E

### NAVIGATION SUBSYSTEM

#### Introduction

The navigation subsystem is used for determining and controlling the heading of the vehicle. Control of the heading is through a feedback system involving a sensing device, a processing network and the rudder. The processing network compares some value received from a sensor to some programmed value. If these two values are **not** the same, an error signal is sent to the rudder causing a heading correction. This section deals with both what is to be sensed and what processing network is required. Much of the preliminary work required to obtain data for final system selection is covered in the sub-appendices. The main body of this appendix provides the rationale for the system selection and presents the final system design.

## System Selection

Several factors influence the selection of the navigation system.

Those considered most important are:

- Unit cost
- Effectiveness
- Resistance to jamming or spoofing
- Programming ease

Effectiveness, although usually directly related to accuracy, is defined as downtime in hours (see Chapter IV, Volume II).

Two basic techniques can be employed to direct the less expensive Type II vehicles to the target area. Either the Type II vehicles are coupled to a leading Type I vehicle by some radiometric link, or they fly their own pattern independent of the Type I vehicles. Many different techniques have been investigated and are discussed in Appendix E-1. Tables E-1 and E-2 summarize the principle approaches available. Of these, three of the approaches are selected as most promising. They are:

- Dead Reckoning (uses geomagnetic field and time)
- Omega (counts omega frequency lanes)
- Loran (uses time differences between signals)

One way of comparing these systems is by the amount of downtime which a given amount of money buys using each of the navigation systems. The cost of achieving this downtime includes the navigation system, the rest of the vehicle, launch cost, and other operating and support cost.

TABLE E-1. SUMMARY OF COUPLED APPROACHES

<u>Approach</u>	<u>Advantage</u>	<u>Disadvantage</u>
Beacon on lead vehicle	Low cost, simple in concept	Can be jammed or spoofed easily, extra beacons needed on trailing vehicles else Type I distinguishable
Beacon on lead vehicle with information updated	Reduces spotlighting of lead vehicle	Jammable, more expensive because of coding
Geomagnetic field and gravity vector synchronization	Relative position to lead vehicle need not be maintained	Requires processor, jammable link
Infra-red	Classical jamming does not hurt	Discrimination of lead vehicle
Ultrasonics	Lead vehicle difficult to determine	Engine noise - does not significantly increase survivability

TABLE E-2. SUMMARY OF INDEPENDENT APPROACHES

<u>Approach</u>	<u>Advantage</u>	<u>Disadvantage</u>
Navigation beacon	Low cost	Beacon very susceptible
Inertial	Not jammable	High cost
Dead Reckoning	Low cost	Inaccurate
Loran	Very accurate	More expensive, jammable
Omega	Low cost	Propagation errors, can be spoofed

This cost is the incremental life-cycle cost and is shown in Table 4-2 Volume II, as \$1327 for dead reckoning and \$1400 for Omega. Loran cost is found to be approximately \$2300 by adding the differences in Loran and Omega the subsystem costs (Appendix E-2) to the Omega subsystem cost. To determine the downtime, program EFFECT is used. Based on Chapter IV, Volume II, eighteen Type I vehicles and seventy-two Type II vehicles are used as representative of a possible wave configuration. The downtime attributable to the Type II vehicles using dead reckoning is obtained from Appendix C-2, Volume II, by subtracting the mean downtime for eighteen Type I waves from the eighteen Type I seventy-two Type II waves. This gives 26.98 hours downtime per seventy-two vehicles or 0.3747 hours downtime per vehicle. The downtime attributable to the Omega and Loran systems is obtained in a similar fashion. Since both Omega and Loran are simulated as having zero navigation error (Appendix E-6, Volume III and Chapter IV, Volume II) the 0.4078 hours downtime per vehicle is the same for each system.

TABLE E-3. HOURS DOWNTIME PER DOLLAR

System	Hours Downtime Per Dollar
Dead Reckoning	0.2824
Omega	0.2912
Loran	0.1773

Table E-3 indicates that either dead reckoning or Omega navigation would be selected over Loran. However, there is no significant difference between dead reckoning and Omega. The 3% difference in downtime-per-dollar is much less than the standard deviation of downtime from Appendix C-2, Volume II, or the cost estimates of Appendix E-2. The

selection between dead reckoning and Omega must be made on a criteria other than cost. Since dead reckoning is completely resistant to jamming or spoofing of any type, it is selected as the navigation system to be used in the Type II vehicle.

### System Design

Pattern. Having selected the method of navigation, the next problem is to define the actual flight requirements of the system. Specifically, this means determining the number of distinct mission legs. All missions begin with a navigation leg taking the vehicle from the launch point to the loiter area, and a repeating pattern is then flown. The simplest pattern has only two legs similar to a long racetrack. A more versatile pattern has four legs and can fly in either a rectangle or a rough 'figure 8'. A stochastic appearing pattern can be formed with eight legs using 135-degree turns. Figure E-1 shows the downtime for various patterns using eighteen Type I and seventy-two Type II vehicles.

A disadvantage of the eight-leg pattern is the number of programming settings required. A disadvantage of the two-leg pattern is, of course, the low downtime. A four-leg pattern is selected as a reasonable compromise between programming difficulty and downtime.

Processing Network. The navigation subsystem is programmed with a heading (magnetic) and a time (in minutes) for each of the mission legs, corrected for predicted wind. The actual magnetic heading is sensed by a two-axis flux-gate magnetometer mounted on the wing. The magnetometer consists of two orthogonal sensing coils which measure the component of the geomagnetic field along the axis of the coil. The magnetometer

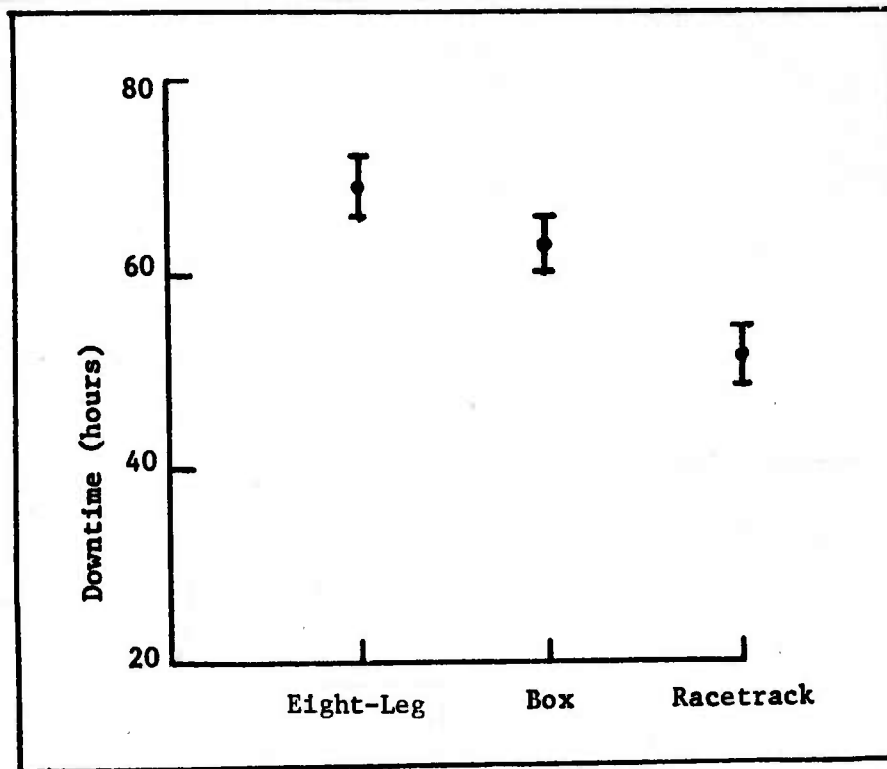


Figure E-1. Loiter Pattern Comparison

is mounted with one coil pointed along the x-axis (nose) of the vehicle and the other coil pointed out the left wing (y-axis). Each coil has an output proportional to the intensity of the magnetic field vector projected on its respective axis. Thus, a heading,  $\theta$ , is defined by the two voltages from the magnetometer. To program the vehicle, a set of variable resistors are adjusted so that the voltage drop across each resistor is related to the voltage output from the magnetometer. The processing circuitry performs the following operation,

$$E = (X - X_{\text{mag}}) - (Y - Y_{\text{mag}}) \quad (\text{E-1})$$

where X is the programmed voltage related to the field parallel to the nose

$X_{\text{mag}}$  is measured voltage related to the field parallel to the nose

Y is the programmed voltage related to the field parallel to the wing

E is the error signal

$Y_{mag}$  is the measured voltage related to the field parallel to the wing

The result of Eq (E-1) is added to the null voltage of the rudder servo so that when e is negative, a right turn is made. Similarly, when e is positive, a left turn is made. In this way the motion of vehicle serves to keep

$$E = (X - X_{mag}) - (Y - Y_{mag}) = 0 \quad (E-2)$$

When a timer has expired, a new heading (X and Y) is selected, and a new timer cycle is initiated. The required circuitry is shown in Figures E-2, E-3, and E-4. All electronics are mounted in a small box as shown in Figure E-5.

#### Summary

For the mission as stated, a dead reckoning system provides downtime comparable to that of the more expensive and more accurate systems. It is inexpensive and can be easily constructed using readily available commercial parts.



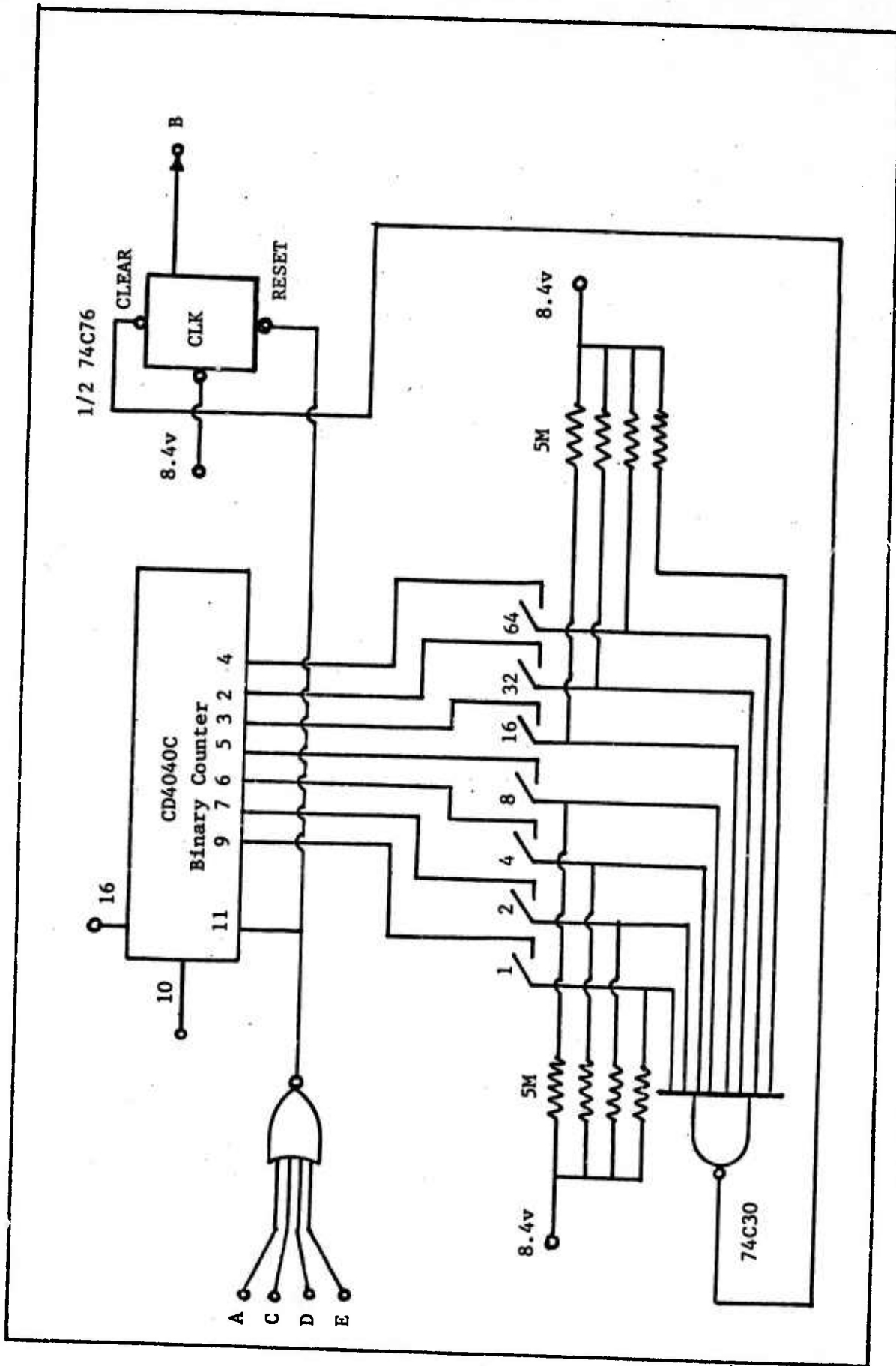
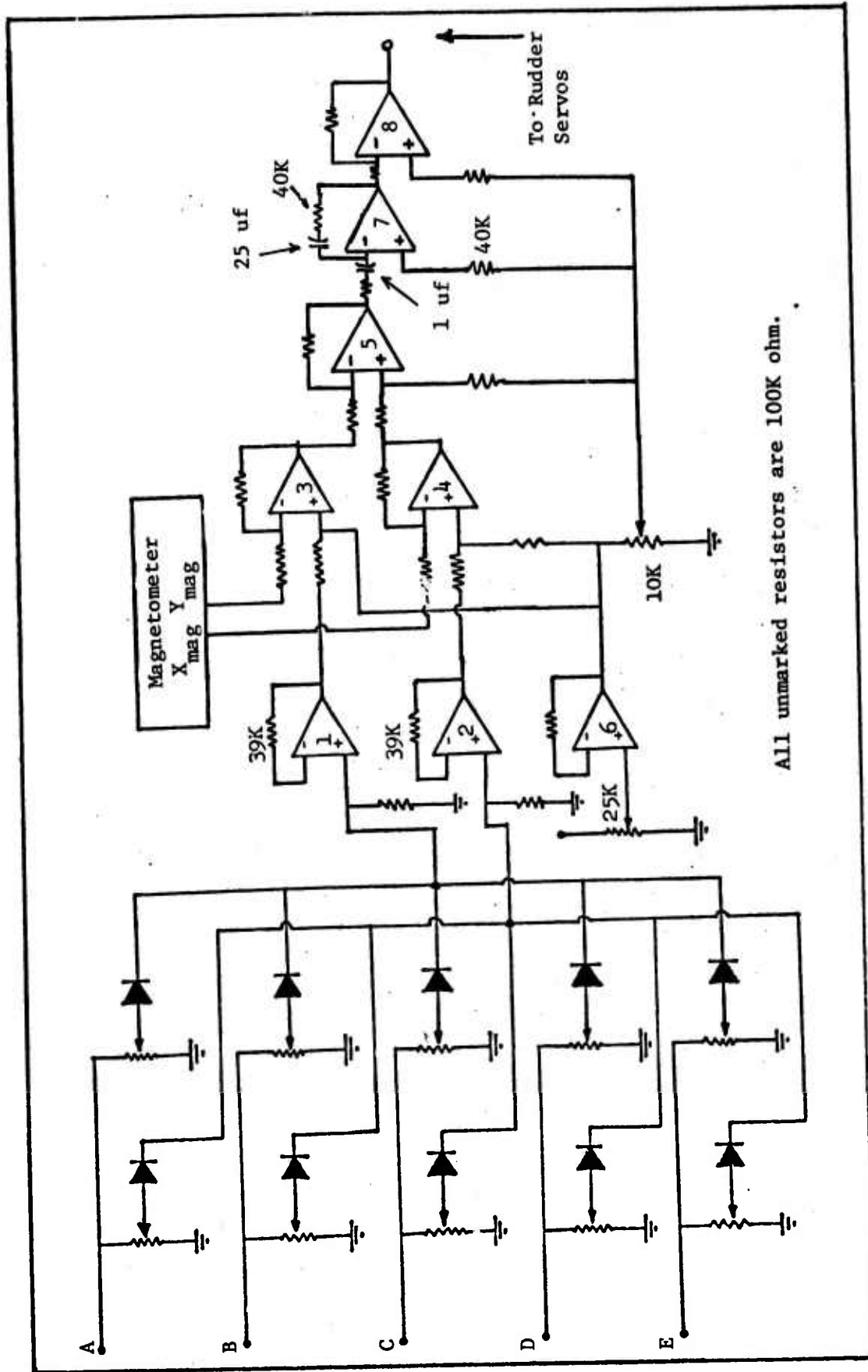


Figure E-3. Timers B through E, Navigation Circuit Final Design



All unmarked resistors are 100K ohm.

Figure E-4. Navigation Final Design

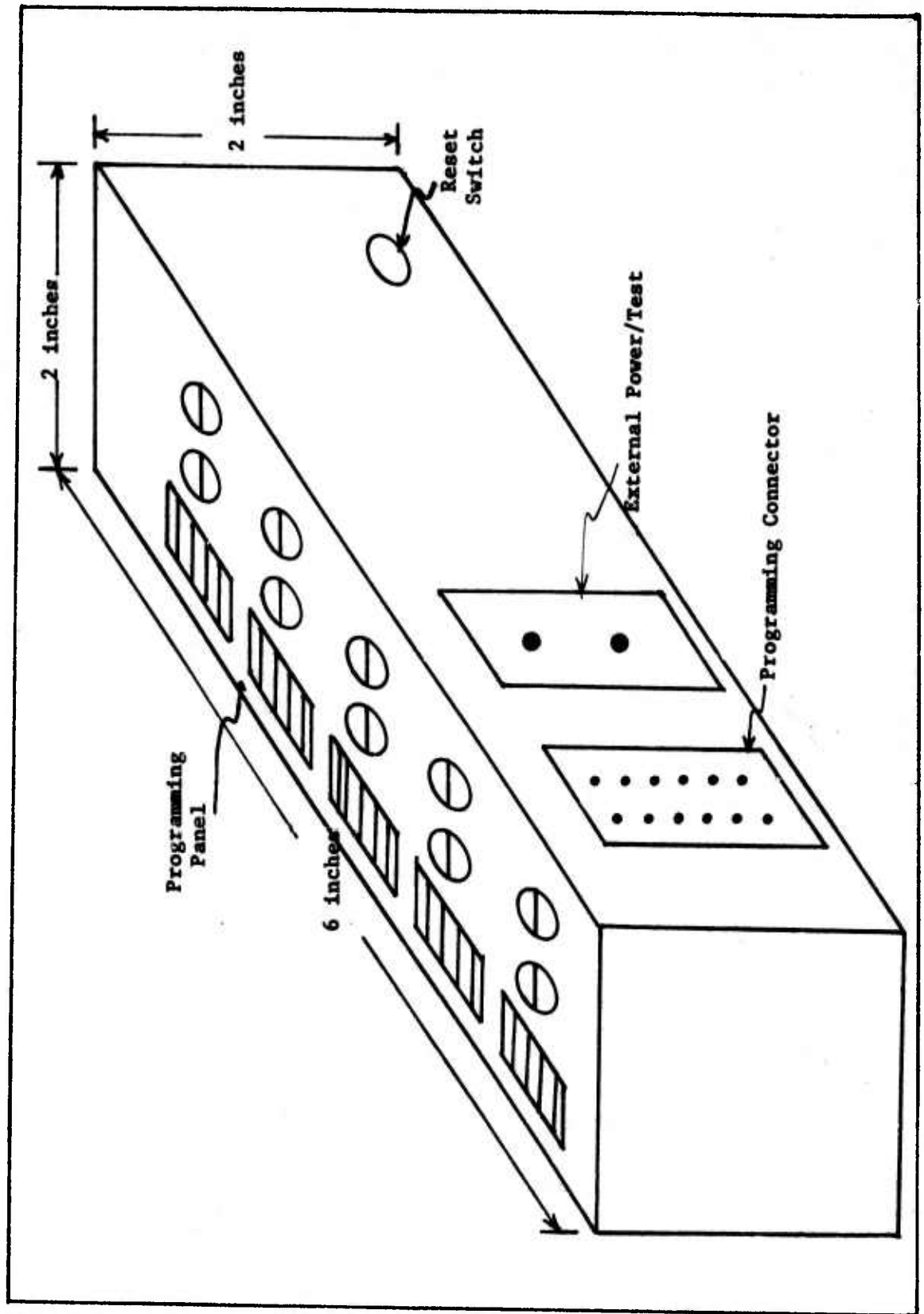


Figure E-5. View of Navigation Set

## APPENDIX E-1

### NAVIGATION TECHNIQUES

#### Coupled Techniques

Many techniques may be employed to direct the less expensive Type II vehicle to the target. Since the Type I vehicle is likely to have an expensive and relatively-accurate navigation system, it may be desirable to create a link of some type between the Type I and the Type II vehicles. Use of such a link could provide two possible advantages. Linkage would eliminate the need for a Type II navigation system; and, by keeping Type II vehicles close to the Type I vehicle, should increase the survivability of the more expensive system. This might be a distinct advantage during terminal maneuvers. Various techniques are considered to achieve such a link.

Navigation Beacon on Lead Vehicle. A small transmitter such as used in survival radios, can be mounted on the Type I vehicle with receivers and a phase discriminator mounted on the Type II vehicles. Since the same altitude is used for both types of vehicle, a simple feedback-control loop consisting of a phase discriminator and turn-command mechanism would keep the Type II vehicle pointed at the signal source. If an amplitude-measuring device is also available, a set distance between the vehicles can be maintained using velocity control. The phase discriminator can be set so that the trailing vehicles track the lead vehicle at different angles with respect to the direction of flight. The spotlighting of the Type I vehicle is eliminated by setting beacons on the trailing vehicles. Using narrow-band-pass filters,

many combinations of "linking" frequencies are produced, each flight of vehicles having its own selected link and broadcast frequencies. One concern is that the trailing vehicles are led away by another vehicle's broadcast frequency or wander aimlessly when the Type I is lost.

Detection of the leader Type I vehicle is possible. The usefulness of Type II vehicles relies heavily on the indistinguishability between the Type I and Type II vehicles. Although the beacon problem is mentioned and solved, others remain. If the lead vehicle attempts abrupt maneuvers or changes in altitude, some time lag occurs before the others follow. This is especially critical in terminal maneuvers. Another way of identifying the Type I vehicle is to use broad band jamming to cause some of the Type II vehicles to follow the false signal.

Navigation Beacon with Update. One way of circumventing several of the problems with the above system is to use a linking signal intermittently. The signal used is coded to reduce jamming problems. A keying code is sent to open the receiving channels and is followed by a pulse used for directional indications. Specially-keyed words command changes in attitude or altitude. This approach requires a mini-processor with a minimum cost of \$500 (Trull, 1975), associated logic, and input/output subsystems. Unfortunately, this approach also is susceptible to broad band continuous-wave jamming. If cost were not considered quite as heavily, a linking frequency, which an opposing force would not try to jam, may be very effective. Such a frequency might be that of his own radar units, between 1,500 and 10,000 meters in wavelength. Type II vehicles can also radiate in a similar manner but at a slightly different frequency. This approach forces the enemy into one or more

response modes: selected jamming, no jamming, disruption of their own radar units, or destruction of all vehicles.

Infra-red. A different approach to the link-jamming problem is infra-red tracking. Such technology has been well demonstrated with the sidewinder missile. Several Type I vehicles would be launched first. Type II vehicles would be launched to follow the engine heat of the previous vehicles. It is important that the heat-seeking device be able to acquire and lock-on a single heat source, to the rejection of all others. Otherwise, Type II vehicles may start following themselves in an uncontrollable fashion. This ambiguity presents a high risk in using this technique which does not appear to be easily overcome either by tactics or technology. Additionally, spoofing of the system through heat flares or other techniques could easily defeat this approach.

Ultrasonics. Another way to conquer the jamming employs sonics, of which ultrasonics are used for illustration. The same type of linking approach as in the radiometric techniques is employed. The Type I vehicle emits a signal and the Type II detects an amplitude and phase difference. Because of the relatively slow propagation speed and rapid amplitude attenuation of the signal, the Type II vehicles need not have their own transmitters. This immediately reduces cost and power requirements on that vehicle, as long as the flight is kept in a tight formation. The difficulty with this approach is the noise created by the engine itself. A significant amount of transmitter power may be required to achieve an acceptable signal to noise ratio. Filters would also be required. The high amount of transmitter power required is certainly advantageous if a jamming threat is to be reduced, since

a powerful jammer would be required to accomplish anything but very localized interference.

Summary of Coupled Systems. Although not requiring an independent navigation system on the Type II vehicle may appear to be an inexpensive idea, there are several serious complications which dim such hopes. The more inexpensive systems are easily jammed. Attempts to code and decipher the communications link increase cost.

#### Uncoupled Independent Techniques

An independent navigation system aboard the Type II vehicle provides several advantages over a coupled approach. Since the Type II vehicle is not dependent on the Type I vehicle, loss of a Type I vehicle does not eliminate the usefulness of the associated Type II vehicles. This means that fewer Type II vehicles are required to achieve some particular concentration due to a longer useful life expectancy. Independent navigation also supplies many more targets, each of which may appear as a threat. Conversely, for a single flight of vehicles in the coupled approach, it is suspected that only one real threat exists. However, increased survivability in the terminal dive is sacrificed with an independent system.

Navigation Beacon. This navigation aid takes on many forms. A beacon is placed at the launch point, nearer the FEBA, or even deposited at the target just as long as it maintains line-of-sight with the vehicle. The transmission character of the beacon can be either omnidirectional or carry directional information, as done with the present TACAN system. Assume first that the beacon is omnidirectional. Wing tip antennas are required, as in the coupled systems, to determine the angle to the beacon. Some type of timing and/or logic circuit is used

to produce a programmed flight path as a function of time and angle with respect to the beacon, with vehicle controls maintaining the proper flight path.

Inertial Systems. Gyros have traditionally been considered the heart of an inertial system. Their operation is very simple as a gyro only tries to maintain a fixed orientation of the angular-momentum vector. When gimbled in a case mounted to the vehicle, changes in the vehicle altitude or direction are read from strain gages as calibrated electrical signals. A gyro is often coupled with accelerometers which give acceleration, then integrated to give velocity, and integrated again for position. Involved with any inertial system for this mission is a microprocessor, which increases costs even further. Other approaches to inertial navigation have better accuracy but are much more expensive (in the \$5,000 range).

Dead Reckoning. A dead-reckoning system is similar to walking with a compass and a stop watch. The earth's magnetic field is used for a reference. A vehicle is programmed to fly on a given heading for a given time, then a different heading for a time, and so forth. The difficulty with such a system is that, if any winds are present, the path through the air mass does not match the ground track. Large errors result when the wind is ignored since the mean wind at 10,000 feet MSL is between 10 and 20 miles-per-hour, depending on the location and season (Carvell, 1975). If forecasts are available, the errors can be significantly reduced. This requires setting the vehicle flight plan not to the ground track, but rather to some corrected setting which, together with the wind, is expected to give the desired ground track. The expected wind can be entered into the vehicle along with the desired ground track, and the vehicle electronics will calculate

the new heading, or the new heading can be precomputed on the ground and entered into the vehicle. The distinctive advantages of dead-reckoning are its complete immunity to jamming and its low expected cost.

LORAN A and C/D. The hyperbolic navigation systems, such as LORAN, operate on the principle that the difference in time of arrival of signals from two stations, observed at a point within the coverage area, is a measure of the difference in distance from the point of observation to each of the stations (see Figure E-6) (Coast Guard, 1974). The locus of all points with the same observed difference in distance is a hyperbola called a line of position (LOP). Normally three stations are required to give a position fix. A few years ago a full-service LORAN-C receiver cost \$20,000 - \$40,000. With the advances in low-cost chips from the calculator industry, the average price of a two-chain receiver is now down to a tenth of the earlier figure (Moss, 1975:58) . LORAN-C is capable of typical fix errors ranging from less than one kilometer to 2500 kilometers over water. LORAN-D is a tactical version of similar accuracy, but limited in range to 800 kilometers (Develco, 1967). Coverage is available as shown in Figures E-7 and E-8 (Teledyne, 1975). LORAN-A coverage is primarily associated with the East Coast U.S. LORAN C and D have very similar pulse trains, lending themselves to a similar receiver. Because of the general unavailability and shorter range of LORAN-A, a system using LORAN-C and D is more useful. Although filters exist to increase discrimination, jamming is possible on a tactical level.

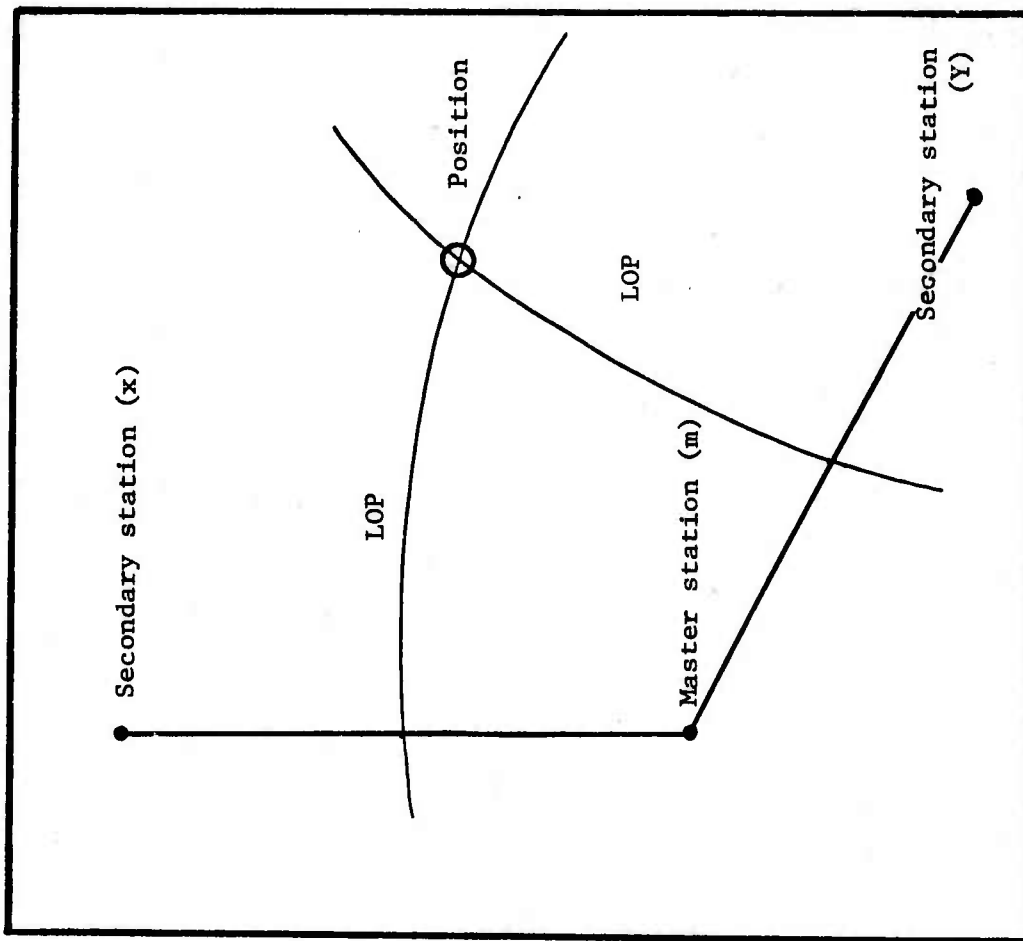
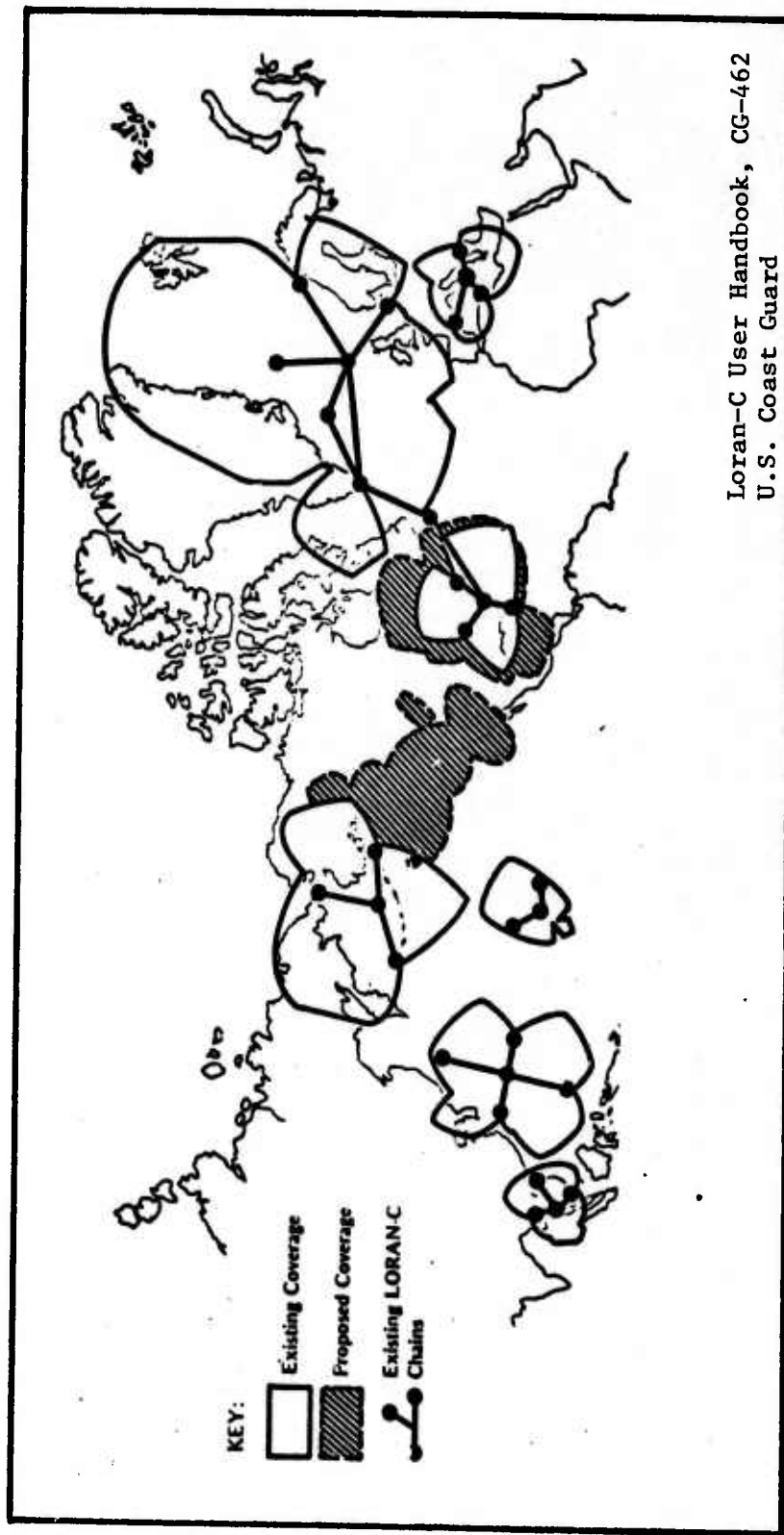


Figure E-6. Three station Loran Position Fix using LOP's



Loran-C User Handbook, CG-462  
 U.S. Coast Guard

Figure E-7 . Loran-C Coverage

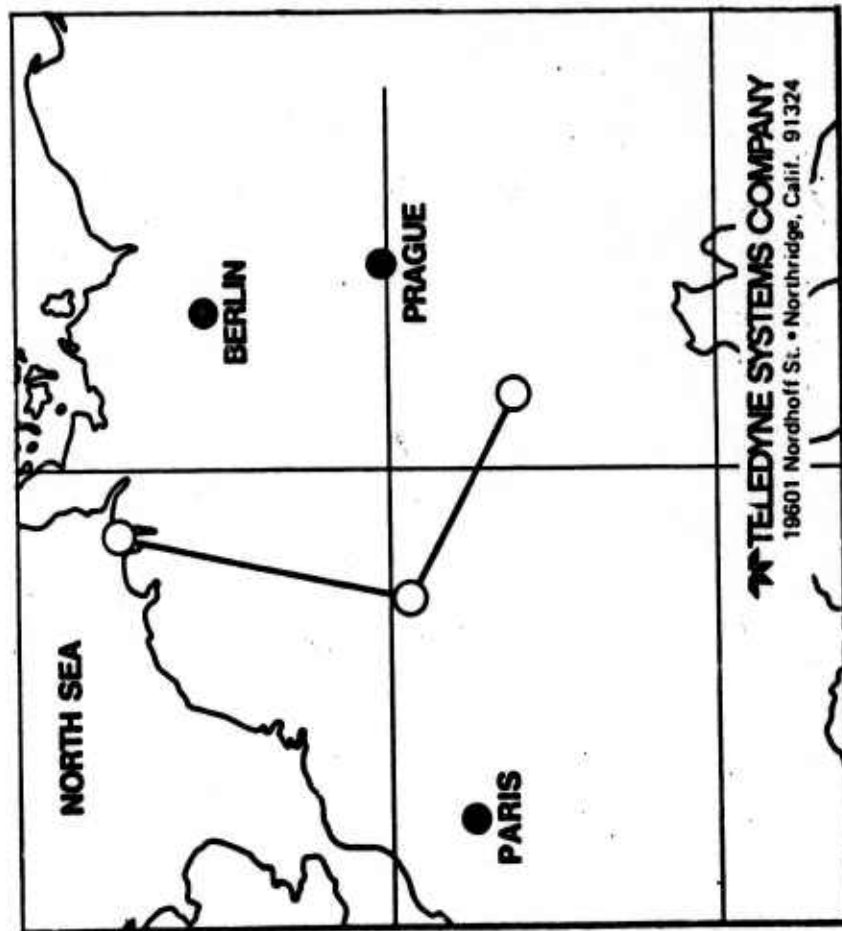


Figure E-8 . Loran-D European Chain  
under Construction

Omega. Omega is a long-range, all-weather navigation system developed by the Navy which is able to provide position within 3 miles over a considerable portion of the earth. The system operates in the very-low-frequency (VLF) range between 10.2 and 13.6 KHz. Four of the eight proposed stations are presently in operation. Omega is basically a Continuous Wave (CW) system, making phase comparisons to determine position, although it uses both time and frequency sharing. The interference patterns from these emissions create ambiguous frequency lanes of 8-15 miles in width. Position is determined by the starting point, present phase angle, and number of lanes of each frequency crossed. Errors are introduced when the wave passes over areas of differing ionospheric characteristics such as night or day, causing predictable errors on the order of kilometers. Sudden ionospheric disturbances, which are yet unpredictable, cause auroral effects that may shift a lane up to 11-12 miles (Beukers, 1973:81). These errors result from a change in the reflection point of the skywave and become important over long ranges moving from one set of stations to another. Over short distances and times they are important only if they occur during the flight--an advantage of lane ambiguities. For this system the diurnal propagation errors can be easily determined from published material and taken into account in the mission planning; thereby substantially reducing processor cost. As noted in the LORAN section, recent technological advances have dramatically reduced the cost of both receiver and logic circuitry (Moss, 1975:58) (Delorme, 1975: 126).

Tactical jamming of the Omega system is practical, but limited in range due to the difficulty of generating the necessary jamming

power at VLF frequencies. Spoofing by building another station can distort the Omega lanes by a few miles (Develco, 1975b).

Summary. Dead-reckoning is the least-expensive independent navigation system, but somewhat inaccurate. Both Loran C/D and Omega are low cost and have accuracies much better than dead-reckoning. Pure inertial systems are not appropriate for this vehicle, primarily because of cost. The use of a navigation beacon involves development cost, provides an easy target, and does not offer any significant advantages over the already-existing Loran or Omega systems.

APPENDIX E-2

COST

Dead Reckoning

Estimating the cost of the system involves more than just adding the cost of a number of parts. Two dead-reckoning sets are costed in this section; a two-direction racetrack and a four-leg pattern, both in addition to the navigation leg. Table E-4 lists the parts and associated costs from current Allied Electronics catalogs. Table E-5 shows similar information for the four-leg pattern. Costs are for more than 100 units.

TABLE E-4  
COMPONENT COSTS (2-LEG PATTERN)

<u>Part</u>	<u>Numbers Required</u>	<u>Cost Each</u>	<u>Total Cost</u>
NAND gates	3	\$ .75	\$ 2.25
15 turn resistors	6	1.21	7.26
Resistors (1%)	21	.14	2.94
Capacitors	7	.04	.28
Diodes	6	.13	.78
Reset switch	1	.42	.42
Bistable timers	2	1.75	3.50
Switch bank	3	2.50	7.50
Test Items			
*22 Pin Connectors	1	2.00	2.00
*Banana Connector (sets)	2	1.44	<u>2.88</u>
TOTAL			\$29.81

\*Parts required for check-out and setting of equipment.

Rather than estimate the number of manhours required and production cost, certain other cost-estimating schemes may be used. One scheme is based on the idea that the component costs make up 10% to 30% of the final installation cost (Johnson, 1975). The most likely estimate is assumed to be 20%. Using this relationship, the following cost estimates for the electronics are found:

High	\$298
Low	99
Most Likely	149

Costs for the four-leg pattern are shown below.

TABLE E-5

COMPONENT COSTS (4-LEG PATTERN)

<u>Part</u>	<u>Numbers Required</u>	<u>Cost Each</u>	<u>Total Cost</u>
NAND gates	6	\$ .75	\$ 4.00
15 turn resistors	10	1.21	12.10
Resistors 1%	23	.14	3.22
Capacitors	9	.04	.36
Diodes	12	.13	1.56
Reset switch	1	.42	.42
7 Switch bank	5	2.00	10.00
Bi-stable timer	5	1.75	1.75
Test items			
*12 Pin Connector (sets)	1	2.00	2.00
*Banana Connectors	2	1.44	<u>2.88</u>
TOTAL			\$45.29

Using the same cost estimating relationships yields for the 4-leg pattern:

High	\$453
Low	251
Most Likely	326

But the magnetometer raises these costs by \$100 each (Dailside, 1975)  
to:

	2-leg	4-leg
High	\$398	\$553
Low	199	251
Most Likely	249	326

The non-recurring production cost is estimated by comparison with a system of similar production complexity, for which an estimate is known, the Omega system. A point estimate of \$50,000 was received (Develco, 1975). High and low estimates are \$45,000 and \$57,000 (Johnson, 1975) based on similar arguments (Rorden, 1975).

Dead-Reckoning Navigation with Omega Station-Keeping

Although this system is not expected to be used, it serves as an intermediate check in both technology and cost in going from DR to Omega.

The costs associated with this system are described as follows:

Magnetometer - Such as Develco 9100C presently selling at \$600 per unit. Available at \$100 per unit in a 5000 unit buy (Dailside, 1975).

Antenna and Coupler - Electric field with coupler, hermetically sealed and molded into airframe. Estimated cost is \$100-200 with less than \$5,000 modification costs from Spears Associates (Burke, 1975).

Receiver and Clock - Constructed using existing integrated circuits.  
 Estimated cost of delivered items if \$100 - \$150 (Gaugler, 1975).

Serial Digital Phase Filter - Supported by USAF, to be produced by RCA as an integrated circuit. Estimated cost of \$5 - \$10 each in large quantities (Gaugler, 1975) (2 required).

Navigation Electronics - Almost the same as the DR system but the leg timer is eliminated. Based on DR, cost is \$50 - \$190 (parts cost from Allied).

	<u>Low</u>	<u>Most Likely</u>	<u>High</u>
Magnetometer	\$100	\$100	\$100
Antenna and Coupler	100	125	200
Receiver and Clock	100	125	150
Other Electronics	<u>70</u>	<u>100</u>	<u>200</u>
TOTALS	\$370	\$455	\$650

#### Omega

Develco, Inc. estimates their design costs at \$400 in lots of 1000 and \$300 in a 5000 unit buy (Develco, 1975a). This price does not include the magnetometer which is estimated at \$100.

#### Loran

The cost for the Loran system, including the antenna, is estimated (firm) at \$1,300 in large quantities (Steelman, 1975). Supporting estimates are available at \$2,000 to \$4,500 (Moss, 1975:58) on a single-unit basis.

## APPENDIX E-3

### WIND MODELS

The choice of navigation systems is dependent on the effect of wind on the vehicle. The objective of this Appendix is to develop a set of models useful in characterizing the wind-velocity vector in the cruise flight regime of the vehicle. Three types of models are considered: climatological, prediction-error, and hourly-change. Each of these models is discussed and its uses indicated below.

The winds are created when large air masses move along the rough, frictional surface of the earth creating a turbulent boundary layer. This boundary layer extends upward some 5,000 feet above the surface. It is within this layer that most day-to-day experience is gained, either from personal observation or from the local weatherman. Fortunately, the vehicle spends only about 10 minutes of its climb in this layer. The remainder of the flight occurs at 10,000 feet in the calmer mesosphere. The air at 10,000 feet is much calmer than the air at the surface of the earth. Clear air turbulence occurs only a short portion of the time (Chalk, 1969:443).

#### Climatological Models

These models illustrate the major trends, such as mean wind velocity and direction. Data is collected over several years and is categorized according to season and location. The types of data available include rainfall, cloudcover, winds, etc., although the present concern is with winds. A summary of the climatological wind data is given in Figure E-9 and E-10 (Carvell, 1975). The standard deviation of the

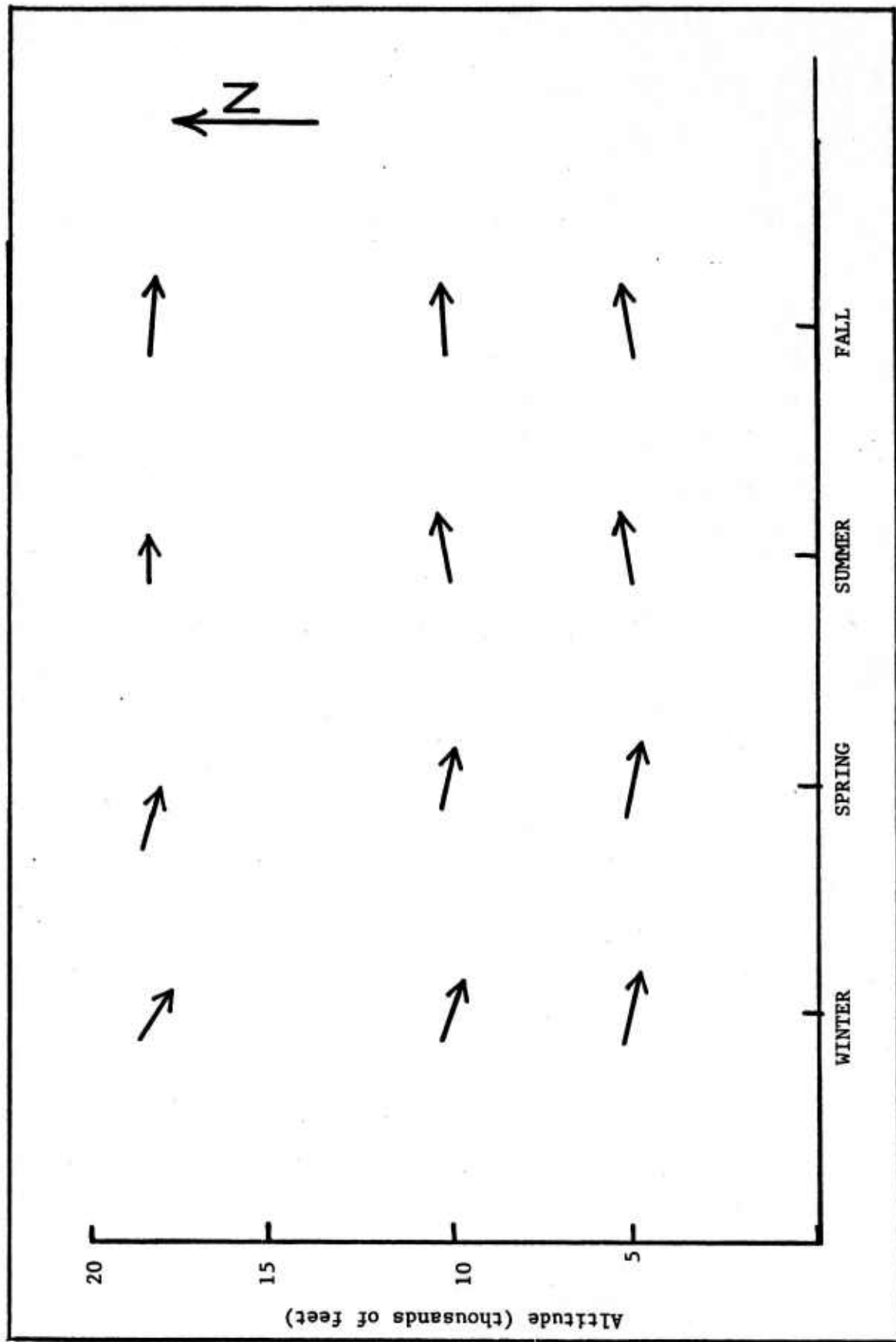


Figure E-9 Prevailing Wind Direction  
 (Central West Germany using  
 Weisbaden Germany 1946-1957)

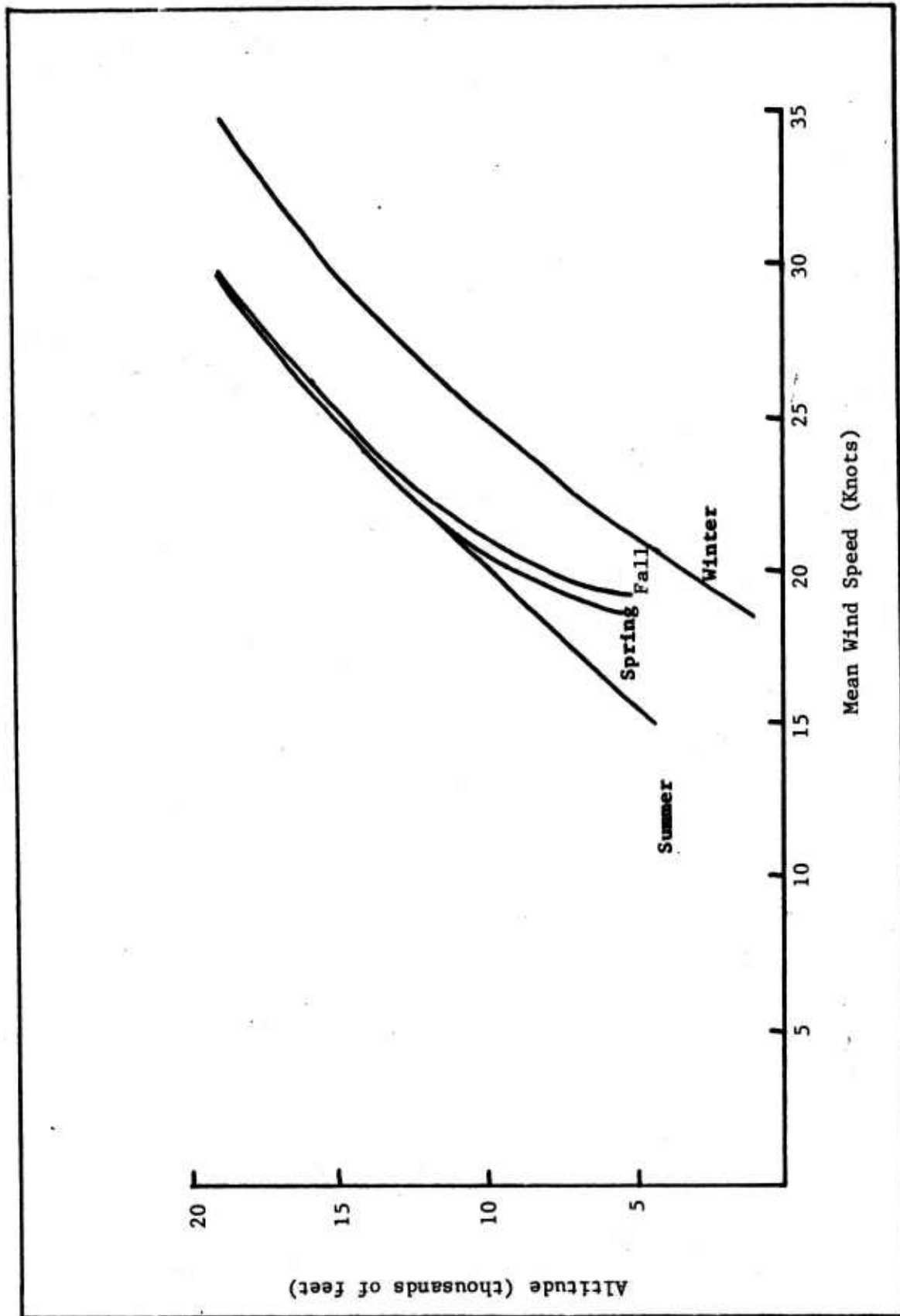


Figure E-10 Mean Wind Speed (Wiesbaden, Germany, 1946-1957)

wind at 10,000 feet is 4.4 meters per sec in speed and 90 degrees in direction. This is obtained from climatological data for Weisbaden, Germany from Air Force Global Weather Control.

Data describing surface weather conditions is recorded on magnetic tapes hourly. Measurements of upper air conditions are generally taken and recorded only every 12 or 24 hours. Extrapolating a model based on one hour surface measurements to higher altitudes is very unwise. Because the wind speeds in the lower (100-meter) layer are uncorrelated with wind speeds in the overlaying layers, their variation at lower levels seldom implies corresponding variations at higher levels (Borisenko, 1967). For a model to be valid using the 10,000 feet data, the length of time between changes in weather should be greater than the sampling period. Since the wind can change significantly in less than 12 hours (Carvell, 1975), the usual meteorological tapes for upper winds taken every 12 hours do not provide data at close enough time increments for a model used to simulate weather over a few hours.

In summary, neither one-hour surface measurements nor 12-hour measurements at 10,000 feet provide a good model for this problem. They do, however, provide information on the general long-term character of the wind for the area.

#### Prediction Error

It is generally thought that having even a poor forecast is better than having none at all. Although the weatherman is taunted for being 50% right 75% of the time, pilots and navigators credit him with mission forecasts generally within 5 mph in a 45-degree cone at altitude. A more quantitative approach is taken to the question of prediction-error

by considering an AFGWC evaluation of the meso-scale prediction model from June 1971 to May 1972 (AFGWC, 1972). This model is used by AFGWC to predict weather in the mesosphere, that area above 5,000 feet but below the ionosphere. The area considered included Canada, United States, and northern Mexico, with approximately 90 stations available for each cycle. Verification statistics are computed by comparing actual data collected by RAWINSONDE stations with previously forecast values of 12 and 24 hours and are shown in Figures E-11 and E-12 for the 12-hour forecast. Table E-6 gives the statistics for the difference between forecast and measured wind for June 1971 to May 1972 at 700 millibars, approximately 10,000 feet altitude.

TABLE E-6. STANDARD DEVIATION OF WIND-PREDICTION ERROR (AFGWC, 1972)

<u>Month</u>	<u>Wind Speed (m/sec)</u>		<u>Wind Direction (degrees)</u>	
	<u>12 hours</u>	<u>24 hours</u>	<u>12 hours</u>	<u>24 hours</u>
June 1971	3.5	4.0	34.2	40
July 1971	3.4	3.9	29.6	37
August 1971	3.4	3.9	32.1	38.8
September 1971	3.8	4.4	33.2	39.3
October 1971	4.1	4.7	31.6	40.0
November 1971	4.3	4.9	26.9	35.9
December 1971	5.4	6.5	29.5	37.9
January 1972	5.1	6.5	23.8	28.5
February 1972	5.1	6.0	27.5	31.7
March 1972	5.0	5.6	29.4	36.0
April 1972	4.7	5.4	31.4	38.7
May 1972	<u>3.9</u>	<u>4.4</u>	<u>33.0</u>	<u>37.8</u>
AVERAGE	4.308	5.017	30.18	36.8

Given the tactical situation, a more accurate forecast than the standard twelve hour forecast should be available. In an attempt to

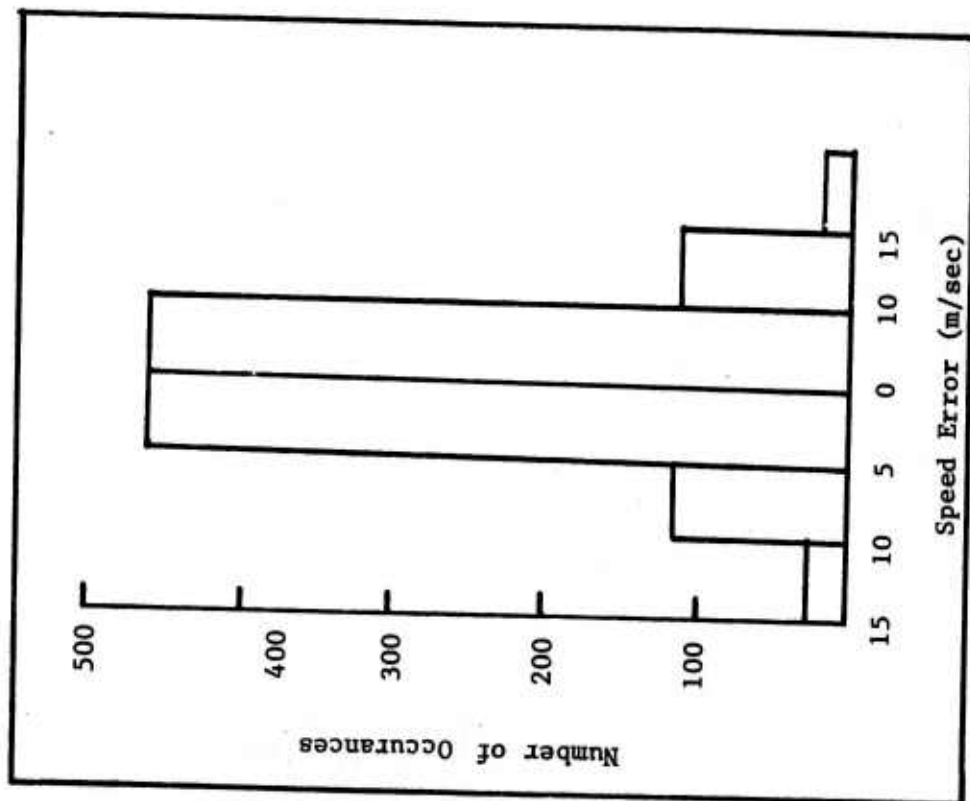


Figure E-11. Mesoscale Speed Prediction Error  
(From 700 millibar data of AFGWC, 1972)

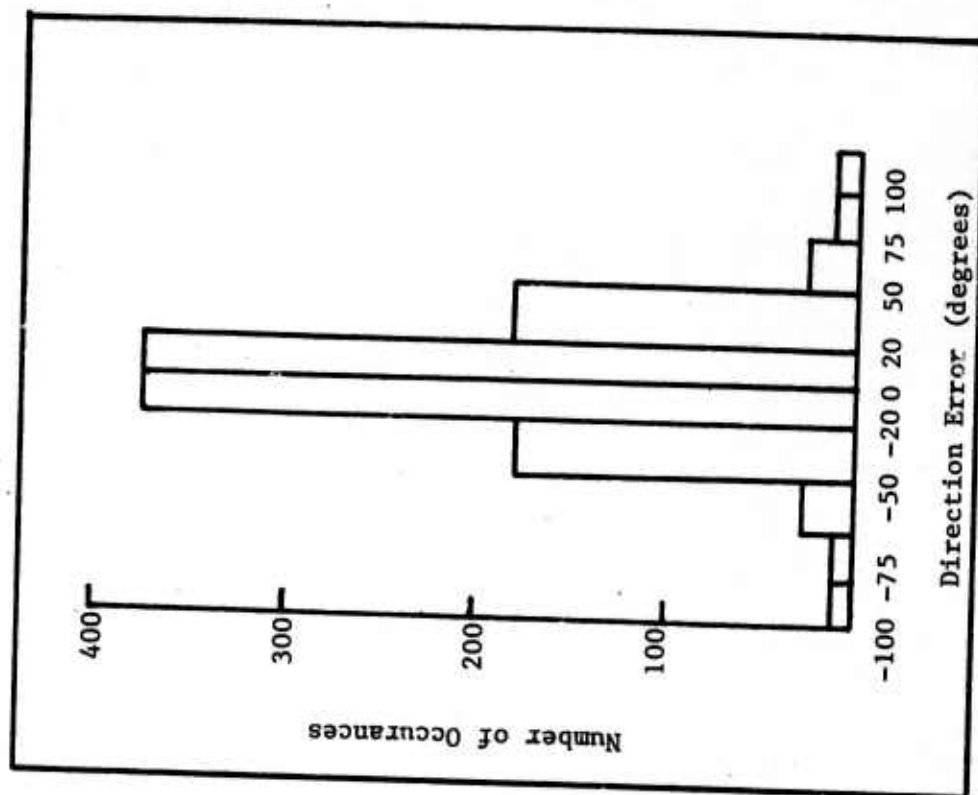


Figure E-12. Mesoscale Direction Prediction Error  
(From 700 millibar data of AFGWC, 1972)

account for this and other possible factors, a linear extrapolation to 6 hours is used for the standard deviation of both speed  $\sigma_s$  and direction  $\sigma_d$ . The prediction error model is for speed  $\sigma_s = 3.9535$  m/sec and for direction  $\sigma_d = 26.87$  degrees. If a normal distribution is assumed for the error, as is normally done (Carvell, 1975), the expected speed error  $\mu_s$  for a 6-hour prediction is  $\mu_s = 2.637$  m/sec = 5.9 mph, and the expected direction  $\mu_d = 17.914$  degrees. It is assumed that the prediction error is constant over the mission time. This model is used in the EFFECT program of Volume II.

#### Hourly Change

Sending a series of vehicles at a target using the same predicted wind does not imply that they arrive at the same place because of slow shifts occurring between launches in the wind conditions both at the launch site and enroute, not accounted for by the prediction. It is desirable to have a model that accounts for these slowly-changing conditions yet does not tamper with the prediction-error model. Although the scarcity of hourly upper-air data is mentioned, the test range at Luke AFB takes hourly readings when the range is operating, about eight hours a day. Approximately 150 Pibal measurements at 11,000 feet MSL are subjected to various statistical tests. The Kolomogorov-Smirnov test and Likelihood Ratio Test for various distributions were also applied using a computer program developed by Prof T. L. Regulinski (1975). Exponential, Weibull, normal, gamma, log normal, beta, and logistic distributions were considered with the normal selected as the most likely distribution based on the Kolomogorov-Smirnov "d" statistic.

The parameters of the normal distribution are  $\sigma_s = 1.6$  m/sec and  $\sigma_d = 25.1$  degrees, with both means equal to zero. These changes are shown in Figures E-13 and E-14.

Another way of grasping the changing nature of the wind is through the auto-correlation function,  $\phi_{xy} = \frac{E[XY] - E[X]E[Y]}{E[XX]}$ . Seventeen strings of five, unbroken data points are used in calculating the auto-correlation function of speed in figure E-15 and direction in Figure E-16. This model is used to slowly change the wind conditions during flight and at launch as explained in Chapter IV of Volume II.

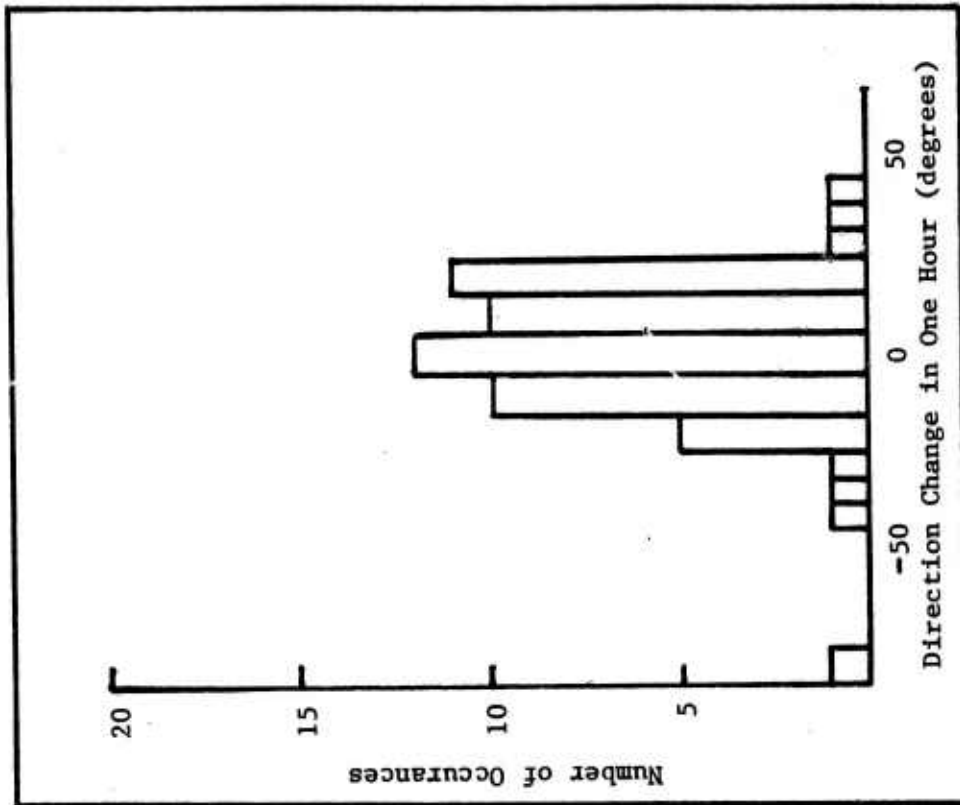


Figure E-14. Hourly Direction Change (1100 ft MSL)

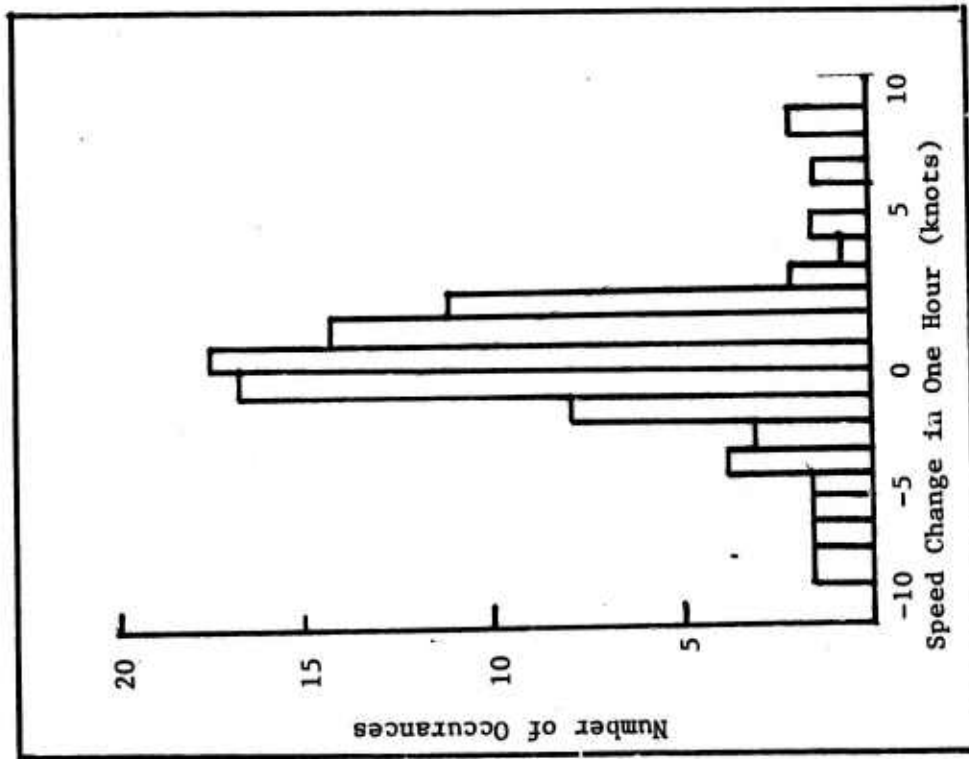


Figure E-13. Hourly Speed Change (1100 ft MSL)

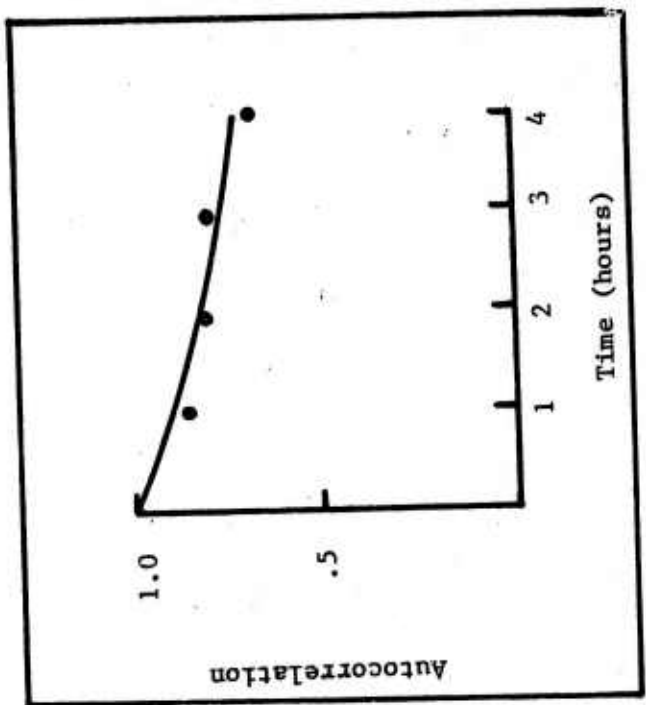


Figure E-16, Direction Change  
(1100 ft MSL)

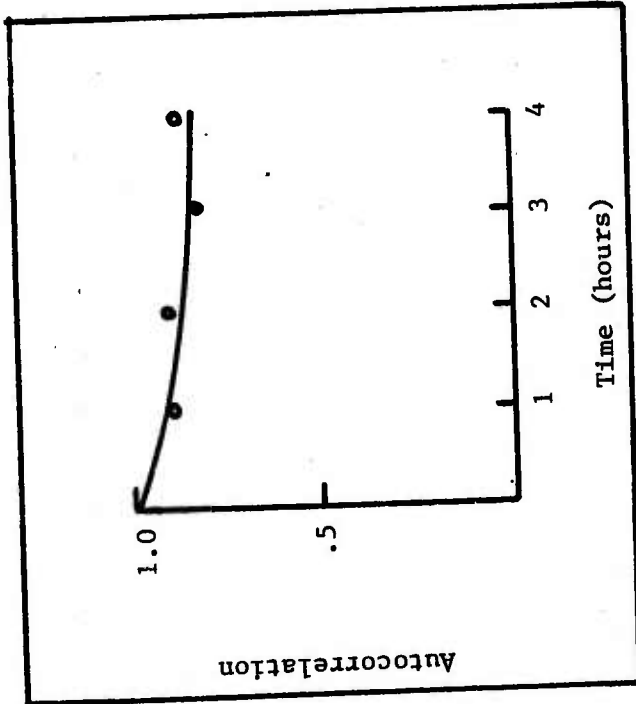


Figure E-15, Speed Change  
(1100 ft MSL)

## APPENDIX E-4

### DEAD RECKONING CIRCUIT DETAILS

A dead reckoning system involves flying a set of given headings for a predetermined length of time. The complexity of the pattern flown depends on the number of pattern legs. A simple navigation scheme is shown in Figure E-17. It consists of flying from the launch site to Point X (Leg A) in the target area and then flying legs B and C repeatedly until fuel depletion. To steer the above track, wind forecasts are used to compute wind triangles (Figure E-18) for each of the pattern legs just prior to launch.

To implement the above scheme, a circuit was constructed (Figure E-19) using both digital and analog integrated circuit technology. This circuit was breadboarded to test the feasibility of the navigational scheme and to quantify the processing accuracies expected from this type of circuit.

#### Circuit Design

The circuit is designed to use two SN72555 integrated circuit timers. These timers use resistors and a capacitor to form one or two RC time constants depending on whether they are configured in a monostable or astable configuration. Timer A is used to time leg A of the navigation pattern; timer B switches back and forth, first timing leg B, then leg C, then leg B again, etc. (Figures E-20 and E-21). A need also exists to program the directions of each leg.

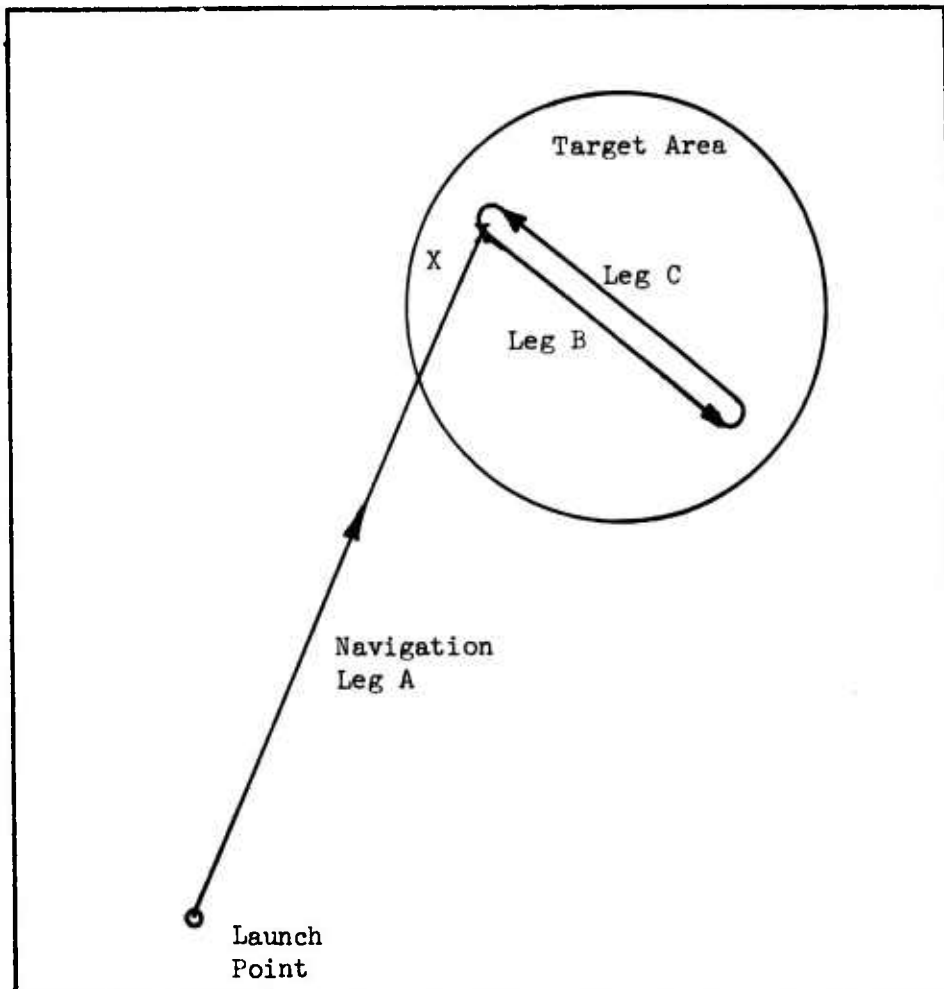


Figure E-17. Navigation Scheme

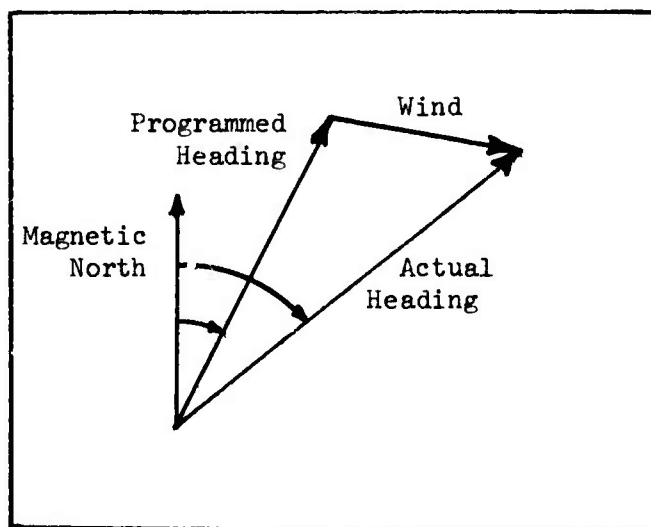


Figure E-18. Wind Triangle

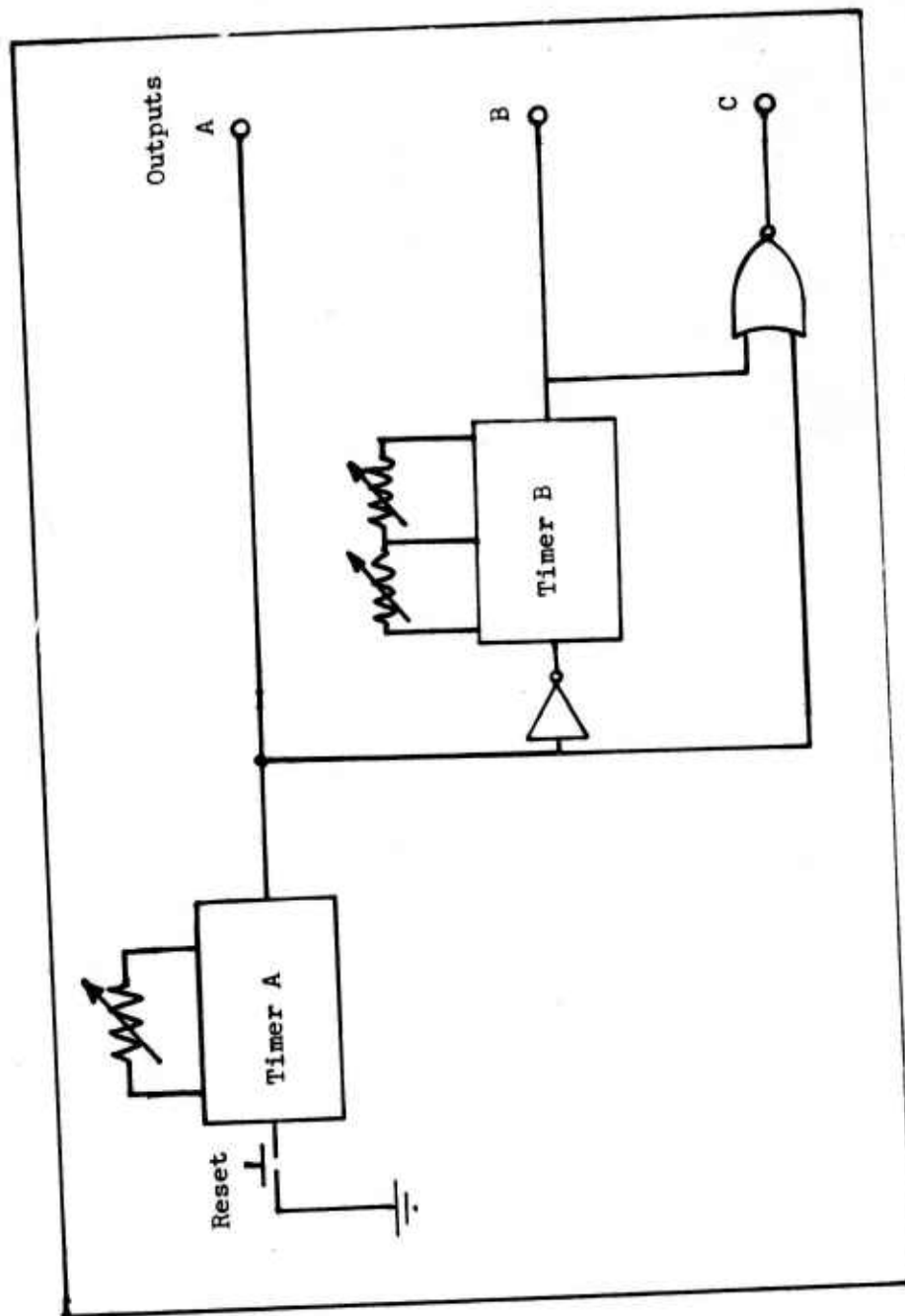


Figure E-19(a). Dead Reckoning Navigation Circuit

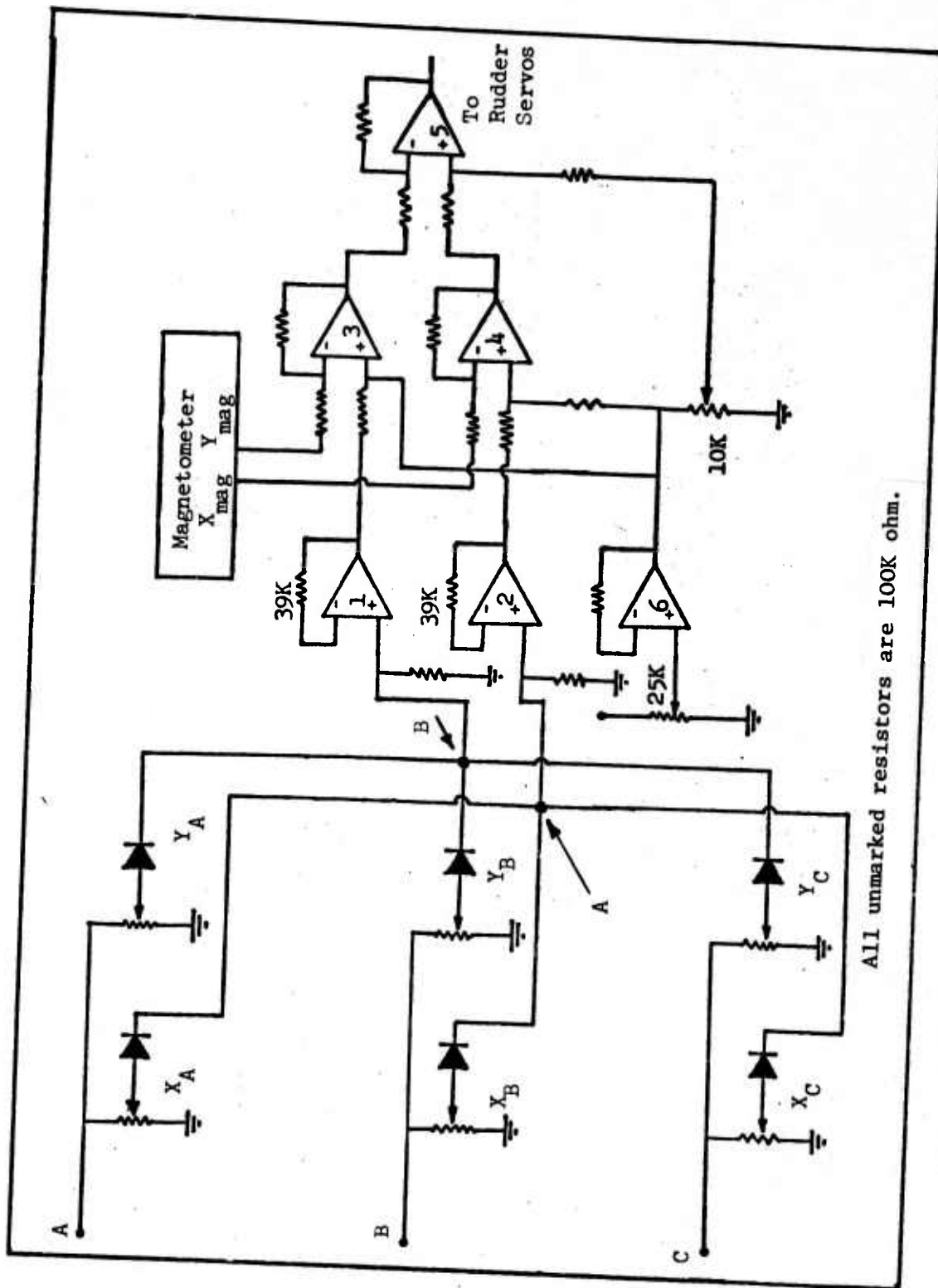


Figure E-19(b). Dead Reckoning Navigation Circuit Diagram (Continued)

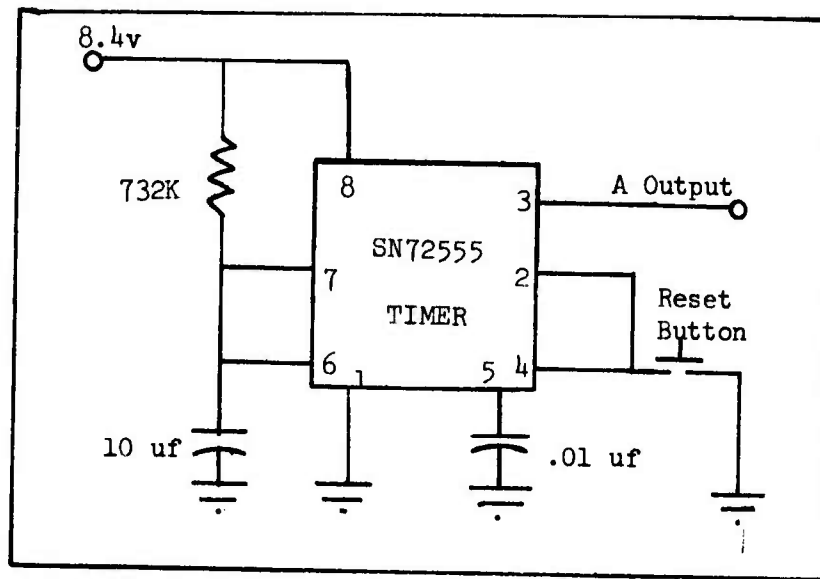


Figure E-20. Timer A, Monostable

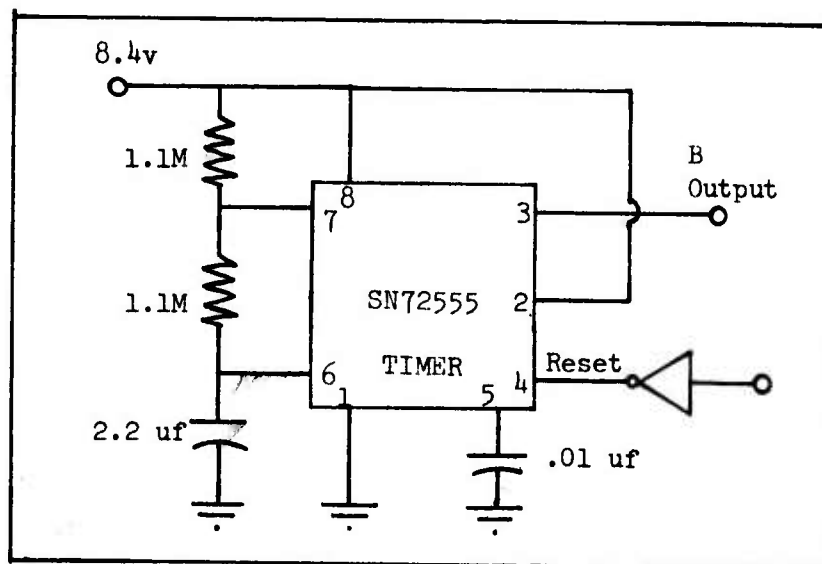


Figure E-21. Timer B, Astable

Direction is sensed by a two-axis, flux-gate magnetometer. The Develco Model 9100C magnetometer was selected, because it is the lowest-cost analog magnetometer available. The output for each of the two orthogonal axes, X and Y, is 0 to +5 volts dc. The zero field bias is +2.5 Vdc. The magnetometer is oriented so that the two axes are in a horizontal plane when the vehicle is cruising in straight-and-level flight. By orienting the magnetometer axes parallel to the Earth's surface, those components of the Earth's magnetic field normal to the surface have minimal effect on the magnetometer.

#### Magnetometer Output

A magnetometer was not available for testing, but it was assumed that the output voltage of the magnetometer has a sinusoidal relationship with the angle between the axes and magnetic north. Given this relationship, it is calculated that the outputs are:

$$(\cos \theta + 1) (2.5) \text{ volts} = X \text{ output} \quad (\text{E-3})$$

$$(\sin \theta + 1) (2.5) \text{ volts} = Y \text{ output} \quad (\text{E-4})$$

where  $\theta$  is the angle between the longitudinal axis of the magnetometer and the magnetic north. Which one of these two equations actually corresponds to the X or Y outputs is arbitrary. The computed outputs for angles of 1 through 360 degrees are contained in Appendix E-10.

#### Programmed Angles

We have thus far established a time length for each navigation leg and have a magnetometer to give the angle from magnetic north which the vehicle is flying. What is left is to find three angles (i.e. pairs of voltages) to compare with the two outputs of the magnetometer. Each pair

of voltages (X and Y) represents the programmed direction the vehicle is to fly. Any of the pairs of voltages from the timer circuit (Figure E-22a) (voltages  $X_{mag}$  and  $Y_{mag}$ ) have a maximum of about 3.4 volts.

### Amplifiers

The above voltages must be amplified so that there is as much as 5.0 volts available (X and Y) to be compared with the output of the magnetometer. This is accomplished by amplifiers 1 and 2 in the circuit in Figure E-19b. From this point, the differences are taken between the magnetometer outputs and the programmed voltages in difference amplifiers 3 and 4. These differences are labeled  $\Delta X$  and  $\Delta Y$ . The difference is then taken between  $\Delta X$  and  $\Delta Y$  in difference amplifier 5. This gives a single overall error as the output of amplifier 5 ( $\Delta Y - \Delta X$ ).

Amplifier Biasing. In a difference amplifier (amplifiers 3, 4, and 5, Figure E-19b) when the voltage at the negative input is more positive than the voltage at the positive input, the voltage at the output is negative (the positive input minus the negative input) (National, 1973: AN20.6). This is true only when the amplifier is connected to both a positive and a negative voltage supply. In this application, only a positive voltage supply is used. Thus, the output cannot go negative. If the input to these amplifiers is given some positive reference voltage (a bias) this voltage becomes the zero-reference point. Positive differences are above this value, and negative differences below. The bias voltage for amplifiers 3 and 4 is arbitrarily picked at 2.500 volts. This also happens to be the zero field bias for the magnetometer. The bias voltage for amplifier 5 is picked to be 1.400 volts, because that is the null voltage for the servos chosen for controlling the rudders.

### Servos

The twin-boom airframe has twin rudders for directional control. Each of the rudders has a movable surface controlled by a Kraft, KPS-16 servo. This servo is chosen, because it is the largest of the line, having a torque of eight inch-pounds. Another reason for choosing this servo is that it is capable of being controlled by either a dc signal or a digital proportional signal. Most other servos of this type, radio controlled (RC) model servos, are not capable of being controlled by a dc signal. The dc control voltage is connected to pin 3 of the servo (Miller, 1975). A voltage swing of 0.6 volts to either side of the null voltage of 1.4 volts results in full deflection of the servo.

### Timer Circuit Components

RC Time Constants. Three fixed-value resistors are used in the prototype circuit in place of the variable-trimmer resistors in the designed circuit. The trimmer resistors are used to set the time for each of the three navigation legs. For the prototype circuit, the values of the resistors and capacitors are chosen to give a time constant of a few seconds so the operation of the timers can be checked. In selecting time constants for the astable configuration, (timer A) the following equation applies:

$$T_A = 1.1 R_A C \quad (\text{Texas, 1973:7-57})$$

where  $T_A$  = Time that timer output is high (sec)

$R_A$  = Resistance (ohms)

$C$  = Capacitance (farads)

for timer B,

$$T_B = 0.693 (R_B + R_C) C$$

$$T_C = 0.693 (R_C) C \text{ (Texas, 1973:7-58)}$$

where  $T_B$  = Time that timer output is high (sec)

$T_C$  = Time that timer output is low (sec)

$R_B + R_C$  controls charging of C

$R_C$  controls discharging of C

C = capacitance (farads)

The values of the RC components are chosen strictly because those are the components available to give time constants of a few seconds.

Figures E-20 and E-21 show the configuration of timers A and B.

Digital Logic. In designing the timer circuitry, two questions arise: how to select one timer output at a time, since Timer A has one output and Timer B has two; and how to keep timer B shut off while Timer A is on. These questions are answered using Boolean algebra (Rhyne, 1973: 30-58) and the Karnaugh mapping technique (Rhyne, 1973:110-133).

Digital Analysis. In the following analysis, A is the output of Timer A when the output is high (a logic one).  $\bar{A}$  represents a logic zero at the output of Timer A. The same holds for Timer B.

Analyzing the second question, both timers are digital devices. That is, their outputs are either zero or one. There are three outputs from the timer circuit, one from Timer A and two from Timer B. The Boolean expression that describes the situation when the vehicle is on is simply A. A Karnaugh map is used to determine the output of the timer

circuit while the vehicle is on navigation leg B is:

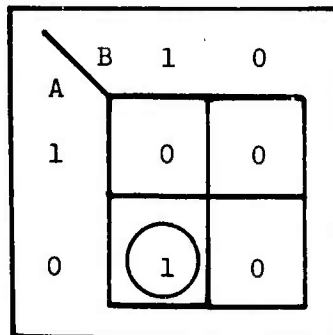


Figure E-22. Karnaugh Map, Navigation Leg B

The Boolean expression derived from this map is:  $\bar{A} \cdot B$ .

On the final leg of the pattern, leg C below,

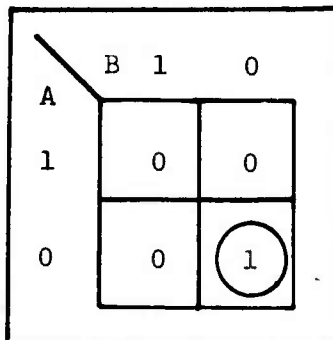


Figure E-23. Karnaugh Map, Navigation Leg C

The derived expression is  $\bar{A} \cdot \bar{B}$ . Negative logic is easier to find and cheaper than positive logic. So using DeMorgan's theorem (Rhyne, 1973: 37),  $\bar{A} \cdot \bar{B} = \overline{A+B}$ . The circuit outputs for the three navigation legs are: A,  $\bar{A} \cdot B$ , and  $\overline{A+B}$ . The logic diagram for these three equations is drawn in Figure E-27 below.

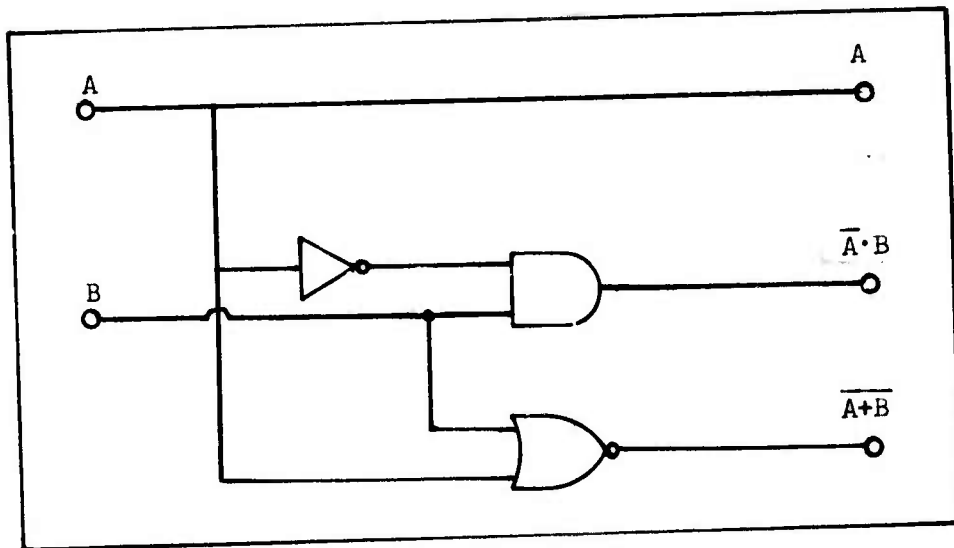


Figure E-24. Prototype Timer Logic Diagram

The above diagram normally requires three logic gates. Looking at the Timer B circuit (Figure E-19a) one finds that by connecting an  $\bar{A}$  signal to the reset of Timer B the timer output becomes  $\bar{A} \cdot B$ , thus eliminating the need for an "AND" gate. Thus, the desired output uses one inverter and one "NOR" gate. These two components are shown in Figure E-19a.

#### Diode Isolation

The diodes used in the timer circuit (Figure E-19b) are needed to isolate each trimmer resistor from the others that are connected together at points A and B, Figure E-19b. If the diodes are not present, each set of three trimmer resistors interacts. Each set of X and Y voltages are then very difficult to program because of the interaction that occurs without the diodes.

### Component Selection

A prototype of the previously described navigation circuit was constructed on a SK-10 universal component socket manufactured by EL Instruments. Resistors with a value of 107.1K ohms at one-percent tolerance were used in place of all 100K ohm resistors in the difference amplifiers (amplifiers 3, 4, and 5 in Figure E-19b). These resistors were used because they were the only one-percent tolerance resistors available with a resistance close to 100K ohms. All other resistors are ten-percent tolerance.

Operational Amplifiers. National Semiconductor LM741 operational amplifiers (op amps) were originally used for the six amplifiers shown in Figure E-19b. These devices are frequency compensated, but they were found to be temperature sensitive. The circuit was reconstructed using National Semiconductor LM324 quad op amps. These are newer devices and are both temperature and frequency compensated.

A rudimentary test of the temperature performance of these op amps was conducted. While monitoring the output of one amplifier under load, circuit cooler was sprayed on the amplifier package. The amplifier output varied less than 0.001 volt for a 5.000 volt output.

Trimmer Resistors. The trimmer resistors should be fifteen-turn trimmers similar to the Weston rectilinear 3/4-inch Cermet trimmer, model #830P, or to the Beckman Helipot, model 89 (Beckman Helipot, 1975). This type trimmer with a resistance of 100K ohm was not available for use in the prototype circuit so 270-degree-turn trimmers were used. This type is very hard to adjust to the accuracy required. The output of the trimmers needs to be within  $\pm 0.001$  volts.

### Circuit Test

The purpose of the test was to find the circuit accuracy and linearity of the difference amplifiers. The magnetometer input was simulated by using a dc power supply. The equipment used are as follows:

SK-10 universal component socket, with circuit

EL Instruments op amp designer

Kepeco, Model ABC7.5-2, 0-7.5V, variable power supply

Fluke, Model 8100B, 3½ digit, digital multimeter

An/USM-398 dual-trace oscilloscope

Measurements. Various angles were assumed and, from the data contained in Appendix E-9, the magnetometer outputs were calculated. The pair of voltages were calculated for input to the circuit at points C and D labeled on Figure E-22b to simulate the magnetometer. This same voltage pair was programmed into the circuit by adjusting one pair of trimmers (shown in Figure E-22b) until the voltages at points A & B were equal to the magnetometer input voltages. The outputs of the three difference amplifiers (3, 4, and 5) were recorded and this data appears in Table E-7.

Test Results. The data sheet for the LM324 op amp (National, 1973) states that the output of these devices goes to ground potential. In the test circuit, a single supply voltage of +15.0 volts was used for the op amps. With this single supply, a potential of 0.038 volts was the lowest potential obtainable. From Appendix E-9, one can see that a value of  $X = 0.038v$  is equivalent to angles of 170 and 190 degrees. This would equate to a ten degree error except that the differences in the Y voltages compensate for this error in less than one degree. To calculate this error, one can see that when X equals zero volts, Y equals 2.500v. For

TABLE E-7. PROTOTYPE CIRCUIT TEST DATA

Heading( $\theta$ )	Op Amp No.	Inputs (volts)		Output (volts)
		(+)	(-)	
180°	3	0.038	0.000	2.545
	4	2.500	2.500	2.501
	5	2.501	2.545	1.354
270°	3	2.500	2.500	2.497
	4	0.038	0.000	2.542
	5	2.542	2.497	1.443
90°	3	2.500	2.500	2.498
	4	5.001	5.000	2.498
	5	2.498	2.498	1.399
0°	3	5.001	5.000	2.491
	4	2.500	2.500	2.501
	5	2.501	2.491	1.408
45°	3	4.270	4.269	2.491
	4	4.269	4.269	2.510
	5	2.510	2.491	1.418
$\theta_{\text{prog}} = 90^\circ$ $\theta_{\text{mag}} = 45^\circ$	3	2.500	4.269	0.723
	4	5.001	4.269	3.240
	5	3.240	0.723	3.096
$\theta_{\text{prog}} = 0^\circ$ $\theta_{\text{mag}} = 45^\circ$	3	5.000	4.269	3.219
	4	2.500	4.269	0.736
	5	0.736	3.219	0.038

an error of 0.038V, Y would have to equal either 2.538 volts or 2.462 volts to compensate. From Equation (E-4),

$$(\text{SIN } \theta + 1) 2.5 \text{ volts} = 2.538$$

$$\text{SIN } \theta = -1 + \frac{2.538}{2.500}$$

$$\text{so, } \theta = 180.87^\circ$$

or, similarly, if the error is compensated in the other direction,

$$\text{SIN } \theta = -1 + \frac{2.462}{2.500}$$

$$\text{so, } \theta = 179.13^\circ$$

In both of the above cases, the error is equal to 0.87 degrees.

The test data compiled in Table E-7 shows that linearity of the LM324 op amps is extremely good around an equilibrium voltage. In the first five sets of data, the magnetometer inputs and the programmed inputs were all set as close as possible to the calculated inputs for the given angles. In all cases, the measured voltages at the amplifier outputs were within 10 millivolts of the actual differences of the input voltages. This relates to the fact that the bias or null voltage for amplifiers 3 and 4 is 2.500 volts and for amplifier 5 is 1.400 volts. Thus, when the inputs to each amplifier are equal, the outputs of amplifiers 4 and 5 should be 2.500 volts and of amplifier 3, 1.400 volts.

The last two sets of data points in Table E-7 were measured to show that the output would command or turn in the correct direction. It was calculated, when the circuit was designed, that a positive error signal (circuit output) commands a turn to the left and negative error signal a right turn. This is verified by the last two data sets.

### Final Circuit Design

The prototype circuit operated properly from the standpoint of the programmed angles and operation of the amplifiers. It was realized during the construction of the prototype that extremely long time constants (on the order of hours) may be required for the timer portion of the circuit. Also, from control analysis of the vehicle it was realized, from the analysis in Appendix B, that a lead-lag compensator is needed between the output of the circuit and the rudder servos. This compensator is needed to stabilize an inherently unstable heading-control loop. It was also decided to use two additional navigation legs, a total of five legs.

Timers. For accuracy in long RC time constants, large capacitors are needed with extremely low leakage. Capacitors of this type are expensive, but a way around this problem is found by using timers with short time constants (less than 10 minutes). The final timer design shown in Figure E-2, uses a time constant of one minute along with a digital counter. This design facilitates the use of switches to program the length of time of each leg instead of adjusting resistors.

The counter logic for each navigation leg is composed of:

one CD4040C, 12-stage ripple-carry binary counter (National, 1975a:  
190-192)

One four-input NOR gate (1/2 CD4002C) (National, 1975a:124-125)

Seven double-pole single throw switches

One eight-input NAND gate (MM74C30) (National, 1975a:11-13)

and one J-K flip-flop with clear and preset (1/2 74C76)

(National, 1975a:22-24)

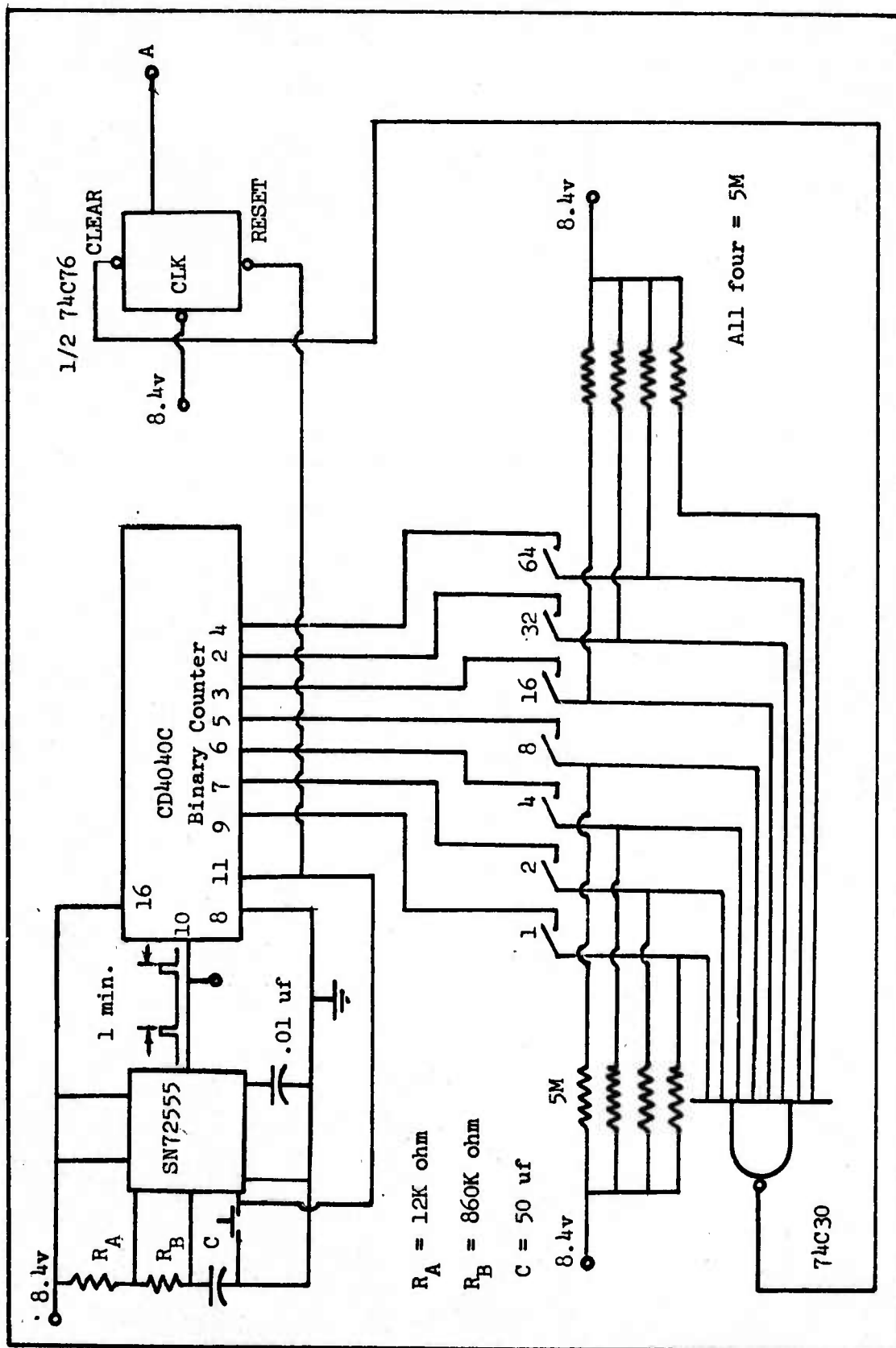


Figure E-2. Timer A for Final Circuit Design

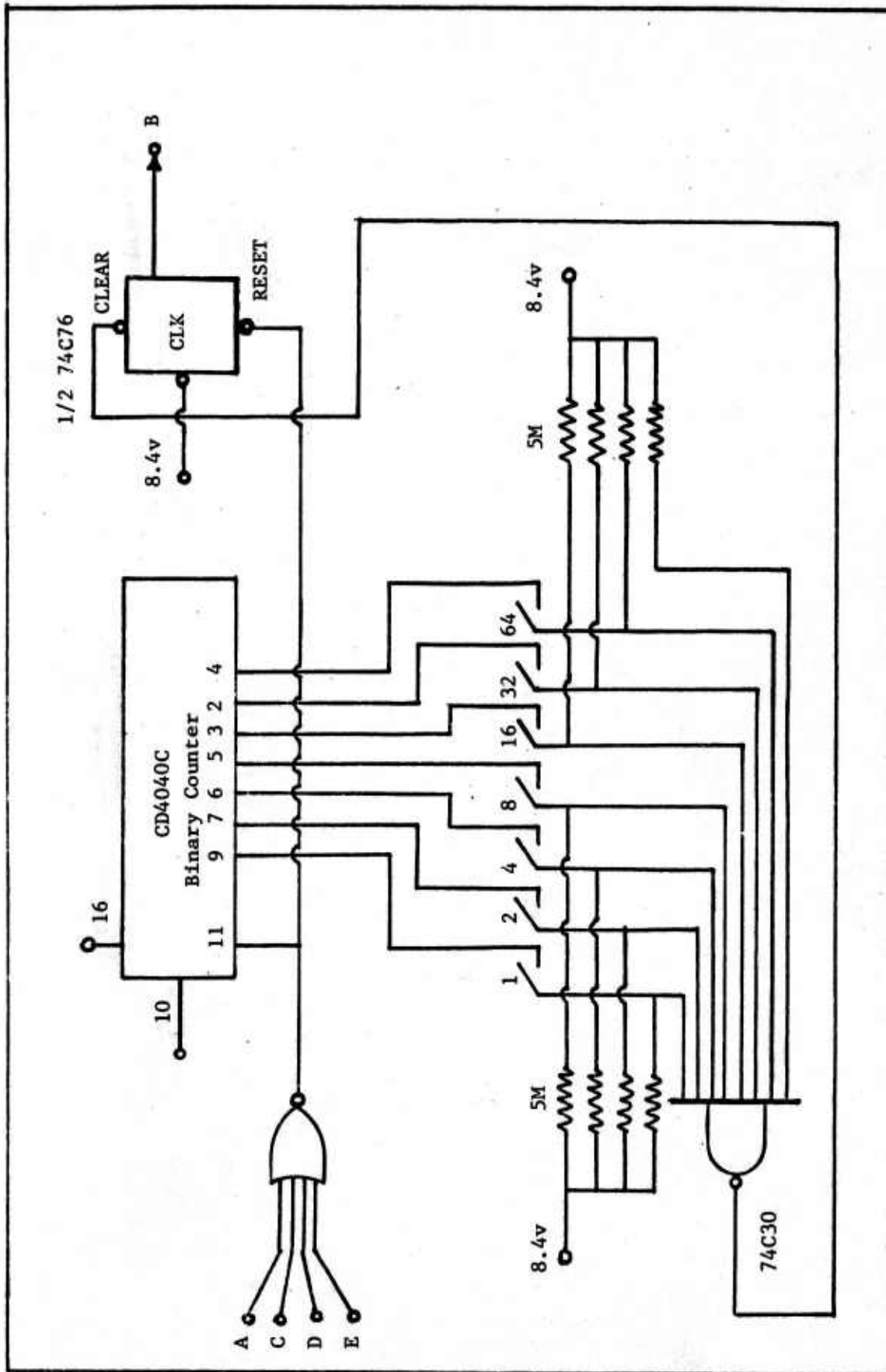


Figure E-3. Timers B through E, Navigation Circuit Final Design

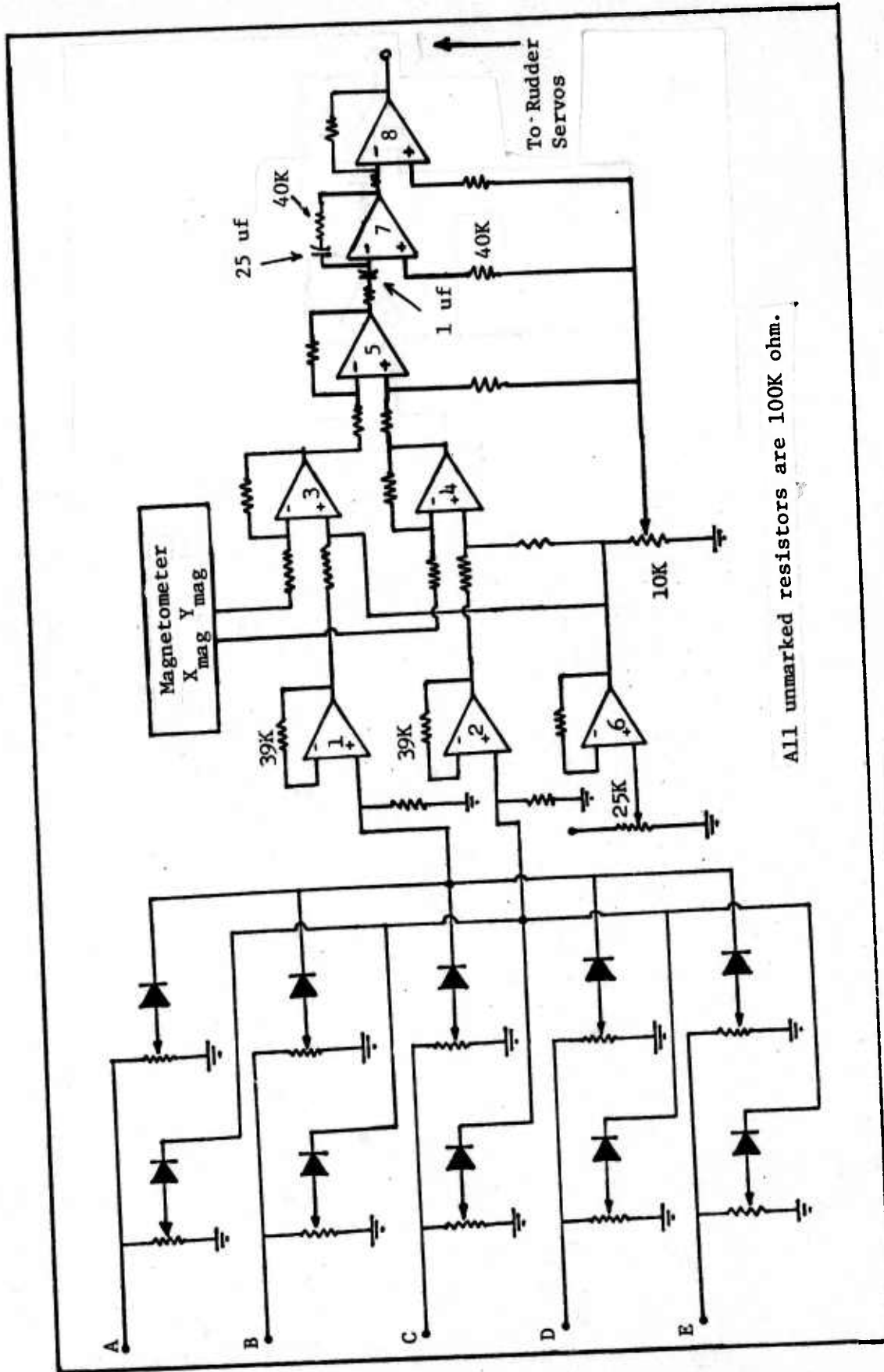


Figure E-4. Navigation Final Design

All of the counters receive an input from a single SN72555 timer with a one-minute time constant.

### Control Compensation

The amplifier circuitry used in the prototype circuit remains virtually unchanged. The only difference in the circuit is the addition of a lead-lag compensation amplifier on the output. The transfer function from the control analysis is  $\frac{0.4(s+1)}{s+10}$

The amplifier circuit needed to accomplish this transfer function is

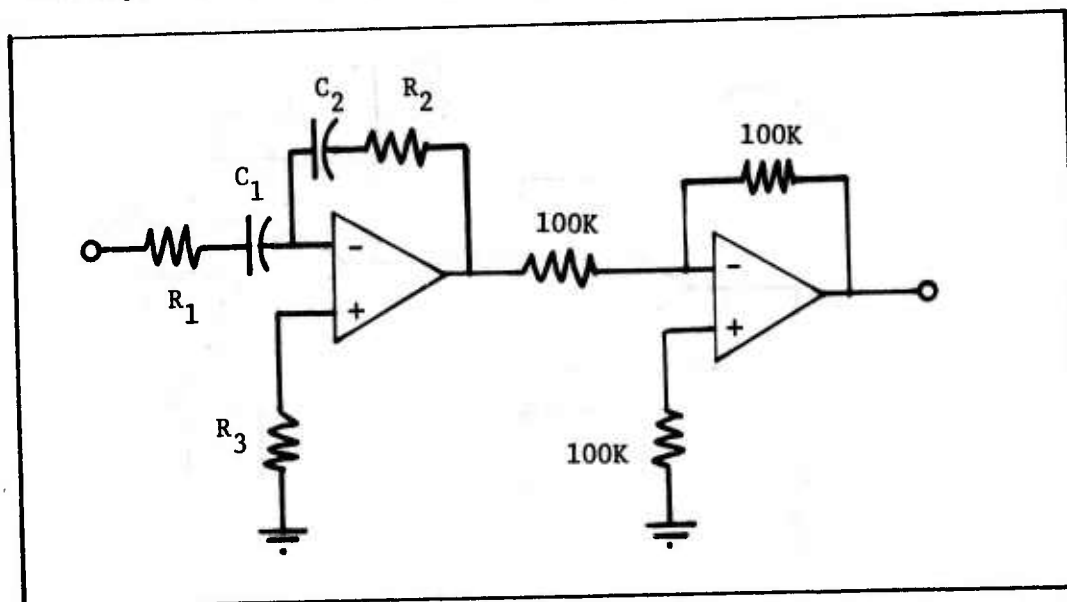


Figure E-25. Heading Control Loop Compensator

where

$$\frac{0.4(s+1)}{s+10} = - \frac{R_2 + \frac{1}{C_2 s}}{R_1 + \frac{1}{C_1 s}}$$

then solving for some reasonable component values yields:

$$C_1 = 1 \text{ uf}$$

$$R_1 = 100K \text{ ohm}$$

$$C_2 = 25 \text{ uf}$$

$$R_2 = R_3 = 40 \text{ K ohm}$$

### Testing of Final Circuit Design.

There are some significant changes in the final circuit that are not in the prototype circuit. This final circuit should be tested to make sure the circuit will operate properly and so that the accuracy of the circuit can be verified. Since the final circuit has not been built and tested, a prototype of this design should be built and tested before any production is contemplated.

Timer Testing. The timer, which uses an RC time constant, might be temperature sensitive. The accuracy of the timer circuit should be measured at 20-degree increments from 70°F down to -30°F. If the results of this test show that there is a significant error at lower temperatures, another type of timer circuit may be needed. A more expensive alternate timer circuit is a crystal-oscillator circuit with a temperature-compensated crystal. The output pulses of the oscillator, although of much higher frequency, would be counted in the same manner as the output of the R-C timer.

Timer Circuit Output. The outputs of the 74C76 flip-flops may not provide enough current to the trimmer resistors used to program the heading angles. This needs to be tested and verified. If the flip-flops do not provide enough current, a buffer stage will have to be added between the flip-flops and the trimmers. Once the timer circuit has been checked out and

is operating properly, the operation of the entire circuit with the magnetometer and servos connected should be tested.

Complete Navigation Circuit Testing. The complete circuit should be tested on a bench with all metal objects moved as far away from the magnetometer as practically possible. At least six different heading angles should be programmed into the circuit and then the magnetometer rotated based on the servo movement. The heading angles and magnetometer alignment should be recorded and analyzed.

If the test results are satisfactory, the system should be test flown. There is no substitute for the actual environment and the effects of actual flight conditions on the navigation circuit performance. Therefore, the navigation system should be installed and tested in a prototype aircraft with radio-control override. Manual intervention of the navigation system will be needed to take over in the event that the navigation system malfunctions and to land the vehicle.

The test flight should be accomplished on a range where the vehicle can be allowed to fly a distance long enough that an adequate measurement of the navigational accuracy can be made, at least 50 miles. The test should be conducted on a low or no-wind day where the data will not reflect wind errors.

Since both magnetometer inputs follow a sine relationship, the smallest change in the inputs per degree change in direction occurs at the peaks of the sine wave. The peak of the sine wave occurs when a given input is either 0.000 volts or 5.000 volts. An error in the other input at either of these two points causes the greatest error in the direction of the vehicle.

At 180 degrees, the X value is 0.000 volts and Y is 2.500 volts. An error of 10 millivolts in the Y signal at this point causes less than one-degree error. Looking only at the X values, it appears that there would be a five degree error ( $x = 0.010$  volts at 185 degrees and 175 degrees). But, the Y value is changing by 0.044 volts per degree at this point and compensates for the 10 millivolt error in less than one-degree change in heading. Thus, the circuit output has to be off by more than 44 millivolts to cause an error of one degree.

## APPENDIX E-5

### RELIABILITY

Reliability is the probability that a system will function in a specified manner for a specified period of time. For the navigation system the specified manner is to perform all functions required to command the vehicle to the desired heading. The specified period is 6 hours. The reliability  $R(6)$  is obtained by developing a model which describes reliability of the system as a function of time. The exponential failure model is frequently used to approximate the reliability of electronic systems and is given as

$$R(t) = e^{-\lambda t} \quad (E-5)$$

where  $\lambda$  is the hazard function associated with failure rate of the system. For this model  $\lambda$  is the sum of the failure rates of the individual components. For simplicity it is assumed that all parts must operate for the entire mission time. Frequently the failure information of a system is expressed as  $1/\lambda$  or the Mean Time Between Failures (MTBF). Obviously the heart of a reliability estimate is obtaining  $\lambda$ .

Because the technology used in both the dead reckoning and Omega systems is quite new, little data exists on the failure rate of any given part. Failure rates under ideal conditions are obtained for each type of part involved from Military Handbook 217-B. Unity stress is used. Environmental factors are then used to provide a more realistic estimate of the part failure rate in its expected operational environment. An environmental factor for an aircraft application would typically be 20; for a missile it would be in the range of 80. Because

of the vibration of the vehicle in flight and the high launch acceleration, an environment factor for this vehicle is expected to be in the range of 50 with bounds of 20 as low and 80 as high. Where failure data is not available on a specific part, the failure rate for a part of similar complexity is used. The failure rate for the magnetometer is estimated at one failure per year (Pierce, 1975), with bounds of one failure every half year as high, to one failure every one and a half years as low (Rose, 1975). An environmental factor of 10 is used for the magnetometer because the MTBF was already based on the operational, though less severe, environment. An estimate of the number of failures during storage is obtained using a powered to unpowered failure ratio of  $10^4$  (Davis, 1975).

Dead Reckoning

Table E-8 illustrates the failure rate results of the electronic components for a two-leg-pattern system.

TABLE E-8. FAILURE RATES FOR DEAD RECKONING ELECTRONICS

<u>Part</u>	<u>Failures Per 10<sup>6</sup> hrs</u>	<u>Environ Factor</u>	<u>Adjusted Failures Per 10<sup>6</sup> hrs</u>	<u>Number of Parts</u>	<u>Total Failures Per 10<sup>6</sup> Hours</u>
Integrated circuits	.5	20	10	5	50.0
Resistors (variable)	.026	20	.52	7	3.64
Connectors	1.	20	20	1	20
Resistors (fixed)	.16	20	3.2	21	67.2
Capacitors	.0065	20	.13	7	.91
Diodes	.015	20	.3	6	1.8
Connections	.00044	20	.0086	40	.352
TOTAL					143.902

Table E-9 summarizes the failure rate for the entire two-leg dead reckoning system.

TABLE E-9. FAILURE SUMMARY (DEAD RECKONING)

	<u>Electr. Failure 10<sup>6</sup> Hrs</u>	<u>Magneto. Failure 10<sup>6</sup> Hrs</u>	<u>Total Powered Failures Per 10<sup>6</sup> Hrs</u>	<u>Total Unpowered Failures Per 10<sup>6</sup> Hrs</u>	<u>Total Unpowered Failures Per Year</u>
Low	144	585	729	.73	.0006
Most Likely	288	878	1166	.117	.001
High	576	1756	2332	.233	.002

This is a most likely system  $\lambda$  of  $.117 \times 10^{-6}$  or an MTBF of 858 hours. From Eq (E-5) the reliability for a 6-hour mission is 0.993. The probability of the navigation system operating properly for 6 hours is 0.993. A similar reliability is expected for the 4-leg system because of only a slight increase in complexity.

Omega

The Omega system is composed of approximately 20 integrated circuits, (IC's) and 20 passive elements (Rorden, 1975), in addition to the magnetometer. A programmable read only memory (PROM) is included as being representative of a possible programming method. The passive elements are approximated by quartz crystals based on complexity considerations.

Table E-9 summarizes the failure rate for the entire two-leg dead reckoning system.

TABLE E-9. FAILURE SUMMARY (DEAD RECKONING)

	Electr. Failure 10 <sup>6</sup> Hrs	Magneto. Failure 10 <sup>6</sup> Hrs	Total Powered Failures Per 10 <sup>6</sup> Hrs	Total Unpowered Failures Per 10 <sup>6</sup> Hrs	Total Unpowered Failures Per Year
Low	144	585	729	.73	.0006
Most Likely	288	878	1166	.117	.001
High	576	1756	2332	.233	.002

This is a most likely system  $\lambda$  of  $.117 \times 10^{-6}$  or an MTBF of 858 hours. From Eq (E-5) the reliability for a 6-hour mission is 0.993. The probability of the navigation system operating properly for 6 hours is 0.993. A similar reliability is expected for the 4-leg system because of only a slight increase in complexity.

#### Omega

The Omega system is composed of approximately 20 integrated circuits, (IC's) and 20 passive elements (Rorden, 1975), in addition to the magnetometer. A programmable read only memory (PROM) is included as being representative of a possible programming method. The passive elements are approximated by quartz crystals based on complexity considerations.

TABLE E-10. FAILURE RATES FOR OMEGA

<u>Part</u>	<u>Failures Per 10<sup>6</sup> Hrs</u>	<u>Environ Factor</u>	<u>Adjusted Failures Per 10<sup>6</sup> Hrs</u>	<u>Number of Parts</u>	<u>Total Failures Per 10<sup>6</sup> Hrs</u>
IC's	.5	20	10	20	200
Passives	.2	20	4	20	80
Connections	.00044	20	.0088	100	.88
ROM	1.5	20	30	1	30
TOTAL					310.88

TABLE E-11. FAILURE SUMMARY FOR OMEGA

	<u>Electr. Failure Per 10<sup>6</sup> Hrs</u>	<u>Magneto. Failure Per 10<sup>6</sup> Hrs</u>	<u>Total Powered Failures Per 10<sup>6</sup> Hrs</u>	<u>Total Unpowered Failures Per 10<sup>6</sup> Hrs</u>	<u>Total Un-Pow'd Failures Per Yr</u>
Low	311	585	895	.09	.00078
Most Likely	622	878	1500	.15	.0013
High	1244	1756	3000	.30	.0026

The MTBF is 667 hours with a 6 hour mission reliability of 0.991.

## APPENDIX E-6

### ACCURACY

A dead-reckoning error analysis is performed to obtain the proper navigation error models for the Program EFFECT simulation, which is to determine downtime. The procedure followed in this section is to identify the source of the errors, quantify the effect of the errors, and place the error in a form which can be approximated in the computer program. For Omega and Loran, a summary of the navigational accuracies is presented at the end of this appendix based on the referenced investigations.

#### Dead Reckoning

The accuracy of the dead-reckoning system is dependent on two major types of errors, those due to winds, and those inherent in the navigation system.

Wind. If the response time of the vehicle to sudden changes in attitude is short, the navigation error due to winds can be modeled as a force acting on a point mass. If the force does not change rapidly, the vehicle soon acquires the additional velocity vector of the wind. The navigation error due to winds,  $E$ , is  $E = \int_0^t W(t) dt$  where  $W(t)$  is the wind velocity vector. The error  $E$  can be reduced by correcting the heading of the vehicle to account for the expected wind. If  $P(t)$  is the predicted wind velocity, the navigation error after the heading adjustment is

$$E_p = \int_0^t (W(t) - P(t)) dt.$$

The model for prediction error,  $(W(t) - P(t))$  developed in Appendix E-3, is used in the computer program EFFECT. It is assumed that the prediction error remains constant throughout each simulation. Using this assumption, an estimate of the circular error probable (CEP) due to wind error is made in Appendix E-7.

Non-Wind Errors. As discussed in Appendix E, the navigation circuitry sends an electrical signal to the rudder servo to force the error to zero, or

$$E = (X - X_{\text{mag}}) - (Y - Y_{\text{mag}}) = 0 \quad (\text{E-1})$$

where  $X$  is the programmed voltage related to the component of the geomagnetic field along the vehicle X axis,

$X_{\text{mag}}$  is the measured voltage from the magnetometer related to the component of the geomagnetic field along the vehicle X axis.

$Y$  is the programmed voltage related to the component of the programmed voltage related to the component of the geomagnetic field in the vehicle Y axis.

and  $Y_{\text{mag}}$  is the measured voltage from the magnetometer related to the component of the geomagnetic field in the vehicle Y axis.

The desired relationship between heading,  $\theta$ , and the X and Y values is illustrated in Figure E-26.

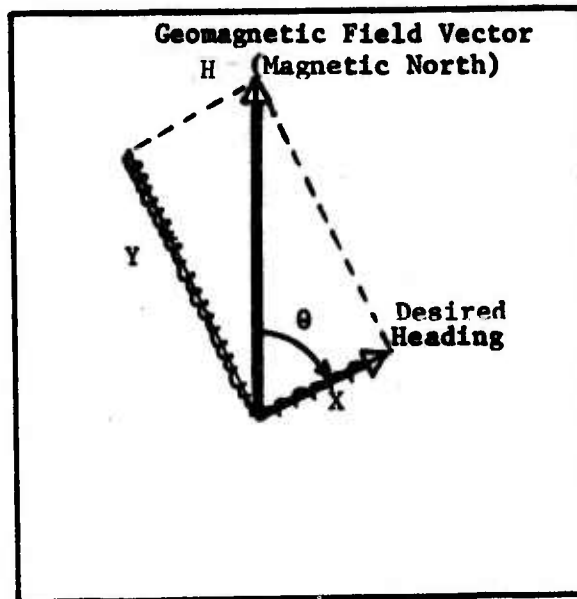


Figure E-26. Relation of Desired Heading  $\theta$  to Preset Values of X and Y

H is the estimated horizontal component of the geomagnetic field vector, which points to magnetic north subject to the declination shown in Figure E-27. However, the navigation system may see a different set of values due to several types of errors. This is shown in Figure E-28.

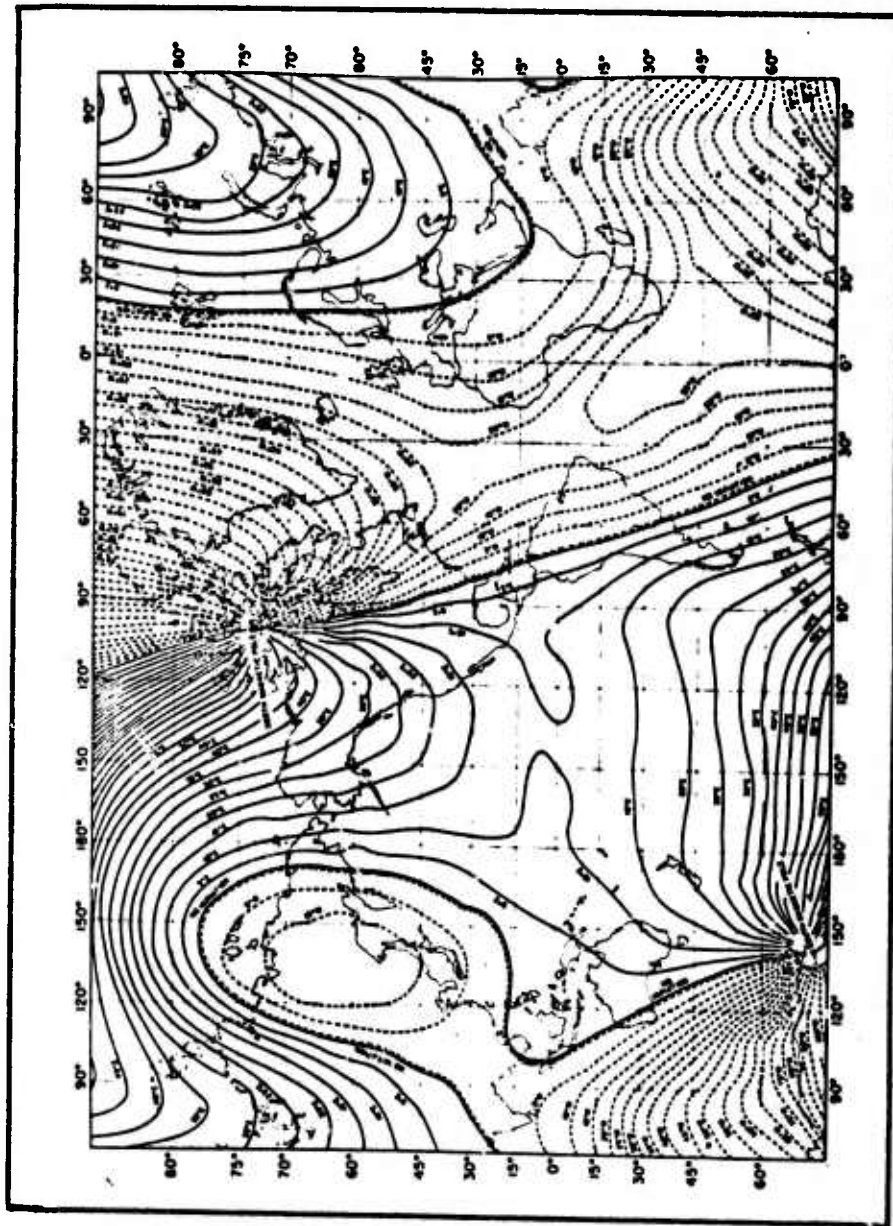


Figure E-27. World Magnetic Chart of Surface Field Declination (Matsushita, 1967:192)

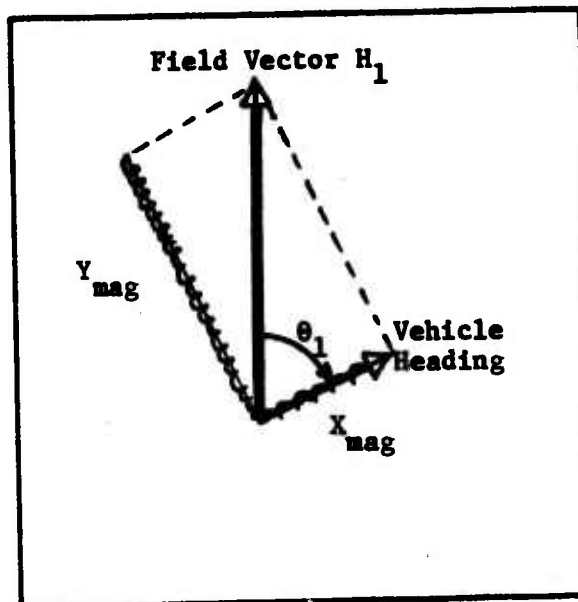


Figure E-28. Values Seen by the Navigation System

where

$$X_{mag} = H_1 \cos \theta$$

$$Y_{mag} = H_1 \sin \theta$$

Some additional explanation of the above terms is in order.

H is the estimated value of the horizontal component of the geomagnetic field at the launch site. This value and the desired vehicle heading,  $\theta$ , (corrected for winds) are used to determine the X and Y values, programmed into the navigation panel.

$H_1$  is the field vector seen by the magnetometers. It may differ from H because of a decrease in the horizontal

field intensity, or because the vehicle is not flying straight and level.  $H_1$  may be either larger or smaller than  $H$  depending on the dip angle of the field vector and the vehicle orientation. A worse case results when  $H_1$  is always considered less than  $H$ . In this way, change in vehicle orientation to a larger  $H_1$  does not cancel some of the error involved with a smaller  $H_1$ .

$\theta_1$  is not necessarily a real value. Rather, it is that value which satisfies Eq (E-9).  $\theta_1$  results when the vehicle changes heading to accommodate an incorrect balance in the programmed and measured field values. When the attitude of the vehicle is not far from straight and level,  $\theta_1$  is a good approximation of the actual heading of the vehicle. For this reason, the error in heading is approximated as  $\theta_1 - \theta$ . For this portion of the analysis, all errors are in degrees from the desired heading,  $\theta$ .

To determine the magnitude of the heading error, Eq (E-1) is rewritten as

$$E = (H \cos \theta - H_1 \cos \theta_1) - (H \sin \theta - H_1 \sin \theta_1) = 0 \quad (E-9)$$

Certain errors are associated with each of these terms. They are the programming error of  $H \cos \theta$  and  $H \sin \theta$ , magnetometer production variance, differences between  $H$  and  $H_1$  and processing errors due to part tolerances.

The use of a digital voltmeter, accurate to one millivolt, programs X and Y to one degree or less. This is illustrated in Appendix E-9 for a field intensity having a maximum magnetometer reading of 2.5 volts. An error in the magnetometer measurements due to manufacturing variance is given by manufacturing specification sheets as  $\pm 1.0$  degrees (Develco, 1975a). The part tolerance error in the processing circuitry gives an error less than 1 degree as discussed in Appendix E-4.

To determine the heading error from the change in the horizontal field component, the difference between H and  $H_1$  due to a location change, is considered.

For the European theatre, for example, the horizontal field intensity, shown in Figure E-29, has almost no change in the east-west direction. In the north-south direction, the change is 0.05 gauss over 800 miles (see Figure E-29). At the center of the continent, a 3% change exists over a north-south distance of 100 miles. As noted earlier, the navigation system will attempt to maneuver the vehicle such that

$$E = H \cos \theta - H_1 \cos \theta_1 - (H \sin \theta_1 - H_1 \sin \theta_1) = 0 \quad (E-9)$$

The maximum error occurs at  $\theta = 0$  degrees since the maximum difference between  $H_1$  and H is detected by aligning X with  $H_1$  which reduces Eq (E-9) to

$$E = H - H_1 \cos \theta - (0 - H_1 \sin \theta_1) = 0$$

Dividing by H gives

$$1 - \frac{H_1}{H} \cos \theta_1 + \frac{H_1}{H} \sin \theta = 0 \quad (E-10)$$

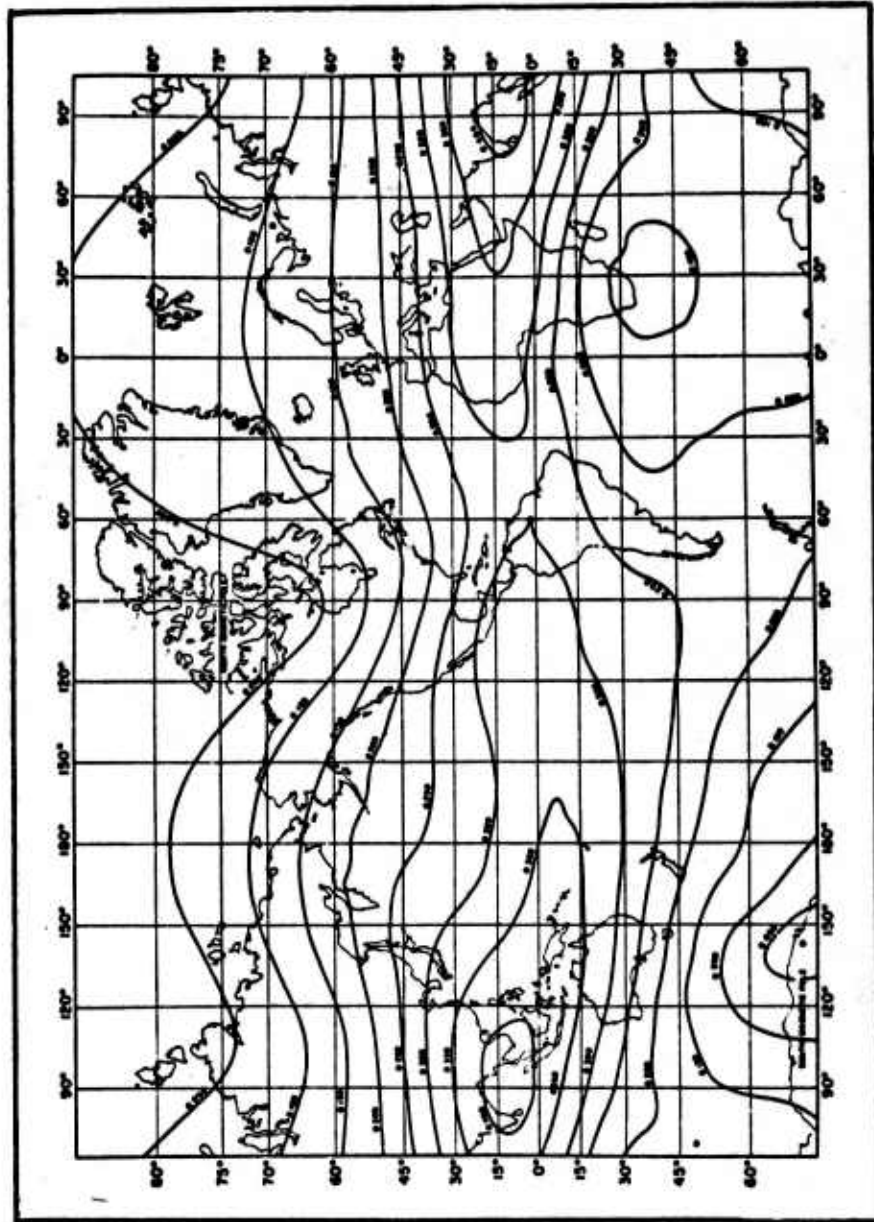


Figure E-29. World Magnetic Chart of Horizontal Field Intensity  
(Matsumita, 1967:193)

Since the maximum change in the horizontal field vector,  $H_1$ , is 3% over 100 miles,  $H_1/H = 0.97$ . Therefore,  $\theta_1 = 1.7$  degrees. Thus, for this particular scenario, the maximum error in heading due to changes in the field intensity is 1.7 degrees.

The second error associated with  $H_1$  occurs when the plane of the magnetometers does not correspond to the local horizontal. This may occur when the vehicle is in a climb, dive, or bank. Let the largest angle between the horizontal and the plane of the magnetometers be defined as the aircraft attitude angle,  $\phi$ . Assume that there is no change in the horizontal field intensity. If the vehicle is in a climb, the value of the field vector,  $H_1$ , read by the magnetometers, is actually  $H \cos \phi$  since only the component of the field vector  $H$  projected onto the plane of the magnetometers is read. Eq (E-9) now becomes

$$E = H \cos \theta - H \cos \phi \cos \theta_1 - H \sin \theta + H \cos \phi \cos \theta_1 \quad (E-11)$$

Again, the maximum error occurs at  $\theta = 0$  reducing Eq (E-11) to

$$E = H - H \cos \phi \cos \theta_1 + H \cos 0 \cos \theta_1 = 0 \quad (E-12)$$

And dividing by  $H \cos \phi$

$$\cos \theta_1 - \sin \theta_1 = \frac{1}{\cos \phi} \quad (E-13)$$

Eq (E-13) shows the relationship between aircraft attitude angle and the maximum heading error due to an incorrect measurement of  $H$ . The solution to Eq (E-13) is given in Figure E-30, as a function of aircraft attitude angle,  $\phi$ . The same results are obtained if the vehicle is heading  $\theta = 90$  degrees in a bank.

Having quantified the individual errors, an estimate of the error expected for the entire mission is formed. Two assumptions

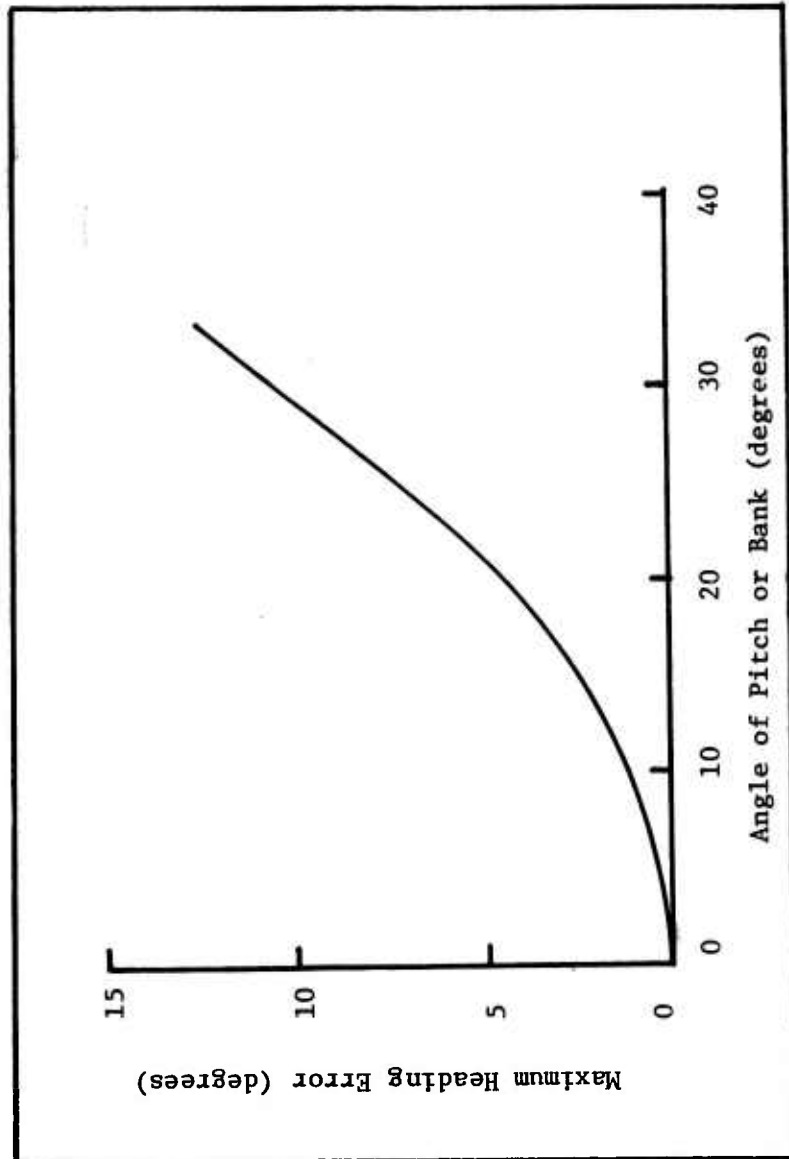


Figure E-30. Heading Error Due to Non-Horizontal Attitude

are now made; the individual errors are independent, and the total error of the system is a linear combination of the individual errors. The error for the system is expressed as

$$\begin{aligned} \text{Error (degrees)} = & \text{programming error} + \text{processing error} + \\ & \text{production error} + \text{horizontal field intensity} \\ & \text{error} + \text{vehicle attitude error} \end{aligned} \quad (\text{E-14})$$

Worst case errors for the first three errors are obtained directly from the above discussion. The vehicle attitude error, the error in heading due to a vehicle not flying straight and level, requires more definition. Three types of attitudes are considered: initial climb, pattern turns, and cruise oscillations.

The angle of climb is not expected to exceed 30 degrees. From Figure E-30, this corresponds to a 10-degree heading error during the 15-minute climb phase. The airframe characteristics of Appendix A indicate that about 30 seconds are required to make a 180-degree turn. If the turn is coordinated, the angle of bank  $\gamma$  is (Kershner, 1968)

$$\text{TAN } \gamma = \frac{2\pi V}{gt} \quad (\text{E-15})$$

where  $t$  is the time to make a 360° turn. Therefore,

$$\text{TAN } \gamma = \frac{2\pi \cdot 110 \text{ fps}}{(32.2)(60)} = 0.3577$$

or

$$\gamma = 19.68 \text{ deg}$$

From Figure E-30, the maximum heading error due to a 20-degree bank is 3 degrees. The actual angle of bank is less than 20 degrees because a slipping turn is used. Even though a stable airframe

is anticipated, flight characteristics, such as phugoid or dutch roll, still create a non-zero aircraft attitudes, pitch or bank angles. The extent of these oscillations is estimated somewhat arbitrarily at one half of the climb angle or 15 degrees. Maximum heading error associated with normal cruise is, then, 2 degrees.

An estimate of the heading error due to the non-horizontal attitude of the vehicle is the summation of the fraction of flight time in the attitude times the error associated with that attitude. Thus, for the navigation phase, if climbing is 25% of the flight time, and cruise is the other 75% the heading error from launch until arriving at the loiter area is new time  $0.25 (10 \text{ deg}) + 0.75 (2 \text{ deg}) = 4 \text{ deg}$  heading error.

Similarly, the heading error during the loiter phase depends on the amount of time spent in turns compared to cruise. The turns are expected to take about 30 seconds while 10 minutes are expected for each pattern leg. Therefore, the heading error is

$$\begin{aligned} & (\text{percent spent in turns})(\text{error in turn}) + (\text{percent spent in} \\ & \text{cruise}) (\text{error in cruise}) \\ & = 0.05 (3) + 0.95 (2) = 2.05 \text{ deg} \end{aligned}$$

The non-wind errors from Eq (E-14) are summarized below.

TABLE E-12. SUMMARY OF ERRORS

ERROR SOURCE	NAVIGATION (DEG)	STATIONKEEPING (DEG)
Magnetometer Manufacture	1.0	1.0
Programming	1.0	1.0
Processing	1.0	1.0
Horizontal Field	1.7	1.7
Vehicle Attitude	<u>4.0</u>	<u>2.05</u>
TOTAL	8.7	6.75

is anticipated, flight characteristics, such as phugoid or dutch roll, still create a non-zero aircraft attitudes, pitch or bank angles. The extent of these oscillations is estimated somewhat arbitrarily at one half of the climb angle or 15 degrees. Maximum heading error associated with normal cruise is, then, 2 degrees.

An estimate of the heading error due to the non-horizontal attitude of the vehicle is the summation of the fraction of flight time in the attitude times the error associated with that attitude. Thus, for the navigation phase, if climbing is 25% of the flight time, and cruise is the other 75% the heading error from launch until arriving at the loiter area is new time  $0.25 (10 \text{ deg}) + 0.75 (2 \text{ deg}) = 4 \text{ deg heading error}$ .

Similarly, the heading error during the loiter phase depends on the amount of time spent in turns compared to cruise. The turns are expected to take about 30 seconds while 10 minutes are expected for each pattern leg. Therefore, the heading error is

$$\begin{aligned} & (\text{percent spent in turns})(\text{error in turn}) + (\text{percent spent in} \\ & \text{cruise}) (\text{error in cruise}) \\ & = 0.05 (3) + 0.95 (2) = 2.05 \text{ deg} \end{aligned}$$

The non-wind errors from Eq (E-14) are summarized below.

TABLE E-12. SUMMARY OF ERRORS

ERROR SOURCE	NAVIGATION (DEG)	STATIONKEEPING (DEG)
Magnetometer Manufacture	1.0	1.0
Programming	1.0	1.0
Processing	1.0	1.0
Horizontal Field	1.7	1.7
Vehicle Attitude	<u>4.0</u>	<u>2.05</u>
TOTAL	8.7	6.75

### Omega

Navigation errors with the Omega system fall into three classes: phase-resolution error, diurnal-propagation error, and sudden ionospheric disturbances. The phase-resolution error, basically noise, has been demonstrated to be 1.5 miles (rms) (Enright, 1969:199). The diurnal-propagation errors occur because the height at which the skywave is reflected from the ionosphere changes from day to night. This change shifts the zero-phase point of the interference pattern up to 11 or 12 miles (Beukers, 1973:81). The time of these shifts is determined from the locations of the Omega stations being used. The diurnal-shift effects on the vehicle are reduced by not launching when a shift is to occur, or by launching a vehicle such that it is shifted into an appropriate area. The sudden ionospheric changes create the same effects as the diurnal-propagation changes but are not predictable.

Both types of propagation errors can be corrected, but it involves a significantly more complex processor, resulting in a more expensive system than acceptable. Even with the above corrections, the vehicle will only be known to stay somewhere within an 11-mile box formed by the intersection of two frequency lanes.

Loran. Numerous tests have shown Loran C is accurate to less than one-half mile (Yonezawa, 1969:67).

## APPENDIX E-7

### CEP ANALYSIS OF DEAD RECKONING

Although a CEP analysis is not sufficient to make a system selection decision, it does provide an analytic tool to identify the major trends expected, major breakpoints, and approximate sensitivity estimates. This analysis is designed to estimate only the effects of wind. The following assumptions are made. For purposes of this appendix only the measure of effectiveness is the time spent over the target area. The target area is a circle with the vehicle starting at its center. The only error in the system is a constant wind-prediction error discussed in Appendix E-2, which is assumed to have normal distribution.

Since a normal distribution is assumed standard normal tables give the probability of a particular speed error. Since a circle is used, direction error does not make any difference. The displacement ( $r$ ) of the vehicle is the prediction error in speed multiplied by time or

$$r(t) = (W(t_1) - P(t_1))(t) \quad (E-6)$$

The diagonal lines on Figure E-31 are values of  $r$  calculated for different probabilities. The probabilities are related to the speed error through the normal distribution, e.g., the mean wind speed is 2.19 m/sec which has the probability of 0.5. Plotting several constant probability lines produces Figure E-31 .

By choosing a target-area radius  $r$ , the probability that the vehicle is still within the distance  $r$  of the center is obtained. Selecting  $r = 20$  miles results in Figure E-32.

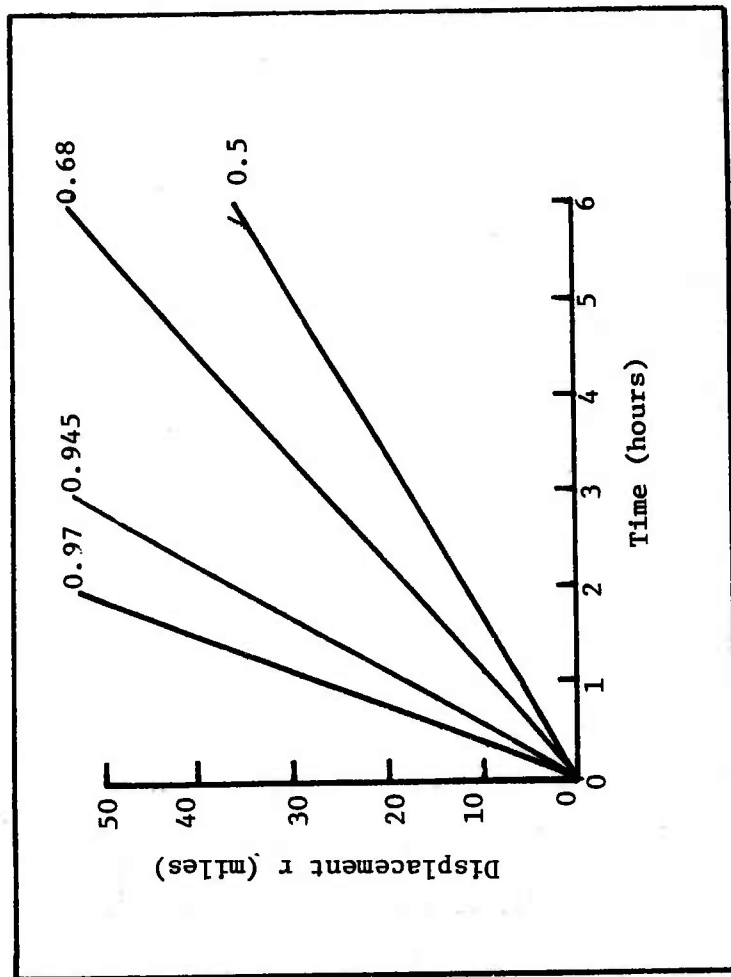


Figure E-31. Probability of Displacement as a Function of Time and Distance

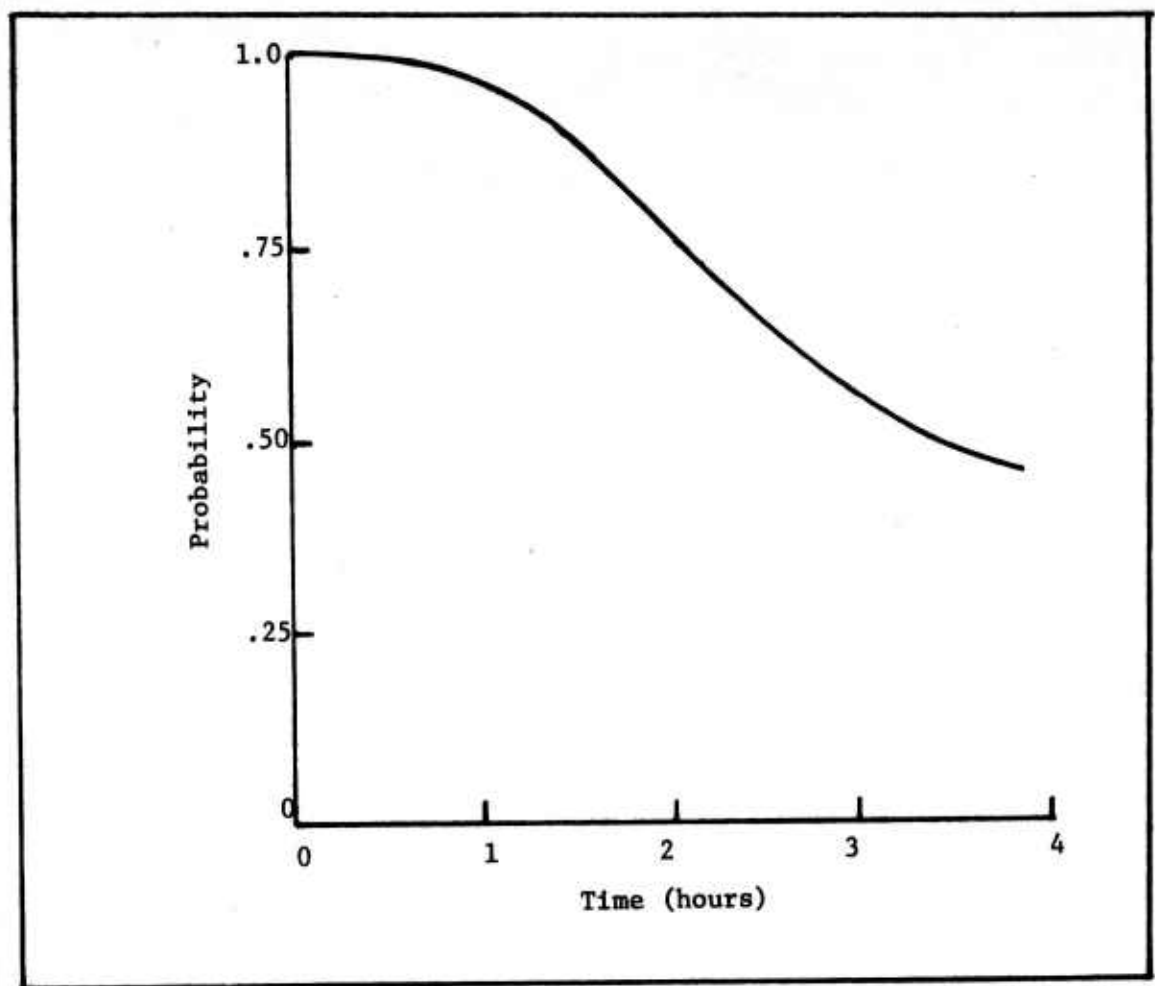


Figure E-32. Probability of Error Less Than  $r$  Versus Time

The changes in better wind prediction are simply illustrated. If the prediction-error variance is increased by a factor of two,  $\sigma$  changes by  $\sqrt{2}$ . This serves merely as a scaling factor to the ordinate of Figure E-31. Appropriate changes are then made in Figure E-31.

This graph is used to compare the dead-reckoning system with the Omega system which is assumed to be able to stay within the target area regardless of the wind. The ratio of the costs of the dead reckoning over Omega is  $\frac{1327}{1400} = 0.947$  (Appendix E). When the probability in Figure E-32 drops below 0.947, the Omega is more cost effective past time  $\tau$ . Thus, Omega is expected to become more cost effective sometime after the vehicle passes a useful life of 2 hours. This, of

course, is only a simple estimate and simulation is done to provide a more accurate result (Chapter IV, Volume II).

It is important to compare the results of this effectiveness measure with the results using the system effectiveness measure of downtime. This appendix indicates that Omega is more cost effective when the expected life of the vehicle is greater than 2 hours. However, this CEP analysis ignored the targeting of many vehicles over the target area. As one vehicle is blown from the area another vehicle may well take its place in creating downtime. The CEP analysis shows that as the expected life of the vehicle increases, an Omega navigation system becomes more cost effective.

APPENDIX E-8

LAUNCH CONTROL CONDITIONS

It is possible that, during launch, the programmed heading is significantly different than the direction of the launcher. As the vehicle is launched, significant rudder commands are given placing unexpected side-forces on the launcher or causing a decrease in altitude immediately after clearing the rail. Rather than trying to determine launch stability under these conditions, a small fix is recommended. Since the vehicle normally attempts to climb, no elevator change is required. A reset timer, inserted in series, commands a given voltage to the rudder maintaining the rudder in a neutral position for several seconds following the power-up of the navigation system. This allows the vehicle to climb to a altitude higher than ten feet above ground level (AGL) before attempting a turn. The simplest approach uses a flip-flop, a bi-stable timer, one resistor to get the appropriate null voltage to the servos, and two resistors and a capacitor to set the time constant on the timer. The actual values are calculated using the same techniques as the leg timers of the DR system. A thirty second pulse of 2.4 volts will null the servo long enough for the launch operations to be completed. If the launch is delayed, a reset switch starts another thirty second pulse.



APPENDIX E-9-2. Computed Outputs

ANGLE IN DEGREES	X OUTPUT IN VOLTS	Y OUTPUT IN VOLTS
1	5.000	2.544
2	4.998	2.587
3	4.997	2.631
4	4.994	2.674
5	4.990	2.718
6	4.986	2.761
7	4.981	2.805
8	4.976	2.848
9	4.969	2.891
10	4.962	2.934
11	4.954	2.977
12	4.945	3.020
13	4.936	3.062
14	4.926	3.105
15	4.915	3.147
16	4.903	3.189
17	4.891	3.231
18	4.878	3.273
19	4.864	3.314
20	4.849	3.355
21	4.834	3.396
22	4.818	3.437
23	4.801	3.477
24	4.784	3.517
25	4.766	3.557
26	4.747	3.596
27	4.728	3.635
28	4.707	3.674
29	4.687	3.712
30	4.665	3.750
31	4.643	3.788
32	4.620	3.825
33	4.597	3.862
34	4.573	3.898
35	4.548	3.934
36	4.523	3.969
37	4.497	4.005
38	4.470	4.039
39	4.443	4.073
40	4.415	4.107
41	4.387	4.140
42	4.358	4.173
43	4.328	4.205
44	4.298	4.237
45	4.268	4.268
46	4.237	4.298
47	4.205	4.328
48	4.173	4.358

ANGLE IN DEGREES	X OUTPUT IN VOLTS	Y OUTPUT IN VOLTS
49	4.140	4.387
50	4.107	4.415
51	4.073	4.443
52	4.039	4.470
53	4.005	4.497
54	3.969	4.523
55	3.934	4.548
56	3.898	4.573
57	3.862	4.597
58	3.825	4.620
59	3.788	4.643
60	3.750	4.665
61	3.712	4.687
62	3.674	4.707
63	3.635	4.728
64	3.596	4.747
65	3.557	4.766
66	3.517	4.784
67	3.477	4.801
68	3.437	4.818
69	3.396	4.834
70	3.355	4.849
71	3.314	4.864
72	3.273	4.878
73	3.231	4.891
74	3.189	4.903
75	3.147	4.915
76	3.105	4.926
77	3.062	4.936
78	3.020	4.945
79	2.977	4.954
80	2.934	4.962
81	2.891	4.969
82	2.848	4.976
83	2.805	4.981
84	2.761	4.986
85	2.718	4.990
86	2.674	4.994
87	2.631	4.997
88	2.587	4.998
89	2.544	5.000
90	2.500	5.000
91	2.456	5.000
92	2.413	4.998
93	2.369	4.997
94	2.326	4.994
95	2.282	4.990
96	2.239	4.986

ANGLE IN DEGREES	X OUTPUT IN VOLTS	Y OUTPUT IN VOLTS
97	2.195	4.981
98	2.152	4.976
99	2.109	4.969
100	2.066	4.962
101	2.023	4.954
102	1.980	4.945
103	1.938	4.936
104	1.895	4.926
105	1.853	4.915
106	1.811	4.903
107	1.769	4.891
108	1.727	4.878
109	1.686	4.864
110	1.645	4.849
111	1.604	4.834
112	1.563	4.818
113	1.523	4.801
114	1.483	4.784
115	1.443	4.766
116	1.404	4.747
117	1.365	4.728
118	1.326	4.707
119	1.288	4.687
120	1.250	4.665
121	1.212	4.643
122	1.175	4.620
123	1.138	4.597
124	1.102	4.573
125	1.066	4.548
126	1.031	4.523
127	.995	4.497
128	.961	4.470
129	.927	4.443
130	.893	4.415
131	.860	4.387
132	.827	4.358
133	.795	4.328
134	.763	4.298
135	.732	4.268
136	.702	4.237
137	.672	4.205
138	.642	4.173
139	.613	4.140
140	.585	4.107
141	.557	4.073
142	.530	4.039
143	.503	4.005
144	.477	3.969

ANGLE IN DEGREES	X OUTPUT IN VOLTS	Y OUTPUT IN VOLTS
145	.452	3.934
146	.427	3.898
147	.403	3.862
148	.380	3.825
149	.357	3.788
150	.335	3.750
151	.313	3.712
152	.293	3.674
153	.272	3.635
154	.253	3.596
155	.234	3.557
156	.216	3.517
157	.199	3.477
158	.182	3.437
159	.166	3.396
160	.151	3.355
161	.136	3.314
162	.122	3.273
163	.109	3.231
164	.097	3.189
165	.085	3.147
166	.074	3.105
167	.064	3.062
168	.055	3.020
169	.046	2.977
170	.038	2.934
171	.031	2.891
172	.024	2.848
173	.019	2.805
174	.014	2.761
175	.010	2.718
176	.006	2.674
177	.003	2.631
178	.002	2.587
179	.000	2.544
180	0.000	2.500
181	.000	2.456
182	.002	2.413
183	.003	2.369
184	.006	2.326
185	.010	2.282
186	.014	2.239
187	.019	2.195
188	.024	2.152
189	.031	2.109
190	.038	2.066
191	.046	2.023
192	.055	1.980

ANGLE IN DEGREES	X OUTPUT IN VOLTS	Y OUTPUT IN VOLTS
193	.064	1.938
194	.074	1.895
195	.085	1.853
196	.097	1.811
197	.109	1.769
198	.122	1.727
199	.136	1.686
200	.151	1.645
201	.166	1.604
202	.182	1.563
203	.199	1.523
204	.216	1.483
205	.234	1.443
206	.253	1.404
207	.272	1.365
208	.293	1.326
209	.313	1.288
210	.335	1.250
211	.357	1.212
212	.380	1.175
213	.403	1.138
214	.427	1.102
215	.452	1.066
216	.477	1.031
217	.503	.995
218	.530	.961
219	.557	.927
220	.585	.893
221	.613	.860
222	.642	.827
223	.672	.795
224	.702	.763
225	.732	.732
226	.763	.702
227	.795	.672
228	.827	.642
229	.860	.613
230	.893	.585
231	.927	.557
232	.961	.530
233	.995	.503
234	1.031	.477
235	1.066	.452
236	1.102	.427
237	1.138	.403
238	1.175	.380
239	1.212	.357
240	1.250	.335

ANGLE IN DEGREES	X OUTPUT IN VOLTS	Y OUTPUT IN VOLTS
241	1.288	.313
242	1.326	.293
243	1.365	.272
244	1.404	.253
245	1.443	.234
246	1.483	.216
247	1.523	.199
248	1.563	.182
249	1.604	.166
250	1.645	.151
251	1.686	.136
252	1.727	.122
253	1.769	.109
254	1.811	.097
255	1.853	.085
256	1.895	.074
257	1.938	.064
258	1.980	.055
259	2.023	.046
260	2.066	.038
261	2.109	.031
262	2.152	.024
263	2.195	.019
264	2.239	.014
265	2.282	.010
266	2.326	.006
267	2.369	.003
268	2.413	.002
269	2.456	.000
270	2.500	0.000
271	2.544	.000
272	2.587	.002
273	2.631	.003
274	2.674	.006
275	2.718	.010
276	2.761	.014
277	2.805	.019
278	2.848	.024
279	2.891	.031
280	2.934	.038
281	2.977	.046
282	3.020	.055
283	3.062	.064
284	3.105	.074
285	3.147	.085
286	3.189	.097
287	3.231	.109
288	3.273	.122

ANGLE IN DEGREES	X OUTPUT IN VOLTS	Y OUTPUT IN VOLTS
289	3.314	.136
290	3.355	.151
291	3.396	.166
292	3.437	.182
293	3.477	.199
294	3.517	.216
295	3.557	.234
296	3.596	.253
297	3.635	.272
298	3.674	.293
299	3.712	.313
300	3.750	.335
301	3.788	.357
302	3.825	.380
303	3.862	.403
304	3.898	.427
305	3.934	.452
306	3.969	.477
307	4.005	.503
308	4.039	.530
309	4.073	.557
310	4.107	.585
311	4.140	.613
312	4.173	.642
313	4.205	.672
314	4.237	.702
315	4.268	.732
316	4.298	.763
317	4.328	.795
318	4.358	.827
319	4.387	.860
320	4.415	.893
321	4.443	.927
322	4.470	.961
323	4.497	.995
324	4.523	1.031
325	4.548	1.066
326	4.573	1.102
327	4.597	1.138
328	4.620	1.175
329	4.643	1.212
330	4.665	1.250
331	4.687	1.288
332	4.707	1.326
333	4.728	1.365
334	4.747	1.404
335	4.766	1.443
336	4.784	1.483

ANGLE IN DEGREES	X OUTPUT IN VOLTS	Y OUTPUT IN VOLTS
337	4.801	1.523
338	4.818	1.563
339	4.834	1.604
340	4.849	1.645
341	4.864	1.686
342	4.878	1.727
343	4.891	1.769
344	4.903	1.811
345	4.915	1.853
346	4.926	1.895
347	4.936	1.938
348	4.945	1.980
349	4.954	2.023
350	4.962	2.066
351	4.969	2.109
352	4.976	2.152
353	4.981	2.195
354	4.986	2.239
355	4.990	2.282
356	4.994	2.326
357	4.997	2.369
358	4.998	2.413
359	5.000	2.456
360	5.000	2.500

APPENDIX F

LAUNCHER

APPENDIX F  
THE LAUNCHER

Introduction

The purpose of this analysis is to select and design a launcher capable of launching the drone from an unprepared area. Several general requirements and guidelines are specified for this effort. These include: aircraft weight of 80 to 150 pounds, minimum launch speed of 50 miles per hour, and minimum launch rate of twelve vehicles per hour. The minimum longitudinal launch load for the proposed vehicle is assumed to be 6 g's.

Two of the more common methods for launching drones and RPV's are the use of the vehicle engine to accelerate it during a ground roll, and the use of a detachable rocket motor to ballistically boost the vehicle into the air without a launch rail. The first is inappropriate because it requires a prepared area in excess of 200 feet. The second requires a rocket motor of high precision and quality to insure aircraft control during launch. This type motor is unacceptable due to its high cost. However, this does not rule out a simple, inexpensive rocket motor used in conjunction with a rail and shuttle. In this application, the rocket would only be used to accelerate the vehicle.

In considering the requirement to launch from unprepared areas, a catapult-type launcher is chosen. Several methods of energy storage are available or are under development. These include compressed air, steam, rubber, nylon cable, and steel springs.

The energy storage elements chosen for investigation in this

study are the inexpensive rocket, rubber, and steel extension springs. Steam and compressed air are eliminated from consideration because of the high cost of providing either of these working fluids at remote sites. The Navy is working on the design and development of a pneumatic launcher utilizing fire hoses and compressed air, which are normally available aboard ship. Also, another pneumatic launcher is commercially available in the \$50,000 price range (Bowen, 1975).

#### Approach

Minimum cost per vehicle launched is used as the criterion for choosing between launchers with adequate performance. With this criterion in mind, the rocket is investigated first. The minimum cost per launch for a rocket system must exceed the cost of the expendable rocket motor. Once the cost of the rocket motor is known, the preliminary design of launchers using other energy elements can be developed provided that their estimated costs do not exceed that of the rocket motor. If one of the other systems can operate at a cost-per-shot below that of the rocket motor, it would be more desirable.

In developing the design of the launcher, a survey of existing launchers was conducted to consider the most sensible designs for application to these requirements. Sizing of the launcher is required so that design of the energy elements can be made. A structural analysis of the launcher is then done to show the feasibility of the launcher configuration. The cost of the launcher and the estimated cost per launch are estimated.

### The Rocket Motor

Since cost per launch is the decision criterion, the most inexpensive rocket motor is desired. A nozzleless rocket motor was suggested, and a preliminary design completed to arrive at an estimated cost. The estimated cost for buys of 10,000 to 15,000 is \$35 with a minimum of \$24 and a maximum of \$52.50 (Koury, 1975). The rocket motor considered here will only supply thrust to the vehicle; a launch rail will also be required for guidance until flying speed is reached and the rocket thrust is estimated. However, only the expendable rocket motor cost is considered for now, and the low estimate of \$24 is used as the benchmark.

### Sizing of Catapult

When rubber or extension springs are used as the energy storage element, the force exerted on the shuttle as it moves is not a constant. For this study the force is considered to be a linear function of the distance traveled.

$$F(x) = FI(1 - \frac{b}{L} x) \quad (F-1)$$

where FI = initial force on shuttle (lbs)

b = 1 - (final force/initial force)

x = distance traveled (ft)

L = total distance force applied

The work done by this force is also a linear function of distance traveled.

$$\begin{aligned} W(L) &= \int_0^L FI (1 - \frac{b}{L} x) dx \\ &= FI (1 - \frac{b}{2}) L \end{aligned} \quad (F-2)$$

The initial program for launcher sizing assumes a frictionless conversion of energy, and uses the following equation.

$$L = \frac{\text{K.E.}}{\text{FI} \left(1 - \frac{b}{2}\right) - \text{AM} \sin \alpha} \quad (\text{F-3})$$

where K.E. = Kinetic Energy of the accelerated mass (ft-lb)

L = length of launcher throw distance (ft )

FI = Initial force on vehicle and shuttle (lbs )

AM = weight of vehicle plus shuttle (lbs )

$\alpha$  = launch angle with respect to level (deg )

b = 1 - FF

FF = final force on shuttle/initial force on shuttle

The output of this program shows that the required launch throw distance for a 6-g, 50 miles per hour launch is approximately 14.3 feet for constant force. With a final force fraction (final force/initial force) of 0.5 the throw distance required is approximately 19.3 feet.

The final program for sizing the spring launch is an expansion that includes the change in kinetic energy and gravitational potential energy of the springs, the work done against sliding friction during launch, and the work done by the net effective thrust of the engine (thrust minus drag). See Appendix F-1 for the computer program.

Assuming a required throw distance of 20 feet, a feasibility design is done for both rubber and spring launcher. A length of 25 feet is chosen for the launcher to allow for the length of a shuttle and for the length of a shock absorber to stop the shuttle.

#### Rubber Launcher Element

Through several discussions and meetings with Dr. Mark Dannis of the B. F. Goodrich Research Center, the following points were brought

forward. Rubber appears to be feasible as an energy storage element. Its main engineering advantage over springs is its large elongation capability which leads to short pieces giving long throw distance. Unfortunately stress-strain hysteresis curves for large elongations and repeated cycles do not exist as this is not a common use of rubber at this time. Additional meetings with members of the Air Force Materials Laboratory and the Firestone Tire and Rubber Company's Central Research confirmed these points (Griffin, 1975) (Weissert, 1975). Dr. Dannis has set up and run tests in an attempt to obtain the required curves. The results of these tests suggest that rubber is not feasible in this application. A permanent deformation of 10% per cycle was seen through the first ten cycles where stabilization of the deformation had been expected after one or two cycles. Failure of the rubber tested occurred at stress levels far below those expected. The required stress-strain curves still are not available. Further consideration of rubber as the energy storage element is not pursued.

#### Spring Launcher

The spring launcher design is developed through the preliminary design stage. The major components of this subsystem are the main structure, the springs (the energy storage element), the shuttle, the shock absorber, transfer elements, and the cocking system.

A drawing of the launcher mounted on a M-36C1 truck is shown in Figure F-1, and an internal view of the launcher is shown in Figure F-2 to show the relative position of components. A similar, but much smaller, launcher is now in use by the Army as a launcher for 10 to 40 pound test vehicles (Powell, 1974).

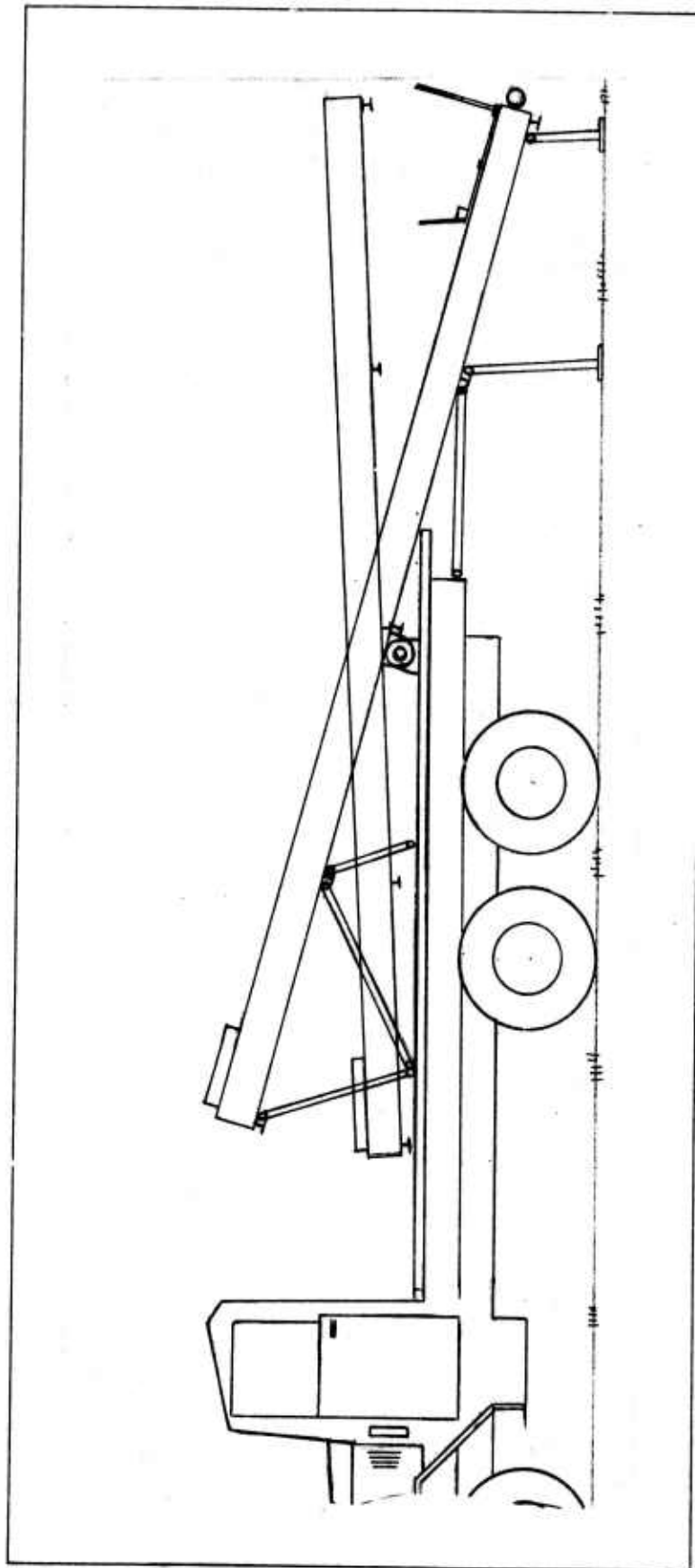


Figure F-1. Launcher Mounted on M-36 Truck

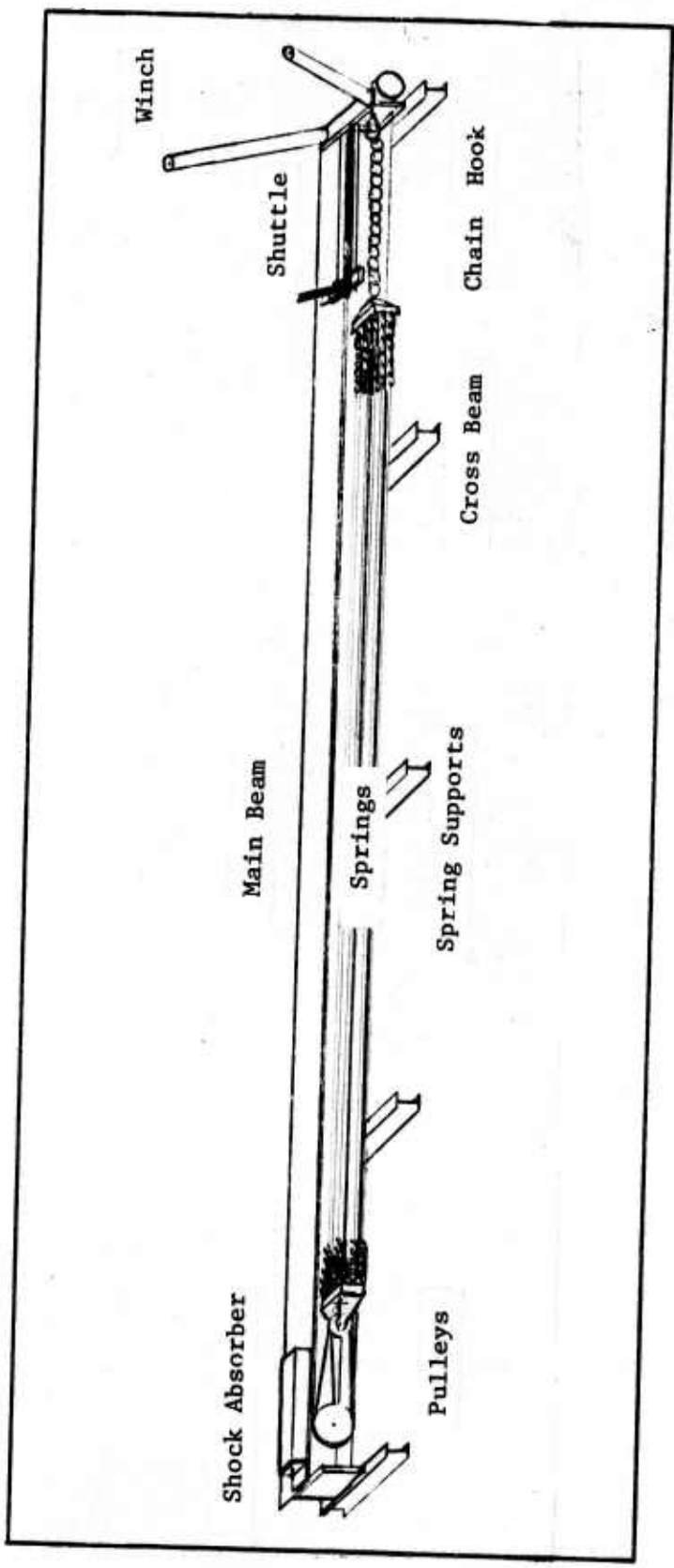


Figure F-2. Major Launcher Components

### Main Structure

The structure is composed of two wide flanged steel beams 10 by 8 inches, 25 feet long. They are connected at the ends by 1-1/2 inch plates. Each beam is attached to cross members at evenly-spaced intervals of approximately 75 inches as shown in Figure F-2.

Steel is chosen for the beams due to the lower cost of material and lack of a bimetallic corrosion problem. The weight of the launcher is approximately 2,400 pounds, and the weight of a similarly designed all aluminum construction (except for the steel springs) would be approximately 1,100 pounds. This decrease in weight is not significant for it is still too heavy to handle easily.

The size of beams chosen for the main beams is dictated by the required space for the springs. The fit is shown in Figure F-3.

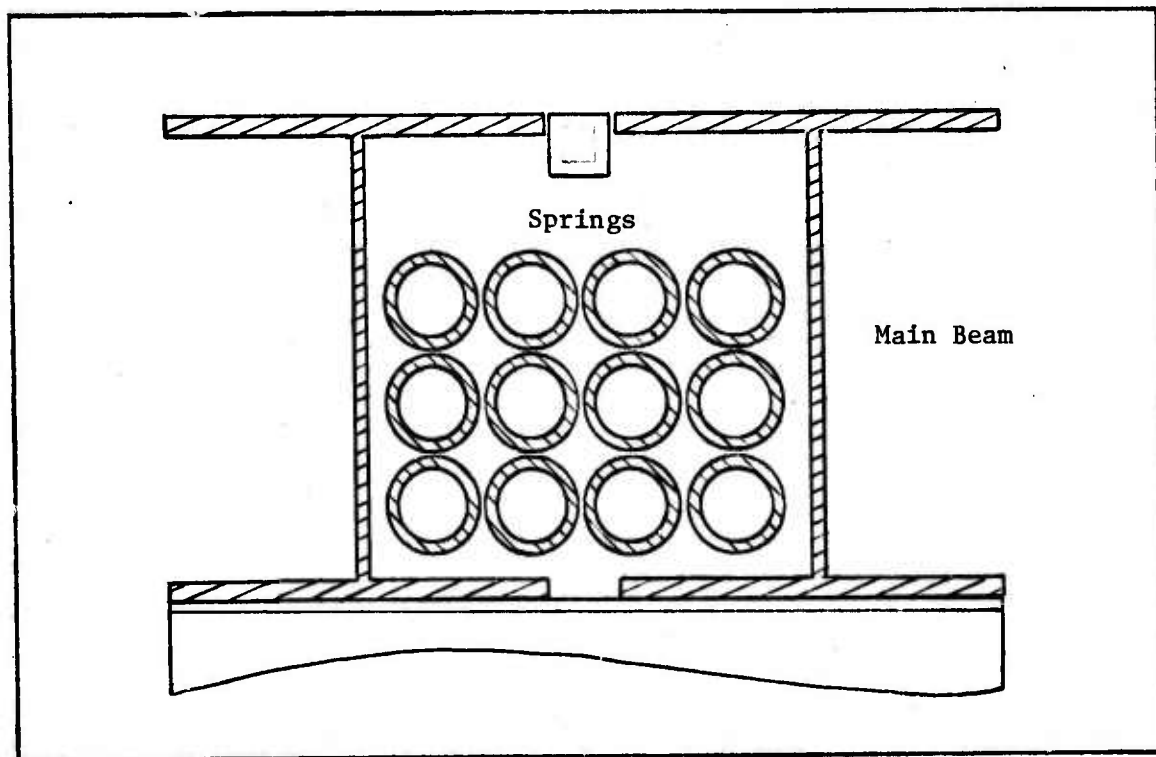


Figure F-3. Cross-Section of Launcher

The aft plate is fitted with a large hook rated at two tons to hold the spring chain. The structural analysis of the main structure is accomplished in Appendix F-3. The analysis considered the main structure as a rigid body loaded axially with moments applied to the weakest direction. Both torsional and lateral buckling are considered, and it is shown that stress levels in the structure are far below those required for failure. The problem of fatigue failure is addressed here. The ultimate tensile strength is reduced by only 10% for 1000 cycles of completely reversed bending stress for typical low carbon steel (Shanley, 1967: 340). The analysis shows that the maximum stress does not reach 10% of yield strength.

The spring component of the launcher is composed of twelve springs, two springs support blocks, and the associated pulleys cable and chain which connect the springs to the main structure and shuttle. A pulley ratio of four to one is used. As shown in Table F-1, this choice allows for the minimum launcher length, and the minimum total spring force for that launcher length.

TABLE F-1. LAUNCHER LENGTH AND SPRING FORCE FOR DIFFERING PULLEY RATIOS

Pulley Ratio	Spring Length(ft) for 20-ft Throw	Launcher Length(ft) Required by Spring*	Launcher Length(ft) Required for Throw**	Minimum Launcher Length(ft)	Maximum Force of Spring Element(lb)
2	20	45	25	45	1800
3	13.3	31.6	25	31.6	2700
4	10	25	25	25	3600
5	8	21	25	25	4500

\* includes requirement for pulley, blocks, chain, etc.

\*\* includes requirement for shuttle and shock absorber length.

### The Spring

For the launcher to have the capability of applying 6 g's to a 150-pound vehicle-shuttle combination, 900 pounds must be transmitted to the shuttle. A total spring force of 3,600 pounds is required to produce this 900 pounds through the four-to-one pulley ratio.

Due to cost, availability, and the relatively benign operating environment, oil tempered spring wire is used in the springs. The size of wire is limited to 0.25 inches due to local manufacturing capability (Pickwell, 1975). The requirement leads to the use of twelve springs. Each spring is constructed of 0.25 inch wire with an outside coil diameter of 2.0 inches and 432 working coils. With this design the spring rate is 2.425 pounds per inch extension and at corrected stress of 98.067 pounds per square inch gives a force of 283.5 pounds. At a load of 300 pounds, the maximum stress level is 103,774 pounds per square inch. These maximum stress levels and a force factor of 0.5 leads to a design life in the first case of between 5000 and 10,000 cycles (Wahl, 1963). Values for minimum, mean, and maximum life expectancy are 1,000, 5,000, and 10,000 cycles respectively (Barnes, 1975) (Pickwell, 1975). The use of twelve springs of this size dictates an area of at least 6.4 by 8.5 inches. This requirement leads to the selection of the main structure beam, W 10x30, which allows for a free area of 7.75 by 9.125 inches to be used (American, 1973: 1-18) (See Figure F-3).

An initial tension of 56 pounds is prescribed and is equivalent to an initial uncorrected stress of 16,000 pounds per square inch. This is readily obtainable in production (Wahl, 1963: 121) (Barnes,

1975).

This spring element of twelve springs operating in parallel has the advantage of flexibility. For a vehicle and shuttle combination whose weight is 125 pounds, two springs may be symmetrically removed from this element. With these two springs removed, the maximum force on the shuttle is reduced to 850 pounds. This produces a maximum g-load of 6 and the desired launch airspeed.

TABLE F-2. LAUNCH WEIGHT, NUMBER OF SPRINGS AND G-LOAD

weight to be accelerated (lb)	number of springs	maximum g-load
150	12	6
125	10	6
100	8	6

The final weight estimate of the drone is 125 pounds; the shuttle, 17. ( See Appendix A for vehicle weight.)

To check the output from the launcher sizing program, another algorithm was written to evaluate spring launcher. This second program calculates the maximum launch g-load and vehicle velocity. Inputs to this computer program are parameters such as launcher component dimensions, net effective thrust, and spring elongation. This program was verified by actual firing data from the small Army launcher (Powell, 1974). This program is in Appendix F-2.

#### Shock Absorber

The shock absorber for the launcher is designed to absorb the kinetic energy of the shuttle and springs, and the work of the final force of the launcher over the distance required to stop the shuttle.

The material used in this design is neoprene rubber with a hardness of 55 BS. For the analysis a worst case of approximately 30,000 inch-pounds of energy with a final force of 465 pounds is used. The material has a cross-sectional area of 24 square inches and a length of 2 feet. At a maximum compression of 12 inches, this shock produces a maximum force of 6000 pounds. The configuration has two rectangular shapes, each 24 inches long, 4.1 inches wide, and 3 inches high. A hole of 0.6 inches in diameter extends for the length of the block to allow a rod to be fitted through it. The analysis of the shock absorber is found in Appendix F-5.

#### Shuttle

The airframe design causes special problems in the design of the shuttle. The propeller, extending 6.5 inches below the main fuselage, requires that the vehicle be held high above the shuttle. The supports hold the vehicle approximately 12 inches above the main beams. The highest fixed item on the shuttle forward of the propeller is located 3.5 inches above the main beams and 32 inches in front of the propeller. The shuttle is made of aluminum to keep the weight to a minimum; it weighs approximately 17 pounds. Views of the shuttle are shown in Figures F-4 and F-5. A cocking bar holds the shuttle in the cocked position by blocking any forward movement of the thrust lever.

A tentative design for the top of the thrust lever and vehicle hard points is presented. The thrust lever is the forward support for the vehicle. Prior to launch, the thrust lever acts as a hold back against engine thrust. During the launch the thrust lever transmits the force from the launcher to the drone while providing a hold-down to prevent premature separation between launcher and drone. Figure F-6(a)

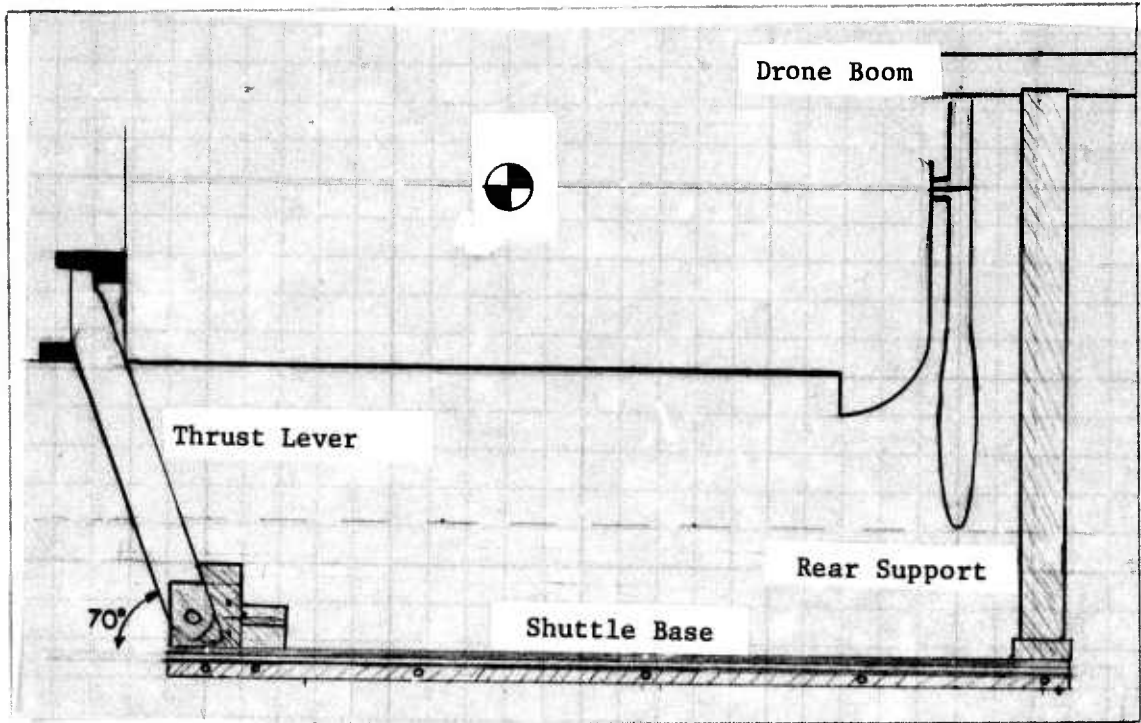


Figure F-4a. Side View of Shuttle

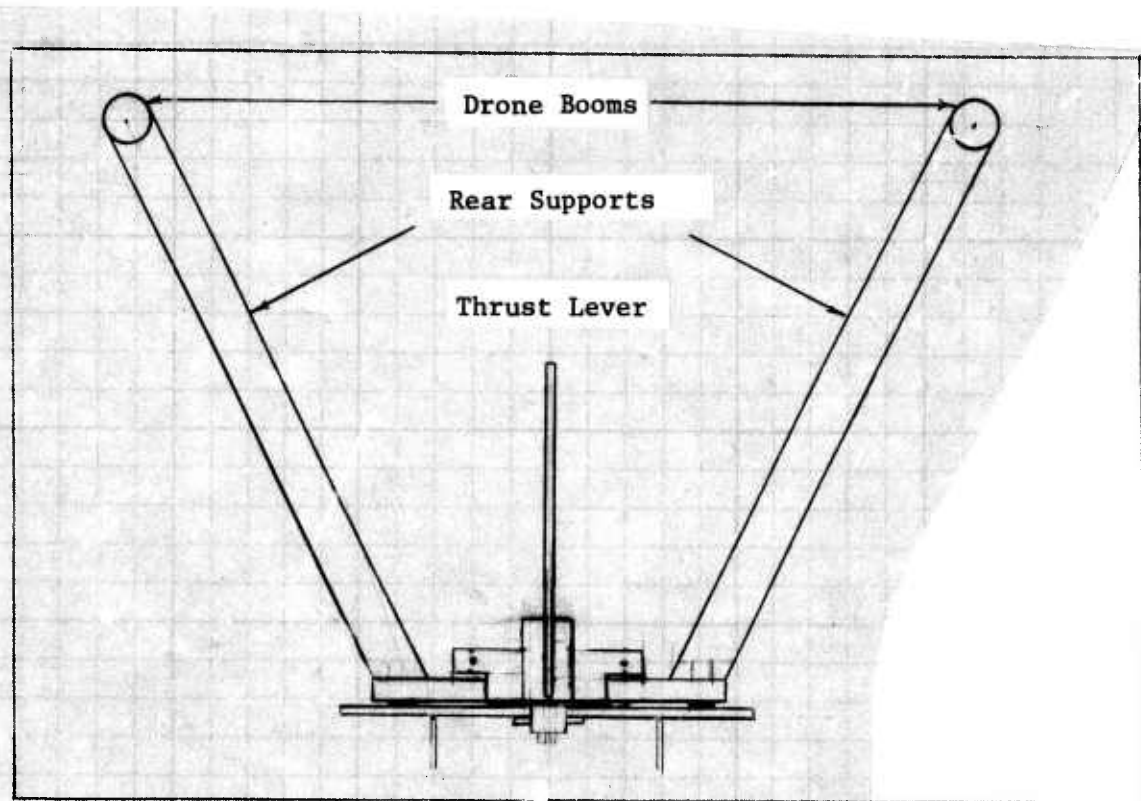


Figure F-4b. Front View of Shuttle

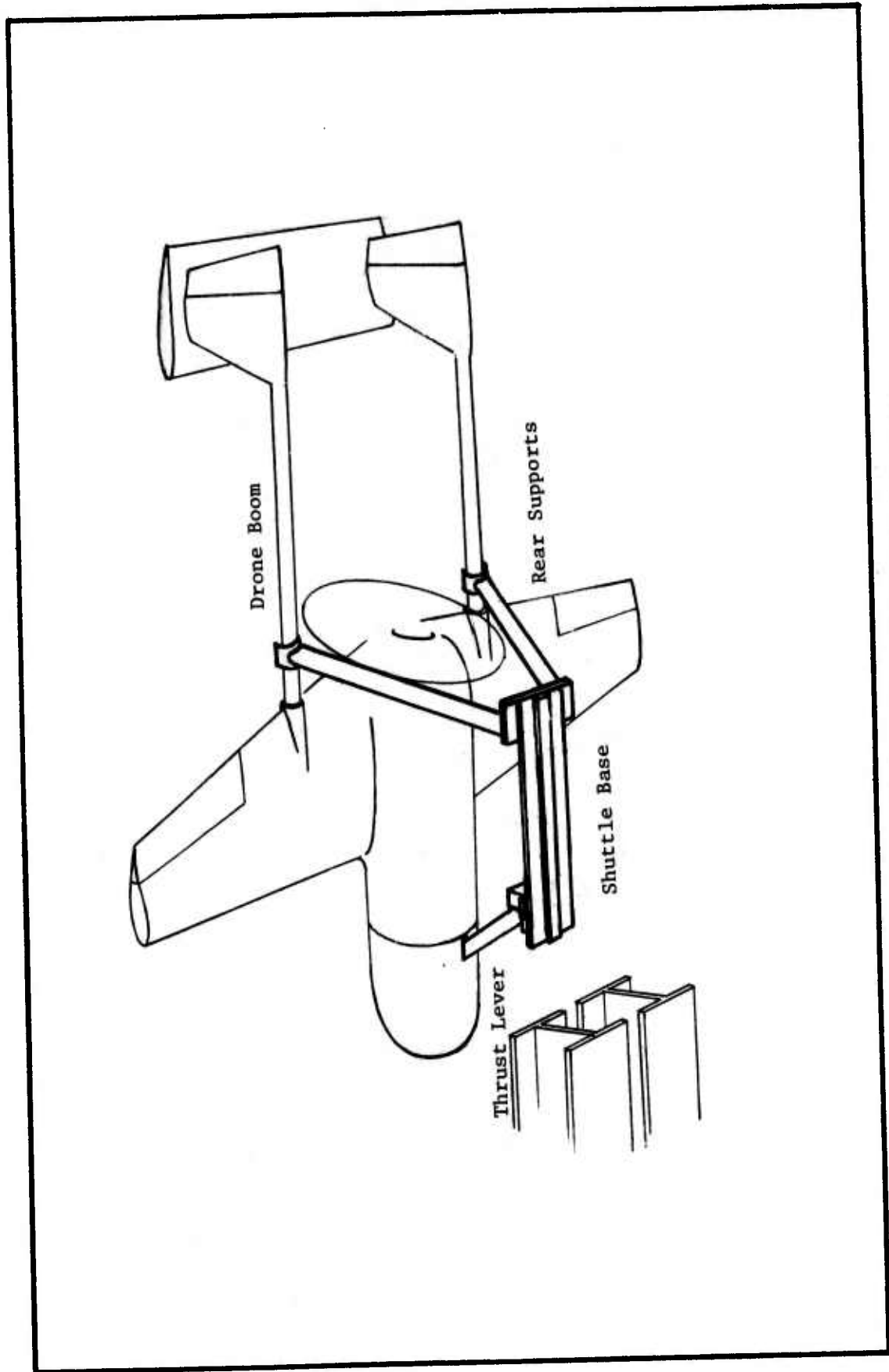


Figure F-5. Oblique View of Shuttle and Drone

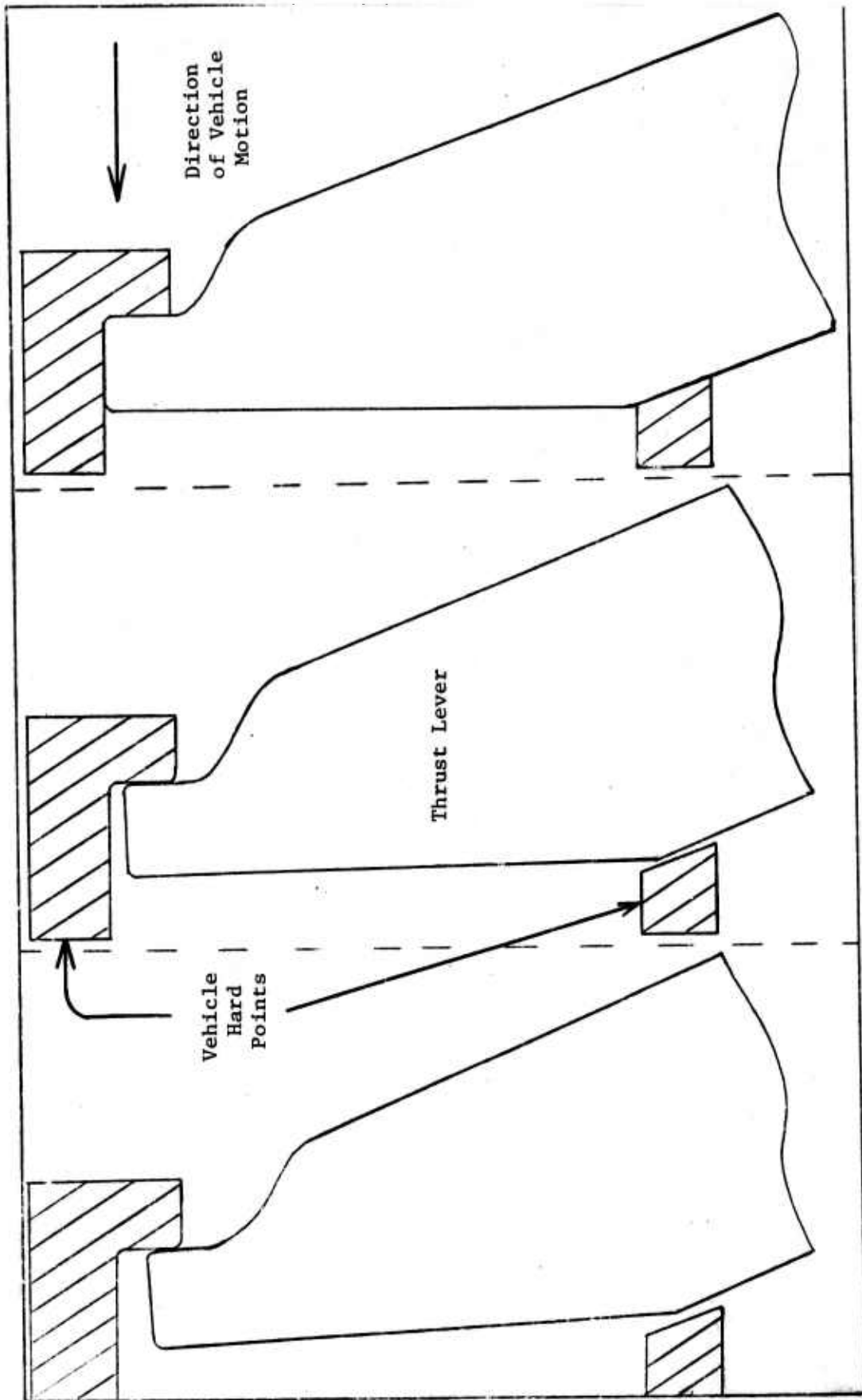


Figure F-6. Views of the Thrust Lever Unlock Sequence

shows the relative positions of the lever and vehicle hard points from the time of load until impact between the shuttle and shock absorber. At impact the thrust lever is unlocked and rotated forward and down by inertia as it withdraws from the vehicle. The initial unlock and rotation of thrust lever is shown in Figure F-6(b) and (c). It will rotate to level from its up position ( $70^{\circ}$ ) in approximately 14 inches of vehicle relative movement. Once down, it is trapped to prevent it bouncing up into the propeller. The two rear supports are 2-inch aluminum tubes, 27 inches long. They are the aft supports for the vehicle and directly support the drone booms aft of the propeller. A structural analysis of the more critical elements of the shuttle is found in Appendix F-6.

This concept of the design for the thrust lever requires close tolerances and may not prove suitable for the one thousand cycle life of the launcher. Other designs using moving parts for the hold down mechanism are possible, but are more complex and heavier. Therefore, if a simple geometric shape will suffice, it should be used.

#### Launch Specification

The vehicle designed for use with this launcher has an estimated longitudinal g-limit in excess of 8-g's and a power-on stall speed of

below 40 miles per hour (Appendix A). Using the launcher evaluation program with a precock elongation of 34 inches, the following g-loads and velocities were derived for various values of net thrust.

TABLE F-3. LAUNCH G AND VELOCITY VERSUS NET THRUST

Net Thrust	G-load	Velocity (ft/sec)	MPH
0	5.98	72.12	49.2
26	6.17	73.64	50.2
38	6.25	74.34	50.7
50	6.33	75.03	51.2

The launcher appears adequate in performance.

#### Cost

The most likely acquisition cost of the launcher is \$5000, with a low of \$4600 and a high of \$5400. A cost breakdown is in Appendix F-6. This cost is based on 120 springs being bought for five launchers and a zero learning curve. The price of \$30 per spring is based on a buy of 120; if only 24 are purchased, the springs would cost \$37.50 each (Barnes, 1975).

The cost per launch for 1000 launches is \$5 with no expected failures of the launcher. The life cycle cost is composed of the acquisition cost plus the sum of the annual maintenance cost. The annual maintenance cost is 10% of the acquisition cost (Jackson, 1975b). This yields a life cycle cost of \$10,000 for a ten year operating life.

### Conclusions and Recommendations

The spring powered launcher appears to be feasible and is more cost effective than the inexpensive rocket powered launcher. It also has the advantage of being adjustable for differing launch weights and, with a shuttle change, differing vehicle designs. Acquisition cost of the spring launcher would be substantially below that of the existing pneumatic launcher.

Although the minimum number of cycles-to-failure of the spring is estimated to be at least 1000 cycles under launch conditions, it is recommended that a test be run to verify the spring failure rate. One launcher would have to be built for this purpose. The shuttle design should be tested to verify the thrust lever concept. Additionally, other shuttle designs should be examined in an effort to reduce shuttle weight.

APPENDIX F-1

COMPUTATION OF REQUIRED LAUNCH THROW

A method for determining the required launch throw distance was needed. To fill this need a program was developed using the concepts of energy conservation and work (the work done is equal to the change in energy). The algorithm used in the final version of this program takes in to account the changes in kinetic and gravitational potential energy of the vehicle, shuttle, and springs. It also considers the work done on the shuttle by the spring force, by sliding friction force and by the net effective thrust of the engine. The net effective thrust is assumed to be a constant. Not considered are the losses due to rotational inertia of pulleys or losses due to cable bending around the pulleys.

The effective spring force on the shuttle is assumed to be a linear function of position.

$$F(x) = FI \left( 1 - \frac{bx}{L} \right) \quad (F-1)$$

where F(x) force as a function of position (lb)  
FI initial force (lb)  
x shuttle position from fully cocked (ft)  
L length of launch throw (ft)  
b 1-FF  
FF final force fraction (final force/FI)

The work done by this force is a linear function of initial force, b, and throw distance.

$$V_{sp} = FI \left( 1 - \frac{b}{2} \right) L \quad (F-2)$$

where  $W_{sp}$  work done by springs on shuttle (ft-lb)

The equation expressing the work done by friction and the net effective thrust of the engine are given below

$$W_f = - (CF) (AM) L \cos\alpha \quad (F-4)$$

$$W_{nt} = (NT) L \quad (F-5)$$

where  $W_f$  work done by friction (ft-lb)

$C_f$  coefficient of friction

AM weight of vehicle and shuttle (lb)

$\alpha$  angle of launch from level (deg)

$W_{nt}$  work done by engine (ft-lb)

NT average thrust minus average drag (lb)

L throw distance (ft)

The gravitational potential energy of vehicle and shuttle, and the springs at the end of the launch throw is given by the following expression (initial energies set at zero).

$$PE = (AM - \frac{M_{sp}}{PR}) L \sin\alpha \quad (F-6)$$

where PE final (ft-lb)

AM weight of vehicle and shuttle (lb)

$M_{sp}$  weight of springs (lb)

L length of launch throw (ft)

PR pulley ratio

$\alpha$  launch angle above level (deg)

The kinetic energy of the shuttle and vehicle at launch is

$$KE_{v+s} = \frac{(AM) V^2}{64.4} \quad (F-7)$$

where  $KE_{v+s}$  kinetic energy of vehicle and shuttle (ft-lb)  
 $V$  velocity of shuttle and vehicle (ft/sec)

The kinetic energy of the springs, as a function of shuttle velocity,  
 is

$$KE_{sp} = \frac{M_{sps} V^2}{6 (PR)^2} \quad (F-8)$$

where  $KE_{sp}$  kinetic energy of spring (ft-lb)  
 $M_{sps}$  mass of spring (slugs)  
 $V$  velocity of shuttle (ft/sec)  
 $PR$  pulley ratio

This expression is derived from summing the kinetic energy of each  
 piece of spring material

$$KE_{sp} = \lim_{n \rightarrow \infty} \sum_{i=1}^n \frac{1/2 M_{sps} V_i^2}{n} \quad (F-9)$$

where  $V_i$  velocity of a spring element (ft/sec)  
 $n$  number of evenly cut elements of a spring  
 $i$  the number of each element from fixed end

$$\text{and } V_i = \frac{V i}{PR n} \quad (F-10)$$

where  $V$  velocity of shuttle (ft/sec)

substituting Eq (F-10) into Eq (F-9) yields

$$KE_{sp} = \frac{1/2 M_{sps}}{N} \sum_{i=1}^N \left( \frac{V i}{(PR)N} \right)^2$$

$$= \frac{M_{sps} V^2}{2N(PR)^2 N^2} \sum_{i=1}^N i^2$$

$$= \frac{M_{\text{sps}} V^2}{2(\text{PR})^2 N^3} \frac{N(N+1)(2N+1)}{6}$$

but  $\lim_{n \rightarrow \infty} \frac{N(N+1)(2N+1)}{6N^3} = \frac{1}{3}$

Therefore  $\text{KE}_{\text{sp}}(V) = \frac{M_{\text{sps}} V^2}{6(\text{PR})^2}$

The algorithm in the launch sizing program is

$$L = \frac{\text{KE}_{\text{vts}} + \text{KE}_{\text{sp}}}{\text{FI}(1 - \frac{b}{2}) + \text{NT} - C_f (\text{AM}) \cos \alpha + \frac{M_{\text{sp}}}{\text{PR}} - \text{AM}) \sin \alpha} \quad (\text{F-11})$$

The program uses inputs of desired velocity, maximum g-load, final force fraction, vehicle-shuttle weight, net thrust, coefficient of friction, spring weight, pulley ratio and launch angle. Use of this program for initial sizing can be accomplished by assuming unknown parameters such as spring weight, coefficient of friction, and net thrust are zero. The program follows.

```

PROGRAM LAUNCH2 (INPUT, OUTPUT, TAPES=INPUT, TAPE6=OUTPUT)
DIMENSION AM(8), V(4), G(5), FF(4), ALPHA(3), X(9,4,5), B(4), BETA(3)
REAL MSP, MSSP, KES
DATA (AM=80., 90., 100., 110., 120., 130., 140., 150.), (V=45., 50., 55., 60.)
+, (G=5., 6., 7., 8., 10.), (FF=.6., .55., .515., .5), (ALPHA=0., 10., 15.)
+, (MSP=397.), (TN=26.), (PR=4.)
DO 100 I=1,4
100 V(I)=(88./60.)*V(I)
DO 200 I=1,3
200 BETA(I)=(3.141592654/180.)*ALPHA(I)
DO 300 I=1,4
300 B(I)=1-FF(I)
DO 500 I=1,8
DO 500 J=1,4
MSSP=MSP/32.2
KES=MSPS*V(J)**2/(6*PR**2)
DO 501 N=1,5
FI=AM(I)*G(N)
Y=V(J)**2/(64.4*G(N))
WKK1=FI*Y
DO 10 L=1,4
DO 10 M=1,3
10 X(N,L,M)=(WKK1+KES)/(FI*(1-B(L)/2.)+(MSP/4-AM(I))*SIN(BETA(M))+TN
+-.1*AM(I)*COS(BETA(M)))
501 CONTINUE

```

```

DO 401 L=1,4
PRINT 701 , AM(I), V(J), FF(L)
PRINT 702 , (G(K), K=1,5)
DO 401 M=1,3
401 PRINT 703, ALPHA(M), (X(K,L,M), K=1,5)
PRINT 704
500 CONTINUE
701 FORMAT (T53,14HTHROW DISTANCE//T30,5HMASS=,F9.2,T45,9HVELOCITY=,F6.
+2//T45,6HFF/FI=,F4.2//
+T10,5HALPHA,T45,4HGMAX)
702 FORMAT (T20,5F10.2)
703 FORMAT (T10,11F10.2)
704 FORMAT (///)
705 FORMAT (T30,5HKES =,3F15.3,2F8.3)
STOP
END

```

THROW DISTANCE

MASS= 140.00 VELOCITY= 73.33

FF/FI= .60

ALPHA	5.00	6.00	GMAX 7.00	8.00	10.00
0.00	20.44	17.09	14.69	12.88	10.33
10.00	20.69	17.27	14.81	12.97	10.39
15.00	20.80	17.35	14.88	13.02	10.42

THROW DISTANCE

MASS= 140.00 VELOCITY= 73.33

FF/FI= .55

ALPHA	5.00	6.00	GMAX 7.00	8.00	10.00
0.00	21.08	17.63	15.15	13.29	10.66
10.00	21.35	17.82	15.29	13.39	10.72
15.00	21.47	17.91	15.35	13.44	10.76

THROW DISTANCE

MASS= 140.00 VELOCITY= 73.33

FF/FI= .52

ALPHA	5.00	6.00	GMAX 7.00	8.00	10.00
0.00	21.56	18.03	15.50	13.59	10.90
10.00	21.84	18.23	15.64	13.70	10.97
15.00	21.97	18.32	15.71	13.75	11.00

THROW DISTANCE

MASS= 140.00 VELOCITY= 73.33

FF/FI= .50

ALPHA	5.00	6.00	GMAX 7.00	8.00	10.00
0.00	21.77	18.21	15.65	13.72	11.01
10.00	22.05	18.41	15.80	13.83	11.08
15.00	22.19	18.50	15.86	13.89	11.11

APPENDIX F-2

EVALUATION OF A SPRING LAUNCHER CAPABILITY

To evaluate a given spring launcher an additional program is needed. This program accepts specific subsystem parameters and computes maximum launch g-load and launch velocity.

The required inputs for the program are

- r spring rate (lb/in)
- IT initial tension (lb)
- MD mean diameter of spring (in)
- WD wire diameter of spring (in)
- NC number of coils per spring
- NS number of springs
- PR pulley ratio
- CF coefficient of friction
- TN net thrust of engine-drag (lb)
- $\alpha$  launch angle (deg)
- X2 elongation of spring at full cock position (in)
- X1 elongation of spring with shuttle at launch end of rail
- X launcher throw distance (ft)
- AM weight of vehicle and shuttle (lb)

The density of the spring steel used in the program is 0.283 pounds per cubic inch.

The outputs of this program are

- FI initial force from spring (lb)
- FJ final force from spring (lb)
- FF final force factor

G max g-load during launch

V velocity of vehicle (ft/sec)

The algorithm used in the program is

$$V = \left[ \frac{W_{sp} + W_{nt} + W_f - PE}{\frac{AM}{64.4} + \frac{M_{sps}}{6(PR)^2}} \right]^{1/2} \quad (F-12)$$

where  $W_{sp}$  work done by spring (ft-lb)

$W_{nt}$  work done by net engine thrust (ft-lb)

$W_f$  work done by friction (ft-lb)

PE final gravitational potential energy (ft-lb)

AM weight of shuttle and vehicle (lb)

$M_{sps}$  mass of springs (slugs)

PR pulley ratio

The program with results for a 125 pound vehicle and both a 15 and a 17 pound shuttle are shown on the following pages.

```

PROGRAM LNEVAL2 (INPUT,OUTPUT)
DIMENSION AM(2),X1(3),X2(3)
REAL MSP,MSPS,MD,MS
DATA (AM=140.,142.), (X1=34.,41.,48.), (X2=94.,101.,108.)
READ *,R,IT,MD,WD,X,PR,NS,NC,CF,TN,ALPHA,N
PI=3.141592654
BETA=PI/180.*ALPHA
PRINT 500
DO 20 I=1,3
DO 20 J=1,2
FJ=(R*X1(I)+IT)*NS/PR
FI=(R*X2(I)+IT)*NS/PR
FF=FJ/FI
B=1.-FF
VOLS=PI**2*WD**2*MD*(NC+2)/4.
MS=VOLS*.283
MSP=MS*NS
MSPS=MSP/32.2
G=(FI+TN)/AM(J)
V=SQRT(X*(FI*(1-B/2)+TN-CF*AM(J)*COS(BETA)+(MSP/PR-AM(J))*SIN(
+BETA))/(AM(J)/64.4+MSPS/(6*PR**2)))
PRINT 501,FI,FJ,FF,G,MSP,X,V,AM(J),NS,TN
20 CONTINUE
500 FORMAT(T20,2HFI,T30,2HFJ,T40,2HFF,T50,1HG,T60,3HMSP,T70,1HX,T80,1H
+V,T90,6HWEIGHT,T100,4H# SP,T110,2HTN)
501 FORMAT(T15,8F10.4,I7,F10.4)
STOP
END

```

FI	FJ	FF	G	X	V	WEIGHT	# SP	TN
850.2600	412.8600	.4856	6.0733	20.0000	72.6431	140.0000	12	0.0000
850.2600	412.8600	.4856	5.9877	20.0000	72.1159	142.0000	12	0.0000
901.2900	463.8900	.5147	6.4378	20.0000	75.6324	140.0000	12	0.0000
901.2900	463.8900	.5147	6.3471	20.0000	75.0869	142.0000	12	0.0000
952.3200	514.9200	.5407	6.8023	20.0000	78.5079	140.0000	12	0.0000
952.3200	514.9200	.5407	6.7065	20.0000	77.9447	142.0000	12	0.0000
FI	FJ	FF	G	X	V	WEIGHT	# SP	TN
850.2600	412.8600	.4856	6.2590	20.0000	74.1812	140.0000	12	26.0000
850.2600	412.8600	.4856	6.1708	20.0000	73.6446	142.0000	12	26.0000
901.2900	463.8900	.5147	6.6235	20.0000	77.1109	140.0000	12	26.0000
901.2900	463.8900	.5147	6.5302	20.0000	76.5563	142.0000	12	26.0000
952.3200	514.9200	.5407	6.9880	20.0000	79.9333	140.0000	12	26.0000
952.3200	514.9200	.5407	6.8896	20.0000	79.3612	142.0000	12	26.0000
FI	FJ	FF	G	X	V	WEIGHT	# SP	TN
850.2600	412.8600	.4856	6.3447	20.0000	74.8804	140.0000	12	38.0000
850.2600	412.8600	.4856	6.2554	20.0000	74.3395	142.0000	12	38.0000
901.2900	463.8900	.5147	6.7092	20.0000	77.7838	140.0000	12	38.0000
901.2900	463.8900	.5147	6.6147	20.0000	77.2251	142.0000	12	38.0000
952.3200	514.9200	.5407	7.0737	20.0000	80.5826	140.0000	12	38.0000
952.3200	514.9200	.5407	6.9741	20.0000	80.0066	142.0000	12	38.0000
FI	FJ	FF	G	X	V	WEIGHT	# SP	TN
850.2600	412.8600	.4856	6.4304	20.0000	75.5732	140.0000	12	50.0000
850.2600	412.8600	.4856	6.3399	20.0000	75.0281	142.0000	12	50.0000
901.2900	463.8900	.5147	6.7949	20.0000	78.4509	140.0000	12	50.0000
901.2900	463.8900	.5147	6.6992	20.0000	77.8881	142.0000	12	50.0000
952.3200	514.9200	.5407	7.1594	20.0000	81.2268	140.0000	12	50.0000
952.3200	514.9200	.5407	7.0586	20.0000	80.6467	142.0000	12	50.0000

APPENDIX F-3

ANALYSIS OF MAIN STRUCTURE

For this analysis it is assumed that the 1-1/2 inch thick end plates, with the maximum load proposed, will insure that the two beams are loaded symmetrically. Therefore, only one beam is used with half the loads. One half the properties of the combined section are

$$\begin{aligned} I_{xx} &= 170.9 \\ I_{yy} &= 255.6 \\ r_x &= 4.2 \\ r_y &= 5.13 \end{aligned} \quad \text{(American, 1973)}$$

The value " $r_x$ " is the controlling radius of gyration for axial load. Since all moment are about the "x-x" axis, failure due to combined axial and moment load will occur about the "x-x" axis.

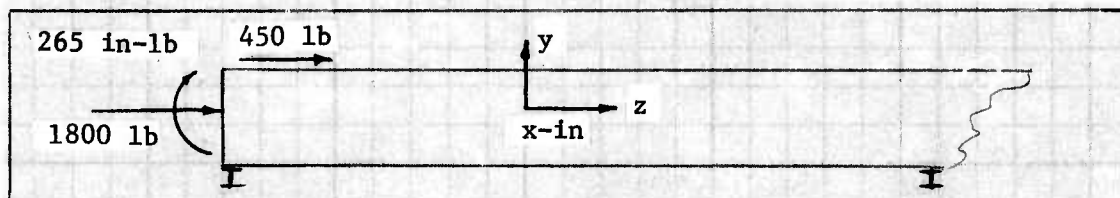


Figure F-7. Beam Loads with Launcher Cocked

The axial load used in analysis is 2250 pounds with a moment of 2515 inch-pounds.

$$P = 1800 + 450 \quad \text{(F-13)}$$

$$M_x = 450(5) + 265 \quad \text{(F-14)}$$

where P axial load (lb)

$M_x$  moment about "x-x" axis (in-lb)

The formula for computing loading conditions for failure of beam-columns under axial and bending loads is (Alcoa, 1956)

$$\frac{f_c}{f_C} + \frac{f_b}{f_B \left[ 1 - \frac{f_c}{f_{CE}} \right]} = D \quad (F-15)$$

where

$f_c$  are compressive stress due to axial load only (lb/in<sup>2</sup>)

$f_C$  critical stress under axial load only (lb/in<sup>2</sup>)

$f_b$  maximum bending stress (M/I) on extreme fiber due to bending moment only (lb/in<sup>2</sup>)

$f_B$  critical bending stress under bending moment only (lb/in<sup>2</sup>)

$f_{CE} = \pi^2 E / (KL/r)^2$  (lb/in<sup>2</sup>)

$\frac{KL}{r}$  effective slenderness ratio for failure in plane of applied moment

E modulus of elasticity (lb/in<sup>2</sup>)

D condition of failure ( $\geq 1$  failure,  $< 1$  no failure)

If the sum is less than one, failure will not occur. All of the above items are easily determined by inspection except  $f_B$ .

$$f_B = F_y \left[ 0.733 - 0.0014 \frac{b_f}{2t_p} \sqrt{F_y} \right] \quad (F-16)$$

where  $F_y$  minimum yield stress (kips/sq in)

$b_f$  flange width (in)

$t_p$  flange thickness (American, 1973)

for  $F_y = 36$  and  $b_f/2t_p = 9.20$ ,  $f_b = 23,606$  pounds per square inch.

$$f_c = \frac{P}{A}$$

$$= 231.1 \text{ lb/in}^2 \quad (\text{F-17})$$

$$f_C = 36,000 \text{ lb/in}^2$$

$$f_b = \frac{M_{xc}}{I_x}$$

$$= \frac{2515(5)}{170.9} \quad (\text{F-18})$$

$$= 73.5 \text{ lb/in}^2$$

Assuming the end support worst case to be the case of one end pinned and the other end allow to translate, dictates  $K = 2$  (American, 1973).

$$SR = \frac{KL}{r} \quad (\text{F-19})$$

where

- SR effective slenderness ratio
- K effective length factor
- L unsupported length (in)
- r radius of gyration (in)

Substituting the appropriate value into Eq (F-19) gives

$$SR_x = \frac{2(75)}{4.2}$$

$$= 35.7 \quad (\text{F-20})$$

and

$$f_{CE} = \frac{\pi^2 E}{SR^2}$$

then

$$f_{CE} = \frac{\pi^2 29.1 \times 10^6}{(35.7)^2}$$

$$= 225.169 \text{ lb/in}^2$$

Substituting the appropriate value into Eq (F-15) yields

$$D = \frac{231.1}{36,000} + \frac{73.5}{23,606 \left(1 - \frac{231.1}{225169}\right)}$$
$$= 0.01$$

Since 0.01 is much less than 1.0, the load is far below those required to produce failure.

Another possible maximum load occurs during shuttle stoppage. With the shock absorber maximum force of 6000 pounds, the single beam will be under a tension load of 3000 pounds from the shock, a compression load 1150 from the springs, and a moment of 3000 lb x 7.5 inches or 22,500 inch-pounds.

$$D = \frac{0}{36000} + \frac{658}{23606(1)} = 0.028$$

Analysis of this beam with only moments applied lead to

$$f = \frac{Mc}{I} \tag{F-21}$$

where f extreme fiber stress (lb/in<sup>2</sup>)

M applied bending moment (in-lb)

c distance to extreme fiber (in)

I moment of inertia (in<sup>4</sup>) (Alcoa, 1956)

The maximum fiber stress is

$$f = \frac{22500 (5)}{170.9}$$
$$= 658 \text{ lb/in}^2$$

This is far below the elastic limit.

Torsional failure must also be considered. The radius of gyration for torsional failure is

$$r_t^2 = \frac{C_s + 0.038 J (KL)^2}{I_x + I_y} \quad (F-22)$$

where  $r_t$  effective radius of gyration for torsional failure (in)

$C_s$  torsion-bending constant (in<sup>6</sup>)

$J$  torsion constant (in<sup>4</sup>)

$I_x + I_y$  sum of moments of inertia (in<sup>4</sup>)

$L$  length unsupported in twist (in)

$K$  factor for end conditions

(Alcoa, 1956)

Substituting appropriate values into Eq (F-22) for a single beam yields

$$r_t^2 = \frac{792 + 0.038 (0.580)(75)^2}{171 + 36.5}$$

$$r_t = 2.1 \text{ in}$$

The effective slenderness ratio is determined by substituting into Eq (F-19). Assume  $K=1$  (ends free to translate but not rotate) and  $L=75$  inches.

$$SR = 35.71$$

Since the effective slenderness ratio for torsional failure is no larger than for lateral failure, torsional failure is no more likely than lateral failure. Therefore the main structure appears very sound, and no failure is expected.

APPENDIX F-4

SPRING DESIGN

Through discussions of the use of springs in this application, it was suggested that at a maximum of 85,000 pounds per square inch stress (uncorrected) and minimum spring index of 7 be used. Oil temper wire is used because of availability, cost, and capabilities (Pickwell, 1975). The stress limit gives a high maximum load without excessively shortening spring life, and the limit on spring index insures a large percentage elongation. The design equations received in the first of these discussions were later confirmed and are listed below (Wahl, 1963).

$$\tau = \frac{8 PD}{\pi d^3} \quad (F-23)$$

$$k = \frac{Gd^4}{8D^3n} \quad (F-24)$$

$$K = \frac{4c - 1}{4c - 4} + \frac{0.615}{c} \quad (F-25)$$

$$\tau' = K\tau \quad (F-26)$$

$$c = \frac{D}{d} \quad (F-27)$$

Where

P = load on spring (lbs)

d = spring wire diameter (in)

D = spring mean coil diameter (in)

$\tau$  = uncorrected stress (psi)

$\tau'$  = corrected shear stress (psi)

K = curvature correction factor

n = number of active coils

k = spring rate (lbs/in)

Initially a maximum wire diameter of 0.25 inches was chosen due to its availability and the fact that it is the largest size that could be worked on machines locally.

The launcher size for a force factor of 0.5 (one half the force left at end of launcher throw) is approximately 20 feet. Therefore a spring length of approximately 10 feet is indicated when a pulley ratio of four to one is used. The four to one pulley ratio and 20-foot throw distance dictate that the spring will contract 5 feet during the throw.

The maximum load attainable under the restrictions of wire size, spring ratio, and stress level is 298 pounds.

$$P = \frac{\pi d^3 \tau}{8D} \quad (F-23)$$

$$P = \frac{\pi(25)^3(85,000)}{8(1.75)} = 298 \text{ lb}$$

The rate is

$$k = \frac{Gd^4}{8D^3n} = \frac{11.5 \times 10^6 (.25)^4}{8(1.75)^3n} \quad (F-24)$$

$$k = \frac{1047.75}{n} = \frac{21.828}{\ell}$$

where  $\ell$  is length in feet of active coils.

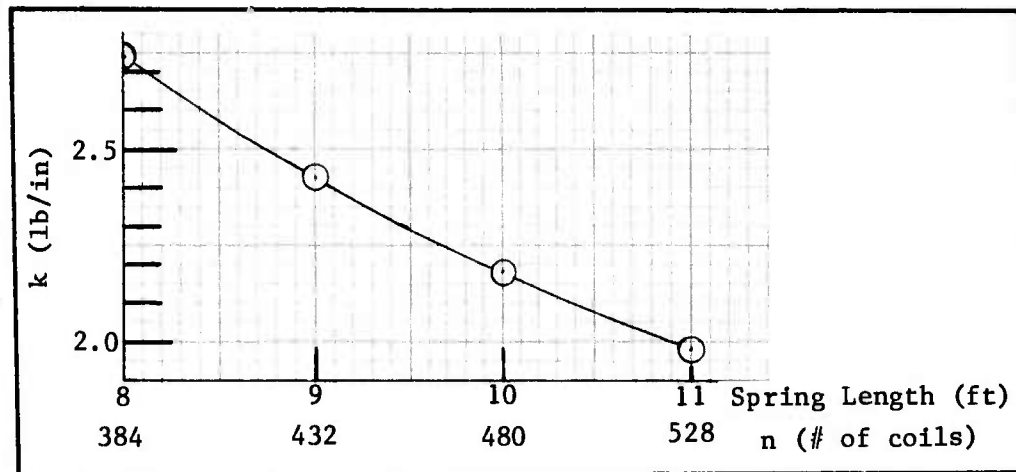


Figure F-8. Spring Rate Versus Number of Coils or Spring Length

The choice of 0.25 inches for wire diameter was reinforced by the fact 0.2508 inch wire diameter was given by an equation for minimum spring weight for these given conditions (Chironis, 1961:18).

An initial tension resulting from initial torsional stress equal to 16,000 pounds per square inch is readily obtainable (Wahl, 1963:121). This initial tension is equal to fifty-six pounds

$$IT = \frac{\pi \tau d^3}{8D} = \frac{\pi(16,000)(.25)^3}{8(1.75)} \quad (F-28)$$

$$= 56 \text{ lb}$$

With an initial tension of 56 pounds, the following graph of spring lengths and elongation for a specific load was constructed.

Minimum launcher length is assumed to be at least 5 feet (arbitrarily) longer than the extended spring length to allow for pulleys, spring supports, and working room in the launcher.

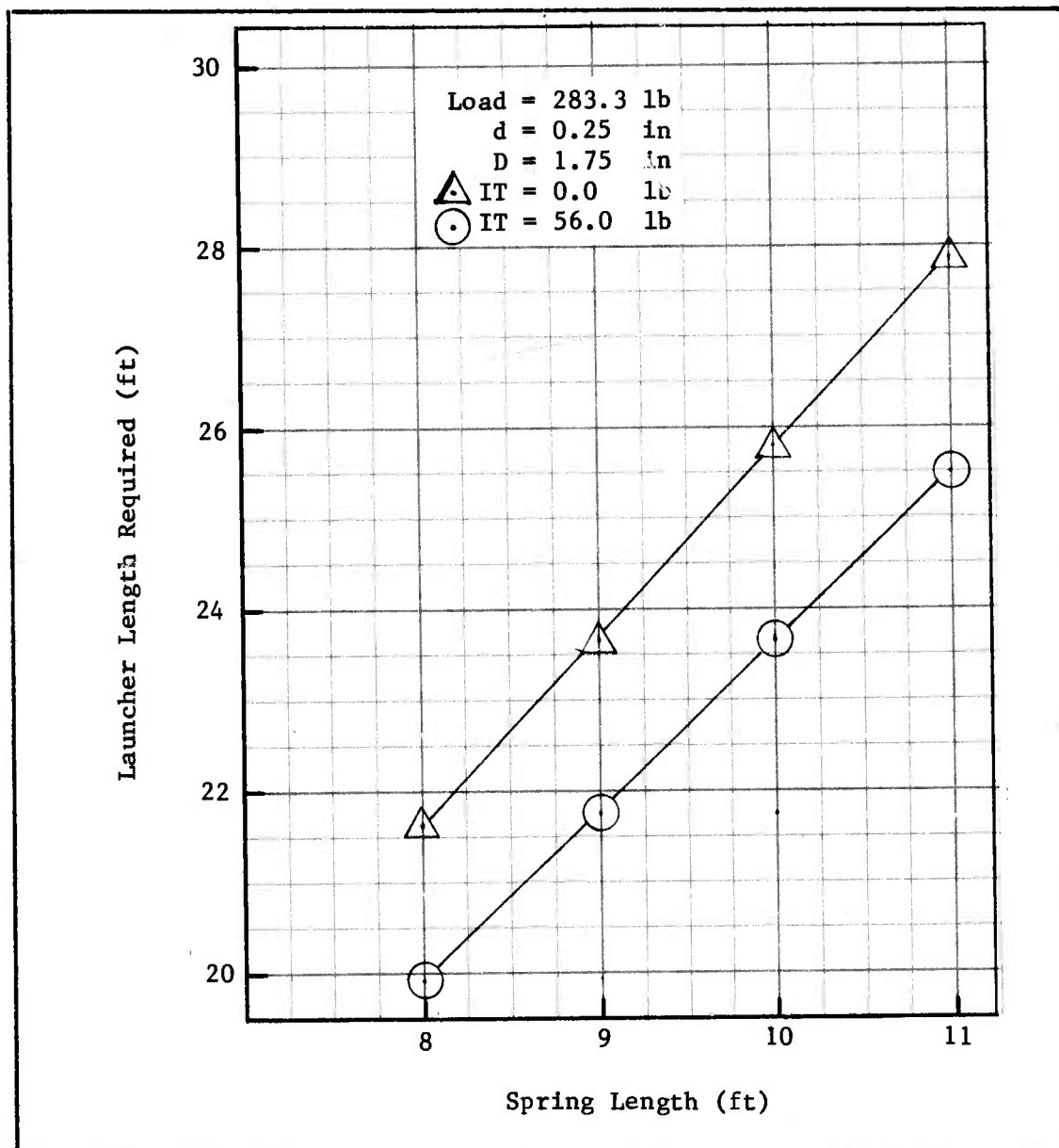


Figure F-9. Minimum Launch Length with Pulley Ratio of 4:1 Versus Spring Length

A 9-foot spring length was chosen with a 25-foot launcher length to insure sufficient travel for a 3-foot shuttle with a 2-foot shock absorber. This length also insured sufficient room to adjust initial pull on the shuttle if the springs did not have the correct initial tension.

From use of the launcher evaluation program it is seen that a reduction in maximum load per spring to 283.3 pounds will suffice to do the required job. This reduces the maximum stress,  $\tau$ , to 80,808 and  $\tau'$  to 98,020. This reduced stress level leads to a mean life greater than 5000, but less than 10,000 cycles (Wahl, 1963:106,107).

APPENDIX F-5

SHOCK ABSORBER ANALYSIS

The shock absorber on the launcher must be able to stop the shuttle without breaking the cable or launcher. The energy levels to be absorbed will vary with the velocity they attain by the shuttle during the launcher firing. The function relating velocity of the shuttle to the total kinetic energy of the launcher components is

$$KE_{sh+sp} = 1/2 \left( M_{sh} + \frac{M_{sp}}{3(PR)^2} \right) V^2 \quad (F-29)$$

where  $M_{sh}$  mass of shuttle (slugs)  
 $M_{sp}$  mass of springs (slugs)  
PR pulley ratio  
 $V$  velocity of shuttle (ft/sec)

This is the maximum kinetic energy that would have to be absorbed to bring the components to rest. The shock absorber will also have to absorb the energy equivalent of the work done by the final force over the distance required to stop the shuttle. Young's modulus for rubber can be determined from hardness number (Payne, 1960:220). The assumption of a constant modulus for strains up to 0.5 is reasonable for this type of material (Griffin, 1975). By selecting rubber with a Young's modulus of 500 pounds per square inch and limiting strain to 0.5, the force of compression equals 500A times strain (A is the original area of rubber.). The work done by compressing this shock absorber is equal to work done by a constant force of 125A over the same distance. See Figure F-10.

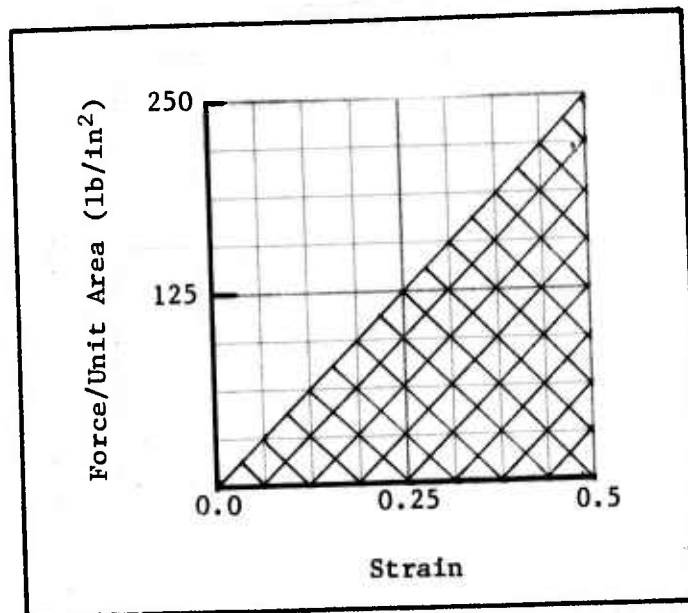


Figure F-10. Work Done by Linear Force

The work done deforming the shock absorber equals the energy to be absorbed. For rubber with the selected modulus and strain restriction, the work done on the material, when the final strain is 0.5, is

$$W_R = 125 A \ell \quad (F-30)$$

where  $W_R$  work done on rubber (in-lb)  
 $A$  original area (in<sup>2</sup>)  
 $\ell$  distance of displacement (in)

The energy to be absorbed consist of the kinetic energy of the shuttle and springs plus the work done by the final force over the displacement distance.

$$W_r = KE_{sh+sp} + (\text{final force}) \ell \quad (F-31)$$

TABLE F-4. KINETIC ENERGY OF SHUTTLE AND SPRINGS

Shuttle Weight (lb)	Shuttle Velocity (ft/sec)		
	73 1/3	75	80
10	18369	19216	21864
15	23381	24457	27826
17	25385	26552	30211

The weight of the shuttle is approximately 17 pounds and chosen launch speed is 74.3 feet per second.

For design of the shock absorber a kinetic energy level of 30,000 inch-pounds is used for a safety margin. Substituting Eq (F-30) into Eq (F-31) yields

$$125 A \ell = 30,000 + 465 \ell \quad (F-32)$$

where  $A$  original area ( $\text{in}^2$ )

$\ell$  displacement distance

leads to

$$\ell = \frac{30,000}{125A-465}$$

A graph showing the displacement for varying area and kinetic energy levels is shown in Figure F-11. The maximum force exerted by the shock is

$$F_{\text{shock}} = 250A \quad (F-33)$$

An area of 24 square inches is arbitrarily selected, and this choice yields a maximum force of 6000 pounds.

The shock absorber consists of two pieces of neoprene rubber, 12.0 inches long and 4.1 by 3.0 inches in cross section. A 0.6-inch diameter hole is drilled through the block to hold a 9/16-inch stiffening rod.

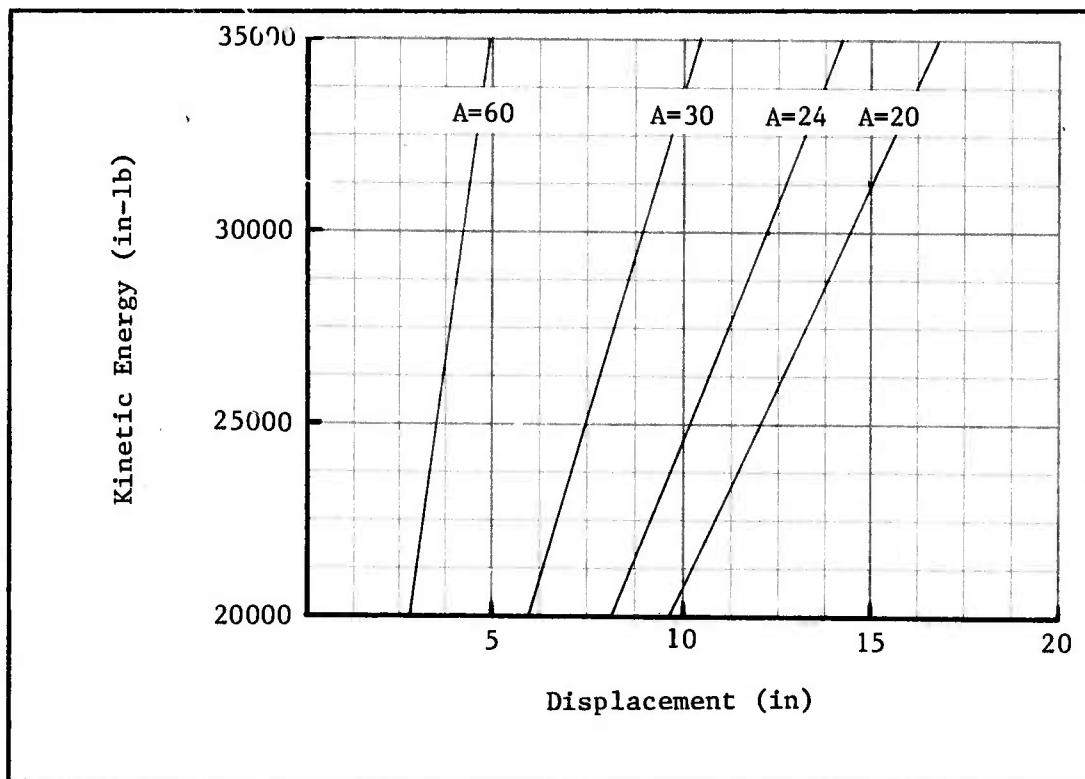


Figure F-11. Distance Required to Bring Shuttle Speed to Zero for Various Areas

The rod is attached through a thin front plate of aluminum and extends through a hole in the mounting brace each on the launcher rails. For analysis to show this rod will prevent the rubber from buckling under load, it is assumed that if the entire load could be carried by the rod, the rubber would not buckle. Two positions are checked, a 6-inch and a 12-inch displacement. This assumes that the ends of the columns are pinned. Using Eqs (F-19, 17 and 20) the following table was constructed.

TABLE F-5. STIFFENING ROD STRESSES

Displacement (in)	12	6
$\frac{KL}{r}$	85 1/3	128
$f_c$ (lb/in <sup>2</sup> )	12,048	6,024
$f_{CE}$ for Al	14,000	6,200
$f_{CE}$ for steel	39,440	17,530

A 9/16 inch steel rod will insure the shock does not buckle.

APPENDIX F-6

ANALYSIS OF CRITICAL SHUTTLE COMPONENTS

The analysis is of the forward thrust lever and rear support columns as these are the most critical to the system.

Thrust Lever

A maximum force of 900 pounds is transmitted through this lever. The lever is a 2 by 1/2 inch bar approximately 14 inches long. The block that prevents the bar from rotating aft during launch is 2 inches above pivot and 9 inches below the airframe block. This condition will create moment of 8,100 inch-pounds during launch in the lever.

The physical characteristics associated with the aluminum thrust lever are listed below:

Weight	Wt.	1.176	(lb/ft)
Area	A	0.500	(in <sup>2</sup> )
Moment of Inertia	I <sub>xx</sub>	0.333	(in <sup>4</sup> )
	I <sub>yy</sub>	0.021	(in <sup>4</sup> )
Sectional Modulus	S <sub>xx</sub>	0.333	(in <sup>3</sup> )
	S <sub>yy</sub>	0.084	(in <sup>3</sup> )
Radius of Gyration	r <sub>x</sub>	0.578	(in)
	r <sub>y</sub>	0.1445	(in)

(Alcoa, 1956)

Bending Analysis of the Thrust Lever. The bending failure would occur about the "x-x" axis if it occurred due to the maximum moment of 8100 inch-pounds.

$$\sigma_{\max} = \frac{M_x}{S_x}$$

(F-34)

(Alcoa, 1956)

$$\begin{aligned}\sigma_{\max} &= \frac{8100}{0.333} \\ &= 24,324 \text{ lb/in}^2\end{aligned}$$

The elastic limit for 6061-T6 aluminum is 35,000 pounds per square inch, and the maximum stress felt under a 900-pound thrust is 24,324. At the impact of the shuttle with shock absorber the bar will rotate forward and down.

Considering the thrust lever as a cantilever beam of 12 inches in length and a load of 846 pounds ( $900 \sin 20^\circ$ ) and the deflection is given by

$$D = \frac{PL^2}{3EI} \tag{F-35}$$

where D deflection (in)

P load (lb)

L distance from support to load (in)

E Young's modulus

I moment of inertia ( $\text{in}^4$ )

(Alcoa, 1956)

The deflection is

$$\begin{aligned}D &= \frac{846 (12)^2}{3(10^7) 0.333} \\ &= 0.012 \text{ in}\end{aligned}$$

The average deflection angle is less than 0.06 degrees. The deflection is not significant.

Torsional Analysis of the Thrust Lever. For the torsional analysis the thrust load is considered to be off-set to the edge of the thrust lever. The maximum shear stress seen in a rectangular section is

$$f_s = \frac{3T}{bt^2} \left(1 + 0.6 \frac{t}{b}\right) \quad (\text{F-36})$$

where  $f_s$  maximum shear (lb/in<sup>2</sup>)  
 $T$  torque (in-lb)  
 $b$  long dimension of rectangular (in)  
 $t$  short dimension rectangular (in)

(Alcoa, 1956)

The maximum shear stress is

$$f_s = \frac{3 (846 \times 0.25)}{2 (0.5)^2} \left(1 + 0.6 \frac{0.5}{2}\right)$$

$$= 1459.4 \text{ lb/in}^2$$

The maximum shear stress is 1,460 pounds per square inch compared to elastic limit of 20,000. The safety factor is greater here than in bending failure.

#### Rear Columns for Vehicle Boom Support

The rear supports for the drone are two 27-inch long aluminum tubes made of alloy 6061-T6. The physical properties of this tube are listed below.

Outside diameter	d	2	(in)
Wall thickness	t	1/16	(in)
Weight	Wt	0.447	(lb/ft)
Area	A	0.380	(in <sup>2</sup> )
Moment of inertia	I	0.179	(in <sup>4</sup> )

Sectional modulus	S	0.179	(in <sup>3</sup> )
Radius of gyration	r	0.685	(in)

(Alcoa, 1956)

Bending Under Maximum Launcher Thrust. The rear supports are located approximately 40 inches aft of the front support and 24 inches above the shuttle base. During a 900 pound thrust, the moment caused by the center of gravity being at most 5.5 inches above the front support is 4950 inch-pounds. Ignoring any counter moment due to engine thrust, the load supported by the rear supports is approximately 124 pounds plus static weight. The maximum total load for each support is approximately 112 pounds vertical. The loading condition for the analysis is 120 pounds axial plus 1456 inch-pound moment (122 x 13). Using the equation for a uniformly loaded cantilever beam, Eq (F-37), the maximum moment due to the rod's weight at 7-g's is 13.6 inch-pounds and is ignored.

$$M_{\max} = \frac{w L^2}{2} \quad (\text{F-37})$$

where  $M_{\max}$  maximum moment (in-lb)  
 $w$  weight per unit length (lb/in)  
 $L$  length of beam (in)

The values for use in Eq (F-15) are

$$f_c = \frac{120}{0.038}$$

$$= 315.8 \text{ lb/in}^2$$

$$\frac{KL}{r} = \frac{2.27}{0.685}$$

$$= 78.83$$

$$f_C = 16,400 \text{ lb/in}^2$$

$$f_{CE} = 16,400 \text{ lb/in}^2$$

$$f_b = \frac{1456}{0.179} = 8,134$$

$$f_B = 35,000 \text{ lb/in}^2$$

Substituting these values into Eq (F-15) yields

$$D = \frac{315.8}{16,400} + \frac{8,134}{35,000 \left(1 - \frac{315.8}{16,400}\right)}$$

$$= 0.256$$

The support rod will not buckle under a 7-g acceleration of launch.

Bending Analysis Under Impact Load. The maximum deceleration force placed on the shuttle by the shock absorber is 6000 pounds. This amounts to a load of 353 g's on the 17-pound shuttle. Using Eq (F-37) with an equivalent weight per unit length for 353 g's, the  $M_{\max}$  is

$$M_{\max} = \frac{0.447 (353)}{2 (12)} (27)^2$$

$$= 4793 \text{ in-lb}$$

The maximum bending stress due to this moment is

$$\sigma = \frac{M}{S}$$

$$= \frac{4793}{0.179}$$

$$= 26,776 \text{ lb/in}^2$$

The stress is below the elastic limit of 35,000 pounds per square inch, therefore no failure will occur to rear supports due to the 353 g-load on the shuttle.

APPENDIX F-7

WINCH AND POWER SUPPLY

An electrical winch is needed to cock the launcher. Superwinch model PM 4000 has sufficient power and speed for this use (See Figure F-13.). The speed, however, does limit the launch interval because of a cocking time of approximately one minute. The power requirement for the winch to operate effectively is a minimum of 9 volts dc at 82 amps, at a maximum load of 900 pounds (Superwinch, 1974).

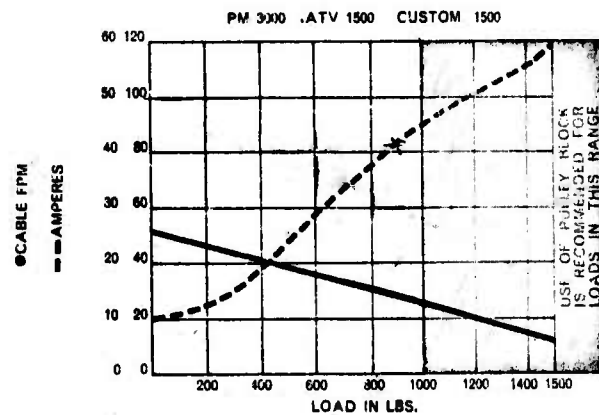


Figure F-12. Capability and Electrical Requirements at 9 Volts dc (Superwinch, 1974)

The selected power supply is the Hobart IRG-450 battery charger. Its capabilities with variable inductive loads are 80 amps at 11.5 volts dc or 120 amps at 9.0 volts. The power supply can run continuously at an output of 95 amps (Heisey, 1975). This combination of winch and power supply will provide sufficient capability for our application.

Test on the power supply are being run at Hobart Brothers of Troy, Ohio, to confirm the battery charger capability as a power supply.

APPENDIX F-8

COST OF LAUNCHER

The cost estimate for material for one launcher is given in the following table.

TABLE F-6. MATERIAL COST FOR A LAUNCHER

Materials	Cost (\$)	Reference
Main Beams	439	(Jackson, 1975a)
Other steel stock	120	(Jackson, 1975a)
Aluminum	25	(Wolfe, 1975)
Rubber	100	(McCarren, 1975)
Springs, 12 each	360	(Barnes, 1975)
Winch	206	(Burlingame, 1975)
Chain, hook, and cable	88	(Grotz, 1975)
Power supply	420	(Heisey, 1975)
Misc.	100	(Wolfe, 1975)
Total	1858	

The estimated direct labor manhours and cost of fabrication are listed in the table below. The skill level required is that of a general machinist. A labor rate of \$6.45 per hour is used with overhead cost of 150 percent of direct labor (Wolfe, 1975).

TABLE F-7. FABRICATION COST AND LABOR HOURS

Cost Element	Low	Most Likely	High
Direct Labor Manhours	170	195	220
Labor and Overhead	\$2741	\$3144	\$3548

## REFERENCES

- Adams, Donald F.  
1971 Airframe Structural Materials for Drone Applications.  
Rand Technical Report R-581/4-ARPA. Santa Monica, CA.  
The Rand Corp, July 1971.
- AFFDL TM-71-1-PTB  
1971 Teleplane Preliminary Design Study. AFFDL TM-71-1-PTB.  
Wright-Patterson AFB, OH: Air Force Flight Dynamics  
Laboratory, December 1971.
- AFGWC  
1972 AFGWC Limited Area Meso-scale Prediction Model. Verification  
Data. Air Force Global Weather Central, 1972.
- AFR 173-10  
1975 USAF Cost and Planning Factors. Washington: Department of  
the Air Force, 6 February 1975.
- AFR 178-1  
1973 Economic Analysis and Program Evaluation for Resource  
Management. Washington: Department of the Air Force,  
20 December 1973.
- AFSC/AFLC Commanders' Working Group on Life Cycle Cost  
1973 Life Cycle Cost Reference Notebook. Wright-Patterson AFB,  
OH: Air Force Aeronautical Systems Division/ACCL,  
August 1973.
- Alan, Hank, Engineer,  
1975 Telephone Conversation. Curtiss-Wright Corporation,  
Woodbridge, NJ, 23 May 1975.
- ALCOA  
1956 Alcoa Structural Handbook, a Design Manual for Aluminum.  
Pittsburgh, PA: Aluminum Company of America, 1956.
- ALCOA  
1975 Telephone Conversation. Alcoa Aluminum Sales Office,  
Dayton, OH, 6 October 1975.
- Alderman, Charles, Unit Supervisor  
1975 Telephone Conversation. Warner-Robbins Air Logistic Center/  
MMURCB, Warner-Robbins AFB, GA, 10 October 1975.

- Allied Electronics Corporation  
1975 Allied Engineering Manual and Purchasing Guide. Elgin, IL: Allied Electronics Corp, 1975.
- Allinkov, Sidney, Materials Engineer  
1975 Personal Interviews. Air Force Materials Laboratory/MXC, Wright-Patterson AFB, OH, 6 May - 23 September 1975.
- American Institute of Steel Construction  
1965 Manual of Steel Construction. New York: American Institute of Steel Construction, Inc., 1965.
- American Institute of Steel Construction  
1973 Manual of Steel Construction (7th edition). New York: American Institute of Steel Construction, Inc., 1973.
- American Radio Relay League  
1974 The Radio Amateur's Handbook (51st edition). Newington, CN: American Radio Relay League, 1974.
- ASD/XR 74-2  
1974 Executive Summary, Drone/RPV Mission Analysis (U). Wright-Patterson AFB, OH: Air Force Aeronautical Systems Division, February 1974. (SECRET)
- Atkins, Alan R., Dr.  
1975 Personal Interviews. Air Force Aeronautical Systems Division/YRPM, Wright-Patterson AFB, OH, 20 September - 25 November 1975.
- Bair, Charles A., Jr.  
1975 Stability and Control of Mini-Remotely Piloted Vehicles. Unpublished Thesis, GAE/AE/75M-1. Wright-Patterson AFB, OH: Air Force Institute of Technology, March 1975.
- Barnes, Bert D., Treasurer  
1975 Telephone Conversation. Yost Superior Manufacturing Co., Springfield, OH, 24 July - 7 November 1975.
- Beckman Helipot  
1975 "Advertisement". Evaluation Engineering, 14, No. 5: (September - October 1975).
- Beukers, J. M.  
1973 "Navigation System Employed in the Differential Mode." Navigation. (Spring, 1973).
- Blakelock, John H.  
1965 Automatic Control of Aircraft and Missiles. New York: John Wiley & Sons, Inc., 1965.
- Blanton, Colleen, Item Manager  
1975 Telephone Conversation. Aerospace Communications Division/MCRMB, McClellan AFB, CA, 10 November 1975.

- Borisenko, M.M., and M.V. Zavaring  
1967 "Vertical Profiles of Wind Speeds From Measurements on High Towers." Air Force Cambridge Research Laboratory Report 68-0653, L.G. Hanscom Field, Bedford, MA, December 1967.
- Bowen, Robert E., Major, USAF  
1975 Personal Interviews. Air Force Aeronautical Systems Division/YRPM, Wright-Patterson AFB, OH, 16 April - 5 November 1975.
- Buchin, S.I.  
1969 Computer Programs for the Analysis of Complex Decision Problems. Harvard University: January 1969.
- Burke, Lawrence G., Marketing Director  
1975 Telephone Conversation. Spears Associates, Needham, MA, 17 October 1975.
- Burlingame, Fenner J., Customer Service Manager  
1975 Telephone Conversation. Superwinch, Inc., Putnam, CT, 6-10 November 1975.
- Carlson, Alan, and others  
1967 Handbook of Analog Computation (2nd Edition). Princeton, NJ: Electronic Associates, Inc., 1967.
- Carvell, Frank  
1975 Personal Interview. Air Force Aeronautical Systems Division/WE, Wright-Patterson AFB, OH, 1 July - 30 September 1975.
- Chalk, C.R., and others  
1969 Background Information and User Guide for Mil-F-8785B (ASG), "Military Specification-Flying Qualities of Piloted Vehicles." AFFDL-TR-69-72, Wright-Patterson AFB, OH, August 1969.
- Chironis, Nicholas P., ed.  
1961 Spring Design and Application. New York: McGraw-Hill Book Co., 1961.
- Coast Guard  
1974 Loran-C User's Guide. Washington: United States Coast Guard, August 1974.
- Coleman, J.J.  
1969 "Silver-Chloride-Magnesium and Cuprous-Chloride-Magnesium Batteries." Standard Handbook for Electrical Engineers (10th Edition). New York: McGraw-Hill Book Co., 1969.
- Comptroller of the Army  
1971 Costing Methodology Handbook. Washington: Department of the Army, April 1971. AD 884835

Corning, Gerald

1953 Airplane Design. College Park, MD: (Printed by Edwards Brothers Inc, Ann Arbor, MI), 1953.

Currie, Caird, Sales Executive

1975 Telephone Conversation. Lawson Power Products, New Holstein, WI, 5 November 1975.

Dailside, Clifford

1975 Telephone Conversations. E-Systems, Inc., Melpar Division, Falls Church, VA: 8 July - 15 September 1975.

Dannis, Mark., PHD, Research Engineer

1975 Personal Interview and Telephone Conversations., B.F. Goodrich Rubber Co./Research Center, Breaksville, OH, 11 June - 7 November 1975.

Davis, Robert, Captain, USAF

1975 Telephone Conversations. Ogden Air Logistic Center, Hill AFB, UT, 2 September - 21 October 1975.

Dayton Plastics

1975 Telephone Conversation. Dayton Plastics Company Sales Office, Dayton, OH, 6 October, 1975.

Delorme, J.F., and A.R. Tuppen

1975 "Low Cost Navigation Processing for Loran-C and Omega." Navigation: (Summer, 1975).

Develco Inc.

1967 "Study Report: A Comparison of Long Range Navigation Systems." Palo Alto, CA: Develco Inc., 1967.

Develco Inc.

1975a "Minimum Essential Omega." Concept Paper 750924. Mountain View, CA: Develco Inc., September 1975.

Develco Inc.

1975b Tactical Jamming of the Omega Navigation System. Technical Note 750922. Mountain View, CA: Develco Inc., 1975.

Diehl, Walter S.

1926 Three Methods of Calculating Range and Endurance of Airplanes. NACA Technical Report 234. Washington: National Advisory Committee for Aeronautics, 1926.

Dommasch, Daniel O., and others  
1951 Airplane Aerodynamics. New York: Pitman Publishing Company,  
1951.

Donahue, J.F.  
1969 "Nickel-Cadmium Batteries." Standard Handbook for Electrical  
Engineers (10th Edition). New York: McGraw-Hill Book  
Company, 1969.

Early, Dwight H., Aeronautical Engineer  
1975 Personal Interviews. Air Force Flight Dynamics Laboratory/  
PTB, Wright-Patterson AFB, OH, 6 March - 19 October 1975.

Enright, J.F.  
1969 "An Economic Evaluation of the Use of Omega Navigation System  
by Merchant Ships." Navigation. (Summer 1969).

Errico, E.F.  
1969 "Zinc-Alkaline-Manganese Dioxide Batteries." Standard  
Handbook for Electrical Engineers (10th Edition). New York:  
McGraw-Hill Book Company, 1969.

E-Systems, Incorporated  
1974a Tactical RPV Final R&D Report. Report No. G3722.18.02C,  
EWO No. 8902-RBBD. Greenville Division: E-Systems Inc.,  
January 1974.

Fisher, Gene H.  
1970 Cost Considerations in Systems Analysis. Report R-490-ASD.  
Santa Monica, CA: The Rand Corp., 1970.

- Gaugler, Gary.  
1975 Personal Interviews. Air Force Avionics Laboratory/TE4,  
Wright-Patterson AFB, OH, 15 April - 30 September 1975.
- Graf, Rudolf F.  
1972 Modern Dictionary of Electronics (Fourth Edition).  
Indianapolis: Howard W. Sams & Co., Inc., 1972.
- Griffin, Warren R., Research Engineer  
1975 Personal Interview. Air Force Materials Laboratory/MBE,  
Wright-Patterson AFB, OH, 6 May - 7 November 1975.
- Grotz, Dale C., Vice President  
1975 Personal Interviews. Material Handling Systems, Inc.,  
Dayton, OH, 30 July - 11 November 1975.
- Hallett, Arthur H.  
1975 Telephone Conversation. 2750 Logistic Squadron/DMTTH,  
Wright-Patterson AFB, OH, 8 October 1975.
- Hammond, Charles, Sales Manager  
1975 Telephone Conversation. McCulloch Corporation, Los Angeles,  
CA, 18 September 1975.
- Hammonds, Carl  
1975 Telephone Conversation. Kraft Systems, Incorporated,  
Vista, CA, 9 October 1975.
- Hartman, Edwin P. and David Bierman  
1938 The Aerodynamic Characteristics of Full-Scale Propellers  
Having 2, 3, and 4 Blades of Clark Y and R.A.F. 6 Airfoil  
Sections. NACA TR 640. Washington: National Advisory  
Committee for Aeronautics, 1938.
- Hayward Distributing Company  
1975 Telephone Conversation. McCulloch Distributors, Columbus,  
OH, 10 October 1975.
- Hedderson, George W.  
1969 "Lead-Acid and Nickel-Cadmium Batteries" Standard Handbook  
for Electrical Engineers (10th Edition). New York: McGraw-  
Hill Book Co., 1969.
- Heisey, Larry E., Development Engineer  
1975 Telephone Conversation. Hubart Brothers Co., Troy, OH,  
11 November 1975.

- Henry, George  
1975b Personal Interviews. Foreign Technology Division/ETTS,  
Wright-Patterson AFB, OH, 15 June - 25 November 1975.
- Horton, Larry K.  
1975 Personal Interview. Air Force Aeronautical Systems  
Division/YRC, Wright-Patterson AFB, OH, 6 October 1975.
- Houpis, Constantine H. and John J. D'Azzo  
1960 Feedback Control System Analysis and Synthesis. New York:  
McGraw-Hill Book Company, 1960.
- Howard, Paul L.  
1969 "Silver Oxide - Cadmium Batteries." Standard Handbook for  
Electrical Engineers (10th Edition). New York: McGraw-  
Hill Book Company, 1969.
- Hoy, Walter, Major, USAF  
1975 Personal Interviews. Air Force Flight Dynamics Laboratory/  
FGSB, Wright-Patterson AFB, OH, 18 February - 21 October 1975.
- Jackson, Ernie C.  
1975a Telephone Conversation. Ryerson Steel Co., Dayton, OH,  
3 November 1975.
- Jackson, Kenneth  
1975b Telephone Conversations. Ogden Air Logistic Center/MMTCP,  
Hill AFB, UT, 18 August - 7 October 1975.
- Jacobs, Eastman N. and others  
1935 The Characteristics of 78 Related Airfoil Sections from  
Tests in the Variable-Density Wind Tunnel. NACA Technical  
Report 460. Washington: National Advisory Committee for  
Aeronautics, 1935.
- Jacobs, Carl R., Division Manager  
1975 Telephone Conversation. Hayward Distributing Company,  
Columbus, OH, 15 October 1975.
- Johnson, Alan  
1975 Telephone Conversation. Air Force Avionics Laboratory/AAI,  
Wright-Patterson AFB, OH, 18 September 1975.
- Joonsar, Heikki, Captain, USAF  
1975 Personal Interviews. Air Force Aeronautical Systems Divi-  
sion/YRPM, Wright-Patterson AFB, OH, 15 January - 25 Nov-  
ember 1975.

- Kershner, William K.  
 1968 The Student Pilot Flight Manual. Iowa State University Press, Ames, IA, 1968.
- Koury, James L., Research Chemist  
 1975 Personal Letter. Air Force Rocket Propulsion Laboratory/ MKMB, Edwards AFB, CA, 20 May 1975.
- Kraft Systems, Incorporated  
 1975 Sales Catalog. Vista, CA: Kraft Systems, Inc., 1975.
- Lander, J.J.  
 1969 "Silver-Zinc Cells." Standard Handbook for Electrical Engineers (10th Edition). New York: McGraw-Hill Book Company, 1969.
- Larsen, Harold C., Head of Aerospace Design  
 1975a Personal Interviews. Air Force Institute of Technology/ END, Wright-Patterson AFB, OH, 12 March - 8 October 1975.
- Larsen, Harold C., Head of Aerospace Design  
 1975b Unpublished Class Notes, AE643. Air Force Institute of Technology, Wright-Patterson AFB, OH, 1975.
- Leggett, A. B., Engineer  
 1975 Personal Letters. US Army Mobility Equipment Research and Development Center/AMXFB-EM, Fort Belvoir, VA, 18 March - 28 November 1975.
- Lentzsch, Craig R., 1Lt, USAF  
 1975 Personal Interview. Air Force Aeronautical Systems Division/ACCC, Wright-Patterson AFB, OH, 21 May 1975.
- Lichty, Lester C.  
 1951 Internal-Combustion Engines (6th Edition). New York: McGraw-Hill Book Company., 1951.
- Lockheed Missles and Space Company, Inc.  
 1974 Test Data of MC101A Engine. Unpublished Paper. Sunnyvale, CA: Lockheed Missles and Space Company, Inc., 1974.
- Lowe, Donald  
 1975 Personal Interviews. Air Force Flight Dynamics Laboratory/ FGSB, Wright-Patterson AFB, OH, 18 February - 21 October 1975.
- Lyman, Jerry  
 1975 "Battery Technology Packaging: More Muscle Into Less Space". Electronics, 48, No. 7: (3 April 1975).

- Main Auto Parts  
1975 Telephone Conversation. Dayton, OH, 22 October 1975.
- Mallory Battery Company  
1975 Price Schedule of Lithium Cells. Terrytown, NY: Mallory Battery Co., 2 January 1975.
- Mandl, Matthew  
1964 Fundamentals of Electric and Electronic Circuits. Englewood Cliffs, NJ: Prentice-Hall, Inc., 1964.
- Matsushita, S., and W. H. Campbell  
1967 Physics of Geomagnetic Phenomena. New York: Academic Press, 1967.
- Maxwell, George  
1975 Telephone Conversation. Air Force Avionics Laboratory/WRA, Wright-Patterson AFB, OH, 12 August 1975.
- McCarren, Paul K., Manager  
1975 Telephone Conversation. Reliable Rubber Products Co., Dayton, OH, 10 November 1975.
- McCulloch Corporation  
1974 McCulloch High Performance 2-Cycle Engines. ADV 150040. Los Angeles, CA: McCulloch Corporation, 1974.
- McCulloch Corporation  
1975 Racing Engines. ADV 150023. Los Angeles, CA: McCulloch Corporation, 1975.
- Meranda, Chuck G.  
1975 Personal Interview. Air Force Aeronautical Systems Division/ACCC, Wright-Patterson AFB, OH, 13 May 1975.
- Messerle, Hugo K.  
1969 Energy Conversion Statistics. New York: Academic Press, 1969.
- MIL-HDBK-217B  
1974 Reliability Prediction of Electronic Equipment. Washington: Department of Defense, 20 September 1974.
- Miller, Dean  
1975 Personal Interview. Air Force Flight Dynamics Laboratory/FSCB. Wright-Patterson AFB, OH, 17 September 1975.

- Morehouse, C.K., and others  
1958 "Batteries." Selected Papers on New Techniques for Energy Conversion, Edited by Sumner N. Levine and others. New York: Dover Publications, Inc., 1961.
- Morrissey, Edward, Materials Research Engineer  
1975 Personal Interviews. Air Force Materials Laboratory/MXC, Wright-Patterson AFB, OH, 6 May - 23 September 1975.
- Moss, Frank T.  
1975 "Understanding Radio Navigation Systems." Yachting: (August 1975).
- Murphy, Edward L.  
1970 Statistical Methods of Measuring the Uncertainty of Cost Estimates. Redstone Arsenal, AL: US Army Missile Command, February 1970. AD 718862
- Myers, George  
1975 Personal Interviews. Air Force Avionics Laboratory/WRA, Wright-Patterson AFB, OH, 15 May - 25 November 1975.
- National Semiconductor Corporation  
1973 Linear Applications Handbook. Santa Clara, CA: National Semiconductor Corp., February, 1973.
- National Semiconductor Corporation  
1974 Transducers - Pressure and Temperature. Santa Clara, CA: National Semiconductor Corp., August, 1974.
- National Semiconductor Corporation  
1975a CMOS Integrated Circuits. Santa Clara, CA: National Semiconductor Corp., 1975.
- National Semiconductor Corporation  
1975b Telephone Conversation. District Sales Office, Dayton, OH, 21 October 1975.
- Nelson, Wilbur C.  
1944 Airplane Propeller Principles. New York: John Wiley Book Company, 1944.
- Owens, F. Scott, Materials Engineer  
1975 Personal Interviews. Air Force Aeronautical Systems Division/YRE, Wright-Patterson AFB, OH, 13 June - 5 October 1975.
- Parry, Thomas, Captain, USAF  
1975 Personal Interview. Air Force Logistics Command/AQMLE, Wright-Patterson AFB, OH, 16 September 1975.
- PARTL  
1974 Heaviside Partial Fraction Expansion and Time Response Program (PARTL). School of Engineering, Air Force Institute of Technology, Wright-Patterson AFB, OH, 1974.

- Payne, Arthur R., and John R. Scott  
1960 Engineering Design with Rubber. New York: Interscience Publishers, Inc., 1960.
- Perkins, Courtland D., and Robert E. Hage  
1949 Airplane Performance, Stability, and Control. New York: John Wiley & Sons, Inc., 1949.
- Pfaff, Don  
1975 Telephone Conversation. Kurz-Kasch, Incorporated, Dayton, OH, 21 October 1975.
- Pierce, J., Phd.  
1975 Telephone Conversation. Develco, Inc., Mountain View, CA, 8 October 1975.
- Pickwell, Glen V., Professional Engineer  
1975 Personal Interviews. Dayton, OH, 10 July - 10 November 1975.
- Poly Paks  
1975 Sales Catalog 211A. South Lynnfield, MA: Poly Paks, September 1975.
- Pope, Alan, and John J. Harper  
1966 Low-Speed Wind Tunnel Testing. New York: John Wiley & Sons, Inc., 1966.
- Powell, Rex B., and others  
1974 A Low Cost TV Guided Weapon Delivery System - FY74 Final Final Report. RD-75-23. Redstone Arsenal, AL: U.S. Army Missile Command, 1 August 1974.
- Power Conversion, Inc.  
1975 O.E.M. Price List for Lithium Organic Electrolyte Batteries. Mt Vernon, NY: Power Conversion, Inc., February, 1975.
- Preist, H. Malcolm and John A. Gilligan  
1965 Design Manual for High-Strength Steels. Pittsburgh, PA: United States Steel Corp., 1965.
- Regulinski, Thaddeus L., Professor  
1975 "Kolomogorov-Smirnov and Likelihood Ratio Tests Computer Program." School of Engineering, Air Force Institute of Technology, Wright-Patterson AFB, OH, 1975.
- Rhyne, V. Thomas  
1973 Fundamentals of Digital Systems Design. Englewood Cliffs, NJ: Prentice-Hall, Inc., 1973.

Rodenroth, Ronald T.

1974 A Preliminary Design Layout and Performance Estimate of a Mini-Remotely Piloted Research Vehicle. Unpublished Thesis, GAE/AE/74D-23. Wright-Patterson AFB, OH: Air Force Institute of Technology, December 1974.

ROOTL

1974 User's Manual for a Digital Computer Routine to Calculate the Root Locus (ROOTL). School of Engineering, Air Force Institute of Technology, Wright-Patterson AFB, OH, 1974.

Rorden, B., Technical Director

1975 Telephone Conversation. Develco, Incorporated, Mountain View, CA: 1 August - 30 October 1975.

Rose, Edward A., Jr.

1975a Telephone Conversations. E-Systems, Inc., Melpar Division, Falls Church, VA: 8 July - 15 September 1975.

Rose, Henry, Engineer

1975b Telephone Conversation. Sensenich Corporation, Lancaster, PA: 14 August 1975.

Ruben, Samuel

1969 "Sealed Zinc-Mercury Batteries." Standard Handbook for Electrical Engineers (10th Edition). New York: McGraw-Hill Book Company, 1969.

Seckel, Edward

1964 Stability and Control of Airplanes and Helicopters. New York: Academic Press, 1964.

Shanley, F. R.

1967 Mechanics of Materials. New York: McGraw-Hill Book Company, 1967.

Small, T. R.

1974 Engine Development Program for the APL Remotely Piloted Vehicle. Report Number TG 1249. Silver Spring, MD: Johns Hopkins University Applied Physics Laboratory, July 1974. AD 787507

Stansberry, Chuck

1975 Personal Letter. American Klegecell Corporation, Corsicana, TX, 28 October 1975.

- Steelman, Larry, Technical Manager  
1975 Telephone Conversation. Teledyne Systems Company, Northridge, CA, 15 September 1975.
- Stengard, Robert A.  
1974 "Integral Skin Urethane Foam." Modern Plastics Encyclopedia, 51: 137-138 (October 1974).
- Superwinch, Incorporated  
1974 Superwinch - The Prime Mover, Sales Catalog 7171, Putnam, Connecticut: Superwinch, Inc., September 1974.
- Sutherland, W.  
1971 Adding Cost Estimates That Are Not Symmetric About the Most Likely Value. RAC-CF-23. McClean, VA: Research Analysis Corporation, April 1971. AD 883232
- Tecumseh Products Company  
1974 1974-75 Replacement Engines Specifications. Grafton, WI: Tecumseh Products Company, 1 October 1974.
- Teledyne Systems Company  
1975 "A Concept for Low Cost Mini-RPV Guidance with Loran C/D." Concept Paper. Northridge, CA: Teledyne Systems Company, June 1975.
- Texas Instruments, Inc.  
1973 The Linear & Interface Circuits Data Book for Design Engineers. Dallas, TX: Texas Instruments, Inc., 1973.
- Thompson, Steven, Captain, USAF  
1975 Personal Interviews. Air Force Aeronautical Systems Division/ACCL, Wright-Patterson AFB, OH, 10 July - 15 August 1975.
- TRANFUN  
1974 Computer Program to Compute Transfer Function of Aircraft Systems (TRANFUN). School of Engineering, Air Force Institute of Technology, Wright-Patterson AFB, OH, 1974.
- Trull, Ronald  
1975 Personal Interview. Air Force Flight Dynamics Laboratory/FGL, Wright-Patterson AFB, OH, 8 April - 6 August 1975.

- Steelman, Larry, Technical Manager  
1975 Telephone Conversation. Teledyne Systems Company, Northridge, CA, 15 September 1975.
- Stengard, Robert A.  
1974 "Integral Skin Urethane Foam." Modern Plastics Encyclopedia, 51: 137-138 (October 1974).
- Superwinch, Incorporated  
1974 Superwinch - The Prime Mover, Sales Catalog 7171, Putnam, Connecticut: Superwinch, Inc., September 1974.
- Sutherland, W.  
1971 Adding Cost Estimates That Are Not Symmetric About the Most Likely Value. RAC-CF-23. McClean, VA: Research Analysis Corporation, April 1971. AD 883232
- Tecumseh Products Company  
1974 1974-75 Replacement Engines Specifications. Grafton, WI: Tecumseh Products Company, 1 October 1974.
- Teledyne Systems Company  
1975 "A Concept for Low Cost Mini-RPV Guidance with Loran C/D." Concept Paper. Northridge, CA: Teledyne Systems Company, June 1975.
- Texas Instruments, Inc.  
1973 The Linear & Interface Circuits Data Book for Design Engineers. Dallas, TX: Texas Instruments, Inc., 1973.
- Thompson, Steven, Captain, USAF  
1975 Personal Interviews. Air Force Aeronautical Systems Division/ACCL, Wright-Patterson AFB, OH, 10 July - 15 August 1975.
- TRANFUN  
1974 Computer Program to Compute Transfer Function of Aircraft Systems (TRANFUN). School of Engineering, Air Force Institute of Technology, Wright-Patterson AFB, OH, 1974.
- Trull, Ronald  
1975 Personal Interview. Air Force Flight Dynamics Laboratory/FGL, Wright-Patterson AFB, OH, 8 April - 6 August 1975.

- Trefzger, C.E., Marketing and Sales Director  
1975 Personal Letter. Georator Corp., Manassas, Virginia,  
8 September 1975.
- Union Carbide Corp.  
1971 Eveready Battery Applications Engineering Data. New York:  
Union Carbide Corp., 1971.
- Wahl, A. M.  
1963 Mechanical Springs (2nd Edition). New York: McGraw-Hill  
Book Co., 1963.
- Waterloo, William C.  
1974 "Extrusion Blow Molding." Modern Plastics Encyclopedia, 51:  
278-284 (October 1974).
- Wedge, A. C.  
1975 Telephone Conversation. Sensenich Corporation, Lancaster,  
PA, 14 August 1975.
- Weissert, Fred, Research Engineer  
1975 Personal Interview and Telephone Conversations. Firestone  
Tire and Rubber Co./Central Research, Akron, OH, 11 June -  
10 September 1975.
- Wolfe, Millard W., Shop Foreman  
1975 Personal Interview. Air Force Institute of Technology/  
SVD, Wright-Patterson AFB, OH, 7 June - 11 November 1975.
- Wright, Wayne F.  
1975 Telephone Conversation. Warner-Robbins Air Logistics  
Center/MMUTCB, Warner-Robbins AFB, GA, 6 November 1975.
- Yonezama, Y., and others  
1969 "Evaluation of Loran-C System by a Manual Receiver -  
Indicator." Navigation. (Spring 1969).